

INTERNATIONAL COUNCIL FOR RESEARCH AND INNOVATION
IN BUILDING AND CONSTRUCTION

WORKING COMMISSION W18 - TIMBER STRUCTURES

CIB - W18

MEETING THIRTY-SEVEN

EDINBURGH

SCOTLAND

AUGUST 2004

Lehrstuhl für Ingenieurholzbau und Baukonstruktionen
Universität Karlsruhe
Germany
Compiled by Rainer Görlacher
2004

ISSN 0945-6996

CONTENTS

0. List of Participants
1. Chairman's Introduction
2. Stresses for Solid Timber
3. Timber Joints and Fasteners
4. Timber Beams
5. Laminated Members
6. Structural Stability
7. Fire
8. Fracture Mechanics
9. Serviceability
10. Loading Codes
11. Joint Committee on Structural Safety
12. Any Other Business
13. Venue and Program for Next Meeting
14. Close
15. List of CIB W18 Papers, Edinburgh, Scotland, UK, 2004
16. Current List of CIB-W18 Papers

CIB-W18 Papers 37-6-1 up to 37-104-1

0 List of Participants

**INTERNATIONAL COUNCIL FOR RESEARCH AND INNOVATION
IN BUILDING AND CONSTRUCTION
WORKING COMMISSION W18 - TIMBER STRUCTURES**

**MEETING THIRTY-SEVEN
Edinburgh, Scotland, 31 August - 3 September 2004**

LIST OF PARTICIPANTS

AUSTRALIA

K Crews University of Technology, Sydney

CANADA

A Asiz University of New Brunswick, Fredericton
Y H Chui University of New Brunswick, Fredericton
F Lam University of British Columbia, Vancouver
E Karacabeyli Forintek, Vancouver
G Lehoux Royal Military College of Canada, Kingston
P Quennville Royal Military College of Canada, Kingston

DENMARK

C Clorius Technical University of Denmark, Lyngby
H J Larsen Copenhagen
J Munch-Andersen Danish Building and Urban Research, Hørsholm

FINLAND

M Kairi Helsinki University of Technology, Helsinki
A Kevarinmäki VTT Technical Research Centre of Finland, Espoo

FRANCE

F Rouger CTBA, Bordeaux

GERMANY

H J Blaß University of Karlsruhe
J Denzler Technical University of Munich
J Ehlbeck Freiburg
P Fellmoser University of Karlsruhe
S Franke Bauhaus University, Weimar
P Glos Technical University of Munich
R Görlacher University of Karlsruhe
M Grosse Bauhaus University, Weimar
P Hamm Technical University of Munich
K Rautenstrauch Bauhaus University, Weimar

IRELAND

A Harte National University of Ireland, Galway

ITALY

M Ballerini University of Trento
A Ceccotti IVALSA-CNR, Florence

JAPAN

K Komatsu
M Noguchi
M Yasumura

Research Institute for Sustainable Humanosphere, Kyoto University
Kyoto University
Shizuoka University

NORWAY

K Solli

Norwegian Institute of Wood Technology, Blindern

SLOVENIA

B Dujic

Faculty of Civil and Geodetic Engineering, Ljubljana

SWEDEN

H Johnsson
B Källander
B Källsner
J König
E Lukaszewska

Lulea University of Technology
Swedish National Testing and Research Institute, Borås
Trätekt, Stockholm
Trätekt, Stockholm
Lulea University of Technology

SWITZERLAND

A Frangi
J Köhler
R Steiger

ETH Zürich
ETH Zürich
EMPA Wood Laboratory, Dübendorf

THE NETHERLANDS

A Jorissen
J W van der Kuilen

TU Eindhoven
TU Delft

UK

M Ansell
F Bradley
A Bahadori Jahromi
F Bruechert
A Lawrence
A Kermani
A Page
J Porteous
D Ridley-Ellis
Y Robert
P Ross
V Tens
B Zhang
J Zang

University of Bath, Bath
University of Strathclyde
Napier University, Edinburgh
Napier University, Edinburgh
ARUP, London
Napier University, Edinburgh
TRADA Technology Ltd
Napier University, Edinburgh
Centre for Timber Engineering, Edinburgh
TRADA Technology Ltd
TRADA Technology Ltd
Napier University, Edinburgh
Napier University, Edinburgh
Napier University, Edinburgh

USA

D M Carradine
B Yeh
T Williamson

Washington State University
American Plywood Association, Tacoma
American Plywood Association, Tacoma

1. **Chairman's Introduction**
2. **Stresses for Solid Timber**
3. **Timber Joints and Fasteners**
4. **Timber Beams**
5. **Laminated Members**
6. **Structural Stability**
7. **Fire**
8. **Fracture Mechanics**
9. **Serviceability**
10. **Loading Codes**
11. **Joint Committee on Structural Safety**
12. **Any Other Business**
13. **Venue and Program for Next Meeting**
14. **Close**

INTERNATIONAL COUNCIL FOR RESEARCH AND INNOVATION
IN BUILDING AND CONSTRUCTION

WORKING COMMISSION W18 - TIMBER STRUCTURES

MEETING THIRTY SEVEN

EDINBURGH SCOTLAND 31 AUGUST - 3 SEPTEMBER 2004

MINUTES
(F Lam)

1 CHAIRMAN'S INTRODUCTION

Chairman Hans Blass opened the 37th CIB W18 meeting and welcomed the delegates to Edinburgh Scotland.

Professor Robin Mackenzie of Napier University also welcomed the delegates to Edinburgh and introduced the new Centre of Timber Engineering of Napier University.

2 STRESSES FOR SOLID TIMBER

37 - 6 - 1 Tensile Strength of Nordic Birch - K H Solli

Presented by: K H Solli

M Ansell asked whether Weibull statistics were considered. Solli answered that it was not yet done. Y Chui asked about the gauge length and the EPI used. It was clarified that the gauge length was ~2 m following EN 1194 and the EPI was an Isocyanite based adhesive. A Jorissen received clarification that the moisture content of the specimens was 12%. H Blass asked about the cost of birch glulam compared to spruce glulam. Solli responded that the birch was more expensive but this product was intended for special structures.

37 - 6 - 2 Effect of Test Piece Orientation on Characteristic Bending Strength of Structural Timber - P Glos, J K Denzler

Presented by J Denzler

H Blass commented this study used knots as grading parameter and asked if it is possible that other grading parameters can determine the grade; if so, how to determine the tension versus compression edge. One such example is the slope of grain. P Glos explained that knots rather than slope of grain tend to be the dominant failure mode. F Lam commented experience in UBC of larger timber cross sections showed slope of grain failures were also commonly noted. K Crews commented the approach of random orientation is used in Australia because other parameters such as slope of grain can determine the grade. B Källander commented this issue depends on sawing pattern.

J Köhler wondered how to quantify the gain in testing efficiency by having a more accurate method compared to the possible loss of the industry from having lower characteristic values.

37 - 6 - 3 *Strength and Stiffness Behaviour of Beech Laminations for High Strength Glulam* - **P Glos, J K Denzler, P W Linsenmann**

Presented by J Denzler

A Jorissen received clarification that the number 1064 in the graphs referred to the specimen number and constant moisture content was used in the tests.

H J Larsen received clarification that Beech is typically not used as structural member because of durability reason. He also questioned the possible application of this work as EN1194 did not refer to nonlinear stress strain laws. P Glos responded that more hard wood will be available in the near future. This project tried to find ways to use more hardwood from an economical aspect. It is part of a joint project between Munich and Karlsruhe to develop design procedures for introduction to EN 1194. H J Larsen further commented that durability should be examined carefully and EN 1194 is based on fitting of results and not on a theoretical model. He would look forward to seeing a proposal based on modelling.

B Zhang received clarification that displacement control tests were performed. Denzler clarified that the smoothness of the bilinear model was based on fitting to the test results and the glue in the fingerjoint was phenol-resorcinol based.

37 - 6 - 4 *A Review of Existing Standards Related to Calculation of Characteristic Values of Timber* - **F Rouger**

Presented by F Rouger

P Glos commented that the main intention of some of the procedures adopted in EN384 was to address the limited sample size. He would like to see the variation of results with limited sample. Rouger answered that some samples had approximately 126 specimens per cell.

P Glos asked which standard gave higher or lower values. Big sample size with 75% TL will give conservative results; therefore ranking approach was taken. Rouger answered that some more detailed results are available in the paper. In general results showed that the difference in the overall approach was small.

H J Larsen questioned why would estimation of characteristic values based on ranking be better than distribution based parameters; after all, distributions are needed in reliability based procedures.

P Glos answered that we had these discussions 15 or so years ago in CIB meetings: 3-P Weibull gives best fit of results; lognormal can be non-conservative for 5th percentile; normal is conservative for 5th percentile. Ranking was equivalent to Weibull but simple. In term of reliability analysis distribution can also be used.

37 - 6 - 5 *Influence of the Rolling-Shear Modulus on the Strength and Stiffness of Structural Bonded Timber Elements* - **P Fellmoser, H J Blass**

Presented by P Fellmoser

M Ansell received clarification that 3 span-to-depth ratios were used and a hammer was used to vibrate the specimen.

A Jorissen asked whether plywood design rules in EN code was considered. H Blass

responded that the cross ply stiffness would be ignored in the plywood standard leading to poor results; therefore, it cannot be used in this case and justifying the need of this work.

3 TIMBER JOINTS AND FASTENERS

37 - 7 - 1 Development of the "Displaced Volume Model" to Predict Failure for Multiple-Bolt Timber Joints - D M Carradine, J D Dolan, C P Heine

Presented by D Carradine

P Quenneville received clarification that brittle failure was encountered.

H J Larsen was critical of the work and commented that the displacement characteristics were ignored and many more tests would be needed.

A Jorissen discussed the concept of the non-linearity adjustment factors and questioned whether they were used to adjust the load-deformation curve.

Carradine answered that 10 tests were conducted to establish the non-linearity adjustment factors.

M Ansell received confirmation that non-linear fracture mechanics approach was not used.

P Quenneville asked whether the tensile stress perpendicular to grain in the wood on the non loaded side of the bolt was considered. Carradine agreed that this could have an impact.

37 - 7 - 2 Mechanical Models of the Knee Joints with Cross-Lapped Glued Joints and Glued in Steel Rods - M Noguchi, K Komatsu

Presented by M Noguchi

H Blass asked whether a certain slip modulus per glue area was used. An example is the rolling shear modulus found by Karlsruhe of 3 N/mm/mm² of area. It would be interesting to compare the results with this approach. Noguchi responded that it was not done and agreed that it would be interesting.

37 - 7 - 3 Simplification of the Neural Network Model for Predicting the Load-Carrying Capacity of Dowel-Type Connections - A Cointe, F Rouger

Presented by F Rouger

H Blass asked how simple can this be used in a code format. Rouger gave an example.

J Köhler received confirmation that nominal values were predicted and one can get characteristic strength from simulation.

C Clorius asked about the mode of loading. Rouger responded that tension compression and angle to grain loading info were available.

C Clorius asked whether all modes of failure were considered. Rouger responded that only capacity, not mode of failure was considered.

A Jorissen commented that the influence of a1 and a2 should be higher. Rouger responded all Jorissen data was considered in the analysis.

Y H Chui asked about the range of values for the parameters and whether sensitivity analysis was done. Rouger agreed that the range of parameter was an important issue and

restated that the model should not be used for extrapolation.

E Karacabeyli commented that seismic design needs stiffness of connections. Rouger stated that the same approach could be used if connection stiffness data base was available.

37 - 7 - 4 Bolted Wood Connections Loaded Perpendicular-to-Grain- A Proposed Design Approach - M C G Lehoux, J H P Quenneville

Presented by G Lehoux

Y Chui asked how were the coefficients, A_b , B_b and C_b , determined. M Lehoux responded that they came from the stress analysis.

C Clorius asked about the interaction between the bolt and the wood connection. Lehoux answered that contact elements were used for the bolt and they provided the contact between the bottom part of the bolt and the wood.

C Clorius commented that the highly non-linear behaviour of the wood at the point of contact with the bolt was ignored. Lehoux answered that it may be of minor concern. Lehoux further pointed out that only the tension perpendicular-to-grain stresses were considered in the stress integral.

H J Larsen asked which and how many parameters were assumed and which were calibrated and questioned the appropriateness of replacing the fracture mechanics approach with a stress approach for a fracture problem. F Lam commented this is a statistical size effect approach that did not require the assumption of the existence of a crack of a certain size in the domain.

37 - 7 - 5 A New Prediction Formula for the Splitting Strength of Beams Loaded by Dowel Type Connections - M Ballerini

Presented by M Ballerini

H J Larsen pointed out that f_w is the effect of distance between two groups and cannot be greater than 2. Ballerini answered that the value of f_w greater than two fitted to the test data but agreed that it should not exceed two.

37 - 7 - 6 Plug Shear Failure: The Tensile Failure Mode and the Effect of Spacing - H Johnsson

Presented by H Johnsson

A Jorissen commented that $B_{\text{effective}}$ value used in this paper should be referenced to thin steel plates therefore it was off by a factor $2^{0.5}$. Johnsson agreed.

37 - 7 - 7 Block Shear Failure Test with Dowel-Type Connection in Diagonal LVL Structure - M Kairi

Presented by M Kairi

C Clorius questioned why the connections were not loaded to 15 mm per code requirements. Kairi responded that they failed already.

H J Larsen asked why failure mode of 3-in-line was more brittle than the 4-in-line. Kairi clarified that they had the same brittle failure mode.

A Kermani asked whether the quality of the inner laminate of worst quality compared to the face. Kairi responded that in the prototype the quality of the face and core veneer were similar.

A Jorissen received clarifications of the number of fasteners in line and the embedment strength of the LVL would be available in a previous 2001 CIB paper. Kairi also clarified the difference between block and plug shear.

37 - 7 - 8 Glued-in Steel Rods: A Design Approach for Axially Loaded Single Rods Set Parallel to the Grain - R Steiger, E Gehri, R Widmann

Presented by R Steiger

H J Larsen commented that these results are for a specific system and generalization must consider other tests. Steiger agreed and will try to combine the data from other sources.

M Ansell questioned why the perpendicular to grain shear strength was higher than that of parallel to grain shear strength and wondered whether this could be caused by oversized holes with thick glue line that gave higher shear strength due to the penetration of glue into the specimen. Steiger explained that these results are for a specific system and the issue of oversized hole was already considered.

J W van de Kuilen asked about the influence of the reinforcements in the pile foundation test set up. Steiger agreed that it could be an important issue.

C Clorius asked whether there was any quantification of influence of reduced cross section of the glue-in-rod. Steiger responded that this information can be found in referenced material.

Steiger invited the delegate to submit articles to a special timber issue in the RILEM Journal of Material of Structures.

37 - 7 - 9 Glued in Rods in Load Bearing Timber Structures - Status regarding European Standards for Test Procedures - B Källander

Presented by B Källander

C Clorius discussed with Källander about PRF and issues related to its ability to bond to steel.

H J Larsen commented about the basis for standardization through the CIB W18 and suggested that more test data should be developed as the CIB W18 group should focus on the evaluation of the test data.

H Blass commented screws can be effectively used in place of the glue-in-rods.

37 - 7 - 10 French Data Concerning Glued-in Rods - C Faye, L Le Magorou, P Morlier, J Surleau

Presented by F Rouger

H Blass asked about the glass transition temperature of the glue T_g . Rouger answered that it was about 50 C and stated that some adhesive with higher T_g can be found.

H Blass asked whether the rods were protruding through the timber in the FEM calculations. Rouger answered that even if the rod were completely covered the same conclusion would be obtained.

P Glos questioned the validity of the temperature model because the model predicted that it took 5 hr for the surface of the wood to reach ambient temperature. It seemed much too slow from his experience. Rouger answered that this is a convection problem and the temperature of the glue line was the main issue. Rouger further clarified that the timber cover to the glue line was 4 cm.

M Ansell commented that room temperature cured epoxy tended to have low T_g and epoxy with high T_g needed to be heated up.

E Karacabeyli asked about the difference between the two DOL models and commented that the DOL factor for the 10 years loading is 0.5. Rouger answered that the difference of threshold level may be the issue.

P Glos noted that there was no moisture effect and suggested that if wood failure was observed then moisture effect should be present. J W van de Kuilen commented that the stress level was related to the short term strength at the respective moisture conditions and therefore masking the moisture effect.

B Källander commented that T_g is more a theoretical measure and one would not know the real characteristic based on T_g . Also high T_g adhesives are available but creep may be an issue with these adhesives. Rouger responded that the short term specimen test results provided the relation between T_g and properties.

J Köhler commented that the stress ratio used in DOL study depended on the equal rank assumption therefore small sample size can lead to errors.

M Ansell commented on the DSC analysis and T_g and that glueline thickness might have been an issue.

P Glos received clarification that the sample size was 10 specimens per series.

37 - 7 - 11 Enhancement of Dowel-Type Fasteners by Glued Connectors - C O Clorius, A Højman

Presented by C Clorius

Clorius provided clarification that the embedment strength of the steel plate was $\frac{1}{2}$ of the ultimate strength according to Euro Code 3, the fasteners were dowels not bolts, and there were no slippage problems.

37 - 7 - 12 Review of Probability Data for Timber Connections With Dowel-Type Fasteners - A J M Leijten, J Köhler, A Jorissen

Presented by J Köhler

F Lam commented that the beta values might be lower if individual data sets were considered.

K Crews commented that single fasteners as dowels were considered and group behaviour should also be studied.

37 - 7 - 13 *Behaviour of Fasteners and Glued-in Rods Produced From Stainless Steel -*
A Kevarinmäki

Presented by A Kevarinmäki

H J Larsen commented that the test results for specialized products such as self tapping screws are needed. Also ordinary screws might also be problematic and the Eurocode is based on 20 year old data.

J König responded that amendment for Eurocode can be considered and a ready proposal should be prepared.

H Blass commented that the Hanssen formula might not be suitable to be generalized for all proprietary products as issues such as connector diameter need to be carefully studied.

J König responded that limitations can be put in the formula.

J Köhler commented that comparisons with code values should be done in a consistent manner; i.e., characteristic values should not be compared to nominal values.

37 - 7 - 14 *Dowel joints in Engineered Wood Products: Assessment of simple fracture mechanics models -* **M Snow, I Smith, A Asiz**

Presented by A Asiz

A Jorissen questioned the test configuration of 88mm by 300 mm (height by length) because the load path for a different configuration can be very different. Asiz responded that the test configuration was ASTM based. Asiz also acknowledged that Eqn 4 was theoretical not empirical.

37 - 7 - 15 *Numerical Modelling of Timber and Connection Elements Used in Timber-Concrete-Composite Constructions -* **M Grosse, K Rautenstrauch**

Presented by M Grosse

J W van de Kuilen asked about the connect element and the friction value. Grosse responded that surface elements were used and the friction value was approximately 0.5 to 0.6.

J Köhler asked about the material properties. Grosse responded that the material properties were based on literature and there were 16 values.

J Zhang asked about load reversal and Grosse clarified that short term experiments were considered without load reversal.

4 TIMBER BEAMS

37 - 10 - 1 *Design of Rim Boards for Use with I-Joists Framing Systems -* **B Yeh, T G Williamson**

Presented by T Williamson

E Karacabeyli asked about the durability of this product. Williamson responded that this is a building envelope issue and not a structural product issue for this standard.

H Blass asked whether there was an OSB production standard in North America. Williamson clarified that OSB production standard in North America is available.

General discussions followed on what type of data is available, EN 300, and perforation would be okay within recommended range.

Williamson extended an invitation to the 9th WCTE 2006 in Oregon.

5 LAMINATED MEMBERS

37 - 12 - 1 Development of Structural LVL from Tropical Wood and Evaluation of Their Performance for the Structural Components of Wooden Houses. Part-1. Application of Tropical LVL to a Roof Truss - K Komatsu, Y Idris, S Yuwasdiki, B Subiyakto, A Firmanti

Presented by K Komatsu

H Blass noted that only the bottom chord of the truss was loaded and commented that as roof truss upper chord loading would be more appropriate. Komatsu agreed and explained that constraints of test equipment limited the load applications to the lower chord only.

P Glos asked for more information on the LVL material used including thickness and bending strength. Komatsu responded the veneer thickness was 1.2 mm and bending and in-plane shear tests of the LVL were also performed but the data is available in different paper.

P Ross questioned why press metal plates not used and as a triangulated truss system why was a less sophisticated approach not used. Komatsu answered that the structural design method was of secondary interest as this is a new material under development; therefore, non-linear FEM was used to get more accurate information.

R Steiger asked whether FEM was used because of geometric nonlinearity. Komatsu responded that its use was academic reason and if the material was already available in the market less sophisticated method would be chosen.

37 - 12 - 2 Reinforcement of LVL Beams With Bonded-in Plates and Rods - Effect of Placement of Steel and FRP Reinforcements on Beam Strength and Stiffness - P Alam, M P Ansell, D Smedley

Presented by M Ansell

F Lam, H J Larsen and Ansell discussed the practicality of these reinforced beams including coast and possible change of failure mode. It was agreed that these beams can be effectively used in repair of structures. 90% of this type of product will be used in repair work.

M Ballerini commented an Italian company has a commercial product available intended for repair and restoration project.

P Glos commented why is there a need for so much repair.

Y H Chui asked about the method of stress strain curve of the adhesive. Ansell replied that it was obtained from experimental tensile and compressive tests on small specimens.

6 STRUCTURAL STABILITY

37 - 15 - 1 Estimating 3D Behavior of Conventional Timber Structures With Shear Walls by Pseudodynamic Tests - M Yasumura, M Uesugi, L Davenne

Presented by M Yasumura

P Quenneville asked whether more tests on different aspect ratios be conducted. Yasumura answered no as the model can be used to predict the response of such systems.

E Karacabeyli observed that the diaphragm without blocking had no nails on the perimeter. Yasumura responded that he wanted to study the more extreme cases for comparison therefore a very flexible system was chosen.

A discussion took place on the assumption of stiffness of the diaphragm between F Lam, A Cecotti and Yasumura. It was agreed that the assumed values gave good results. As the response of pseudo dynamic tests is dependent on the assumed stiffness, refinements to the model could be taken.

37 - 15 - 2 Testing of Racking Behavior of Massive Wooden Wall Panels - B Dujič, J Pucelj, R Žarnić

Presented by B Dujič

C Clorius commented that new anchorage system is available.

A Cecotti commented that AC24 protocol for steel connection and European document and ISO standards for joints are available.

P Quenneville asked with such a rigid system whether tests should focus on the connection only. Dujič responded that the diagonal deformations of the wall were also measured. P Quenneville suggested that as the rigidity of the wall is now known further information on design should be based on connection behaviour.

37 - 15 - 3 Influence of Framing Joints on Plastic Capacity of Partially Anchored Wood-Framed Shear Walls - B Källsner, U A Girhammar

Presented by B Källsner

B Dujič and Källsner discussed the concept of fully vertical shear capacity.

R Steiger commented that in the lower bound plasticity method equilibrium must be fulfilled; however, he felt that the boundary condition should also be considered. Källsner answered that in plastic method deformations were not considered as only the strength of the system was considered.

R Steiger commented that the elastic solution should consider deformation. Källsner agreed.

B J Yeh asked if it is possible that the vertical load contributed to the friction of the test setup. Källsner answered one cannot use friction forces in this case.

H Blass commented that it does not matter whether one anchored the tensile stud or put the vertical load onto the tensile stud. E Karacabeyli further commented on the difference between the fully anchored and partially held down cases with respect to the contribution of vertical load. He further explained that similar approach was developed in the Canadian code. Källsner agreed that it was done independently. H Blass commented that one of the objectives of this work is to obtain a unified approach in the European code.

37 - 15 - 4 Bracing of Timber Members in Compression - J Munch-Andersen

Presented by J Munch-Andersen

P Quenneville asked whether the bracing members acting only in compression. Andersen answered no as both tension and compression forces can be considered in the bracing members.

37 - 15 - 5 Acceptance Criteria for the Use of Structural Insulated Panels in High Risk Seismic Areas - B Yeh, T D Skaggs, T G Williamson Z A Martin

Presented by B Yeh

F Lam commented that the shake table experience of some of these walls was brittle.

H Blass asked how large were the sip. Yeh answered that they can be up to 8x24 ft or 16x24 ft but 8x8 ft wall sizes were tested.

H Blass commented it needs the presence of splines otherwise they will not work.

B Dujč commented displacement control was used and this system could behave differently after peak load under load control and some of the brittle failures mention by F Lam may be observed. B J Yeh answered that he would like to take a look at the over strength factor.

Y H Chui asked whether dynamic test is considered in the acceptance criteria. B J Yeh answered that this acceptance criteria is in effect today. Length of wall tested is 8 ft and brittle walls may be caught by the ductility criteria.

Discussion took place between F Lam and Yeh on the issue of vertical load going through the sheathing because of possible lacking of vertical studs. B J Yeh answered that this acceptance criteria cover a wide range of loading conditions including vertical and out of plane loading. The issue of cost of testing versus more complicated acceptance criteria was also discussed.

P Glos commented that the paper missed information on the structure of the product tested. Yeh responded that the work takes the code limitation today and demonstrates one has the simulated dynamic behaviour. A Cecotti commented in Eurocode 8 such walls would not be banned but allowed.

37 - 15 - 6 Predicting Load Paths in Shearwalls - Hongyong Mi, Ying-Hei Chui, I Smith, M Mohammad

Presented by Y Chui

P Quenneville received confirmation that all shear walls in model house were connected the same way.

J M Andersen asked why 4 load cells were needed. Chui answered 4 load cells were needed to catch the up-down action observed.

P Ross asked about the conclusion that the capacity of vertically sheathed wall and the wall with opening behaved similarly. Chui responded that the wall with opening had extra framing around the opening.

H Blass asked about the deformation of the horizontal sheathed shearwalls. Chui responded that the information is available in the paper.

H Blass asked about the gaps between panels in the horizontal sheathed shearwalls. Chui

responded that such gaps were maintained per Canadian practice.

E Karacabeyli commented that the conclusions should be limited to the specimens tested and should not be generalized e.g. conclusion on the shearwall with opening.

BJ Yeh received clarification that the horizontal shear wall was unblocked and method of loading used.

T Williamson discussed with Chui the issue of hold down in the unblocked shearwall.

K Crews asked why 3 D load cells were used for a 2 D specimen with in plane loading. Chui answered that out of plane loading will be performed in further studies.

7 FIRE

37 - 16 - 1 *Effective Values of Thermal Properties of Timber and Thermal Actions During the Decay Phase of Natural Fires* - **J König**

Presented by J König

B Källander suggested that the possibility of large volume of moisture in the wood escaping in form of water vapor cooled the medium. And he asked about the issue of heat of evaporation. König responded that the water diffused into the wood rather than escaping from the wood. Experimental results are available and some theoretical work is available. The issue of heat of evaporation is considered in the heat capacity.

37 - 16 - 2 *Fire Tests on Timber Connections With Dowel-type Fasteners* - **A Frangi, A Mischler**

Presented by A Frangi

C Clorius asked how was failure defined and whether deformation criterion was used.

Frangi answered that every failure mode can be observed. It is very difficult to check all of the mode behaviour of the serious damage. Main importance is the loss of cross section.

P Glos asked what additional information was gained from this study as results agreed with previous studies in Germany. Frangi explained that before these tests one did not know the 30 minute rating and now we know the performance of these connections subject to fire more accurately.

P Glos asked whether the German results were referenced. Frangi answered that these tests were done before the German tests but this is the 1st chance that the results were presented and that they were aware of the German results.

Y H Chui asked about the test set up. Frangi answered that the standard ISO test set up was used with the exception that they have to enclose the specimen and they measured the temperature on the surface and made sure that it is standard fire exposure.

J König commented that this work is the most comprehensive set of connection fire test that he has seen. They have the complete set of code reference tests. Test referenced in the Eurocode had only few reference tests so these are weaknesses. Eurocode seemed to be too conservative for this type of dowel connection. He is glad that the improvement due to fire protection agreed well with the Eurocode expression.

A Jorissen expressed surprises at the results of the cover specimen. Frangi explained that in some cases the cover started to fall down quickly leading to variation in the results.

P Glos commented that this would depend on the density of the cover. Frangi answered

that more or less the same boards were used and it was just the randomness in the experiment.

R Steiger asked why a reduced load level was used. Frangi responded that 0.3 is the assumed load ratio and other higher levels were reference from the Eurocode.

8 FRACTURE MECHANICS

37 - 19 - 1 Determination of Fracture Mechanics Parameters for Wood with the Help of Close Range Photogrammetry - S Franke, B Franke, K Rautenstrauch

Presented by S Franke

A Asiz received clarification on the resistance curves.

B Yeh asked about the costs. S Franke responded that the costs of the equipment are less than 10000 Euro and the costs per test is 3 Euro.

9 SERVICEABILITY

37 - 20 - 1 A New Design Method to Control Vibrations Induced by Foot Steps in Timber Floors - Lin J Hu, Y H Chui

Presented by Y H Chui

F Rouger commented that the upper part of the regression curve has as many accepted as unacceptable floors. Chui answered that this is a common issue with the acceptance criteria for serviceability studies.

P Glos commented that different countries have different acceptance criteria and this work only refers to acceptance based on Canadian surveys and experience.

T Williamson asked whether floor joist types were considered. Chui answered yes and the information is available in the paper.

B J Yeh asked how was the influence of dead weight and partition walls considered in the survey and the acceptance criteria. Chui answered that it is a sensitive issue and a large number of new construction were also considered in the survey. Furniture loads were not considered in the design proposal.

37 - 20 - 2 Serviceability Limit States of Wooden Footbridges. Vibrations Caused by Pedestrians - P Hamm

Presented by P Hamm

H Blass noted high damping factor was observed for simple beam. Hamm answered that concrete topped mechanical connections did not seem to have a large role in the damping. Hamm agreed that more tests should be done to check whether dowels or screws would make a difference.

C Clorius received clarification of framework bridge and truss beam bridge.

K Crews received confirmation that the dampers were installed under the bridge.

Y H Chui asked whether there would be an influence of the exciter used in the test to determine damping. He found in floor vibration test that the human exciter can make a big difference. Hamm answered that the mass of the exciter was too low compared to the bridge to make a difference.

F Lam asked whether ambient vibration techniques have been considered. Hamm answered that the exciter is the more direct method.

A Cecotti asked whether the 0.3% damping for the cable found by measurement as it seemed to low. Hamm answered that they were measured results and they were surprisingly low.

P Ross shared his experience with a bridge design by his firm that has a fn of 1.5 Hz and low damping. This bridge would be okay with few people. The assumption for a lot of people was that the randomness of the movement from the people could make the bridge response still acceptable. They found out that this assumption was wrong and dampers were added to remediate.

A discussion took place between point-wise applications of the exciter versus exciting the bridge over the whole span. Hamm found a moving excitation versus fixed excitation factor of 0.75 which is dependent on the damping and the bridge length.

K Crews commented that this issue of position of excitation would depend on the mode of excitation.

10 LOADING CODES

37 - 101 -1 Action Combination Processing for the Eurocodes Basis of Software to Assist the Engineer - Y Robert, A V Page, R Thépaut, C J Mettem

Presented by Y Robert

J Köhler asked whether the loads are taken random or from loading codes. Robert answered that they are taken from codes.

Zhang asked if only U.L.S is considered. Robert clarified that also S.L.S. is taken into account.

11 JOINT COMMITTEE ON STRUCTURAL SAFETY

37 - 104 - 1 Proposal for a Probabilistic Model Code for Design of Timber Structures - J Köhler, H Faber

Presented by J Köhler

R Steiger asked whether the Probabilistic Code is used as a design code or for calibration. Köhler answered that it supports the engineers in their decision as well as it is a basis for decision in code drafting.

P Glos stated that the probabilistic design code is important but that he cannot see any progress in the last 20 years. There are data available to check the model and find out which accuracy of information is really needed. The existing system for designing structures is good.

H Blass answered that off-shore structures are designed according to the probabilistic design methods.

J Köhler added that it is also important to compare the different building materials.

K Crews added that there is also an application for bridges.

12 ANY OTHER BUSINESS

J König proposed to define again criteria for the goal of the CIB-W 18 group. The problem is that in the last meetings there were too many papers, many participants and restrictions of the numbers of pages of the papers. He suggested accepting papers only if they are in direct relation to standards of codes.

There was a general support to that and H Blass said that for the next call for papers the criteria for accepting papers are mentioned and that he will refuse abstracts or papers which do not fulfil the criteria. Everybody agreed on that.

13 VENUE AND PROGRAMME FOR NEXT MEETING

Next meeting will be held in Karlsruhe, Germany from 29. - 31. August 2005 (three days).

For the meeting 2006 there is an invitation by A Ceccotti to Florence (Italy) and for 2007 there is an invitation by B Dujic to Slovenia.

14 CLOSE

Professor Robin Mackenzie of Napier University thanked all delegates for joining the meeting at Napier University.

H Blass thanked the host for successfully hosting the 37th CIB W18 Meeting and he thanked the participants for attending the meeting.

**15. List of CIB-W18 Papers,
Edinburgh, Scotland, UK 2004**

List of CIB-W18 Papers, Edinburgh, Scotland 2004

- 37 - 6 - 1 Tensile Strength of Nordic Birch - **K H Solli**
- 37 - 6 - 2 Effect of Test Piece Orientation on Characteristic Bending Strength of Structural Timber - **P Glos, J K Denzler**
- 37 - 6 - 3 Strength and Stiffness Behaviour of Beech Laminations for High Strength Glulam - **P Glos, J K Denzler, P W Linsenmann**
- 37 - 6 - 4 A Review of Existing Standards Related to Calculation of Characteristic Values of Timber - **F Rouger**
- 37 - 6 - 5 Influence of the Rolling-Shear Modulus on the Strength and Stiffness of Structural Bonded Timber Elements - **P Fellmoser, H J Blass**
- 37 - 7 - 1 Development of the "Displaced Volume Model" to Predict Failure for Multiple-Bolt Timber Joints - **D M Carradine, J D Dolan, C P Heine**
- 37 - 7 - 2 Mechanical Models of the Knee Joints with Cross-Lapped Glued Joints and Glued in Steel Rods - **M Noguchi, K Komatsu**
- 37 - 7 - 3 Simplification of the Neural Network Model for Predicting the Load-Carrying Capacity of Dowel-Type Connections - **A Cointe, F Rouger**
- 37 - 7 - 4 Bolted Wood Connections Loaded Perpendicular-to-Grain- A Proposed Design Approach - **M C G Lehoux, J H P Quenneville**
- 37 - 7 - 5 A New Prediction Formula for the Splitting Strength of Beams Loaded by Dowel Type Connections - **M Ballerini**
- 37 - 7 - 6 Plug Shear Failure: The Tensile Failure Mode and the Effect of Spacing - **H Johnsson**
- 37 - 7 - 7 Block Shear Failure Test with Dowel-Type Connection in Diagonal LVL Structure - **M Kairi**
- 37 - 7 - 8 Glued-in Steel Rods: A Design Approach for Axially Loaded Single Rods Set Parallel to the Grain - **R Steiger, E Gehri, R Widmann**
- 37 - 7 - 9 Glued in Rods in Load Bearing Timber Structures - Status regarding European Standards for Test Procedures - **B Källander**
- 37 - 7 - 10 French Data Concerning Glued-in Rods - **C Faye, L Le Magorou, P Morlier, J Surleau**
- 37 - 7 - 11 Enhancement of Dowel-Type Fasteners by Glued Connectors - **C O Clorius, A Højman**
- 37 - 7 - 12 Review of Probability Data for Timber Connections with Dowel-Type Fasteners - **A J M Leijten, J Köhler, A Jorissen**
- 37 - 7 - 13 Behaviour of Fasteners and Glued-in Rods Produced From Stainless Steel - **A Kevarinmäki**
- 37 - 7 - 14 Dowel joints in Engineered Wood Products: Assessment of Simple Fracture Mechanics Models - **M Snow, I Smith, A Asiz**

- 37 - 7 - 15 Numerical Modelling of Timber and Connection Elements Used in Timber-Concrete-Composite Constructions - **M Grosse, K Rautenstrauch**
- 37 - 10 - 1 Design of Rim Boards for Use with I-Joists Framing Systems - **B Yeh, T G Williamson**
- 37 - 12 - 1 Development of Structural LVL from Tropical Wood and Evaluation of Their Performance for the Structural Components of Wooden Houses. Part-1. Application of Tropical LVL to a Roof Truss - **K Komatsu, Y Idris, S Yuwasdiki, B Subiyakto, A Firmanti**
- 37 - 12 - 2 Reinforcement of LVL Beams With Bonded-in Plates and Rods - Effect of Placement of Steel and FRP Reinforcements on Beam Strength and Stiffness - **P Alam, M P Ansell, D Smedley**
- 37 - 15 - 1 Estimating 3D Behavior of Conventional Timber Structures with Shear Walls by Pseudodynamic Tests - **M Yasumura, M Uesugi, L Davenne**
- 37 - 15 - 2 Testing of Racking Behavior of Massive Wooden Wall Panels - **B Dujič, J Pucelj, R Žarnić**
- 37 - 15 - 3 Influence of Framing Joints on Plastic Capacity of Partially Anchored Wood-Framed Shear Walls - **B Källsner, U A Girhammar**
- 37 - 15 - 4 Bracing of Timber Members in Compression - **J Munch-Andersen**
- 37 - 15 - 5 Acceptance Criteria for the Use of Structural Insulated Panels in High Risk Seismic Areas - **B Yeh, T D Skaggs, T G Williamson Z A Martin**
- 37 - 15 - 6 Predicting Load Paths in Shearwalls - **Hongyong Mi, Ying-Hei Chui, I Smith, M Mohammad**
- 37 - 16 - 1 Effective Values of Thermal Properties of Timber and Thermal Actions During the Decay Phase of Natural Fires - **J König**
- 37 - 16 - 2 Fire Tests on Timber Connections with Dowel-type Fasteners - **A Frangi, A Mischler**
- 37 - 19 - 1 Determination of Fracture Mechanics Parameters for Wood with the Help of Close Range Photogrammetry - **S Franke, B Franke, K Rautenstrauch**
- 37 - 20 - 1 A New Design Method to Control Vibrations Induced by Foot Steps in Timber Floors - **Lin J Hu, Y H Chui**
- 37 - 20 - 2 Serviceability Limit States of Wooden Footbridges. Vibrations Caused by Pedestrians - **P Hamm**
- 37 - 101 -1 Action Combination Processing for the Eurocodes Basis of Software to Assist the Engineer - **Y Robert, A V Page, R Thépaut, C J Mettem**
- 37 - 104 - 1 Proposal for a Probabilistic Model Code for Design of Timber Structures - **J Köhler, H Faber**

16. Current List of CIB-W18(A) Papers

CURRENT LIST OF CIB-W18(A) PAPERS

Technical papers presented to CIB-W18(A) are identified by a code CIB-W18(A)/a-b-c, where:

- a denotes the meeting at which the paper was presented.
Meetings are classified in chronological order:
- 1 Princes Risborough, England; March 1973
 - 2 Copenhagen, Denmark; October 1973
 - 3 Delft, Netherlands; June 1974
 - 4 Paris, France; February 1975
 - 5 Karlsruhe, Federal Republic of Germany; October 1975
 - 6 Aalborg, Denmark; June 1976
 - 7 Stockholm, Sweden; February/March 1977
 - 8 Brussels, Belgium; October 1977
 - 9 Perth, Scotland; June 1978
 - 10 Vancouver, Canada; August 1978
 - 11 Vienna, Austria; March 1979
 - 12 Bordeaux, France; October 1979
 - 13 Otaniemi, Finland; June 1980
 - 14 Warsaw, Poland; May 1981
 - 15 Karlsruhe, Federal Republic of Germany; June 1982
 - 16 Lillehammer, Norway; May/June 1983
 - 17 Rapperswil, Switzerland; May 1984
 - 18 Beit Oren, Israel; June 1985
 - 19 Florence, Italy; September 1986
 - 20 Dublin, Ireland; September 1987
 - 21 Parksville, Canada; September 1988
 - 22 Berlin, German Democratic Republic; September 1989
 - 23 Lisbon, Portugal; September 1990
 - 24 Oxford, United Kingdom; September 1991
 - 25 Åhus, Sweden; August 1992
 - 26 Athens, USA; August 1993
 - 27 Sydney, Australia; July 1994
 - 28 Copenhagen, Denmark; April 1995
 - 29 Bordeaux, France; August 1996
 - 30 Vancouver, Canada; August 1997
 - 31 Savonlinna, Finland; August 1998
 - 32 Graz, Austria; August 1999
 - 33 Delft, The Netherlands; August 2000
 - 34 Venice, Italy; August 2001
 - 35 Kyoto, Japan; September 2002
 - 36 Colorado, USA; August 2003
 - 37 Edinburgh, Scotland; August 2004

b denotes the subject:

- 1 Limit State Design
- 2 Timber Columns
- 3 Symbols
- 4 Plywood
- 5 Stress Grading
- 6 Stresses for Solid Timber
- 7 Timber Joints and Fasteners
- 8 Load Sharing
- 9 Duration of Load
- 10 Timber Beams
- 11 Environmental Conditions
- 12 Laminated Members
- 13 Particle and Fibre Building Boards
- 14 Trussed Rafters
- 15 Structural Stability
- 16 Fire
- 17 Statistics and Data Analysis
- 18 Glued Joints
- 19 Fracture Mechanics
- 20 Serviceability
- 21 Test Methods
- 100 CIB Timber Code
- 101 Loading Codes
- 102 Structural Design Codes
- 103 International Standards Organisation
- 104 Joint Committee on Structural Safety
- 105 CIB Programme, Policy and Meetings
- 106 International Union of Forestry Research Organisations

c is simply a number given to the papers in the order in which they appear:

Example: CIB-W18/4-102-5 refers to paper 5 on subject 102 presented at the fourth meeting of W18.

Listed below, by subjects, are all papers that have to date been presented to W18. When appropriate some papers are listed under more than one subject heading.

LIMIT STATE DESIGN

- 1-1-1 Limit State Design - H J Larsen
- 1-1-2 The Use of Partial Safety Factors in the New Norwegian Design Code for Timber Structures - O Brynildsen
- 1-1-3 Swedish Code Revision Concerning Timber Structures - B Noren
- 1-1-4 Working Stresses Report to British Standards Institution Committee BLC/17/2
- 6-1-1 On the Application of the Uncertainty Theoretical Methods for the Definition of the Fundamental Concepts of Structural Safety - K Skov and O Ditlevsen
- 11-1-1 Safety Design of Timber Structures - H J Larsen
- 18-1-1 Notes on the Development of a UK Limit States Design Code for Timber - A R Fewell and C B Pierce
- 18-1-2 Eurocode 5, Timber Structures - H J Larsen
- 19-1-1 Duration of Load Effects and Reliability Based Design (Single Member) - R O Foschi and Z C Yao
- 21-102-1 Research Activities Towards a New GDR Timber Design Code Based on Limit States Design - W Rug and M Badstube
- 22-1-1 Reliability-Theoretical Investigation into Timber Components Proposal for a Supplement of the Design Concept - M Badstube, W Rug and R Plessow
- 23-1-1 Some Remarks about the Safety of Timber Structures - J Kuipers
- 23-1-2 Reliability of Wood Structural Elements: A Probabilistic Method to Eurocode 5 Calibration - F Rouger, N Lheritier, P Racher and M Fogli
- 31-1-1 A Limit States Design Approach to Timber Framed Walls - C J Mettem, R Bainbridge and J A Gordon
- 32 -1-1 Determination of Partial Coefficients and Modification Factors- H J Larsen, S Svensson and S Thelandersson
- 32 -1-2 Design by Testing of Structural Timber Components - V Enjily and L Whale
- 33-1-1 Aspects on Reliability Calibration of Safety Factors for Timber Structures – S Svensson and S Thelandersson
- 33-1-2 Sensitivity studies on the reliability of timber structures – A Ranta-Maunus, M Fonselius, J Kurkela and T Toratti

TIMBER COLUMNS

- 2-2-1 The Design of Solid Timber Columns - H J Larsen
- 3-2-1 The Design of Built-Up Timber Columns - H J Larsen
- 4-2-1 Tests with Centrally Loaded Timber Columns - H J Larsen and S S Pedersen
- 4-2-2 Lateral-Torsional Buckling of Eccentrically Loaded Timber Columns- B Johansson
- 5-9-1 Strength of a Wood Column in Combined Compression and Bending with Respect to Creep - B Källsner and B Norén
- 5-100-1 Design of Solid Timber Columns (First Draft) - H J Larsen
- 6-100-1 Comments on Document 5-100-1, Design of Solid Timber Columns - H J Larsen and E Theilgaard
- 6-2-1 Lattice Columns - H J Larsen
- 6-2-2 A Mathematical Basis for Design Aids for Timber Columns - H J Burgess
- 6-2-3 Comparison of Larsen and Perry Formulas for Solid Timber Columns- H J Burgess

- 7-2-1 Lateral Bracing of Timber Struts - J A Simon
- 8-15-1 Laterally Loaded Timber Columns: Tests and Theory - H J Larsen
- 17-2-1 Model for Timber Strength under Axial Load and Moment - T Poutanen
- 18-2-1 Column Design Methods for Timber Engineering - A H Buchanan, K C Johns, B Madsen
- 19-2-1 Creep Buckling Strength of Timber Beams and Columns - R H Leicester
- 19-12-2 Strength Model for Glulam Columns - H J Blaß
- 20-2-1 Lateral Buckling Theory for Rectangular Section Deep Beam-Columns- H J Burgess
- 20-2-2 Design of Timber Columns - H J Blaß
- 21-2-1 Format for Buckling Strength - R H Leicester
- 21-2-2 Beam-Column Formulae for Design Codes - R H Leicester
- 21-15-1 Rectangular Section Deep Beam - Columns with Continuous Lateral Restraint - H J Burgess
- 21-15-2 Buckling Modes and Permissible Axial Loads for Continuously Braced Columns - H J Burgess
- 21-15-3 Simple Approaches for Column Bracing Calculations - H J Burgess
- 21-15-4 Calculations for Discrete Column Restraints - H J Burgess
- 22-2-1 Buckling and Reliability Checking of Timber Columns - S Huang, P M Yu and J Y Hong
- 22-2-2 Proposal for the Design of Compressed Timber Members by Adopting the Second-Order Stress Theory - P Kaiser
- 30-2-1 Beam-Column Formula for Specific Truss Applications - W Lau, F Lam and J D Barrett
- 31-2-1 Deformation and Stability of Columns of Viscoelastic Material Wood - P Becker and K Rautenstrauch
- 34-2-1 Long-Term Experiments with Columns: Results and Possible Consequences on Column Design – W Moorkamp, W Schelling, P Becker, K Rautenstrauch
- 34-2-2 Proposal for Compressive Member Design Based on Long-Term Simulation Studies – P Becker, K Rautenstrauch
- 35-2-1 Computer Simulations on the Reliability of Timber Columns Regarding Hygrothermal Effects- R Hartnack, K-U Schober, K Rautenstrauch
- 36 - 2 - 1 The Reliability of Timber Columns Based on Stochastical Principles - K Rautenstrauch, R Hartnack

SYMBOLS

- 3-3-1 Symbols for Structural Timber Design - J Kuipers and B Norén
- 4-3-1 Symbols for Timber Structure Design - J Kuipers and B Norén
- 28-3-1 Symbols for Timber and Wood-Based Materials - J Kuipers and B Noren
- 1 Symbols for Use in Structural Timber Design

PLYWOOD

- 2-4-1 The Presentation of Structural Design Data for Plywood - L G Booth
- 3-4-1 Standard Methods of Testing for the Determination of Mechanical Properties of Plywood - J Kuipers

- 3-4-2 Bending Strength and Stiffness of Multiple Species Plywood - C K A Stieda
- 4-4-4 Standard Methods of Testing for the Determination of Mechanical Properties of Plywood - Council of Forest Industries, B.C.
- 5-4-1 The Determination of Design Stresses for Plywood in the Revision of CP 112 - L G Booth
- 5-4-2 Veneer Plywood for Construction - Quality Specifications - ISO/TC 139. Plywood, Working Group 6
- 6-4-1 The Determination of the Mechanical Properties of Plywood Containing Defects - L G Booth
- 6-4-2 Comparison of the Size and Type of Specimen and Type of Test on Plywood Bending Strength and Stiffness - C R Wilson and P Eng
- 6-4-3 Buckling Strength of Plywood: Results of Tests and Recommendations for Calculations - J Kuipers and H Ploos van Amstel
- 7-4-1 Methods of Test for the Determination of Mechanical Properties of Plywood - L G Booth, J Kuipers, B Norén, C R Wilson
- 7-4-2 Comments Received on Paper 7-4-1
- 7-4-3 The Effect of Rate of Testing Speed on the Ultimate Tensile Stress of Plywood - C R Wilson and A V Parasin
- 7-4-4 Comparison of the Effect of Specimen Size on the Flexural Properties of Plywood Using the Pure Moment Test - C R Wilson and A V Parasin
- 8-4-1 Sampling Plywood and the Evaluation of Test Results - B Norén
- 9-4-1 Shear and Torsional Rigidity of Plywood - H J Larsen
- 9-4-2 The Evaluation of Test Data on the Strength Properties of Plywood - L G Booth
- 9-4-3 The Sampling of Plywood and the Derivation of Strength Values (Second Draft) - B Norén
- 9-4-4 On the Use of the CIB/RILEM Plywood Plate Twisting Test: a progress report - L G Booth
- 10-4-1 Buckling Strength of Plywood - J Dekker, J Kuipers and H Ploos van Amstel
- 11-4-1 Analysis of Plywood Stressed Skin Panels with Rigid or Semi-Rigid Connections- I Smith
- 11-4-2 A Comparison of Plywood Modulus of Rigidity Determined by the ASTM and RILEM CIB/3-TT Test Methods - C R Wilson and A V Parasin
- 11-4-3 Sampling of Plywood for Testing Strength - B Norén
- 12-4-1 Procedures for Analysis of Plywood Test Data and Determination of Characteristic Values Suitable for Code Presentation - C R Wilson
- 14-4-1 An Introduction to Performance Standards for Wood-base Panel Products - D H Brown
- 14-4-2 Proposal for Presenting Data on the Properties of Structural Panels - T Schmidt
- 16-4-1 Planar Shear Capacity of Plywood in Bending - C K A Stieda
- 17-4-1 Determination of Panel Shear Strength and Panel Shear Modulus of Beech-Plywood in Structural Sizes - J Ehlbeck and F Colling
- 17-4-2 Ultimate Strength of Plywood Webs - R H Leicester and L Pham
- 20-4-1 Considerations of Reliability - Based Design for Structural Composite Products - M R O'Halloran, J A Johnson, E G Elias and T P Cunningham
- 21-4-1 Modelling for Prediction of Strength of Veneer Having Knots - Y Hirashima

- 22-4-1 Scientific Research into Plywood and Plywood Building Constructions the Results and Findings of which are Incorporated into Construction Standard Specifications of the USSR - I M Guskov
- 22-4-2 Evaluation of Characteristic values for Wood-Based Sheet Materials - E G Elias
- 24-4-1 APA Structural-Use Design Values: An Update to Panel Design Capacities - A L Kuchar, E G Elias, B Yeh and M R O'Halloran

STRESS GRADING

- 1-5-1 Quality Specifications for Sawn Timber and Precision Timber - Norwegian Standard NS 3080
- 1-5-2 Specification for Timber Grades for Structural Use - British Standard BS 4978
- 4-5-1 Draft Proposal for an International Standard for Stress Grading Coniferous Sawn Softwood - ECE Timber Committee
- 16-5-1 Grading Errors in Practice - B Thunell
- 16-5-2 On the Effect of Measurement Errors when Grading Structural Timber- L Nordberg and B Thunell
- 19-5-1 Stress-Grading by ECE Standards of Italian-Grown Douglas-Fir Dimension Lumber from Young Thinnings - L Uzielli
- 19-5-2 Structural Softwood from Afforestation Regions in Western Norway - R Lackner
- 21-5-1 Non-Destructive Test by Frequency of Full Size Timber for Grading - T Nakai
- 22-5-1 Fundamental Vibration Frequency as a Parameter for Grading Sawn Timber - T Nakai, T Tanaka and H Nagao
- 24-5-1 Influence of Stress Grading System on Length Effect Factors for Lumber Loaded in Compression - A Campos and I Smith
- 26-5-1 Structural Properties of French Grown Timber According to Various Grading Methods - F Rouger, C De Lafond and A El Quadrani
- 28-5-1 Grading Methods for Structural Timber - Principles for Approval - S Ohlsson
- 28-5-2 Relationship of Moduli of Elasticity in Tension and in Bending of Solid Timber - N Burger and P Glos
- 29-5-1 The Effect of Edge Knots on the Strength of SPF MSR Lumber - T Courchene, F Lam and J D Barrett
- 29-5-2 Determination of Moment Configuration Factors using Grading Machine Readings - T D G Canisius and T Isaksson
- 31-5-1 Influence of Varying Growth Characteristics on Stiffness Grading of Structural Timber - S Ormarsson, H Petersson, O Dahlblom and K Persson
- 31-5-2 A Comparison of In-Grade Test Procedures - R H Leicester, H Breitingner and H Fordham
- 32-5-1 Actual Possibilities of the Machine Grading of Timber - K Frühwald and A Bernasconi
- 32-5-2 Detection of Severe Timber Defects by Machine Grading - A Bernasconi, L Boström and B Schacht
- 34-5-1 Influence of Proof Loading on the Reliability of Members – F Lam, S Abayakoon, S Svensson, C Gyamfi
- 36-5-1 Settings for Strength Grading Machines – Evaluation of the Procedure according to prEN 14081, part 2 - C Bengtsson, M Fonselius
- 36-5-2 A Probabilistic Approach to Cost Optimal Timber Grading - J Köhler, M H Faber
- 36-7-11 Reliability of Timber Structures, Theory and Dowel-Type Connection Failures - A Ranta-Maunus, A Kevarinmäki

STRESSES FOR SOLID TIMBER

- 4-6-1 Derivation of Grade Stresses for Timber in the UK - W T Curry
- 5-6-1 Standard Methods of Test for Determining some Physical and Mechanical Properties of Timber in Structural Sizes - W T Curry
- 5-6-2 The Description of Timber Strength Data - J R Tory
- 5-6-3 Stresses for EC1 and EC2 Stress Grades - J R Tory
- 6-6-1 Standard Methods of Test for the Determination of some Physical and Mechanical Properties of Timber in Structural Sizes (third draft) - W T Curry
- 7-6-1 Strength and Long-term Behaviour of Lumber and Glued Laminated Timber under Torsion Loads - K Möhler
- 9-6-1 Classification of Structural Timber - H J Larsen
- 9-6-2 Code Rules for Tension Perpendicular to Grain - H J Larsen
- 9-6-3 Tension at an Angle to the Grain - K Möhler
- 9-6-4 Consideration of Combined Stresses for Lumber and Glued Laminated Timber - K Möhler
- 11-6-1 Evaluation of Lumber Properties in the United States - W L Galligan and J H Haskell
- 11-6-2 Stresses Perpendicular to Grain - K Möhler
- 11-6-3 Consideration of Combined Stresses for Lumber and Glued Laminated Timber (addition to Paper CIB-W18/9-6-4) - K Möhler
- 12-6-1 Strength Classifications for Timber Engineering Codes - R H Leicester and W G Keating
- 12-6-2 Strength Classes for British Standard BS 5268 - J R Tory
- 13-6-1 Strength Classes for the CIB Code - J R Tory
- 13-6-2 Consideration of Size Effects and Longitudinal Shear Strength for Uncracked Beams - R O Foschi and J D Barrett
- 13-6-3 Consideration of Shear Strength on End-Cracked Beams - J D Barrett and R O Foschi
- 15-6-1 Characteristic Strength Values for the ECE Standard for Timber - J G Sunley
- 16-6-1 Size Factors for Timber Bending and Tension Stresses - A R Fewell
- 16-6-2 Strength Classes for International Codes - A R Fewell and J G Sunley
- 17-6-1 The Determination of Grade Stresses from Characteristic Stresses for BS 5268: Part 2 - A R Fewell
- 17-6-2 The Determination of Softwood Strength Properties for Grades, Strength Classes and Laminated Timber for BS 5268: Part 2 - A R Fewell
- 18-6-1 Comment on Papers: 18-6-2 and 18-6-3 - R H Leicester
- 18-6-2 Configuration Factors for the Bending Strength of Timber - R H Leicester
- 18-6-3 Notes on Sampling Factors for Characteristic Values - R H Leicester
- 18-6-4 Size Effects in Timber Explained by a Modified Weakest Link Theory- B Madsen and A H Buchanan
- 18-6-5 Placement and Selection of Growth Defects in Test Specimens - H Riberholt
- 18-6-6 Partial Safety-Coefficients for the Load-Carrying Capacity of Timber Structures - B Norén and J-0 Nylander
- 19-6-1 Effect of Age and/or Load on Timber Strength - J Kuipers
- 19-6-2 Confidence in Estimates of Characteristic Values - R H Leicester

- 19-6-3 Fracture Toughness of Wood - Mode I - K Wright and M Fonselius
- 19-6-4 Fracture Toughness of Pine - Mode II - K Wright
- 19-6-5 Drying Stresses in Round Timber - A Ranta-Maunus
- 19-6-6 A Dynamic Method for Determining Elastic Properties of Wood - R Görlacher
- 20-6-1 A Comparative Investigation of the Engineering Properties of "Whitewoods" Imported to Israel from Various Origins - U Korin
- 20-6-2 Effects of Yield Class, Tree Section, Forest and Size on Strength of Home Grown Sitka Spruce - V Picardo
- 20-6-3 Determination of Shear Strength and Strength Perpendicular to Grain - H J Larsen
- 21-6-1 Draft Australian Standard: Methods for Evaluation of Strength and Stiffness of Graded Timber - R H Leicester
- 21-6-2 The Determination of Characteristic Strength Values for Stress Grades of Structural Timber. Part 1 - A R Fewell and P Glos
- 21-6-3 Shear Strength in Bending of Timber - U Korin
- 22-6-1 Size Effects and Property Relationships for Canadian 2-inch Dimension Lumber - J D Barrett and H Griffin
- 22-6-2 Moisture Content Adjustements for In-Grade Data - J D Barrett and W Lau
- 22-6-3 A Discussion of Lumber Property Relationships in Eurocode 5 - D W Green and D E Kretschmann
- 22-6-4 Effect of Wood Preservatives on the Strength Properties of Wood - F Ronai
- 23-6-1 Timber in Compression Perpendicular to Grain - U Korin
- 24-6-1 Discussion of the Failure Criterion for Combined Bending and Compression - T A C M van der Put
- 24-6-3 Effect of Within Member Variability on Bending Strength of Structural Timber - I Czmocho, S Thelandersson and H J Larsen
- 24-6-4 Protection of Structural Timber Against Fungal Attack Requirements and Testing- K Jaworska, M Rylko and W Nozynski
- 24-6-5 Derivation of the Characteristic Bending Strength of Solid Timber According to CEN-Document prEN 384 - A J M Leijten
- 25-6-1 Moment Configuration Factors for Simple Beams- T D G Canisius
- 25-6-3 Bearing Capacity of Timber - U Korin
- 25-6-4 On Design Criteria for Tension Perpendicular to Grain - H Petersson
- 25-6-5 Size Effects in Visually Graded Softwood Structural Lumber - J D Barrett, F Lam and W Lau
- 26-6-1 Discussion and Proposal of a General Failure Criterion for Wood - T A C M van der Put
- 27-6-1 Development of the "Critical Bearing": Design Clause in CSA-086.1 - C Lum and E Karacabeyli
- 27-6-2 Size Effects in Timber: Novelty Never Ends - F Rouger and T Fewell
- 27-6-3 Comparison of Full-Size Sugi (*Cryptomeria japonica* D.Don) Structural Performance in Bending of Round Timber, Two Surfaces Sawn Timber and Square Sawn Timber - T Nakai, H Nagao and T Tanaka
- 28-6-1 Shear Strength of Canadian Softwood Structural Lumber - F Lam, H Yee and J D Barrett
- 28-6-2 Shear Strength of Douglas Fir Timbers - B Madsen

- 28-6-3 On the Influence of the Loading Head Profiles on Determined Bending Strength - L Muszyński and R Szukala
- 28-6-4 Effect of Test Standard, Length and Load Configuration on Bending Strength of Structural Timber- T Isaksson and S Thelandersson
- 28-6-5 Grading Machine Readings and their Use in the Calculation of Moment Configuration Factors - T Canisius, T Isaksson and S Thelandersson
- 28-6-6 End Conditions for Tension Testing of Solid Timber Perpendicular to Grain - T Canisius
- 29-6-1 Effect of Size on Tensile Strength of Timber - N Burger and P Glos
- 29-6-2 Equivalence of In-Grade Testing Standards - R H Leicester, H O Breitingner and H F Fordham
- 30-6-1 Strength Relationships in Structural Timber Subjected to Bending and Tension - N Burger and P Glos
- 30-6-2 Characteristic Design Stresses in Tension for Radiata Pine Grown in Canterbury - A Tsehaye, J C F Walker and A H Buchanan
- 30-6-3 Timber as a Natural Composite: Explanation of Some Peculiarities in the Mechanical Behaviour - E Gehri
- 31-6-1 Length and Moment Configuration Factors - T Isaksson
- 31-6-2 Tensile Strength Perpendicular to Grain According to EN 1193 - H J Blaß and M Schmid
- 31-6-3 Strength of Small Diameter Round Timber - A Ranta-Maunus, U Saarelainen and H Boren
- 31-6-4 Compression Strength Perpendicular to Grain of Structural Timber and Glulam - L Damkilde, P Hoffmeyer and T N Pedersen
- 31-6-5 Bearing Strength of Timber Beams - R H Leicester, H Fordham and H Breitingner
- 32-6-1 Development of High-Resistance Glued Robinia Products and an Attempt to Assign Such Products to the European System of Strength Classes - G Schickhofer and B Obermayr
- 32-6-2 Length and Load Configuration Effects in the Code Format - T Isaksson
- 32-6-3 Length Effect on the Tensile Strength of Truss Chord Members - F Lam
- 32-6-4 Tensile Strength Perpendicular to Grain of Glued Laminated Timber - H J Blaß and M Schmid
- 32-6-5 On the Reliability-based Strength Adjustment Factors for Timber Design - T D G Canisius
- 34-6-1 Material Strength Properties for Canadian Species Used in Japanese Post and Beam Construction - J D Barrett, F Lam, S Nakajima
- 35-6-1 Evaluation of Different Size Effect Models for Tension Perpendicular to Grain Design - S Aicher, G Dill-Langer
- 35-6-2 Tensile Strength of Glulam Perpendicular to Grain - Effects of Moisture Gradients - J Jönsson, S Thelandersson
- 36-6-1 Characteristic Shear Strength Values Based on Tests According to EN 1193 - P Glos, J Denzler
- 37-6-1 Tensile Strength of Nordic Birch - K H Solli
- 37-6-2 Effect of Test Piece Orientation on Characteristic Bending Strength of Structural Timber - P Glos, J K Denzler
- 37-6-3 Strength and Stiffness Behaviour of Beech Laminations for High Strength Glulam - P Glos, J K Denzler, P W Linsenmann

- 37-6-4 A Review of Existing Standards Related to Calculation of Characteristic Values of Timber - F Rouger
- 37-6-5 Influence of the Rolling-Shear Modulus on the Strength and Stiffness of Structural Bonded Timber Elements - P Fellmoser, H J Blass

TIMBER JOINTS AND FASTENERS

- 1-7-1 Mechanical Fasteners and Fastenings in Timber Structures - E G Stern
- 4-7-1 Proposal for a Basic Test Method for the Evaluation of Structural Timber Joints with Mechanical Fasteners and Connectors - RILEM 3TT Committee
- 4-7-2 Test Methods for Wood Fasteners - K Möhler
- 5-7-1 Influence of Loading Procedure on Strength and Slip-Behaviour in Testing Timber Joints - K Möhler
- 5-7-2 Recommendations for Testing Methods for Joints with Mechanical Fasteners and Connectors in Load-Bearing Timber Structures - RILEM 3 TT Committee
- 5-7-3 CIB-Recommendations for the Evaluation of Results of Tests on Joints with Mechanical Fasteners and Connectors used in Load-Bearing Timber Structures - J Kuipers
- 6-7-1 Recommendations for Testing Methods for Joints with Mechanical Fasteners and Connectors in Load-Bearing Timber Structures (seventh draft) - RILEM 3 TT Committee
- 6-7-2 Proposal for Testing Integral Nail Plates as Timber Joints - K Möhler
- 6-7-3 Rules for Evaluation of Values of Strength and Deformation from Test Results - Mechanical Timber Joints - M Johansen, J Kuipers, B Norén
- 6-7-4 Comments to Rules for Testing Timber Joints and Derivation of Characteristic Values for Rigidity and Strength - B Norén
- 7-7-1 Testing of Integral Nail Plates as Timber Joints - K Möhler
- 7-7-2 Long Duration Tests on Timber Joints - J Kuipers
- 7-7-3 Tests with Mechanically Jointed Beams with a Varying Spacing of Fasteners - K Möhler
- 7-100-1 CIB-Timber Code Chapter 5.3 Mechanical Fasteners;CIB-Timber Standard 06 and 07 - H J Larsen
- 9-7-1 Design of Truss Plate Joints - F J Keenan
- 9-7-2 Staples - K Möhler
- 11-7-1 A Draft Proposal for International Standard: ISO Document ISO/TC 165N 38E
- 12-7-1 Load-Carrying Capacity and Deformation Characteristics of Nailed Joints - J Ehlbeck
- 12-7-2 Design of Bolted Joints - H J Larsen
- 12-7-3 Design of Joints with Nail Plates - B Norén
- 13-7-1 Polish Standard BN-80/7159-04: Parts 00-01-02-03-04-05.
"Structures from Wood and Wood-based Materials. Methods of Test and Strength Criteria for Joints with Mechanical Fasteners"
- 13-7-2 Investigation of the Effect of Number of Nails in a Joint on its Load Carrying Ability - W Nozynski
- 13-7-3 International Acceptance of Manufacture, Marking and Control of Finger-jointed Structural Timber - B Norén
- 13-7-4 Design of Joints with Nail Plates - Calculation of Slip - B Norén
- 13-7-5 Design of Joints with Nail Plates - The Heel Joint - B Källsner

- 13-7-6 Nail Deflection Data for Design - H J Burgess
- 13-7-7 Test on Bolted Joints - P Vermeijden
- 13-7-8 Comments to paper CIB-W18/12-7-3 "Design of Joints with Nail Plates"-
B Norén
- 13-7-9 Strength of Finger Joints - H J Larsen
- 13-100-4 CIB Structural Timber Design Code. Proposal for Section 6.1.5 Nail Plates -
N I Bovim
- 14-7-1 Design of Joints with Nail Plates (second edition) - B Norén
- 14-7-2 Method of Testing Nails in Wood (second draft, August 1980) - B Norén
- 14-7-3 Load-Slip Relationship of Nailed Joints - J Ehlbeck and H J Larsen
- 14-7-4 Wood Failure in Joints with Nail Plates - B Norén
- 14-7-5 The Effect of Support Eccentricity on the Design of W- and WW-Trussed with Nail Plate
Connectors - B Källsner
- 14-7-6 Derivation of the Allowable Load in Case of Nail Plate Joints Perpendicular to Grain - K
Möhler
- 14-7-7 Comments on CIB-W18/14-7-1 - T A C M van der Put
- 15-7-1 Final Recommendation TT-1A: Testing Methods for Joints with Mechanical Fasteners in
Load-Bearing Timber Structures. Annex A Punched Metal Plate Fasteners - Joint
Committee RILEM/CIB-3TT
- 16-7-1 Load Carrying Capacity of Dowels - E Gehri
- 16-7-2 Bolted Timber Joints: A Literature Survey - N Harding
- 16-7-3 Bolted Timber Joints: Practical Aspects of Construction and Design; a Survey -
N Harding
- 16-7-4 Bolted Timber Joints: Draft Experimental Work Plan - Building Research Association of
New Zealand
- 17-7-1 Mechanical Properties of Nails and their Influence on Mechanical Properties of Nailed
Timber Joints Subjected to Lateral Loads - I Smith, L R J Whale,
C Anderson and L Held
- 17-7-2 Notes on the Effective Number of Dowels and Nails in Timber Joints - G Steck
- 18-7-1 Model Specification for Driven Fasteners for Assembly of Pallets and Related Structures
- E G Stern and W B Wallin
- 18-7-2 The Influence of the Orientation of Mechanical Joints on their Mechanical Properties - I
Smith and L R J Whale
- 18-7-3 Influence of Number of Rows of Fasteners or Connectors upon the Ultimate Capacity of
Axially Loaded Timber Joints - I Smith and G Steck
- 18-7-4 A Detailed Testing Method for Nailplate Joints - J Kangas
- 18-7-5 Principles for Design Values of Nailplates in Finland - J Kangas
- 18-7-6 The Strength of Nailplates - N I Bovim and E Aasheim
- 19-7-1 Behaviour of Nailed and Bolted Joints under Short-Term Lateral Load - Conclusions
from Some Recent Research - L R J Whale, I Smith and B O Hilson
- 19-7-2 Glued Bolts in Glulam - H Riberholt
- 19-7-3 Effectiveness of Multiple Fastener Joints According to National Codes and Eurocode 5
(Draft) - G Steck
- 19-7-4 The Prediction of the Long-Term Load Carrying Capacity of Joints in Wood Structures -
Y M Ivanov and Y Y Slavic
- 19-7-5 Slip in Joints under Long-Term Loading - T Feldborg and M Johansen

- 19-7-6 The Derivation of Design Clauses for Nailed and Bolted Joints in Eurocode 5 - L R J Whale and I Smith
- 19-7-7 Design of Joints with Nail Plates - Principles - B Norén
- 19-7-8 Shear Tests for Nail Plates - B Norén
- 19-7-9 Advances in Technology of Joints for Laminated Timber - Analyses of the Structural Behaviour - M Piazza and G Turrini
- 19-15-1 Connections Deformability in Timber Structures: A Theoretical Evaluation of its Influence on Seismic Effects - A Ceccotti and A Vignoli
- 20-7-1 Design of Nailed and Bolted Joints-Proposals for the Revision of Existing Formulae in Draft Eurocode 5 and the CIB Code - L R J Whale, I Smith and H J Larsen
- 20-7-2 Slip in Joints under Long Term Loading - T Feldborg and M Johansen
- 20-7-3 Ultimate Properties of Bolted Joints in Glued-Laminated Timber - M Yasumura, T Murota and H Sakai
- 20-7-4 Modelling the Load-Deformation Behaviour of Connections with Pin-Type Fasteners under Combined Moment, Thrust and Shear Forces - I Smith
- 21-7-1 Nails under Long-Term Withdrawal Loading - T Feldborg and M Johansen
- 21-7-2 Glued Bolts in Glulam-Proposals for CIB Code - H Riberholt
- 21-7-3 Nail Plate Joint Behaviour under Shear Loading - T Poutanen
- 21-7-4 Design of Joints with Laterally Loaded Dowels. Proposals for Improving the Design Rules in the CIB Code and the Draft Eurocode 5 - J Ehlbeck and H Werner
- 21-7-5 Axially Loaded Nails: Proposals for a Supplement to the CIB Code - J Ehlbeck and W Siebert
- 22-7-1 End Grain Connections with Laterally Loaded Steel Bolts A draft proposal for design rules in the CIB Code - J Ehlbeck and M Gerold
- 22-7-2 Determination of Perpendicular-to-Grain Tensile Stresses in Joints with Dowel-Type Fasteners - A draft proposal for design rules - J Ehlbeck, R Görlacher and H Werner
- 22-7-3 Design of Double-Shear Joints with Non-Metallic Dowels A proposal for a supplement of the design concept - J Ehlbeck and O Eberhart
- 22-7-4 The Effect of Load on Strength of Timber Joints at high Working Load Level - A J M Leijten
- 22-7-5 Plasticity Requirements for Portal Frame Corners - R Gunnewijk and A J M Leijten
- 22-7-6 Background Information on Design of Glulam Rivet Connections in CSA/CAN3-086.1-M89 - A proposal for a supplement of the design concept - E Karacabeyli and D P Janssens
- 22-7-7 Mechanical Properties of Joints in Glued-Laminated Beams under Reversed Cyclic Loading - M Yasumura
- 22-7-8 Strength of Glued Lap Timber Joints - P Glos and H Horstmann
- 22-7-9 Toothed Rings Type Bistyp 075 at the Joints of Fir Wood - J Kerste
- 22-7-10 Calculation of Joints and Fastenings as Compared with the International State - K Zimmer and K Lissner
- 22-7-11 Joints on Glued-in Steel Bars Present Relatively New and Progressive Solution in Terms of Timber Structure Design - G N Zubarev, F A Boitemirov and V M Golovina
- 22-7-12 The Development of Design Codes for Timber Structures made of Compositive Bars with Plate Joints based on Cylindrical Nails - Y V Piskunov

- 22-7-13 Designing of Glued Wood Structures Joints on Glued-in Bars - S B Turkovsky
- 23-7-1 Proposal for a Design Code for Nail Plates - E Aasheim and K H Solli
- 23-7-2 Load Distribution in Nailed Joints - H J Blass
- 24-7-1 Theoretical and Experimental Tension and Shear Capacity of Nail Plate Connections - B Källsner and J Kangas
- 24-7-2 Testing Method and Determination of Basic Working Loads for Timber Joints with Mechanical Fasteners - Y Hirashima and F Kamiya
- 24-7-3 Anchorage Capacity of Nail Plate - J Kangas
- 25-7-2 Softwood and Hardwood Embedding Strength for Dowel type Fasteners - J Ehlbeck and H Werner
- 25-7-4 A Guide for Application of Quality Indexes for Driven Fasteners Used in Connections in Wood Structures - E G Stern
- 25-7-5 35 Years of Experience with Certain Types of Connectors and Connector Plates Used for the Assembly of Wood Structures and their Components- E G Stern
- 25-7-6 Characteristic Strength of Split-ring and Shear-plate Connections - H J Blass, J Ehlbeck and M Schlager
- 25-7-7 Characteristic Strength of Tooth-plate Connector Joints - H J Blass, J Ehlbeck and M Schlager
- 25-7-8 Extending Yield Theory to Screw Connections - T E McLain
- 25-7-9 Determination of k_{def} for Nailed Joints - J W G van de Kuilen
- 25-7-10 Characteristic Strength of UK Timber Connectors - A V Page and C J Mettem
- 25-7-11 Multiple-fastener Dowel-type Joints, a Selected Review of Research and Codes - C J Mettem and A V Page
- 25-7-12 Load Distributions in Multiple-fastener Bolted Joints in European Whitewood Glulam, with Steel Side Plates - C J Mettem and A V Page
- 26-7-1 Proposed Test Method for Dynamic Properties of Connections Assembled with Mechanical Fasteners - J D Dolan
- 26-7-2 Validatory Tests and Proposed Design Formulae for the Load-Carrying Capacity of Toothed-Plate Connected Joints - C J Mettem, A V Page and G Davis
- 26-7-3 Definitions of Terms and Multi-Language Terminology Pertaining to Metal Connector Plates - E G Stern
- 26-7-4 Design of Joints Based on in V-Shape Glued-in Rods - J Kangas
- 26-7-5 Tests on Timber Concrete Composite Structural Elements (TCCs) - A U Meierhofer
- 27-7-1 Glulam Arch Bridge and Design of its Moment-Resisting Joints - K Komatsu and S Usuku
- 27-7-2 Characteristic Load - Carrying Capacity of Joints with Dowel - type Fasteners in Regard to the System Properties - H Werner
- 27-7-3 Steel Failure Design in Truss Plate Joints - T Poutanen
- 28-7-1 Expanded Tube Joint in Locally DP Reinforced Timber - A J M Leijten, P Ragupathy and K S Viridi
- 28-7-2 A Strength and Stiffness Model for the Expanded Tube Joint - A J M Leijten
- 28-7-3 Load-carrying Capacity of Steel-to Timber Joints with Annular Ring Shank Nails. A Comparison with the EC5 Design Method - R Görlacher
- 28-7-4 Dynamic Effects on Metal-Plate Connected Wood Truss Joints - S Kent, R Gupta and T Miller

- 28-7-5 Failure of the Timber Bolted Joints Subjected to Lateral Load Perpendicular to Grain - M Yasumura and L Daudeville
- 28-7-6 Design Procedure for Locally Reinforced Joints with Dowel-type Fasteners - H Werner
- 28-7-7 Variability and Effects of Moisture Content on the Withdrawal Characteristics for Lumber as Opposed to Clear Wood - J D Dolan and J W Stelmokas
- 28-7-8 Nail Plate Capacity in Joint Line - A Kevarinmäki and J Kangas
- 28-7-9 Axial Strength of Glued-In Bolts - Calculation Model Based on Non-Linear Fracture Mechanics - A Preliminary Study - C J Johansson, E Serrano, P J Gustafsson and B Enquist
- 28-7-10 Cyclic Lateral Dowel Connection Tests for seismic and Wind Evaluation - J D Dolan
- 29-7-1 A Simple Method for Lateral Load-Carrying Capacity of Dowel-Type Fasteners - J Kangas and J Kurkela
- 29-7-2 Nail Plate Joint Behaviour at Low Versus High Load Level - T Poutanen
- 29-7-3 The Moment Resistance of Tee and Butt - Joint Nail Plate Test Specimens - A Comparison with Current Design Methods - A Reffold, L R J Whale and B S Choo
- 29-7-4 A Critical Review of the Moment Rotation Test Method Proposed in prEN 1075 - M Bettison, B S Choo and L R J Whale
- 29-7-5 Explanation of the Translation and Rotation Behaviour of Prestressed Moment Timber Joints - A J M Leijten
- 29-7-6 Design of Joints and Frame Corners using Dowel-Type Fasteners - E Gehri
- 29-7-7 Quasi-Static Reversed-Cyclic Testing of Nailed Joints - E Karacabeyli and A Ceccotti
- 29-7-8 Failure of Bolted Joints Loaded Parallel to the Grain: Experiment and Simulation - L Davenne, L Daudeville and M Yasumura
- 30-7-1 Flexural Behaviour of GLT Beams End-Jointed by Glued-in Hardwood Dowels - K Komatsu, A Koizumi, J Jensen, T Sasaki and Y Iijima
- 30-7-2 Modelling of the Block Tearing Failure in Nailed Steel-to-Timber Joints - J Kangas, K Aalto and A Kevarinmäki
- 30-7-3 Cyclic Testing of Joints with Dowels and Slotted-in Steel Plates - E Aasheim
- 30-7-4 A Steel-to-Timber Dowelled Joint of High Performance in Combination with a High Strength Wood Composite (Parallam) - E Gehri
- 30-7-5 Multiple Fastener Timber Connections with Dowel Type Fasteners - A Jorissen
- 30-7-6 Influence of Ductility on Load-Carrying Capacity of Joints with Dowel-Type Fasteners - A Mischler
- 31-7-1 Mechanical Properties of Dowel Type Joints under Reversed Cyclic Lateral Loading - M Yasumura
- 31-7-2 Design of Joints with Laterally Loaded Dowels - A Mischler
- 31-7-3 Flexural Behaviour of Glulam Beams Edge-Jointed by Lagscrews with Steel Splice Plates - K Komatsu
- 31-7-4 Design on Timber Capacity in Nailed Steel-to-Timber Joints - J Kangas and J Vesa
- 31-7-5 Timber Contact in Chord Splices of Nail Plate Structures - A Kevarinmäki
- 31-7-6 The Fastener Yield Strength in Bending - A Jorissen and H J Blaß

- 31-7-7 A Proposal for Simplification of Johansen's Formulae, Dealing With the Design of Dowelled-Type Fasteners - F Rouger
- 31-7-8 Simplified Design of Connections with Dowel-type fasteners - H J Blaß and J Ehlbeck
- 32-7-1 Behaviour of Wood-Steel-Wood Bolted Glulam Connections - M Mohammad and J H P Quenneville
- 32-7-2 A new set of experimental tests on beams loaded perpendicular-to-grain by dowel-type joints- M Ballerini
- 32-7-3 Design and Analysis of Bolted Timber Joints under Lateral Force Perpendicular to Grain - M Yasumura and L Daudeville
- 32-7-4 Predicting Capacities of Joints with Laterally Loaded Nails - I Smith and P Quenneville
- 32-7-5 Strength Reduction Rules for Multiple Fastener Joints - A Mischler and E Gehri
- 32-7-6 The Stiffness of Multiple Bolted Connections - A Jorissen
- 32-7-7 Concentric Loading Tests on Girder Truss Components - T N Reynolds, A Reffold, V Enjily and L Whale
- 32-7-8 Dowel Type Connections with Slotted-In Steel Plates - M U Pedersen, C O Clorius, L Damkilde, P Hoffmeyer and L Esklidsen
- 32-7-9 Creep of Nail Plate Reinforced Bolt Joints - J Vesa and A Kevarinmäki
- 32-7-10 The Behaviour of Timber Joints with Ring Connectors - E Gehri and A Mischler
- 32-7-11 Non-Metallic, Adhesiveless Joints for Timber Structures - R D Drake, M P Ansell, C J Mettem and R Bainbridge
- 32-7-12 Effect of Spacing and Edge Distance on the Axial Strength of Glued-in Rods - H J Blaß and B Laskewitz
- 32-7-13 Evaluation of Material Combinations for Bonded in Rods to Achieve Improved Timber Connections - C J Mettem, R J Bainbridge, K Harvey, M P Ansell, J G Broughton and A R Hutchinson
- 33-7-1 Determination of Yield Strength and Ultimate Strength of Dowel-Type Timber Joints – M Yasumura and K Sawata
- 33-7-2 Lateral Shear Capacity of Nailed Joints – U Korin
- 33-7-3 Height-Adjustable Connector for Composite Beams – Y V Piskunov and E G Stern
- 33-7-4 Engineering Ductility Assessment for a Nailed Slotted-In Steel Connection in Glulam– L Stehn and H Johansson
- 33-7-5 Effective Bending Capacity of Dowel-Type Fasteners - H J Blaß, A Bienhaus and V Krämer
- 33-7-6 Load-Carrying Capacity of Joints with Dowel-Type Fasteners and Interlayers - H J Blaß and B Laskewitz
- 33-7-7 Evaluation of Perpendicular to Grain Failure of Beams caused by Concentrated Loads of Joints – A J M Leijten and T A C M van der Put
- 33-7-8 Test Methods for Glued-In Rods for Timber Structures – C Bengtsson and C J Johansson
- 33-7-9 Stiffness Analysis of Nail Plates – P Ellegaard
- 33-7-10 Capacity, Fire Resistance and Gluing Pattern of the Rods in V-Connections – J Kangas
- 33-7-11 Bonded-In Pultrusions for Moment-Resisting Timber Connections – K Harvey, M P Ansell, C J Mettem, R J Bainbridge and N Alexandre
- 33-7-12 Fatigue Performance of Bonded-In Rods in Glulam, Using Three Adhesive Types - R J Bainbridge, K Harvey, C J Mettem and M P Ansell
- 34-7-1 Splitting Strength of Beams Loaded by Connections Perpendicular to Grain, Model Validation – A J M Leijten, A Jorissen

- 34-7-2 Numerical LEFM analyses for the evaluation of failure loads of beams loaded perpendicular-to-grain by single-dowel connections – M Ballerini, R Bezzi
- 34-7-3 Dowel joints loaded perpendicular to grain - H J Larsen, P J Gustafsson
- 34-7-4 Quality Control of Connections based on in V-shape glued-in Steel Rods – J Kangas, A Kevarinmäki
- 34-7-5 Testing Connector Types for Laminated-Timber-Concrete Composite Elements – M Grosse, S Lehmann, K Rautenstrauch
- 34-7-6 Behaviour of Axially Loaded Glued-in Rods - Requirements and Resistance, Especially for Spruce Timber Perpendicular to the Grain Direction – A Bernasconi
- 34-7-7 Embedding characteristics on fibre reinforcement and densified timber joints - P Haller, J Wehsener, T Birk
- 34-7-8 GIROD – Glued-in Rods for Timber Structures – C Bengtsson, C-J Johansson
- 34-7-9 Criteria for Damage and Failure of Dowel-Type Joints Subjected to Force Perpendicular to the Grain – M Yasumura
- 34-7-10 Interaction Between Splitting and Block Shear Failure of Joints – A J M Leijten, A Jorissen, J Kuipers
- 34-7-11 Limit states design of dowel-fastener joints – Placement of modification factors and partial factors, and calculation of variability in resistance – I Smith, G Foliente
- 34-7-12 Design and Modelling of Knee Joints - J Nielsen, P Ellegaard
- 34-7-13 Timber-Steel Shot Fired Nail Connections at Ultimate Limit States - R J Bainbridge, P Larsen, C J Mettem, P Alam, M P Ansell
- 35-7-1 New Estimating Method of Bolted Cross-lapped Joints with Timber Side Members - M Noguchi, K Komatsu
- 35-7-2 Analysis on Multiple Lag Screwed Timber Joints with Timber Side Members - K Komatsu, S Takino, M Nakatani, H Tateishi
- 35-7-3 Joints with Inclined Screws - A Kevarinmäki
- 35-7-4 Joints with Inclined Screws - I Bejtka, H J Blaß
- 35-7-5 Effect of distances, Spacing and Number of Dowels in a Row on the Load Carrying Capacity of Connections with Dowels failing by Splitting - M Schmid, R Frasson, H J Blaß
- 35-7-6 Effect of Row Spacing on the Capacity of Bolted Timber Connections Loaded Perpendicular-to-grain - P Quenneville, M Kasim
- 35-7-7 Splitting Strength of Beams Loaded by Connections, Model Comparison - A J M Leijten
- 35-7-8 Load-Carrying Capacity of Perpendicular to the Grain Loaded Timber Joints with Multiple Fasteners - O Borth, K U Schober, K Rautenstrauch
- 35-7-9 Determination of fracture parameter for dowel-type joints loaded perpendicular to wooden grain and its application - M Yasumura
- 35-7-10 Analysis and Design of Modified Attic Trusses with Punched Metal Plate Fasteners - P Ellegaard
- 35-7-11 Joint Properties of Plybamboo Sheets in Prefabricated Housing - G E Gonzalez
- 35-7-12 Fiber-Reinforced Beam-to-Column Connections for Seismic Applications - B Kasal, A Heiduschke, P Haller
- 36-7-1 Shear Tests in Timber-LWAC with Screw-Type Connections - L Jorge, H Cruz, S Lopes
- 36-7-2 Plug Shear Failure in Nailed Timber Connections: Experimental Studies - H Johnsson
- 36-7-3 Nail-Laminated Timber Elements in Natural Surface-Composite with Mineral Bound Layer - S Lehmann, K Rautenstrauch

- 36-7-4 Mechanical Properties of Timber-Concrete Joints Made With Steel Dowels - A Dias, J W G van de Kuilen, H Cruz
- 36-7-5 Comparison of Hysteresis Responses of Different Sheathing to Framing Joints - B Dujič, R Zarnić
- 36-7-6 Evaluation and Estimation of the Performance of the Nail Joints and Shear Walls under Dry/Humid Cyclic Climate - S Nakajima
- 36-7-7 Beams Transversally Loaded by Dowel-Type Joints: Influence on Splitting Strength of Beam Thickness and Dowel Size - M Ballerini, A Giovanella
- 36-7-8 Splitting Strength of Beams Loaded by Connections - J L Jensen
- 36-7-9 A Tensile Fracture Model for Joints with Rods or Dowels loaded Perpendicular-to-Grain - J L Jensen, P J Gustafsson, H J Larsen
- 36-7-10 A Numerical Model to Simulate the Load-Displacement Time-History of Multiple-Bolt Connections Subjected to Various Loadings - C P Heine, J D Dolan
- 36-7-11 Reliability of Timber Structures, Theory and Dowel-Type Connection Failures - A Ranta-Maunus, A Kevarinmäki
- 37-7-1 Development of the "Displaced Volume Model" to Predict Failure for Multiple-Bolt Timber Joints - D M Carradine, J D Dolan, C P Heine
- 37-7-2 Mechanical Models of the Knee Joints with Cross-Lapped Glued Joints and Glued in Steel Rods - M Noguchi, K Komatsu
- 37-7-3 Simplification of the Neural Network Model for Predicting the Load-Carrying Capacity of Dowel-Type Connections - A Cointe, F Rouger
- 37-7-4 Bolted Wood Connections Loaded Perpendicular-to-Grain- A Proposed Design Approach - M C G Lehoux, J H P Quenneville
- 37-7-5 A New Prediction Formula for the Splitting Strength of Beams Loaded by Dowel Type Connections - M Ballerini
- 37-7-6 Plug Shear Failure: The Tensile Failure Mode and the Effect of Spacing - H Johnsson
- 37-7-7 Block Shear Failure Test with Dowel-Type Connection in Diagonal LVL Structure - M Kairi
- 37-7-8 Glued-in Steel Rods: A Design Approach for Axially Loaded Single Rods Set Parallel to the Grain - R Steiger, E Gehri, R Widmann
- 37-7-9 Glued in Rods in Load Bearing Timber Structures - Status regarding European Standards for Test Procedures - B Källander
- 37-7-10 French Data Concerning Glued-in Rods - C Faye, L Le Magorou, P Morlier, J Surleau
- 37-7-11 Enhancement of Dowel-Type Fasteners by Glued Connectors - C O Clorius, A Højman
- 37-7-12 Review of Probability Data for Timber Connections with Dowel-Type Fasteners - A J M Leijten, J Köhler, A Jorissen
- 37-7-13 Behaviour of Fasteners and Glued-in Rods Produced From Stainless Steel - A Kevarinmäki
- 37-7-14 Dowel joints in Engineered Wood Products: Assessment of Simple Fracture Mechanics Models - M Snow, I Smith, A Asiz
- 37-7-15 Numerical Modelling of Timber and Connection Elements Used in Timber-Concrete-Composite Constructions - M Grosse, K Rautenstrauch

LOAD SHARING

- 3-8-1 Load Sharing - An Investigation on the State of Research and Development of Design Criteria - E Levin
- 4-8-1 A Review of Load-Sharing in Theory and Practice - E Levin

- 4-8-2 Load Sharing - B Norén
- 19-8-1 Predicting the Natural Frequencies of Light-Weight Wooden Floors - I Smith and Y H Chui
- 20-8-1 Proposed Code Requirements for Vibrational Serviceability of Timber Floors - Y H Chui and I Smith
- 21-8-1 An Addendum to Paper 20-8-1 - Proposed Code Requirements for Vibrational Serviceability of Timber Floors - Y H Chui and I Smith
- 21-8-2 Floor Vibrational Serviceability and the CIB Model Code - S Ohlsson
- 22-8-1 Reliability Analysis of Viscoelastic Floors - F Rouger, J D Barrett and R O Foschi
- 24-8-1 On the Possibility of Applying Neutral Vibrational Serviceability Criteria to Joisted Wood Floors - I Smith and Y H Chui
- 25-8-1 Analysis of Glulam Semi-rigid Portal Frames under Long-term Load - K Komatsu and N Kawamoto
- 34-8-1 System Effect in Sheathed Parallel Timber Beam Structures – M Hansson, T Isaksson
- 35-8-1 System Effects in Sheathed Parallel Timber Beam Structures part II. - M Hansson, T Isaksson

DURATION OF LOAD

- 3-9-1 Definitions of Long Term Loading for the Code of Practice - B Norén
- 4-9-1 Long Term Loading of Trussed Rafters with Different Connection Systems - T Feldborg and M Johansen
- 5-9-1 Strength of a Wood Column in Combined Compression and Bending with Respect to Creep - B Källsner and B Norén
- 6-9-1 Long Term Loading for the Code of Practice (Part 2) - B Norén
- 6-9-2 Long Term Loading - K Möhler
- 6-9-3 Deflection of Trussed Rafters under Alternating Loading during a Year - T Feldborg and M Johansen
- 7-6-1 Strength and Long Term Behaviour of Lumber and Glued-Laminated Timber under Torsion Loads - K Möhler
- 7-9-1 Code Rules Concerning Strength and Loading Time - H J Larsen and E Theilgaard
- 17-9-1 On the Long-Term Carrying Capacity of Wood Structures - Y M Ivanov and Y Y Slavic
- 18-9-1 Prediction of Creep Deformations of Joints - J Kuipers
- 19-9-1 Another Look at Three Duration of Load Models - R O Foschi and Z C Yao
- 19-9-2 Duration of Load Effects for Spruce Timber with Special Reference to Moisture Influence - A Status Report - P Hoffmeyer
- 19-9-3 A Model of Deformation and Damage Processes Based on the Reaction Kinetics of Bond Exchange - T A C M van der Put
- 19-9-4 Non-Linear Creep Superposition - U Korin
- 19-9-5 Determination of Creep Data for the Component Parts of Stressed-Skin Panels - R Kliger
- 19-9-6 Creep an Lifetime of Timber Loaded in Tension and Compression - P Glos
- 19-1-1 Duration of Load Effects and Reliability Based Design (Single Member) - R O Foschi and Z C Yao
- 19-6-1 Effect of Age and/or Load on Timber Strength - J Kuipers

- 19-7-4 The Prediction of the Long-Term Load Carrying Capacity of Joints in Wood Structures - Y M Ivanov and Y Y Slavic
- 19-7-5 Slip in Joints under Long-Term Loading - T Feldborg and M Johansen
- 20-7-2 Slip in Joints under Long-Term Loading - T Feldborg and M Johansen
- 22-9-1 Long-Term Tests with Glued Laminated Timber Girders - M Badstube, W Rug and W Schöne
- 22-9-2 Strength of One-Layer solid and Lengthways Glued Elements of Wood Structures and its Alteration from Sustained Load - L M Kovaltchuk, I N Boitemirova and G B Uspenskaya
- 24-9-1 Long Term Bending Creep of Wood - T Toratti
- 24-9-2 Collection of Creep Data of Timber - A Ranta-Maunus
- 24-9-3 Deformation Modification Factors for Calculating Built-up Wood-Based Structures - I R Kliger
- 25-9-2 DVM Analysis of Wood. Lifetime, Residual Strength and Quality - L F Nielsen
- 26-9-1 Long Term Deformations in Wood Based Panels under Natural Climate Conditions. A Comparative Study - S Thelandersson, J Nordh, T Nordh and S Sandahl
- 28-9-1 Evaluation of Creep Behavior of Structural Lumber in Natural Environment - R Gupta and R Shen
- 30-9-1 DOL Effect in Tension Perpendicular to the Grain of Glulam Depending on Service Classes and Volume - S Aicher and G Dill-Langer
- 30-9-2 Damage Modelling of Glulam in Tension Perpendicular to Grain in Variable Climate - G Dill-Langer and S Aicher
- 31-9-1 Duration of Load Effect in Tension Perpendicular to Grain in Curved Glulam - A Ranta-Maunus
- 32-9-1 Bending-Stress-Redistribution Caused by Different Creep in Tension and Compression and Resulting DOL-Effect - P Becker and K Rautenstrauch
- 32-9-2 The Long Term Performance of Ply-Web Beams - R Grantham and V Enjily
- 36-9-1 Load Duration Factors for Instantaneous Loads - A J M Leijten, B Jansson

TIMBER BEAMS

- 4-10-1 The Design of Simple Beams - H J Burgess
- 4-10-2 Calculation of Timber Beams Subjected to Bending and Normal Force - H J Larsen
- 5-10-1 The Design of Timber Beams - H J Larsen
- 9-10-1 The Distribution of Shear Stresses in Timber Beams - F J Keenan
- 9-10-2 Beams Notched at the Ends - K Möhler
- 11-10-1 Tapered Timber Beams - H Riberholt
- 13-6-2 Consideration of Size Effects in Longitudinal Shear Strength for Uncracked Beams - R O Foschi and J D Barrett
- 13-6-3 Consideration of Shear Strength on End-Cracked Beams - J D Barrett and R O Foschi
- 18-10-1 Submission to the CIB-W18 Committee on the Design of Ply Web Beams by Consideration of the Type of Stress in the Flanges - J A Baird
- 18-10-2 Longitudinal Shear Design of Glued Laminated Beams - R O Foschi
- 19-10-1 Possible Code Approaches to Lateral Buckling in Beams - H J Burgess

- 19-2-1 Creep Buckling Strength of Timber Beams and Columns - R H Leicester
- 20-2-1 Lateral Buckling Theory for Rectangular Section Deep Beam-Columns - H J Burgess
- 20-10-1 Draft Clause for CIB Code for Beams with Initial Imperfections - H J Burgess
- 20-10-2 Space Joists in Irish Timber - W J Robinson
- 20-10-3 Composite Structure of Timber Joists and Concrete Slab - T Poutanen
- 21-10-1 A Study of Strength of Notched Beams - P J Gustafsson
- 22-10-1 Design of Endnotched Beams - H J Larsen and P J Gustafsson
- 22-10-2 Dimensions of Wooden Flexural Members under Constant Loads - A Pozgai
- 22-10-3 Thin-Walled Wood-Based Flanges in Composite Beams - J König
- 22-10-4 The Calculation of Wooden Bars with flexible Joints in Accordance with the Polish Standart Code and Strict Theoretical Methods - Z Mielczarek
- 23-10-1 Tension Perpendicular to the Grain at Notches and Joints - T A C M van der Put
- 23-10-2 Dimensioning of Beams with Cracks, Notches and Holes. An Application of Fracture Mechanics - K Riipola
- 23-10-3 Size Factors for the Bending and Tension Strength of Structural Timber - J D Barret and A R Fewell
- 23-12-1 Bending Strength of Glulam Beams, a Design Proposal - J Ehlbeck and F Colling
- 23-12-3 Glulam Beams, Bending Strength in Relation to the Bending Strength of the Finger Joints - H Riberholt
- 24-10-1 Shear Strength of Continuous Beams - R H Leicester and F G Young
- 25-10-1 The Strength of Norwegian Glued Laminated Beams - K Solli, E Aasheim and R H Falk
- 25-10-2 The Influence of the Elastic Modulus on the Simulated Bending Strength of Hyperstatic Timber Beams - T D G Canisius
- 27-10-1 Determination of Shear Modulus - R Görlacher and J Kürth
- 29-10-1 Time Dependent Lateral Buckling of Timber Beams - F Rouger
- 29-10-2 Determination of Modulus of Elasticity in Bending According to EN 408 - K H Solli
- 29-10-3 On Determination of Modulus of Elasticity in Bending - L Boström, S Ormarsson and O Dahlblom
- 29-10-4 Relation of Moduli of Elasticity in Flatwise and Edgewise Bending of Solid Timber - C J Johansson, A Steffen and E W Wormuth
- 30-10-1 Nondestructive Evaluation of Wood-based Members and Structures with the Help of Modal Analysis - P Kuklik
- 30-10-2 Measurement of Modulus of Elasticity in Bending - L Boström
- 30-10-3 A Weak Zone Model for Timber in Bending - B Källsner, K Salmela and O Ditlevsen
- 30-10-4 Load Carrying Capacity of Timber Beams with Narrow Moment Peaks - T Isaksson and J Freysoldt
- 37-10-1 Design of Rim Boards for Use with I-Joists Framing Systems - B Yeh, T G Williamson

ENVIRONMENTAL CONDITIONS

- 5-11-1 Climate Grading for the Code of Practice - B Norén
- 6-11-1 Climate Grading (2) - B Norén

- 9-11-1 Climate Classes for Timber Design - F J Keenan
- 19-11-1 Experimental Analysis on Ancient Downgraded Timber Structures - B Leggeri and L Paolini
- 19-6-5 Drying Stresses in Round Timber - A Ranta-Maunus
- 22-11-1 Corrosion and Adaptation Factors for Chemically Aggressive Media with Timber Structures - K Erler
- 29-11-1 Load Duration Effect on Structural Beams under Varying Climate Influence of Size and Shape - P Galimard and P Morlier
- 30-11-1 Probabilistic Design Models for the Durability of Timber Constructions - R H Leicester
- 36-11-1 Structural Durability of Timber in Ground Contact – R H Leicester, C H Wang, M N Nguyen, G C Foliente, C McKenzie

LAMINATED MEMBERS

- 6-12-1 Directives for the Fabrication of Load-Bearing Structures of Glued Timber - A van der Velden and J Kuipers
- 8-12-1 Testing of Big Glulam Timber Beams - H Kolb and P Frech
- 8-12-2 Instruction for the Reinforcement of Apertures in Glulam Beams - H Kolb and P Frech
- 8-12-3 Glulam Standard Part 1: Glued Timber Structures; Requirements for Timber (Second Draft)
- 9-12-1 Experiments to Provide for Elevated Forces at the Supports of Wooden Beams with Particular Regard to Shearing Stresses and Long-Term Loadings - F Wassipaul and R Lackner
- 9-12-2 Two Laminated Timber Arch Railway Bridges Built in Perth in 1849 - L G Booth
- 9-6-4 Consideration of Combined Stresses for Lumber and Glued Laminated Timber - K Möhler
- 11-6-3 Consideration of Combined Stresses for Lumber and Glued Laminated Timber (addition to Paper CIB-W18/9-6-4) - K Möhler
- 12-12-1 Glulam Standard Part 2: Glued Timber Structures; Rating (3rd draft)
- 12-12-2 Glulam Standard Part 3: Glued Timber Structures; Performance (3 rd draft)
- 13-12-1 Glulam Standard Part 3: Glued Timber Structures; Performance (4th draft)
- 14-12-1 Proposals for CEI-Bois/CIB-W18 Glulam Standards - H J Larsen
- 14-12-2 Guidelines for the Manufacturing of Glued Load-Bearing Timber Structures - Stevin Laboratory
- 14-12-3 Double Tapered Curved Glulam Beams - H Riberholt
- 14-12-4 Comment on CIB-W18/14-12-3 - E Gehri
- 18-12-1 Report on European Glulam Control and Production Standard - H Riberholt
- 18-10-2 Longitudinal Shear Design of Glued Laminated Beams - R O Foschi
- 19-12-1 Strength of Glued Laminated Timber - J Ehlbeck and F Colling
- 19-12-2 Strength Model for Glulam Columns - H J Blaß
- 19-12-3 Influence of Volume and Stress Distribution on the Shear Strength and Tensile Strength Perpendicular to Grain - F Colling
- 19-12-4 Time-Dependent Behaviour of Glued-Laminated Beams - F Zaupa

- 21-12-1 Modulus of Rupture of Glulam Beam Composed of Arbitrary Laminae - K Komatsu and N Kawamoto
- 21-12-2 An Appraisal of the Young's Modulus Values Specified for Glulam in Eurocode 5- L R J Whale, B O Hilson and P D Rodd
- 21-12-3 The Strength of Glued Laminated Timber (Glulam): Influence of Lamination Qualities and Strength of Finger Joints - J Ehlbeck and F Colling
- 21-12-4 Comparison of a Shear Strength Design Method in Eurocode 5 and a More Traditional One - H Riberholt
- 22-12-1 The Dependence of the Bending Strength on the Glued Laminated Timber Girder Depth - M Badstube, W Rug and W Schöne
- 22-12-2 Acid Deterioration of Glulam Beams in Buildings from the Early Half of the 1960s - Preliminary summary of the research project; Overhead pictures - B A Hedlund
- 22-12-3 Experimental Investigation of normal Stress Distribution in Glue Laminated Wooden Arches - Z Mielczarek and W Chanaj
- 22-12-4 Ultimate Strength of Wooden Beams with Tension Reinforcement as a Function of Random Material Properties - R Candowicz and T Dziuba
- 23-12-1 Bending Strength of Glulam Beams, a Design Proposal - J Ehlbeck and F Colling
- 23-12-2 Probability Based Design Method for Glued Laminated Timber - M F Stone
- 23-12-3 Glulam Beams, Bending Strength in Relation to the Bending Strength of the Finger Joints - H Riberholt
- 23-12-4 Glued Laminated Timber - Strength Classes and Determination of Characteristic Properties - H Riberholt, J Ehlbeck and A Fewell
- 24-12-1 Contribution to the Determination of the Bending Strength of Glulam Beams - F Colling, J Ehlbeck and R Görlacher
- 24-12-2 Influence of Perpendicular-to-Grain Stressed Volume on the Load-Carrying Capacity of Curved and Tapered Glulam Beams - J Ehlbeck and J Kürth
- 25-12-1 Determination of Characteristic Bending Values of Glued Laminated Timber. EN-Approach and Reality - E Gehri
- 26-12-1 Norwegian Bending Tests with Glued Laminated Beams-Comparative Calculations with the "Karlsruhe Calculation Model" - E Aasheim, K Solli, F Colling, R H Falk, J Ehlbeck and R Görlacher
- 26-12-2 Simulation Analysis of Norwegian Spruce Glued-Laminated Timber - R Hernandez and R H Falk
- 26-12-3 Investigation of Laminating Effects in Glued-Laminated Timber - F Colling and R H Falk
- 26-12-4 Comparing Design Results for Glulam Beams According to Eurocode 5 and to the French Working Stress Design Code (CB71) - F Rouger
- 27-12-1 State of the Art Report: Glulam Timber Bridge Design in the U.S. - M A Ritter and T G Williamson
- 27-12-2 Common Design Practice for Timber Bridges in the United Kingdom - C J Mettem, J P Marcroft and G Davis
- 27-12-3 Influence of Weak Zones on Stress Distribution in Glulam Beams - E Serrano and H J Larsen
- 28-12-1 Determination of Characteristic Bending Strength of Glued Laminated Timber - E Gehri
- 28-12-2 Size Factor of Norwegian Glued Laminated Beams - E Aasheim and K H Solli
- 28-12-3 Design of Glulam Beams with Holes - K Riipola

- 28-12-4 Compression Resistance of Glued Laminated Timber Short Columns- U Korin
- 29-12-1 Development of Efficient Glued Laminated Timber - G Schickhofer
- 30-12-1 Experimental Investigation and Analysis of Reinforced Glulam Beams - K Oiger
- 31-12-1 Depth Factor for Glued Laminated Timber-Discussion of the Eurocode 5 Approach - B Källsner, O Carling and C J Johansson
- 32-12-1 The bending stiffness of nail-laminated timber elements in transverse direction- T Wolf and O Schäfer
- 33-12-1 Internal Stresses in the Cross-Grain Direction of Wood Induced by Climate Variation – J Jönsson and S Svensson
- 34-12-1 High-Strength I-Joist Compatible Glulam Manufactured with LVL Tension Laminations – B Yeh, T G Williamson
- 34-12-2 Evaluation of Glulam Shear Strength Using A Full-Size Four-Point Test Method – B Yeh, T G Williamson
- 34-12-3 Design Model for FRP Reinforced Glulam Beams – M Romani, H J Bläß
- 34-12-4 Moisture induced stresses in glulam cross sections – J Jönsson
- 34-12-5 Load Carrying Capacity of Nail-Laminated Timber under Concentrated Loads – V Krämer, H J Bläß
- 34-12-6 Determination of Shear Strength Values for GLT Using Visual and Machine Graded Spruce Laminations – G Schickhofer
- 34-12-7 Mechanically Jointed Beams: Possibilities of Analysis and some special Problems – H Kreuzinger
- 35-12-1 Glulam Beams with Round Holes – a Comparison of Different Design Approaches vs. Test Data - S Aicher L Höfflin
- 36-12-1 Problems with Shear and Bearing Strength of LVL in Highly Loaded Structures - H Bier
- 36-12-2 Weibull Based Design of Round Holes in Glulam - L Höfflin, S Aicher
- 37-12-1 Development of Structural LVL from Tropical Wood and Evaluation of Their Performance for the Structural Components of Wooden Houses. Part-1. Application of Tropical LVL to a Roof Truss - K Komatsu, Y Idris, S Yuwasdiki, B Subiyakto, A Firmanti
- 37-12-2 Reinforcement of LVL Beams With Bonded-in Plates and Rods - Effect of Placement of Steel and FRP Reinforcements on Beam Strength and Stiffness - P Alam, M P Ansell, D Smedley

PARTICLE AND FIBRE BUILDING BOARDS

- 7-13-1 Fibre Building Boards for CIB Timber Code (First Draft)- O Brynildsen
- 9-13-1 Determination of the Bearing Strength and the Load-Deformation Characteristics of Particleboard - K Möhler, T Budianto and J Ehlbeck
- 9-13-2 The Structural Use of Tempered Hardboard - W W L Chan
- 11-13-1 Tests on Laminated Beams from Hardboard under Short- and Longterm Load - W Nozynski
- 11-13-2 Determination of Deformation of Special Densified Hardboard under Long-term Load and Varying Temperature and Humidity Conditions - W Halfar
- 11-13-3 Determination of Deformation of Hardboard under Long-term Load in Changing Climate - W Halfar
- 14-4-1 An Introduction to Performance Standards for Wood-Base Panel Products - D H Brown
- 14-4-2 Proposal for Presenting Data on the Properties of Structural Panels - T Schmidt

- 16-13-1 Effect of Test Piece Size on Panel Bending Properties - P W Post
- 20-4-1 Considerations of Reliability - Based Design for Structural Composite Products - M R O'Halloran, J A Johnson, E G Elias and T P Cunningham
- 20-13-1 Classification Systems for Structural Wood-Based Sheet Materials - V C Kearley and A R Abbott
- 21-13-1 Design Values for Nailed Chipboard - Timber Joints - A R Abbott
- 25-13-1 Bending Strength and Stiffness of Izopanel Plates - Z Mielczarek
- 28-13-1 Background Information for "Design Rated Oriented Strand Board (OSB)" in CSA Standards - Summary of Short-term Test Results - E Karacabeyli, P Lau, C R Henderson, F V Meakes and W Deacon
- 28-13-2 Torsional Stiffness of Wood-Hardboard Composed I-Beam - P Olejniczak

TRUSSED RAFTERS

- 4-9-1 Long-term Loading of Trussed Rafters with Different Connection Systems - T Feldborg and M Johansen
- 6-9-3 Deflection of Trussed Rafters under Alternating Loading During a Year - T Feldborg and M Johansen
- 7-2-1 Lateral Bracing of Timber Struts - J A Simon
- 9-14-1 Timber Trusses - Code Related Problems - T F Williams
- 9-7-1 Design of Truss Plate Joints - F J Keenan
- 10-14-1 Design of Roof Bracing - The State of the Art in South Africa - P A V Bryant and J A Simon
- 11-14-1 Design of Metal Plate Connected Wood Trusses - A R Egerup
- 12-14-1 A Simple Design Method for Standard Trusses - A R Egerup
- 13-14-1 Truss Design Method for CIB Timber Code - A R Egerup
- 13-14-2 Trussed Rafters, Static Models - H Riberholt
- 13-14-3 Comparison of 3 Truss Models Designed by Different Assumptions for Slip and E-Modulus - K Möhler
- 14-14-1 Wood Trussed Rafter Design - T Feldborg and M Johansen
- 14-14-2 Truss-Plate Modelling in the Analysis of Trusses - R O Foschi
- 14-14-3 Cantilevered Timber Trusses - A R Egerup
- 14-7-5 The Effect of Support Eccentricity on the Design of W- and WW-Trusses with Nail Plate Connectors - B Källsner
- 15-14-1 Guidelines for Static Models of Trussed Rafters - H Riberholt
- 15-14-2 The Influence of Various Factors on the Accuracy of the Structural Analysis of Timber Roof Trusses - F R P Pienaar
- 15-14-3 Bracing Calculations for Trussed Rafter Roofs - H J Burgess
- 15-14-4 The Design of Continuous Members in Timber Trussed Rafters with Punched Metal Connector Plates - P O Reece
- 15-14-5 A Rafter Design Method Matching U.K. Test Results for Trussed Rafters - H J Burgess
- 16-14-1 Full-Scale Tests on Timber Fink Trusses Made from Irish Grown Sitka Spruce - V Picardo
- 17-14-1 Data from Full Scale Tests on Prefabricated Trussed Rafters - V Picardo
- 17-14-2 Simplified Static Analysis and Dimensioning of Trussed Rafters - H Riberholt

- 17-14-3 Simplified Calculation Method for W-Trusses - B Källsner
- 18-14-1 Simplified Calculation Method for W-Trusses (Part 2) - B Källsner
- 18-14-2 Model for Trussed Rafter Design - T Poutanen
- 19-14-1 Annex on Simplified Design of W-Trusses - H J Larsen
- 19-14-2 Simplified Static Analysis and Dimensioning of Trussed Rafters - Part 2 - H Riberholt
- 19-14-3 Joint Eccentricity in Trussed Rafters - T Poutanen
- 20-14-1 Some Notes about Testing Nail Plates Subjected to Moment Load - T Poutanen
- 20-14-2 Moment Distribution in Trussed Rafters - T Poutanen
- 20-14-3 Practical Design Methods for Trussed Rafters - A R Egerup
- 22-14-1 Guidelines for Design of Timber Trussed Rafters - H Riberholt
- 23-14-1 Analyses of Timber Trussed Rafters of the W-Type - H Riberholt
- 23-14-2 Proposal for Eurocode 5 Text on Timber Trussed Rafters - H Riberholt
- 24-14-1 Capacity of Support Areas Reinforced with Nail Plates in Trussed Rafters - A Kevarinmäki
- 25-14-1 Moment Anchorage Capacity of Nail Plates in Shear Tests - A Kevarinmaki and J. Kangas
- 25-14-2 Design Values of Anchorage Strength of Nail Plate Joints by 2-curve Method and Interpolation - J Kangas and A Kevarinmaki
- 26-14-1 Test of Nail Plates Subjected to Moment - E Aasheim
- 26-14-2 Moment Anchorage Capacity of Nail Plates - A Kevarinmäki and J Kangas
- 26-14-3 Rotational Stiffness of Nail Plates in Moment Anchorage - A Kevarinmäki and J Kangas
- 26-14-4 Solution of Plastic Moment Anchorage Stress in Nail Plates - A Kevarinmäki
- 26-14-5 Testing of Metal-Plate-Connected Wood-Truss Joints - R Gupta
- 26-14-6 Simulated Accidental Events on a Trussed Rafter Roofed Building - C J Mettem and J P Marcroft
- 30-14-1 The Stability Behaviour of Timber Trussed Rafter Roofs - Studies Based on Eurocode 5 and Full Scale Testing - R J Bainbridge, C J Mettern, A Reffold and T Studer
- 32-14-1 Analysis of Timber Reinforced with Punched Metal Plate Fasteners- J Nielsen
- 33-14-1 Moment Capacity of Timber Beams Loaded in Four-Point Bending and Reinforced with Punched Metal Plate Fasteners – J Nielsen
- 36-14-1 Effect of Chord Splice Joints on Force Distribution in Trusses with Punched Metal Plate Fasteners - P Ellegaard
- 36-14-2 Monte Carlo Simulation and Reliability Analysis of Roof Trusses with Punched Metal Plate Fasteners - M Hansson, P Ellegaard
- 36-14-3 Truss Trouble – R H Leicester, J Goldfinch, P Paevere, G C Foliente

STRUCTURAL STABILITY

- 8-15-1 Laterally Loaded Timber Columns: Tests and Theory - H J Larsen
- 13-15-1 Timber and Wood-Based Products Structures. Panels for Roof Coverings. Methods of Testing and Strength Assessment Criteria. Polish Standard BN-78/7159-03
- 16-15-1 Determination of Bracing Structures for Compression Members and Beams - H Brüninghoff

- 17-15-1 Proposal for Chapter 7.4 Bracing - H Brüninghoff
- 17-15-2 Seismic Design of Small Wood Framed Houses - K F Hansen
- 18-15-1 Full-Scale Structures in Glued Laminated Timber, Dynamic Tests: Theoretical and Experimental Studies - A Ceccotti and A Vignoli
- 18-15-2 Stabilizing Bracings - H Brüninghoff
- 19-15-1 Connections Deformability in Timber Structures: a Theoretical Evaluation of its Influence on Seismic Effects - A Ceccotti and A Vignoli
- 19-15-2 The Bracing of Trussed Beams - M H Kessel and J Natterer
- 19-15-3 Racking Resistance of Wooden Frame Walls with Various Openings - M Yasumura
- 19-15-4 Some Experiences of Restoration of Timber Structures for Country Buildings - G Cardinale and P Spinelli
- 19-15-5 Non-Destructive Vibration Tests on Existing Wooden Dwellings - Y Hirashima
- 20-15-1 Behaviour Factor of Timber Structures in Seismic Zones. - A Ceccotti and A Vignoli
- 21-15-1 Rectangular Section Deep Beam - Columns with Continuous Lateral Restraint - H J Burgess
- 21-15-2 Buckling Modes and Permissible Axial Loads for Continuously Braced Columns- H J Burgess
- 21-15-3 Simple Approaches for Column Bracing Calculations - H J Burgess
- 21-15-4 Calculations for Discrete Column Restraints - H J Burgess
- 21-15-5 Behaviour Factor of Timber Structures in Seismic Zones (Part Two) - A Ceccotti and A Vignoli
- 22-15-1 Suggested Changes in Code Bracing Recommendations for Beams and Columns - H J Burgess
- 22-15-2 Research and Development of Timber Frame Structures for Agriculture in Poland- S Kus and J Kerste
- 22-15-3 Ensuring of Three-Dimensional Stiffness of Buildings with Wood Structures - A K Shenghelia
- 22-15-5 Seismic Behavior of Arched Frames in Timber Construction - M Yasumura
- 22-15-6 The Robustness of Timber Structures - C J Mettem and J P Marcroft
- 22-15-7 Influence of Geometrical and Structural Imperfections on the Limit Load of Wood Columns - P Dutko
- 23-15-1 Calculation of a Wind Girder Loaded also by Discretely Spaced Braces for Roof Members - H J Burgess
- 23-15-2 Stability Design and Code Rules for Straight Timber Beams - T A C M van der Put
- 23-15-3 A Brief Description of Formula of Beam-Columns in China Code - S Y Huang
- 23-15-4 Seismic Behavior of Braced Frames in Timber Construction - M Yasumura
- 23-15-5 On a Better Evaluation of the Seismic Behavior Factor of Low-Dissipative Timber Structures - A Ceccotti and A Vignoli
- 23-15-6 Disproportionate Collapse of Timber Structures - C J Mettem and J P Marcroft
- 23-15-7 Performance of Timber Frame Structures During the Loma Prieta California Earthquake - M R O'Halloran and E G Elias
- 24-15-2 Discussion About the Description of Timber Beam-Column Formula - S Y Huang

- 24-15-3 Seismic Behavior of Wood-Framed Shear Walls - M Yasumura
- 25-15-1 Structural Assessment of Timber Framed Building Systems - U Korin
- 25-15-3 Mechanical Properties of Wood-framed Shear Walls Subjected to Reversed Cyclic Lateral Loading - M Yasumura
- 26-15-1 Bracing Requirements to Prevent Lateral Buckling in Trussed Rafters - C J Mettem and P J Moss
- 26-15-2 Eurocode 8 - Part 1.3 - Chapter 5 - Specific Rules for Timber Buildings in Seismic Regions - K Becker, A Ceccotti, H Charlier, E Katsaragakis, H J Larsen and H Zeitter
- 26-15-3 Hurricane Andrew - Structural Performance of Buildings in South Florida - M R O'Halloran, E L Keith, J D Rose and T P Cunningham
- 29-15-1 Lateral Resistance of Wood Based Shear Walls with Oversized Sheathing Panels - F Lam, H G L Prion and M He
- 29-15-2 Damage of Wooden Buildings Caused by the 1995 Hyogo-Ken Nanbu Earthquake - M Yasumura, N Kawai, N Yamaguchi and S Nakajima
- 29-15-3 The Racking Resistance of Timber Frame Walls: Design by Test and Calculation - D R Griffiths, C J Mettem, V Enjily, P J Steer
- 29-15-4 Current Developments in Medium-Rise Timber Frame Buildings in the UK - C J Mettem, G C Pitts, P J Steer, V Enjily
- 29-15-5 Natural Frequency Prediction for Timber Floors - R J Bainbridge, and C J Mettem
- 30-15-1 Cyclic Performance of Perforated Wood Shear Walls with Oversize Oriented Strand Board Panels - Ming He, H Magnusson, F Lam, and H G L Prion
- 30-15-2 A Numerical Analysis of Shear Walls Structural Performances - L Davenne, L Daudeville, N Kawai and M Yasumura
- 30-15-3 Seismic Force Modification Factors for the Design of Multi-Storey Wood-Frame Platform Construction - E Karacabeyli and A Ceccotti
- 30-15-4 Evaluation of Wood Framed Shear Walls Subjected to Lateral Load - M Yasumura and N Kawai
- 31-15-1 Seismic Performance Testing On Wood-Framed Shear Wall - N Kawai
- 31-15-2 Robustness Principles in the Design of Medium-Rise Timber-Framed Buildings - C J Mettem, M W Milner, R J Bainbridge and V. Enjily
- 31-15-3 Numerical Simulation of Pseudo-Dynamic Tests Performed to Shear Walls - L Daudeville, L Davenne, N Richard, N Kawai and M Yasumura
- 31-15-4 Force Modification Factors for Braced Timber Frames - H G L Prion, M Popovski and E Karacabeyli
- 32-15-1 Three-Dimensional Interaction in Stabilisation of Multi-Storey Timber Frame Buildings - S Andreasson
- 32-15-2 Application of Capacity Spectrum Method to Timber Houses - N Kawai
- 32-15-3 Design Methods for Shear Walls with Openings - C Ni, E Karacabeyli and A Ceccotti
- 32-15-4 Static Cyclic Lateral Loading Tests on Nailed Plywood Shear Walls - K Komatsu, K H Hwang and Y Itou
- 33-15-1 Lateral Load Capacities of Horizontally Sheathed Unblocked Shear Walls – C Ni, E Karacabeyli and A Ceccotti
- 33-15-2 Prediction of Earthquake Response of Timber Houses Considering Shear Deformation of Horizontal Frames – N Kawai
- 33-15-3 Eurocode 5 Rules for Bracing – H J Larsen

- 34-15-1 A simplified plastic model for design of partially anchored wood-framed shear walls – B Källsner, U A Girhammar, Liping Wu
- 34-15-2 The Effect of the Moisture Content on the Performance of the Shear Walls – S Nakajima
- 34-15-3 Evaluation of Damping Capacity of Timber Structures for Seismic Design – M Yasumura
- 35-15-1 On test methods for determining racking strength and stiffness of wood-framed shear walls - B Källsner, U A Girhammar, L Wu
- 35-15-2 A Plastic Design Model for Partially Anchored Wood-framed Shear Walls with Openings - U A Girhammar, L Wu, B Källsner
- 35-15-3 Evaluation and Estimation of the Performance of the Shear Walls in Humid Climate - S Nakajima
- 35-15-4 Influence of Vertical Load on Lateral Resistance of Timber Frame Walls - B Dujič, R Žarnić
- 35-15-5 Cyclic and Seismic Performances of a Timber-Concrete System - Local and Full Scale Experimental Results - E Fournely, P Racher
- 35-15-6 Design of timber-concrete composite structures according to EC5 - 2002 version - A Ceccotti, M Fragiaco, R M Gutkowski
- 35-15-7 Design of timber structures in seismic zones according to EC8- 2002 version - A Ceccotti, T Toratti, B Dujič
- 35-15-8 Design Methods to Prevent Premature Failure of Joints at Shear Wall Corners - N Kawai, H Okiura
- 36-15-1 Monitoring Light-Frame Timber Buildings: Environmental Loads and Load Paths – I Smith et al.
- 36-15-2 Applicability of Design Methods to Prevent Premature Failure of Joints at Shear Wall Corners in Case of Post and Beam Construction - N Kawai, H Isoda
- 36-15-3 Effects of Screw Spacing and Edge Boards on the Cyclic Performance of Timber Frame and Structural Insulated Panel Roof Systems - D M Carradine, J D Dolan, F E Woeste
- 36-15-4 Pseudo-Dynamic Tests on Conventional Timber Structures with Shear Walls - M Yasumura
- 36-15-5 Experimental Investigation of Laminated Timber Frames with Fiber-reinforced Connections under Earthquake Loads - B Kasal, P Haller, S Pospisil, I Jirovsky, A Heiduschke, M Drdacky
- 36-15-6 Effect of Test Configurations and Protocols on the Performance of Shear Walls - F Lam, D Jossen, J Gu, N Yamaguchi, H G L Prion
- 36-15-7 Comparison of Monotonic and Cyclic Performance of Light-Frame Shear Walls - J D Dolan, A J Toothman
- 37-15-1 Estimating 3D Behavior of Conventional Timber Structures with Shear Walls by Pseudodynamic Tests - M Yasumura, M Uesugi, L Davenne
- 37-15-2 Testing of Racking Behavior of Massive Wooden Wall Panels - B Dujič, J Pucelj, R Žarnić
- 37-15-3 Influence of Framing Joints on Plastic Capacity of Partially Anchored Wood-Framed Shear Walls - B Källsner, U A Girhammar
- 37-15-4 Bracing of Timber Members in Compression - J Munch-Andersen
- 37-15-5 Acceptance Criteria for the Use of Structural Insulated Panels in High Risk Seismic Areas - B Yeh, T D Skaggs, T G Williamson Z A Martin
- 37-15-6 Predicting Load Paths in Shearwalls - Hongyong Mi, Ying-Hei Chui, I Smith, M Mohammad

FIRE

- 12-16-1 British Standard BS 5268 the Structural Use of Timber: Part 4 Fire Resistance of Timber Structures
- 13-100-2 CIB Structural Timber Design Code. Chapter 9. Performance in Fire
- 19-16-1 Simulation of Fire in Tests of Axially Loaded Wood Wall Studs - J König
- 24-16-1 Modelling the Effective Cross Section of Timber Frame Members Exposed to Fire - J König
- 25-16-1 The Effect of Density on Charring and Loss of Bending Strength in Fire - J König
- 25-16-2 Tests on Glued-Laminated Beams in Bending Exposed to Natural Fires - F Bolonius Olesen and J König
- 26-16-1 Structural Fire Design According to Eurocode 5, Part 1.2 - J König
- 31-16-1 Revision of ENV 1995-1-2: Charring and Degradation of Strength and Stiffness - J König
- 33-16-1 A Design Model for Load-carrying Timber Frame Members in Walls and Floors Exposed to Fire - J König
- 33-16-2 A Review of Component Additive Methods Used for the Determination of Fire Resistance of Separating Light Timber Frame Construction - J König, T Oksanen and K Towler
- 33-16-3 Thermal and Mechanical Properties of Timber and Some Other Materials Used in Light Timber Frame Construction - B Källsner and J König
- 34-16-1 Influence of the Strength Determining Factors on the Fire Resistance Capability of Timber Structural Members – I Totev, D Dakov
- 34-16-2 Cross section properties of fire exposed rectangular timber members - J König, B Källsner
- 34-16-3 Pull-Out Tests on Glued-in Rods at High Temperatures – A Mischler, A Frangi
- 35-16-1 Basic and Notional Charring Rates - J König
- 37 - 16 - 1 Effective Values of Thermal Properties of Timber and Thermal Actions During the Decay Phase of Natural Fires - J König
- 37 - 16 - 2 Fire Tests on Timber Connections with Dowel-type Fasteners - A Frangi, A Mischler

STATISTICS AND DATA ANALYSIS

- 13-17-1 On Testing Whether a Prescribed Exclusion Limit is Attained - W G Warren
- 16-17-1 Notes on Sampling and Strength Prediction of Stress Graded Structural Timber - P Glos
- 16-17-2 Sampling to Predict by Testing the Capacity of Joints, Components and Structures - B Norén
- 16-17-3 Discussion of Sampling and Analysis Procedures - P W Post
- 17-17-1 Sampling of Wood for Joint Tests on the Basis of Density - I Smith, L R J Whale
- 17-17-2 Sampling Strategy for Physical and Mechanical Properties of Irish Grown Sitka Spruce - V Picardo
- 18-17-1 Sampling of Timber in Structural Sizes - P Glos
- 18-6-3 Notes on Sampling Factors for Characteristic Values - R H Leicester
- 19-17-1 Load Factors for Proof and Prototype Testing - R H Leicester
- 19-6-2 Confidence in Estimates of Characteristic Values - R H Leicester

- 21-6-1 Draft Australian Standard: Methods for Evaluation of Strength and Stiffness of Graded Timber - R H Leicester
- 21-6-2 The Determination of Characteristic Strength Values for Stress Grades of Structural Timber. Part 1 - A R Fewell and P Glos
- 22-17-1 Comment on the Strength Classes in Eurocode 5 by an Analysis of a Stochastic Model of Grading - A proposal for a supplement of the design concept - M Kiesel
- 24-17-1 Use of Small Samples for In-Service Strength Measurement - R H Leicester and F G Young
- 24-17-2 Equivalence of Characteristic Values - R H Leicester and F G Young
- 24-17-3 Effect of Sampling Size on Accuracy of Characteristic Values of Machine Grades - Y H Chui, R Turner and I Smith
- 24-17-4 Harmonisation of LSD Codes - R H Leicester
- 25-17-2 A Body for Confirming the Declaration of Characteristic Values - J Sunley
- 25-17-3 Moisture Content Adjustment Procedures for Engineering Standards - D W Green and J W Evans
- 27-17-1 Statistical Control of Timber Strength - R H Leicester and H O Breitingen
- 30-17-1 A New Statistical Method for the Establishment of Machine Settings - F Rouger
- 35-17-1 Probabilistic Modelling of Duration of Load Effects in Timber Structures - J Köhler, S Svenson

GLUED JOINTS

- 20-18-1 Wood Materials under Combined Mechanical and Hygral Loading - A Martensson and S Thelandersson
- 20-18-2 Analysis of Generalized Volkersen - Joints in Terms of Linear Fracture Mechanics - P J Gustafsson
- 20-18-3 The Complete Stress-Slip Curve of Wood-Adhesives in Pure Shear - H Wernersson and P J Gustafsson
- 22-18-1 Perspective Adhesives and Protective Coatings for Wood Structures - A S Freidin
- 34-18-1 Performance Based Classification of Adhesives for Structural Timber Applications - R J Bainbridge, C J Mettem, J G Broughton, A R Hutchinson
- 35-18-1 Creep Testing Wood Adhesives for Structural Use - C Bengtsson, B Källander

FRACTURE MECHANICS

- 21-10-1 A Study of Strength of Notched Beams - P J Gustafsson
- 22-10-1 Design of Endnotched Beams - H J Larsen and P J Gustafsson
- 23-10-1 Tension Perpendicular to the Grain at Notches and Joints - T A C M van der Put
- 23-10-2 Dimensioning of Beams with Cracks, Notches and Holes. An Application of Fracture Mechanics - K Riipola
- 23-19-1 Determination of the Fracture Energie of Wood for Tension Perpendicular to the Grain - W Rug, M Badstube and W Schöne
- 23-19-2 The Fracture Energy of Wood in Tension Perpendicular to the Grain. Results from a Joint Testing Project - H J Larsen and P J Gustafsson
- 23-19-3 Application of Fracture Mechanics to Timber Structures - A Ranta-Maunus
- 24-19-1 The Fracture Energy of Wood in Tension Perpendicular to the Grain - H J Larsen and P J Gustafsson

- 28-19-1 Fracture of Wood in Tension Perpendicular to the Grain: Experiment and Numerical Simulation by Damage Mechanics - L Daudeville, M Yasumura and J D Lanvin
- 28-19-2 A New Method of Determining Fracture Energy in Forward Shear along the Grain - H D Mansfield-Williams
- 28-19-3 Fracture Design Analysis of Wooden Beams with Holes and Notches. Finite Element Analysis based on Energy Release Rate Approach - H Petersson
- 28-19-4 Design of Timber Beams with Holes by Means of Fracture Mechanics - S Aicher, J Schmidt and S Brunold
- 30-19-1 Failure Analysis of Single-Bolt Joints - L Daudeville, L Davenne and M Yasumura
- 37 - 19 - 1 Determination of Fracture Mechanics Parameters for Wood with the Help of Close Range Photogrammetry - S Franke, B Franke, K Rautenstrauch

SERVICEABILITY

- 27-20-1 Codification of Serviceability Criteria - R H Leicester
- 27-20-2 On the Experimental Determination of Factor k_{def} and Slip Modulus k_{ser} from Short- and Long-Term Tests on a Timber-Concrete Composite (TCC) Beam - S Capretti and A Ceccotti
- 27-20-3 Serviceability Limit States: A Proposal for Updating Eurocode 5 with Respect to Eurocode 1 - P Racher and F Rouger
- 27-20-4 Creep Behavior of Timber under External Conditions - C Le Govic, F Rouger, T Toratti and P Morlier
- 30-20-1 Design Principles for Timber in Compression Perpendicular to Grain - S Thelandersson and A Mårtensson
- 30-20-2 Serviceability Performance of Timber Floors - Eurocode 5 and Full Scale Testing - R J Bainbridge and C J Mettem
- 32-20-1 Floor Vibrations - B Mohr
- 37 - 20 - 1 A New Design Method to Control Vibrations Induced by Foot Steps in Timber Floors - Lin J Hu, Y H Chui
- 37 - 20 - 2 Serviceability Limit States of Wooden Footbridges. Vibrations Caused by Pedestrians - P Hamm

TEST METHODS

- 31-21-1 Development of an Optimised Test Configuration to Determine Shear Strength of Glued Laminated Timber - G Schickhofer and B Obermayr
- 31-21-2 An Impact Strength Test Method for Structural Timber. The Theory and a Preliminary Study - T D G Canisius
- 35-21-1 Full-Scale Edgewise Shear Tests for Laminated Veneer Lumber- B Yeh, T G Williamson

CIB TIMBER CODE

- 2-100-1 A Framework for the Production of an International Code of Practice for the Structural Use of Timber - W T Curry
- 5-100-1 Design of Solid Timber Columns (First Draft) - H J Larsen
- 5-100-2 A Draft Outline of a Code for Timber Structures - L G Booth
- 6-100-1 Comments on Document 5-100-1; Design of Solid Timber Columns - H J Larsen and E Theilgaard

- 6-100-2 CIB Timber Code: CIB Timber Standards - H J Larsen and E Theilgaard
- 7-100-1 CIB Timber Code Chapter 5.3 Mechanical Fasteners; CIB Timber Standard 06 and 07 - H J Larsen
- 8-100-1 CIB Timber Code - List of Contents (Second Draft) - H J Larsen
- 9-100-1 The CIB Timber Code (Second Draft)
- 11-100-1 CIB Structural Timber Design Code (Third Draft)
- 11-100-2 Comments Received on the CIB Code
U Saarelainen; Y M Ivanov, R H Leicester, W Nozynski, W R A Meyer, P Beckmann; R Marsh
- 11-100-3 CIB Structural Timber Design Code; Chapter 3 - H J Larsen
- 12-100-1 Comment on the CIB Code - Sous-Commission Glulam
- 12-100-2 Comment on the CIB Code - R H Leicester
- 12-100-3 CIB Structural Timber Design Code (Fourth Draft)
- 13-100-1 Agreed Changes to CIB Structural Timber Design Code
- 13-100-2 CIB Structural Timber Design Code. Chapter 9: Performance in Fire
- 13-100-3a Comments on CIB Structural Timber Design Code
- 13-100-3b Comments on CIB Structural Timber Design Code - W R A Meyer
- 13-100-3c Comments on CIB Structural Timber Design Code - British Standards Institution
- 13-100-4 CIB Structural Timber Design Code. Proposal for Section 6.1.5 Nail Plates - N I Bovim
- 14-103-2 Comments on the CIB Structural Timber Design Code - R H Leicester
- 15-103-1 Resolutions of TC 165-meeting in Athens 1981-10-12/13
- 21-100-1 CIB Structural Timber Design Code. Proposed Changes of Sections on Lateral Instability, Columns and Nails - H J Larsen
- 22-100-1 Proposal for Including an Updated Design Method for Bearing Stresses in CIB W18 - Structural Timber Design Code - B Madsen
- 22-100-2 Proposal for Including Size Effects in CIB W18A Timber Design Code - B Madsen
- 22-100-3 CIB Structural Timber Design Code - Proposed Changes of Section on Thin-Flanged Beams - J König
- 22-100-4 Modification Factor for "Aggressive Media" - a Proposal for a Supplement to the CIB Model Code - K Erler and W Rug
- 22-100-5 Timber Design Code in Czechoslovakia and Comparison with CIB Model Code - P Dutko and B Kozelouh

LOADING CODES

- 4-101-1 Loading Regulations - Nordic Committee for Building Regulations
- 4-101-2 Comments on the Loading Regulations - Nordic Committee for Building Regulations
- 37-101-1 Action Combination Processing for the Eurocodes Basis of Software to Assist the Engineer - Y Robert, A V Page, R Thépaut, C J Mettem

STRUCTURAL DESIGN CODES

- 1-102-1 Survey of Status of Building Codes, Specifications etc., in USA - E G Stern
- 1-102-2 Australian Codes for Use of Timber in Structures - R H Leicester
- 1-102-3 Contemporary Concepts for Structural Timber Codes - R H Leicester

- 1-102-4 Revision of CP 112 - First Draft, July 1972 - British Standards Institution
- 4-102-1 Comparison of Codes and Safety Requirements for Timber Structures in EEC Countries - Timber Research and Development Association
- 4-102-2 Nordic Proposals for Safety Code for Structures and Loading Code for Design of Structures - O A Brynildsen
- 4-102-3 Proposal for Safety Codes for Load-Carrying Structures - Nordic Committee for Building Regulations
- 4-102-4 Comments to Proposal for Safety Codes for Load-Carrying Structures - Nordic Committee for Building Regulations
- 4-102-5 Extract from Norwegian Standard NS 3470 "Timber Structures"
- 4-102-6 Draft for Revision of CP 112 "The Structural Use of Timber" - W T Curry
- 8-102-1 Polish Standard PN-73/B-03150: Timber Structures; Statistical Calculations and Designing
- 8-102-2 The Russian Timber Code: Summary of Contents
- 9-102-1 Svensk Byggnorm 1975 (2nd Edition); Chapter 27: Timber Construction
- 11-102-1 Eurocodes - H J Larsen
- 13-102-1 Program of Standardisation Work Involving Timber Structures and Wood-Based Products in Poland
- 17-102-1 Safety Principles - H J Larsen and H Riberholt
- 17-102-2 Partial Coefficients Limit States Design Codes for Structural Timberwork - I Smith
- 18-102-1 Antiseismic Rules for Timber Structures: an Italian Proposal - G Augusti and A Ceccotti
- 18-1-2 Eurocode 5, Timber Structures - H J Larsen
- 19-102-1 Eurocode 5 - Requirements to Timber - Drafting Panel Eurocode 5
- 19-102-2 Eurocode 5 and CIB Structural Timber Design Code - H J Larsen
- 19-102-3 Comments on the Format of Eurocode 5 - A R Fewell
- 19-102-4 New Developments of Limit States Design for the New GDR Timber Design Code - W Rug and M Badstube
- 19-7-3 Effectiveness of Multiple Fastener Joints According to National Codes and Eurocode 5 (Draft) - G Steck
- 19-7-6 The Derivation of Design Clauses for Nailed and Bolted Joints in Eurocode5 - L R J Whale and I Smith
- 19-14-1 Annex on Simplified Design of W-Trusses - H J Larsen
- 20-102-1 Development of a GDR Limit States Design Code for Timber Structures - W Rug and M Badstube
- 21-102-1 Research Activities Towards a New GDR Timber Design Code Based on Limit States Design - W Rug and M Badstube
- 22-102-1 New GDR Timber Design Code, State and Development - W Rug, M Badstube and W Kofent
- 22-102-2 Timber Strength Parameters for the New USSR Design Code and its Comparison with International Code - Y Y Slavik, N D Denesh and E B Ryumina
- 22-102-3 Norwegian Timber Design Code - Extract from a New Version - E Aasheim and K H Solli
- 23-7-1 Proposal for a Design Code for Nail Plates - E Aasheim and K H Solli

- 24-102-2 Timber Footbridges: A Comparison Between Static and Dynamic Design Criteria - A Ceccotti and N de Robertis
- 25-102-1 Latest Development of Eurocode 5 - H J Larsen
- 25-102-1A Annex to Paper CIB-W18/25-102-1. Eurocode 5 - Design of Notched Beams - H J Larsen, H Riberholt and P J Gustafsson
- 25-102-2 Control of Deflections in Timber Structures with Reference to Eurocode 5 - A Martensson and S Thelandersson
- 28-102-1 Eurocode 5 - Design of Timber Structures - Part 2: Bridges - D Bajolet, E Gehri, J König, H Kreuzinger, H J Larsen, R Mäkipuro and C Mettem
- 28-102-2 Racking Strength of Wall Diaphragms - Discussion of the Eurocode 5 Approach - B Källsner
- 29-102-1 Model Code for the Probabilistic Design of Timber Structures - H J Larsen, T Isaksson and S Thelandersson
- 30-102-1 Concepts for Drafting International Codes and Standards for Timber Constructions - R H Leicester
- 33-102-1 International Standards for Bamboo – J J A Janssen
- 35-102-1 Design Characteristics and Results According to EUROCODE 5 and SNiP Procedures - L Ozola, T Keskküla
- 35-102-2 Model Code for the Reliability-Based Design of Timber Structures - H J Larsen
- 36-102-1 Predicted Reliability of Elements and Classification of Timber Structures - L Ozola, T Keskküla
- 36-102-2 Calibration of Reliability-Based Timber Design Codes: Choosing a Fatigue Model - I Smith

INTERNATIONAL STANDARDS ORGANISATION

- 3-103-1 Method for the Preparation of Standards Concerning the Safety of Structures (ISO/DIS 3250) - International Standards Organisation ISO/TC98
- 4-103-1 A Proposal for Undertaking the Preparation of an International Standard on Timber Structures - International Standards Organisation
- 5-103-1 Comments on the Report of the Consultation with Member Bodies Concerning ISO/TC/P129 - Timber Structures - Dansk Ingeniorforening
- 7-103-1 ISO Technical Committees and Membership of ISO/TC 165
- 8-103-1 Draft Resolutions of ISO/TC 165
- 12-103-1 ISO/TC 165 Ottawa, September 1979
- 13-103-1 Report from ISO/TC 165 - A Sorensen
- 14-103-1 Comments on ISO/TC 165 N52 "Timber Structures; Solid Timber in Structural Sizes; Determination of Some Physical and Mechanical Properties"
- 14-103-2 Comments on the CIB Structural Timber Design Code - R H Leicester
- 21-103-1 Concept of a Complete Set of Standards - R H Leicester

JOINT COMMITTEE ON STRUCTURAL SAFETY

- 3-104-1 International System on Unified Standard Codes of Practice for Structures - Comité Européen du Béton (CEB)
- 7-104-1 Volume 1: Common Unified Rules for Different Types of Construction and Material – CEB

37-104-1 Proposal for a Probabilistic Model Code for Design of Timber Structures - J Köhler, H Faber

CIB PROGRAMME, POLICY AND MEETINGS

1-105-1 A Note on International Organisations Active in the Field of Utilisation of Timber - P Sonnemans

5-105-1 The Work and Objectives of CIB-W18-Timber Structures - J G Sunley

10-105-1 The Work of CIB-W18 Timber Structures - J G Sunley

15-105-1 Terms of Reference for Timber - Framed Housing Sub-Group of CIB-W18

19-105-1 Tropical and Hardwood Timbers Structures - R H Leicester

21-105-1 First Conference of CIB-W18B, Tropical and Hardwood Timber Structures Singapore, 26 - 28 October 1987 - R H Leicester

INTERNATIONAL UNION OF FORESTRY RESEARCH ORGANISATIONS

7-106-1 Time and Moisture Effects - CIB W18/IUFRO 55.02-03 Working Party

INTERNATIONAL COUNCIL FOR RESEARCH AND INNOVATION
IN BUILDING AND CONSTRUCTION

WORKING COMMISSION W18 - TIMBER STRUCTURES

TENSILE STRENGTH OF NORDIC BIRCH

K H Solli

Norwegian Institute of Wood Technology

NORWAY

Presented by: K H Solli

M Ansell asked whether Weibull statistics were considered. Solli answered that it was not yet done. Y Chui asked about the gauge length and the EPI used. It was clarified that the gauge length was ~2 m following EN 1194 and the EPI was an Isocyanate based adhesive. A Jorissen received clarification that the moisture content of the specimens was 12%. H Blass asked about the cost of birch glulam compared to spruce glulam. Solli responded that the birch was more expensive but this product was intended for special structures.

TENSILE STRENGTH OF NORDIC BIRCH

Kjell Helge Solli, Norwegian Institute of Wood Technology

1. Introduction

Structural timber and timber structures are familiar concepts in Norway and the other Nordic countries. Traditionally, structural timber in the Nordic countries is equivalent to spruce (*Picea abies*) and/or pine (*Pinus sylvestris*). But sometimes other species are also used.

At the end of the 90s, a Norwegian church was built using structural birch glulam roof trusses. In 2000 a building, including an insurance company, was also erected using structural birch glulam. In both these structures birch was chosen for architectural reasons.

However, no characteristic strength or stiffness values existed, neither for structural birch nor for glulam made of birch. The designer presupposed that glulam made of birch had at least the same characteristic values as the corresponding values of glulam made of spruce. And at all critical details, such as mechanical joints, finger joints etc. the calculated coefficients of utilization were quite low.

Since the demand for structural birch in general, and structural birch glulam especially, increased, one decided to establish a project that could reveal some of the missing information.

This birch project had the following main goals

1. Define the basic parameters of two visual strength grades (laminations).
2. Determine the requisite characteristic strength and stiffness values which correspond to the two visual strength grades.
3. Prescribe a recommended finger geometry (based on tests).
4. Prescribe a recommended type of glue (based on tests).
5. Give an estimate (based on tests) of strength and stiffness of glulam beams produced according to the mentioned prescriptions.

This paper will present the first results from part 1 and 2.

2. Materials

The birch timber was from the following geographical areas:

- Southern part of Norway
- Middle part of Norway
- Southern part of Sweden
- Middle part of Sweden

These parts are considered as the most representative areas in Norway and Sweden regarding structural birch laminations.

The birch laminations were sawn at mills in Norway (2) and Sweden (3). After drying the laminations to a moisture content equal to 12 % and planing, the project ended up with the following sample:

30 mm x 150 mm x 2700 mm (300 laminations)
36 mm x 150 mm x 2700 mm (1200 laminations)

3. Data registration

The sample consisted of a random distribution of side boards, pit-side boards and heart planks. For every lamination the location of the pit and the location of knots and other (visual) defects were registered on a full size cross section scheme. The registration was done in the expected critical section. If failure occurred outside the expected critical section, a complete drawing of the true critical section was made during the testing procedure.

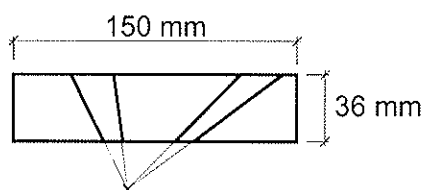


Figure 1. Example of registration on a cross section scheme

In addition to the pit and knots, the following features were also registered for each lamination:

- Thickness and width
- Annual ring width
- Slope of grain (both on face and edge)
- Curly grained wood
- Spike knot/top rupture
- Read heart
- Ring shakes
- Hard decay
- Rot
- Bark pocket
- Bark
- Wane (both on face and edge)
- Shakes
- Insect damage

4. Preliminary grading

To get a total view of the strength properties of Norwegian/Swedish birch laminations, it was important to have a representative distribution from low to high strength quality. The first step to reach this aim was to define two rough classes based on visual grading of knot sizes.

Class S

Knot sizes corresponding to the Nordic class ¹ T2 and better, i.e. T2 and T3.

In Class S the knots should be equal to or smaller than the following limitations:

- Edge: 1/2 of thickness
- Face: 1/4 of width, but max. 50 mm
- Knot cluster (length of 150 mm): Maximum sum of knots equal to largest permitted edge knot + largest permitted face knot

The laminations without any visual defects ("clear pieces") were mainly taken out of the sample. In practise, clear pieces of birch will be used for other products than structural birch glulam, e.g. knife handles, furniture etc. The strength and stiffness properties of the "clear pieces" would not contribute to the definition of the grading limitation, i.e. knot sizes etc.

Class L:

Knot sizes corresponding to the Nordic class T1 and lower, i.e. T1, T0 and Reject ².

In Class L the knots should be bigger than the given limitations of Class S.

The total birch lamination sample ended up with approx. 50 % in Class S and 50 % in Class L.

¹ INSTA 142 Nordic visual strength grading rules for timber [1]

² From "Reject" a small number of laminations with extreme defects were taken out of the sample.

5. Test method

- All birch glulam laminations were tested on tension parallel to the grain according to EN 408 [2] and EN 1194 [3].
- MOE was measured on two sides of the test specimen.
- Density and moisture content were recorded as close to failure as possible.
- If failure occurred outside the expected critical section, a complete drawing of the true critical section was made during the testing procedure.
- Each failure was photographed.
- The reason for failure was recorded in the lamination's data file.

5. Preliminary results

The results based on the “rough grading” in Class S (i.e. knots according to T2 and better) and Class L (i.e. knots with maximum diameter including T1) show that there is no problem in grading structural birch timber regarding tension strength.

However, it might be a problem to separate the corresponding high and low MOE, and it will indeed be a problem to grade high and low density by visual methods.

		Class L	Class S	D30	D35	D50
Tension strength						
f_{t0} -mean	N/mm ²	40,0	51,0			
Std	N/mm ²	11,1	11,9			
CoV	%	27,8	23,3			
$f_{t0,05}$	N/mm ²	21,1	30,8	18,0	21,0	30,0
Modulus of Elasticity						
E_{t0} -mean	N/mm ²	13 300	14 100	10 000	10 000	14 000
Std	N/mm ²	3 115	1 980			
CoV	%	23,4	14,0			
$E_{t0,05}$	N/mm ²	8 030	10 750	8 000	8 700	11 800
Density						
ρ_{mean}	kg/m ³	620	627	640	670	780
Std	kg/m ³	42,9	46,8			
CoV	%	6,9	7,5			
ρ_k	kg/m ³	550	550	530	560	650

Table 1. Results ³ from tension tests of birch laminations compared with requirements for D30, D35 and D50 (hardwood species) stated in EN 338.

The results show that Class L and Class S, based on the “rough” grading, meets the requirements of respectively D35 and D50 regarding the (preliminary) characteristic tension strength value and mean value of MOE.

However, if the above stated values should become the conclusion of this project, birch lamination from Norway and Sweden graded in Class L and Class S would be assigned to D30 because of the characteristic value of density.

Figure 2 and 3 show typical failures in knots. Figure 4 shows a failure caused by the slope of grain. The dark lines on the specimens define the Critical Section.

³ The results given in Table 1 are based on about 500 pieces



Figure 2. Tension failure at Critical Section in lamination no. L11131 (36 mm x 151 mm)
Tension stress at failure: $f_{t,0} = 65,7 \text{ N/mm}^2$



Figure 3. Tension failure at Critical Section in lamination no. L11159 (36 mm x 153 mm)
Tension stress at failure: $f_{t,0} = 57,2 \text{ N/mm}^2$

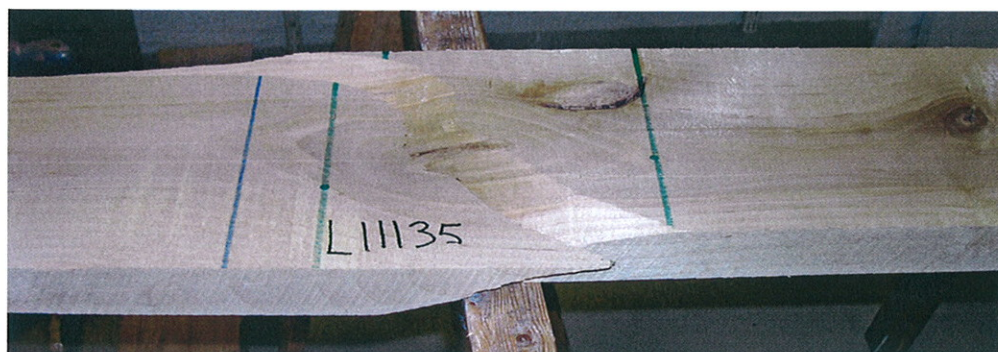


Figure 4. Tension failure at Critical Section in lamination no. L11135 (36 mm x 151 mm)
Tension stress at failure: $f_{t,0} = 14,4 \text{ N/mm}^2$

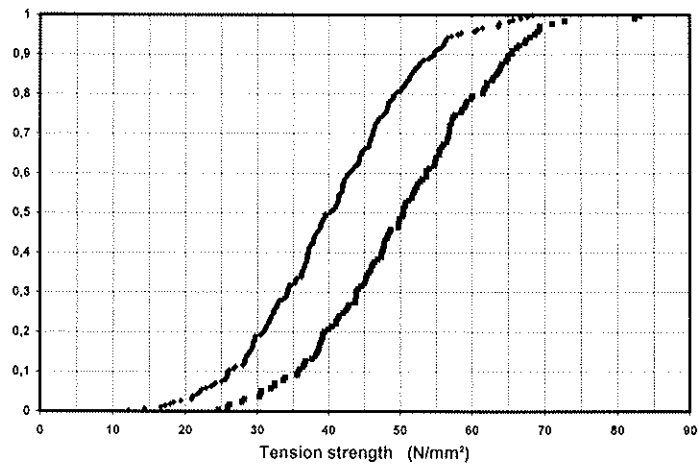


Figure 5. Cumulative distribution of Class L and Class S, Tension strength.

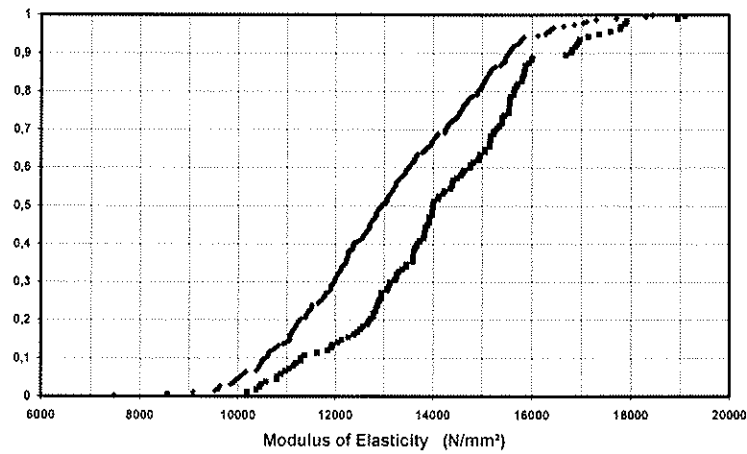


Figure 6. Cumulative distribution of Class L and Class S, MOE.

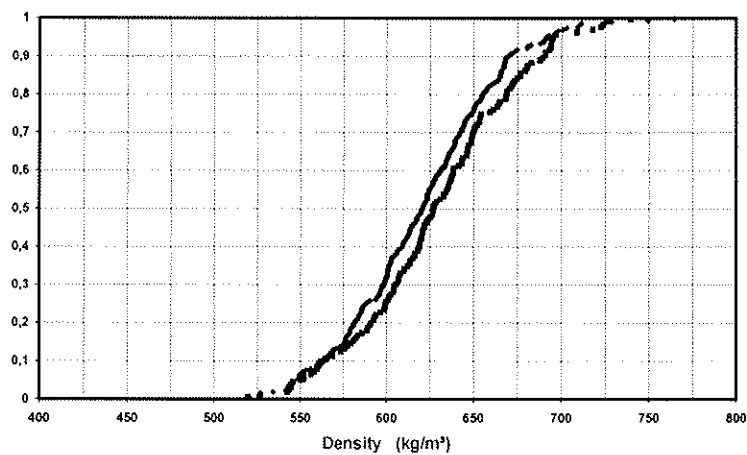


Figure 7. Cumulative distribution of Class L and Class S, Density.

Figure 5, 6 and 7 show in a very clear way that tension strength MOE easily can be separated in (strength) classes. MOE is also quite well separated. Density is not separated in the two classes.

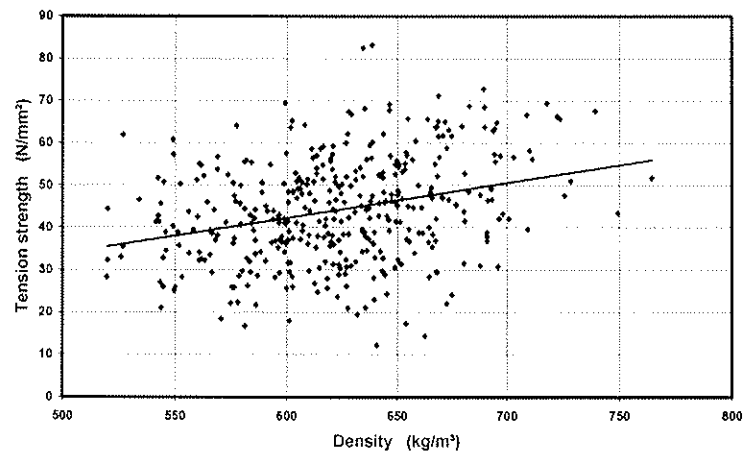


Figure 8. Correlation between density (X) and tension strength (Y).

$$f_{t,0} = 0,08 \cdot \rho - 7,8 \quad (R^2 = 0,09)$$

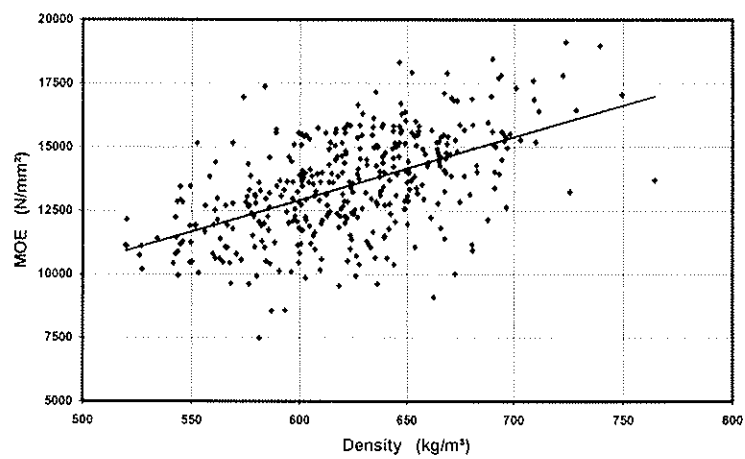


Figure 9. Correlation between density (X) and MOE (Y).

$$MOE = 24,8 \cdot \rho - 1963 \quad (R^2 = 0,30)$$

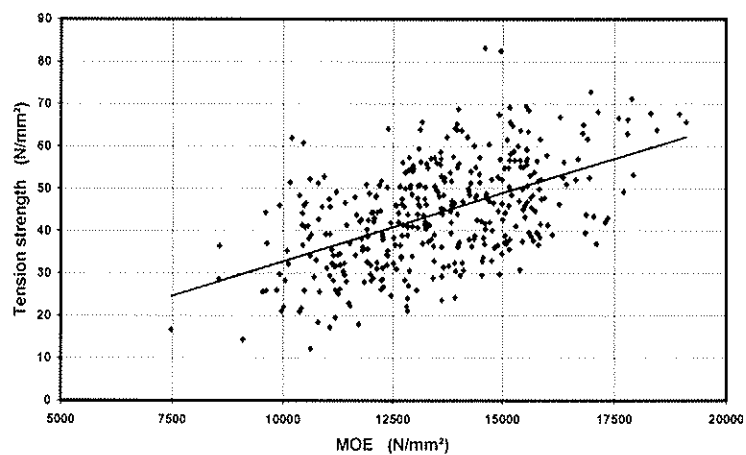


Figure 10. Correlation between MOE (X) and tension strength (Y).

$$f_{t,0} = 3,2 \cdot 10^{-3} \cdot MOE - 0,5 \quad (R^2 = 0,28)$$

6. Simulated strength grading

Since a large amount of data is recorded for each piece, it is possible to simulate grading based on other conditions than those who generated Class L and Class S.

Table 2 shows the results from the grading classes T3, T2 and T1, defined in INSTA 142, based on simulated grading.

		T3	T2	T1	T1+T2
Tension strength		(45 %)	(37 %)	(18 %)	(55 %)
$f_{t0\text{-mean}}$	N/mm ²	53,0	42,0	36,8	40,3
Std	N/mm ²	9,1	9,8	9,0	9,8
CoV	%	17,2	23,4	24,4	24,3
$f_{t0,05}$	N/mm ²	36,7	24,2	19,7	23,1
Modulus of Elasticity					
$E_{t0\text{-mean}}$	N/mm ²	15 130	13 015	12 270	12 920
Std	N/mm ²	1 650	2 055	2 030	2 040
CoV	%	10,9	15,8	16,0	15,8
$E_{t0,05}$	N/mm ²	12 175	9 300	8 860	9 360
Density					
ρ_{mean}	kg/m ³	630	630	625	630
Std	kg/m ³	48,0	46,0	42,0	45,0
CoV	%	7,6	7,1	6,6	7,1
ρ_k	kg/m ³	550	555	555	555

Table 2. Results from simultaneous grading of the Nordic classes T3, T2 and T1

By grading in the two classes T3 and T1+T2, the yield will be approximately the same in both classes.

Both the characteristic value of the tension strength and the mean value of MOE of T3 exceed the requirements given to D60.

Both the characteristic value of the tension strength and the mean value of MOE of T1+T2 exceed the requirements given to D35.

However, the density is still the weakest link in this combination. The visual grading rules defined in INSTA 142 do not separate the different levels of density regarding birch. All the different grade combinations (T3, T2, T1 and T1+T2) give the same results of both mean and characteristic density.

7. Conclusion

The results from the tension tests of birch laminations show that birch grown in Norway and Sweden can effectively be graded regarding tension strength and stiffness by the Nordic rules of visual strength grading, INSTA 142.

The consequences of such visual grading might be

- a characteristic tension strength value of T3 between 35 and 40 N/mm².
- a corresponding mean MOE value of approximately 15000 N/mm².
- a characteristic tension strength value of T1+T2 between 20 and 24 N/mm².
- a corresponding mean MOE value of approximately 13000 N/mm².

However, the visual grading based on INSTA 142 do not separate the different density levels.

The D classes given in EN 338 do not correspond to structural birch grown in Norway and Sweden because of the density requirements.

The conclusion of this will be one of the two following alternatives.

- a) Due to the density properties of Nordic grown birch laminations, all laminations that meet the requirements of the grading classes T1, T2 and T3 defined in INSTA 142, can be assigned to strength class D30 in EN 338.
- b) Due to the density properties of Nordic grown birch laminations, it is not reasonable to classify the birch laminations in the standardised strength classes given in EN 338. Instead a set of special classes will be generated in accordance to the rules given in EN 408, EN 1194, EN 384 [4] and prEN 14081-1 [5].

Postscript

The final results and recommendation will be available when all the testing (i.e. laminations, finger joints and glulam beams), calculations and evaluations are finished.

References

- [1] INSTA 142 Nordic visual strength grading rules for timber (1997)
- [2] EN 408 Timber structures – Structural timber and glued laminated timber – Determination of some physical and mechanical properties (2003)
- [3] EN 1194 Timber structures – Glued laminated timber – Strength classes and determination of characteristic values (1999)
- [4] EN 384 Structural timber – Determination of characteristic values of mechanical properties and density (1995)
- [5] prEN 14081 Timber structures – Strength graded structural timber with rectangular cross section – Part 1: General requirements

INTERNATIONAL COUNCIL FOR RESEARCH AND INNOVATION
IN BUILDING AND CONSTRUCTION

WORKING COMMISSION W18 - TIMBER STRUCTURES

EFFECT OF TEST PIECE ORIENTATION ON CHARACTERISTIC
BENDING STRENGTH OF STRUCTURAL TIMBER

P Glos

J K Denzler

Holzforschung München

GERMANY

Presented by J Denzler

H Blass commented this study used knots as grading parameter and asked if it is possible that other grading parameters can determine the grade; if so, how to determine the tension versus compression edge. One such example is the slope of grain. P Glos explained that knots rather than slope of grain tend to be the dominant failure mode. F Lam commented experience in UBC of larger timber cross sections showed slope of grain failures were also commonly noted. K Crews commented the approach of random orientation is used in Australia because other parameters such as slope of grain can determine the grade. B Källander commented this issue depends on sawing pattern.

J Köhler wondered how to quantify the gain in testing efficiency by having a more accurate method compared to the possible loss of the industry from having lower characteristic values.

Effect of Test Piece Orientation on Characteristic Bending Strength of Structural Timber

P. Glos, J.K. Denzler

Holzforschung München, Germany

1 Introduction

Characteristic strength and stiffness values for structural sawn timber shall be determined according to EN 384 on the basis of tests carried out in accordance with EN 408. In bending tests the test piece shall be positioned with the critical section between the load points and the tension edge shall be selected at random. The random orientation of the test piece is intended to simulate the real situation in a structure. However, this is not the most economic way to determine the 5-percentile value of the bending strength, as in this case more pieces than required have to be tested to determine the 5-percentile value with a given degree of accuracy. This is due to the fact, that pieces with the critical defect at the compression edge will usually exhibit a higher bending strength than a similar piece with the critical defect at the tension edge. Therefore it might be more economic to concentrate on tests where the test piece is oriented systematically with the critical defect at the tension edge.

This paper investigates the effect of the orientation of the test pieces and analyses which bending strength percentile value of a sample tested systematically with the critical defect at the tension edge corresponds to the 5-percentile value of a sample with random orientation of the test pieces.

2 Theoretical Considerations

A sample of size $2 \cdot n$ with random orientation of the test pieces can be assumed to consist of a sub-sample 1 of size n with the critical defect at the tension edge and a second sub-sample 2 of size n with the critical defect at the compression edge. Figure 1 outlines the test configuration of both samples; Figure 2 shows the hypothetical frequency distribution.

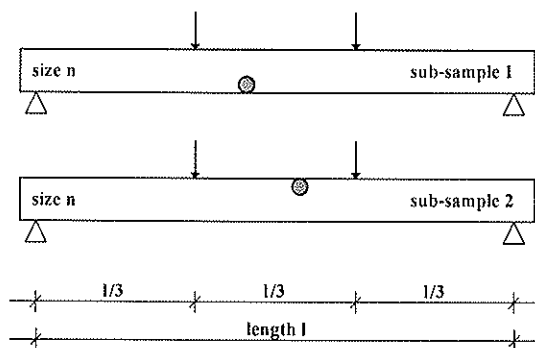


Fig. 1: Test configuration of a fictitious sample.

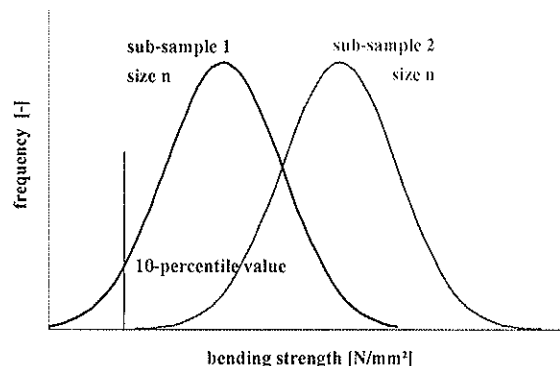


Fig. 2: Frequency distribution of the fictitious sub-samples.

Assuming that the weakest piece of sub-sample 2, i.e. the sub-sample with the critical defect at the compression edge, has a higher bending strength than the 10 % weakest pieces of sub-sample 1, i.e. the sub-sample with the critical defect at the tension edge, the 5-percentile bending strength value of the total sample would be equivalent to the 10-percentile value of sub-sample 1. As there is a probability that some pieces of sub-sample 2 might be weaker than 90 % of sub-sample 1, a percentile value of sub-sample 1 above 5 and below 10 percent might be an appropriate conservative guess of the 5-percentile value of the random sample.

In order to investigate this relationship 609 bending tests of Sitka Spruce and 164 bending tests of Norway spruce were analysed. This paper presents the results of this investigation and wants to start a discussion about an amendment to EN 384.

2 Material and Methods

The results of bending tests from 3 different projects were used in this investigation. Sample 1 consisted of 609 pieces of Sitka spruce (*Picea sitchensis*), machine graded to strength class C 16. Sample 2 consisted of 61 pieces of Norway spruce (*Picea abies*) visually graded to S 10 according to DIN 4074 which corresponds to C 24. Sample 3 consisted of 103 ungraded pieces of Norway spruce (*Picea abies*).

The cross-sections of the test pieces ranged from 38 x 75 mm² to 75 x 225 mm² (see Table 2). Table 1 shows the mean strength, stiffness and density values as well as the 5-percentile bending strength of the 3 samples.

All knots of the test pieces between the inner load points were measured. Knot size was calculated as total knot area ratio (total KAR) and margin knot area ratio (margin KAR). Total KAR is the ratio of the sum of projected cross sectional areas of all knots within 15 cm piece length to the total cross-sectional area of the piece. Margin KAR is the ratio of the sum of the projected cross-sectional areas of all knots or portions of knots within 15 cm piece length in a margin at the compression or tension edge, where the margin occupies one-quarter of the total cross-sectional area of the piece (see Figure 3).

Tab. 1: Strength, stiffness and density of test pieces.

sample no.	species	no.	bending strength			MOE	density	strength
			$f_{m,mean}$	COV	$f_{m,k}$	$E_{0,mean}$	ρ_{mean}	class
[-]	[-]	[-]	[N/mm ²]	[-]	[N/mm ²]	[N/mm ²]	[kg/m ³]	[-]
1	Sitka spruce	609	30.4	30 %	16.1	8 555	404	C 16
2	Norway spruce	61	45.7	24 %	26.0	12 453	439	C 24
3	Norway spruce	103	40.4	33 %	21.1	12 210	457	ungraded

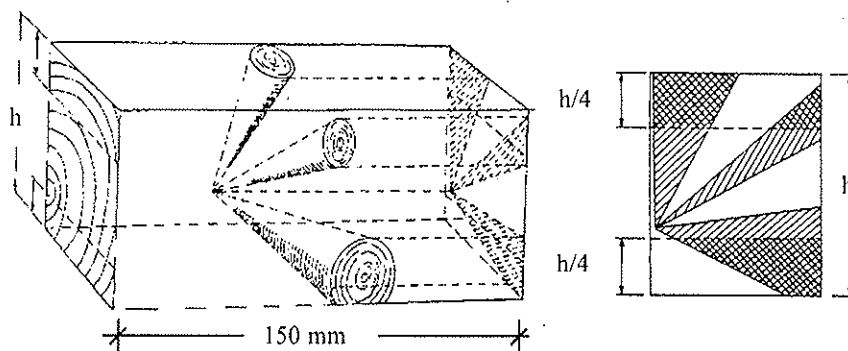


Fig. 3: Calculation of Knot Area Ratios: total KAR and margin KAR.

Based on the measured knot sizes all samples were divided into 2 sub-samples: one sub-sample comprised all pieces with the maximum margin KAR at the tension edge. The other sub-sample comprised all pieces with the maximum margin KAR at the compression edge. The number of pieces in these two sub-samples is given in Table 2, separated for each sample and each cross-section.

Table 2 shows that in all samples the requirement of random orientation was met, as the maximum margin KAR was equally distributed over the tension and compression edge.

In the following analysis the bending strength percentile values of two different samples were compared: the “random samples”, comprising all pieces of each group, e.g. 609 pieces of sample no.1 and the “oriented samples”, comprising the pieces with the maximum margin KAR at the tension edge, e.g. 295 pieces of sample no.1 (see Table 2).

The percentile values were determined non-parametric according to EN 384 clause 5.3.1.

Tab. 2: Assignment of specimens into sub-groups of cross-sections and test piece orientation.

sample no. [-]	species [-]	cross-section [mm ²]	number of specimens		
			total [-]	with margin KAR at the tension edge [-]	compression edge [-]
1	Sitka spruce	38 x 75	96	40	56
		38 x 100	51	27	24
		47 x 100	97	48	49
		47 x 150	102	48	54
		47 x 250	55	24	31
		75 x 100	54	30	24
		75 x 150	54	23	31
		75 x 225	100	55	45
		total	609	295	314
2	Norway spruce	38 x 89	20	9	11
		38 x 140	21	12	9
		38 x 183	20	10	10
		total	61	31	30
3	Norway spruce	50 x 175	103	49	54
		total	103	49	54
			773	375	398

4 Results

4.1 Sitka spruce

Random samples and oriented samples were formed separate for each cross-section. As an example, the random sample of pieces with cross-section 38 x 75 mm² comprised 96 pieces and the oriented sample comprised 40 pieces (see Table 2). For each random sample the 5-percentile strength value was calculated according to EN 384. The values are given in Table 3. For each oriented sample 5-, 6-, 7-, 8-, 9- and 10-percentile strength values were calculated following the method given in EN 384. Figure 4 shows for each cross-section the deviation between the 5-percentile strength value of the random sample and the 5- to 10-percentile values of the oriented sample.

Figure 5 shows the deviation between the characteristic strength value of the random sample ($n = 609$) and the percentile values of the corresponding oriented sample ($n = 295$) both determined as the weighted mean of the percentile values of the 8 sub-samples.

Figure 5 shows that the 7.5-percentile of the oriented sample corresponds best to the 5-percentile value of the random sample. Figure 4 shows that in 6 out of 8 cases the 7.5-percentile of the oriented sample is conservative in relation to the 5-percentile value of the random sample. In two cases (sub-samples 47 x 100 mm² and 38 x 75 mm²) the values are non-conservative, but the deviation from the 5-percentile value of the corresponding random sample does not exceed the variation of the 5-percentile values of the 8 random samples (see Table 3).

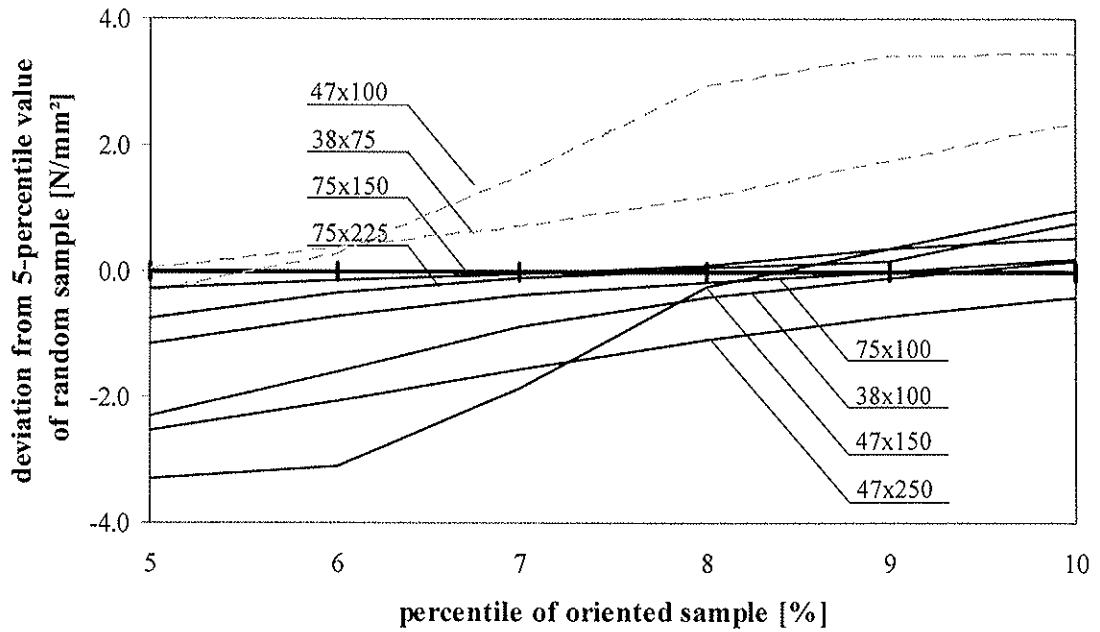


Fig. 4: Sample no. 1: Deviation of 5- to 10-percentile strength values of oriented samples from 5-percentile strength value of random sample separated for each cross-section.

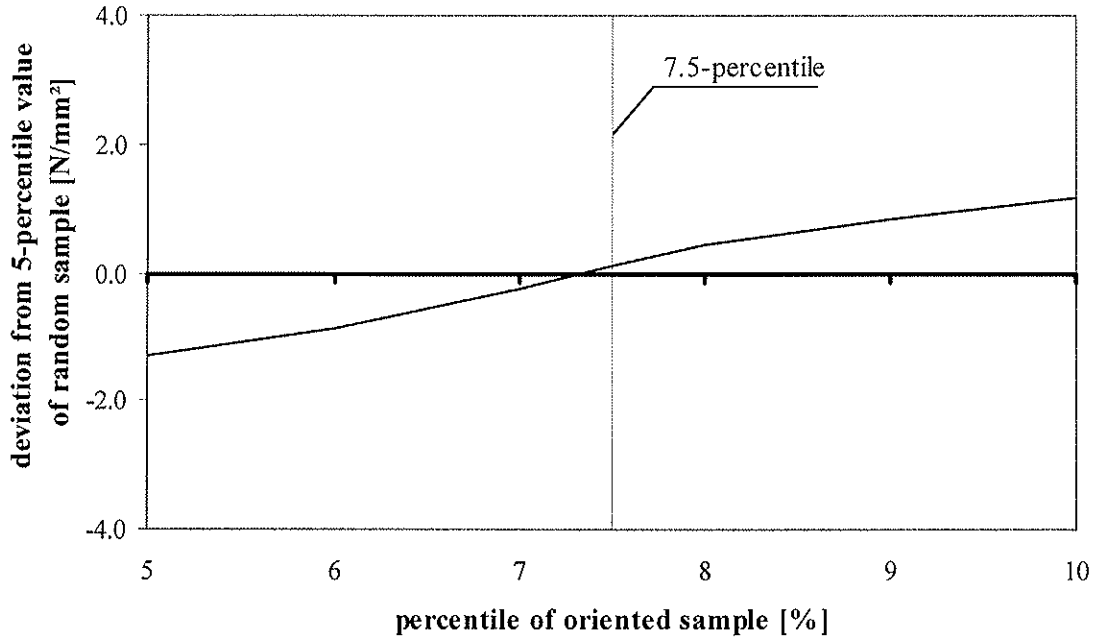


Fig. 5: Sample no. 1: Deviation of 5- to 10-percentile strength values of oriented sample ($n = 295$) from characteristic strength value of random sample ($n = 609$).

Tab. 3: Sample no. 1: 5-percentile values of random samples in comparison to 7.5-percentile values of oriented samples.

		percentile	height [mm]				
			75	100	150	225	250
width [mm]	38	5 th	16.3	17.2			
		7.5 th	17.2	16.5			
	47	5 th		15.3	18.5		15.8
		7.5 th		17.5	17.5		14.5
	75	5 th		16.7	13.4	14.7	
		7.5 th		16.4	13.4	14.7	

4.2 Norway spruce

Two different samples of Norway spruce were analysed. Sample no. 2 comprised 61 pieces with 3 different cross-sections (see Table 2). Due to the small number of pieces these could not be analysed separately for each cross section. Therefore only the random sample comprising all 61 pieces and the oriented sample comprising all 31 pieces with the maximum margin KAR at the tension edge were compared.

The result is shown in Figure 6: The 5-percentile strength value of the random sample is 26.0 N/mm². The 5-, 6-, 7-, 8-, 9- and 10-percentile strength values of the oriented samples range from 19.4 N/mm² to 30.0 N/mm². The 8.5-percentile value of the oriented sample corresponds best to the 5-percentile value of the random sample. Hence, in this case the 7.5-percentile value of the oriented sample is a conservative estimate.

Sample no. 3 comprised 103 pieces of 1 cross section. The oriented sub-sample with the maximum margin KAR at the tension edge comprised 49 pieces. In Figure 7 the 5-percentile strength value of the random sample (21.1 N/mm²) is compared with the 5-, 6-, 7-, 8-, 9- and 10-percentile strength values of the oriented sample.

Figure 7 shows that in this case the 8.5-percentile value corresponds best to the 5-percentile value of the random sample. The 7.5-percentile value is a conservative estimate.

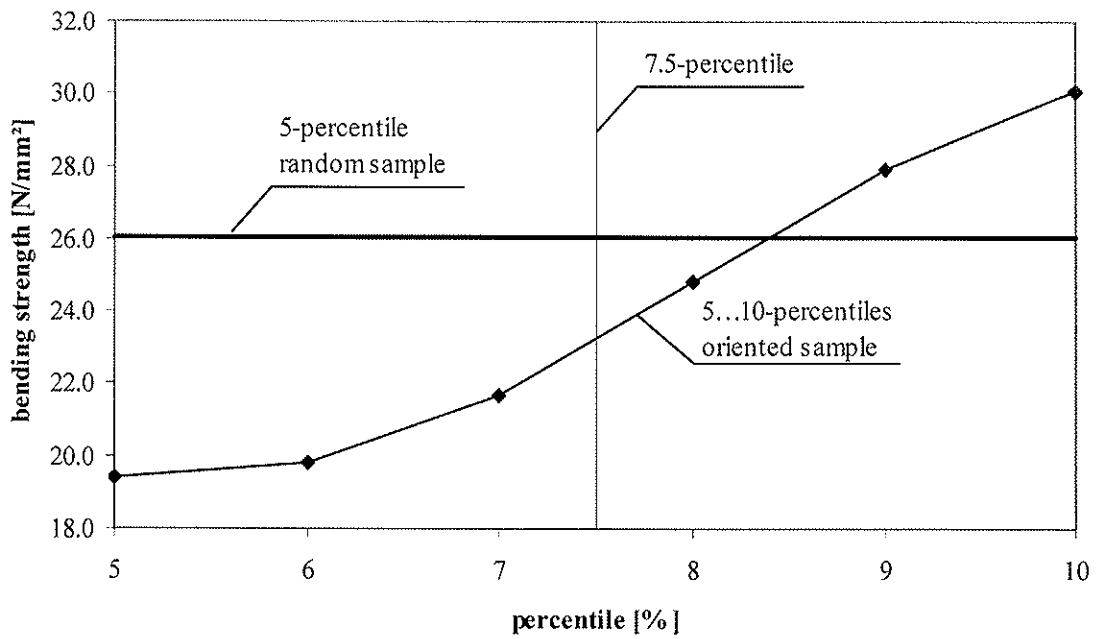


Fig. 6: Sample no. 2: Comparison of 5-percentile strength value of random sample with 5- to 10-percentile strength values of oriented sample.

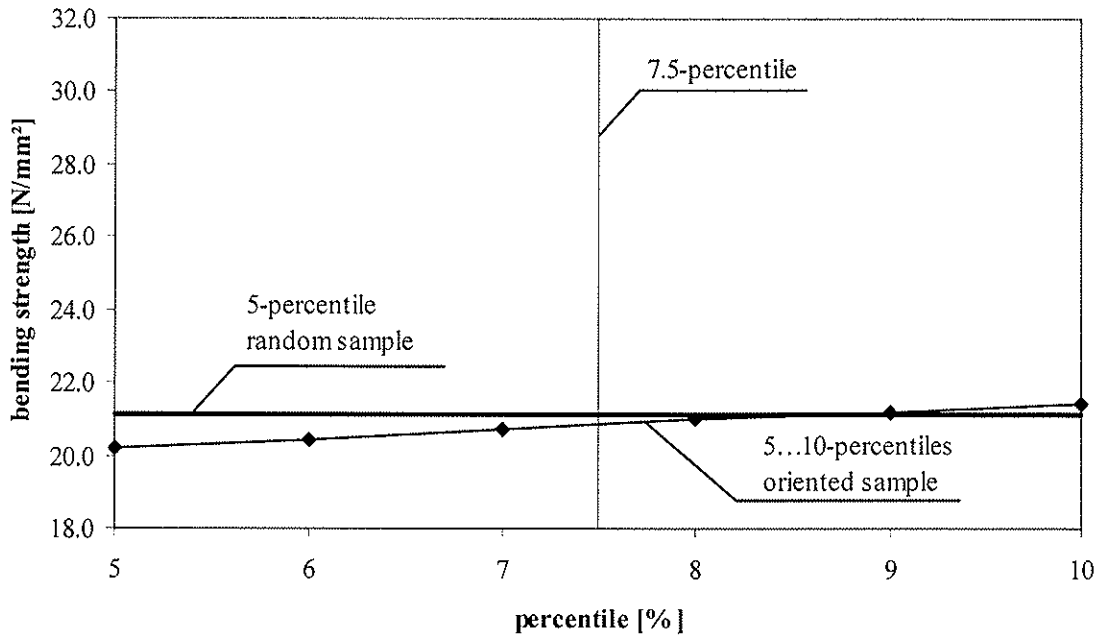


Fig. 7: Sample no. 3: Comparison of 5-percentile strength value of random sample with 5- to 10-percentile strength values of oriented sample.

5 Conclusions

According to EN 384 bending tests shall be carried out as follows: The test piece shall be positioned with the critical section between the inner load points and the tension edge shall be selected at random.

The analysis of 3 samples comprising 2 different species has shown that the 5-percentile bending strength value of a sample of structural sawn timber with random orientation of the pieces in the bending test corresponds to the 7.5-percentile strength value of a sample where the critical defect, i.e. the maximum margin knot area, is generally located at the tension edge of the pieces.

From this follows that based on the same amount of test pieces characteristic strength values can be determined with a higher degree of accuracy or that less test pieces are required to determine characteristic strength values with the same degree of accuracy when the tests are always carried out with the critical defect at the tension edge.

However, the relationship between the percentile strength values of “random” and “oriented” samples depends on wood quality. The effect of the orientation may get smaller the higher the strength class of the timber. So far the results cover structural sawn timber up to strength class C 24. Research to investigate this relationship for timber of higher strength classes is underway.

7 Summary

Based on the results of 773 bending tests of structural sawn timber (*Picea sitchensis* and *Picea abies*) from 3 different projects the effect of test piece orientation, i.e. random orientation or testing with the critical defect at the tension edge, was investigated.

This study showed that the characteristic bending strength value of a sample with random orientation is equivalent to the 7.5-percentile strength value of a sample whose pieces are generally oriented with the critical defect at the tension edge.

So far this result is limited to timber up to strength class C 24. Research to verify this relationship for timber belonging to strength classes above C 24 is underway.

8 Literature

- [1] EN 384: 2004-01
Structural timber – Determination of characteristic values of mechanical properties
- [2] EN 408: 2003-08
Timber structures – Structural timber and glued laminated timber – Determination of some physical and mechanical properties.

INTERNATIONAL COUNCIL FOR RESEARCH AND INNOVATION
IN BUILDING AND CONSTRUCTION

WORKING COMMISSION W18 - TIMBER STRUCTURES

STRENGTH AND STIFFNESS BEHAVIOUR OF BEECH LAMINATIONS
FOR HIGH STRENGTH GLULAM

P Glos

J K Denzler

P W Linsenmann

Holzforschung München

GERMANY

Presented by J Denzler

A Jorissen received clarification that the number 1064 in the graphs referred to the specimen number and constant moisture content was used in the tests.

H J Larsen received clarification that Beech is typically not used as structural member because of durability reason. He also questioned the possible application of this work as EN1194 did not refer to nonlinear stress strain laws. P Glos responded that more hard wood will be available in the near future. This project tried to find ways to use more hardwood from an economical aspect. It is part of a joint project between Munich and Karlsruhe to develop design procedures for introduction to EN 1194. H J Larsen further commented that durability should be examined carefully and EN 1194 is based on fitting of results and not on a theoretical model. He would look forward to seeing a proposal based on modelling.

B Zhang received clarification that displacement control tests were performed. Denzler clarified that the smoothness of the bilinear model was based on fitting to the test results and the glue in the fingerjoint was phenol-resorcinol based.

Strength and Stiffness Behaviour of Beech Laminations for High Strength Glulam

P. Glos, J.K. Denzler, P.W. Linsenmann
Holzforschung München, Germany

1 Introduction

The European Standard EN 1194 specifies a system of strength classes and gives characteristic values for structural glued laminated timber. This standard is currently limited to softwood glued laminated timber.

The objective of this paper is to widen the scope of the glulam standard EN 1194 in order to include glulam made of beech (*Fagus silvatica*). Glued laminated timber made of beech laminations has a potential for significantly higher strength and stiffness properties than traditional glulam made of softwood laminations. As a basis for modelling the strength and stiffness properties of glued laminated timber made of beech the stress-strain relationship of solid and finger-jointed beech lamination elements loaded in tension and compression was investigated. The element length is 150 mm. The stress-strain-relationship of each element is described as a function of the characteristics density and knot size or density and finger-joint respectively (Figure 1). Moreover, the density and knot size variation within and between boards was determined.

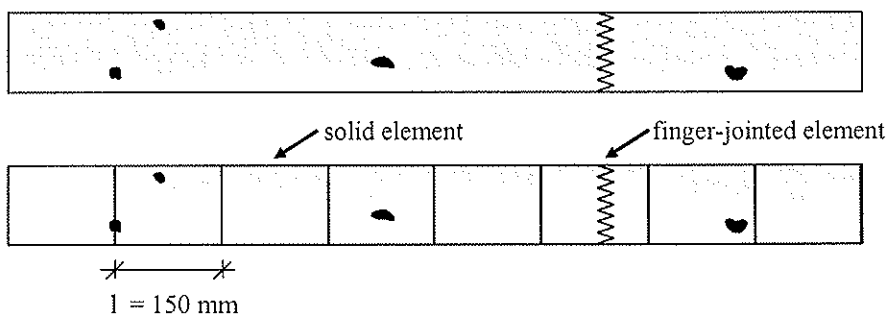


Fig. 1: Modelling of a beech lamination by 150 mm long elements.

2 Material and Methods

350 beech boards with four cross-sections (25x100, 35x100, 25x150 and 35x150 mm²) were collected at random in a hardwood sawmill after creaming off premium boards for joinery. The boards were free of pith. Their length varied from 3500 to 5000 mm. The boards were kiln-dried to a target moisture content of 12 %. Density of the boards and of individual elements was determined according to ISO 3131. Knot size was calculated as total knot area ratio (KAR), i.e. the ratio of the sum of projected cross-sectional areas of all knots within 15 cm board length to the total cross-sectional area of the board.

After measuring each board's density and knots along the board length the total amount of 350 boards was divided into two sub-samples: Sub-sample 1 consisted of 20 boards to investigate the within board variation of density and compression strength and of 30 boards to investigate the within board variation of tensile strength. Sub-sample 2 included 300 boards to determine the strength and stiffness behaviour.

3 Results

3.1 Variation of knot size and density between and within boards

To investigate the knot variation between and within boards the knots of 350 boards were measured. The boards were virtually divided into 150 mm long elements and the knot area ratio (KAR) of each element was calculated. Figure 2 shows the distribution of KAR in 9079 elements. In 94.6 % the KAR values are smaller than or equal to 0.1. This shows that there are less and smaller knots in these boards as compared to spruce boards.

Additionally the variation of knot sizes within each board was analysed. Figure 3 shows the probability of appearance of the size of KAR in an element as dependent on the KAR value of the previous element in the same board.

Figure 4 shows the variation of density within 5 boards. The distribution of the mean density of 350 boards is shown in Figure 5. The within board density variation of 20 boards is shown in Figure 6. This Figure shows the deviation of the density of individual 200 mm long sections within a board from the mean density of the corresponding board. Here a section length of 200 mm instead of 150 mm was chosen because these sections should additionally be used for compression tests and these required a test piece length of 200 mm (see Figures 7 and 8).

3.2 Strength and stiffness values of solid and finger-jointed elements

Four different types of test pieces were produced from 300 boards: Solid elements for compression and tension tests and finger-jointed elements for compression and tension tests (see Figure 7). The geometry of the compression and tension specimens is shown in Figure 8. The dotted lines define the area for the MOE measurement. The element length is extended to 200 mm to insure an undistributed deformation reading for the MOE measurement and to be able to fix the deformation gauge. The total length of a tension specimen includes two 300 mm long clamping areas necessary to introduce the tension force.

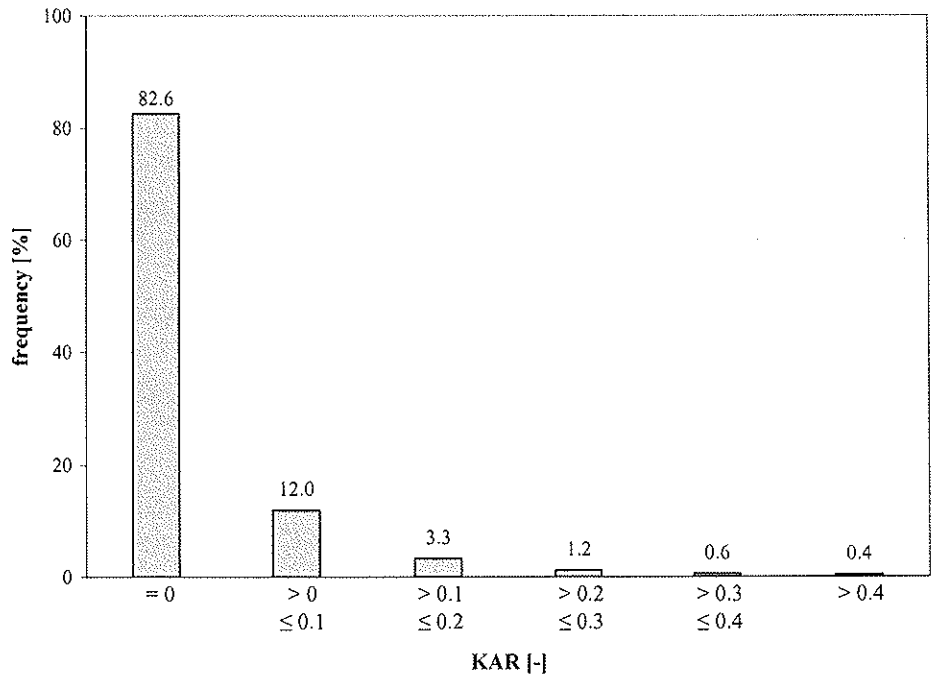


Fig. 2: Knot size distribution (KAR) in 9079 elements of length $l = 150$ mm in 350 boards.

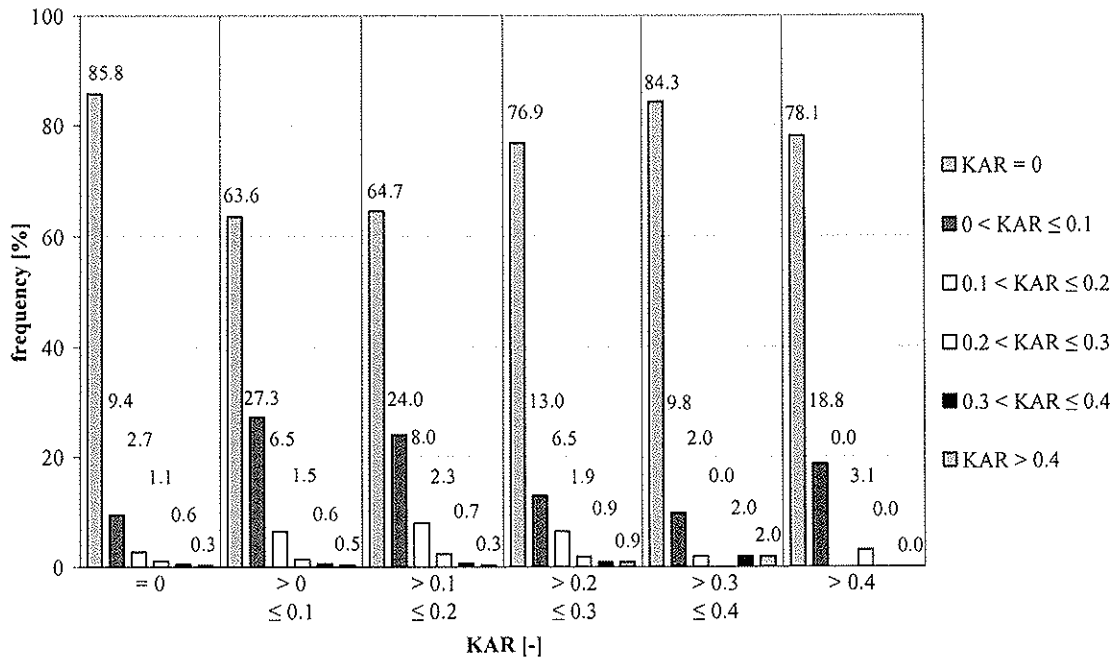


Fig. 3: Probability of appearance of knot area ratio (KAR) in an element as dependant on the KAR value of the previous element, $n = 350$ boards; 9079 elements, length $l = 150$ mm.

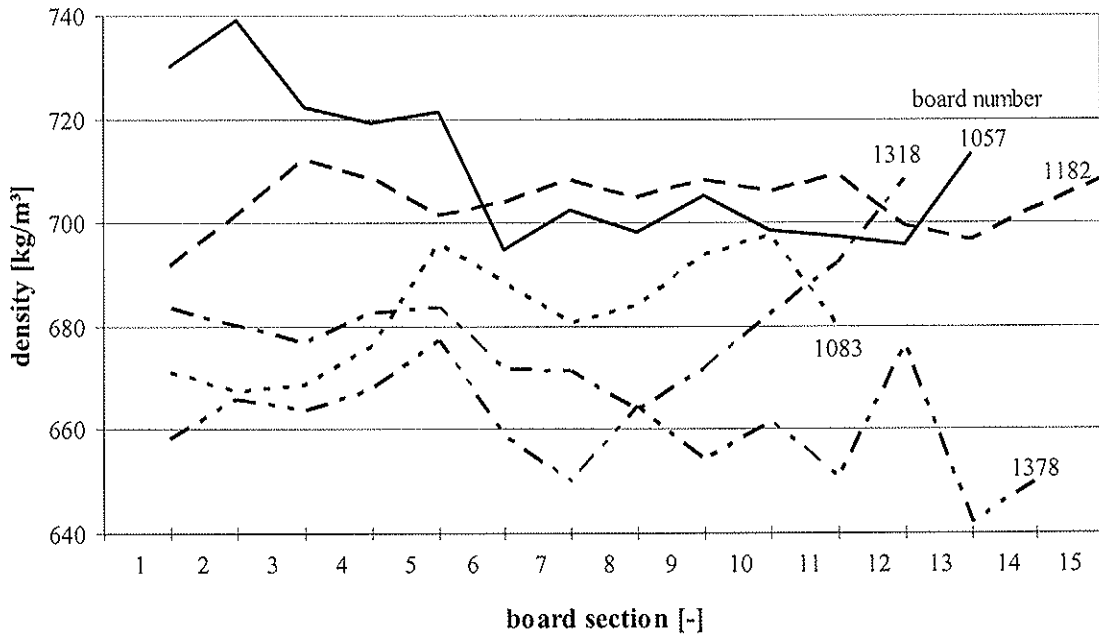


Fig. 4: Density variation within a board, $n = 5$ boards, section-length $\ell = 200$ mm.

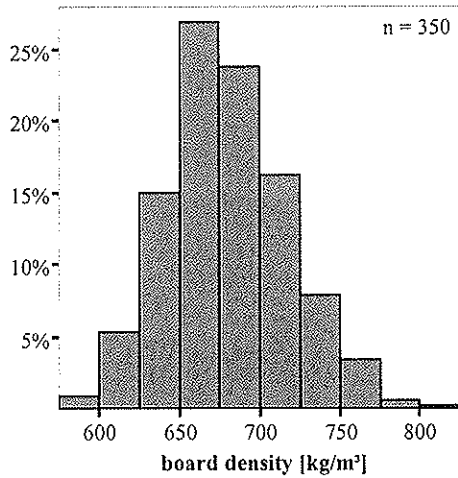


Fig. 5: Density distribution of $n = 350$ boards.

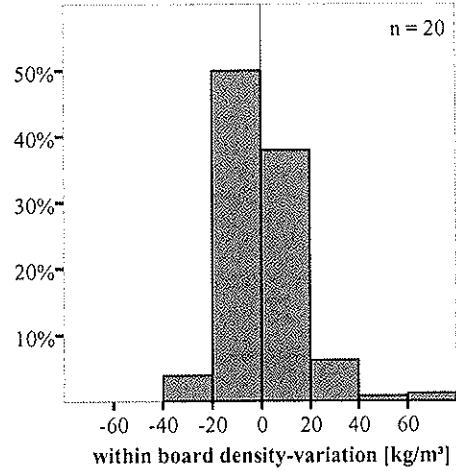


Fig. 6: Within board density variation, $n = 20$ boards, length $\ell = 200$ mm.

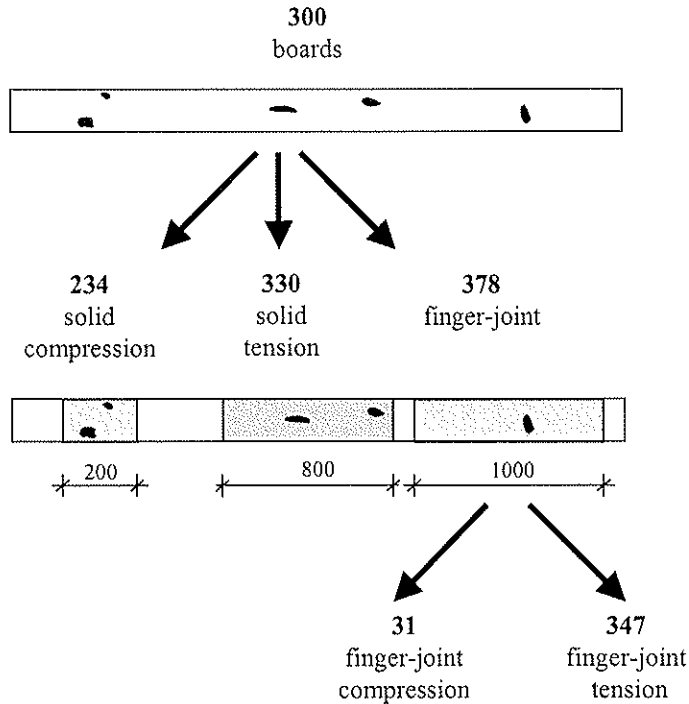


Fig. 7: Preparing of specimens for compression and tension tests from 300 boards of sub-sample 2.

The finger-jointed specimens were produced as follows: 1000 mm long sections were cut out from the boards, ensuring that 100 mm along both ends of the section were free of knots. These sections were finger-jointed in a commercial glulam plant in a random order using a profile 15x3.8 mm and the adhesive “Kauramin 681/Hardener 686” (see Figure 9). From this finger-jointed lamination tension and compression specimens with the same geometry as the solid specimens shown in Figure 8 were cut out. In total 234 solid compression and 330 solid tension specimens and 31 finger-jointed compression and 347 finger-jointed tension specimens were produced from 300 boards.

Table 1 shows the compression and tension test results of the solid elements. Mean values and standard deviation of strength, MOE, density and knot size are given for all 234 compression and 330 tension specimens as well as for the 66 compression and 102 tension specimens that were free of knots (KAR=0). Table 2 summarizes the results of the finger-jointed test pieces.

The results in Table 1 show the significant effect of knots on tension strength. The comparison of the results in Table 2 with these in Table 1 show that on average the compression and tension strength of finger-jointed elements is similar to that of solid elements, whereas MOE of finger-jointed elements is about 15 % higher than that of solid elements. In comparison to knot free solid elements the tensile strength of finger-jointed elements is only 2/3, whereas MOE is nearly the same. From this follows that finger-joints are “critical sections” of glulam laminations similar to what it is well known from softwood laminations. This must be taken into account when establishing requirements for end joints of hardwood laminations.

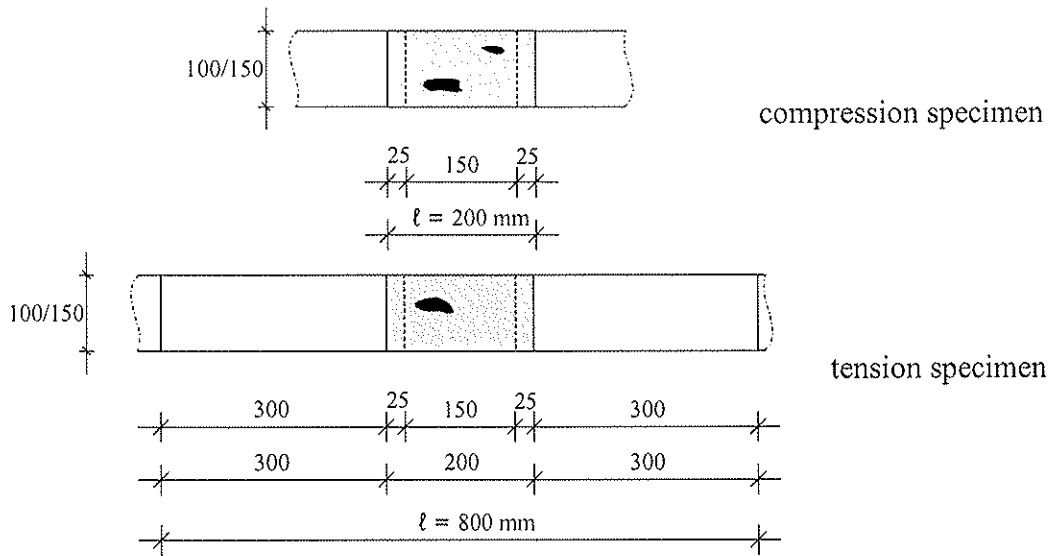


Fig. 8: Specimen geometry for compression and tension tests.

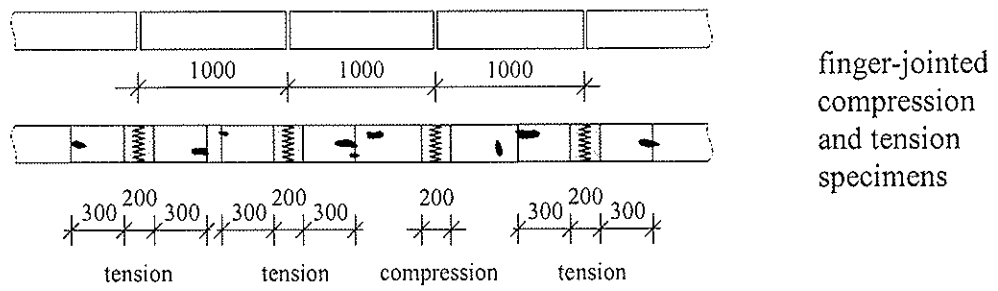


Fig. 9: Specimen geometry for compression and tension finger-joint tests.

Tab. 1: Strength, MOE, density and KAR for solid compression and tension specimens.
a) all pieces b) pieces with KAR = 0

			mean value	standard deviation
solid compression	a) 234	f_c [N/mm ²]	45.5	7.3
		E_c [N/mm ²]	11 500	2 700
		$\rho_{0,c}$ [kg/m ³]	680	39
		KAR_c [-]	0.09	0.10
	b) 66	f_c [N/mm ²]	50.8	6.2
		E_c [N/mm ²]	13 500	2 200
		$\rho_{0,c}$ [kg/m ³]	674	36
		KAR_c [-]	-	-
solid tension	a) 330	f_t [N/mm ²]	69.6	34.1
		E_t [N/mm ²]	13 100	3 500
		$\rho_{0,t}$ [kg/m ³]	679	37
		KAR_t [-]	0.11	0.14
	b) 102	f_t [N/mm ²]	99.9	30.7
		E_t [N/mm ²]	15 400	2 600
		$\rho_{0,t}$ [kg/m ³]	683	39
		KAR_t [-]	-	-

Tab. 2: Strength, MOE and density of finger-jointed compression and tension specimens.

			mean value	standard deviation
finger-joints compression	31	$f_{c,fj}$ [N/mm ²]	47.9	5.2
		$E_{c,fj}$ [N/mm ²]	13 200	2 100
		$\rho_{0,c,fj}^{*)}$ [kg/m ³]	665	37
		$KAR_{c,fj}$ [-]	-	-
finger-joints tension	347	$f_{t,fj}$ [N/mm ²]	65.8	14.1
		$E_{t,fj}$ [N/mm ²]	15 000	1 800
		$\rho_{0,t,fj}^{*)}$ [kg/m ³]	655	29
		$KAR_{t,fj}$ [-]	-	-

*) lower value of the two parts of the finger-jointed specimen

3.3 Bi-linear model for the stress-strain relationship of glulam laminations

A bi-linear model of the stress-strain relationship of beech elements under tensile and compressive loads requires 4 parameters: tensile and compressive strength and tensile and compressive MOE, both for solid and finger-jointed elements (Figure 10). Table 3 shows the correlation coefficients of strength and stiffness with density and knot area ratio. Table 4 shows the regression equations for compressive and tensile strength and stiffness of solid elements with KAR and density as independent parameters as well as the corresponding regression equations for finger-jointed elements with density as an independent parameter. KAR is not included in the equations for finger-jointed elements as no knots are allowed near finger-joints.

The results show that in contrast to softwoods the correlation between strength and density and MOE and density is very low. This is due to the fact that density of beech varies much less than the density of softwoods. Therefore KAR is the most important parameter for strength and stiffness prediction. This is also indicated by the correlation coefficients of the regression equations in Table 4: they are not much higher than the correlation coefficient between strength and KAR or MOE and KAR alone (see Table 3).

MOE is stronger correlated with strength than KAR and density (see Table 3). This indicates that mechanical grading of beech boards will provide better yields than visual grading.

Density has a small effect on MOE and on compression strength of finger-jointed elements. It has no effect on tensile strength of finger-jointed elements.

When this model is used to simulate the strength and stiffness behaviour of glulam beams the autocorrelation of strength and stiffness has to be taken into account. As an example Figure 11 shows the correlation of the residuals of compressive strength and compressive MOE, Figure 12 shows the correlation of the residuals of tensile strength and tensile MOE.

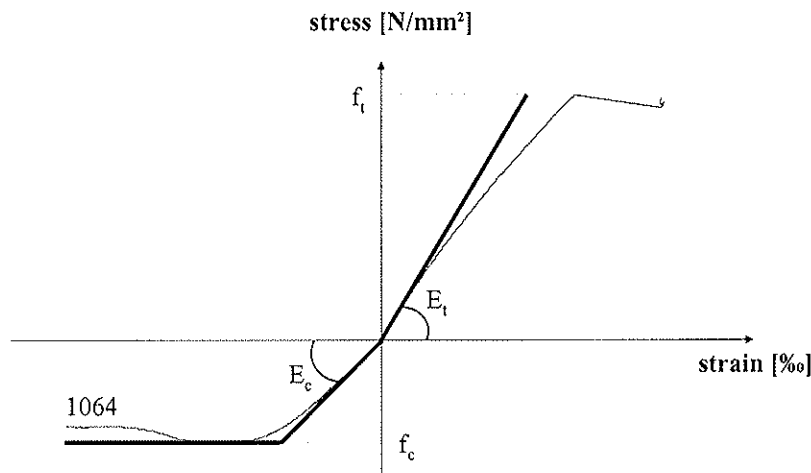


Fig. 10: Bi-linear model of stress-strain relationship of beech laminations as compared to the stress-strain-curve of specimen no. 1064.

Tab. 3: Correlation coefficients for strength, stiffness, density and knot size of solid and finger-jointed elements.

			$\rho_0^{*})$ [kg/m ³]	KAR [-]	E [N/mm ²]
solid n = 234	f_c	[N/mm ²]	0.01	-0.66	0.89
	E_c	[N/mm ²]	-0.05	-0.68	1.00
solid n = 330	f_t	[N/mm ²]	0.19	-0.67	0.80
	E_t	[N/mm ²]	0.23	-0.70	1.00
finger-joints n = 31	$f_{c,fj}$	[N/mm ²]	0.37	-	0.66
	$E_{c,fj}$	[N/mm ²]	0.11	-	1.00
finger-joints n = 347	$f_{t,fj}$	[N/mm ²]	0.07	-	0.33
	$E_{t,fj}$	[N/mm ²]	0.26	-	1.00

*) for finger-joints: lower value of the two parts of the finger-jointed specimens

Tab. 4: Linear regression formulas for bi-linear compression and bi-linear tension strength model.

compression (solid elements n=234; finger-jointed elements n=31)				r	
f_c [N/mm ²]	=	+ 29.0	- 48.4·KAR [-]	+ 0.031· ρ_0 [kg/m ³]	0.68
$f_{c,fj}$ [N/mm ²]	=	+13.0		+0.052· ρ_0 [kg/m ³]	0.37
E_c [N/mm ²]	=	+ 8 035	- 17 831·KAR [-]	+ 7.41· ρ_0 [kg/m ³]	0.69
$E_{c,fj}$ [N/mm ²]	=	+9 115		+6.15· ρ_0 [kg/m ³]	0.11

tension (solid elements n=330; finger-jointed elements n=347)				r	
f_t [N/mm ²]	=	+ 3.6	- 162.5·KAR [-]	+ 0.125· ρ_0 [kg/m ³]	0.68
$f_{t,fj}$ [N/mm ²]	=	+44.6		+0.032· ρ_0 [kg/m ³]	0.07
E_t [N/mm ²]	=	+ 4 066	- 17 267·KAR [-]	+ 16.21· ρ_0 [kg/m ³]	0.72
$E_{t,fj}$ [N/mm ²]	=	+3 947		+16.79· ρ_0 [kg/m ³]	0.26

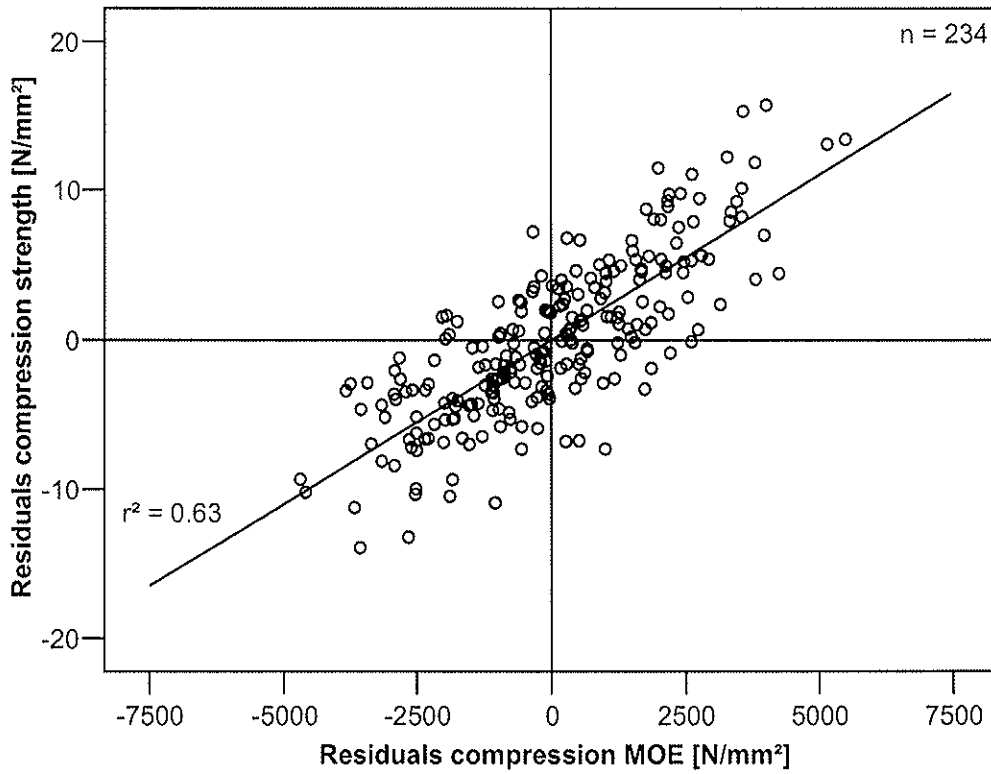


Fig. 11: Correlation between residuals of regression equations (Table 4) for compression strength f_c and compression MOE E_c .

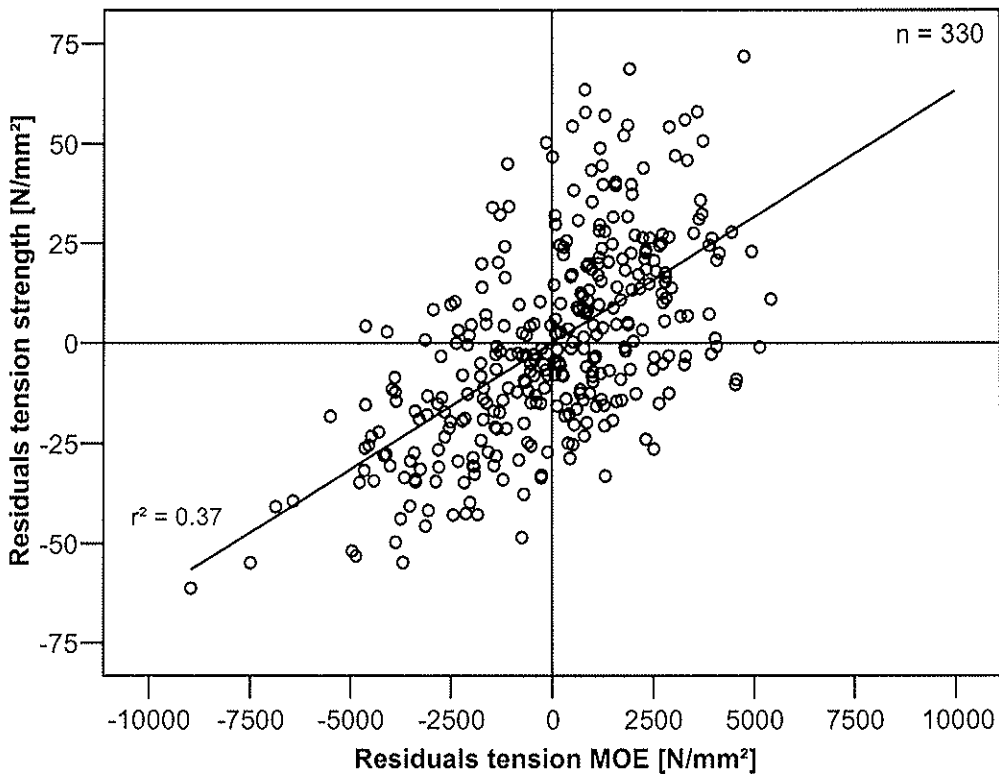


Fig. 12: Correlation between residuals of regression equations (Table 4) for tension strength f_t and tension MOE E_t .

3.4 Non-linear model for the stress-strain relationship in compression

Figure 13 shows a non-linear model for the description of the stress-strain relationship of beech elements under compressive load. The model was developed by GLOS 1978 for softwood elements. It requires 4 parameters which can be expressed as functions of compressive strength f_c , MOE, strain at maximum stress ϵ_c and asymptotic stress $f_{c,end}$. The equations are given in Annex A. This model fits the stress-strain-curve of beech elements very well when the coefficient N is chosen as $N = 4$. The regression equations for f_c , $f_{c,end}$, MOE and ϵ_c are shown in Table 5.

Tab. 5: Linear regression formulas for multivariate compression strength model.

<u>compression strength of solid elements (n = 234)</u>				r	
f_c [N/mm ²]	=	+ 29.0	- 48.4·KAR [-]	+ 0.031· ρ_0 [kg/m ³]	0.68
$f_{c,end}$ [N/mm ²]	=	+ 15.3	- 27.7·KAR [-]	+ 0.035· ρ_0 [kg/m ³]	0.56
E_c [N/mm ²]	=	+ 8 035	- 17 831·KAR [-]	+ 7.41· ρ_0 [kg/m ³]	0.69
ϵ_c [‰]	=	+3.62	+4.39·KAR[-]	-0.003· ρ_0 [kg/m ³]	0.57

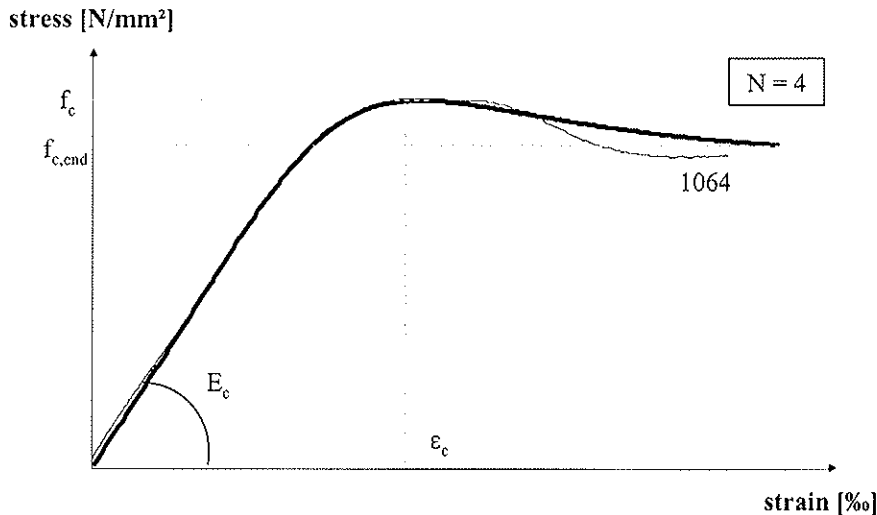


Fig. 13: Non-linear model of stress-stain relationship of beech laminations loaded in compression as compared to the stress-strain-curve of specimen no. 1064.

4 Conclusions

A bi-linear and a non-linear model is proposed to describe the stress-strain-relationship of solid and finger-jointed beech board elements loaded in tension and compression as a function of the wood characteristics density and knot size.

Strength and stiffness are mainly determined by the knot area ratio of the elements. Due to the low variation of density (COV~5%) it does not contribute significantly to the strength and stiffness prediction of solid and finger-jointed boards.

The best single predictor of strength is MOE. This indicates that mechanical grading of beech boards will provide better yields than visual grading.

On average the MOE-strength ratio of finger-jointed specimens is about 15 % higher than that of solid elements, both in tension and compression. Compared to knot-free tension pieces the strength of finger-jointed pieces is only 67 % whereas the MOE value remains unchanged. Opposite to knot areas where the strength reduction is combined with a lower MOE value, finger-joints are exposed to higher stresses due to the high MOE value. This must be taken into account when establishing requirements for end joints of hardwood laminations.

5 Literature

- [1] EN 1194:1999-04
Timber structures – Glued laminated timber – Strength classes and determination of characteristic values
- [2] ISO 3131:1975-11
Wood; Determination of density for physical and mechanical tests
- [2] GLOS, P. (1978): Zur Bestimmung des Festigkeitsverhaltens von Brettschichtholz bei Druckbeanspruchung aus Werkstoff- und Einwirkungskenngrößen. Berichte zur Zuverlässigkeitstheorie der Bauwerke, Laboratorium für den Konstruktiven Ingenieurbau (LKI), Technische Universität München. 35 (1978) 335.

Annex A

$$\sigma_c = \frac{\varepsilon + k_1 \cdot \varepsilon^4}{k_2 + k_3 \cdot \varepsilon + k_4 \cdot \varepsilon^4}$$

$$k_1 = \frac{f_{c,end}}{3 \cdot E_c \cdot \varepsilon_c^4 \cdot \left(1 - \frac{f_{c,end}}{f_c}\right)}$$

$$k_2 = \frac{1}{E_c}$$

$$k_3 = \frac{1}{f_c} - \frac{4}{3} \cdot \frac{1}{E_c \cdot \varepsilon_c}$$

$$k_4 = \frac{1}{3 \cdot E_c \cdot \varepsilon_c^4 \cdot \left(1 - \frac{f_{c,end}}{f_c}\right)}$$

Conditions:

$$f_{c,end} \leq f_c - 1$$

$$\varepsilon_c \geq \frac{4}{3} \cdot \frac{f_c}{E_c}$$

INTERNATIONAL COUNCIL FOR RESEARCH AND INNOVATION
IN BUILDING AND CONSTRUCTION

WORKING COMMISSION W18 - TIMBER STRUCTURES

A REVIEW OF EXISTING STANDARDS RELATED TO
CALCULATION OF CHARACTERISTIC VALUES OF TIMBER

F Rouger

CTBA

Bordeaux

FRANCE

Presented by F Rouger

P Glos commented that the main intention of some of the procedures adopted in EN384 was to address the limited sample size. He would like to see the variation of results with limited sample. Rouger answered that some samples had approximately 126 specimens per cell.

P Glos asked which standard gave higher or lower values. Big sample size with 75% TL will give conservative results; therefore ranking approach was taken. Rouger answered that some more detailed results are available in the paper. In general results showed that the difference in the overall approach was small.

H J Larsen questioned why would estimation of characteristic values based on ranking be better than distribution based parameters; after all, distributions are needed in reliability based procedures.

P Glos answered that we had these discussions 15 or so years ago in CIB meetings: 3-P Weibull gives best fit of results; lognormal can be non-conservative for 5th percentile; normal is conservative for 5th percentile. Ranking was equivalent to Weibull but simple. In term of reliability analysis distribution can also be used.

A review of existing standards related to calculation of characteristic values of timber.

F Rouger

1 Abstract

Different standards currently exist to calculate characteristic values for wood based materials. In the case of solid timber, the calculation involves sampling issues as well as statistical approaches which differ upon the standards. In all cases, the underlying methods have been mainly calibrated by using Monte-Carlo simulations. The purpose of this paper is to test these methods on a real database, to compare the results and to propose a unique approach that could give equivalence factors.

The database which has been used in this investigation comprises more than 10 000 test pieces, from 10 different species and 4 grades.

Four different standards have been investigated :

- EN 384 : applicable for solid timber
- EN 14358 : applicable for wood based products
- ISO 13910 : applicable for solid timber
- ISO 12491 : applicable to building products

EN 384 relies on stratified sampling and on ranking. ISO 13910 proposes to calculate the characteristic value as the lower bound estimate, given by Weibull distribution, of the sample fifth percentile, given by ranking. ISO 12491 proposes to calculate the 5th percentile as the lower bound estimate by assuming a normal distribution. EN 14358 follows basically the same approach as ISO 12491, but assuming a log-normal distribution and an unknown coefficient of variation.

The investigations show that EN 14358 and EN 384 give the same results. If only one European standard is maintained, one suggests that EN 14358 is kept, since it is applicable to all wood-based products and that it is much more easy to use. We should only slightly modify it in order to have a minimum sampling (e.g. 200 specimens, made of 5 distinct samples).

Despite ISO 12491 is applicable to all building materials, we suggest not to use it, since it gives a big scatter.

In ISO 13910, there is an equivalence factor with EN 384, which varies from 1,0 to 1,3, depending on the strength property, the size and the quality of timber, taking into account different test methods. Our simulations show that the way of calculating the fifth percentiles gives another correction factor, which encounters the previous one. By combining both factors, we could use a straightforward correspondence between both standards.

2 Introduction

Different methods exist currently to calculate characteristic values. In the case of solid timber, the calculation involves sampling issues as well as statistical approaches which differ upon the standards. The purpose of this paper is to test these methods on a real database, and exhibit each of the issues.

The database which has been used in this investigation is the following :

- A grand total of 10 442 test pieces
- 10 different species
- 19 different regions
- 4 different grades

By combining this sampling, we get the following base for the investigation :

- 32 grade/species samples for which a characteristic value for the grade might be performed.
- 126 samples (grade/species/region) which can be used when performing stratified sampling.

Table 1 gives the details of the database. In this table, the following code has been used for the regions :

Alsace	(1)
Aquitaine	(2)
Auvergne	(3)
Basse Normandie	(4)
Bourgogne	(5)
Bretagne	(6)
Bretagne (1)	(7)
Bretagne (2)	(8)
Centre	(9)
Champagne Ardennes	(10)
Corse	(11)
Franche Comté	(12)
Haute Normandie	(13)
Languedoc Roussillon	(14)
Limousin	(15)
Lorraine	(16)
Midi-Pyrénées	(17)
Normandie	(18)
Provence Alpes côte d'azur	(19)
Rhône Alpes	(20)

For the analysis on sub-samples, the minimum sample size has been taken larger or equal than 20. The sub-samples which are taken in the analysis are bolded. The other ones are only used for the so-called “global analysis” which considers the grade/species as the unit.

NB MOR		Region																				Total
Essence	Grade	(1)	(2)	(3)	(4)	(5)	(6)	(7)	(8)	(9)	(10)	(11)	(12)	(13)	(14)	(15)	(16)	(17)	(18)	(19)	(20)	
Douglas Fir	Rejet			53	146	64				26			60	132	151							632
	ST1			8	21	6				9			24	17	14							99
	ST2			36	125	54				49			37	91	96							488
	ST3			64	179	54				24			56	114	152							643
Sub-Total				161	471	178				108			177	354	413							1862
Spruce	Rejet	14	29	18						19	51	13	21	40	17						132	354
	ST1	19	6	11						8	56	6	26	1							90	223
	ST2	40	31	39						30	129	24	12	68	11						205	589
	ST3	23	30	17						19	72	15	9	51	17						116	369
Sub-Total		96	96	85						76	308	58	42	185	46						543	1535
Sitka Spruce	Rejet							113	113													226
	ST2							7	196													203
	ST3							65	222													287
Sub-Total								185	531													716
Dorskamp Poplar	Rejet									54												54
	ST2									42												42
	ST3									53												53
Sub-Total										149												149
Corsican Pine	Rejet									115	124									126		365
	ST1									28	81									26		135
	ST2									116	177									51		344
	ST3									83	86									74		243
Sub-Total										342	468									277		1087
Maritime Pine	Rejet	141																				141
	ST1	15																				15
	ST2	30																				30
	ST3	48																				48
Sub-Total		234																				234
Black Pine	Rejet			63						47		141	58		139	127						575
	ST1			1						12		5	2		9	2						31
	ST2			9						30		31	9		79	34						192
	ST3			26						35		71	51		93	51						327
Sub-Total				99						124		248	120		320	214						1125
Scots Pine	Rejet	152	238							258			71		143							862
	ST1	25	68							38			10		4							145
	ST2	148	200							162			52		88							650
	ST3	92	131							158			39		67							487
Sub-Total		417	637							616			172		302							2144
Fir	Rejet	50	37	7								71	18	95	29						99	406
	ST1	30	21	3								107	33	42	34						62	332
	ST2	58	30	17								176	24	99	42						126	572
	ST3	32	31	14								47	16	54	16						69	279
Sub-Total		170	119	41								401	91	290	121						356	1589
Total		683	234	852	161	696	178	185	531	1215	200	468	709	177	397	568	595	580	277	622	1113	10441

Table 1 : Database used for the investigation

The investigation has three objectives :

- Investigate the effect of stratified sampling
- Investigate the statistical assumptions (ranking, curve fitting, confidence intervals)
- Compare the standards to give correspondence factors

3 Review of the standards.

Four different standards have been investigated :

- EN 384 : applicable for solid timber [1]
- EN 14358 : applicable for wood based products [2]
- ISO 13910 : applicable for solid timber [3]
- ISO 12491 : applicable to building products [4]

3.1 EN 384

EN 384 relies on stratified sampling [5]. Minimum sample size is 40, and it is advisable to have at least 5 samples. For each sample, the 5% fractile, denoted f_{05} , is calculated by ranking. Then, the characteristic value is calculated as the weighted mean of the samples 5th percentiles :

$$\overline{f_{05}} = \frac{\sum_j n_j f_{05,j}}{\sum_j n_j} \quad (1)$$

where :

n_j is the size of the j^{th} sample,

$f_{05,j}$ is the 5th percentile of the j^{th} sample,

$\overline{f_{05}}$ is the weighted mean value of samples' fifth percentiles

Then, the characteristic value has to be calculated according to :

$$f_k = \text{Min} \left\{ \overline{f_{05}}, 1.2 \text{Min}_j f_{05,j} \right\} \quad (2)$$

Furthermore, f_k may have to be corrected to take account of the cross-sectional dimensions of the timber and of the number and sizes of samples.

This standard is the only one that relies on stratified sampling.

3.2 ISO 13910

ISO 13910 proposes to calculate the characteristic value as the lower bound estimate of the fifth percentile.

The fifth percentile, f_{05} , is calculated by ranking. Then, the lower tail (the lowest 15 values, or the lowest 15 percent, whichever is the larger) is fitted by a Weibull distribution.

The 2 parameters Weibull distribution function is given by :

$$F(z) = 1 - \exp \left[- \left(\frac{z}{w_1} \right)^k \right] \quad (3)$$

where :

F(z) is the distribution function (cumulative percentiles)
z is the variate
k is the shape parameter
w₁ is the « characteristic smallest value »

This distribution can be fitted according to a transformation of equation (3) :

$$\text{Ln} \left\{ -\text{Ln} [1 - F(z)] \right\} = k [\text{Ln}(z) - \text{Ln}(w_1)] \quad (4)$$

This equation shows that *k* is the slope of $\text{Ln} \left\{ -\text{Ln} [1 - F(z)] \right\}$ as a function of $\text{Ln}(z)$.

The coefficient of variation of the 2-P Weibull distribution is given by :

$$1 + CV^2 = \frac{\Gamma(1 + 2/k)}{\Gamma^2(1 + 1/k)} \quad (5)$$

In ISO 13910, a simplification is proposed :

$$V_{tail} = k^{-0,92} \quad (6)$$

Surprisingly, these equations give exactly the same results, as illustrated in Figure 1.

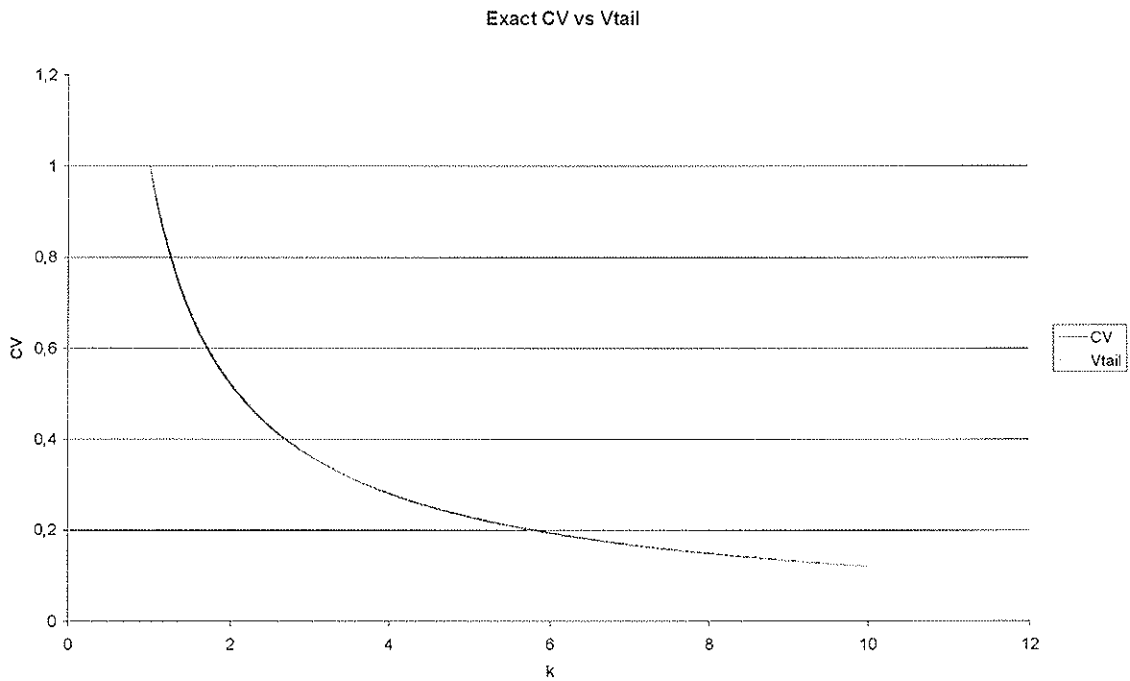


Figure 1 : Comparaison between CV (exact) and Vtail (approximation) as a function of k

Furthermore, the characteristic value is given as the lower bound estimate of the 5th percentile value :

$$f_k = \left[1 - 2,7 \frac{V_{tail}}{\sqrt{N}} \right] f_{05} \quad (7)$$

This lower bound estimate equation has been calibrated by numerical simulation [6], since there are no exact formulas for confidence intervals for a fractile in the case of a Weibull distribution.

3.3 ISO 12491

In ISO 12491, the characteristic value is deducted from the mean value and the standard deviation according to :

$$f_k = \bar{x} + k_s s \quad (8)$$

where :

- f_k is the characteristic value
- \bar{x} is the sample mean
- s is the sample standard deviation
- k_s is a correction factor, see below

This equation corresponds to a lower bound estimate at a given confidence of the fractile, assuming a normal distribution. The confidence interval is denoted by α . In general, $\alpha = 75\%$ is recommended.

Despite exact formula for k_s is not given in the standard (only tables are presented), it can be found in the literature [7].

k_s is given by :

$$k_s = -\frac{k}{\sqrt{n}} \quad (9)$$

where :

- n is the sample size
- k is the α -percentile of the non-central t distribution with n degrees of freedom and the non-centrality parameter λ , given by :

$$\lambda = \Phi^{-1}(1-p) \sqrt{n} \quad (10)$$

where :

- Φ is the standardised normal distribution function.
- p is the fractile level (i.e. $p = 5\%$)

This approach is valid when the population standard deviation, σ , is unknown. When it is known, equation (8) is replaced by :

$$f_k = \bar{x} + k_\sigma \sigma \quad (11)$$

where

$$k_\sigma = \Phi^{-1}(1-p) - \frac{\Phi^{-1}(\alpha)}{\sqrt{n}} \quad (12)$$

3.4 EN 14358

EN 14358 follows basically the same approach as ISO 12491, but assuming a log-normal distribution and an unknown coefficient of variation. Therefore, equation (8) is replaced by :

$$f_k = \exp(\bar{x} + k_s s) \quad (13)$$

where :

$$\bar{x} = \frac{1}{n} \sum_{i=1}^n \ln(x_i) \quad (14)$$

and

$$s = \sqrt{\frac{1}{n-1} \sum_{i=1}^n (\ln(x_i) - \bar{x})^2} \quad (15)$$

4 Effect of stratified sampling

The first effect we want to investigate is the effect of stratification. For this investigation, we define a so-called stratified fractile and a global fractile. We calculate the stratified fractile for a grade/species combination as the weighted mean of the individual fractiles for each region, each of these fractiles being calculated according to the relevant standard, ie :

- EN 384 : ranking
- EN 14358 : 75% lower bound, log normal
- ISO 12491 : 75% lower bound, normal
- ISO 13910 : 75% lower bound, Weibull

We calculate the global fractile by cumulating all the regions for a grade/species combination, and calculating the fractile according to the relevant standard.

The coefficients of correlation of the different standards are the following :

- EN 384 : 0.977
- EN 14358 : 0.996
- ISO 13910 : 0.983
- ISO 12491 : 0.995

The relationships between those fractiles are illustrated in Figure 2 to Figure 5.

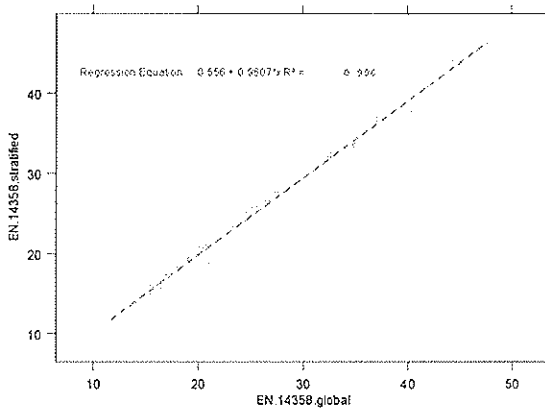


Figure 2

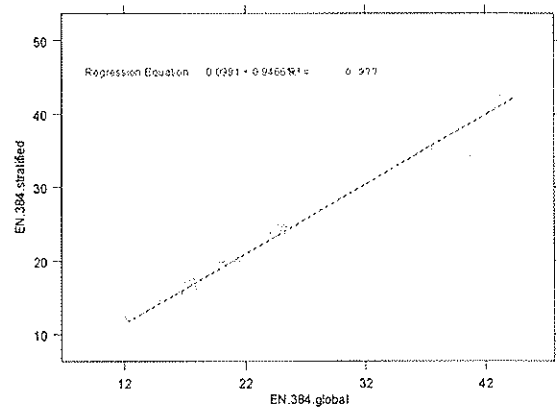


Figure 3

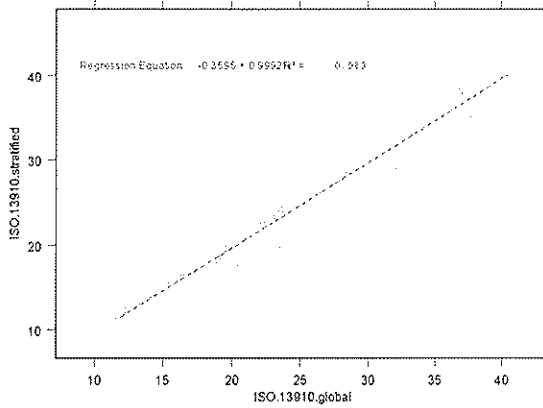


Figure 4

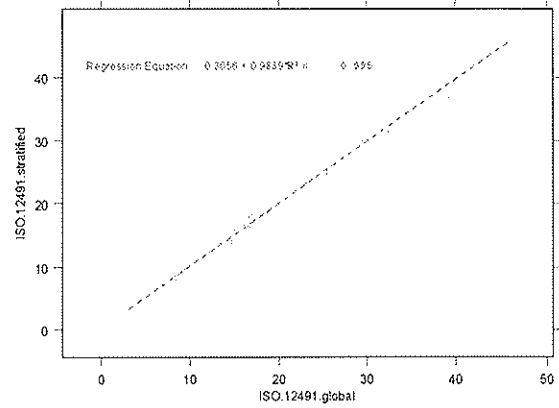


Figure 5

By looking at the regression equations and coefficients, one can conclude that it is not necessary to go through a stratified calculation, since the difference between the global and stratified approach is less than 5% on the fractile. The only case which gives a difference EN 384, for which the stratified value is 5.4% lower than the global value.

However, we still think that a stratified sampling is necessary to represent to variability of timber.

5 Effect of assumed distribution.

We can perform this comparison on regions/species/grade combinations (126 values, average sample size = 80) or on species/grade combinations (32 values, average sample size = 325). These comparisons are both interesting since the sample size might have an influence. But we only report the comparison for small sample sizes, since all the methods should give the same results for large samples.

The difference between the four methods are illustrated in Figure 6 to Figure 11.

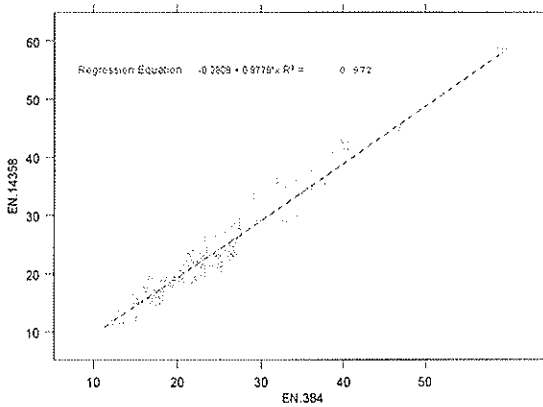


Figure 6

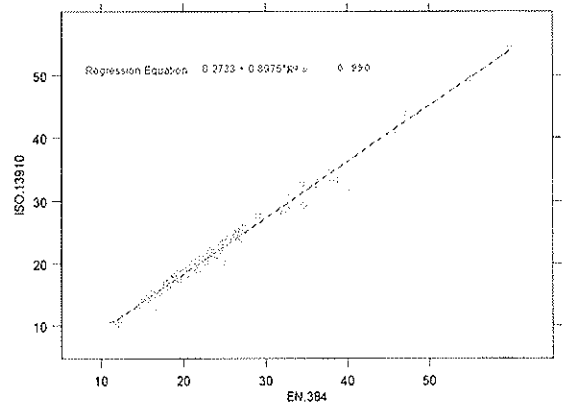


Figure 7

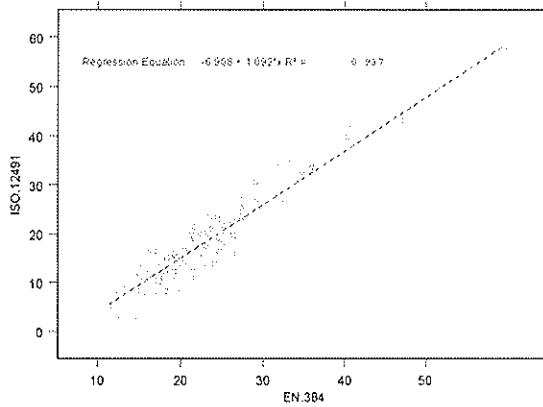


Figure 8

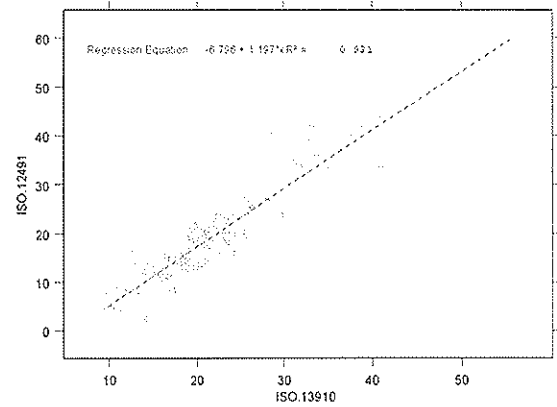


Figure 9

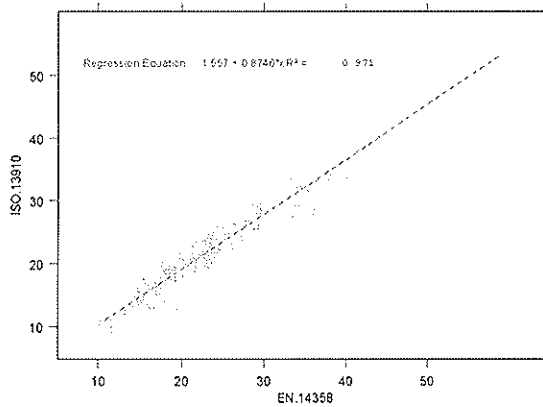


Figure 10

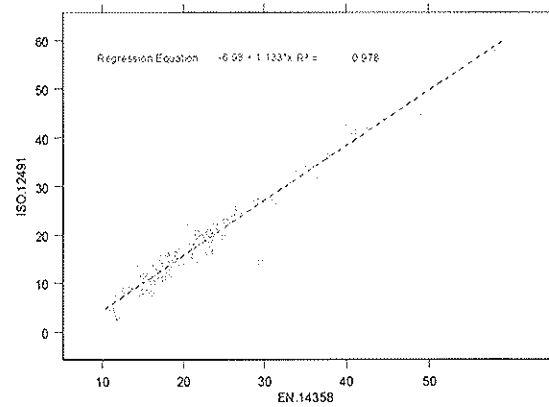


Figure 11

Based on these figures, one can conclude that, for the fractile calculation :

Normal distribution > Ranking > Log Normal distribution > Weibull distribution.

The difference can be as large as 20%, which represents a gap up to two strength classes in the European system.

Another point is that the normal distribution assumption gives a big scatter as compared to other assumptions.

6 Comparison between standards.

This section relates to a combination of both previous sections, since there is a mixture of stratified/non stratified approach and assumptions on distributions :

- EN 384 : stratified, ranking
- EN 14358 : non stratified, Log Normal
- ISO 13910 : non stratified, Weibull
- ISO 12491 : non stratified, Normal

The following figures illustrate the differences between standards on the grade/species combinations.

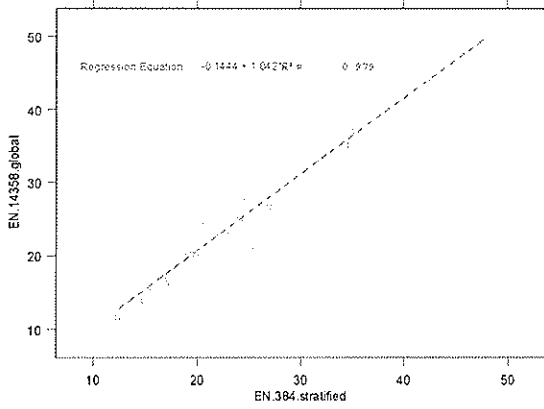


Figure 12

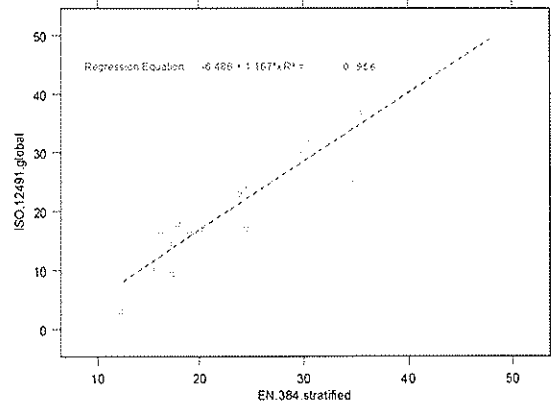


Figure 13

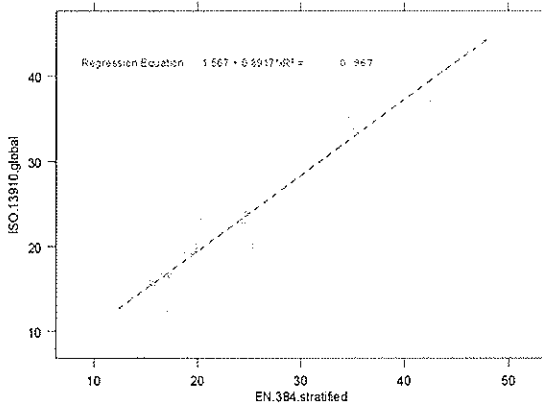


Figure 14

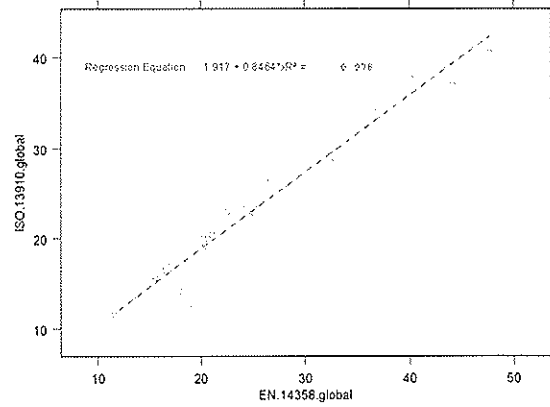


Figure 15

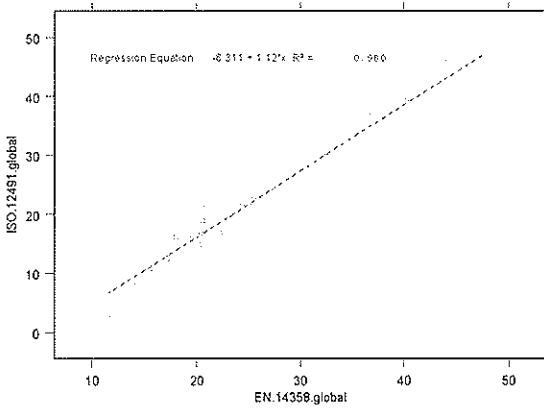


Figure 16

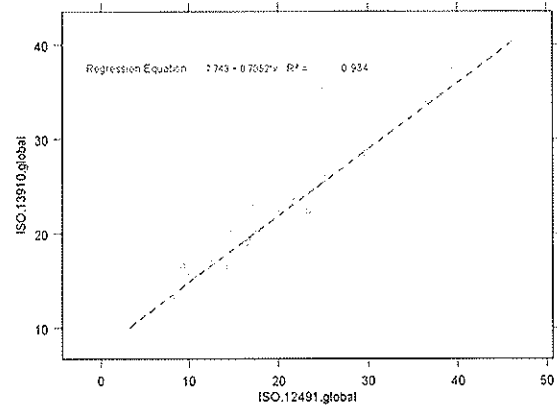


Figure 17

Regarding those figures, we can propose the following relationships :

$$f_{05,EN384} = f_{05,EN14358} \quad (16)$$

$$f_{05,ISO 12491} = 1.15 f_{05,EN14358} \quad (17)$$

$$f_{05,ISO 13910} = 0.85 f_{05,EN14358} \quad (18)$$

$$f_{0.05, \text{ISO 13910}} = 0.7 f_{0.05, \text{ISO 12491}} \quad (19)$$

If only one European standard is maintained, one suggests that EN 14358 is kept, since it is applicable to all wood-based products. We should only slightly modify it in order to have a minimum sampling (e.g. 200 specimens, made of 5 distinct samples).

Despite ISO 12491 is applicable to all building materials, we suggest not to use it, since it gives a big scatter.

Regarding ISO 13910, we have to remember that there is already a correspondence with EN 384, given by :

$$f_{\text{ISO}, 0.05} = k_{\text{eq}} f_{\text{EN}, 0.05} \quad (20)$$

The correction factor, which varies from 1,0 to 1,3, depending on the strength property, the size and the quality of timber, accounts for different test methods. In EN 384, in the case of bending, a worst defect has to be located in the central third, whereas in ISO 13910, the test specimen can be placed in any position.

By combining equations (18) and (20), we could give two options :

- Either we disregard correction factors between ISO and EN
- Or we reduce current factors by 0.85

This has to be decided in ISO TC 165.

7 Final checks by Monte-Carlo simulations

In order to check our conclusions, we performed Monte-Carlo simulations, according to the following procedure :

- Generate a parent population of 100 000 specimens, according to a given distribution
- For n times, extract samples of a given size m
 - For these samples, calculate the 5th percentile according to the four methods
- Calculate the ratios between these methods

The results are not presented in this paper, since they are very much dependent on the assumed distribution, on n and m . But we observed that EN 14358 and EN 384 are very close to each other, and that the values are close to the exact 5th percentile. Therefore, we are still confident to our conclusions.

8 Conclusions

The investigations show that EN 14358 and EN 384 give the same results. If only one European standard is maintained, one suggests that EN 14358 is kept, since it is applicable to all wood-based products and that it is much more easy to use. We should only slightly modify it in order to have a minimum sampling (e.g. 200 specimens, made of 5 distinct samples).

Despite ISO 12491 is applicable to all building materials, we suggest not to use it, since it gives a big scatter.

In ISO 13910, there is an equivalence factor with EN 384, which varies from 1,0 to 1,3, depending on the strength property, the size and the quality of timber, taking into account different test methods. Our simulations show that the way of calculating the fifth percentiles gives another correction factor, which encounters the previous one. By combining both factors, we could use a straightforward correspondence between both standards.

9 References

- [1] EN 384 – Structural timber – Determination of characteristic values of mechanical properties
- [2] EN 14358 – Timber structures – Fasteners and wood-based products – Calculation of characteristic 5-percentile value and acceptance criteria for a sample.
- [3] ISO 13910 – Structural timber – Sampling, full size testing, and evaluation of the characteristic values of strength graded timber
- [4] ISO 12491 – Statistical methods for quality control of building materials and components.
- [5] Notes on sampling and strength prediction of stress graded structural timber. P. Glos – 1983 - Proceedings of 16th conference of CIBW18, Lillehammer, Norway
- [6] Confidence in estimates of characteristic values. R.H. Leicester – 1986 – Proceedings of 19th conference of CIBW18, Firenze, Italy
- [7] Methods of structural safety. H.O. Madsen, S. Krenk, N.C. Lind – Prentice Hall Inc., 1986

INTERNATIONAL COUNCIL FOR RESEARCH AND INNOVATION
IN BUILDING AND CONSTRUCTION

WORKING COMMISSION W18 - TIMBER STRUCTURES

INFLUENCE OF ROLLING SHEAR MODULUS ON STRENGTH AND
STIFFNESS OF STRUCTURAL BONDED TIMBER ELEMENTS

P Fellmoser

H J Blaß

University of Karlsruhe

GERMANY

Presented by P Fellmoser

M Ansell received clarification that 3 span-to-depth ratios were used and a hammer was used to vibrate the specimen.

A Jorissen asked whether plywood design rules in EN code was considered. H Blass responded that the cross ply stiffness would be ignored in the plywood standard leading to poor results; therefore, it cannot be used in this case and justifying the need of this work.

Influence of rolling shear modulus on strength and stiffness of structural bonded timber elements

P. Fellmoser, H.J. Blaß

Lehrstuhl für Ingenieurholzbau und Baukonstruktionen

Universität Karlsruhe, Germany

1 Introduction

Rolling shear is defined as shear stress leading to shear strains in a plane perpendicular to the grain direction. Due to the very low rolling shear stiffness of timber significant shear deformations may occur. Fig. 1 shows a schematic representation of rolling shear stresses.

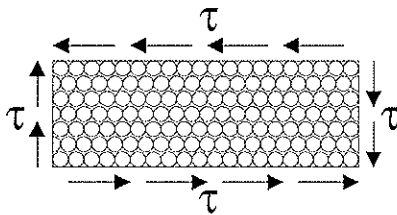


Fig. 1: Stress due to rolling shear

In prEN 1995-1-1 – Design of timber structures (final draft 2004) a ratio of $G_{R,mean} / G_{mean} = 0,10$ is defined for softwood. For the rolling shear strength a common characteristic value of $f_{R,k} = 1,0 \text{ N/mm}^2$ is given independent of the strength class.

Neuhaus [9] determined the rolling shear modulus of spruce as 48 N/mm^2 for a moisture content of 9 % through torsion tests. *Aicher et al.* [1] analysed the rolling shear modulus for different annual ring orientations in the cross-section using the Finite Element Method. Depending on the annual ring orientation he found values between about 50 N/mm^2 and 200 N/mm^2 . Experiments by *Aicher et al.* [2] resulted in a rolling shear modulus of 50 N/mm^2 .

Fig. 2 shows rolling shear failure in structural bonded timber elements.

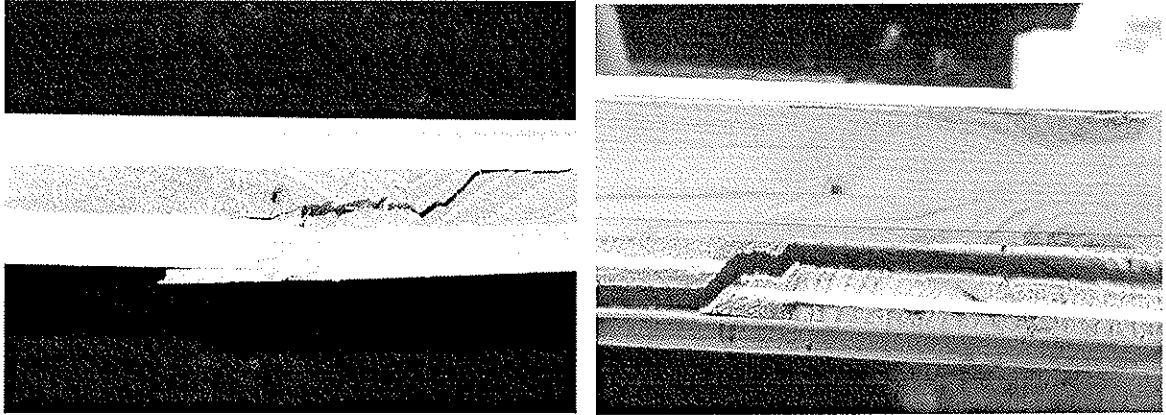


Fig. 2: Failure due to rolling shear

2 Determination of rolling shear modulus

2.1 Experimental investigations

For determining the rolling shear modulus of spruce specimens, the dynamic method of measuring the frequencies of a bending vibration was used. A method for the determination of the modulus of elasticity perpendicular to the grain and the rolling shear modulus was derived from the method for determining the modulus of elasticity parallel to the grain.

Görlacher describes in [5] the determination of the modulus of elasticity parallel to the grain direction via measuring the frequencies of a bending vibration. Fig. 3 shows the schematic representation of the experimental set-up. An approximate solution of the differential equation of a flexural vibration is given taking into account the shear modulus.

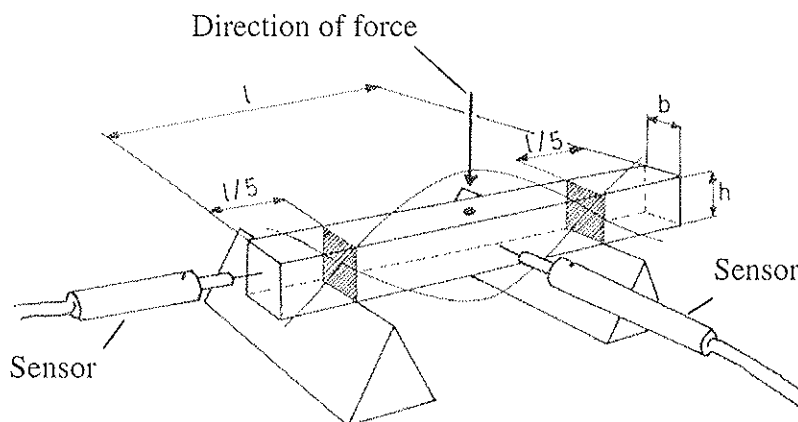


Fig. 3: Measuring the frequencies of a bending vibration

The modulus of elasticity may be determined from the frequency of a 1. order flexural mode using equation (1):

$$E = \frac{4 \cdot \pi^2 \cdot \ell^4 \cdot f_0^2 \cdot \rho}{500,6 \cdot i^2} \cdot \left(1 + \frac{i^2}{\ell^2} \cdot \left(49,48 + 12,3 \cdot s \cdot \frac{E}{G} \right) - \frac{4 \cdot \pi^2 \cdot s \cdot i^2 \cdot f_0^2 \cdot \rho}{G} \right) \quad (1)$$

where

ℓ = length of test specimen

f_0 = frequency of bending vibration

ρ = density

i = radius of inertia

E = modulus of elasticity

G = shear modulus

s = form factor (according to *Hearmon* [7] for wood: $s = 1,06$)

For test specimens with large span to depth ratios (ℓ/h) and / or small modulus of elasticity to shear modulus ratios (E/G) the influence of shear modulus (or E/G , respectively) is small. In this case a rough estimate for the shear modulus is sufficient. Alternatively, the shear modulus may be determined for a known modulus of elasticity using specimens with small span to depth ratios and / or large ratios of modulus of elasticity to shear modulus.

First tests from *Görlacher* [6] showed that both, rolling shear modulus and modulus of elasticity perpendicular to the grain, significantly depend on the annual ring orientation. Based on these tests the rolling shear modulus and the modulus of elasticity perpendicular to the grain of spruce were determined in this study.

2.2 Test set-up and specimens

Different solid wood panels with cross layers (nominal thickness 21mm, 32 mm and 52 mm) were dismantled for testing. From every board of the middle layers a specimen (width 10 mm) was prepared. Consequently, three test series were performed depending on the thickness of the solid wood panels. The specimens were conditioned in a constant climate of 20° C and 65 % relative humidity. The average moisture content was 12,2 %.

Test series 1: L x B x H = 104 mm x 10 mm x 6 mm

Test series 2: L x B x H = 46 mm x 10 mm x 17 mm

Test series 3: L x B x H = 53 mm x 10 mm x 17 mm

The specimens were forced to bending vibrations in grain direction (see Fig. 4 left) and perpendicular to grain direction (see Fig. 4 right). For both bending vibrations the frequencies were measured.

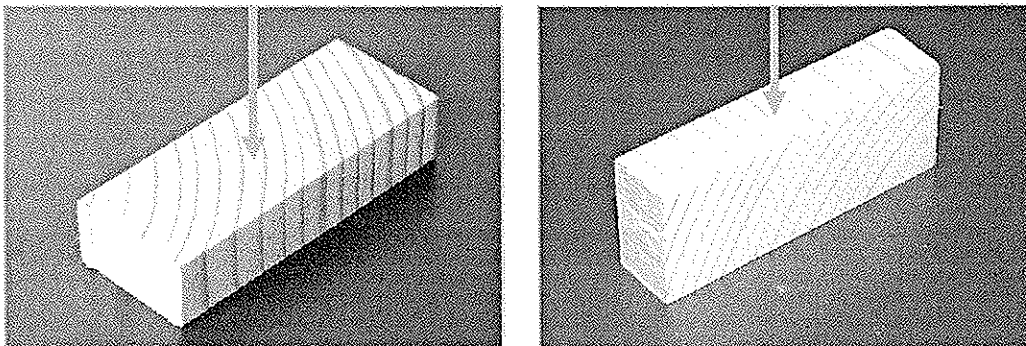


Fig. 4: Specimen with force in grain direction and perpendicular to grain direction

2.3 Results

For bending vibration in grain direction the shear modulus has a lower influence on the modulus of elasticity. Consequently a value of $G = 500 \text{ N/mm}^2$ was assumed in equation (1). The modulus of elasticity perpendicular to grain may be determined using the measured frequency of bending vibration parallel to the grain (Fig. 4 left).

For bending vibration perpendicular to grain the influence of shear modulus is large. Rolling shear modulus may be calculated according to the following procedure: in equation (1) the modulus of elasticity from the bending vibration parallel to grain of the same specimen as well as the measured frequency from bending vibration perpendicular to grain is inserted and the rolling shear modulus is calculated.

For determining the rolling shear modulus of spruce 112 specimens were analysed using the dynamic method of measuring the frequencies of a bending vibration. Fig. 5 and Fig. 6 show the modulus of elasticity perpendicular to grain and the rolling shear modulus versus density. Four specimens were excluded from the analysis because of knots and marked in Fig. 5 and Fig. 6. Common values of rolling shear modulus of spruce are between 40 N/mm^2 and 80 N/mm^2 . The results confirm specifications of prEN 1995-1-1 – Design of timber structures (final draft 2004) where a ratio of $G_{R,\text{mean}} / G_{\text{mean}} = 0,10$ is defined for softwood.

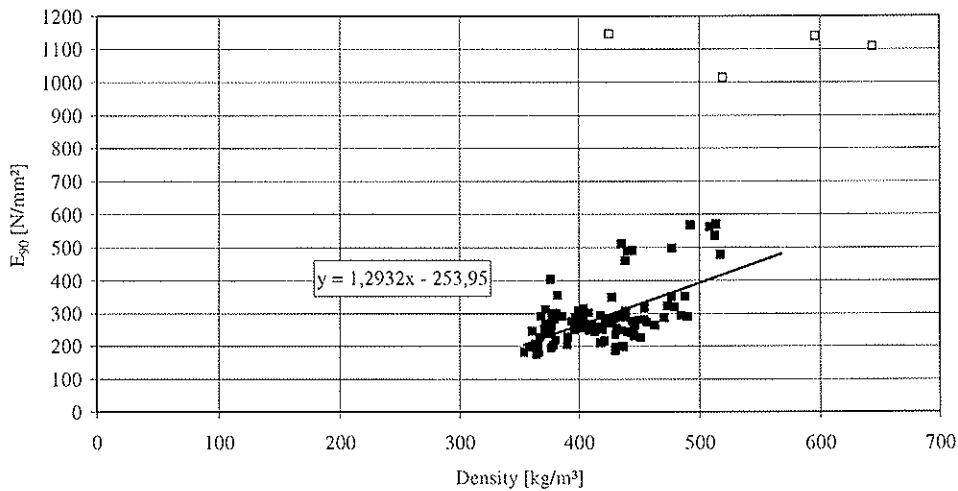


Fig. 5: Modulus of elasticity perpendicular to the grain versus density

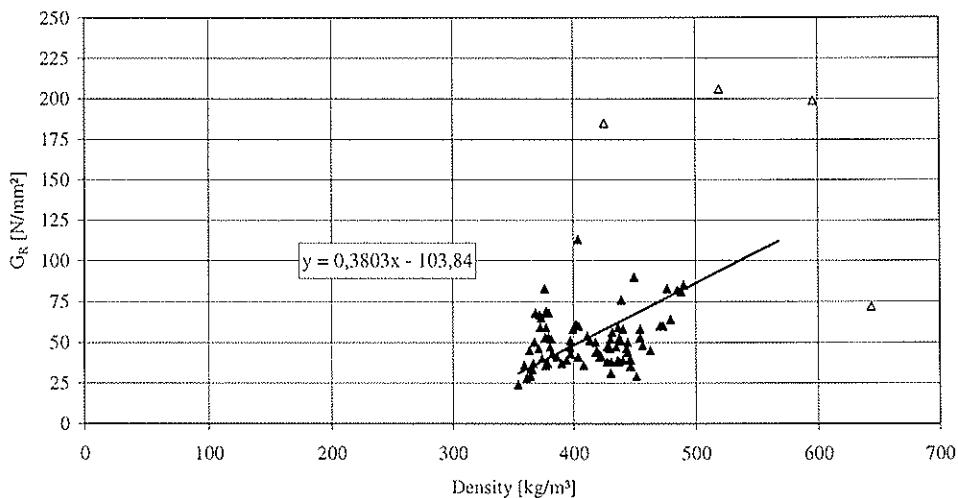


Fig. 6: Rolling shear modulus versus density

The influence of annual ring orientation on modulus of elasticity perpendicular to the grain and the rolling shear modulus was analysed by *Görlacher* [6] based on the Finite Element Method and on the transformation of constitutive equations. For small deviations of the annual ring orientation from 0° and 90°, respectively, the modulus of elasticity perpendicular to the grain is decreasing significantly and the rolling shear modulus remains almost constant. For an annual ring orientation of about 45° the rolling shear modulus is increasing significantly (up to a factor of about 4) and the modulus of elasticity perpendicular to the grain remains almost constant.

Because of curved annual rings in the specimens, the influence of annual ring orientation on the rolling shear modulus cannot be determined. Consequently, the theoretical results from FEM with straight annual rings in the cross-section cannot be confirmed by the method of measuring the frequencies of bending vibrations.

3 Design of solid wood panels with cross layers

The stress distribution in and the deformation behaviour of solid wood panels with cross layers loaded perpendicular to the plane both depend on the shear deformation. Due to the very low rolling shear modulus, shear deformation increases significantly depending on the thickness of the rolling shear layer. Bernoulli's hypothesis of plane cross-sections remaining plane and a linear stress-strain relationship may not be assumed because of shear deformations. Fig. 7 shows the normal and shear stress distribution in solid wood panels with 5 layers for bending perpendicular to the plane and parallel / perpendicular to the grain direction of outer skins.

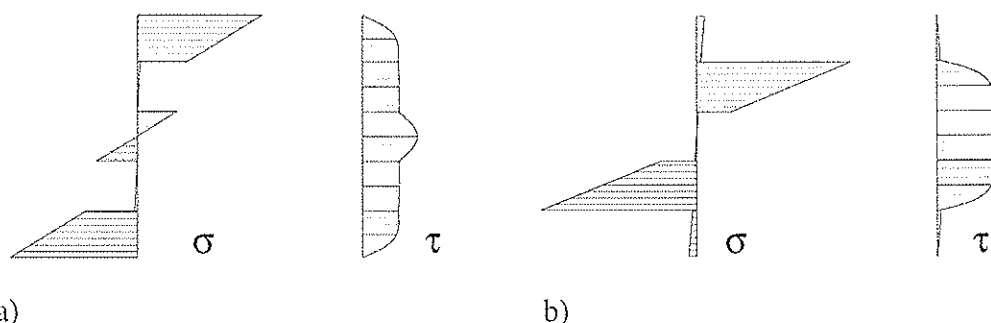


Fig. 7a and b: Bending stress and shear stress of solid wood panel with 5 layers when bending perpendicular to the plane a) parallel b) perpendicular to the grain direction of outer skins

The stress distribution in and the deformation behaviour of solid wood panels with cross layers were analysed using the shear analogy method by *Kreuzinger* [8]. Both different moduli of elasticity and shear moduli of single layers may be considered for any system configuration. Also the number of layers within a panel is unlimited in the shear analogy method.

The following properties were used as input for modelling solid wood panels with cross layers:

Modulus of elasticity parallel to the grain:	$E_0 = 12.500 \text{ N/mm}^2$
Modulus of elasticity perpendicular to the grain:	$E_{90} = E_0 / 30$
Shear modulus:	$G = 500 \text{ N/mm}^2$
Rolling shear modulus:	$G_R = 50 \text{ N/mm}^2$

Tab. 1 summarises the build-up of the solid wood panels with cross layers that were analysed using the shear analogy method.

Tab. 1: Build-up of analysed solid wood panels with cross layers

Type of solid wood panel	Nominal thickness	Build-up
3 layers	21 mm	6,9 / 7,2 / 6,9
3 layers	60 mm	6,9 / 46,2 / 6,9

The span was varied for the modelling of the solid wood panels and the calculation of the effective modulus of elasticity when bending perpendicular to the plane. The effective modulus of elasticity is the effective bending stiffness over the second moment of inertia. The influence of the span on the effective modulus of elasticity of solid wood panels is shown in Fig. 8. The solid wood panels with a nominal thickness of 21 mm and 60 mm were analysed for bending perpendicular to the plane and parallel to the grain direction of the outer skins.

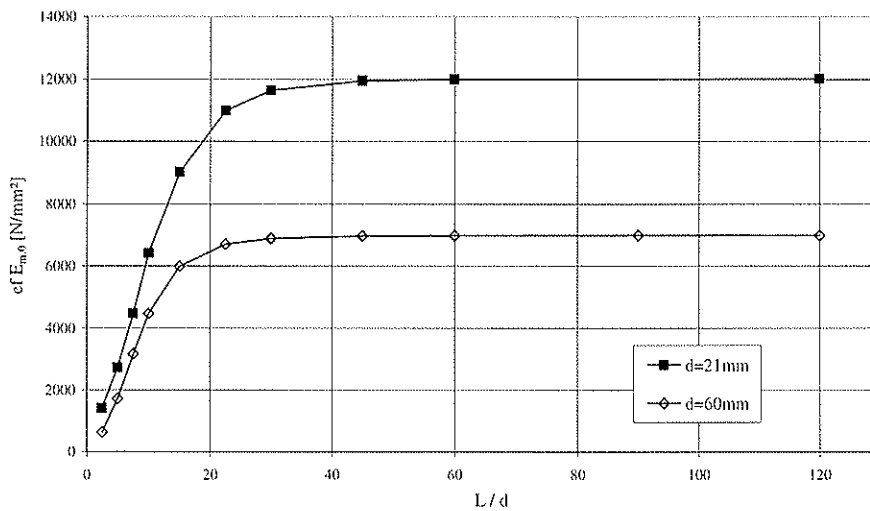


Fig. 8: Effective modulus of elasticity versus span to depth ratio for bending perpendicular to the plane and parallel to the grain direction of outer skins

Shear influence was observed for span to depth ratios smaller than 30 when bending perpendicular to the plane and parallel to the grain direction of outer skins: for decreasing span to depth ratios shear influence is increasing. Consequently the effective modulus of elasticity is decreasing.

For bending perpendicular to the plane and perpendicular to the grain direction of outer skins shear influence is not as distinctive as for loading parallel to the grain direction of outer skins. Shear influence was observed for span to depth ratios smaller than 20 for bending perpendicular to the plane and perpendicular to the grain direction of outer skins.

Fig. 9 shows the ratios of shear and bending deformation for a solid wood panel (nominal thickness 60 mm) for bending perpendicular to the plane and parallel to the grain direction of outer skins. Due to the very low rolling shear modulus, the proportion of shear deformation increases significantly for decreasing span to depth ratios. For small span to depth ratios shear deformation in cross layers hence have to be taken into account.

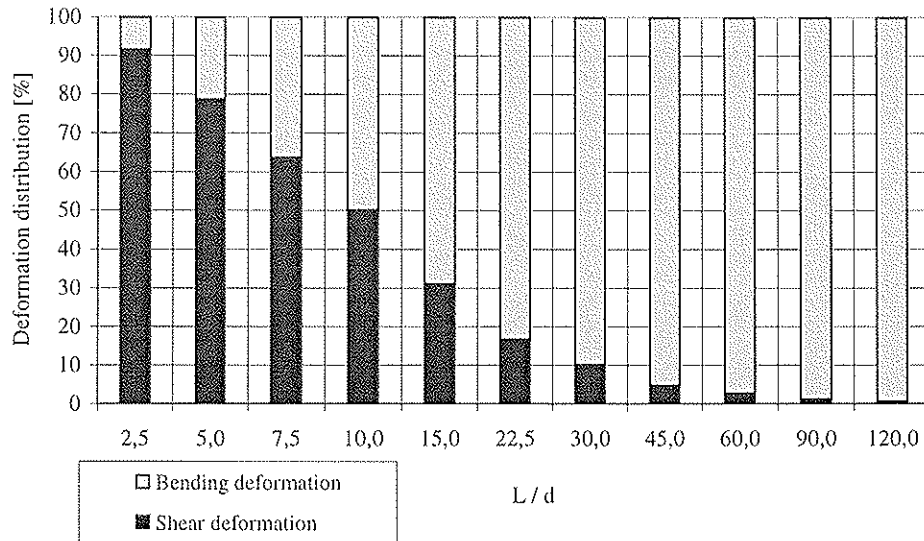


Fig. 9: Proportion of shear and bending deformation versus span to depth ratio for solid wood panel (nominal thickness 60 mm) when bending perpendicular to the plane and parallel to the grain direction of outer skins

In [3] and [4] different methods for the design of solid wood panels with cross layers are presented. The theory of mechanically jointed beams may be used for the design of solid wood panels with cross layers taking into account shear deformations. Instead of joint slip the shear deformation of cross layers is taken into account by the reduction factor γ_i when calculating the effective bending stiffness and the resulting stresses. The shear analogy method is a more precise calculation method for the design of solid wood panels with cross layers taking into account shear deformations. Both different moduli of elasticity and shear moduli of single layers may be considered. Using the composite theory for the design of solid wood panels with cross layers, shear deformations are not taken into account. Consequently the composite theory may only be used for high span to depth ratios for the design of solid wood panels with cross layers.

4 Summary

The stress distribution in and the deformation behaviour of solid wood panels with cross layers loaded perpendicular to the plane both depend on shear deformation. Due to the very low rolling shear modulus, shear deformation increases significantly depending on the thickness of the rolling shear layer.

The dynamic method of measuring the frequencies of a bending vibration was used for determining the rolling shear modulus of spruce. From the well known method for determining the modulus of elasticity parallel to the grain, a method to determine the modulus of elasticity perpendicular to the grain and the rolling shear modulus was derived. Rolling shear modulus and modulus of elasticity perpendicular to the grain both depend on annual ring orientation. Common values for the rolling shear modulus of spruce are between 40 N/mm² and 80 N/mm².

The load bearing performance of solid wood panels with cross layers loaded perpendicular to the plane was analysed using the shear analogy method. Shear influence was determined for different build-ups of solid wood panels depending on the type of stress and span to

depth ratio. For decreasing span to depth ratios, shear deformation increases significantly due to the very low rolling shear modulus. Significant shear influence was observed for span to depth ratios smaller than 30 for bending perpendicular to the plane and parallel to the grain direction of outer skins and for span to depth ratios smaller than 20 for bending perpendicular to the plane and perpendicular to the grain direction of outer skins.

5 Literature

- [1] Aicher, S, Dill-Langer, G. (2000): Basic Considerations to Rolling Shear Modulus in Wooden Boards. Annual Journal on Research and Testing of Materials 11, p. 157-165
- [2] Aicher, S, Dill-Langer, G., Höfflin, L. (2001): Effect of polar anisotropy of wood loaded perpendicular to grain. Journal of Materials in Civil Engineering, 01,02/2001
- [3] Blaß, H.J., Görlacher, R. (2002): Brettsperrholz – Berechnungsgrundlagen. Holzbau Kalender 2003, S. 580-598
- [4] Blaß, H.J., Fellmoser, P. (2003): Bemessung von Mehrschichtplatten. Bauen mit Holz, 08/2003 and 09/2003
- [5] Görlacher, R. (1984): Ein neues Messverfahren zur Bestimmung des Elastizitätsmoduls von Holz. Holz als Roh- und Werkstoff 42, S. 219-222
- [6] Görlacher, R. (2002): Ein Verfahren zur Ermittlung des Rollschubmoduls von Holz. Holz als Roh- und Werkstoff 60, S. 317-322
- [7] Hearmon, R.F.S. (1966): Vibration Testing of Wood. Forest Products Journal 16, p. 29-40
- [8] Kreuzinger, H. (1999): Flächentragwerke – Platten, Scheiben und Schalen – ein Berechnungsmodell für gängige Statikprogramme. Bauen mit Holz 01/1999, S.34-39
- [9] Neuhaus, F.H. (1981): Elastizitätszahlen von Fichtenholz in Abhängigkeit von der Holzfeuchtigkeit. Bochum, Ruhr-Universität, Technisch-wissenschaftliche Mitteilungen Nr. 81-8

INTERNATIONAL COUNCIL FOR RESEARCH AND INNOVATION
IN BUILDING AND CONSTRUCTION

WORKING COMMISSION W18 - TIMBER STRUCTURES

DEVELOPMENT OF THE "DISPLACED VOLUME MODEL" TO
PREDICT FAILURE FOR MULTIPLE-BOLT TIMBER JOINTS

D M Carradine

J D Dolan

Wood Materials and Engineering Laboratory
Washington State University, Pullman

UNITED STATES

C P Heine

Bosch Power Tool Division, Leinfelden-Echterdingen

GERMANY

Presented by D Carradine

P Quenneville received clarification that brittle failure was encountered.

H J Larsen was critical of the work and commented that the displacement characteristics were ignored and many more tests would be needed.

A Jorissen discussed the concept of the non-linearity adjustment factors and questioned whether they were used to adjust the load-deformation curve.

Carradine answered that 10 tests were conducted to establish the non-linearity adjustment factors.

M Ansell received confirmation that non-linear fracture mechanics approach was not used.

P Quenneville asked whether the tensile stress perpendicular to grain in the wood on the non loaded side of the bolt was considered. Carradine agreed that this could have an impact.

Development of the “Displaced Volume Model” to Predict Failure for Multiple-Bolt Timber Joints

D. M. Carradine¹, J. D. Dolan, P. E.¹ and C. P. Heine, P. E.²

Abstract

Modern timber structures are typically engineered such that elastic and inelastic deformations, and eventually failure occur in the connections securing wooden members together rather than as a failure in the wood members themselves. While bolts are often employed in modern engineered timber structures due to simplicity, ease of use, and effectiveness, they are extremely complex regarding response mechanisms to various loading. This is mainly due to the inherent anisotropic and variable characteristics of surrounding wood. A general model (MULTBOLT) was created that predicts load-displacement relationships, load distributions, capacities, and energy absorption characteristics of multiple-bolt timber joints of various configurations and subjected to reversed cyclic displacing functions. Fundamental parameters of the model are load and displacement levels at which material strengths are exceeded and stress concentrations become critical, leading to joint failure. The “Displaced Volume Method” (DVM) was developed to determine stresses around bolts using a closed-form computation of local forces for both slender and rigid bolts in wood. In combination with stress computations and appropriate failure criteria, failure is predicted as a function of parameters such as fastener spacing and end distance, fastener diameter, yield mode, member thickness, member width, and general material properties. Development and verification of the DVM through experimental testing is discussed for predicting failure in multiple-bolt timber joints.

Introduction

As the need for low to medium-rise residential structures continues to increase throughout the world, timber structures need to become more reliable in terms of performance, safer regarding resistance to natural disasters such as earthquakes, and more efficient in terms of amount of material consumed. Accomplishing this requires that the performance and response of each structural component, as well as interactions with other components in the structure, be thoroughly understood and accurately predicted.

One of the most important elements of a timber structure is the connector, and it is well established that the overall response of a wooden structure is a function of the performance of its connectors. Based on the brittle failure characteristics of wood in tension, and the much more ductile failure of steel, modern buildings are engineered such that elastic and inelastic deformations, and eventually failure occur in the connection rather than the wood members. Based on simplicity, ease of use, and effectiveness, metal dowel-type fasteners in particular, such as nails, screws and bolts, are commonly utilized

¹ Research Engineer and Professor, respectively, Wood Materials and Engineering Laboratory, Washington State University, Pullman, WA 99164, United States.

² Senior Product Manager, Bosch Power Tool Division, Leinfelden-Echterdingen, Germany.

connectors in modern engineered timber structures. While easily installed, bolts are extremely complex regarding response mechanisms to various loading cases. This is mainly due to the inherent anisotropic and variable characteristics of the surrounding wood. For example, while the mechanics of a single-bolt joint are complex enough to require comprehensive three dimensional finite element analysis to predict stresses (see Patton-Mallory, 1996), the response of an array of bolts in a joint is even more complex and far from being completely understood and predictable.

Constituting the simplest loading condition and joint configuration, single-bolt joints tested under unidirectional loading have attracted much research. Significant information on bolts available today is therefore based on single-bolt connections subjected to unidirectional displacing functions. Past research, however, demonstrated that the behavior of single-bolt joints cannot simply be extrapolated to predict the response of multiple-bolt configurations. This is especially true for stiffer bolts, which cause stress concentrations that may reach material strength and prematurely fail a joint.

An additional consideration when developing an accurate method for predicting connection behavior is that joints exhibit different and much more complex deformation mechanisms under cyclic or dynamic loading than when exposed to unidirectional forces. One characteristic that provides much difficulty for prediction models is the response dependency on loading history of joints in wood, also referred to as the “memory effect”. Load history dependency describes the case where hole oversize or parts of the hole may grow because the elastic limit in the wood is exceeded in a previous cycle and the surrounding wood fibers are crushed locally. Also, when loaded cyclically, a multiple-bolt joint whose holes are drilled oversize turns into a slack system, which is notoriously difficult to predict for timber, and no prediction models could be identified that accomplished such a task.

In view of improving the understanding of single- and multiple-bolt joints in timber, a theoretical model that furnishes scientists and designers alike with accurate information of load-displacement relation, not tied to a single input function, would be beneficial. Therefore, MULTBOLT, a generic model that predicts the load-displacement behavior of multiple-bolt joints under reversed cyclic and other displacement functions within the elastic *and* inelastic response range up to maximum load, was developed. MULTBOLT is an array of five models that have been interfaced and are solved numerically. A new mathematical hysteresis model describes the force of the individual bolt at each time step increment; a mechanically based structural stiffness model accounts for the interaction of one bolt with another bolt within the joint; an analytically based failure model computes the stresses at each time step and initiates failure if crack length equals fastener spacing; a stochastic model varies main input parameters; and a system identification routine estimates hysteresis parameters. Specific details on development of the model are found in Heine (2001). MULTBOLT was written in FORTRAN and is limited to joints that consisted of two members connected with one or more bolts configured in one row, where the abutting surfaces of the two members form the shear plane and that effects attributed to ‘time effects’ such as moisture content variations, as well as creep, weathering, and aging, were not considered.

The connection failure model employed for MULTBOLT, is the “Displaced Volume Method” (DVM). The DVM was developed to determine stresses around bolts using a closed-form computation of local forces for both slender and rigid bolts in wood.

In combination with stress computations and appropriate material failure criteria, failure of connections can be predicted as a function of parameters such as fastener spacing and end distance, fastener diameter, yield mode, member thickness, member width, and general material properties.

Objective

The objective of this paper is to present the development and verification of the DVM based on theoretical stress determinations and experimental test results conducted on single and multiple-bolt connections in wood.

Displaced Volume Method (DVM)

A critical facet to the development of an accurate prediction model for bolted connections in wood subject to cyclic loading is the displacement levels at which material strength would be exceeded, especially in multiple-bolt joints where changes in fastener spacing and number could induce stress concentrations and result in catastrophic failure. The DVM is used to compute stresses around slender and rigid bolts. DVM evades the difficulty of computing stresses in orthotropic materials for cases where the plane stress assumption is not valid such as slender bolts. The great advantage of DVM is that it allows the relative simple closed-form computation of local forces for both slender and rigid bolts. Once forces are identified, stress distributions can be computed and a failure criterion applied. Based on the Yield Theory, Jorissen's crack model (Jorissen, 1998), and a mechanics approach, DVM provides a robust method whose equations are comparatively easily programmed. In combination with stress computations and appropriate failure criteria, failure is predicted as a function of fastener spacing and end distance, fastener diameter, yield mode, member thickness, member width, and general material properties.

The concept behind DVM is similar to a buoyancy problem. If it is assumed that the wood foundation is a collection of individual, independent linear springs, then the reactive force exerted by the foundation on a body that is pushed into it is proportional to the displaced volume. The proportionality factor is the three-dimensional foundation modulus. The fact that the wood foundation is modeled by linear springs, despite the well established notion that that wood generally exhibits non-linear behavior, is no limitation since only failure is of interest. Catastrophic failure is described by a single point on the load-slip curve of the joint. How that point is reached, whether by linear or non-linear behavior is immaterial in this case.

If the foundation can be visualized as an array of an infinite number of independent linear springs, and if it is assumed that the dowel is infinitely stiff along its length, then the reaction force of a dowel with diameter d , plotted in three-dimensional space as a function of length (z -direction), deformation (x -direction), dowel diameter, and reaction per unit length (p -direction) resembles a triangular plane as depicted in Figure 1. The net force necessary to rotate the dowel about the point predicted by the Yield Theory is equal to the more darkly shaded area. However, the total force on the dowel equals the area of all triangular planes along its length. Observe that all forces act in the x - z -plane parallel to the x -axis. As the joint is displaced, the bolt rotates and ultimately deforms similar to one of the modes described by the Yield Theory. For example, rotating in accordance to Mode II, the bolt displaces a volume as it is pressed into the wood

foundation as depicted in Figure 2. If the foundation modulus is known, total reaction force of the foundation can be computed and from it, shear stresses and stresses perpendicular to the grain are obtained.

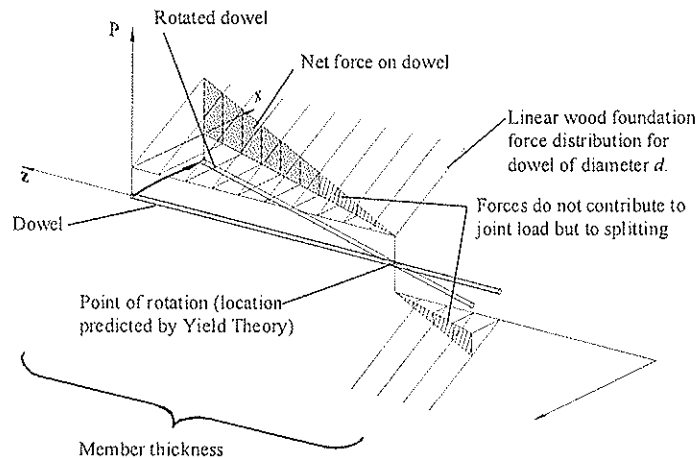


Figure 1. Reaction Force Determined by Displaced Volume of Dowel where Foundation is Modeled as an Array of Linear, Independent Springs

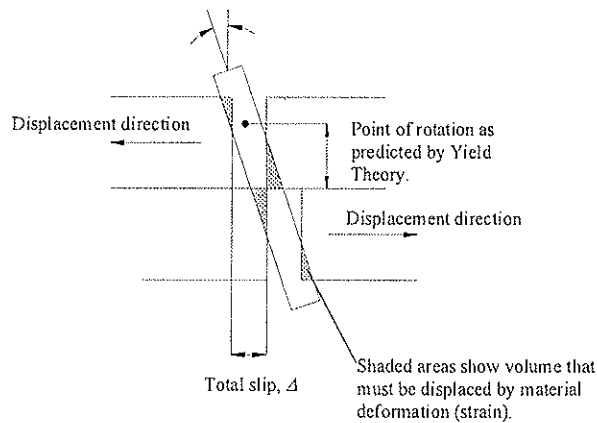


Figure 2. Example of Displaced Volume for Mode II Deformation

In multiple-bolt joints, failure typically occurs due to a combination of perpendicular to grain stresses and shear stresses. Experiments confirm that joint failure can be most frequently classified as row tear-out or splitting. When a bolt is pressed into a wood foundation (real foundation, not approximated by independent springs), stresses perpendicular to the grain develop, attributed to the resultants of the reaction forces on the surface of the dowel. Furthermore, depending on the angle of friction, some fibers are deviated around the bolt, whereas others are crushed underneath it, ultimately leading to the formation of two cracks as the bolt gets pushed farther into the foundation. According to Jorissen (1998), the width of the compression region parallel to the grain may be determined by the following equation:

$$\delta = 2(r_{bolt})\sin\phi = d_{bolt}(\sin\phi) \quad (1)$$

where,

- δ = width of compression region, (mm),
- r_{bolt} = fastener radius (mm),
- φ = angle of friction, and
- d_{bolt} = fastener diameter (mm).

Therefore, as a result of friction between the bolt–wood interface, one may assume that there are pronounced “regions” as shown in Figure 3, where the foundation is stressed parallel and perpendicular to the grain, respectively. Acting shear stresses can then be computed based on the volume displaced within the compression region parallel to the grain, while stresses perpendicular to the grain can be determined in relation to the volume displaced within the compression region perpendicular to the grain.

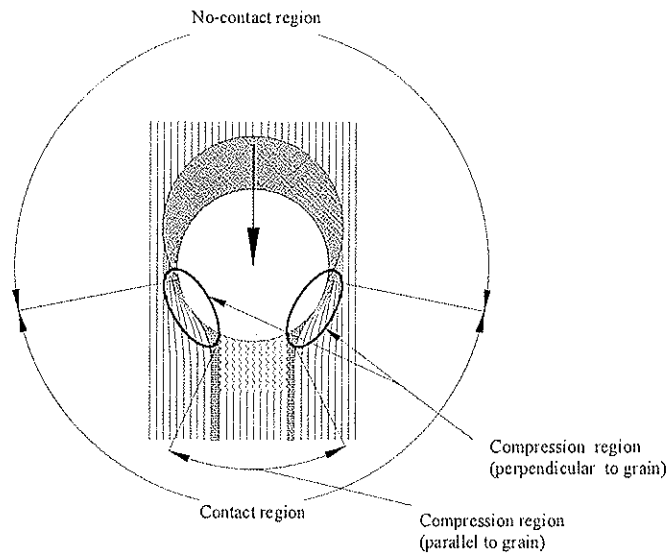


Figure 3. Regions Where Stresses Parallel to the Grain Dominate and Where Stresses Perpendicular to the Grain Dominate

When implemented in MULTBOLT, displaced volumes are directly related to their cross-sectional areas, which are derived first. Slack and differences in slack between directions of movement in the connection are included in all derivations although the exact location of the bolt within the hole was not known. Total slack in positive ($slack_p$) and negative ($slack_n$) direction of movement are known. It was further assumed that slack did not affect the point of rotation as predicted by the Yield Theory. Both area and volume output were verified by the graphical program AutoCAD R14.

In plane view (parallel to the shear plane of the joint), a round bolt pushing into a wood foundation of an oversized hole may be abstracted as two intersecting circles with different diameters, which aids in the simplification of the analysis. Actual cross section of the rotated bolt in plane view is an ellipse. Heine (2001) presented derivations for determining the area, A^* , which represented the crescent shaped region that occurred within the area of the bolt cross section, yet outside of the bolt hole where the bolt was embedded within the wood, as shown by the dotted line in Figure 4. The following

equations provide reasonable estimations of the areas of strain parallel and perpendicular to the grain, which are shown in Figure 4:

$$A_{\text{parallel}} = d_{\text{bolt}}(\sin\phi)\Delta \quad (2)$$

$$A_{\text{perp}} = (A^* - A_{\text{parallel}})/2 \quad (3)$$

where,

Δ = joint displacement, (mm).

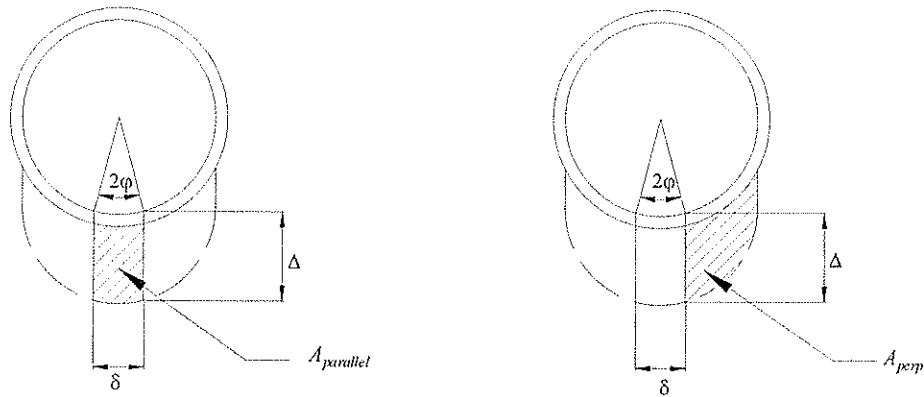


Figure 4. Strain Areas for Parallel and Perpendicular to Grain

Displaced volumes for Yield Modes I, II, III, and IV were derived (Heine, 2001) in terms of strain areas perpendicular and parallel to grain, joint displacement, hole oversize, member thickness, member embedment strength, yield mode predictions, and the yielding moment of the bolts. Displaced volumes are computed based on the assumption that the bolt cross section remained circular if viewed in the shear plane when, in fact, the cross section was an ellipse whose main axis elongated with increasing rotation angle. This assumption introduces two errors. First, the computed strain area is smaller than the actual strain area and second, the calculated heights from the edges of the members to the point where bolt bearing started are shorter than actual, resulting in a displaced volume that was too small. To rectify the problem and diminish the error, two adjustment factors are introduced (obviously, the factors are not applied to Mode I yield) and included when displaced volumes determined. Note that the error is not completely compensated for because the strain area derived is a segment rather than a sector of a circle, and the proportionality to an elliptic area is only approximate.

If it is assumed that the wood foundation resembles a Winkler foundation in that it is an array of linear independent springs, then the same displaced volume always produces the same reactive force, no matter what the projected area is. To account for nonlinear deformations perpendicular and parallel to the grain, the nonlinearity factor Ω , is introduced. Furthermore, the ratio of E_{para} to E_{perp} is assumed fixed at 15 and the ratio of E_{para} to G_{para} is assumed fixed at 16 (Bodig and Jayne, 1982). The pseudo foundation modulus perpendicular to the grain is modeled as a composite of both local and global stiffness effects to include the impact of changing member width relative to fastener diameter. Global stiffness effects are obtained based on beam-on-elastic-foundation theory. In order to account for local effects, the global stiffness is arranged in series with the material, or local, stiffness. The pseudo foundation modulus parallel to grain takes into account the shear strain distribution along the crack planes. If a bolt is laterally

loaded, the surrounding wood counteracts the load, and ideally, forces are shared equally on either side of the bolt due to symmetry. Key to deriving the foundation modulus was the insight that forces parallel to the grain act across the area of the segment between the crack planes. Moreover, the summation of shear stress over the crack plane area between two bolts, or between a bolt and a member free end, counteracts the force parallel to the grain.

Having derived the pseudo foundation moduli, it is possible to compute the reaction force caused by a displaced volume. Each bolt displaces several volumes and hence causes more than one reaction force. The number of volumes displaced per bolt changes depending on yield mode. To compute failure stresses, the reaction forces obtained are added or subtracted based on their direction of application. Perpendicular to grain reaction forces all act in the same direction and are therefore added (in this case, due to symmetry, only half of the joint cut perpendicular to the shear plane is considered). Attributed to their different directions and interactions, parallel to the grain forces (used to compute shear stresses) for each segment between bolts or between a bolt and a member end are computed by the following (see Figure 5):

$$F_{para1(shear),member1} = -F_{para11(shear),bolt1}$$

$$F_{para2(shear),member1} = F_{para12(shear),bolt1} - F_{para11(shear),bolt2} \quad (4)$$

for Member 1 and negative direction of movement. Other forces are obtained accordingly. Depending on yield mode, some forces depicted in Figure 5 may be zero. However, for Modes II and III, parallel to grain forces are higher than the net force in the segments between the member ends and the bolt, increasing splitting potential at that location.

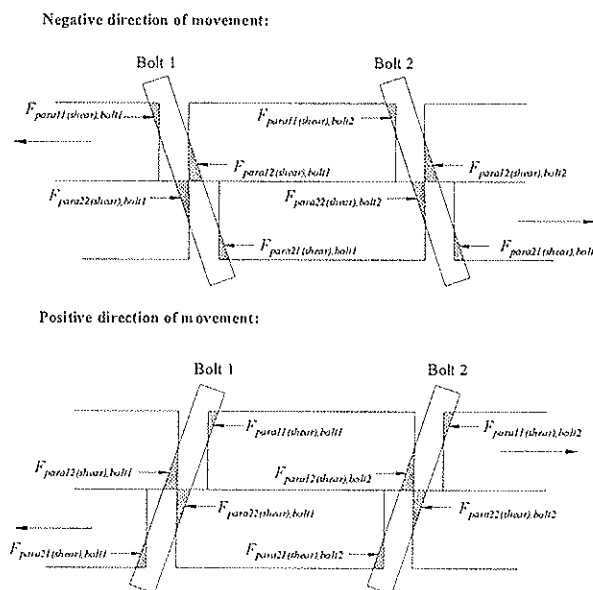


Figure 5. Example Joint (Mode II) to Demonstrate Direction and Consequent Summation of Forces Parallel to Grain Caused by Displaced Volumes (Shaded Areas)

Stress Distributions

Shear and perpendicular to grain stresses are identified in the crack planes because it is assumed that failure occurs at this location. As elaborated previously, catastrophic failure is primarily due to a combination of perpendicular to grain stress and shear stress. Stresses do not act independently, however, which means that normal stress parallel to the grain needs to be accounted for as well. Based on the same assumptions as employed to derive the foundation modulus perpendicular to the grain, stresses perpendicular are obtained using semi-infinite beam on elastic foundation theory and the principle of superposition to account for multiple fasteners. It is important to realize that unlike the force computed with the displaced volume method, the sum of the stresses perpendicular to the grain over the beam length is not affected by the foundation modulus. However, stress distribution changes as the foundation modulus relative to beam stiffness changes. Figure 6 shows stresses perpendicular to grain for individual bolts, and the resulting total stress computed by MULTBOLT, for a three-fastener joint.

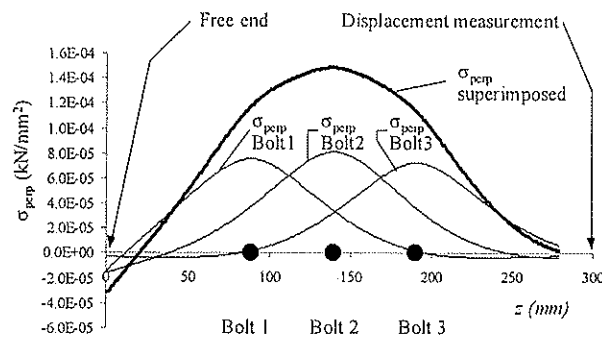


Figure 6. Stresses Perpendicular to Grain and Computed Superimposed Stress for Three-Bolt Connection

Shear stresses are computed based on the shear strain distribution and the effect of bolt hole diameter is included. Similar to the pseudo foundation modulus, stresses parallel to the grain are computed along the length, $L = \text{spacing} - \text{hole diameter}$, rather than using the spacing. Figure 7 (left) reveals the shear stress distribution of Member 1, for positive and negative displacements and bolts yielding in Mode II. There is no interaction between the shear stresses caused by the individual fasteners. The segments between the bolts and between a bolt and a member end are confined by two free ends and are thus completely isolated such that no shear forces are transferred to the next segment.

Parallel to grain stresses are computed based on the average normal force acting in the member within each segment. Parallel to grain stress distribution is a stepwise function along the length of the member. Figure 7 (right) shows the computed parallel to grain stresses for Member 1 in a three-bolt joint with bolts yielding in Mode II for negative and positive displacements. Step size is not constant and depends on the resisted force at each bolt.

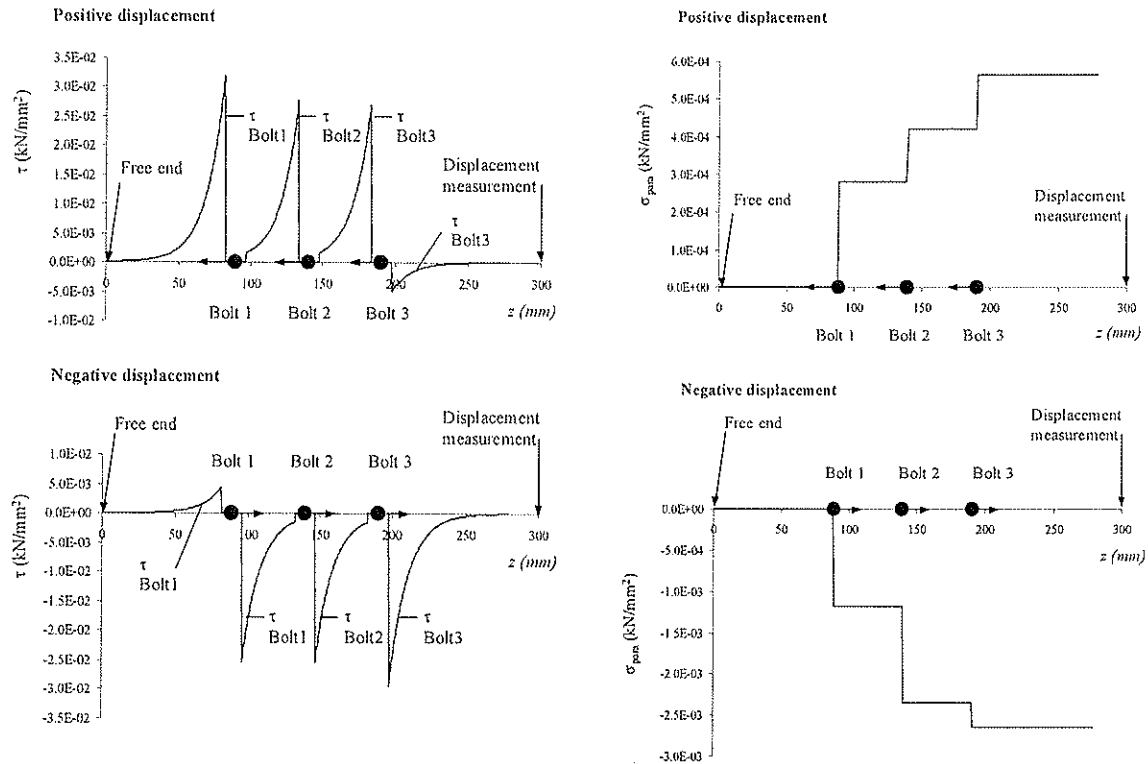


Figure 7. Shear Stress Distributions (Left) and Parallel to Grain Stress Distributions (Right) as Computed by MULTBOLT for Three-Bolt Connections

Failure Criteria

It has long been suspected that stresses in principal directions influence each other and therefore affect material failure. Especially for fibrous materials, stress interaction may change failure mode and failure stress. The Tsai-Wu failure criterion is an interactive failure theory that has been used mostly for fiber reinforced materials and was derived from the well known von Mises criterion for isotropic materials. A comprehensive discussion of the Tsai-Wu Criterion for fiber reinforced composite materials (also applicable to wood) can be found in Hyer (1997). In light of the fact that the stresses computed along the member of a multiple-bolt joint are not constant, and given the desire for the failure criterion to account for crack development and growth, the Tsai-Wu criterion and its application were somewhat modified. Stress variability along member length and inclusion of crack development made it necessary to check for failure in each direction separately by keeping all other stresses constant. For all but the direction under consideration, the average stress over a given segment between two fasteners, or a fastener and a member end, is computed. The Tsai-Wu criterion is subsequently applied to each length increment of the stress grid varying only the relevant stress per increment. The procedure is repeated for each direction. Stresses computed by MULTBOLT may exceed material strength of any given direction and stress combination (expressed as $Tsai-Wu \leq 1.0$). In this case, it is assumed that a crack is forming. MULTBOLT then checks whether the section without a crack is capable of absorbing

additional force. Thus, if area A_2 , which represents the potential strength still stored in the material, is less than area A_1 , catastrophic failure occurs.

Failure Model Calibration

The failure model was calibrated with the average test data obtained from ten tests of a single bolt joint yielding in Mode II. Details on the experimental connection testing are provided by Anderson (2001). All validation predictions were for multiple-bolt connections and were made prior to obtaining experimental results. Mode II was selected because failure is of a brittle nature. Good results were achieved with $\Omega_{shear} = 2.61$ and $\Omega_{perp} = 0.37$. A Ω_{perp} of less than 1.0 signals that failure stresses perpendicular to the grain needed to be amplified by increasing the foundation modulus perpendicular to the grain to produce the desired results. The reason probably lies in the fact that no local peak stresses are included in the stress derivation. Shear stresses are effectively reduced by dividing the foundation modulus by $\Omega_{shear} > 1.0$, which may be attributed to the assumption that the entire shear force is transferred by the crack planes only. The calibration relies on the assumption that shear strength and perpendicular-to-grain strength equally affect connection failure. Exact contributions of each strength property are extremely difficult to obtain.

Summary and Conclusions

Formulation of a model for accurately predicting the load displacement behavior of multiple-bolt connections in wood (MULTBOLT) included the development of the DVM, which is utilized to compute stresses around bolts and predict failure of the joints. The DVM in combination with the European Yield Theory, a modified Tsai-Wu failure criterion, and modified stress computations based on the approach advanced by Jorissen (1998), provides an effective means of simulating brittle failure of multiple-bolt joints in timber. The failure model predicts failure of rigid and slender fasteners alike, inserted in tight-fit or oversized holes and was validated using data from single shear single- and multiple-bolt joints subject to unidirectional and cyclic displacing functions.

References

- Anderson, G. T. 2001. *Experimental Investigation of Group Action Factor for Bolted Wood Connections*. MS Thesis, Virginia Polytechnic and State University, Blacksburg, VA. 300 pp.
- Bodig, J. and B.A. Jayne. 1982. *Mechanics of Wood and Wood Composites*. Van Nostrand Reinhold Co. New York, NY. 712 pp.
- Heine, P. C. 2001. *Simulated Response of Degrading Hysteretic Joints with Slack Behavior*, Ph. D. Thesis, Virginia Polytechnic and State University, Blacksburg, VA. 292 pp.
- Hyer, M.W. 1997. *Stress Analysis of Fiber Reinforced Composite Materials*. WCB/McGraw-Hill. New York, NY. 627 pp.
- Jorissen, A.J.M. 1998. *Double Shear Timber Connections with Dowel Type Fasteners*. Ph. D. Thesis, Delft University Press, Delft, Netherlands. 264 pp.
- Patton-Mallory, M. 1996. *The Three Dimensional Mechanics and Failure of Single Bolt Wood Connections*. Ph. D. Thesis, Colorado State University, Fort Collins, CO, USA. 310 pp.

INTERNATIONAL COUNCIL FOR RESEARCH AND INNOVATION
IN BUILDING AND CONSTRUCTION

WORKING COMMISSION W18 - TIMBER STRUCTURES

MECHANICAL MODELS OF THE KNEE JOINTS WITH CROSS-LAPPED
GLUED JOINTS AND GLUED IN STEEL RODS

M Noguchi

Graduate school of Agriculture, Kyoto University

K Komatsu

Research Institute for Sustainable Humanosphere, Kyoto University

JAPAN

Presented by M Noguchi

H Blass asked whether a certain slip modulus per glue area was used. An example is the rolling shear modulus found by Karlsruhe of 3 N/mm/mm² of area. It would be interesting to compare the results with this approach. Noguchi responded that it was not done and agreed that it would be interesting.

Mechanical Models of the Knee Joints with Cross-Lapped Glued Joints and Glued in Steel Rods

Masahiro Noguchi* and Kohei Komatsu†

*Graduate school of Agriculture, Kyoto University, Japan

†Research Institute for Sustainable Humanosphere, Kyoto University Japan

1 Introduction

Adhesive joints are used widely, especially in combination with glued in steel rods. However, there are some problems with the design methods when applied for moment transmitting application. In this paper, new design methods of glued in steel rods (GIR) joints, and cross-lapped glued joints (CLJ) are proposed for transmitting bending moments.

First, five knee joint types were tested, using GIR, CLJ and combinations some having three others having five parallel members. The results show that the strengths of the GCJ joint having three parallel members is higher than the bending strength of a solid beam with the same cross-section (GCJ=combination of GIR and CLJ). The strengths of the other joints are 0.7 to 0.8 times the bending strength of a solid beam. While, the rigidity of CLJ is much smaller than that of GIR. The rigidity of GCJ is in between the rigidity of the CLJ and GIR joint. The aim is to derive a new design method taking into account the behaviour mechanism of these joints. A new mechanical model for the CLJ and GIR joint for moment transmitting are proposed.

We tried to find out the reason why the rotational rigidity of the CLJ is not infinite as tests indicate? As the glue lines can be thought of too thin and too brittle to deform, it can be assumed that the glue lines are rigid bodies. Therefore, the deformation components are caused by only bending and shear of timber members. The stresses occur in both deformed parts (timber members) and at the interface between the rigid body (glued area). We assume that the stresses in the rigid body are equal to that of the stresses at the interface. From this, we made the hypothesis that both rotational deformation of CLJ and the stresses of glue line are dependent of the bending and shearing deformation of the timber. A orthogonal co-ordinate system at the interface is considered. With the hypothesis and Kelvin's theorem - half the torque is taken by the shear stresses in x-direction while the other half is taken by the components in the y-direction CLJ was modelled. Moreover, the effect of number of glue lines is taken in account.

In GIR, not only the pulling component of rod but also shearing component of rod can be taken in account using "theory of the beam on an elastic foundation". In old models, the lateral force components were ignored. Split failures occurs due to the lateral force component. Therefore, it was thought that the lateral force component is the significant factor for estimating of the split failure as well as to estimate the exact rotational rigidity.

From the comparisons between calculations and experimental results, it was recognized that the stiffness and strength in CLJ, and GIR could be predicted using our models.

2 Experiments

Fig. 1 and 2 show the specimens used in this study. Five types of specimens were chosen. Type A specimens were assembled with three member layers (each width is 35 mm), Fig. 1 (a). Type B specimens were assembled in the same way however two layers were connection using glued in rod joints, Fig. 1(b). Type C specimens were assembled with five layers (each width is 20 mm), Fig. 1(c). Type D specimens were assembled with five layers with glued in rod joints as shown in, Fig. 1(d). Type E specimens were assembled traditionally with one layer, Fig. 1(e).

All specimens were made of Sugi glulam having JAS (Japanese Agricultural Standard) strength grade of E65 – f 220 (MOE = 6500kg/mm² and MOR= 22 MPa), the average moisture content of 11 %, and the mean density of xxx kg/m³. The glued in rod joints were located as given in Fig. 2. An epoxy resin adhesive was used. The insert length of the rod in each member was set to 100 mm. The rod diameter is 16 mm and the predrilled holes 18 mm. The time to cure was at least two weeks.

Monotonic loads were applied to failure by applying a lateral force at the top of the specimens, as illustrated in Fig. 3.

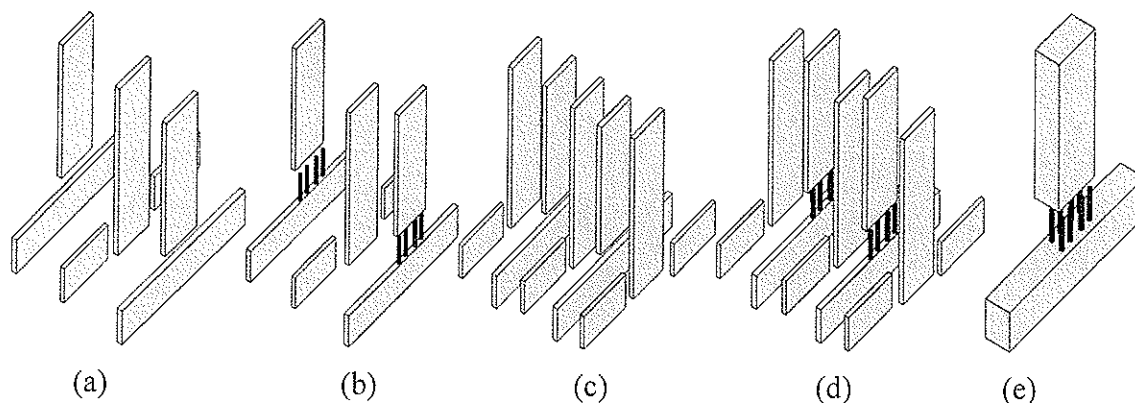


Fig. 1 Specimen

3 Results and Discussions

Fig. 4 shows the bending capacity of the joints. The strength of Type B was higher than that of bending capacity of a solid beam with the same cross-section. The strengths of the others are from 0.7 to 0.8 times the bending strength of the solid beam. The strength of Type D was less than Type C. The reason is that the splits originated from the holes. It might be that the holes were too large in comparison to the width of layers. Fig. 5 shows the results of the rotational stiffness of the joints. Rotational stiffness of Type A and B (CLJ) were much smaller than that of type E (GIR). The rigidity of type B and D (GCJ) were much higher than CLJ. Summarising the stiffness, GCJ was much more rigid than CLJ with the same number of layers. The stiffness of CLJs are less than those of GIR.

In the Japanese code, the span of timber beams is limited to 12 times the height of the beam to avoid a detailed structural analysis. Taking this span to depth ratio as a starting point and the rotational stiffness R from the experiments a factor, which

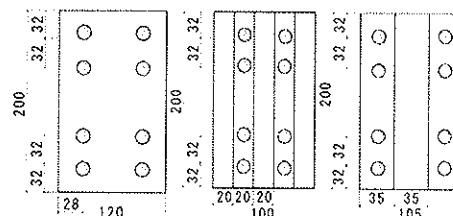


Fig. 2 Rod arrangement

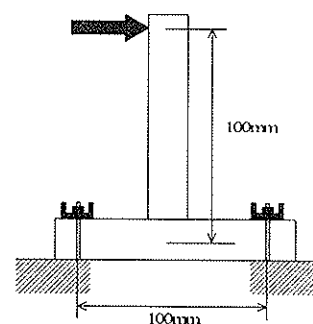


Fig. 3 Test set up

relates the rotation to the bending stiffness is the value, $\beta_r (= \frac{RI}{EI})$ here equal to 10.4, for type A. The deflection of a beam in case of fixed ends is 0.2 times that of a simply supported beam. When span was increased $\sqrt[3]{5}$ times, β_r becomes equal to 17.7. In reality β_r ranges from 10 to 17.7. As there are cases that adhesive joints cannot be assumed rigid in vertical load ^{1, 2, 3)}, it significantly affects the stress distribution, a method to judge whether the joints can be assumed as rigid or not is important. While in Japan, the story drifts, in horizontal load (seismic design), is the most governing criteria in timber portal frame structures, it also is significant to make a suitable method to estimate the story drift precisely. Therefore, we tried to make a mechanical model to estimate both stiffness and strength of the CLJ and GIR.

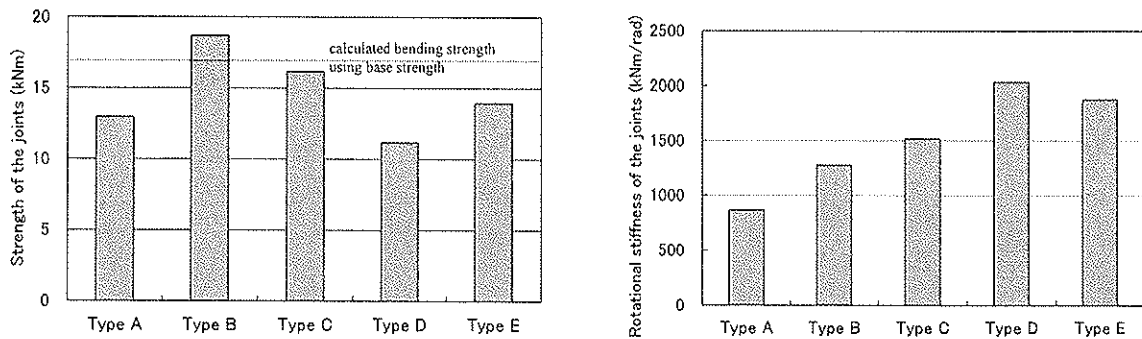


Fig. 4 Strength of the joints by tests Fig. 5 Rotational stiffness of the joints by tests

4 proposal of Mechanical Model

The tested knee joints consists of a number of timber members with glued joints and joints with glued in rods. It means that it is necessary to consider the properties of all components, i.e., each member, each glued joint, and the glued in rods. In our model, each component was modelled as simple as possible, and it is focussed to bring out the mechanism of the joint deformation.

4.1 The knee joint model for GIR

To explain the reason why GIR is more rigid than CLJ, all possible component must be considered. Fig. 6 shows the vertical and horizontal normal stress distribution and deformation. From this figure it is clear that we need to consider both axial and lateral components in the rod.. So, in the model below, the axial and lateral components were considered.

In general, moment transmitting joints transmit the moment from a member to another member. In GIR applied as a column-beam joint the glued in steel rods must transmit the bending moment and shear forces. This means that the moments and axial forces in the rods must be in equilibrium at interface between beam and column (in Fig. 6 (e)). Also the axial forces in the rods at interface must be in equilibrium with the axial force resulting from the longitudinal stress components along the rods in each member. Similarly, the bending moment in each individual rod at interface also must be equilibrium to the bending moment resulting from the lateral stress components along the rods. Using the above concept, a mechanical model was derived.

4.1.1 Resisting moment due to lateral component

The moment resulted from the lateral component of rods inserted in the beam M_{oi} is expressed as:

$$M_{oi} = \int_0^{t_{ij}} \sigma_{xij} x_{ij} dx_{ij} = \int_0^{t_{ij}} k_{ij} v_{ij}(x_{ij}) x_{ij} dx_{ij} \dots (1)$$

To differentiate Eq. (1) two times, Eq. (2) was obtained.

$$\frac{d^4 v_{ij}(x_{ij})}{dx_{ij}^4} + 4k_{ij} v_{ij}(x_{ij}) = 0 \dots (2)$$

General solution:

$$v_{ij}(x_{ij}) = O_{ij} \sin \lambda_{ij} x_{ij} \cdot \cos \lambda_{ij} x + P_{ij} \sinh \lambda_{ij} x_{ij} \cdot \cos \lambda_{ij} x_{ij} + Q_{ij} \sin \lambda_{ij} x_{ij} \cdot \cosh \lambda_{ij} x_{ij} + R_{ij} \sinh \lambda_{ij} x_{ij} \cdot \cosh \lambda_{ij} x_{ij}$$

where, t_{ij} : is the embedment length of the rod in the column, s_{ijx} : the bearing displacement of rod at x_{ij} , k_{ij} : the bearing constant of i -th rod in vertical member, σ_{xij} : resisting force per unit area, x_{ij} : the distance from the interface

between beam and column, $\lambda_{ij} = \sqrt[4]{\frac{k_{ij} d_i}{4(EI)_{si}}}$,

$(EI)_{si}$: bending stiffness of rod, d_i : the diameter of rod,

Eq. (2) expresses 'the theory of the beam on an elastic foundation'. It means that the bending components due to the lateral resistance of the rod are clearly depended on the deformation of the rods.

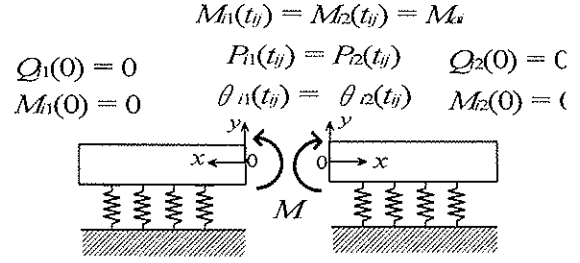


Fig. 7 Boundary conditions

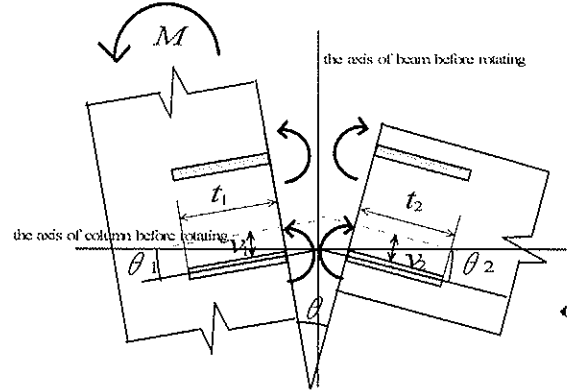


Fig. 8 definition of rotational angle

Fig. 7 shows the boundary conditions. At the interface between beam and column, the equilibrium condition of both bending moment and shear force and the capability of the rotation angle were set. The moment is introduced at the interface as a load. The ends of the rods away from the interface can be assumed as free so both shear force and bending moment are equal to zero.

Here, rotational angle of the knee joint can be defined using v_i and t_i as follows (Fig. 8):

$$\theta = \theta_1 + \theta_2, \quad \text{where, } \theta_{ij} = \frac{v_{ij}}{t_{ij}} \dots (3)$$

$$\text{where, } v_{i1} = \frac{-M}{2\lambda^2 EI_s} \cdot \frac{B(F - H - 2D)\mu^2 + E(C - 1)\lambda\mu + A(G - C)\lambda^2}{B(G - C)\mu^2 + A(C + H + 2D)\lambda^2}$$

$$A = \cos \lambda_2 t_2 \sin \lambda_2 t_2 - \cosh \lambda_2 t_2 \sinh \lambda_2 t_2, \quad B = \cos \lambda_2 t_2 \sin \lambda_2 t_2 + \cosh \lambda_2 t_2 \sinh \lambda_2 t_2$$

$$C = \cosh^2 \lambda_1 t_1 + \cos^2 \lambda_1 t_1, \quad D = \cos \lambda_1 t_1 \sin \lambda_1 t_1 \cosh \lambda_1 t_1 \sinh \lambda_1 t_1, \quad E = \cosh^2 \lambda_2 t_2 - \cos^2 \lambda_2 t_2$$

$$F = \cosh^2 \lambda_1 t_1 - \cos^2 \lambda_1 t_1, \quad G = \cosh^4 \lambda_1 t_1 + \cos^4 \lambda_1 t_1, \quad H = \cosh^4 \lambda_1 t_1 - \cos^4 \lambda_1 t_1$$

In case of calculating using v_{i2} , subscript 1 and 2 should be exchanged.

Above all, M_{oi} is calculated as:

$$M_a = \sum M_{ai} \dots (4)$$

4.1.2 Resisting moment due to axial component

The moment due to axial component M_o is expressed as:

$$M_o = \sum P_i l_{mi} \dots (5) \text{ where, } l_{mi}: \text{ the length between the neutral axis of } i\text{-th rod}$$

In this paper, the model of Koizumi and Sasaki et al. were applied. See the reference (15)

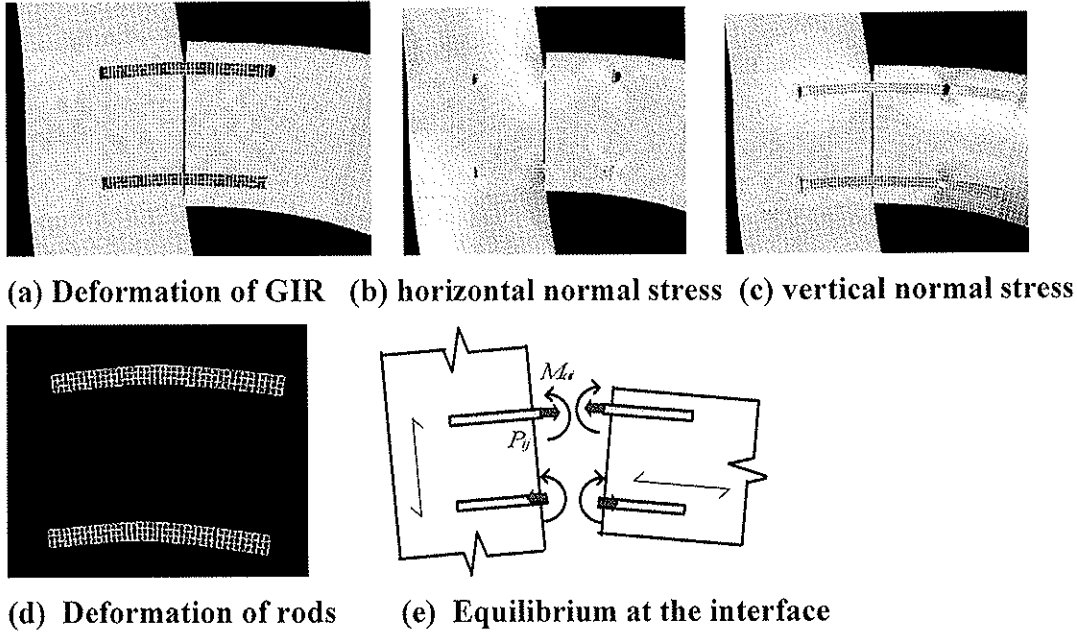


Fig. 6 GIR: stress and deformation distribution

4.1.2 Combined, bending moment due to axial and lateral components

The moment of the knee joint was defined as the sum of the moment due to axial and lateral components at the same rotational angle.

$$M = M_a + M_o \dots (6)$$

4.1.3 Strength of GIR

Splitting failure due to Glued in rod

Using Eq. (2), the shear forces of the rod at interface caused by the applied moment was derived as:

$$P_i = \frac{-2\mu M}{\lambda^2} \cdot \frac{E(2D + H - F)\lambda - BH\mu}{B(G - C)\mu^2 + A(2D - F - H)\lambda^2} \dots (7)$$

At the zones circled in Figure 9 (panel zone), the moment distributions are changed remarkably. This means that the shear forces and shear stresses are concentrated at the panel zone. Therefore, it was taken in account to consider the panel zone as an area prone to shear failure (Fig. 9).

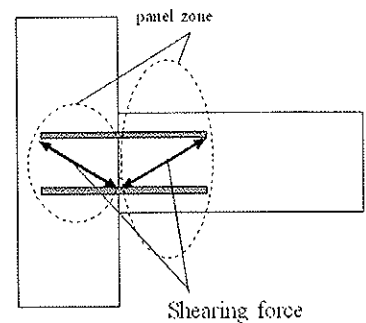


Fig. 9 panel zone in GIR

$$M = \tau_{wood} t h_1 t_2 \dots (8)$$

4.2 The knee joint model of CLJ

Two main torsion theories exist, Coulomb's torsion theory and Saint Venant's torsion theory⁴⁾. One may think that the torsion of glue lines can be explained using Coulomb's torsion theory because the glue lines can be thought of as very thin. According to Goodier's hypothesis⁴⁾, the torsion of arbitrary cross-section with infinitely small length can be explained using Coulomb's torsion theory. However, as the modulus of elasticity and rigidity of timber are not high compared to the modulus of elasticity and rigidity of the adhesive, the adhesive will force local deformation of the timber very close to the glue line. This local phenomenon is called the effective width. When the stress distribution in the glue line is considered, it cannot be thought that the effective width of glue lines are very small. Therefore, it is thought that the stress distribution of glue line should not be explained using the Coulomb's torsion theory. The effective width of timber to the torsion of glue lines cannot be thought large enough to applying the Saint Venant's torsion theory. Actually, it can be thought that the stress distributions of glue lines have the characteristics of both theories.

The characteristic of Saint Venant's torsion theory is that the stress at shorter sides is much higher than that at longer sides. Kelvin⁵⁾ founds the necessary condition of this phenomenon. According to Kelvin and others. (demonstrated by Timosienko⁴⁾), it was found that half the torque was due to the x -components of the shear stress and the other half to the y -components in Saint Venant's torsion theory. To extend Kelvin's hypothesis, we made a hypothesis that the moment due to x -components of shear forces is equal to that

due to y -components.
$$M_x = \frac{1}{2} M, \quad M_y = \frac{1}{2} M \quad \dots (9)$$

The characteristic of Coulomb's torsion theory (based on Goodier's hypothesis) is that the stress distribution is in proportionally related to the rigid body displacement of side members. Doing so, we made the hypothesis that the stress of glue line occur due to the bending and shearing deformation of timber.

We thought that the rotational characteristic of CLJ was governed by the above two hypotheses. The theory proposed was derived as follows:

The aim of this theory is to explain the stiffness of CLJ. First, the parameters of deformation were identified. Fig. 10 shows the all-possible deformations. As the glue lines can be thought too thin and brittle to deform, it can be assumed

that the glue lines are rigid bodies. Therefore, the deforming components are defined as the only the bending and shear deformation of timber.

Fig. 11 shows the axial stress and shear stress distribution of each member. From this figure, bending moment and shear stress is distributed approximately in conformity with basic beam theory. In other words, the bending and shear deformation of each member at panel zone is assumed to behave as the basic theory predicts. In general, the stresses appear where deformations occur. It can be thought that the stress acts to prevent the solid bodies from deforming and fracture. Therefore, in CLJ, shear stresses in the glue line occur to

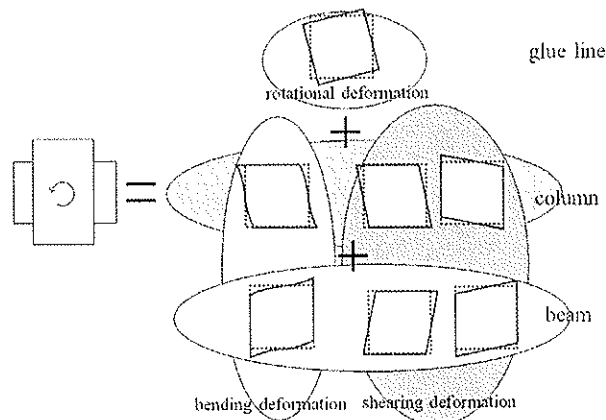


Fig. 10 Deformation factors of CLJ

prevent timber from deforming, because glue lines can be thought as rigid bodies. As the glue lines prevent the members to deform locally.

Next, it is discussed why the torsion-like stresses occur at the glue lines. Corresponding to the cross lapped joints, it had been recognized that beams or columns transmit bending moment at panel zone. Therefore, it can be reasonably assumed that each member is subjected to a bending moment M , which introduces a coupling moment M in the panel zone, which formed a torque M to resist the glue lines. Therefore, the glue lines are twisted by the torque M .

4.2.1 Timber deformation

At panel zone, the bending moment between timber members is transmitted. So, the moment of the panel zone changed along its length. It is assumed that at the panel zone only the moment works. The final aim of this model is derived design method. In order to simplify the design equation, the distribution of the shear stress due to a moment was assumed as constant. First, the shear deformations of panel zone were considered, focussing on the timber member. Therefore, δ_{js} could be expressed as follows.

$$\delta_{js} = \beta \frac{M_j}{G_j t_j b_j h_j} x_j \quad \dots (10)$$

where, G_j : shear modulus of j -th member, t_j : width of j -th member, b_j : height of j -th member, h_j : the length of the panel zone of j -th member, β : undetermined coefficient, which means the effect to prevent the timber deformation due to the glue lines.

Considering timber bending deformation at panel zone, each member is considered as a beam. Using basic beam theory, the following relationship holds:

$$Q_j(x_j) = \frac{M_j}{h_j} = \frac{d^3 \delta_j}{dx_j^3} \quad \dots (11)$$

Meanwhile, the centre of panel zone is assumed to be symmetric, The following boundary conditions are possible:

$$M_j(0) = 0, \delta_j(0) = 0, \text{ and } \theta_j(0) = 0. \quad \dots (12)$$

Using these boundary conditions and Eq. (11), the deflections of the beam due to bending moment $\delta_j(x_j)$ can be derived as follows:

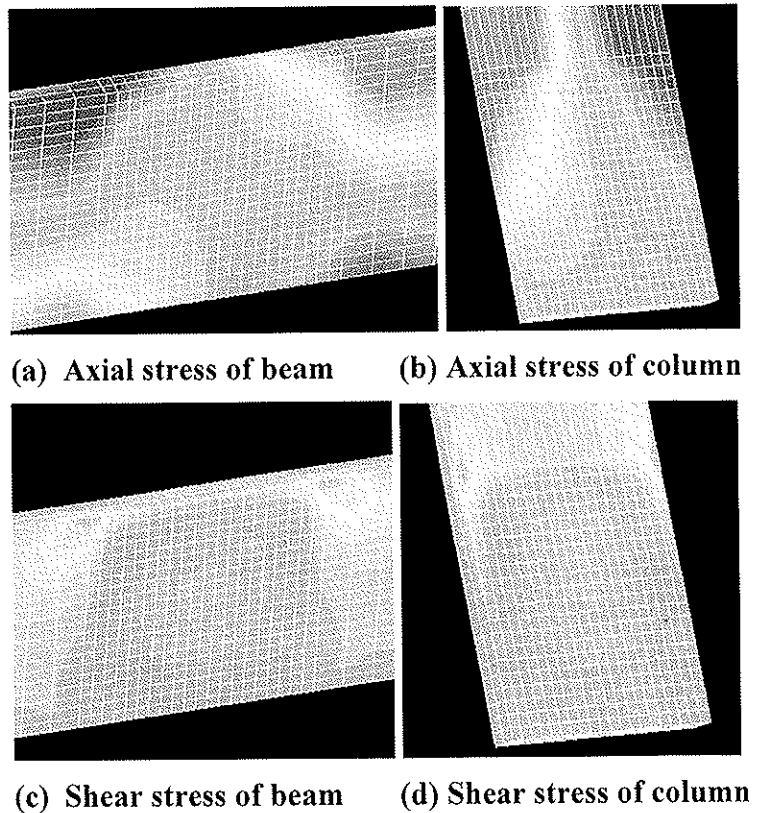


Fig. 11 Stress distribution of CLJ

$$\delta_j(x_j) = \beta_j \frac{M_j}{6h_j E_j I_j} x_j^3 \quad \dots (13)$$

Next, the stress distribution of the glue line was considered, focussing on the glue line.

From Fig. 10, the total displacement is obtained as:

$$\delta_i = \left(\beta \frac{M_j}{G_j t_j b_j h_j} x + \beta \frac{M_2}{G_2 t_2 b_2 h_2} x + \beta \frac{M_j}{6h_j E_j I_j} x_j^3 \right) \quad \dots (14)$$

Corresponding to x -component, the shear stress of τ_{xMi} must be in proportional with the deformation of the member. Here, the moment of beam at panel zone must be equal to that of column. From this, τ_{ij} can be expressed as follows:

$$\tau_{ix} = \alpha \left(\frac{M}{G_j t_j b_j h_j} x + \frac{M}{G_2 t_2 b_2 h_2} x + \frac{M}{6h_j E_j I_j} x_j^3 \right) \quad \dots (15)$$

where, α : undetermined coefficient

As the applied moment must be equal to the sum of the internal stress, moment due to x -component must be satisfied:

$$M = \iint \tau_{ix} x \, dx dy \quad \dots (16)$$

From Eq. (15), Eq. (16), by eliminating α , τ_x , τ_y can be obtained:

$$\begin{aligned} \tau_x &= \frac{30E_1 I_1 x + 5G_2 t_2 b_2^2 x^3 + 5G_1 t_1 b_1^2 x^3}{20E_2 I_2 b_2 h_2^3 + 2G_2 t_2 b_2 2h_2^5 + 2G_1 t_1 b_1^2 h_2^5} M \\ \tau_y &= \frac{30E_2 I_2 y + 5G_2 t_2 b_2^2 y^3 + 5G_1 t_1 b_1^2 y^3}{20E_2 I_2 b_2 h_2^3 + 2G_2 t_2 b_2 2h_2^5 + 2G_1 t_1 b_1^2 h_2^5} M \quad \dots (17) \end{aligned}$$

4.2.3 Rotational stiffness of cross lapped joints

Estimation of rotational stiffness of cross-lapped joints will be derived as follows.

The apparent rotational deformation of CLJ result from local deformation of each member at panel zone. Therefore, the energy method was used. The internal potential energy of panel zone was expressed as: (Total energy U at joint is :)

$$U = \frac{1}{2} \int \frac{M^2}{EI} dx + \frac{1}{2} \int \frac{\gamma^2}{G} dx dy dz \quad \dots (18)$$

Here, the influence of the glue lines must be considered, in order to explain the reason why the CLJs with five layers were more rigid than CLJs with three layers.

It can, focusing on the member, be thought that the glue lines work to change the moment of timber along the length at panel zone. Therefore, it was assumed that the direct effect of the glue lines was taken in account by considering the moment distribution along the panel zone length. However, there are certain differences between the member with single-side glue line and two-sided glue lines. It appeared as the effect of the width direction. Assuming that the stress distribution along the width is constant, the average deformation along the width with two-sides glue line members are a half as large as that with single-side glue line geometrically (Fig. 12). The relative effect of the difference was taken in

account afterwards, introducing width-direction-effect factor to divide the deformation of the member with two-side glue lines by two single glue lines.

Using above and Castilian's first theorem, the rotational stiffness R was as follows:

$$R = \frac{1}{\sum_{\text{sin glue-side-glue-line}} \left(\frac{h_j}{G_j b_j t_j} + \frac{h_j^3}{6E_j I_j} \right) + \sum_{\text{both-side-glue-line}} \left(\frac{h_j}{4G_j b_j t_j} + \frac{h_j^3}{24E_j I_j} \right)} \quad \dots (19)$$

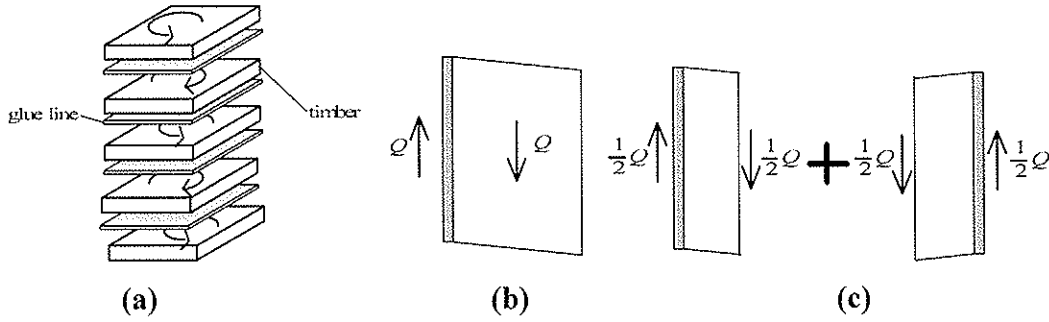


Fig. 12 Concept of deformation of CLJ

4.2.4 Strength of cross-lapped joints

The maximum shear stress of glued line at, $h_1/2$ and $y=h_2/2$ must be appeared.

Substituting $h_1/2$ and $y=h_2/2$ into Eq. (17), those equations are expressed as:

$$\tau_x = \varphi M \quad \tau_y = \psi M \quad \dots (20)$$

$$\text{where, } \varphi = \frac{15E_1 I_1 h_1 + 0.625G_2 t_2 b_2^2 h_1^3 + 0.625G_1 t_1 b_1^2 h_1^3}{20E_2 I_2 b_2 h_2^3 + 2G_2 t_2 b_2 2h_2^5 + 2G_1 t_1 b_1^2 h_2^5}, \quad \psi = \frac{15E_2 I_2 h_2 + 0.625G_2 t_2 b_2^2 h_2^3 + 0.625G_1 t_1 b_1^2 h_2^3}{20E_2 I_2 b_2 h_2^3 + 2G_2 t_2 b_2 2h_2^5 + 2G_1 t_1 b_1^2 h_2^5}$$

The shear stress of the glue lines was calculated using Eq. (21).

$$\tau_i = \sqrt{\tau_{xi}^2 + \tau_{yi}^2} = M \sqrt{\varphi^2 + \psi^2} \quad \dots (21)$$

Now, as the CLJ is brittle, the maximum moment M_{\max} was defined as the moment which arbitrary shear stress reached the shearing strength. M_{\max} is expressed as:

$$M_y = \frac{\tau_y}{\sqrt{\varphi^2 + \psi^2}} \quad \dots (22)$$

Moreover, it was taken in account to consider the panel zone of shear failure (Fig. 13).

$$M = \tau_{\text{wood}} t_i h_i b_i \quad \dots (23)$$

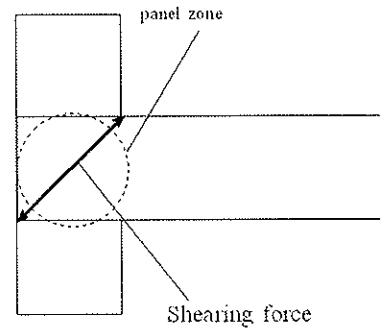


Fig. 13 Panel zone of CLJ

τ_{wood} : shear strength of timber,

Finally, bending failure of the members just outside the panel zone area must be considered. Because in CLJ the effective thickness of each member at interface are much smaller than that at non-panel zone. As the distance of interface is very small, the strength cannot be predicted using strength of timber (not clear wood). In the case of very small area, the probability that the member at the interface have fatal defects compared to the defects along the beam is very small. For this reason only the clear wood strength for this

particular case was used. Using ‘a basic beam theory’, the equation of bending failure at panel zone was derived:

$$M_b = \sigma_{clear} Z_{effective} \dots (24)$$

5 Comparison between Test and Estimation

For the mechanical properties the following values were thought to apply: $E = 6.5$ GPa, $G = 430$ MPa ($G = E/15$), bearing constant k (embedment) in this case, double the compression.(used calculated by Komatsu⁶⁾), the bending strength of clear wood 65 MPa (according to Japanese old code), shear stress of glue line 4 MPa, axial characteristics of GIR: slip modulus: 50 kN/mm (Aicher et al⁷⁾), lateral strength of GIR: (calculated using according to Blass and et al.⁸⁾), shear failure of panel zone: reference(9)

Table 1 shows the strength and stiffness values using test and our theory. From this table, it was recognized that the stiffness and strength in CLJ, and GIR could be predicted using our models. The strength criterion of CLJ was the bending failure of interface. The strength criterion of GIR was the split criteria at panel zone due to pulling components of rod. Both criteria were consistent with the failure modes of tests. In this case, the split criterion due to lateral components in the rod was not governing, but the shear force was reached at 80% of the strength (8.5 kN). The ratio of the stiffness due to lateral component in the rod to total stiffness was 25 % in GIR. Therefore, it was thought that the lateral component in the rod is a significant factor for stiffness and strength estimation of GIR.

Table 1 Comparison between Test and Estimation

	strength (kNm)			stiffness (kNm/rad)				
	test	theory	test/theory	test	theory	test/theory	vertical component	horizontal component
Type A	12.95	14.30	0.91	867	937	0.93		
Type C	16.15	17.33	0.93	1517	1338	1.13		
Type E	13.94			1800	1572	1.15	1184	388

6 Conclusions

The design methods of knee joints using glued in steel rods, and cross-lapped glued joints were proposed. In CLJ, we made the hypothesis that both rotational deformation of CLJ and the stress of glue line occurred due to the bending and shear deformation of timber. In GIR, not only the pulling component of rod but also shear component of rod can be taken in account using “theory of the beam on an elastic foundation”. From the comparisons between calculations and experimental result, it was recognized that the stiffness and strength in CLJ, and GIR are in good agreement and can therefore be predicted using our models. Therefore, it was thought that the lateral component in the rod is a significant factor for stiffness and strength estimation of GIR.

References

- 1) A. J. M. Leijten: Proceedings of IUFRO S5.02, Turku, 1988, p.168-170
- 2) P. Racher (edited by H. Blass at al): Moment resisting connection, Timber Engineering STEP 1, Dusseldorf, 1995, pp. C16/1-C16/11
- 3) prEN 1993: Eurocode 3, 1999
- 4) Timoshenko S., Goodier J. N.1951, Theory of Elasticity, Kogakuaha, Tokyo, pp 258-263
- 5) Kelvin and Tait: Treatise on Natural Philosophy, vol. 2, 1912, p267-268
- 6) K. Komatsu (edited by AIJ): Structural Design Note for Timber Structures, Maruzen, Tokyo, 1995. p. 184-221 (in Japanese)
- 7) H. Blass, R. Görlacher, B. Laskewitz (edited by C Bengtsson and C.J. Johansson): GIROD-Glued in Rods for timber structures, SMT4-CT97-2199, SP report, 2002 , p.34-43
- 8) S. Aicher, P.J. Gustafsson, M. Wolf : Proceedings of 1st RILEM Symposium on timber Engineering, Stockholm, Sweden, p.369-378
- 9) M. Noguchi K. Komatsu: Proceedings of the WCTE, Lahich, 2004, vol. 3 p. 301-304

INTERNATIONAL COUNCIL FOR RESEARCH AND INNOVATION
IN BUILDING AND CONSTRUCTION

WORKING COMMISSION W18 - TIMBER STRUCTURES

SIMPLIFICATION OF THE NEURAL NETWORK MODEL FOR
PREDICTING THE LOAD CARRYING CAPACITY OF
DOWEL-TYPE CONNECTIONS

A Cointe

LRBB

F Rouger

CTBA

FRANCE

Presented by F Rouger

H Blass asked how simple can this be used in a code format. Rouger gave an example.

J Köhler received confirmation that nominal values were predicted and one can get characteristic strength from simulation.

C Clorius asked about the mode of loading. Rouger responded that tension compression and angle to grain loading info were available.

C Clorius asked whether all modes of failure were considered. Rouger responded that only capacity, not mode of failure was considered.

A Jorissen commented that the influence of a_1 and a_2 should be higher. Rouger responded all Jorissen data was considered in the analysis.

Y H Chui asked about the range of values for the parameters and whether sensitivity analysis was done. Rouger agreed that the range of parameter was an important issue and restated that the model should not be used for extrapolation.

E Karacabeyli commented that seismic design needs stiffness of connections. Rouger stated that the same approach could be used if connection stiffness data base was available.

Simplification of the neural network model for predicting the load carrying capacity of dowel-type connections

By A. Cointe, ¹ PhD, LRBB, F. Rouger, ² Research Manager, CTBA

Abstract: Our study focuses on predicting the ultimate short-term load carrying capacity of timber-to-timber connections with dowel-type fasteners. The wide range of possible configurations in practice makes the resolution of these values by tests unrealistic. Moreover, different current regulations do not consider some specific failure mechanisms. In many countries, the reduction of resistance involved by this phenomenon is taken into account by considering an effective number of dowels (n_{ef}) smaller than the actual number of dowels (n) in the connection. However, these different regulations disagree on the values of n_{ef} and on other points (spacing, partial coefficient of security, formulas). These discrepancies in design rules impede the fundamental research on this topic and, therefore, new methods are sought in order to estimate the load carrying capacities of connections. In the light of these, our approach consists of modelling the load carrying capacity with the neural network numerical tool. The results obtained by this analysis tool are satisfactory, although the model remains complex. Subsequently, we focus on the simplification of this numerical model with classical regression techniques.

¹Laboratoire de Rhéologie du Bois de Bordeaux, Domaine de l'Hermitage, 69 route d'Arcachon, 33612 Cestas Cedex.

Tel : +33 (0)5 57 12 28 12

Fax : +33 (0)5 56 68 07 13

Email : cointe@lrbb3.pierroton.inra.fr

²Centre Technique du Bois et de l'Ameublement, Allée de Boutaut, BP 227, 33028 Bordeaux cedex.

Tel : +33 (0)5 56 43 63 73

Fax : +33 (0)5 56 43 64 86

Email : Frederic.Rouger@ctba.fr

Key Words: connection, timber, dowel, neural network, experimental design, variance analysis

Introduction

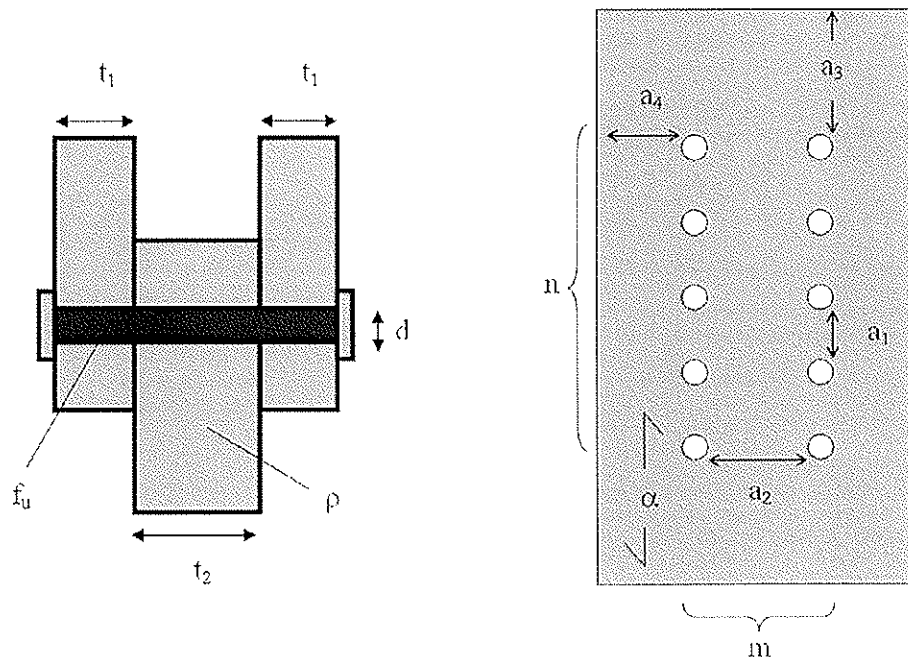
Connections in timber structures often determine the load carrying capacity of the whole structure. As a result of the complexity of designing connections, the thesis prepared in conjunction with LRBB and CTBA only deals with the short-term load carrying capacity, in double shear under static loading, of single and multiple-doweled-type timber-to-timber connections. Our approach consists of modelling the load carrying capacity with the neural network numerical tool. The first step of using the neural networks consisted in creating a database related to our study as an input for the network.

1. Creation of a Database

We reviewed several test results and picked up the common parameters (cf. figure 1) available from the literature (Jorissen 1998, Vermeyden 1980, Vincent 1988, Wilkinson 1986):

- ✓ the mean density of wood (kg/m^3): ρ
- ✓ the angle between the loading direction and the grain direction (rad): α
- ✓ the dowel diameter (mm): d
- ✓ the thickness of connected elements (mm): t_1, t_2
- ✓ the number of dowel rows: m
- ✓ the number of bolts in a row: n
- ✓ the different spacings in the connections (mm): a_1, a_2, a_3, a_4
- ✓ the characteristic tensile strength of the metallic dowel (MPa): f_u

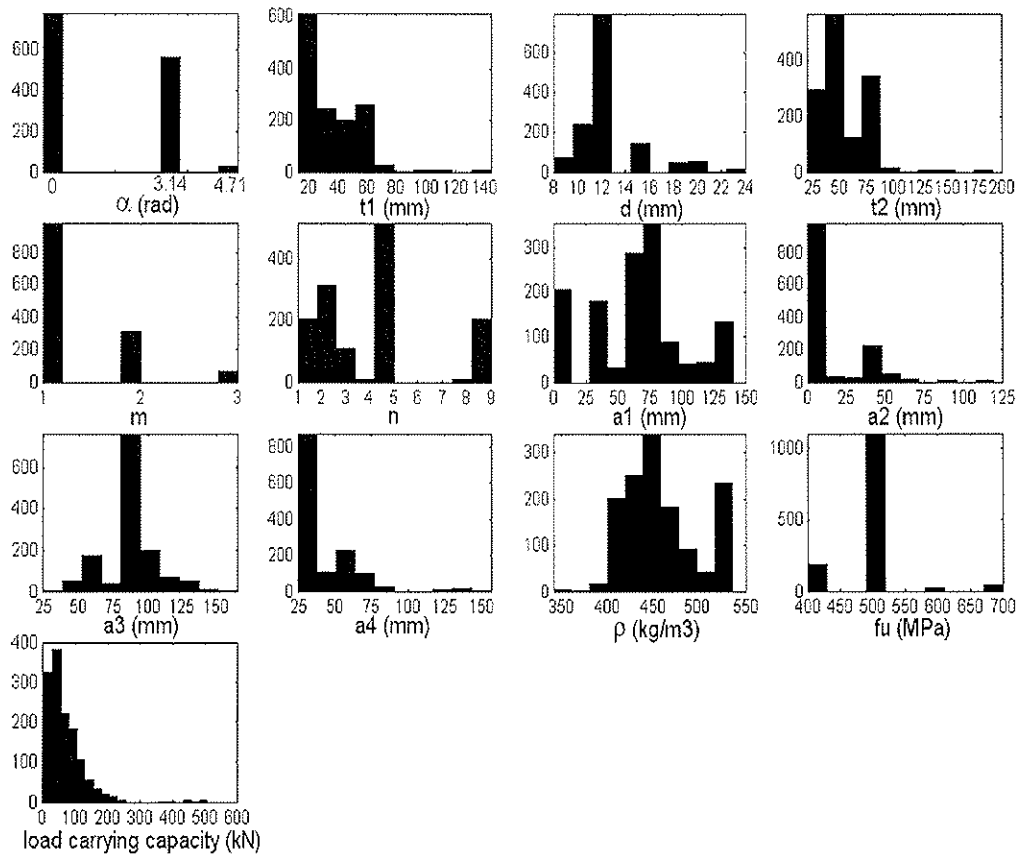
Figure 1. Studied Configurations



The spacings a_1 and a_2 are taken equal to zero when the number of rows and the number of bolts in a row are equal to one respectively. The wood species are mainly spruce and pine. Using this

approach, we listed 1368 configurations of connections with the corresponding ultimate values of the load carrying capacity (Cointe and Rouger 2001, Cointe 2003). The following figure 2 shows a summary of the parametric variability of connections.

Figure 2. Statistical Distribution of the Database Parameters



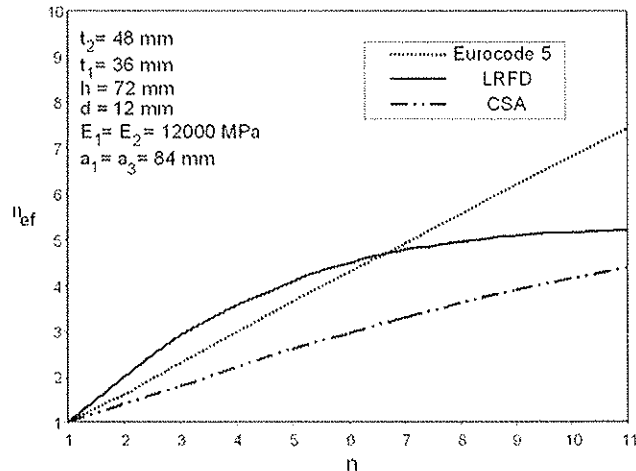
It can be seen that there are many gaps in this database. We thus appeal to authors who work on this topic to fill in these gaps and thus to improve the homogeneity of the database and the strength of the model given by the neural network.

2. Design Approach

Many approaches were developed since Johansen proposed the Yield Theory in 1949. The past fifty years have seen elastic analyses (Wilkinson 1986), a coupling between the Yield Theory and Fracture Mechanics (Jorissen 1998) and elasto-plastic analyses being developed. Nevertheless, there is no actual convergence between these approaches. Moreover, if the design codes are considered (CSA 086.1-94 1994, LRFD 1991, prEN 1995-1-1 2002), more discrepancies can be found. These design rules agree with the Yield Theory formulation for only one dowel in the connection but disagree when the number of dowels increases. In fact, the load carrying capacity of a connection with several dowels is smaller than the one of the same connection with only one dowel multiplied by the number of dowels. It is, therefore, a widespread practice to take into account an effective number (n_{ef}) smaller than the actual number (n) of dowels in the connection. In his thesis, Jorissen illustrated the differences on n_{ef} between the three design codes (CSA, LRFD, Eurocode 5). The

comparison of Jorissen was modified with new values of n_{ef} for Eurocode 5, as can be seen in figure 3.

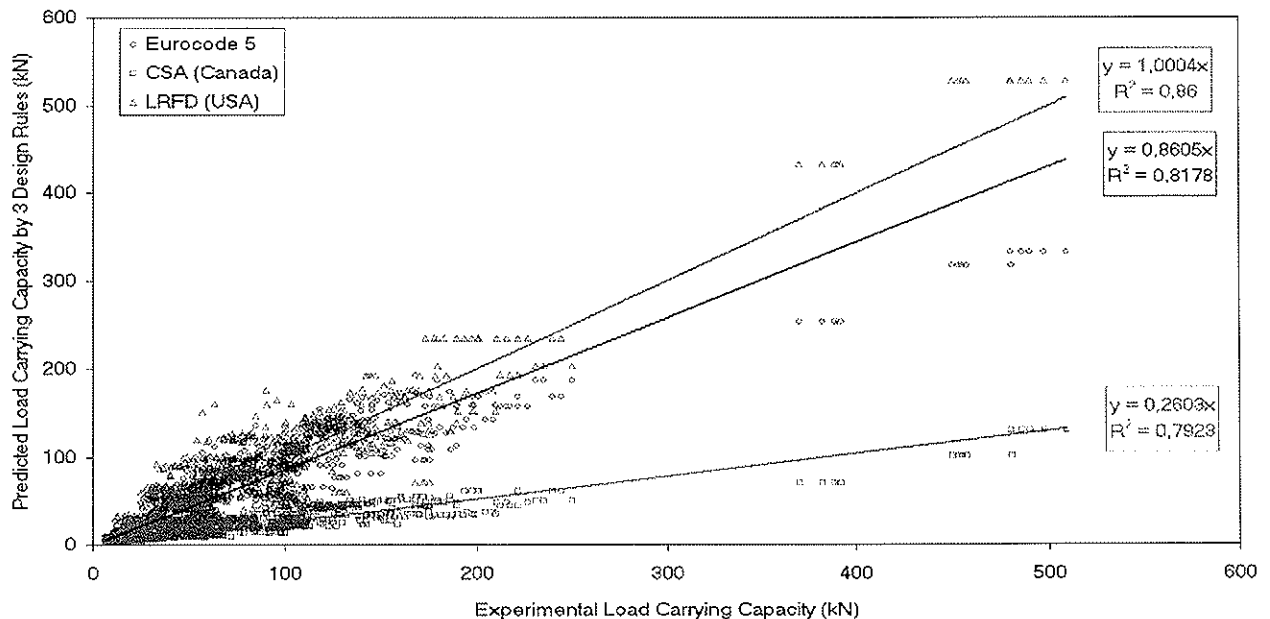
Figure 3. Comparison of the Effective Number of Dowels according to Design Rules



It is clear that no agreement exists on the design values for n_{ef} . n_{ef} according to Eurocode 5 can be two times higher than n_{ef} according to the Canadian code.

Moreover, differences between the standards on the minimum spacing in a connection to abide by in order to avoid brittle failures, on the determination of the embedment strength of the wood f_{ib} , on the formulation of the unitary strength and at last on the coefficients for the number of dowel rows (m) can also be found. Because of the lack of equations rendering specific mechanisms, the design rules do not explain well the cases when brittle failures occur in the connection, even if the design measures are satisfied. These differences on the whole database are shown in figure 4.

Figure 4. Comparison of the Predicted Load Carrying Capacity According to Design Rules



The mean load carrying capacity given by the American (LRFD), Canadian (CSA) and European (Eurocode 5) regulations on our database are compared. It is important to note that the values shown in the figure 4 take into account the geometric data but it does not represent the final design values. The modification factors for the duration of loading, the environmental conditions (temperature, humidity) and the partial coefficients of security on materials properties are disregarded to compare the mean values. The considerations for minimum spacing are not necessarily respected in order to make the comparison as large as possible. Finally, the Canadian design code appears to be too conservative because the load carrying capacities shown are the characteristic values and not the average ones. According to authors, it is not easy to switch from one to another.

3. Modelling by Neural Networks

3.1. Justification

In order to predict more accurately the load carrying capacity of connections, the neural network approach implemented by a commercially available software package (Matlab®) was used. The justification for this approach lies in the fact that the determination of the load carrying capacity by way of tests is quite impossible, the regulations in use are not uniform, and eventually, neural networks present interesting properties. Neural networks are defined as sparing models: if an approximation with a given precision is needed, the neural networks will use less adjustable parameters than the other common approximators like polynomials, or developments in Fourier series. Neural networks represent a quick way to approximate non-linear functions, and are less noise sensitive on input data than the other methods. Moreover, the direct switch from input data to predictors does not necessitate formulation of any hypothesis on the model.

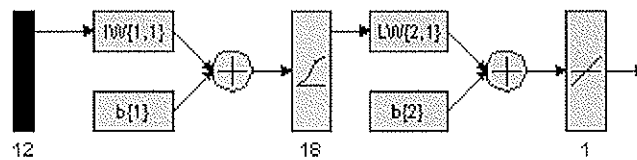
3.2. Principle of Functioning

There are different types of neural networks, and their area of application varies according to their topology. Among these, the networks with layers of neurons that are mainly used to solve problems relating to modelling, classification or function approximation are common. This kind of structure was implemented in this study. The principle of functioning is quite simple, knowing that a neural network is an automaton made up of elementary cells: the neurons. The neurons perform a mathematical function of input data: “a formal neuron performs a weighted sum of action potentials that reached it and then bustles about according to this weighted sum”. Each neuron is associated with coefficients (weight, bias) weighting input data. The neuron realizes a function (called transfer function) of this weighted input and produces a scalar output. Neurons can be associated in a network linked by connexions weighted by coefficients. It has to be noted that both weight and bias are adjustable scalar parameters of the neuron. The central idea of neural networks is that such parameters can be adjusted so that the network would exhibit a desired or interesting behaviour. Thus, the network can be trained to do a particular job by adjusting the weight or bias parameters. This is the learning principle (generally done on the two thirds of the database). The input data are presented to the network which is asked to modify the weights and biases so that it finds the desired output by successive iterations. The network compares the calculated output with the desired one and modifies its weights so that the error is minimal. Once the learning is done, the weights and the biases of the network are fixed and we can submit a new set of examples to verify the ability of the network to answer correctly to new data that are not in the learning sample (generally done on one third of the database).

3.3. Choice of the Neural Network Topology

To determine the optimum topology of the network, several parameters were adjusted: the number of neuron layers, the number of neurons in each layer, the transfer functions, the learning rule and the initialization of the weights and the biases. The chosen network is a feed forward one with two layers of neurons. The twelve input parameters in the database are connected to the first layer whose transfer function is tan sigmoid. This layer contains eighteen neurons connected to the linear output layer that is made up of one neuron (because only one output is needed, namely the load carrying capacity of the connection). The learning rule is based on the scaled-conjugate gradient algorithm. An overview of this network is shown in figure 5.

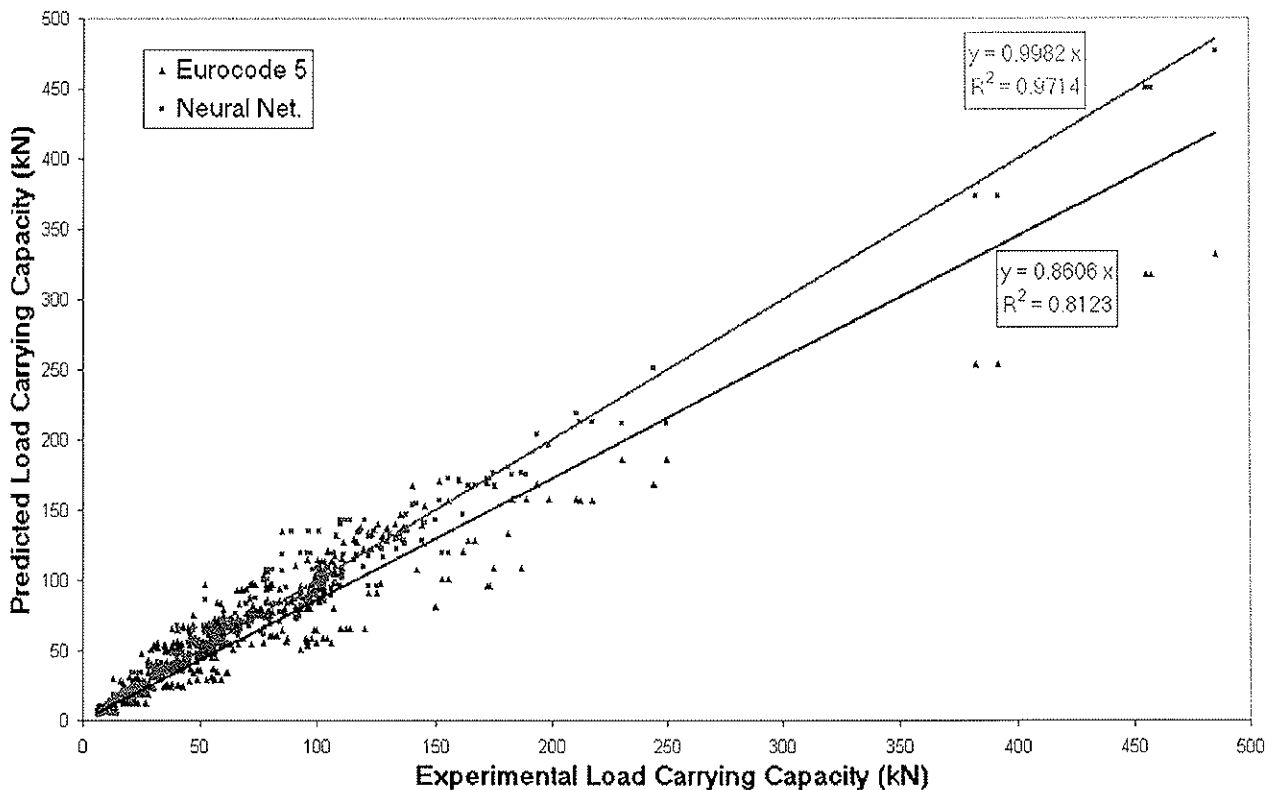
Figure 5. Overview of the Neural Network Used



3.4. Results

The results showed that neural networks could be a useful tool to estimate the load carrying capacity of connections. A comparison of prediction between the neural network and the Eurocode 5 on the generalization sample has been carried out and showed in the following figure 6.

Figure 6. Comparison between the Neural Network and the Eurocode 5 Values



Filling in the gaps in the database could improve the results of the model. Unlike the standards, neural networks allow estimation of the load carrying capacity without any restrictions on the dimensions of connections. Any possible configuration in the range of data can be generated with the corresponding strength without resorting to experimentation that is usually very tedious and expensive. However, the model provided by the neural network remains too complex to be incorporated into a design code.

4. Simplification of the Neural Network Model

4.1. Eurocode 5-Type Model

In order to simplify the neural network model, it was supposed that the load carrying capacity of a multiple-dowel-type connection can be expressed as a Eurocode 5-type model:

$$R_{multiple} = n_{ef} \cdot R_{simple}$$

For each multiple dowel-type connection, the same configuration with only one dowel was generated and the corresponding strength was simulated by way of the neural network. The above ratio for each connection was then calculated and a correlation between this ratio and the input parameters was sought. However, there were no correlations between n_{ef} and the input data. Indeed, the maximum correlation coefficient is equal to $2.92e^{-02}$.

The original hypothesis was thus rejected. This particular point challenges the relevance of using an effective number of dowels to calculate the multiple dowel-type connection strength from the one of a connection with a unique dowel. In the light of this conclusion, it was decided to split up the database into three parts: connections with only one dowel, connections with one row of dowels and connections with multiple rows of dowels.

4.2. Experimental Design

In order to study the sensitivity of the neural network output to the input parameters, it was resorted to the experimental design. These designs are based on multifactor experiments and on a statistical processing of results with the help of multiple regressions and analyses of variance. In order to achieve this, a full design of experiments and fractional Plackett-Burman designs that are more accessible were used. For each split database, full experimental design with three levels per parameter (low, mid and high levels) were carried out and a variance analysis was undertaken to obtain the most influential parameters according to the Fisher-Snedecor test. An illustration of the results is shown in the figures 7 and 8. The following Pareto charts of the standardized effects show the decreasing influences of the parameters on the neural network outputs.

Figure 7. Pareto Charts of the Standardized Effects

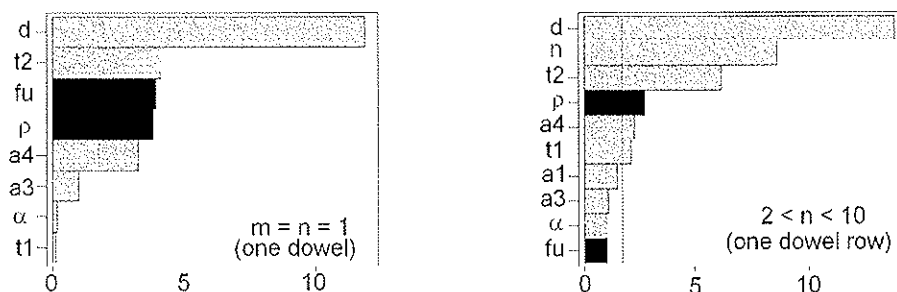
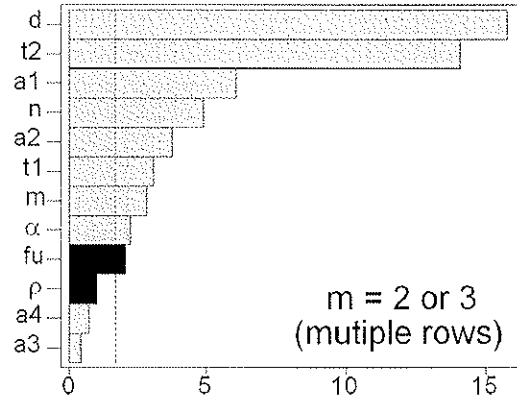


Figure 8. Pareto Charts of the Standardized Effects



We notice that the influence of material properties (ρ , f_u) is giving way to geometric properties when the number of dowels in the connection increases.

From the variance analysis, the most influential parameters and their interactions were calculated. A multiple regression model for each database was created this way. The models showed quite good predictions for parameter levels that are taken into account in the design of experiments but as soon as these level values are different, the models become not robust enough and the prediction results are poor when a random database is considered. The provided models thus present a poor ability to generalization. Moreover, with this analysis, the quadratic influences of input data remain unclear.

4.3. Stepwise Regression

A stepwise regression tool that allows consideration of these quadratic effects was thus used. To reach this goal, three random sets of five thousand configurations were generated. Three full quadratic generalized models (forty four, sixty five and ninety terms respectively) were formed from the input data (eight for the connections with only one dowel, ten for the connections with only one row of dowels and twelve for connections with more than one row of dowels), its interactions and its quadratic effects. Starting with a full quadratic model and eliminating one by one the terms that have a negligible influence on the load carrying capacity, a reasonable number of terms in the simplified models was reached. The coefficients associated to these terms were determined afterwards by constrained optimization. For each random database, simplified models that are less and less complex (models with 20, 18, 16, 12 and 8 terms plus a constant) were obtained. A simplified multiple-dowel-type connection model is formulated as:

$$R_{simp} = A_0 + A_1^T X + X^T A_2 X \text{ with}$$

$A_0 = \text{constant}$,

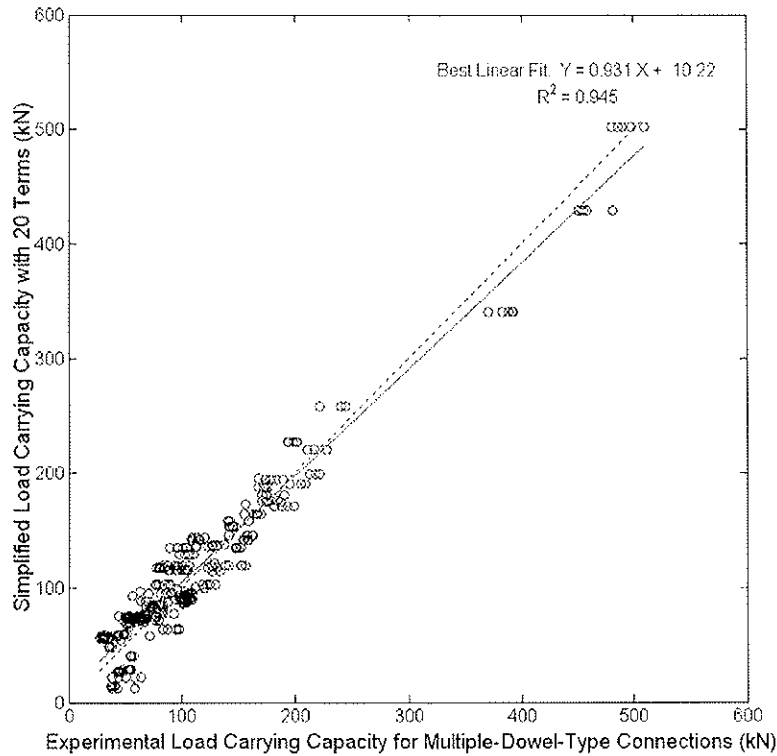
$A_1^T = \text{vector } [1 \times 12]$,

$A_2 = \text{matrice } [12 \times 12]$,

$X^T = [\alpha \ t_1 \ d \ t_2 \ m \ n \ a_1 \ a_2 \ a_3 \ a_4 \ \rho \ f_u]$.

This model shows satisfactory results, particularly for multiple-dowel-type connections (cf. figure 9).

Figure 9. Comparison between the Neural Network and the Eurocode 5 Values



The regression quality here is less reliable than the neural network one, but the models are simpler to interpret and the predictions improve the Eurocode 5 rule. The results for connections with only one dowel are a little bit less convincing because of the lack of data and a collection of other experimental values should improve these results.

Conclusions

Database development presented a long and tedious task, but now other authors who work on this topic can use it. The initial idea that consisted in predicting the load carrying capacity of multiple dowel-type connections with neural networks was ratified. Nevertheless, it should be noted that neural networks are good interpolators but their ability to extrapolate remains doubtful. Conclusions obtained from a simplified Eurocode 5-type model challenge the relevance of using an effective number of dowels we have to consider in order to estimate the load carrying capacity of a multiple dowel-type connection from the one of the same connection with only one dowel. Moreover, it was shown that the influence of material properties (ρ , f_u) is giving way to geometric properties when the number of dowels in the connection increases. Even if the simplified quadratic models are less accurate than the neural network ones, they remain closer to experimental values than the Eurocode 5. Finally, expanding the method with other types of connections e.g. steel to timber connections, screws and nails could be considered. A further possibility would be using probabilistic neural networks to include some notions of reliability.

Appendix. References

Canadian Standards Association (1994), "Engineering Design in Wood (limit states design). A national standard of Canada," CSA 086.1-94.

Cointe, A. (2003), "Prévision de résistances d'assemblages bois par organes multiples à l'aide des réseaux de neurones," PhD thesis, Div. of Mechanics, Bordeaux I University, Bordeaux, France.

Cointe, A., Rouger, F. (2001), "Predicting the load carrying capacity of dowel-type connections by using the neural network approach," International Rilem Symposium on Joints in Timber Structures, PRO 22, Stuttgart, Germany, 51-61.

Jorissen, A. (1998), "Double shear timber connections with dowel type fasteners," Delft University Press, Mekelweg 4, 2628 CD Delft, the Netherlands.

Load and Resistance Factor Design (1991), "Specification for engineered wood construction. Guidelines for developing reference resistance", LRFD.

prEN 1995-1-1, Eurocode 5 (2002), "Design of timber structures, part 1-1, general rules and rules for buildings, final draft," Document CEN/TC 250/SC 5 : N 195.

Vermeyden, P. (1980), "Test on bolted joints," CIB W18 (13-7-7), meeting 13, Otaniemi, Finland.

Vincent, B. (1988), "Analyse et modélisation du comportement mécanique des assemblages bois boulonnés ou cloués," PhD thesis, Div. of Civil Engrg., CUST, Clermont II University, Clermont-Ferrand, France.

Wilkinson, T.L. (1986), "Load distribution among bolts parallel to load," *Journal of Structural Engineering*, ASCE, 112(4), 835-852.

Appendix. Notation

The following symbols are used in this paper:

a_1	=	spacing between dowels in a row;
a_2	=	spacing between dowel rows;
a_3	=	end distance spacing;
a_4	=	edge distance spacing;
d	=	dowel diameter;
f_h	=	embedment strength of the wood;
f_u	=	characteristic tensile strength of the metallic dowel;
m	=	number of rows;
n	=	number of dowels in a row;
n_{ef}	=	effective number of dowels;
t_1	=	lateral thickness of wood members;
t_2	=	median thickness of wood member;
α	=	angle between the loading and the grain directions;
ρ	=	mean density of wood.

INTERNATIONAL COUNCIL FOR RESEARCH AND INNOVATION
IN BUILDING AND CONSTRUCTION

WORKING COMMISSION W18 - TIMBER STRUCTURES

BOLTED WOOD CONNECTIONS LOADED PERPENDICULAR-TO-GRAIN
A PROPOSED DESIGN APPROACH

M C G Lehoux

J H P Quenneville

Royal Military College of Canada

CANADA

Presented by G Lehoux

Y Chui asked how were the coefficients, A_b , B_b and C_b , determined. M Lehoux responded that they came from the stress analysis.

C Clorius asked about the interaction between the bolt and the wood connection. Lehoux answered that contact elements were used for the bolt and they provided the contact between the bottom part of the bolt and the wood. C Clorius commented that the highly non-linear behaviour of the wood at the point of contact with the bolt was ignored. Lehoux answered that it may be of minor concern. Lehoux further pointed out that only the tension perpendicular-to-grain stresses were considered in the stress integral.

H J Larsen asked which and how many parameters were assumed and which were calibrated and questioned the appropriateness of replacing the fracture mechanics approach with a stress approach for a fracture problem. F Lam commented this is a statistical size effect approach that did not require the assumption of the existence of a crack of a certain size in the domain.

Bolted Wood Connections Loaded Perpendicular-to-Grain A Proposed Design Approach

MCG Lehoux
JHP Quenneville

Royal Military College of Canada, CANADA

1 Introduction

A design approach to estimate the load-carrying capacity of bolted timber connections loaded perpendicular-to-grain is presented in this paper. The proposed method follows the concept of Foschi with riveted timber connections presently used in the current Canadian wood design code, CSA Standard O86-01.

The current design procedures of bolted connections consist of calculating the resistances of the ductile failure modes based on the European Yield Model (EYM) originally proposed by Johansen (1949) and further refined by Larsen (1973). This theory has been validated to be accurate for a connection that exhibit a ductile behaviour but its ability to correctly predict the ultimate load of multi-bolt connections is rather weak since most of them fails in a brittle manner. The EYM theory does not take into consideration the failure of the connection by brittle fracture of the wood. To overcome this setback, the current Canadian wood design code uses an adjustment factor based on the number of rows in the connection loaded perpendicular-to-grain.

In the CSA O86-01, the method used to design timber rivet connections is based on Foschi and Longworth's theory (1975). They used a finite element model to predict stresses around the cluster of rivets. The ultimate load capacity of the timber rivets connection is limited by either the yielding strength of the rivets with localized wood crushing or the wood strength. This approach takes into consideration both modes of failure: brittle and ductile.

The research program described consists of experimental studies and stress analysis using finite element computer modeling. Experimental studies were carried out at the Royal Military College of Canada during the last 5 years. Many groups of Glulam specimens were tested with two wood species (Douglas fir or Spruce-Pine), various connection configurations and different beam sizes. Stress analyses to estimate the ultimate strength of the connections were performed using the finite element modeling programme ANSYS 6.1. The results are presented and the new design approach to predict the failure modes and the ultimate strength of bolted connection is described.

2 Objectives

The two main objectives of this research were: 1) to carry out stress analyses of bolted connections in glulam loaded perpendicular-to-grain using finite element computer modeling and 2) to develop a design approach to predict the failure modes (brittle or ductile) and the ultimate strength of a bolted connection loaded perpendicular-to-grain.

3 Background- Riveted Connections Loaded Perpendicular-to-Grain

In the Canadian wood design code, the method utilized to design timber riveted connections is based on Foschi and Longworth's theory (1975). The ultimate load capacity of the connections is limited by either the yielding strength of the rivets with localized wood crushing or wood strength. Foschi and Longworth first used a finite element model to predict stresses around the cluster of rivets [5], [6].

To verify the yielding strength of the rivets, Foschi determined that the rivets at both ends of the connection carry more load than the ones in the center of the connection. While these end rivets reach their maximum capacity, the excess of the applied load is transferred to the rivets in the middle of the connections. Ultimately, each rivet carries its ultimate capacity leading to the maximum load-carrying capacity of the entire connection, q_{yr} . Obviously, q_{yr} can be attainable if the wood under the applied load does not split prematurely. It was found that riveted connections loaded perpendicularly failed usually by wood splitting rather than by rivet yielding or wood crushing.

The computation of wood failure loads q_{wr} is not as simple as that of rivet failure loads q_{yr} . It requires a three-dimensional stress analysis of the connection. Equilibrium exists between the applied load and both the tensile stresses at the head of the rivets and the shear stresses along the sides of the connection width. However, it was observed that tensile stresses controlled the design; consequently, the shear stresses were not considered. The ultimate load capacity of a riveted connection, according to Foschi [6], is the smaller of the two values given by the following equations:

$$\text{Rivet Capacity} = q_{yr} = n_R \times n_C \times P^* \quad (1)$$

$$\text{Wood Capacity} = q_{wr} = \frac{\sigma A_t}{K_{tp} \beta_{tp} \beta_D} \quad (2)$$

Where n_R is the number of rows, n_C is the number of fasteners per row, P^* is the maximum load-carrying capacity for a single rivet in ductile failure mode, σ is the ultimate normal stress of the wood in tension perpendicular to the grain, A_t is the area of timber influenced by applied load (connection width X rivet length), and K_{tp} , β_{tp} and β_D are coefficients that depend on the connection configuration.

To evaluate the value of the ultimate normal stress of wood (σ), Foschi first started with finite element analyses [6]. While these analyses enhanced the understanding of riveted connection behaviour, they did not give an accurate value of allowable maximum stress under perpendicular-to-grain loading. Size effects were not considered in Foschi's first analyses [4]. To determine the strength of riveted connections loaded perpendicular-to grain, including size effects, Barrett, Foschi and Fox [4] applied the Weibull's theory of brittle failure, which is described by:

$$\sigma_M[s] = \sigma^* [s] \left(\int_V G^k dv \right)^{-1/k} \quad (3)$$

From his finite element analysis, Foschi showed that normal maximum stress occurs at the surface of the beam just above the top of the cluster of rivets and diminishes abruptly over the depth of rivet penetration and end distance. The stress intensity is also influenced by the location of the connection with reference to the depth of the beam. The stress distribution function $G[x,y,z]$ was determined by Barrett et al. to be:

$$G[x, y, z] = \left(e^{-\frac{1.151x^2}{W^2}} \right) \left(1 - \frac{y^2}{e_p^2} \right) \left(e^{-\frac{2.08z}{p}} \right) \quad (4)$$

Where e_p is the unloaded edge distance, p is the penetration length of the rivet, W is the width of the connection along the length of the beam and (x, y, z) is the Cartesian coordinates along the length, the depth and thickness of the beam. By incorporating equation (4) into (3) and using a k -value of 4.63 (found by Barrett [4]), the maximum normal stress at the surface of the beam for any riveted connections was determined as:

$$\sigma = \sigma^* (0.030545 n_s D W p)^{-1/4.63} \quad (5)$$

Where n_s is the number of shear planes. As a result, for a survival probability of 95%, ($\sigma^* = 267$ psi or 1842 kN/m² found by Barrett et al.) the stress value for a riveted connection is given as:

$$\sigma = 1722.31 (n_s D W p)^{-1/5} \text{ kN/m}^2 \quad (6)$$

4 Experimental Procedures

The scope of this research was to undertake laboratory testing, perform computer modeling using a finite element method, and carry out a theoretical evaluation of the failure behaviour and the ultimate load capacity in order to develop a new design approach for a bolted connection loaded perpendicular-to-grain.

The extent of the laboratory work was to test ten specimens of each joint configuration up to failure and to record the ultimate loads at which the failure occurred. Laboratory testing was conducted in accordance with the American Society for Testing and Material (ASTM) standard procedures [1], [3]. Ultimate load capacities were calculated for each joint configuration using the 5th percentile approach consistent with the ASTM standard procedures [2]. Twenty-five configurations were selected to complete the research. All joint configurations selected were loaded perpendicular-to-grain, subjected to monotonic loading, consisted of steel-wood-steel type connections, and had the connection group located in the middle of the specimen.

The twenty-five joint configurations selected were modeled in three dimensions using a finite element software (ANSYS 6.1). By taking advantage of the geometric symmetry in two planes, only one quarter of the beam was modeled. The normal stress distribution in all directions (X, Y, Z) was recorded then plotted for each joint configuration selected.

5 Results

From the finite element analysis it was found that the maximum normal stress is always located below the middle edge of the bolt hole slightly beneath the surface of the beam. Where there are more than one bolt in a row, the maximum stress is located at the top bolt. The normal stress values are taken following the three axes shown in Figure 1.

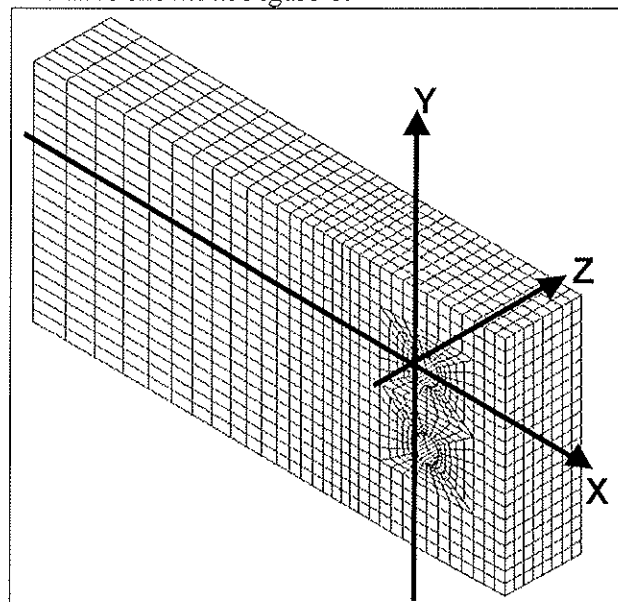


Figure 1 - Bolts Connection – Cartesian System

6 Development of Design Approach

To develop a design approach to predict the mode of failure and the ultimate strength of a bolted connection loaded perpendicular-to-grain one must keep in mind the fact that the EYM theory gives accurate results for a ductile failure. Therefore, only a new equation corresponding to the brittle failure mode is required. Hence, the EYM equations are equivalent to q_{yr} for the rivets (eq 1) and a new equation corresponding to q_{wr} is needed (eq 2). The procedure to develop the design equation of a connection with rivets failing in a brittle mode, developed by Foschi et al., is followed to create the new equation for a connection with bolts.

6.1 Normal Stress Distribution

As it was found by Foschi [6], the maximum normal stress in a connection with rivets occurs at the surface of the beam, in the middle of the connection width, just above the top of the cluster of rivets. From the finite element analysis on bolted connections the maximum normal stress is located very close to the surface of the beam, left or right of the bolt holes and located at the bolt hole farthest to the loaded edge. It is clear that both types of connections, bolts and rivets, behave differently under loads perpendicular-to-grain. As a result, the stress distribution function $G [x, y, z]$ of a bolted connection will be different to the one of a riveted connection. It was decided to derive the function $G [x, y, z]$ using the stress distribution curves of 1 row, 1 bolt configuration because the stress distributions for each group configuration is similar to one another in each direction of the Cartesian axes (Figures 2 to 4).

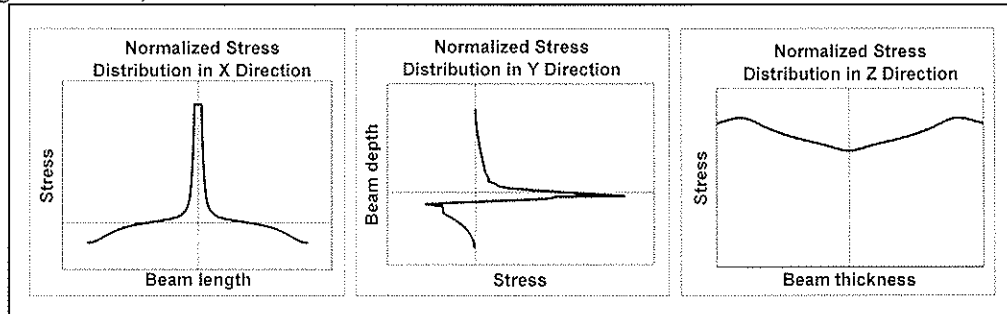


Figure 2 – Normal Stress Distribution for a Connection With 1 Row, 1 Bolt

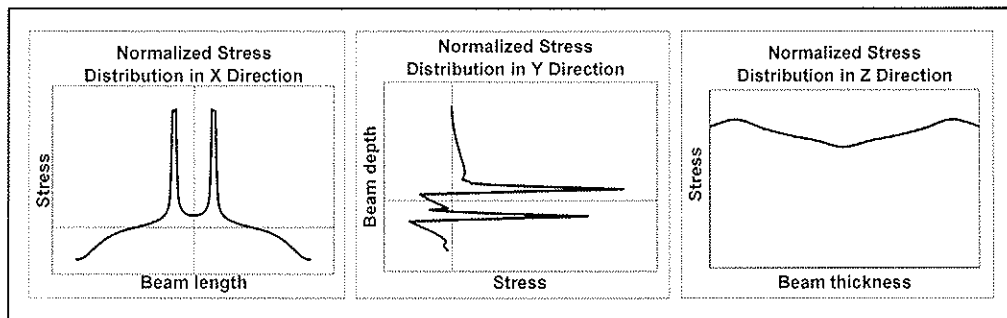


Figure 3–Normal Stress Distribution for a Connection with 2 Rows, 2 Bolts per Row

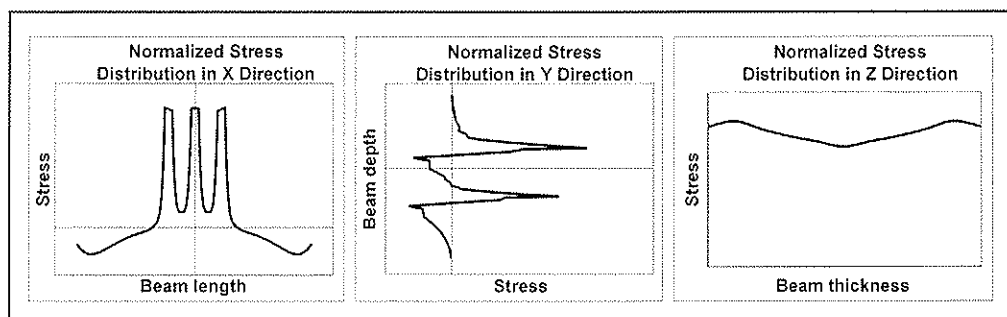


Figure 4–Normal Stress Distribution for a Connection with 3 Rows, 2 Bolts per Row

6.1.1 Stress Distribution in X-Direction

Similar to the connection with rivets and for the sake of simplicity, it is assumed that the length of the beam extends to infinity on either side of the connection with bolts. The equation of the stress distribution in the x-direction is therefore integrated from the edge of the bolt hole (half of the bolt hole diameter) to infinity ($d/2$ to ∞). The equation is determined to be:

$$X = 0.3824 \left(\frac{x}{d} \right)^{-2} \quad \text{from } d/2 \text{ to } +\infty \quad (7)$$

Equation (7) is multiplied by the number of rows (n_R) present in the bolted joint.

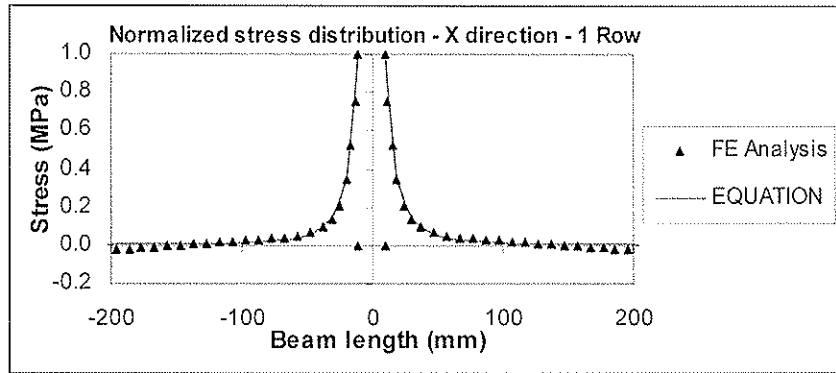


Figure 5 –Normal Stress Distribution in X-Direction

6.1.2 Stress Distribution in Y-Direction

Contrary to the rivets where the stress distribution equation is a function of the unloaded edge, the equation for a connection with bolts depends on the bolt diameter. To simplify the equation, only the linear portion of the stress distribution is represented by the equation. In fact, the curved portion of the stress distribution appears only at the location of the top bolt and is not present in all connection groups. The integration is performed from the center of the bolt hole to the edge of the bolt (0 to $d/2$). Only the wood in tension is considered in the equation.

$$Y = -1.3865 \left(\frac{x}{d} \right) + 1 \quad \text{from } 0 \text{ to } d/2 \quad (8)$$

Equation (8) is multiplied by the number of bolts in a row (n_c).

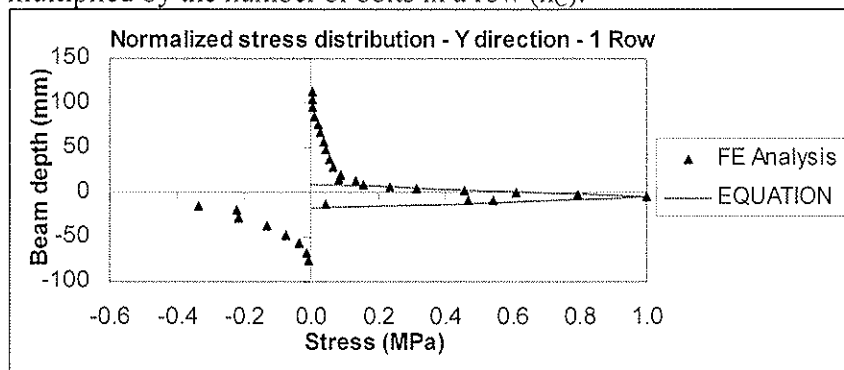


Figure 6 - Normal Stress Distribution in Y-Direction

6.1.3 Stress Distribution in Z-Direction

The maximum normal stress occurs close to the surface of the beam. The stress distribution in the z-direction of a bolted connection is influenced mostly by the thickness of the beam, similar to that of the connection with rivets. The integration is performed from the surface to half of the thickness of the beam (0 to $t/2$). Half of the curve is represented by the following equation:

$$Z = e^{-0.5 \frac{z}{t}} \quad \text{from } 0 \text{ to } t/2 \quad (9)$$

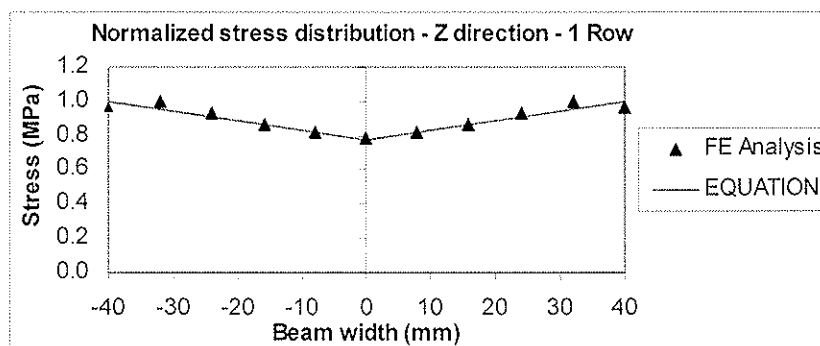


Figure 7 – Normal Stress Distribution in Z-Direction

6.2 Global Stress Distribution Function

Once the three equations are assembled (7 to 9), the tension stress distribution function $G[x, y, z]$ of a bolted connection is determined to be:

$$G[x, y, z] = \left(0.3824 \left(\frac{x}{d} \right)^{-2} \right) \left(-1.3865 \left(\frac{y}{d} \right) + 1 \right) \left(e^{-0.5 \frac{z}{t}} \right) \quad (10)$$

The following relation can be derived when equation (10) is incorporated into equation (3):

$$\sigma = \sigma^* \left(\int_v \left(\left(0.3824 \left(\frac{x}{d} \right)^{-2} \right) \left(-1.3865 \left(\frac{y}{d} \right) + 1 \right) \left(e^{-0.5 \frac{z}{t}} \right) \right)^k dv \right)^{-1/k} \quad (11)$$

6.3 Equation Development to represent wood failure

Each equation (7 to 9) is integrated only over half of each axis. These equations must be multiplied by 2 to obtain the complete area under each curve. In the x-direction, the stress distribution is dependent on the number of rows (n_R) and bolt diameter. The number of bolts per row and the bolt diameter influence the stress distribution in the y-direction. Finally, the stress distribution in the z-direction is a function of the thickness. With the evaluation of the integral of equation 11, equation 12 below is obtained:

$$\sigma = \sigma^* ((2 \times 0.433097 n_R d)(2 \times 0.12794 \ln_c d)(2 \times 0.297115 t))^{-1/4.63} \text{ kN/m}^2 \quad (12)$$

The strength of a unit volume in uniform tension perpendicular-to-grain (σ^*), at a probability of survival of 95%, is equal to 1842 kN/m² (as found by Barrett [4]). Similar to the connection with rivets, for simplicity, one can round the value of 1/4.63 to a value of 1/5 and convert the units from kN/m² into MPa, and the units inside the parentheses from metres to millimetres; in doing this, the following relation can be approximated:

$$\sigma = 200(n_c n_R d^2 t)^{-1/5} \text{ MPa} \quad (13)$$

Equation 13 is developed to predict characteristic values with a normal load duration. These predicted values are then used to calculate the ultimate load of the bolted connection that can be compared to the experimental values transformed to a normal load duration. The area of the wood under the influence of the load from the bolts is taken as: (the number of rows) x (the bolt diameter) x (the thickness of the beam). Therefore, the wood capacity in a bolted connection loaded perpendicular-to-grain can be given as:

$$\text{Bolted connection: } q_{wb} = \frac{\overbrace{\sigma \times n_R \times d \times t}^{\text{Area}}}{A_b B_b C_b} \quad (14)$$

As a result, by incorporating equation 13 into 14, with the notation of the three coefficients based on the bolted connection geometry as being: A_b , B_b and C_b , the ultimate wood capacity of a bolted connection is:

$$q_{wb} = \frac{200(n_R \times d \times t)^{0.8}}{A_b B_b C_b \times 10^3 \times (n_c \times d)^{0.2}} \text{ kN} \quad (15)$$

6.4 Coefficients A_b , B_b , C_b

The values of coefficients A_b , B_b and C_b were evaluated in light of the experimental results of the twenty-five connection groups.

6.4.1 Coefficient A_b

Coefficient A_b is a function of the number of rows (n_R) and the number of bolts in a row (n_C). The values are illustrated on Figure 8. The value of the coefficient A_b can be represented by the following equation:

$$A_b = 0.85 - ((n_C - 1) \times 0.10) + ((n_R - 1) \times 0.25) \quad (16)$$

The variation of the coefficient A_b adheres to observations made from previous studies on the behaviour of a bolted connection loaded perpendicular-to-grain. The load-carrying capacity of two or three rows of bolt(s) is less than the sum of the capacity of the individual rows. As it is represented in Figure 8, when n_R increases, A_b increases, which decreases the value of the load-carrying capacity. The number of bolts per row has a smaller influence on the load-carrying capacity than the number of rows, as Reshke observed [8].

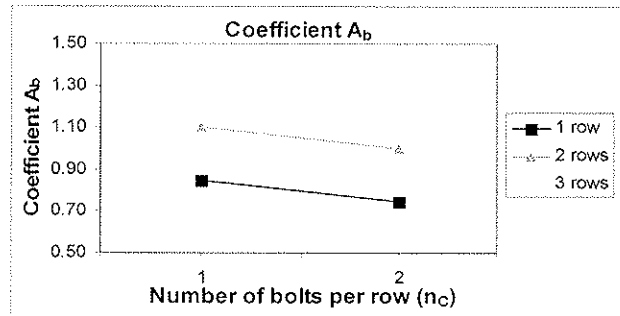


Figure 8 – Coefficient A_b

6.4.2 Coefficient B_b

Because many of the twenty-five configurations had a bolt spacing of 57mm ($3d$) and had two rows, the relation between coefficient B_b and the row spacing can be determined precisely only for these cases. More experimental testing is required in order to obtain results on different joint configurations (i.e. 2 rows $S_Q=38$ mm and 3 rows $S_Q=57$ mm), to increase the number of data points and generate more reliable regressions. At this point, a preliminary equation is developed to calculate the value of B_b for a two-row bolted connection, assuming that the linear slope of the relation between B_b and different S_Q is equal to the slope where $S_Q=57$ mm. The values of the coefficient B_b can be represented by equation 17 and are illustrated in Figure 9.

$$B_b = 1.28 + ((S_Q - 38) \times 0.014) - (S_p \times 0.0034) \quad (17)$$

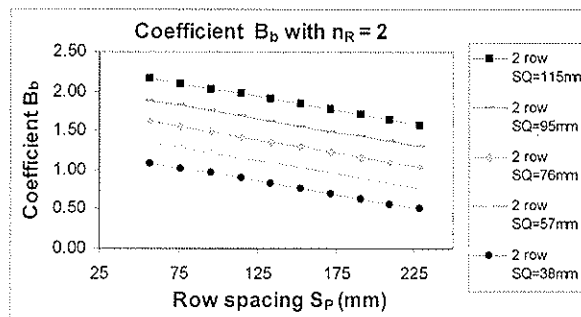


Figure 9 – Coefficient B_b with $n_R = 2$

With an increase of row spacing, B_b diminishes and the load-carrying capacity increases. This corroborates the observation made by Kasim that the resistance of the joint increases when the spacing between the rows increases [7].

6.4.3 Coefficient C_b

Coefficient C_b is a function of the ratio of the distance from the line of bolts farthest to the loaded edge to the loaded edge ($e_Q + S_Q$) over the depth of the beam. When the ratio is larger, the load-carrying capacity is higher. Coefficient C_b is represented in Figure 10 and is calculated with the following equation:

$$C_b = 11.41e^{-3.08r} \quad \text{where } r = \left(\frac{e_Q + S_Q}{\text{depth}} \right) \quad (18)$$

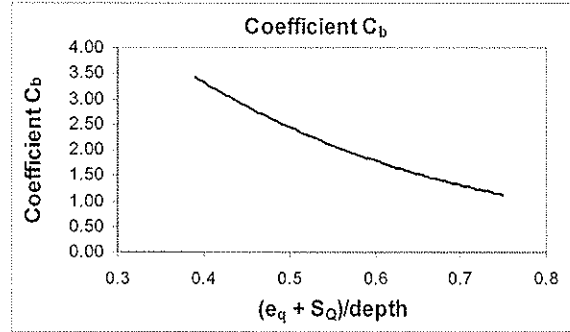


Figure 10 – Coefficient C_b

6.5 Comparison Between Experimental and Theoretical Values

The final results of the connection load capacity of the twenty-five configurations calculated with the proposed equation (q_b) are given in Table 1.

Table 1 – Theoretical vs Experimental Load Values

Group Ref no.	s_Q mm	s_R mm	n_C --	n_R --	t mm	d mm	$A_b B_b C_b$ --	q_{wb} kN	q_{yb} kN	q_b		Ratio q_b/P_{exp}
										Minimum (q_{wb} or q_{yb}) kN	Exp load $P^{(1)}$ kN	
1	57	76	2	2	80	19.1	1.70	34.9	47.7	34.9	34.9	1.00
2	57	133	2	2	130	19.1	1.44	60.9	77.5	60.9	57.0	1.07
3	57	95	2	3	130	19.1	1.81	66.8	116.2	66.8	64.9	1.03
4	57	76	2	3	80	19.1	2.39	34.3	71.5	34.3	34.9	0.98
5	57	76	2	2	80	19.1	3.82	15.5	47.7	15.5	14.0	1.11
6	57	155	2	2	80	19.1	3.02	19.6	47.7	19.6	21.0	0.93
7	57	225	2	2	80	19.1	2.31	25.7	47.7	25.7	31.8	0.81
8	57	76	2	2	80	19.1	1.68	35.3	47.7	35.3	39.1	0.90
9	76	76	2	2	80	19.1	2.30	25.8	47.7	25.8	27.6	0.93
10	76	76	2	2	80	19.1	2.30	25.8	47.7	25.8	23.8	1.08
11	0	0	1	1	80	19.1	2.54	15.4	11.9	11.9	16.0	0.75
12	57	0	2	1	80	19.1	0.74	46.0	23.8	23.8	32.2	0.74
13	57	95	2	2	130	19.1	1.61	54.4	77.5	54.4	52.0	1.05
14	57	95	2	3	130	19.1	1.55	77.9	116.2	77.9	56.1	1.39
15	57	95	2	3	130	19.1	3.36	36.0	116.2	36.0	43.3	0.83
16	57	77	2	2	80	19.1	3.78	15.7	53.1	15.7	16.0	0.98
17	57	225	2	2	80	19.1	2.28	25.9	53.1	25.9	33.0	0.79
18	57	0	2	1	80	19.1	1.65	20.7	23.8	20.7	21.6	0.95
19	57	0	2	1	80	19.1	0.73	46.5	23.8	23.8	41.5	0.58
20	38	152	2	2	130	12.7	2.05	33.3	50.6	33.3	33.9	0.98
21	0	95	1	2	130	19.1	3.04	33.1	38.7	33.1	31.4	1.05
22	57	95	2	2	130	19.1	1.38	63.5	77.5	63.5	64.9	0.98
23	57	320	2	2	80	19.1	1.35	44.0	47.7	44.0	33.6	1.31
24	57	225	2	2	80	19.1	1.01	58.4	47.7	47.7	47.0	1.01
25	38	38	2	2	80	9.5	1.57	24.8	26.5	24.8	24.4	1.02

(1) Normal duration, 5th percentile value

The smallest value between the load calculated with the EYM theory (q_{yb}) and the new equation (q_{wb}) represents the ultimate load capacity of the bolted connection under load perpendicular-to-grain (q_b). To summarize, the proposed design procedure of a bolted three-member connection loaded perpendicular-to-grain is the following:

$$q_b = \text{minimum} \begin{cases} q_{wb} \\ q_{yb} \end{cases}$$

$$\text{where } q_{wb} = \frac{200(n_R \times d \times t)^{0.8}}{A_b B_b C_b \times 10^3 \times (n_C \times d)^{0.2}} \quad (19)$$

$$q_{yb} = \text{EYM theory}$$

Figure 11 represents the comparison between the theoretical values of the proposed approach and the experimental values. It illustrates the ductile (q_{yb}) and brittle (q_{wb}) resistances of each twenty-five configurations (black dots and grey squares). The circle represents the ultimate load capacity of each connection, which is the minimum value between q_{yb} and q_{wb} .

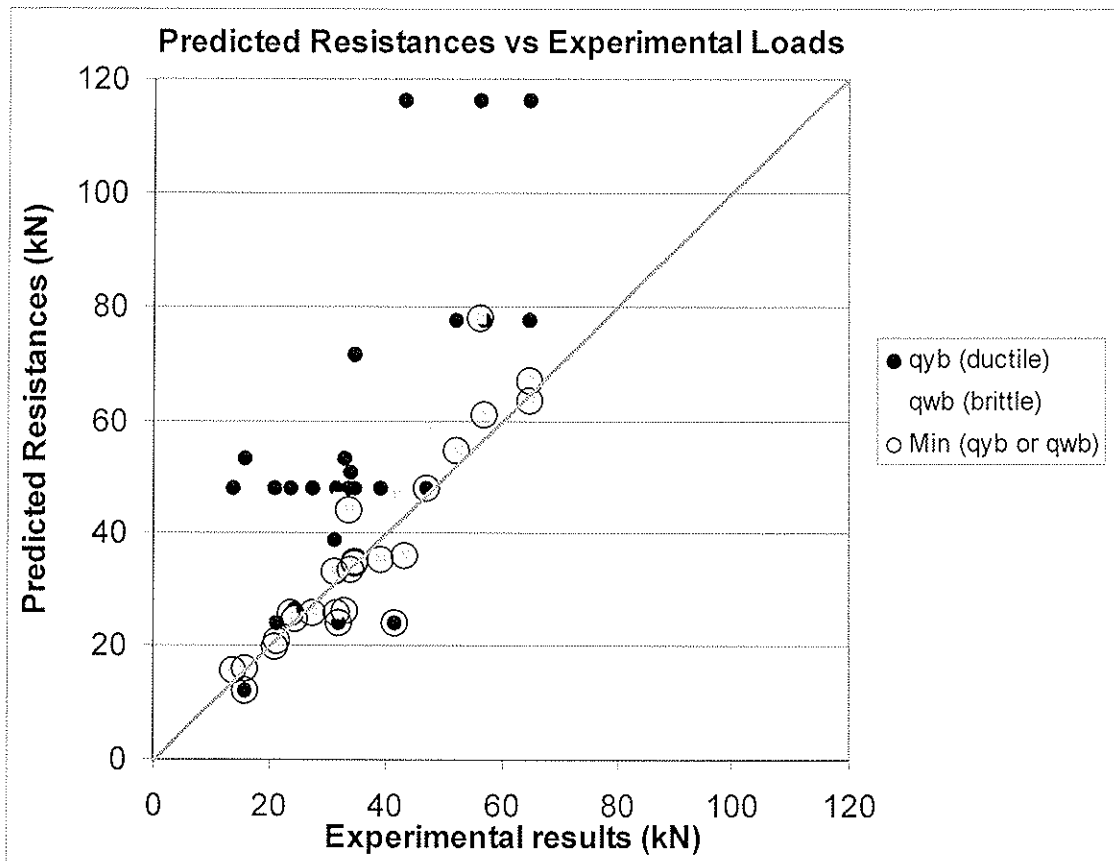


Figure 11 – Predicted Resistances vs Experimental Results

The proposed design approach gives much better results than the equation of the Canadian wood design code. From these twenty-five groups, an overall percentage of error of 37% is obtained between the experimental values and the values calculated with the design equation of the CSA O86-01. A better accuracy is reached with the theoretical values of the proposed equation, where the percentage of error is 12%.

7 Conclusions and Recommendations

Based on the results and discussion, the following specific conclusions can be drawn:

- a. The proposed design approach permits the differentiation between ductile and brittle failure mode.
- b. A good accuracy is reached with the proposed design approach. An overall percentage error of 12% is obtained between the experimental values and the theoretical values of the proposed design equations.
- c. The proposed equation is a function of the: number of rows, number of bolts in a row, spacing between the rows, spacing between the bolts in a row, distance from the line of bolts farthest to the loaded edge to the loaded edge, bolt diameter, thickness of the beam and depth of the beam.

While the proposed design method of this research provides good results in predicting the failure mode and the ultimate strength of a bolted connection loaded perpendicular-to-grain, additional research is required to validate its accuracy. To increase the reliability of the proposed equation, further groups of different configurations need to be tested.

Different types of bolted connection should be tested to validate the proposed equation, such as having the connection group located at the end of the member rather than located in the middle of the member, having a two-member connection (wood-wood and steel-wood) or a three-member connection (wood-wood-wood and wood-steel-wood), testing sawn lumber instead of glulam, and testing different wood species.

8 References

- [1] ASTM, “*Standard test methods for mechanical fasteners in wood*”, Standard D1761-88, American Society for Testing and Material, Philadelphia, Pa., 2000, pp. 294-305.
- [2] ASTM, “*Standard specification for computing the reference resistance of wood-based materials and structural connections for load and resistance factor design*”, Standard D5457-93, American Society for Testing and Material, Philadelphia, Pa., 1998, pp. 561-567.
- [3] ASTM, “*Standard Test Methods for Bolted Connections in Wood and Wood-Based Products*”, Standard D5652-95, American Society for Testing and Material, Philadelphia, Pa., 2000, pp. 561-567.
- [4] Barrett, J.D., Foschi, R.O., and Fox, S.P., “*Perpendicular-to-grain Strength of Douglas-Fir*”, Canadian Journal of Civil Engineering, 2, 1975, pp. 50-57.
- [5] Foschi, R.O., “*Stress analysis and design of glulam rivet connections for parallel-to-grain loading of wood*” Information Report VP-X-116, Department of the Environment, Canadian Forestry Service, 1973.
- [6] Foschi, R.O., “*Stress analysis and design of glulam rivet connections for perpendicular-to-grain loading of wood*” Information Report VP-X-117, Department of the Environment, Canadian Forestry Service, 1973.
- [7] Kasim, M.H., “*Bolted timber connections loaded perpendicular-to-grain: effect of row spacing on resistance*”, M.Sc. Thesis, Department of Civil Engineering, Royal Military College of Canada, Kingston, Ontario, 2002.
- [8] Reshke, R. “*Bolted timber connections loaded perpendicular-to-grain: influence of joint configuration parameters on strength*”, M.Sc. Thesis, Department of Civil Engineering, Royal Military College of Canada, Kingston, Ontario, 1999.

INTERNATIONAL COUNCIL FOR RESEARCH AND INNOVATION
IN BUILDING AND CONSTRUCTION

WORKING COMMISSION W18 - TIMBER STRUCTURES

A NEW PREDICTION FORMULA FOR THE SPLITTING STRENGTH
OF BEAMS LOADED BY DOWEL-TYPE CONNECTIONS

M Ballerini

University of Trento, Department of Mechanics & Structural Engineering

ITALY

Presented by M Ballerini

H J Larsen pointed out that f_w is the effect of distance between two groups and cannot be greater than 2. Ballerini answered that the value of f_w greater than two fitted to the test data but agreed that it should not exceed two.

A new prediction formula for the splitting strength of beams loaded by dowel-type connections

M. Ballerini

University of Trento, Department of Mechanics & Structural Engineering, Italy

Abstract: The paper presents a new semi-empirical prediction formula for the splitting strength of beams loaded perpendicular-to-grain by dowel-type connections. The formula is derived on the basis of the results of the main experimental researches carried out by different authors by means of the analysis of the influence of different parameters. It takes into account the influence of both the beams' size and the connections' geometry. The formula is initially derived for beams loaded by single-dowel connections and then corrected to cover the case of beams loaded by multiple-dowel connections. The prediction ability of the formula is illustrated, discussed and compared with the ones of prediction formulas available from literature which have been adopted in the new European and German design codes for timber structures. Finally, a design proposal is simply derived and compared with experimental results.

1 Introduction

Beams loaded on their depth by dowel-type connections can lead to failure for splitting at load levels which may be considerable lower than the ones of the connections or of the beams. This is particularly true when the distance from the loaded edge of the furthest row of fasteners (h_e) is small compared to the beam height (h).

Due to this reason such engineering solution for the transmission of forces should be avoided or adequately designed by means of properly reinforcements as suggested by Blass & Bejtka in [1].

Nevertheless by the presence of possible reinforcements, the need of a valid prediction formula for the splitting strength of beams loaded by dowel-type connections is widely recognised. Unfortunately, the evaluation of the splitting strength is a difficult task due to the large number of involved parameters.

The most recent drafts for the new European (EC5, 2002 [2]) and German (E DIN 1052, 2002 [3]) design codes for timber structures suggest two different design formulae which take into account the several parameters in a very different way.

The design formula embodied in the draft of the new EC5 is based on the work originally developed by Van der Put ([4, 5]), on the basis of an energetic approach in the framework of the Linear Elastic Fracture Mechanics, and recently put forward again by Leijten in [6]. Essentially, this formula assumes a linear relationship with the beam thickness and an influence of the square root of the distance of the furthest row of fasteners from the loaded edge of the beam (h_e). On the contrary, it neglects any influence of the connection geometry.

The design formula embodied in the draft of new E DIN 1052 is an evolution of the prediction formula derived by Ehlbeck, Görlacher & Werner [7], which was based on both empirical and theoretical considerations. With respect to the Van der Put formula, it assumes a different influence of the loaded edge distance (by means of the non-dimensional

parameter $\alpha = h_o/h$) and also a different non-linear influence of both the beam thickness (b) and the beam height (h) as a result of the assumed Weibull failure theory. Moreover, it explicitly considers the influence of the joint configuration on the splitting strength.

Both prediction formulae seem to have some correct and some wrong assumptions.

The formula of Van der Put seems to be able to predict more correctly the influence of the beam height (and also of the beam thickness), as reported in the recent experimental and numerical researches of Ballerini [8, 9, 10] and Yasumura [11] performed on beams loaded by single-dowel connections. Nevertheless, it doesn't take into consideration the effect of the joint geometry which is instead clearly detectable in all the experimental researches: from the oldest (Möhler & Lautenschläger [12], Möhler & Siebert [13], Ehlbeck & Görlacher [14]) to the more recent ones (Ballerini & Giovanella [9], Reske [15], Reske, Mohammad & Quenneville [16], Quenneville & Mohammad [17], Kasim & Quenneville [18]).

On the other side, the formula embodied in the recent draft of the new German design code for timber structures correctly takes into account the effect of the joint geometry, however it seems less reliable from the viewpoint of the influence of beam height and thickness.

In the present paper a new semi-empirical prediction formula is derived on the basis of theoretical considerations and on the main outcomes of the different experimental researches. Initially, the formula is derived for the case of beams loaded by single-dowel connections. Afterwards, the formula is corrected to cover the case of beams loaded by multiple-dowel connections. This second step is developed considering initially the effect of the width of the connection and then the effect of the connection height.

Afterwards the prediction capability of the proposed formula is illustrated, discussed and compared with the one of the prediction formula of Van der Put and of the design formula of E DIN 1052.

Finally, from the proposed prediction formula a design proposal is simply derived and compared with experimental results.

2 The experimental data sets and main outcomes

The experimental data sets taken into account in this work are reported in table 1. The table shows also the number of tests (or available tests data) and the main characteristics of each experimental programme. A total amount of 627 test results have been considered in this study. In this research, only the data concerning beam specimens in different configurations (simply supported and loaded by the connection in the mid-span, or simply supported with the connection at one or both ends, or in a cantilever configuration and loaded at the end by the connection) have been considered.

More in detail, with respect to the main parameters which can affect the beams splitting strength, the following characteristic of each experimental research should be noticed:

- h - this parameter has been quite widely investigated up to the height of 400 mm, above this height there are only the tests of Möhler & Siebert (600 and 1200 mm high beams, only 1 test/configuration) and of Ballerini & Giovanella (800 mm, 3 tests/configuration);
- b - the beam thickness has been investigated by Ehlbeck & Görlacher (80, 100 and 120 mm thick beams, 3 tests/configuration), by Reske and Reske, Mohammad & Quenneville (80 and 130 mm, 10 tests/configuration) and by Ballerini & Giovanella (80, 120, 160 and 200 mm thick beams, 3 tests/configuration);
- α - this parameter ($\alpha = h_o/h$) has been investigated partially in all researches and extensively in the research of Möhler & Lautenschläger (from 0.16 to 0.58, 3 tests/configuration) and of Ballerini & Faccincani and Ballerini & Giovanella (from 0.10 to 0.70, 3 tests/confi-

- guration);
- h_m - the connection height (in combination with the number of rows n) has been extensively investigated by Möhler & Lautenschläger (from 0 to 76 mm, 3 tests/configuration), partially by Möhler & Siebert (from 80 to 500 mm, only 1 test/configuration) and by Reske, Mohammad & Quenneville (from 0 to 89 mm, 10 tests/configuration);
 - l_r - the connection width (in combination with the number of fasteners per row m) has been investigated by Möhler & Lautenschläger (from 0 to 76 mm, 3 tests/configuration), by Reske, Mohammad & Quenneville (from 0 to 190 mm, 10 tests/configuration), and by Kasim & Quenneville (from 0 to 700 mm, 10 tests/configuration, only mean data available);
 - l_1 - the distance between clusters of fasteners has been deeply investigated by Ehlbeck & Görlacher (from 0 to 240 mm, 3 tests/configuration) on simply supported beams with connection at mid-span, by Reske, Mohammad & Quenneville (from 0 to 268 mm, 10 tests/configuration) on cantilever beams or on supported beams with the connection at one end, and by Yasumura, Murata & Sakai (from 0 to 784 mm, only mean data available).

In the above experimental researches the joints were made essentially by dowels ranging from 10 to 30 mm in diameter. Some researches were carried out on specimens with nailed connections (Ehlbeck & Görlacher and Möhler & Lautenschläger), and the research of Möhler & Siebert had some specimens with Appel connectors 65 mm in diameter.

From the tests results the following main outcomes can be driven:

- in tests characterised by α ratios up to 0.7, failure occurs as a consequence of the development of a crack in correspondence of the furthest row of fasteners from the loaded edge of the beam;
- the splitting strength is essentially proportional to the beams thickness b [9] as shown clearly by the graph of figure 1;

Table 1 – Experimental data sets

<i>Authors</i>	<i>year</i>	<i>n.</i> <i>of tests</i>	<i>beams' size</i> <i>and main investigated parameters</i>	<i>Reference</i>
Möhler & Lautenschläger	1978	52	40 x 120 and 180 ; α, h_m, n, l_r, l_1	[12]
Möhler & Siebert	1980	28	100 x 600 and 1200 ; α, h_m, n, d	[13]
Ehlbeck & Görlacher	1983	57	80 – 100 – 120 x 250 – 400 $\alpha, b, L, h_m, n, l_r, l_1$	[14]
Yasumura, Murata & Sakai	1987	18	80 x 304 ; α, n, l_r, l_1	[22]
Ballerini & Faccincani	1999	47	40 x 196 and 397 ; α, h_m, n	[8]
Reske	1999	138	80 – 130 x 190 – 228 ; α, b, h_m, n, l_r	[15]
Reske, Mohammad & Quenneville	2000	105	80 – 130 x 190 – 228 $\alpha, b, h_m, n, l_r, d, l_1$	[16, 17]
Quenneville	2001	89	80 x 190 – 228 ; $\alpha, h_m, n, l_r, d, l_1$	[21]
Yasumura	2001	10	64 x 224 – 336 – 448 $\alpha, b, L, h_m, n, l_r$	[11]
Kasim & Quenneville	2002	11	80 x 190 – 228 ; α, n, l_r	[18]
Ballerini & Giovanella	2003	72	80 – 120 – 160 – 200 x 800 40 x 200 and 400 ; α, b, h, n, l_r, d	[9, 20]

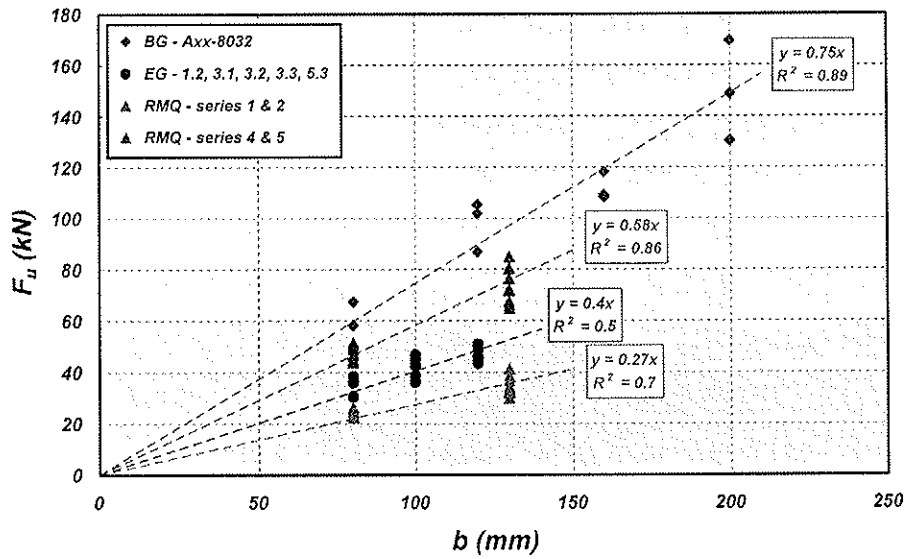


Fig. 1 – Influence of beams' width (b)

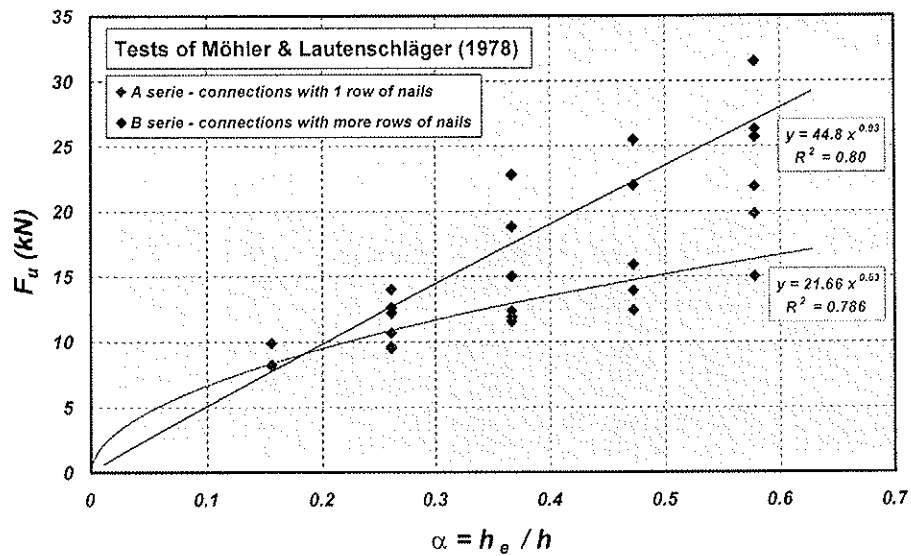


Fig. 2 – Influence of α (h_e/h) and of connection's height (h_m)

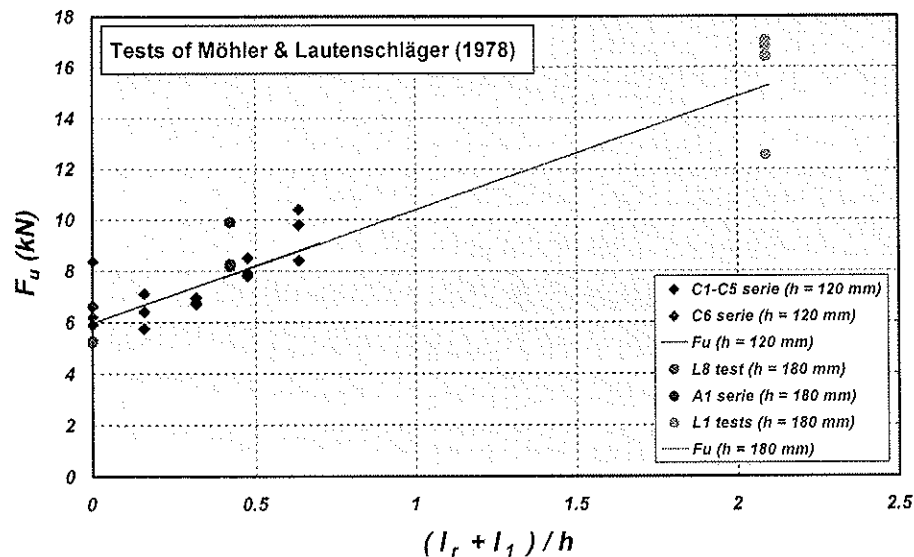


Fig. 3 – Influence of connection width (l_r) and of the distance between clusters of fasteners (l_1)

- the splitting strength depends greatly (but not linearly) by the distance from the loaded edge of the furthest row of fasteners h_e or for the same beam height h by the ratio α (see the red line of figure 2 related to connections with a row of 5 nails);
- the splitting strength is greatly influenced from the number of rows n of the connection and consequently from the connection height h_m (see the blue line of figure 2 concerning connections respectively with 2, 3, 4 and 5 rows of 5 nails);
- the strength is also influenced by the connection width l_r and, for connections made by means of different clusters of fasteners by the distance between clusters l_l (see figure 3);
- on the other side, the strength seems not influenced by type and size of fasteners and also by the slenderness (L_{test}/h) of beams.

3 The strength of beams loaded by single-dowel connections

From the results of the experimental tests reported above, the formula of Van der Put, which assumes a plane stress state and consequently a linear relationship with the beam thickness, has been considered firstly.

It can be written as follows:

$$F_u = 2b \cdot k \cdot \sqrt{\frac{h_e}{1-\alpha}} \quad (1)$$

On the basis of a fit on the mean strengths of beams loaded by single-dowel connections a value of $k = \sqrt{GG_c}/0.6 = 11.6 \text{ N/mm}^{1.5}$ has been derived. The result of the fitting is shown in figures 4 and 5. From figure 4 it is possible to notice that the model describes quite well the mean experimental results of beams 200 and 400 mm high which represent quite completely the whole database. This fact confirms that the Van der Put model is able to predict correctly the influence of beams height. However, from the graph it is also possible to notice that the model tends to underestimate the average strength for lower α values and to overestimate it for the higher ones.

This fact is confirmed from the graph of figure 5 which shows clearly a marked residual influence of parameter α on the ratio F_u/F_{pre} with the only exception of the data of Yasumura.

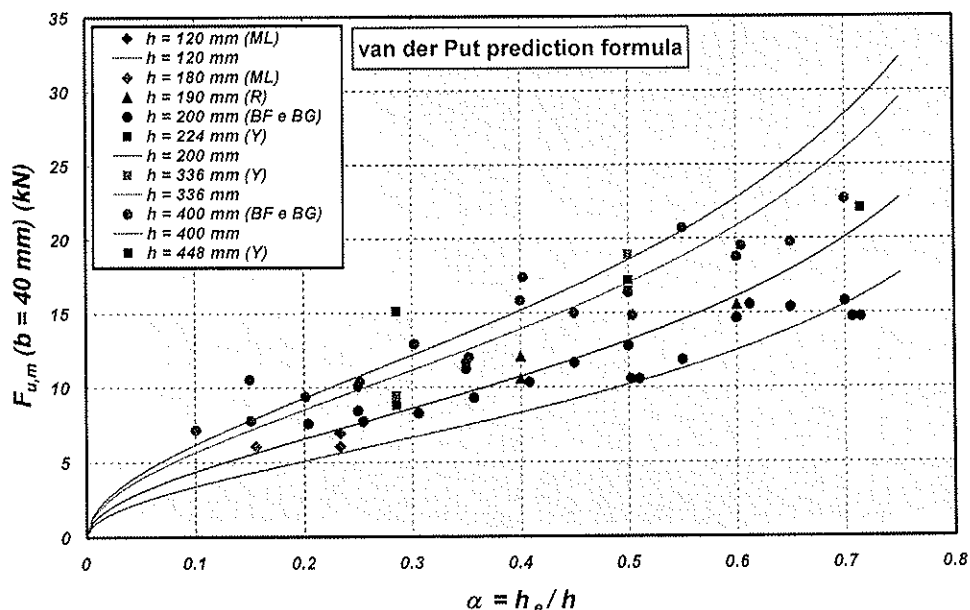


Fig. 4 – Van der Put model for beams loaded by single-dowel connections

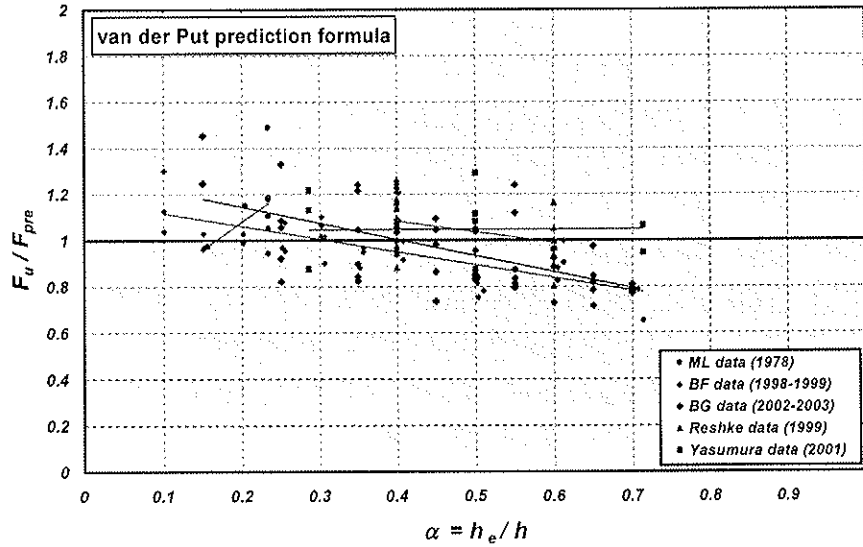


Fig. 5 – Van der Put model: values of F_u / F_{pre} versus α

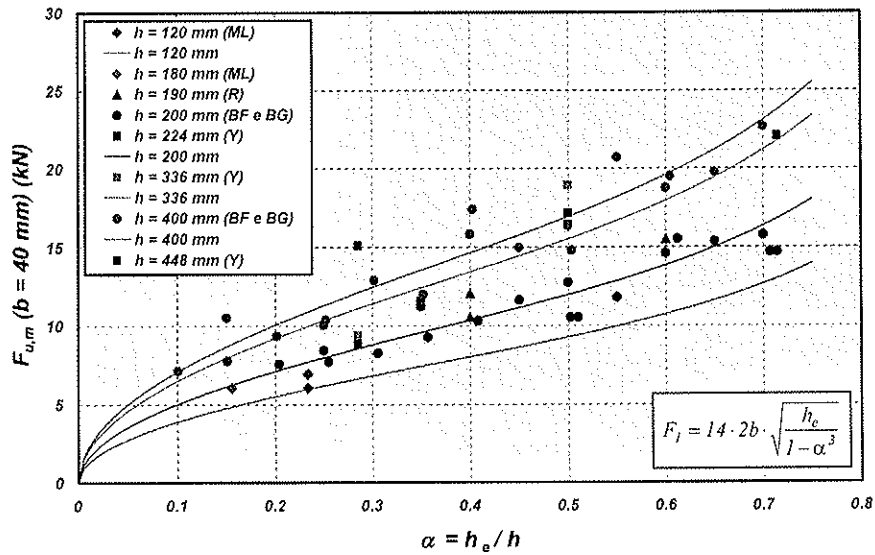


Fig. 6 – proposed model for beams loaded by single-dowel connections

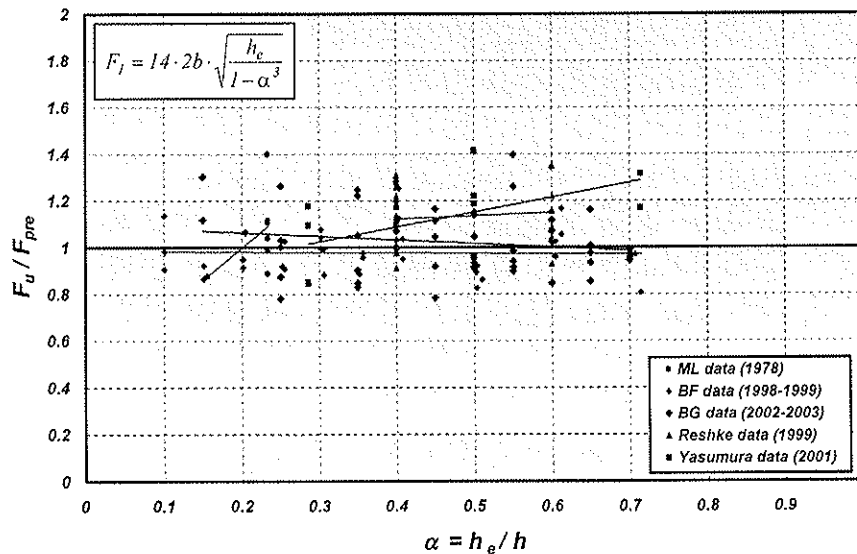


Fig. 7 – proposed model: values of F_u / F_{pre} versus α

To correct this residual influence, the following prediction formula can be assumed:

$$F_{u,I} = 2b \cdot k \cdot \sqrt{\frac{h_e}{1-\alpha^3}} \quad (2)$$

Eq. (2) maintains the good properties of eq. (1) but it allows to increase the strength of specimens with lower α values and to decrease the one of specimens with the higher ones. Although eq. (2) has been derived by fitting of experimental data, it is in line with the equation originally developed by Van der Put in [4, 5] and also with the one found by Jensen in [19], which takes into account a different distribution of bending moments in the cracked beam due to the presence of the axial force.

Eq. (2) has been calibrated on the mean data of the experimental researches of Ballerini (BF and BG) which, as already mentioned, represent quite the whole database for beams with single-dowel connections. As a result, a value of $14 \text{ N/mm}^{1.5}$ has been found for the coefficient k . Graphically, the good prediction capability of eq. (2) is shown in figures 6 and 7.

Finally, for comparison purposes only, the data of beams loaded by single-dowel connections have been compared with the model embodied in the new German design code for timber structures (BEKS). For single dowel connections, it can be written as:

$$F_u = (6.5 + 18 \cdot \alpha^2) \cdot (b \cdot h)^{0.8} f_{t,90,m} \quad (3)$$

The results of the comparison are shown in figures 8 and 9; for the comparison, a value of 0.86 MPa for the average strength perpendicular-to-grain of wood, resulting from the best fit on the whole set of data, has been assumed.

From figure 8 it appears clearly that this formula predicts quite perfectly the data of beams with an height of 200 mm but it overestimates greatly the ones of 400 mm high beams.

This seems to confirm that BEKS model is not able to predict correctly the influence of beams height.

The graph of figure 9 confirms the results of figure 8.

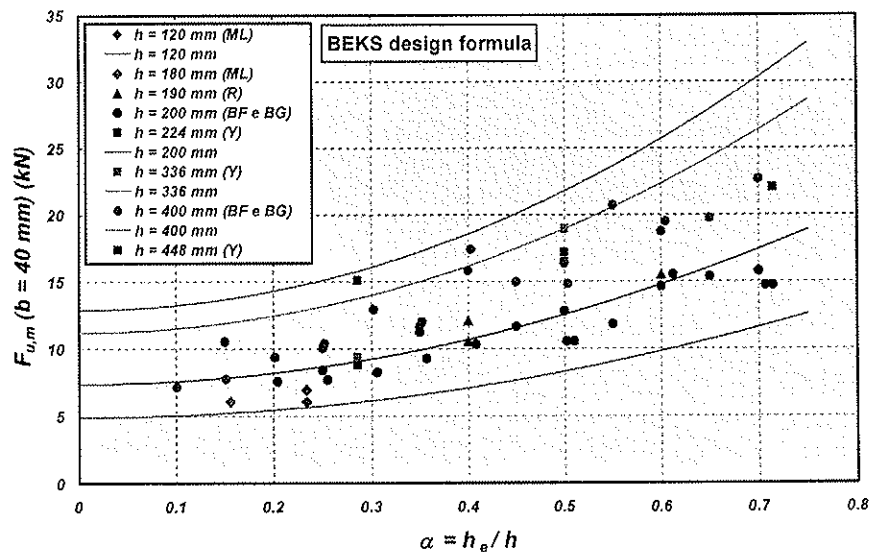


Fig. 8 – BEKS model for beams loaded by single-dowel connections

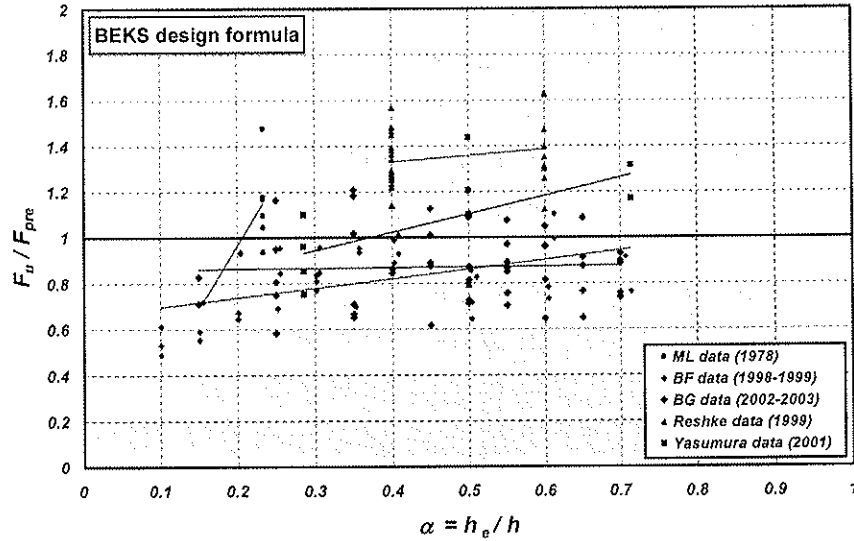


Fig. 9 – BEKS model: values of F_u/F_{pre} versus α

4 The influence of the connection geometry

4.1 The effect of connections width and of the distance between clusters of fasteners

To investigate the influence of the width of connections and of the distance between clusters of fasteners, the data of tests with 1 row of fasteners have been considered.

These data concerns tests on simply supported beams with the connection in the mid-span and tests with the connection at one end (or both ends) on simply supported beams or on cantilever beams. In the former case the specimens are usually characterised by different connections widths (l_r) and by the absence of clusters of fasteners (consequently $l_l = 0$); the latter case instead can be regarded as one half of a mid-span connection, therefore it is always characterised by non-zero l_l values (l_l is in this case twice the distance between the connections centre and beams end).

The average values of tests results divided by the predicted strength of specimens with single-dowel connections (F_I), have been plotted versus the following non-dimensional parameters: $(l_r+l_l)/h$, $(l_r+l_l)/h_e$, $(l_r+l_l)/h_l$, where in the latter case h_l is the distance between the unloaded beam edge and the nearest row of fasteners.

Figure 10 shows the data $F_{u,m} / F_I$ versus $(l_r+l_l)/h$, which is the parameter with the better correlation with tests data. In the same figure, together with the data of specimens with one row of fasteners (solid dots), are plotted the ones of specimens with more rows and same connection geometry (cross dots).

In spite of the big scatter, from the picture it is possible to notice a considerable increase of the splitting strength of beams with respect to the one of single-dowel connections. Moreover, cross dots (representing the average strength of specimens with more rows) shows generally a strength higher than the one of solid dots (1 row) as expected.

From the figure, a general trend for the increase of the splitting strength of beams with 1 row of fasteners can be detected. It is represented by the solid line in figure 10 which can be written as follows:

$$f_w(l_r, l_l, h) = \min \left\{ \begin{array}{l} 1 + 0.75 \left(\frac{l_r + l_l}{h} \right) \\ 2.2 \end{array} \right. \quad (4)$$

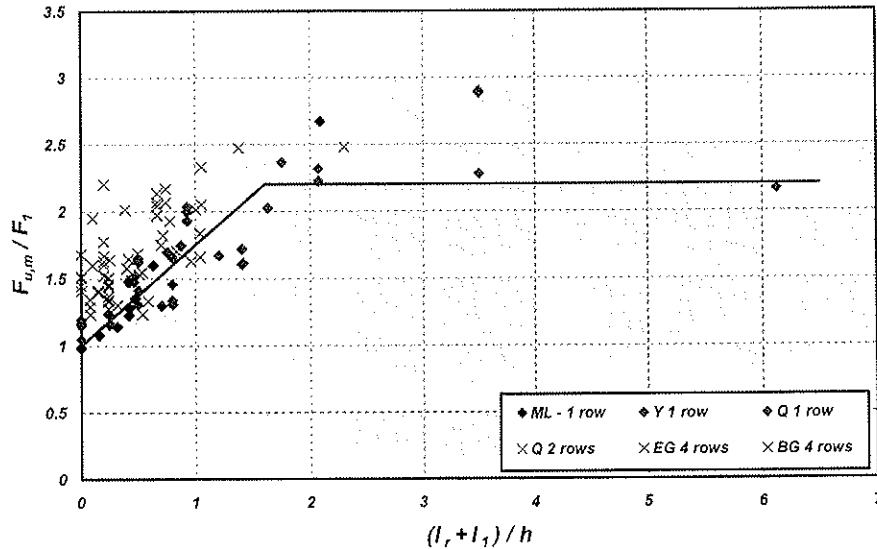


Fig. 10 – Average strength increase of specimens with 1 row of fasteners (solid dots) and of the ones with more rows (cross dots) versus connections width and the distance between clusters of fasteners

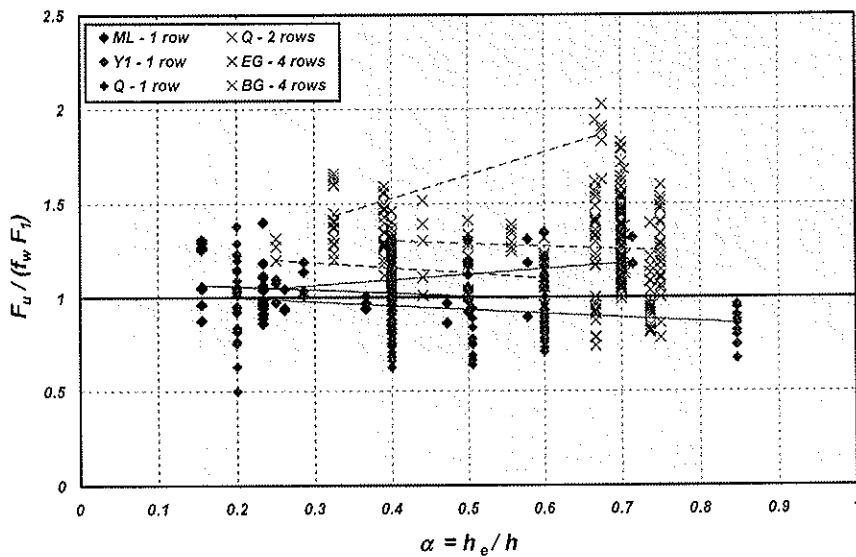


Fig. 11 – Values of $F_u/(f_w F_1)$ versus α for specimens with one row of fasteners (solid dots) and for the ones with more rows of fasteners (cross dots)

Figure 11 shows the data $F_u/(f_w F_1)$ versus α . Besides the big scatter, it is possible to notice a quite good estimation of specimens with one row of fasteners.

4.2 The effect of connections height and of the number of rows

To investigate the influence of connections height the whole database has been taken into account.

The average data of each configuration have been divided by the predicted strength for the specimens with 1 row of fasteners ($f_w F_1$) to eliminate the influences of parameters b , h , α , l_r and l_1 . The resulting set of data has been plotted versus different non-dimensional parameters to find out the better correlation.

Accordingly with the findings of the experimental researches, the investigated parameters were proportional to the connection depth h_m or to the number of rows n , and inversely

proportional to the beams height h , to the distance of the furthest row of fasteners from the loaded edge of the beam h_e , or to the distance of the same row of fasteners from the unloaded edge of the beam h_l .

In detail, the investigated parameters were: h_m/h , h_m/h_e , h_m/h_l , $n h_m/h$, and other more complex combinations of n and h_m/h_l like the ones which can be obtained with different approximations of the row factor $1/k_r$ defined by Ehlbeck, Görlacher & Werner in [7] and embodied in the new E DIN 1052 [3].

Among the above non-dimensional parameters, the one which gives the better correlation is h_m/h_e ; its graphs is shown in figure 12. In spite of this, as it is possible to notice, the correlation is again quite poor.

The better correlation has been found with the following dimensional parameter: $n h_m/1000$. Its correlation with the data set computed from the average strengths is reported in figure 13. From the picture it is evident a quite good correlation with the data even if a quite large scatter is apparent for values of $n h_m/1000$ lesser than 0.25.

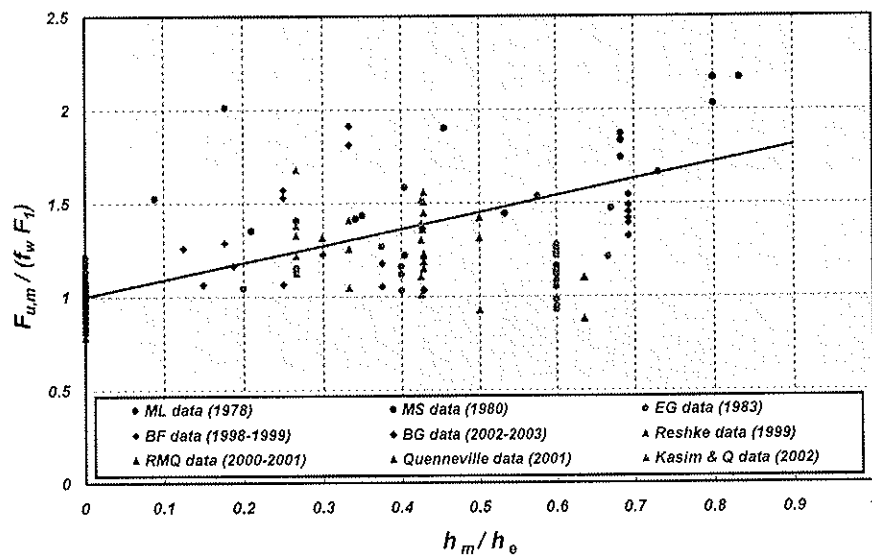


Fig. 12 – Strength increase due to connections height versus h_m/h_e

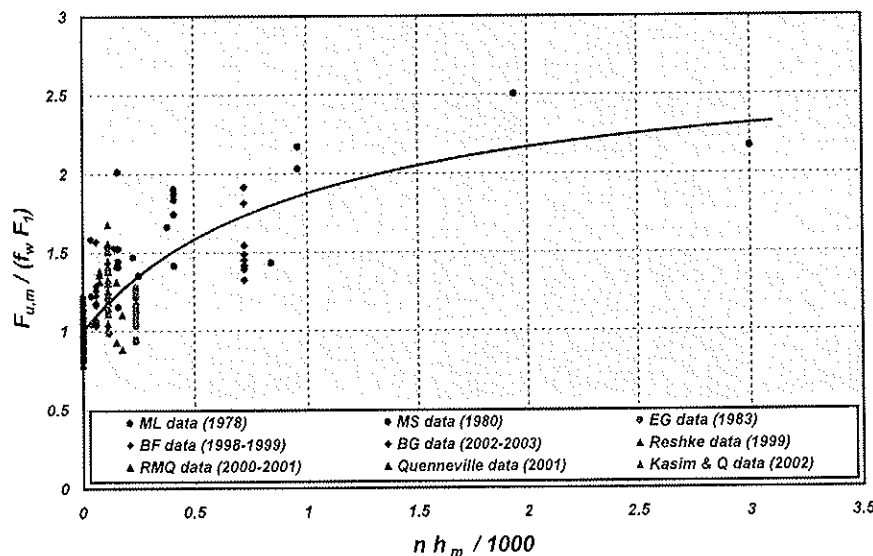


Fig. 13 – Strength increase due to connections height versus $n h_m / 1000$

In figure 13, the solid line represents the effect of the connection height or of the number of rows f_r . Its equation is:

$$f_r(n, h_m) = 1 + 1.75 \frac{\kappa}{1 + \kappa} \quad \text{where} \quad \kappa = \frac{n \cdot h_m}{1000} \quad (5)$$

5 Comparison with design code formulae

The capability prediction of the derived model has been compared with the one of the Van der Put model embodied in the new EC5, and with the one of Ehlbeck, Görlacher & Werner embodied in the new German code with some changes (BEKS).

For comparison purposes, the above models have been calibrated on the whole database. As a result of the calibration an average value of $\sqrt{GG_c}/0.6$ equal to 16.6 N/mm^{1.5} has been found for the Van der Put model (G and G_c are respectively the shear modulus and the energy release rate of timber parallel-to-grain), and an average value of 0.89 MPa for $f_{t,90,m}$ has been found for the BEKS one. The above values are respectively 2.37 and 1.8 times the characteristic values suggested in the design codes.

The results of the comparison are summarized in table 2 and in figures 14, 15 and 16. In table 2 for each model, for each experimental data set and for the whole database, the mean values, the standard deviation, the maximum and the minimum values of ratios F_u/F_{pre} are reported.

From figures 14, 15 and 16 appear clearly that the model of Van der Put is the one with the lower prediction capability. Indeed, in spite of its good ability in predicting the strength of beams with different height and thickness, neglecting any influence of the connection geometry it is not able to catch the strength in those situations where the connection geometry has a relevant effect, like high values of l_j/h (F_u/F_{pre} equal to 2.55 and 2.2, ML tests) or large number of rows (F_u/F_{pre} equal to 1.5, 1.7 and 2.1 for connections with 4 rows, MS tests). On the other side, to catch the average effect of connections geometry, the model is forced to underestimate the strength of beams with single-dowel connection.

Due to the high value of the standard deviation of ratios F_u/F_{pre} of the whole set of data, 0.29 as reported in table 2, the characteristic strength it is only about 42% of the average one.

Table 2 – Statistical parameters of different prediction models

experimental data set	Van der Put model				BEKS model				proposed model			
	mean	s.d.	max	min	mean	s.d.	max	min	mean	s.d.	max	min
ML	1.14	0.44	2.55	0.66	1.00	0.16	1.42	0.69	1.08	0.17	1.57	0.83
MS	1.38	0.28	2.09	0.92	1.01	0.17	1.35	0.76	1.20	0.24	1.81	0.80
EG	0.94	0.13	1.29	0.66	0.94	0.12	1.26	0.71	0.86	0.12	1.16	0.59
Y1	0.73	0.10	0.90	0.61	1.03	0.21	1.39	0.72	1.12	0.18	1.41	0.85
BF	0.71	0.11	1.12	0.46	0.78	0.14	1.06	0.47	1.01	0.12	1.43	0.81
R	0.90	0.17	1.34	0.56	1.04	0.19	1.57	0.64	1.10	0.17	1.55	0.67
RMQ	1.07	0.27	1.69	0.57	1.07	0.24	1.57	0.60	0.99	0.21	1.58	0.64
Q	1.03	0.21	1.64	0.58	1.04	0.23	1.60	0.51	0.90	0.17	1.38	0.50
Y2	1.30	0.31	1.84	0.78	1.17	0.20	1.41	0.79	1.10	0.11	1.32	0.92
KQ	1.16	0.24	1.54	0.79	1.02	0.13	1.23	0.81	1.09	0.16	1.42	0.86
BG	0.83	0.27	1.34	0.50	0.87	0.15	1.18	0.56	0.98	0.15	1.40	0.69
all data	1.00	0.29	2.55	0.46	1.00	0.20	1.60	0.47	1.03	0.19	1.81	0.50

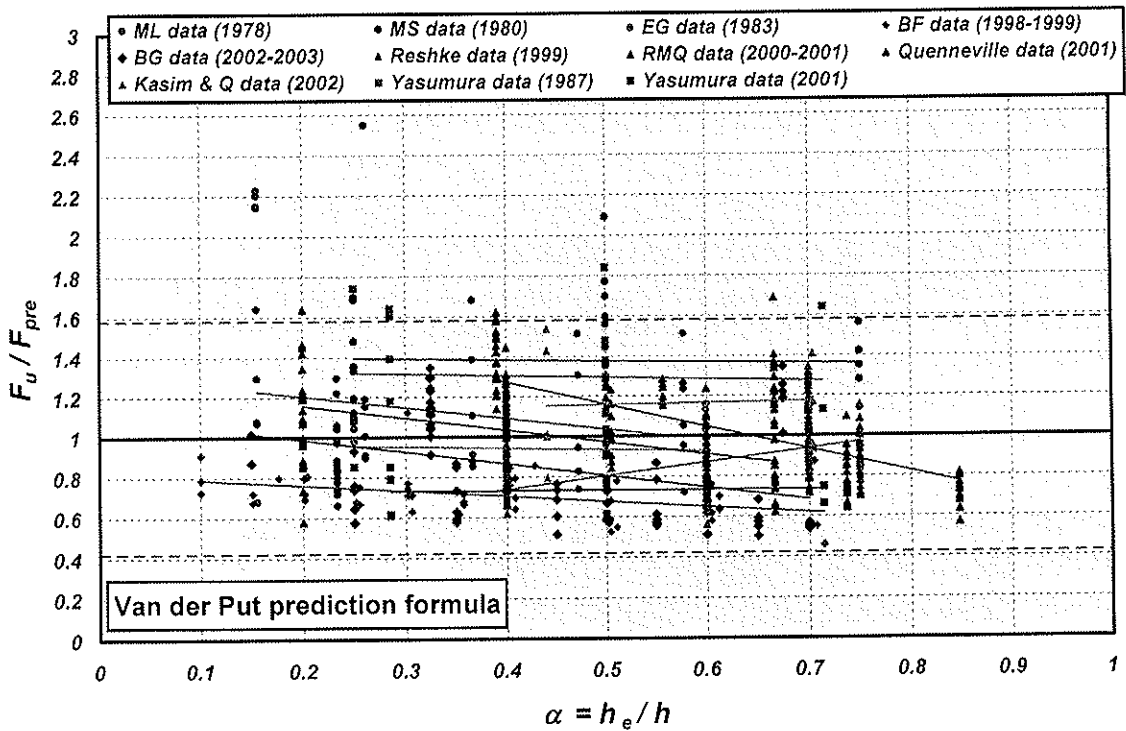
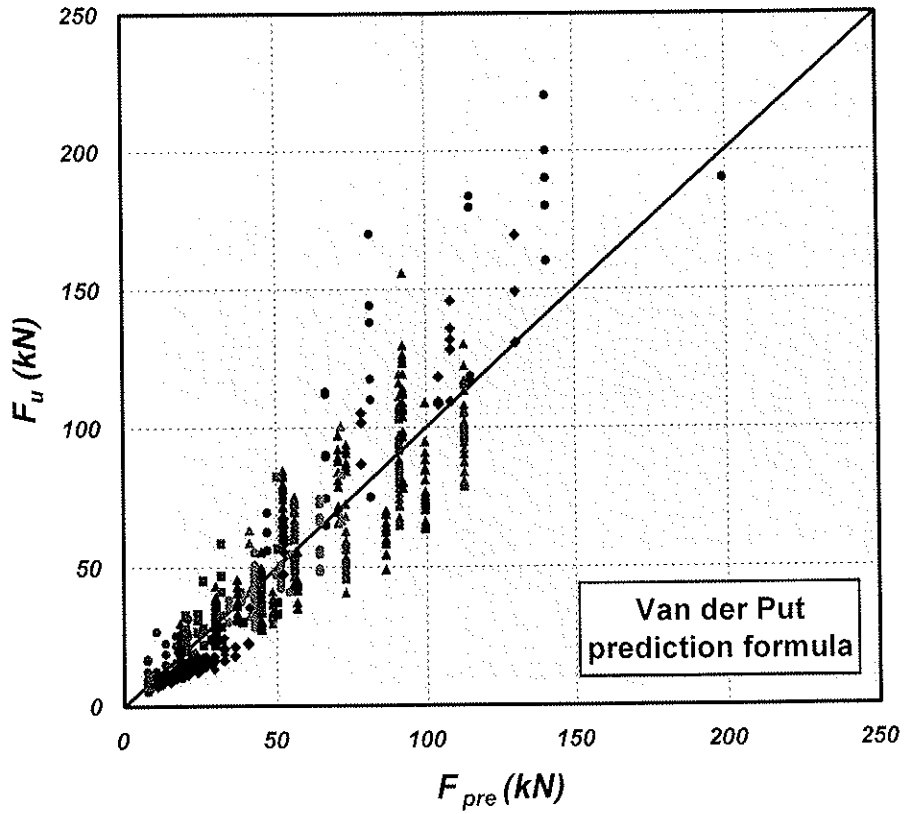


Fig. 14 – Van der Put model ($\sqrt{GG_c/0.6} = 16.6 \text{ N/mm}^{1.5}$): strength prediction capability (above), F_u/F_{pre} values versus α with the lower and upper characteristic values (bottom)

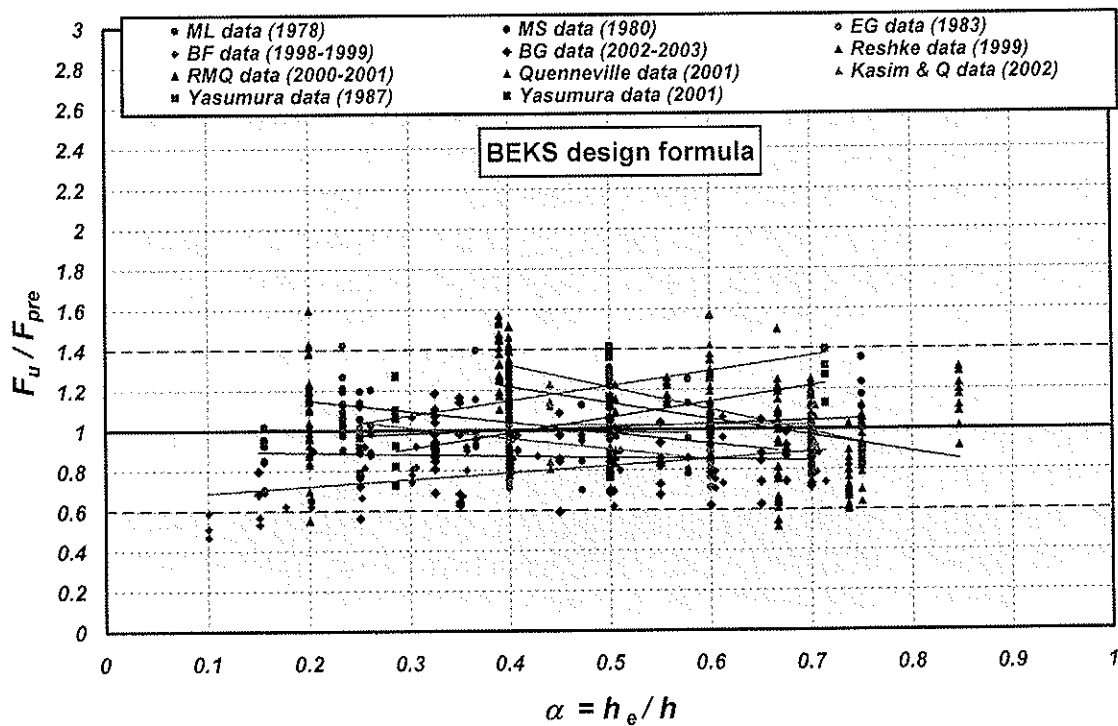
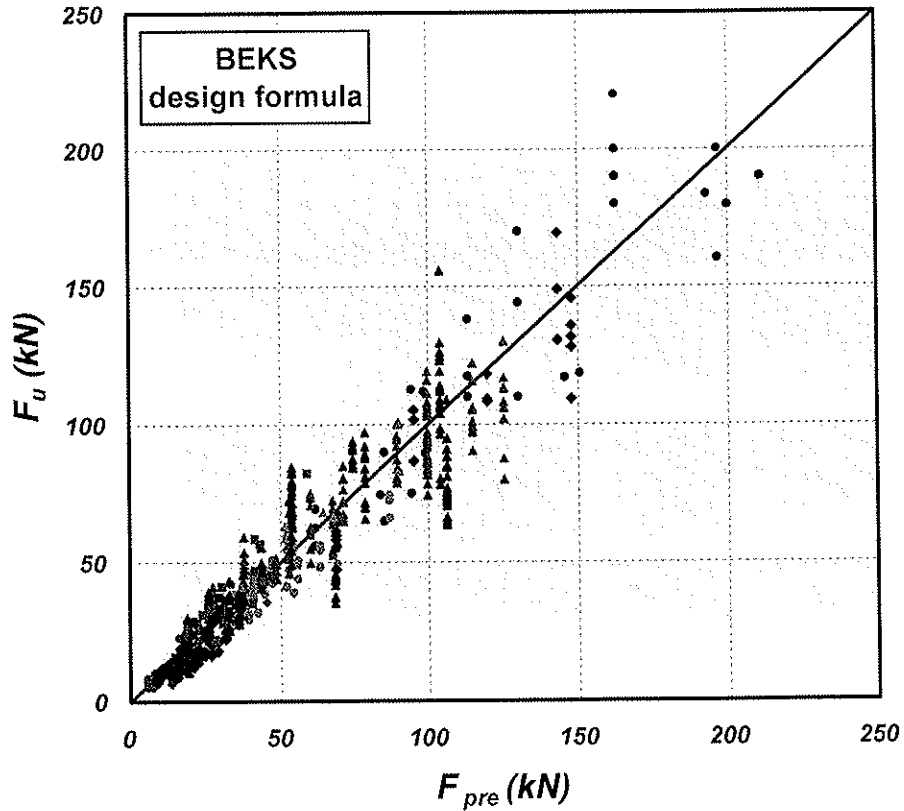


Fig. 15 – BEKS model ($f_{t,90,m} = 0.89$ MPa): strength prediction capability (above), F_u / F_{pre} values versus α with the lower and upper characteristic values (bottom)

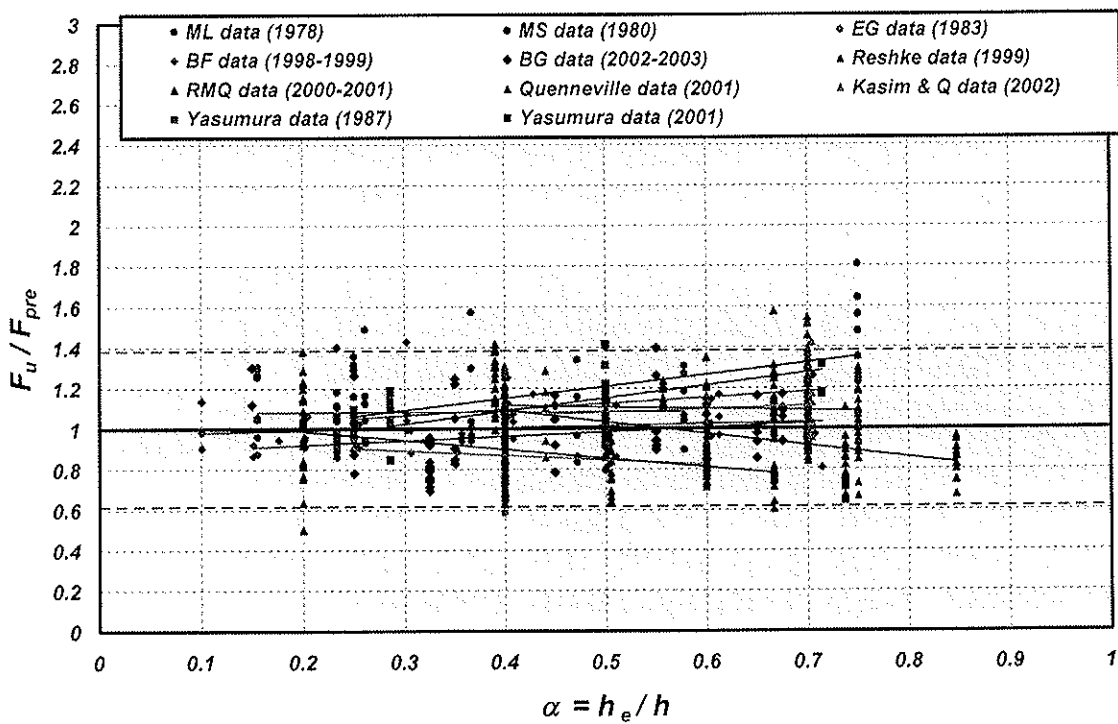
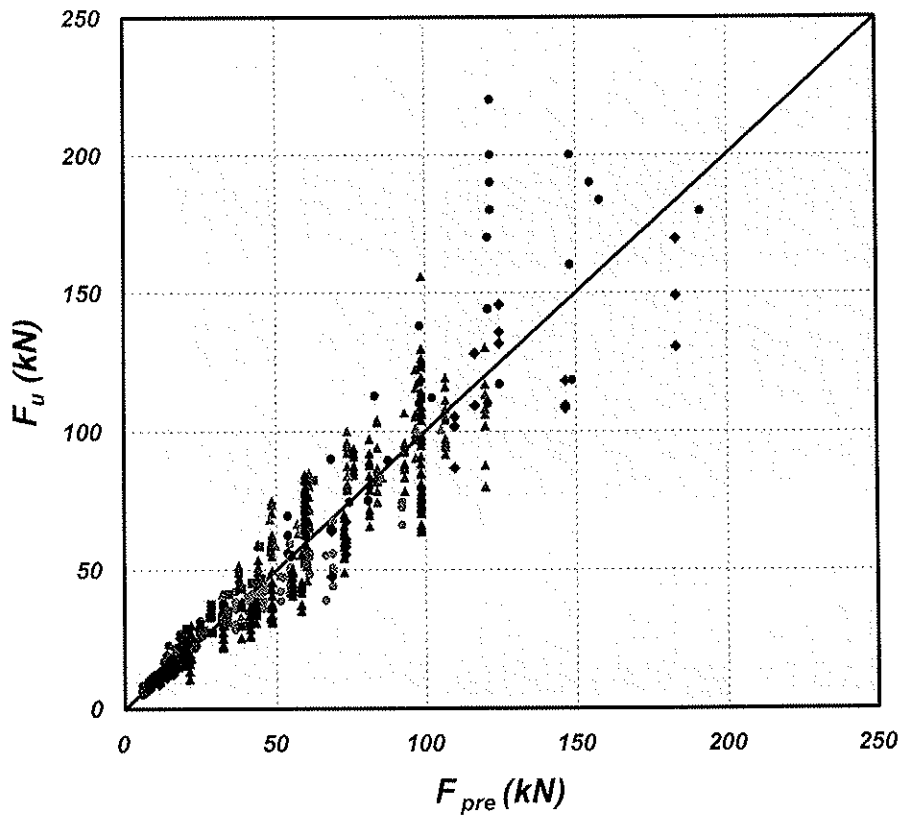


Fig. 16 – proposed model: strength prediction capability (above), F_u/F_{pre} values versus α with the lower and upper characteristic values (bottom)

In spite of the fact it is not very reliable for beams with single-dowel connections, the BEKS model has a considerable prediction capability. The values of ratios F_u / F_{pre} differ generally not more than ± 0.4 from the average. Some exceptions are due to Canadian data (maximum value 1.6) and to some data of Ballerini researches for beams 400 mm high, low α values and single dowel connections (minimum value 0.47). As it is possible to see from table 2, the BEKS model generally predicts better the data sets for which it was originally developed (ML, MS and EG data sets). The standard deviation of F_u / F_{pre} of the whole database is 0.2, then the characteristic strength is about 60% the average one.

The proposed model has substantially the same level of prediction ability of BEKS model. The data of F_u / F_{pre} are generally confined in the range ± 0.4 from the average. The exceptions are limited to some values of the Canadian data sets (whose data are very far from the average strength of identical specimens) and to some data of ML and MS data sets (also in this case the data are quite far from the average strength of identical specimens or the data are very high with respect to similar specimens, MS data). Different from the BEKS model, the proposed one predicts generally better the strength of beams with single-dowel connections and the one of Canadian researches. The standard deviation of the whole experimental data set is about 0.19 and consequently the characteristic strength is 62% the average one.

6 Design proposal

From the developed model for the prediction of the splitting strength of beams loaded with multiple-dowel connections a design proposal can be easily derived.

The characteristic strength can be written as:

$$F_{90,Rk} = 2b \cdot 8.6 \cdot \sqrt{\frac{h_e}{1-\alpha^3}} \cdot f_w \cdot f_r \quad (6)$$

with f_w and f_r are defined respectively by equations (4) and (5).

From equation (4) it can be easily noticed that when the total width of a connection made with two clusters of fasteners ($l_r + l_l$) is greater than $1.6 h$ (f_w greater than 2.2), the connection should be considered made by two independent connections and the splitting strength computed separately for each connection. While, if the length of the connection is lesser than $1.6 h$, the clusters of fasteners should be regarded as a single connection and the strength computed according to equation (6).

The comparison between the predicted characteristic splitting strength of beams and the experimental data is shown in figure 17. From the figure appears clearly that the average strength is about 1.7 times the characteristic one and that the most part of experimental data have a strength not greater than 2.4 times the one predicted by eq. (6).

7 Conclusions

The derivation of a new semi-empirical prediction formula for the splitting strength of beams loaded by dowel-type connections has been illustrated in detail. The formula is based on the results of some theoretical and numerical works of different authors and on the data of a large number of experimental researches.

The prediction capability of the new formula has been compared with the one of two different design formulae embodied in the new Eurocode 5 and in the new E DIN 1052.

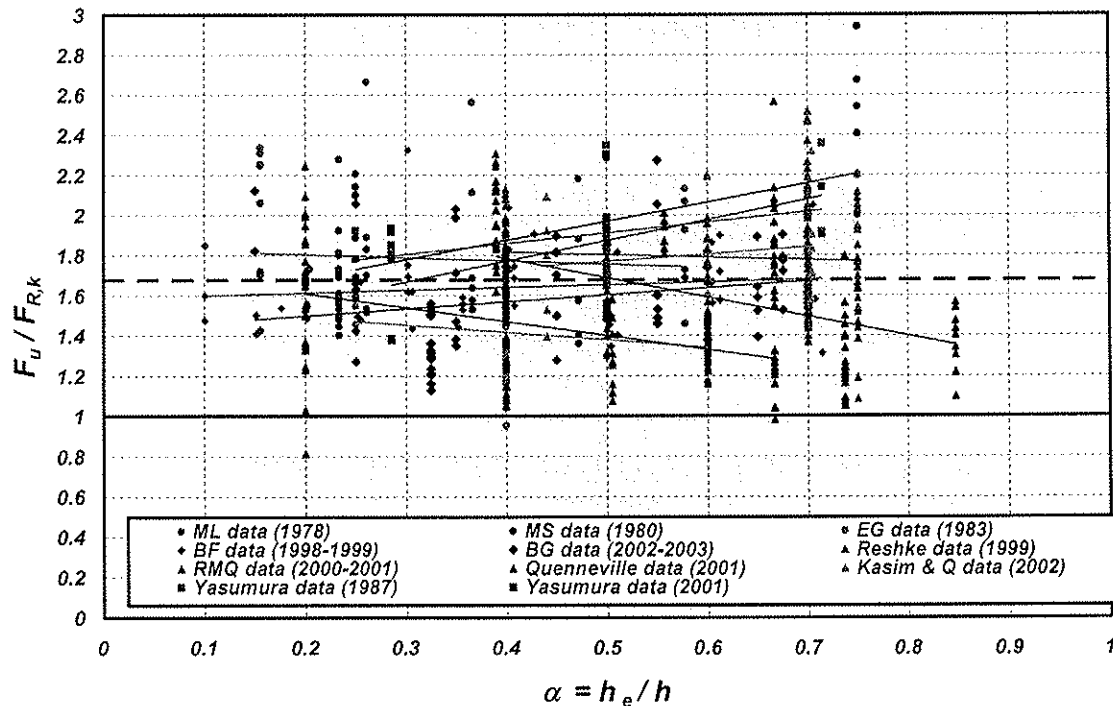


Fig. 17 – Values of $F_u / F_{90,Rk}$ versus α

As a result of the comparison the following drawings can be derived:

- the prediction formula of Van der Put is able to predict quite well the strengths of beams loaded by single-dowel connections but it is prevented to predict the ones of beams loaded by multiple-dowel connections since it doesn't take into account the effect of the joint geometry;
- the prediction formula embodied in the new E DIN 1052 (BEKS) is not very reliable in the prediction of the strength of beams with different heights, however it is able to predict well the strength of a large set of data and globally of the whole set of experimental data;
- the new prediction formula has the same prediction ability of the BEKS formula, it predicts better the strength of beams with single-dowel connections but it is less effective with respect to some experimental data set (particularly the EG data set and some tests of the MS data set).

Finally, since the new formula is very easy and it has a good level of prediction ability, a simple design proposal has been derived and compared with experimental data.

References

- [1] **Blass H.J., Bejtka I.** (2004): *Reinforcements perpendicular to grain using self-tapping screws*. Proceedings of 8th World Timber Engineering Conference, WCTE 2004, Lahti, Finland.
- [2] **prEN 1995-1-1** (2002): *Eurocode 5 - Design of timber structures. Part 1-1: General rules and rules for buildings*. CEN/TC 250/SC 5, N 195, Final Draft, 2002-10-09.
- [3] **E DIN 1052** (2002): *Entwurf, Berechnung und Bemessung von Holzbauwerken*. Schlussentwurf Bemessungsnorm Holzbau BEKS-2002, Ingenieurholzbau, Karlsruher Tage, Bruderverlag, Universität Karlsruhe, 13-7-2002.

- [4] **Van der Put T.A.C.M.**, 1990: *Tension perpendicular to the grain at notches and joints*. CIB-W18 Conference, paper 23-10-1, Lisbon, Portugal.
- [5] **Van der Put T.A.C.M.**, 1992: *Energy approach for fracture of joints loaded perpendicular to the grain*. COST 508, Workshop on fracture mechanics in wooden structures, Bordeaux, France.
- [6] **Leijten A.J.M.**, 2002: *Splitting strength of beams loaded by connection, model comparison*. CIB-W18 Conference, paper 35-7-7, Kyoto, Japan.
- [7] **Ehlbeck J., Görlacher R., Werner H.**, 1989: *Determination of perpendicular-to-grain tensile stresses in joints with dowel-type fasteners: a draft proposal for design rules*. CIB-W18 Conference, paper 22-7-2, Berlin, German Democratic Republic.
- [8] **Ballerini M.**, 1999: *A new set of experimental tests on beam loaded perpendicular-to-grain by dowel-type joints*. CIB-W18 Conference, paper 32-7-2, Graz, Austria.
- [9] **Ballerini M., Giovanella A.**, 2003: *Beams transversally loaded by dowel-type joints: influence on splitting strength of beam thickness and dowel size*. CIB-W18 Conference, paper 36-7-7, Estes Park, Colorado, USA.
- [10] **Ballerini M., Bezzi R.**, 2001: *Numerical LEM analyses for the evaluation of failure loads of beams loaded perpendicular-to-grain by single-dowel connections*. CIB-W18 Conference, paper 34-7-6, Venice, Italy.
- [11] **Yasumura M.**, 2001: *Criteria for damage and failure of dowel-type joints subjected to force perpendicular-to-grain*. CIB-W18 Conference, paper 34-7-9, Venice, Italy.
- [12] **Möhler K., Lautenschläger R.**, 1978: *Großflächige Queranschlüsse bei Brett-schichtholz*. Forschungsbericht des Lehrstuhls für Ingenieurholzbau und Baukon-struktionen, Universität Karlsruhe.
- [13] **Möhler K., Siebert W.**, 1980: *Ausbildung von Queranschlüssen bei angehängten Lasten an Brett-schichtholzträger*. Forschungsbericht des Lehrstuhls für Ingenieur-holzbau und Baukonstruktionen, Universität Karlsruhe.
- [14] **Ehlbeck J., Görlacher R.**, 1983: *Tragverhalten von Queranschlüssen mittels Stahl-blechformteilen, insbesondere Balkenschuhe, im Holzbau*. Forschungsbericht der Versuchsanstalt für Stahl, Holz und Steine, Abt. Ingenieurholzbau, Universität Karlsruhe.
- [15] **Reske R.G.**, 1999: *Bolted timber connections loaded perpendicular-to-grain: influ-ence of joint configuration parameters on strength*. M. Sc. Thesis. Dept. of Civil Engineering, Royal Military College of Canada, Kingston, Ontario, Canada.
- [16] **Reske R.G., Mohammad M., Quenneville J.H.P.**, 2000: *Influence of joint configu-ration parameters on strength of perpendicular-to-grain bolted timber connections*. Proceedings of 6th World Timber Engineering Conference, WCTE 2000, Whistler, B.C., Canada.
- [17] **Quenneville J.H.P., Mohammad M.**, 2001: *A proposed Canadian design approach for bolted connections loaded perpendicular-to-grain*. Proceedings of the International RILEM Symposium "Joints in Timber Structures", Stuttgart, Germany.
- [18] **Kasim M., Quenneville J.H.P.**, 2002: *Effect of row spacing on the capacity of bolted timber connections loaded perpendicular-to-grain*. CIB-W18 Conference, paper 35-7-6, Kyoto, Japan.
- [19] **Jensen J.L.**, 2003: *Splitting strength of beams loaded by connections*. CIB-W18 Conference, paper 36-7-8, Estes Park, Colorado, USA.
- [20] **Giovanella A.**, 2002: *Experimental investigation on the splitting strength of beams*

loaded perpendicular to grain by dowel-type connections (in Italian). Degree Thesis, University of Trento, Faculty of Engineering, 27-3-2002.

- [21] **Quenneville J.H.P.**, 2001: Personal communication.
- [22] **Yasumura M., Murota T., Sakai H.**, 1987: *Ultimate properties of bolted joints in glued-laminated timber*. CIB-W18 Conference, paper 20-7-3, Dublin, Ireland.

INTERNATIONAL COUNCIL FOR RESEARCH AND INNOVATION
IN BUILDING AND CONSTRUCTION

WORKING COMMISSION W18 - TIMBER STRUCTURES

PLUG SHEAR FAILURE: THE TENSILE FAILURE MODE
AND THE EFFECT OF SPACING

H Johnsson

Luleå University of Technology

SWEDEN

Presented by H Johnsson

A Jorissen commented that $B_{\text{effective}}$ value used in this paper should be referenced to thin steel plates therefore it was off by a factor 20.5. Johnsson agreed.

Plug Shear Failure: The Tensile Failure Mode and the Effect of Spacing

Ph.D. Helena Johnsson

Luleå University of Technology, Sweden

Abstract

Plug shear failure in nailed timber connections is a brittle failure mode, which limits the capacity for nailed joints loaded in tension parallel to the grain. The limiting strength parameter for plug shear failure is for most cases the shear strength of timber. However, for short joints a tensile failure mode is possible. The occurrence of plug shear failure is closely linked to the spacing between the nails and in particular to the spacing perpendicular to the grain.

Plug shear failure was studied in short-term experiments on nailed steel-to-timber joints. The occurrence of the tensile failure mode was shown as well as the effect of increased spacing, which increases the resistance and alters the course of failure. A prediction model is proposed for the tensile failure mode. A complete prediction model for plug shear failure in nailed joints is presented together with recommendations on nail spacing.

1 Introduction

When timber is stressed by a group of fasteners loaded in tension parallel to the grain it results in both tension and shear stresses parallel to the grain, Fig. 1, where the bottom and side faces of the plug are in shear. The resistance of the joint is the lowest value of the nail embedding and the plug shear resistance, which involves tensile, R_t , and shear, R_v , capacities. In Johnsson (2003) the earlier models of Kangas and Vesa (1998) and Foschi and Longworth (1975) were evaluated and a model was proposed for predicting the plug shear resistance based on experimental evidence, Eqn. 1.

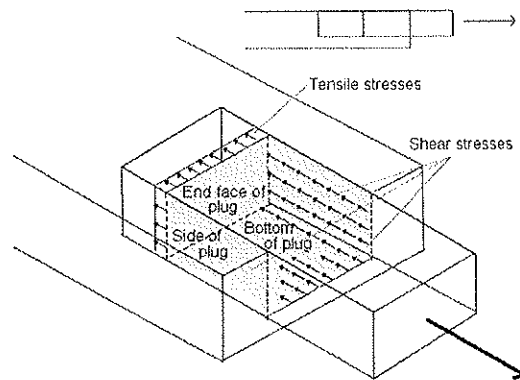


Figure 1: Schematic Plug Shear Failure

$$R_v = b \cdot l \cdot f_v \quad \text{where } f_v = K(b \cdot l)^{-0.25} \quad (1)$$

In Eqn. 1 b is the width of the plug, l is the length of the plug including the end distance and f_v is the shear strength of timber. The parameter K describes the volume effect of shear strength and was experimentally determined to $K = 64.5$. Eqn. 1 describes the resistance of

the shear failure mode of plug shear failure and in Johnsson (2004) the course of plug shear failure was described:

1. A crack develops internally along one side of the plug, Fig. 1. The failure is initiated at the nail farthest from the free end.
2. The crack reaches the free end and is visible on the edge. The same development goes for the other side of the plug. This occurs in two-thirds of the experiments before the ultimate load is reached.
3. The end face of the plug fails in tension.
4. The final failure occurs when a shear crack along the bottom face of the plug joins the two side cracks.

For short (in the direction parallel to the grain) joints, a tensile failure mode should be possible. In short joints, the area loaded in shear is small and the capacity according to Eqn. 1 is lower than the tensile capacity of the end face of the plug. The first aim with this paper is to investigate the occurrence of the tensile failure mode in nailed timber joints.

The second aim with this paper is to study the effect of spacing on the occurrence of plug shear failure. This study is limited to comparing cases where spacing is either $7d/3.5d$ or $10d/5d$, where d is the diameter of the nail. In the expression $7d/3.5d$, $7d$ is the spacing parallel to the grain and $3.5d$ is the spacing perpendicular to the grain.

2 Experimental methods

Full size joints in glulam (*Picea Abies*) were tested in tension parallel to grain, Table 1. The timber member cross section was $90 \times 225 \text{ mm}^2$ from glulam of strength class GL32, Eurocode 5 (1998). The timber member length varied between 650 and 850 mm. In the RECTX series the thickness of the member, H , varied between 66 mm (RECTX1 series), 78 mm (RECTX2 series) and 90 mm (RECTX0 series).

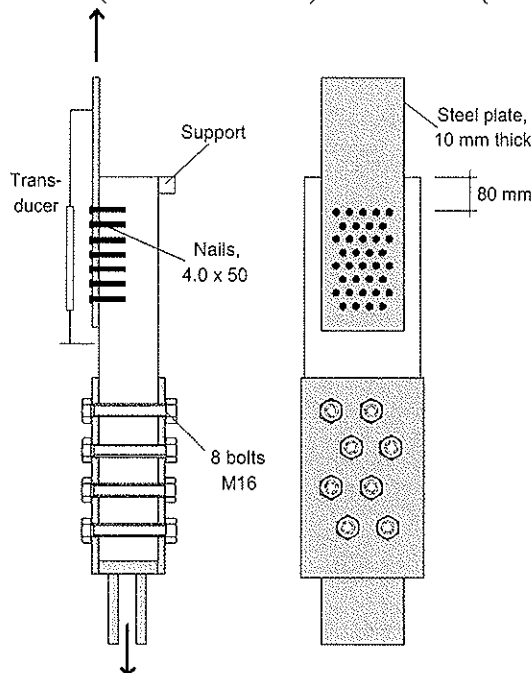


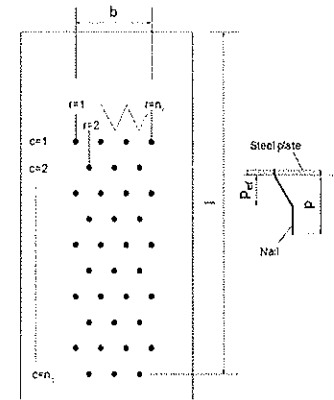
Figure 2: Experimental set-up

One joint consisted of one steel plate 5 or 10 mm thick with a yield strength, $f_y = 355$ MPa, annular ringed shank nails with diameter, $d = 4.0$ mm, and nail penetration depth, $p = 40$ mm. Nail holes were pre-drilled. The investigation comprised 9 series with a grand total of 45 specimens. The nail patterns varied between the different series, Table 1. The basic nail pattern is designed with distances between nails parallel to grain of $10d$ and perpendicular to grain of $5d$ ($10d/5d$). A reduction of the distances with a factor 0.7 was also tested ($7d/3.5d$). The specimens were conditioned to a temperature of 20°C and a relative humidity of 65 % according to ISO 6891 (1983). The tests were conducted with a time to failure between 8 and 15 minutes using a servo hydraulic testing machine with a maximum load of 600 kN and a maximum error of 1 % over the entire measuring range.

During the tests, displacements were measured by displacement transducers (LVDT, 0 - 50 mm, Vishay) placed centrally in the joint region. Data was sampled with a frequency of 2 Hz. The density and moisture content of the wood were determined according to ISO 3131 (1975) and ISO 3130 (1975) respectively. Measurements were made on two samples taken in the inner lamellas of the joints. The size of the samples was $40 \times 40 \times 40 \text{ mm}^3$.

Table 1: Specimen characteristics

Series	No.	n_c	n_r	No. of nails	Nail pattern	b/b_{ef} [mm]	l [mm]
RECTS	5	14	9	59	7d/3.5d	56/40	248
RECTL	5	15	19	143	7d/3.5d	126/90	276
RECTX	15	29	19	276	7d/3.5d	126/90	452
NORMS	3	10	7	35	10d/5d	64/48	240
NORML	3	11	13	72	10d/5d	124/96	260
NORMX	3	21	15	157	10d/5d	136/108	460
SPREAD	5	15	19	143	10d/3.5d	126/90	336
TENSS	3	3	13	21	7d/3.5d	88/60	88
TENSL	3	4	33	66	7d/3.5d	228/164	102



In Table 1 specimen characteristics are presented where n_c denotes the number of columns of nails in the direction perpendicular to grain and n_r is the number of rows in the direction parallel to grain. The width b/b_{ef} , includes/excludes the nail diameters and the length, l , includes the end distance. The end distance was 60-80 mm for all test series. The effective penetration depth, p_{ef} , is calculated as the distance between the plastic hinges for mode III according to Johansen (1949), following a concept presented by Kangas and Väänänen (1996) and can be evaluated as $p_{ef} = \sqrt{(2M_y)/(f_h d)} = 16\text{-}17 \text{ mm}$ for these specimens.

3 Results

Table 2: Experimental results

Series	Ultimate load, R [kN]	Ult. displacement, u_u [mm]	Density, ρ [kg/m^3]	Moisture content, w [%]
RECTS	76.2, 84.5, 92.1, 94.1, 94.9	1.7, 1.4, 1.5, 1.8, 1.5	473, 392, 425, -, 413	11.2, 11.0, 10.3, -, 10.6
RECTL	150, 158, 162, 167, 171	1.2, 1.2, 1.8, 1.7, 1.3	467, 450, 415, 488, 431	11.1, 10.7, 10.5, 10.7, 11.3
RECTX0	224, 233, 252, 262, 281	2.9, 2.2, 1.8, 2.3, 2.4	441, 431, 456, 420, 455	10.0, 9.30, 10.0, 9.44, 10.1
RECTX1	169, 184, 203, 222, 224	2.2, 2.6, 2.0, 3.0, 2.1	418, 382, 448, 454, 366	10.3, 10.2, 10.8, 10.7, 10.1
RECTX2	214, 231, 248, 285, 306	1.9, 1.5, 1.8, 2.2, 1.9	436, 476, 457, 471, 432	10.2, 10.5, 10.4, 10.6, 10.3
NORMS	92.6, 102, 95.5	6.2, 8.8, 7.8	400, 472, 479	10.3, 10.0, 9.90
NORML	175, 190, 168	5.3, 3.8, 3.0	462, 445, 479	10.3, 11.2, 9.58
NORMX	276, 297, 305	2.8, 3.5, 3.9	414, 444, 487	9.10, 9.53, 10.56
SPREAD	245, 246, 250, 261, 264	2.7, 3.0, 2.2, 2.6, 2.2	490, 455, 489, 446, 473	10.2, 9.86, 11.1, 9.69, 9.33
TENSS	61.4, 57.5, 58.1	7.6, 7.4, 8.3	484, 418, 399	10.5, 9.47, 10.1
TENSL	153, 130, 126	4.0, 5.0, 2.4	446, 460, 457	10.2, 10.6, 10.7

The ultimate displacement in Table 2 is the displacement at the ultimate load. In Table 2, the RECTS, -L and -X series are designed to have the same outer measurements of the nail layout as the NORMS, -L and -X series, i.e. the nail group has the same width b and length l , but with denser spacing. During the tests observations were made of the failure mode of the specimens, which is summarised as follows:

- RECTS and RECTL series failed in plug shear failure. A bottom shear face formed in both cases.
- The RECTX0 series failed in plug shear failure with a bottom shear face.
- A type of tensile failure was observed for the RECTX1 and RECTX2 series where the thickness of the specimen was 66 and 78 mm respectively. For these joints the side shear crack protruded right through the timber thickness as shown in Fig. 3a. Tensile failure of the end face of the plug was observed.
- For the NORMS series, one specimen failed in a ductile failure mode and two in plug shear failure with a bottom shear face.
- In the NORML series with spacing $10d/5d$ a small plug formed and the remaining nails failed in a ductile manner, which is shown in Fig. 3b.
- In the NORMX series the plug was divided in several smaller plugs forming sequentially during loading.
- The SPREAD series failed in plug shear failure with a bottom shear face.
- In the TENSS series two specimens failed in a ductile manner while in one specimen a small plug was formed and the remaining nails failed ductile.
- In the TENSL series, many smaller plugs formed sequentially during loading, the first one being placed centrally in the joint region, Fig. 4b. The course of failure did not follow the general description in section 1, since neither side shear cracks formed, nor bottom shear cracks, indicating that the failure mode has shifted from shear failure of the bottom shear face to tensile failure of the end face of the plug.

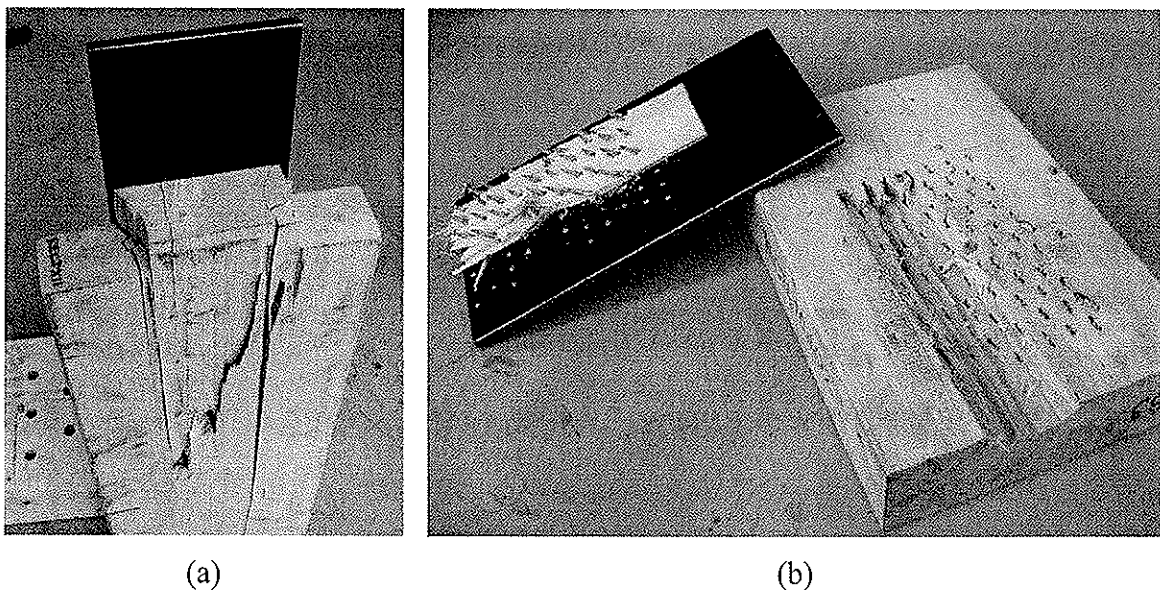


Figure 3: a) RECTX11 specimen b) NORML02 specimen

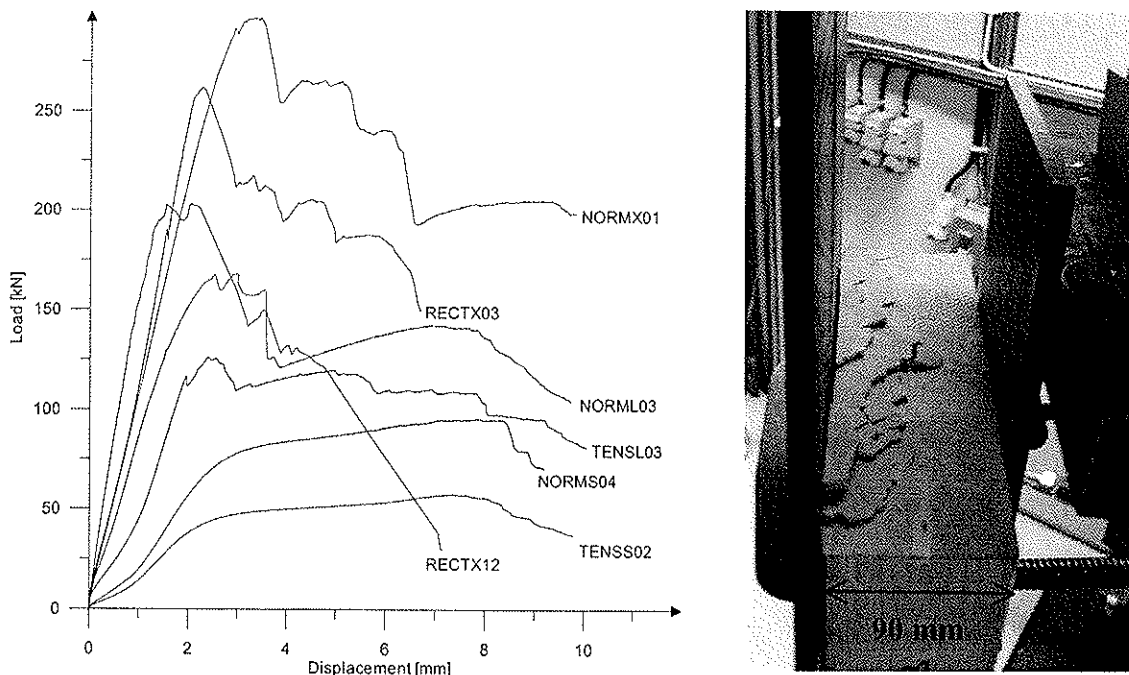


Figure 4: a) Typical load-displacement curves from experiments b) TENSLO1 specimen

Observations from the experiments point to the fact that with smaller spacing perpendicular to the grain, the nails will interact stronger and an integrate plug is formed, while an increase of the cross-grain spacing (the NORM- series) triggers a more ductile behaviour and the formation of many smaller plugs. Typical load-displacements curves are shown in Fig. 4a.

4 Analysis

4.1 Tensile failure mode

It is clear from the experimental observations that a tensile failure mode of plug shear failure is possible and that it occurs for short and wide joints. The tensile failure mode is not included in the prediction model presented in Eqn. 1, which only deals with the shear resistance of the bottom face of the plug. The tensile resistance of the end face can be stated in several hypotheses, Eqn. 2.

$$R_t = \text{either} \begin{cases} b \cdot p \cdot f_t & \text{(a)} \\ b_{ef} \cdot p \cdot f_t & \text{(b)} \\ b \cdot p_{ef} \cdot f_t & \text{(c)} \\ b_{ef} \cdot p_{ef} \cdot f_t & \text{(d)} \\ b \cdot H \cdot f_t & \text{(e)} \end{cases} \quad (2)$$

where b is the width of the connection, b_{ef} is the width of the connection reduced by the nail diameters, H is the thickness of the timber member and f_t is the tensile strength of wood. The penetration depth, p , and the effective penetration depth, p_{ef} , are defined in Table 1.

To estimate the different proposals for a prediction formula in Eqn. 2 an estimate of the tensile strength parallel to grain is needed. Johansson (1998) tested the tensile strength of glulam laminations of Nordic origin (*Picea Abies*). The results showed $f_t = 37.7$ MPa in the outer laminations and $f_t = 28.4$ MPa in the inner. All joints reported in Table 1 are mounted in the inner laminations. When the laminations are assembled to a glulam beam, the apparent tensile strength increases, Colling and Falk (1993), due to a lamination effect. In their study, Colling and Falk (1993) separates the different constituents of the lamination effect, λ , into; i) the effect of test procedure, ii) the reinforcements of defects and iii) the dispersion of low-strength lumber, Eqn. 3.

$$\lambda = \frac{f_{m,beam}}{f_{t,lam}} = k_{test} \cdot k_{reinf} \cdot k_{disp} \Rightarrow f_t = f_{t,lam} \cdot k_{test} \cdot k_{reinf} = 28.4 \cdot 1.2 \cdot 1.2 = 40.9 \text{ MPa} \quad (3)$$

Tensile failure in the outmost lamination is most often governing in bending failures and therefore $\lambda = f_t / f_{t,lam}$ is tentatively valid. Guidelines for selecting the factors k_{test} , k_{disp} and k_{reinf} are presented in Colling and Falk (1993). The dispersion effect is dependent on the amount of laminations in the beam, $k_{disp} > 1.0$, while the volume effect is also related to the size of the loaded area, but will decrease the apparent strength as the size increases. These two phenomena counteract one another and will tentatively be of the same magnitude. Therefore, they are both ignored at this stage, but in future studies, where larger joints are tested, this could be an area of interest to consider. In Fig. 5 the different hypotheses in Eqn. 2 are compared to the test results failing in the tensile failure mode reported in Table 2.

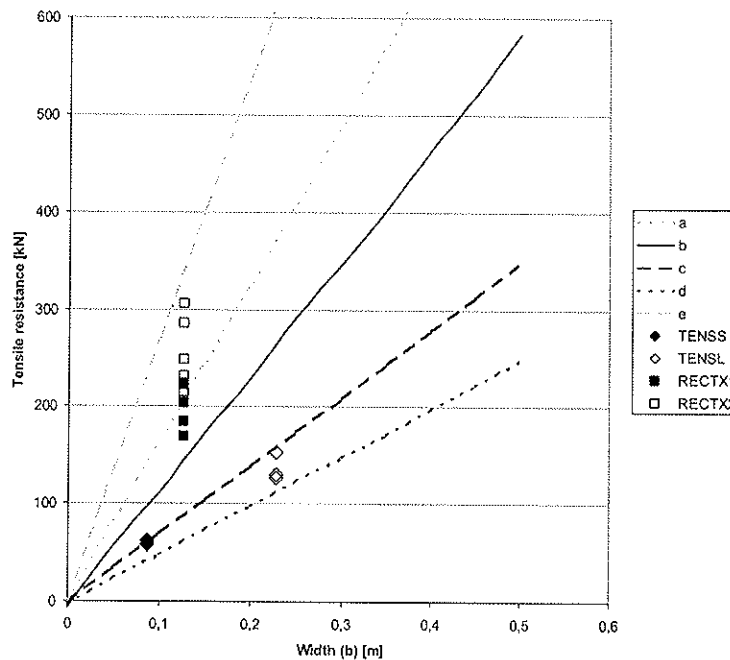


Figure 5: Comparison between Eqn. 2 and test results

In the TENS- series, where no side shear cracks form, the resistance is best predicted by either hypotheses *c* or *d*. It seems as though the effective penetration depth, p_{ef} , can be used as a depth measure for the tensile failure mode. In Fig. 4b, the depth of the plugs varies between 15-45 mm, where the plugs forming initially are smallest with a depth close to the effective penetration depth ($p_{ef} = 17$ mm). Furthermore, hypothesis *d* points to the fact that it is sound to reduce the cross section with the width of the nail holes. However, current test results are not so many as to be able to differ between the hypotheses *c* and *d* with any

statistical certainty, so until further studies have been made, a proposal for the tensile resistance of plug shear failure is:

$$R_t = b_{ef} \cdot p_{ef} \cdot f_t \quad (4)$$

The tensile resistance of the RECTX series is much higher than predicted by Eqn. 4. The many small plugs in Fig. 4b did not form, instead an integrate plug was pulled away from the specimen, with almost the entire cross-sectional depth contributing to the tensile area of the end face, Fig. 3a. The test results from the RECTX1 and RECTX2 series should logically fall in the region between hypotheses *a* and *e*, which they do according to Fig. 5. Comparing the RECTX0 -1 and -2 series, a limit for the occurrence of the tensile failure mode with respect to timber thickness is found. When the ratio p/H (penetration depth/timber thickness) is larger than 0.5 a tensile failure mode will occur. This is concluded through comparing the RECTX0 and RECTX1 series where p/H increases from 0.44 to 0.51 and the failure mode changes from shear failure of the bottom face of the plug to tensile failure of the end face of the plug.

4.2 Influence of fastener spacing

In several of the experiments, the fastener spacing has been chosen as $7d/3.5d$. Presumably, joints with larger nail spacing are less prone to fail in plug shear failure since stress concentrations are smaller than in closer spaced joints. Joints with the same area $b \cdot l$ as the RECT- series, but with different spacing were studied in the NORMS, NORML and NORMX series. The average resistance increased between 9-17% compared to the RECT-series, Table 3. The failure mode was still plug shear failure, but small, separate plugs formed instead of one integrate.

Table 3: Comparison between joints with different spacing (average values given)

Series	Ult.load [kN]	Series	Ult.load [kN]	Increase [%]	Note
RECTS	88.4	NORMS	96.7	9.4	On the limit to ductile
RECTL	162	NORML	178	10	Small plug, then ductile
RECTX	250	NORMX	293	17	Many smaller plugs

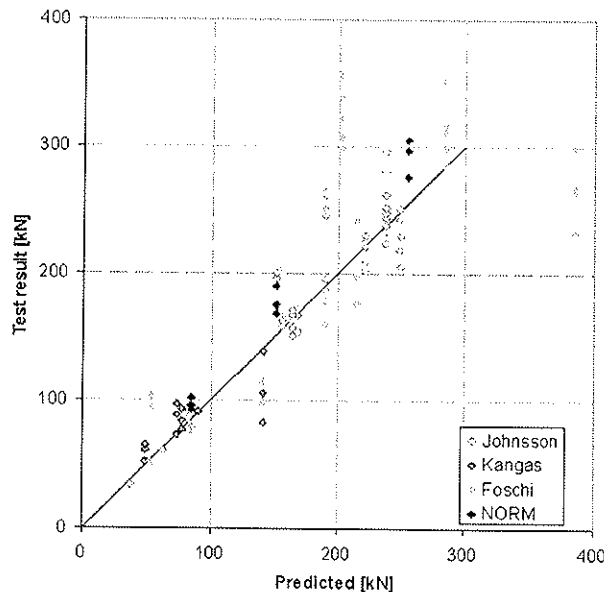


Figure 6: Test results versus predicted resistance.

In Fig. 6, the NORM- series are shown in a Test-Predicted plot, where the model in Eqn. 1 is plotted against test results from Johnsson (2003), Kangas et al. (1997) and Foschi and Longworth (1975). Fig. 6 shows that the resistance is indeed higher for the NORM- series. However, the difference is not larger than the scatter already existing between the different test series. The model $R_v = b/f_v$ will give results on the safe side. The suggestion is that the model in Eqn. 1 is left unchanged, as far as nail spacing within the studied domain is concerned.

5 Discussion

Having established Eqn. 1 for the shear failure mode and tentatively Eqn. 4 for the tensile failure mode of plug shear failure it is necessary to determine the limit length for the tensile failure mode to occur. This can be accomplished through equalling Eqns. 1 and 4 after inserting the constant ratio $b_{ef}/b = 5/7$ in Eqn. 4 and $f_v = K(b \cdot l)^{-0.25}$ in Eqn. 1.

$$R_v = K(b \cdot l)^{0.75} \text{ and } R_t = \frac{5}{7} b \cdot p_{ef} \cdot f_t \Rightarrow l_{lim} = \left(\frac{5}{7} \frac{b^{0.25} p_{ef} \cdot f_t}{K} \right)^{4/3} \quad (5)$$

If using hypothesis c, Eqn. 5 will have the same expression except for the factor 5/7. Two plots of the limit length depending on the width of the connection are shown in Fig. 7, corresponding to hypotheses c and d. All joints with a length that falls below the line will be prone to failing in the tensile failure mode.

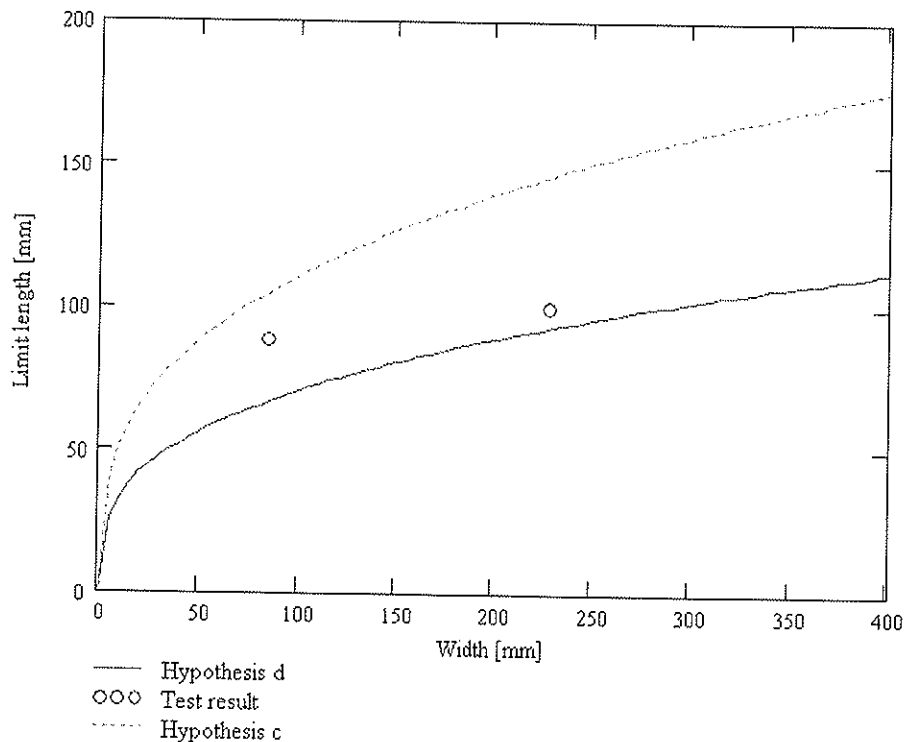


Figure 7: Limit length between tensile and shear failure mode, Eqn. 5.

From Fig. 7 it is evident that the limit length is quite small – it also includes the end distance, which according to Eurocode 5 (1998) can be taken as $15d = 60$ mm for the current nail type. The tensile failure mode will therefore seldom occur in any applications. The TENS- series are shown in the graph as circles. Both test series showed failures in the tensile failure mode, although they do not fall below the line in Fig. 7. This could be due to

the natural variations in timber properties or the difference between the estimated tensile strength f_t and the real tensile strength in the specimen.

The result from the NORM- series points to the fact that the nails interact less when the spacing is larger. The same tendency was found in the investigation by Quenneville and Mohammad (2000), where it is stated that decreasing the distance from $5d$ to $3d$ between parallel rows changes the failure mode from row shear-out to group tear-out. Comparing test series RECTX and SPREAD, these experiments showed similar behaviour with one single plug withdrawn from the timber member, although the SPREAD series had larger spacing parallel to the grain. An efficient way of reducing the risk for plug shear failure and still keep the joint small, would be to allow the spacing parallel to grain to be $7d$, but keep the limit on the perpendicular to grain spacing at $5d$. To obtain joints with higher ductility and safety and to decrease the risk for plug shear failure it is recommended that the reduction by multiplying the spacing with 0.7 for steel-to-timber joints in Eurocode 5 (1998) be not used. Note that for loading in other directions than in tension parallel to the grain, the reduction might still be appropriate.

A prediction model for plug shear failure, differing between a shear failure mode and a tensile failure mode would be formulated as:

$$\begin{aligned} \text{If } p/H < 0.5: \quad R_{\text{plug}} &= \max \begin{cases} R_v = b \cdot l \cdot f_v \text{ where } f_v = K \cdot (b \cdot l)^{-0.25} \\ R_t = b_{\text{ef}} \cdot p_{\text{ef}} \cdot f_t \end{cases} \\ \text{If } p/H \geq 0.5: \quad R_{\text{plug}} &= R_t = b_{\text{ef}} \cdot p_{\text{ef}} \cdot f_t \end{aligned} \quad (6)$$

The model in Eqn. 6 will give results on the safe side for joints in thin timber members experiencing a tensile failure mode. The model will also give results well on the safe side for joints where the spacing is taken as $10d/5d$. The result in Eqn. 6 is similar to the approach presented by Biger et al. (2000) and Mohammad and Quenneville (1999), who both performed research on bolted joints and also separated between a shear and a tensile failure mode.

6 References

ISO 6891 (1983). *Timber Structures - Joints made with mechanical fasteners - General principles and determination of strength and deformation characteristics.*

Eurocode 5 (1998). *Eurocode 5 - Design of Timber Structures.* ENV 1995-1-1:1993.

Biger, J.P., Bocquet, J.F. and Racher, P. (2000). Testing and Designing the Joints for the Pavilion of Utopia. *World Conference on Timber Engineering*, paper 4.3.3, Whistler, Canada, 2000.

Colling, F. and Falk, R.H. (1993). Investigation of Laminating Effects in Glued Laminated Timber. *International Council for Research and Innovation in Building and Construction, Working Commission CIB-W18*, paper 26-12-3, Athens, Georgia, U.S.A.

Foschi, R.O. and Longworth, J. (1975). *Analysis and Design of Grippam Nailed Connections.* Journal of the Structural Division 101(12): 2537-2555.

Johansen, K.W. (1949). *Theory of Timber Connections*. International Association of Bridge and Structural Engineering 9: 249-262.

Johansson, C.-J. (1998). *Laminations for Glued Laminated Timber: Establishment of Strength Classes for Visual Strength Grades and Machine Settings for Glulam Laminations of Nordic Origin*. SP Report 1998:38, SP, Borås, Sweden.

Johnsson, H. (2003). Plug Shear Failure in Nailed Timber Connections: Experimental Studies. *International Council for Research and Innovation in Building and Construction, Working Commission CIB-W18*, 36-7-2, Estes Park, Colorado, USA

Johnsson, H. (2004). *Plug Shear Failure in Nailed Timber Connections - Avoiding Brittle and Promoting Ductile Failures*. Doctoral, Div. of Timber Structures, Luleå University of Technology, 2004:03.

Kangas, J., Aalto, K. and Kevarinmäki, A. (1997). Modelling of the Block Tearing Failure in Nailed Steel-to-Timber Joints. *International Council for Research and Innovation in Building and Construction, Working Commission CIB-W18*, paper 30-7-2, Vancouver, British Columbia, Canada

Kangas, J. and Vesa, J. (1998). Design on Timber Capacity in Nailed Steel-to-Timber Joints. *International Council for Research and Innovation in Building and Construction, Working Commission CIB-W18*, paper 31-7-4, Savonlinna, Finland

Kangas, J. and Väänänen, H. (1996). The Capacity of Multiple-Nail-Connector/Kerto-LVL Joints. *International Wood Engineering Conference*, New Orleans, USA

Mohammad, M. and Quenneville, J.H.P. (1999). Behaviour of Wood-Steel-Wood Bolted Glulam Connections. *International Council for Research and Innovation in Building and Construction, Working Commission CIB-W18*, paper 32-7-1, Graz, Austria, August 1999.

Quenneville, J.H.P. and Mohammad, M. (2000). *On the Failure Modes and Strength of Steel-Wood-Steel Bolted Timber Connections Loaded Parallel to Grain*. Canadian Journal of Civil Engineering 27(4): 761-773.

INTERNATIONAL COUNCIL FOR RESEARCH AND INNOVATION
IN BUILDING AND CONSTRUCTION

WORKING COMMISSION W18 - TIMBER STRUCTURES

BLOCK SHEAR FAILURE TEST WITH DOWEL-TYPE CONNECTION IN
DIAGONAL LVL STRUCTURE

M Kairi

Laboratory of Wood Technology
Helsinki University of Technology

FINLAND

Presented by M Kairi

C Clorius questioned why the connections were not loaded to 15 mm per code requirements. Kairi responded that they failed already.

H J Larsen asked why failure mode of 3-in-line was more brittle than the 4-in-line. Kairi clarified that they had the same brittle failure mode.

A Kermani asked whether the quality of the inner laminate of worst quality compared to the face. Kairi responded that in the prototype the quality of the face and core veneer were similar.

A Jorissen received clarifications of the number of fasteners in line and the embedment strength of the LVL would be available in a previous 2001 CIB paper. Kairi also clarified the difference between block and plug shear.

Block shear failure test with dowel-type connection in diagonal LVL structure

Matti Kairi
Laboratory of Wood Technology
Helsinki University of Technology (HUT)
Finland

1. Introduction

The low transverse tensile strength of wood in contrast to the tensile strength in grain direction is a common problem in dowel-type connections. Several alternative solutions have been presented, mainly based on the strengthening of the connection area with special plywood (Werner 1993 and 1995, 9; Leitjen and Rodd 1998), fibre reinforcement and densified timber (Haller (2001) or nail plates (Kevarinmäki 1998). According to Kairi (2001) the transverse tensile strength of the basic material could be strengthened already in the production stage of the Laminated Veneer Lumber (LVL) by bedding the veneers diagonally.

Two new versions, LVL-DA and LVL-DB, has been developed to diagonal LVL. Their bending and tensile capacity as beam system are essentially higher than those of previously presented diagonal LVL (Kairi 2001).

The failure modes of wood with dowel-type connection, when wood is loaded with tensile force, are presented in Figure 1. The failure mode is dependent on (prEN 1995-1-1 2002, 72-80):

- edge and end distances of the dowels
- the slenderness of the dowels in relation to the thickness of wood
- the number of the dowel next to each other and in a row and also on distances between them

- Embedment failure (plastic displacement $> 0,02 \cdot d$)
- Splitting failure in grain direction
- Plug shear failure
- Block shear failure
- Tension failure

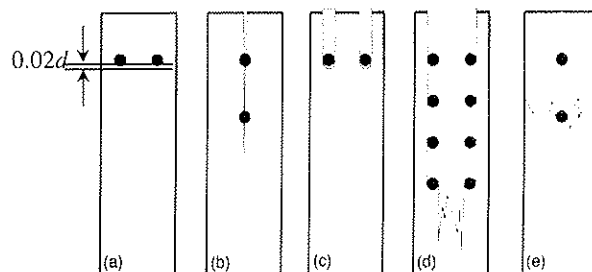


Figure 1. Failure modes in wood for connection with dowel-type fasteners according Fahlbusch (1949).

The primary aim is to avoid the occurrence of block shear failure (Ranta-Maunus and Kevarinmäki 2003), which is considered critical by using the new LVL structure. In this study the failure mode of a jointing area consisting unbending bolts is analysed with two different LVL –structure. The results are compared with LVL standard structure.

Because solid wood and also standard LVL are brittle materials, the joint will behave brittle as well. The only way in this situation is to provide ductility with mechanical fasteners forming plastic hinges. The connections are design on terms of wood so that the slenderness and the number of the dowels are optimised. The aim is to reach the yield point of the steel

before failure of wood. Analysing the ductility of the joint Gehri (1996) has developed a concept for ratio of ductility D_s , figure 2. It is a ratio between the plastic and elastic displacement. Mischler (2000) recommend for a good connection the ratio of $D_s > 3$:

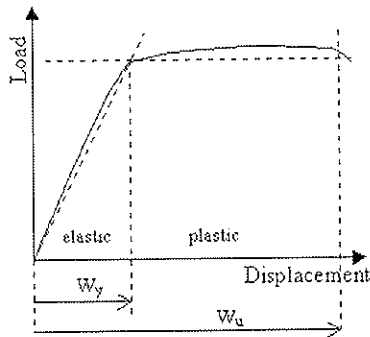


Figure 2. Principal drawing of ductility ratio according Gehri (1996).

$$D_s = W_u / W_y \quad (1)$$

where: D_s is ductility ratio
 W_y is elastic displacement
 W_u is elastic+plastic displacement

The other aim of the study is to achieve a stiff dowel –type connection by using stiff pins in a way that the connection acts according to the principal presented by Gerhi

2 New Diagonal LVL Structure

For the bending and connection tests 3 different panel structures were glued in the Laboratory of Wood Technology (Helsinki University of Technology, HUT). The size of the panels was $850 \times 850 \text{ mm}^2$, and the thickness was 39mm.

1. LVL standard; all the veneers were 3mm thick spruce veneers; reference pieces
2. LVL-DA
3. LVL-DB

After the conditioning the panels the specimens were sawn up. Then the specimens were conditioned over 4 weeks in RH 65% and 20 °C before tests.

3 Testing arrangements and results

3.1 Bending tests

2 specimens from both sides of the panel (together 4 specimens /panel) were tested on the edge according to following experimental arrangement.

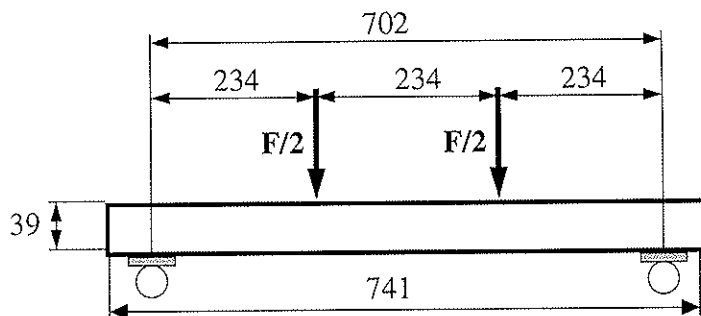


Figure 3. The loading arrangement in bending test according to EN 408.

The test results show that while using diagonal veneers the bending stiffness on the edge decreases 6-8% but at the same time the standard deviation decreases. With such small test series the decrease of the standard deviation can not be explained. However the final result is

that the bending strength and the modulus of elasticity do not essentially change while moving over from LVL standard to LVL-DA and LVL-DB structures.

Table 1. Modulus of rupture (MOR) and Modulus of elasticity (MOE) on the edge with three different LVL structure.

LVL	Number n	MOR \bar{x} N/mm ²	MOR stdev N/mm ²	MOR COV %	MOR f_{bk} N/mm ²	MOE \bar{x} N/mm ²	MOE stdev N/mm ²	MOE COV %
Spruce	19	68,6	6,6	9,6	58,1	10 650	482	4,5
LVL-DA	19	63,4	2,7	4,3	59,1	10 601	555	5,2
LVL-DB	16	64,6	3,8	5,9	58,5	10 494	381	3,6

3.1 Test with dowel-type connection

The tests were done according to EN 26891 in the Laboratory of Structural Engineering and Building Physics (HUT). Testing arrangements are presented in figure 4. M10 8,8 bolts were used in the test, the actual measured thickness of the bolts were 9,7 mm. CNC technique was used for the drillings of the specimens and the steel plates. The wood was drilled with a high speed steel cutter \varnothing 9,7 mm in diameter and the steel plate with \varnothing 10,0 mm cutter. The bolts were so tight that they had to be hammered into the drill holes in wood. The distances between the bolts and the distribution of the bolts are presented in figure 4. The aim was to bring out all the failure modes. Therefore the number of bolts in a row was the variable. Cases with $n = 3, 4$ and 5 samples were tested.

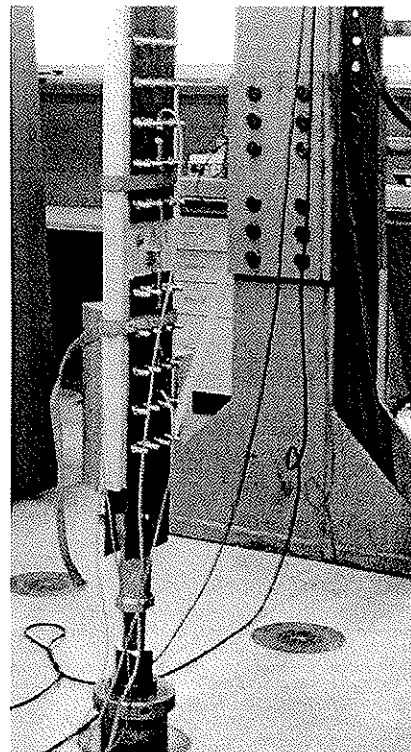
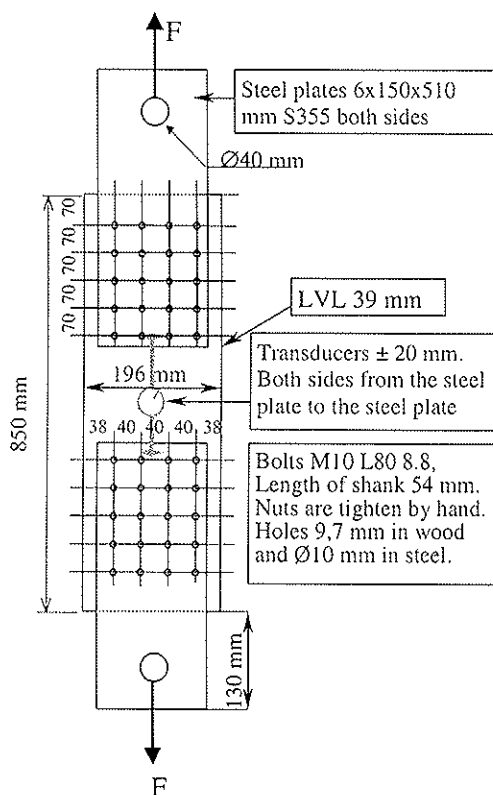


Figure 4. Test set-up in tension parallel to the grain direction of the face veneer..

The expected values can be calculated using the formulas (8.13 case 1) and (8.33) in prEN 1995-1-1 (2002, 67-78):

$$R_k = 0,5 f_{h,2,k} t_2 d \quad (2)$$

where: R_k is the characteristic design value of the bolt/shear plane
 $f_{h,2,k}$ is the characteristic embedment strength of the wood
 t_2 is the timber thickness
 d is the fastener diameter

$$n_{ef} = n^{0,9} \sqrt[4]{a_1 / 13d} \quad (3)$$

where: n_{ef} is effective number of bolts parallel to the grain direction
 n is number of bolts parallel to the grain direction
 a_1 is the spacing distance in the grain direction

The calculated values are given in next table:

Table 2. Calculated failure load of tested connections.

Number of bolts mxn	$R_{k, total}$ kN	Test result with LVL standard \bar{x} kN
4x5	216	243
4x4	177	215
4x3	136	158

The test results are on the safe side compared with the calculated values. This was also expected, because the preparing of test samples in laboratory conditions is accurate. There is almost no initial displacement in the curves, figures 5 and 6.

All results are presented in the following table. In the calculations of tensile strength the part of the holes has been deducted from the cross-section of wood. Thereafter the typical transition curves have been collected as functions of the structures and the numbers of bolts.

Table 3. Summary of the tension test with three different LVL structure using 4x5, 4x4 and 4x3 bolts with ϕ 10 mm diameter.

Number of bolts $m \times n$	LVL stand. Failure mode test piece	F_{max} kN	b mm	l mm	Failure of wood N/mm^2	LVL-DA Failure mode test piece	F_{max} kN	b mm	l mm	Failure of wood N/mm^2	LVL-DB Failure mode test piece	F_{max} kN	b mm	l mm	Failure of wood N/mm^2
4x5	B/P 2.2	268,32	38,4	196,3	44,71	T 6.1	276,40	38,5	196,0	46,02	T 11.1	296,93	38,2	195,5	49,99
4x5	B/S 3.3	246,00	39,3	194,4	40,54	T 7.2	276,95	38,5	196,4	45,99	T 12.2	290,36	38,3	196,2	48,54
4x5	B/S 4.2	220,73	38,9	196,1	36,35	T 8.3	248,34	39,2	194,8	40,93	T 13.3	321,30	38,3	185,0	57,86
4x5	B/P 14.1	238,39	38,9	196,1	39,26	T 9.1	285,00	39,0	196,4	46,72	T 15.2	288,12	38,0	196,1	48,57
4x5						T 10.2	255,26	38,1	196,4	42,84					
	mean	243			40,2	mean	268			44,5	mean	299			51,2
	stdev	19,7			3,5	stdev	15,7			2,5	stdev	15,2			4,5
	COV (%)	8,1			8,6	COV (%)	5,9			5,6	COV (%)	5,1			8,7
4x4	B/P 1.2	202,76	38,6	195,9	33,69	T 6.2	268,99	38,2	196,3	45,05	E/T 11.2	312,18	37,9	196,0	52,80
4x4	B/S 2.3	225,08	38,8	178,0	42,04	T 7.3	286,81	38,5	193,5	48,53	E/T 13.1	289,75	38,0	196,1	48,85
4x4	B/P 3.1	222,80	38,8	196,2	36,76	T 8.1	281,82	38,6	197,0	46,50	E/T 15.3	289,75	37,8	190,7	50,86
4x4	B/P 4.3	232,81	38,9	191,9	39,40	T 9.2	281,08	38,2	196,4	47,05					
4x4	B/P 14.2	193,10	38,5	192,2	32,95	T 10.3	249,65	38,2	190,9	43,31					
	mean	215			37,0	mean	274			46,1	mean	297			50,8
	stdev	16,6			3,8	stdev	14,9			2,0	stdev	12,9			2,0
	COV (%)	7,7			10,3	COV (%)	5,5			4,3	COV (%)	4,4			3,9
4x3	B 1.3	146,01	38,8	190,9	24,94	E/P 6.3	213,60	38,2	194,8	36,12	E/B 11.3	211,06	38,7	196,2	34,92
4x3	B 2.1	166,85	38,6	195,8	27,74	E/P 7.1	213,17	38,5	196,2	35,45	E/T 12.1	211,33	38,4	196,0	35,28
4x3	B 3.2	143,79	39,1	196,2	23,54	E/T 8.2	209,36	38,6	197,1	34,52	E/P 13.2	206,03	38,0	196,0	34,76
4x3	B 4.1	159,64	38,8	195,8	26,41	E/T 9.3	220,75	38,1	198,4	36,58	E/P 15.1	207,98	37,9	195,8	35,22
4x3	B 14.3	173,77	38,5	188,1	30,48	E/T 10.1	206,75	38,7	196,2	34,20					
	mean	158			26,6	mean	213			35,4	mean	209			35,0
	stdev	13,0			2,7	stdev	5,3			1,0	stdev	3,0			0,2
	COV (%)	8,2			10,0	COV (%)	2,5			2,9	COV (%)	1,4			0,7

Failure modes are given in each case:

E = Embedment failure (plastic displacement > 0,02-d)

S = Splitting failure in grain direction

P = Plug shear failure

B = Block shear failure

T = Tension failure

The moisture content of LVL

\bar{x} =

stdev =

COV =

8,7 %

0,56 %

6,4 %

Figure 5. LVL standard; 4x5 bolts

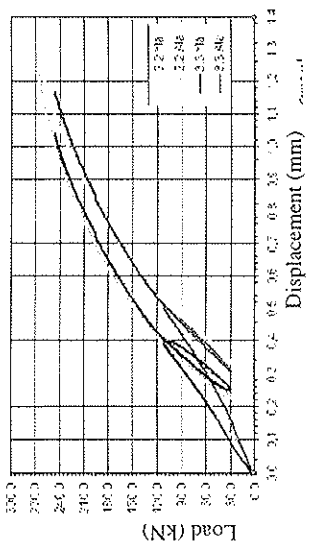


Figure 6. LVL standard; 4x4 bolts

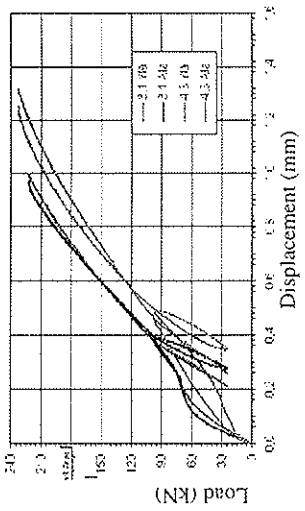


Figure 7. LVL standard; 4x3 bolts

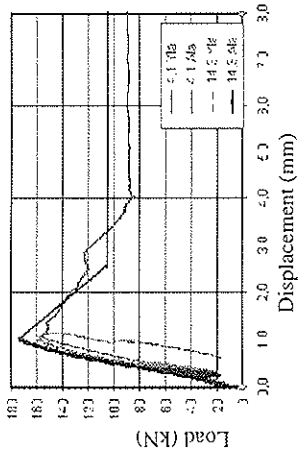


Figure 8. LVL-DA; 4x5 bolts

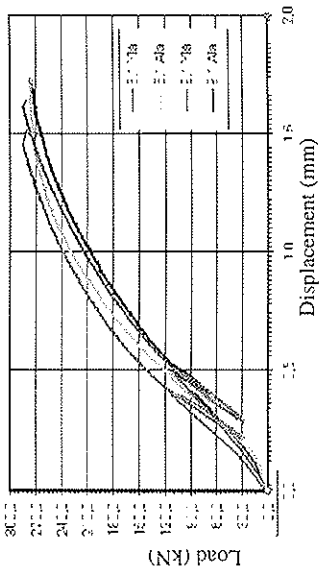


Figure 9. LVL-DA; 4x4 bolts

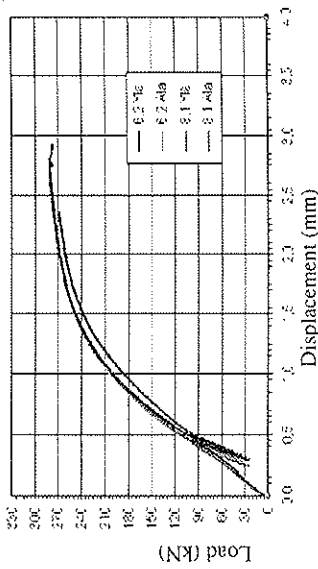


Figure 10. LVL-DA; 4x3 bolts

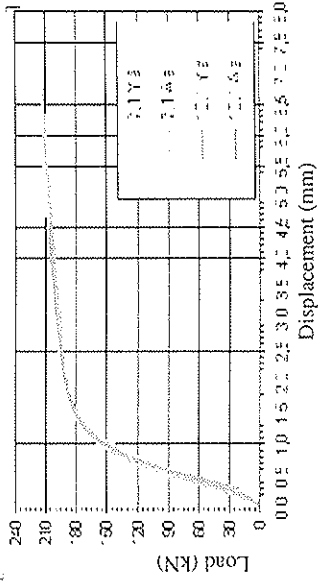


Figure 11. LVL-DB; 4x5 bolts

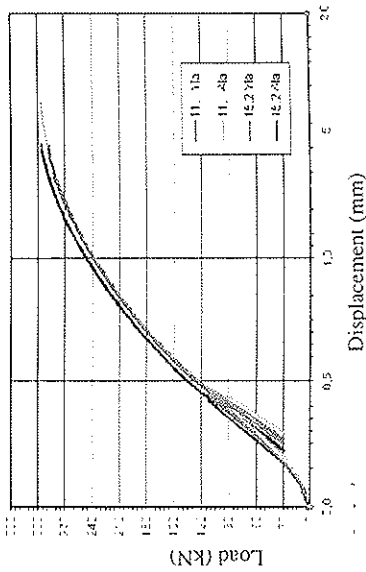


Figure 12. LVL-DB; 4x4 bolts

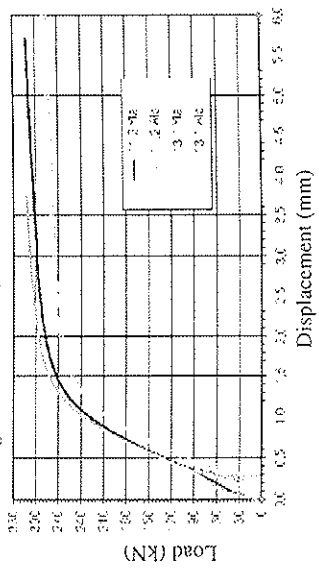
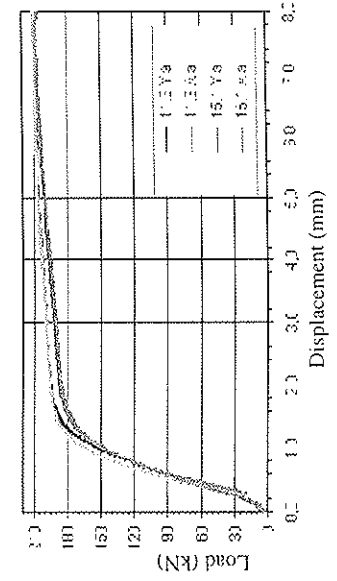


Figure 13. LVL-DB; 4x3 bolts



4 Conclusion

With the new LVL-D structure the block shear failure can be avoided by using stiff fasteners in dowel-type connections with wood. Also the ductility ratio of 4 can be reached; figure 2, 10, 12 and 13. The new structure can reach up to 40 % higher characteristic failure load in tension than LVL standard. The relative capacity of one bolt with each structure is shown in next figure. The 4x4 bolts in serie LVL-DB gives the optimum result. LVL standard had in all cases brittle failure; figures 5-7. In LVL-DA and LVL-DB series there was no use to have the fifth row of bolts.

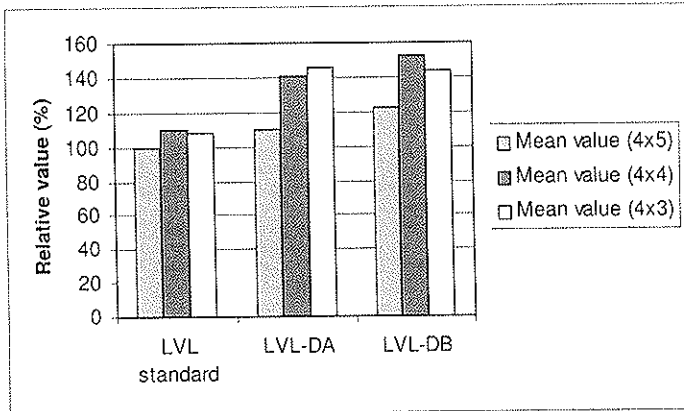


Figure 14. Relative capacity of one bolt with each structure and number of bolts. The basic is LVL standard with 4x5 bolts =100.

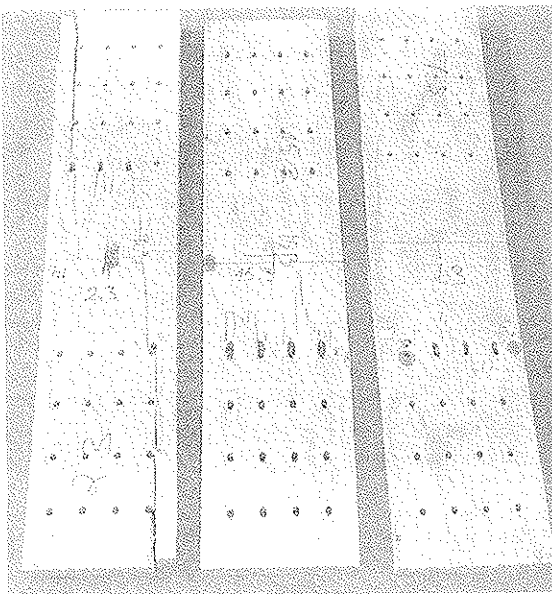


Figure 15. From the left LVL standard with block shear failure; figure 6, LVL-DA with tension failure, figure 9 and LVL-DB with first embedment failure and later tension failure, figure 12.

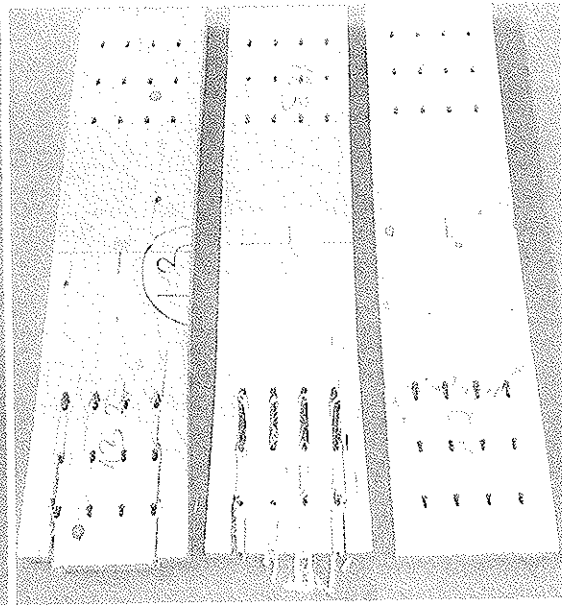


Figure 16. LVL-DB first with embedment failure and after that block shear, plug shear and tension failure, figure 13.

References

- prEN 1995-1-1, 2002, Eurocode 5 – Design of timber structures, Part 1.1: General rules and rules for buildings, Final Draft 2002-10-09. Document CEN/TC 250/SC 5: N 195.
- Fahlbusch, H., 1949. Ein Beitrag zur Frage der Tragfähigkeit von Bolzen in Holz bei statischer Belastung. Braunschweig: Institut für Maschinenkonstruktion und Leichtbau, Technische Hochschule Braunschweig. Bericht Nr. 49-9.
- Gehri, E., 1996. Design of joints and frame corners using dowel-type fasteners. Proceedings CIB W18, paper 29-7-6. Bordeaux, France.
- Haller, P., Wehsener, J. and Birk, T., 2001. Embedding characteristics on fibre reinforcement and densified timber joints. Proceedings of CIB/W18, paper 34-7-14, Venice
- Kairi, M. 1987. Kertopuun ladonnassa käytettävä menetelmä ja laite (Method and equipment used in lay upping of Kerto[®]-LVL). Finnish patent 73163.
- Kairi, M., 2001. Diagonal Laminated Veneer Lumber (LVL-D) gives ductility to dowel-type connection, Joints in Timber Structures, 55th Rilem Annual Week, Stuttgart, Germany
- Kevarinmäki, A., Kangas, J., Nokelainen, T., and Kanerva, P. 1995. Nail-plate reinforced bolt joints of Kerto-LVL structures. Publication 51, Helsinki University of Technology/LSEBP, ISSN 0783-9634. 23 p.
- Mischler, A., 2000. Die Bemessung von Stabdübel-Verbindungen, Verbindungstechnik im Holzbau, 32. SAH-Fortbildungskurs, Schweizerische Arbeitsgemeinschaft für Holzforschung, Zürich, ISBN 3-906703-12-6, 71-91
- Leijten, A. and Rodd, P., 1998. The development of moment resisting timber joints densified veneer wood, Cost C1, Control of the semi-rigid behaviour of civil engineering structural connactions, Proceedings of the international conference, Liège, EUR 18854 EN
- Werner, H., 1993. Tragfähigkeit von Holz-Verbindungen mit stiftförmigen Verbindungsmitteln unter Berücksichtigung streuender Einflußgrößen. Karlsruhe: Versuchsanstalt für Stahl, Holz und Steine, Abt. Ingenieurholzbau, Universität Karlsruhe (TH), Heft 48.
- Werner, H., 1995. Stiftverbindungen – Spalteffekte und Verstärkungsmaßnahmen. STEP 3. Arbeitsgemeinschaft Holz e.V. ISSN-Nr. 0446-2114

INTERNATIONAL COUNCIL FOR RESEARCH AND INNOVATION
IN BUILDING AND CONSTRUCTION

WORKING COMMISSION W18 - TIMBER STRUCTURES

GLUED-IN STEEL RODS: A DESIGN APPROACH FOR AXIALLY LOADED
SINGLE RODS SET PARALLEL TO THE GRAIN

R Steiger
E Gehri
R Widmann

Swiss Federal Laboratories for Materials Testing and Research EMPA

SWITZERLAND

Presented by R Steiger

H J Larsen commented that these results are for a specific system and generalization must consider other tests. Steiger agreed and will try to combine the data from other sources.

M Ansell questioned why the perpendicular to grain shear strength was higher than that of parallel to grain shear strength and wondered whether this could be caused by oversized holes with thick glue line that gave higher shear strength due to the penetration of glue into the specimen. Steiger explained that these results are for a specific system and the issue of oversized hole was already considered.

J W van de Kuilen asked about the influence of the reinforcements in the pile foundation test set up. Steiger agreed that it could be an important issue.

C Clorius asked whether there was any quantification of influence of reduced cross section of the glue-in-rod. Steiger responded that this information can be found in referenced material.

Steiger invited the delegate to submit articles to a special timber issue in the RILEM Journal of Material of Structures.

Glued-in steel rods: A design approach for axially loaded single rods set parallel to the grain

R. Steiger ¹⁾, E. Gehri ²⁾, R. Widmann ¹⁾

¹⁾ Swiss Federal Laboratories for Materials Testing and Research EMPA, Switzerland

²⁾ Prof. em. ETH, Switzerland

1 Introduction

Steel rods bonded in glulam elements are very efficient to introduce high forces into timber structural members as well as to strengthen timber perpendicular to the grain. Research on bonded-in rods started in the late eighties of the last century and attempts to develop design methods and to optimize the application were intensified within the last 10 years. A good compilation of existing knowledge, including lists of basic literature can be found in the proceedings PRO 22 of the 2001 RILEM Symposium on “Joints in Timber Structures” and in the proceedings of the CIB W18-Meetings 28 and 32 – 34.

Several design approaches and code models have been published. By comparing these models and approaches, some discrepancy and partly even contradictions between the models, especially regarding the treatment of isolated parameters, can be found. On this background, a small test program was initiated, to study the influence of a selection of these parameters, known or supposed to be determinant on the pull-out strength of single, axially loaded steel rods with a metric screw-thread, bonded with an epoxy-type adhesive in glulam made of spruce. The tests were focused to determine the influence of timber density ρ , rod-to-grain angle (0° or 90°), length ℓ and diameter d of the rod (or the corresponding drill-hole d_h respectively), represented by the slenderness ratio $\lambda = \ell/d_h$ on the pull-out strength of glued-in rods.

Important objectives of the test program were that it should be based on practical situations and dimensions and that it should enable a comparison with similar test series. These objectives could only be reached by permitting certain compromises regarding the test layout. Although for example in practice the use of one single rod will not or hardly ever be the normal case, all tests described here were carried out on connections with one single rod, because the examination of such a connection provides a good basis to study the influence of isolated parameters. The tested GSA[®]-system was “optimized” (type of adhesive and rod, geometry) in a way that failure was forced into the timber. The test results and conclusion are therefore specifically valid for the tested system and loading configuration (On the influence of the loading configuration see: [1]). A generalisation of the conclusions will not be possible and a comparison to other test series has to be done with some restraint. Nevertheless it is possible to quantify the influence of the parameters focused by the present study on the pull-out strength of axially loaded rods and to propose an adequate design model.

2 Review of existing approaches

2.1 Influence of the timber density

Since most of the mechanical properties of timber are known to be more or less directly related to the density of the timber, it is to be supposed that the pull-out strength of glued-in steel rods depends on the timber density, if steel and adhesive failure is prevented. For screws and screw nails, the influence of the density on the pull-out strength was shown for example by [2-5] to exist and was taken into account by a power function of the density (ρ^c) with exponents c up to 2.5.

The pull-out strength of glued-in rods could therefore be supposed to exhibit a similar dependence on the density. But compared to screws and screw nails, glued-in rods introduce the shear forces into the timber in a different way. While the screws rely on direct contact between the timber and the flanks of the thread and therefore on a kind of compression perpendicular to the grain, the glued-in rods transfer the force that way only in the interface between rod and adhesive. The load transfer between the adhesive and the timber is governed mainly by shear forces without much indenting. Being aware of this, a certain dependence of the pull-out strength of glued-in rods on the timber density can be expected, but compared to screws and screw nails the influence should be less significant because the shear strength of timber is affected by the density not as much as the compression strength.

Researchers have different opinions on the influence of the timber density on the pull-out strength of glued-in rods. While some of them (for example: [6, 7]) derived such an influence from their test results, others asserted the pull-out strength to be independent of timber density [8] or to exhibit poor correlation [1, 9, 10]. Design models derived from the tests take care of the density influence by power functions ρ^c with exponents c in the range of 0 to 1.5 according to the rod-to-grain angle [9-17]. All of these design models consider the dependence on the density, if taken into account at all, to be marked more for rods set parallel to the grain, than for those set perpendicular to the grain.

2.2 Influence of length and diameter of the anchorage zone

The diameter and the length of the rod or of the hole respectively (which is the correct way of analysing data derived from tests with clear failure in the timber) were shown by different studies (for example by [6, 9, 12, 15, 16, 18, 19] to be of dominant influence on the pull-out strength of glued-in rods. In [11] and [20] it was found, that a variation of the strength depending on the anchorage length of rods glued-in perpendicular to the grain was not given or just moderate.

The glued length $\ell + \ell_v$ (ℓ corresponds to the anchorage length, where the load is actually transmitted from the rod to the timber; ℓ_v is a sinking length without any load transmission capacity; see 3.1.3 and annex A.1) and the diameter d_h of the drill-hole can be combined in a single parameter called slenderness ratio $\lambda = \ell/d_h$. The advantage of using λ is a certain simplification of the design models. The disadvantage of combining ℓ and d_h in one single parameter is, that a possible different degree of influence of the single parameters ℓ and d_h on the pull-out strength of the rods might be hidden. In [9] a very strong effect of absolute size of the rod and also of the rod's slenderness is stated for brittle adhesives.

2.3 Influence of rod-to-grain angle (0° or 90°)

Timber subjected to stresses parallel or perpendicular to the grain exhibits completely different behaviour. Joints with rods set perpendicular to the grain are governed by the tension strength of the timber perpendicular to the grain. To be able to compare the capacity of rods set perpendicular to the grain to such set parallel, the failure must be forced to the anchorage zone and early failures due to high stresses perpendicular to the grain within the joint have to be prevented by an adequate geometrical design or by a reinforcement of the joint perpendicular to the grain. Specimens with rods glued-in parallel to the grain tend to split due to forces perpendicular to the grain. Early splitting can be prevented by providing sufficiently dimensioned edge distances of the rods or by strengthening the anchorage zone perpendicular to the grain.

Since the type of failure directly affects the load levels reached within the different test series, the scientists' opinions on the influence of rod-to-grain angle (0° and 90°) exhibit considerable differences (see for example [6, 7, 13, 16, 18, 21]).

3 Tests

3.1 Material properties

3.1.1 Timber

The tests described in this paper were carried out on glued-laminated timber made of Swiss spruce lamellas with a thickness of 44 mm and a width of 175 mm. The lamellas were free from any finger-joints or significant anatomical defects such as big knots and deviations of grain angle, in order to avoid negative influence of the results by these parameters. The glulam members with a cross-section of 160 x 480 mm were assembled using an urea formaldehyde (UF) resin adhesive. Two glulam beams were produced from lamellas with clearly distinct distributions of density (fig. 1), in order to quantify the influence of the timber density on the pull-out strength of the rods.

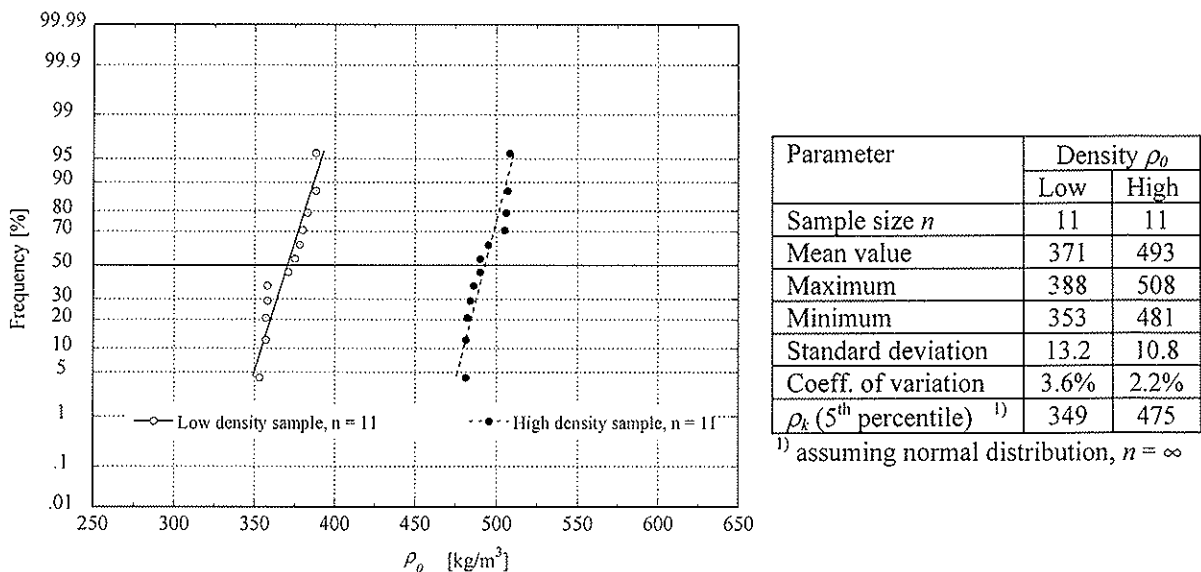


Figure 1: Normal probability plot and sample statistics of lamellae's densities ρ_0

3.1.2 Adhesive

The rods were set using a system called GSA[®] by n'H (Neue Holzbau AG, Switzerland) [22]. For the GSA[®]-system a special epoxy-type adhesive, free from any solvent and curing at ambient temperature has been developed by ASTORit AG, Switzerland. This adhesive performs well, as was shown by testing the shear strength between two threaded steel surfaces bonded together, where shear strengths up to 35 N/mm² were reached. Tests on threaded steel rods bonded in ash established nominal shear strengths of 16 to 18 N/mm².

3.1.3 Steel rods

In practice, joints with glued-in rods should be designed in a way that steel failure occurs and not wood- or adhesive failure in order to achieve a ductile rather than a brittle rupture. The GSA[®]-system considers this fact by reducing the cross-section of the steel rods within a certain length ℓ_v , which is an investigation based on tests by Fabris [23]. By turning off the rod's thread within the length ℓ_v the anchorage zone is shifted away from the surface more to the interior. Stress concentrations are reduced and local splitting due to shear forces and stresses perpendicular to the grain is prevented [19, 23, 24]. Although the drill-hole on its whole length $\ell + \ell_v$ was filled with glue, any contribution of the sinking length ℓ_v to the pull-out resistance was disregarded due to the lack of mechanical indenting of rod and adhesive in that zone. The sinking length ℓ_v was taken to be 5·d.

The steel rods with metric threads M12 and M20 were zinc coated and corresponded to quality 8.8 (nominal yielding point: $f_y \approx 640$ N/mm² / $\varepsilon_y \approx 3$ ‰ and nominal ultimate tensile strength: $f_u \approx 800$ N/mm²), in order to force timber failure rather than steel failure. They were set in pre-bored holes with diameters d_h of 2 mm more than that of the rod itself (M12: $d_h = 14$ mm; M20: $d_h = 22$ mm). The anchorage lengths ℓ and the resulting slenderness ratios $\lambda = \ell/d_h$ are listed in annex A.1.3.

3.2 Specimens, equipment and procedure

3.2.1 Specimens

The rods set parallel to the grain were tested in a double-ended (pull-pull) configuration (Annex A.1.1). To give the joints an optimal performance both the timber and the steel elements should have similar stiffness ($A_{Timber} \cdot E_{Timber} \approx A_{Steel} \cdot E_{Steel}$) [19, 23]. The ratio A_{Timber} / A_{Steel} should therefore be at least equal or even bigger than the ratio E_{Steel} / E_{Timber} which is approximately 16 to 20 for spruce. From the practical point of view, high ratios of A_{Timber} / A_{Steel} are unattractive because of a poor performance of the joint itself, regarding the resulting tensile stress in the glulam element. In order to prevent early splitting of timber due to stress concentrations, the M12 specimens were of cross-section 55 x 55 mm (thus had an edge distance of 2.29 d) and the M20 specimens cross-section measured 95 x 95 mm (edge distance 2.38 d), which represents a ratio of A_{Timber} / A_{Steel} of 36 to 37.

The rods set perpendicular to the grain were tested in a single-ended configuration (pull-compression) according to annex A.1.2. This type of loading configuration produces a situation, where the tensile force in the steel rod is balanced by shear stresses in the timber. In order to avoid crushing due to excessive compression perpendicular to the grain caused by the reaction forces, four screws of type SFS WR 9 x 300 (M12-series) and four steel rods M12 (M20-series) were set around the rod, acting like a "pile foundation" with a length equal to that of the tested rod. Thus crushing of the timber perpendicular to the

grain was prevented and an optimised (homogeneous) shear zone (more or less uniform field of shear stresses) within the timber could be assumed.

3.2.2 Equipment and procedure

All of the tests were carried out on a universal tension testing machine with a maximal error of the force measurement < 1 %. The loading scheme was taken from EN 26891 [25].

4 Results

4.1 General

A compilation of all test results is given in annex A.2. Except the specimens M12 perpendicular to the grain with the longest anchorage length ℓ (175 mm), all other specimens failed by pull-out of the rods. The above mentioned specimens failed due to steel failure within the area of the reduced diameter d_{red} of the rod. The rods set perpendicular to the grain achieved pull-out strengths which were about 20% – 40% higher than those of the rods set parallel to the grain. Therefore rod-to-grain angle is regarded to be a parameter which cannot be neglected when designing joints with glued-in rods.

Even though it was not verified in detail, there was strong evidence that the pull-out of the rods occurred due to shear failure of the wood around the glue-zone of the rods. Regarding the pull-pull tests on rods set parallel to the grain visible splitting and cracking occurred on about 50% of all specimens. However, there were no significant differences between the failure loads of specimens with and without external signs of cracking/splitting found. Cracking should therefore not have influenced the achieved pull-out strengths and is regarded as being a consequence of the internal shear failure of the wood.

4.2 Influence of timber density

The test results (see for example fig. 3) show, that the pull-out strength of glued-in rods depends on the timber density. The influence is clearly visible regarding the rods set parallel to the grain but not as marked for those set perpendicular to the grain. The mean values of calculated exponents c_i from $(F_1/F_2) = (\rho_1/\rho_2)^{c_i}$ comparing the high-density glulam sample (F_1, ρ_1) with the low-density sample (F_2, ρ_2) are $c_{mean,0} = 0.51$ and $c_{mean,90} = 0.29$. Carrying out the same analysis based on the density of the lamellas located within the anchorage zone of the rods leads to exponents of $c_{mean,0} = 0.48$ and $c_{mean,90} = 0.28$. Design models should therefore take into account the timber density at least when the rods are set parallel to the grain. There an exponent of $c_0 = 1/2$ seems to be appropriate. For rods set perpendicular to the grain the density influence can either be disregarded or considered by applying an exponent of $c_{90} = 1/4$.

4.3 Influence of anchorage length and of drill-hole diameter

As already mentioned before, the tests were planned to follow a certain range of geometrical proportions in terms of drill-hole diameter d_h and anchorage length ℓ , represented by the parameter $\lambda = \ell/d_h$. Besides analysing the test results with regard to λ , the influences of the single parameters ℓ and d_h will be studied, in order to get an idea on their power. The nominal shear strength $f_{v,mean}$ is calculated assuming a constant

distribution of the shear stresses over the anchorage length ℓ . This assumption is valid for the rods set perpendicular to the grain. In case of gluing in the rods parallel to the grain, the stress distribution is uneven with peaks at both ends of the anchorage zone [10, 26, 27].

4.3.1 Influence of the anchorage length ℓ

Regarding the influence of the anchorage length on the pull-out strength of the rods, it has to be stated, that this influence is marked for rods set parallel to the grain (fig. 2-left). There an approach based on $\ell^{-1/3}$ could be suggested. In the case of rods glued-in perpendicular to the grain (fig. 2-right) the results are not conclusive. While the M20-series shows a dependence on the anchorage length, the M12-series does not. It's therefore not possible to give an overall approach.

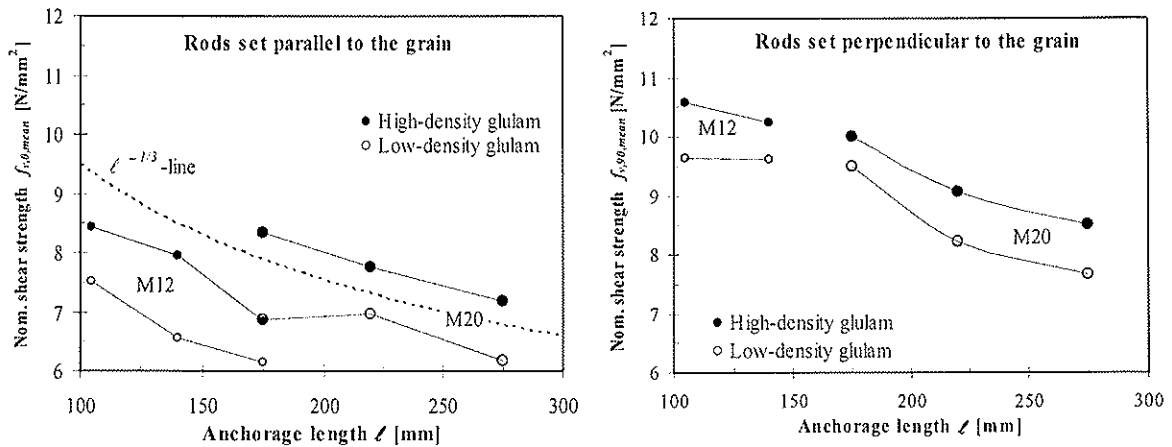


Figure 2: Nominal shear strength $f_{v,mean}$ versus anchorage length ℓ for rods set parallel to the grain (left) and for rods set perpendicular to the grain (right)

4.3.2 Influence of slenderness ratio $\lambda = \ell/d_h$

Regarding the influence of the slenderness ratio $\lambda = \ell/d_h$ on the nominal shear strength $f_{v,mean}$, this influence is marked more for the 0°-series than for the 90°-series (fig. 3). A power function $\lambda^{-1/3}$ fits the test results of the 0°-series well, whereas such a model does not approximate the test values for rods set perpendicular to the grain well enough.

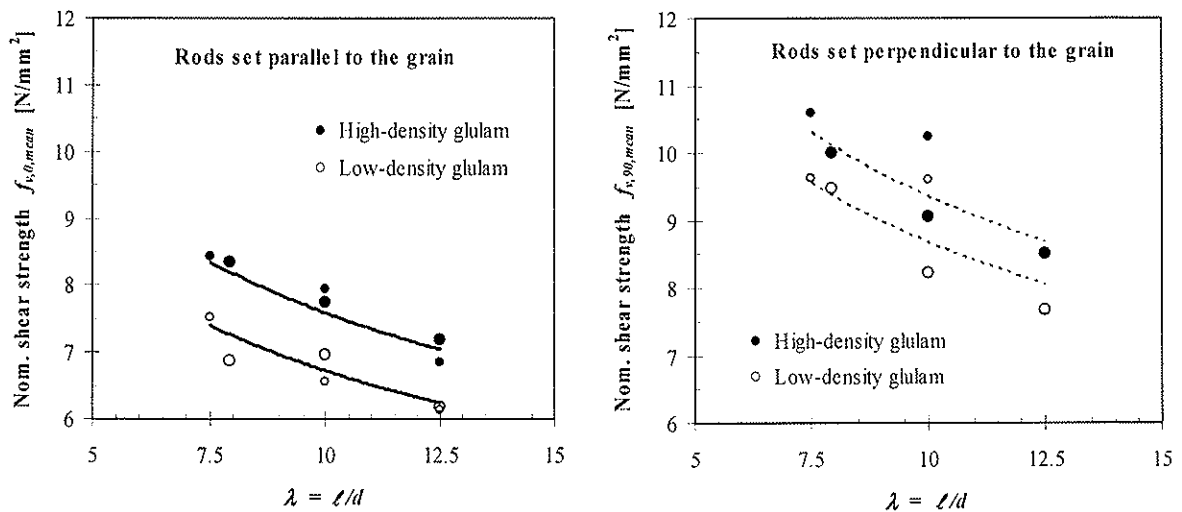


Figure 3: Nominal shear stress vers. slenderness ratio. The curves represent $\lambda^{-1/3}$ -functions.

4.3.3 Influence of drill-hole diameter d_h

Since the leading parameter of the test series was not the drill-hole diameter d_h but much more the slenderness ratio λ , there is only a few test data with an equal anchorage length ℓ available to quantify the influence of the hole diameter d_h . For the data-analysis all test results were transformed to an identical density base ($\rho_{ref} = 480 \text{ kg/m}^3$) by adjusting the values of both the low-density and the high-density sample with factors $x_0 = (480/\rho_i)^{0.5}$ and $x_{90} = (480/\rho_i)^{0.25}$. (On the exponents $c_0 = 1/2$ and $c_{90} = 1/4$: see section 4.2.)

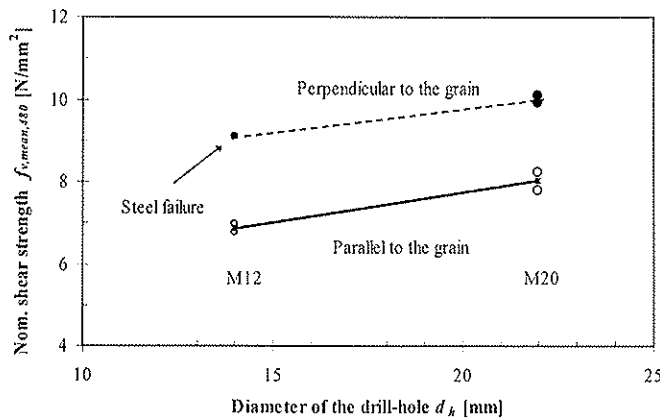


Figure 4:
Nominal shear strength $f_{v,mean,480}$
versus diameter of the drill-hole
 d_h (Series with $\ell = 175 \text{ mm}$ only)

According to figure 4, which shows only the results of the tests with an equal anchorage length $\ell = 175 \text{ mm}$, it can be stated, that the nominal shear strength $f_{v,mean,480}$ perpendicular to the grain is about 25 % higher than that parallel to the grain and that in the latter case the nominal shear strength increases with increasing diameter d_h . Due to occurring steel failures in the M12-series a similar dependence on the drill-hole diameter can not be postulated in case of rods set perpendicular to the grain. In table 1 an analysis on the influence of the drill-hole's diameter is shown, which covers all test values of the 0° -series adjusted to a timber density of $\rho_{ref} = 480 \text{ kg/m}^3$ and grouped according to their slenderness ratios λ .

Table 1: Comparison of nominal, density-adjusted pull-out shear strengths $f_{v,0,mean,480}$ [N/mm^2] for different slenderness ratios $\lambda = \ell/d_h$ and drill-hole diameters d_h

Series		$f_{v,0,mean,480}$ [N/mm^2] (Mean value of density-adjusted high- and low-density samples)		
		$\lambda = 7.5$ ¹⁾	$\lambda = 10$	$\lambda = 12.5$
0°	M12	8.41	7.65	6.92
	M20	8.24 ¹⁾	7.83	7.11
	M20/M12	1.02	1.02	1.03

¹⁾ The M20-tests with an anchorage length $\ell = 175 \text{ mm}$ correspond to a slenderness ratio of $\lambda = \ell/d = 7.955$. A multiplication of the M20- $f_{v,0,mean,480}$ -values by a factor $x = (7.5/7.955)^{-1/3} = 1.02$ (see section 4.3.2) in order to adjust those values to $\lambda = 7.5$ was applied.

According to table 1 the pull-out strength ratio M20/M12 is approximately 1 for all three slenderness ratios. This means that a variation in shear strength can be explained by the variation in λ , a result, which was already found in 4.3.2. Based on an approach $\lambda^{-1/3}$, the influence of the hole-diameter d_h on the pull-out strength of rods set parallel to the grain needs to be $d_h^{1/3}$ in case of constant length. This can not be proven due to lacking of further test results with other diameters but it can at least be verified by comparing the M12- and the M20 series with an equal anchorage length of $\ell = 175 \text{ mm}$ directly (table 2).

Table 2: Comparison of nominal, density-adjusted pull-out shear strengths $f_{v,0,mean,480}$ [N/mm²] for anchorage length $\ell = 175$ mm

Series		$f_{v,0,mean,480}$ [N/mm ²] (Mean value of density-adjusted high- and low-density samples)	Calculation of function
0°	M12	0.5 (7.08 + 6.76) = 6.92	$\left(\frac{d_{h,1}}{d_{h,2}}\right)^{c_0} = \left(\frac{22}{14}\right)^{c_0} = \text{ratio} \frac{M20}{M12}$
	M20	0.5 (7.92 + 8.23) = 8.08	
	M20/M12	1.17	$c_0 = 0.35$

In general it can be stated, that if the single parameters anchorage length ℓ and diameter of the drill-hole d_h are taken as base for the determination of the pull-out strength $f_{v,0,mean}$ of rods set parallel to the grain, both would have to be considered and both with different powers. An approach on base of slenderness λ therefore seems to be the better solution.

4.4 Load transmission capacity for rods set parallel to the grain

A comparison of the tensile stresses in the timber members shows, that the load transmission capacity steel to timber of the M20 rods set parallel to the grain is about 15 % less than that of the M12 rods.

5 Conclusions

Based on the test results it can be stated, that for the used GSA[®]-system:

- the pull-out strength of rods bonded in glulam made of spruce depends on the density of the timber around the anchorage zone. For rods set parallel to the grain, the influence of the density is stronger and can be covered by a power function ρ^c with an exponent of $c_0 = 1/2$. Rods set perpendicular to the grain exhibit a smaller dependence on the timber density. There the influence of the density could be taken into account with an exponent $c_{90} = 0.25$ or could be disregarded.
- there is a difference of about 20 to 40 % in pull-out strengths according to the rod-to-grain angle (0° or 90°), which should be considered by design models.
- the influence of the anchorage length ℓ is marked more for rods set parallel to the grain, than for those set perpendicular. In the case of rods set parallel to the grain, an adjustment based on $\ell^{-1/3}$ is a good approach.
- the 0°-series show a dependence on the slenderness ratio $\lambda = \ell/d$, which can be quantified by $\lambda^{-1/3}$. If a design model is based on λ , the influence of the drill-hole diameter on the pull-out strength, which is about $d_h^{1/3}$, is automatically taken into account.
- with regard to an optimal load transmission capacity steel to timber, rods with smaller diameter should be given preference.

6 Design rule proposal for single, axially loaded rods

6.1 Nominal shear strength of rods set parallel to the grain

Based on the test results presented in this paper, the nominal shear strength of single, axially loaded rods set parallel to grain may be calculated as:

$$f_{v,0,mean} = k_0 \cdot \lambda^{-1/3} \cdot \left(\frac{\rho}{480}\right)^{1/2}$$

$$\text{or } f_{v,0,mean} = k_0 \cdot d^{1/3} \cdot \ell^{-1/3} \cdot \left(\frac{\rho}{480}\right)^{1/2}$$

$f_{v,0,mean}$	[N/mm ²]
ρ	[kg/m ³]
λ	[-]
ℓ	[mm]
d	[mm]

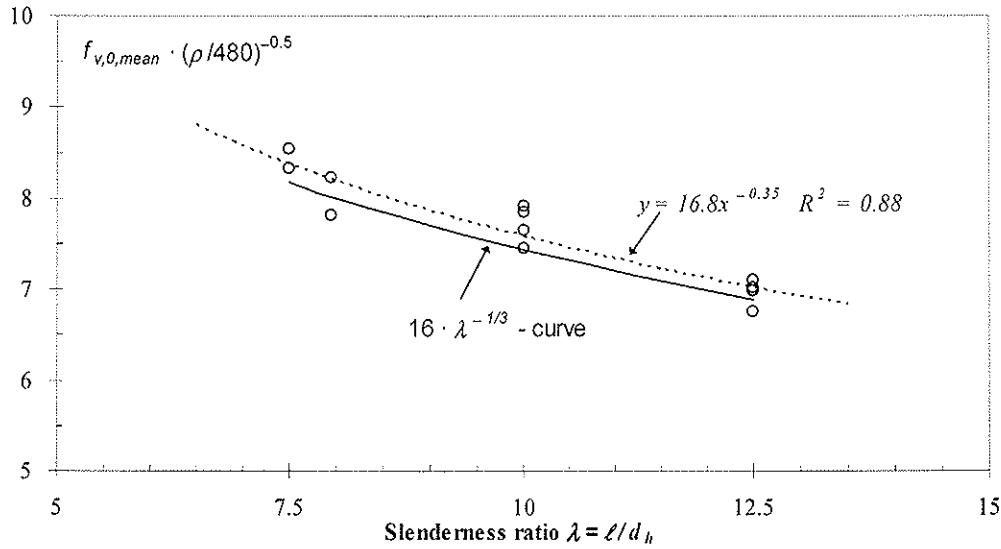


Figure 5: Design model to calculate the nominal shear strength of single, axially loaded rods glued-in parallel to the grain together with the test results

Figure 5 shows, that this design model with a value of $k_0 = 16$ fits the test results well. The use of the model is restricted to:

- single rods glued-in parallel to the grain and loaded axially in tension
- slenderness ratios $\lambda = \ell/d_h$ in the range of $7.5 \leq \lambda \leq 12.5$
- rod diameters of 12 to 20 mm
- sinking length $\ell_v = 5d$
- glulam made of spruce or other coniferous timber with similar properties and a characteristic values of density in the range of 350 to 500 kg/m³.

In addition a control of the stresses in the steel bar and in the timber member (net cross-section) is necessary. In practice however the above design model only allows to optimize the joint and to take full advantage of the system. The joint should actually be designed in such a way that (ductile) steel failure rather than (brittle) timber or adhesive failure occurs.

6.2 Pull-out strength of rods set perpendicular to the grain

Concerning rods set perpendicular to the grain, due to occurring steel failures it's not possible to propose an adequate design model. But the tests show that the pull-out strength of rods set perpendicular to the grain depends on the timber density by $\rho^{1/4}$.

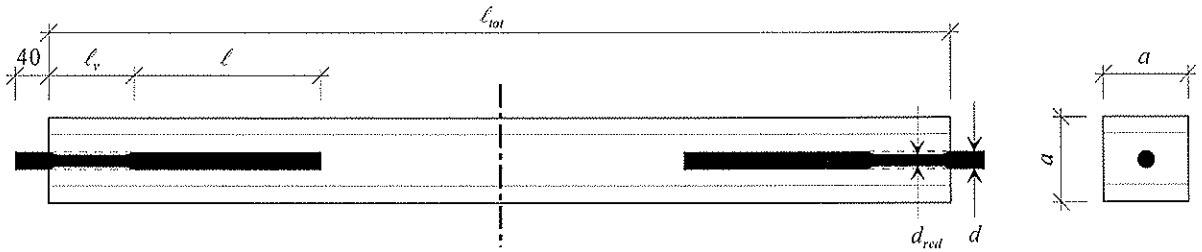
7 References

1. **Bengtsson C., Johansson C.-J.:** Test methods for glued-in rods for timber structures. Paper 33-7-8 in: Proceedings of CIB W18-Meeting Thirty-Three. (2000). Delft, The Netherlands.
2. **Ehlbeck J.:** Versuche mit Sondernägeln für den Holzbau. Holz als Roh- und Werkstoff 34 (1976), Nr. 7, p. 205-211.
3. **Meierhofer U.:** Schraubenauszugfestigkeit und Tragfähigkeit von Fichten- und Tannenholz. Holz als Roh- und Werkstoff 46 (1988), Nr. 1, p. 15-17.
4. **Görlacher R.:** Untersuchungen an altem Konstruktionsholz: Die Ausziehwidstandsmessung. bauen mit holz 92 (1990), Nr. 12, p. 904-908.
5. **Werner H., Siebert W.:** Neue Untersuchungen mit Nägeln für den Holzbau. Holz als Roh- und Werkstoff 49 (1991), Nr. 5, p. 191-198.
6. **Gerold M.:** Verbund von Holz und Gewindestangen aus Stahl. Bautechnik 69 (1992), p. 167-178.
7. **Serrano E.:** Glued-in rods for timber structures - An experimental study of softening behaviour. Materials and Structures 34 (2001), p. 228-234.
8. **Kemmsies M.:** Comparison of pull-out strengths of 12 adhesives for glued-in rods for timber structures. (1999). SP Swedish National Testing and Research Institute. Borås. Report 1999:20. pp. 26.
9. **Aicher S., Gustafsson P. J., Wolf M.:** Load displacement and bond strength of glued-in rods in timber influenced by adhesive, wood density, rod slenderness and diameter. In: Proceedings of 1999-International RILEM Symposium on "Timber Engineering". (1999). Stockholm, Sweden. pp. 10.
10. **Bernasconi A.:** Behaviour of axially loaded glued-in rods - Requirements and resistance, especially for spruce timber perpendicular to the grain direction. Paper 34-7-6 in: Proceedings of CIB W18-Meeting Thirty-Four. (2001). Venice, Italy.
11. **Riberholt H.:** Glued bolts in glulam - Proposal for CIB code. Paper 21-7-2 in: Proceedings of CIB W18-Meeting Twenty-One. (1988). Parksville, Vancouver Island, Canada.
12. **Gerold M.:** Anwendung von in Holz eingebrachten, in Schafrichtung beanspruchten Gewindestangen aus Stahl. Bautechnik 70 (1993), Nr. 10, p. 603-613.
13. **Gehri E.:** Krafterleitung mittels Stahlanker. In: Proceedings of the 28th SAH-Fortbildungskurs "Brettschichtholz". (1996). Weinfelden, Switzerland. p. 111-143.
14. **CEN:** Eurocode 5 - Design of timber structures. Part 2: Bridges. (1997). pp. 45.
15. **Kangas J.:** Capacity, fire resistance and gluing pattern of the rods in V-connections. Paper 33-7-10 in Proceedings of CIB W18-Meeting Thirty-Three. (2000). Delft, The Netherlands.
16. **Gustafsson P.-J., Serrano E., Aicher S., Johansson C.-J.:** A strength design equation for glued-in rods. In: Proceedings of 2001-International RILEM Symposium on "Joints in Timber Structures". (2001). Stuttgart, Germany. p. 323-332.
17. **Gehri E.:** Background paper on glued-in rods in prENV 1995-2: 1997. CEN/TC 250/SC 5-Document Nr. 108 rev. (1997). pp. 8.
18. **Möhler K., Hemmer K.:** Eingeleimte Gewindestangen. bauen mit holz 83 (1981), Nr. 5, p. 296-298.
19. **Gehri E.:** Klassische Verbindungen neu betrachtet. In: Proceedings of the 17th Dreiländer Holztagung "Holz: Architecture - Research - Technology". (2000). Lucerne, Switzerland. p. 43-50.
20. **Bernasconi A.:** Axially loaded glued-in rods for high capacity joints - Behaviour and resistance. In: Proceedings of 2001-International RILEM Symposium on "Joints in Timber Structures". (2001). Stuttgart, Germany. p. 373-381.
21. **Belchior-Gaspard P., Colling F., Siebert W.:** Karlsruher Forschung im Ingenieurholzbau 1987, 3. Teil: Eingeleimte Gewindestangen unter Axialbelastung. bauen mit holz 89 (1987), Nr. 8, p. 504-512.
22. **Strahm T.:** Das entwurfsfreundliche und leistungsfähige GSA-Ankersystem. In: Proceedings of the 32th SAH-Fortbildungskurs "Verbindungstechnik im Holzbau". (2000). Weinfelden, Switzerland.
23. **Fabris A.:** Verbesserung der Zugeigenschaften von Bauholz parallel zur Faser mittels Verbund mit profilierten Stahlstangen. PhD thesis. (2001). ETH Zürich, Professur für Holztechnologie. pp. 265.
24. **Gehri E.:** Ductile behaviour and group effect of glued-in steel rods. In: Proceedings of 2001-International RILEM Symposium on "Joints in Timber Structures". (2001). Stuttgart, Germany. p. 333-342.
25. **CEN:** EN 26891: Timber structures - Joints made with mechanical fasteners: General principles for the determination of strength and deformation characteristics. (1991). pp. 4.
26. **Del Senno M., Piazza M., Tomasi R.:** Axial glued-in steel timber joints - Experimental and numerical analysis. Holz als Roh- und Werkstoff 62 (2004), p. 137-146.
27. **Deng J.X., Moss P. J., Buchanan A. H.:** Glued bolts in glulam - An analysis of stress distribution. In: Proceedings of the 5th World Conference on Timber Engineering. (1998). Volume 2. Lausanne, Switzerland. p. 206-213.

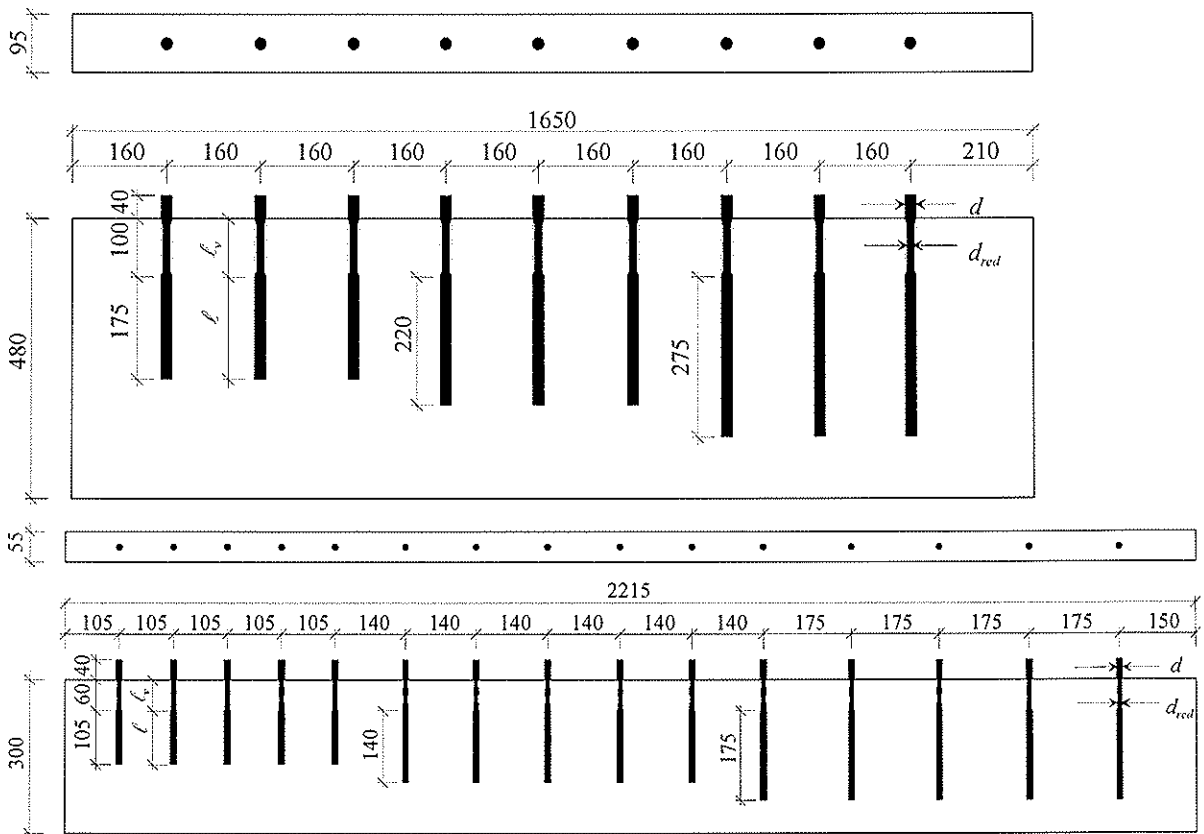
Annexes 1 - 2

A.1 Test set up

A.1.1 Test specimens with rods set parallel to the grain (pull-pull)



A.1.2 Test specimens with rods set perpendicular to the grain (pull-compression)



A.1.3 Geometrical properties

Series	a [mm]	d [mm]	Reduced diameter d_{red} [mm]	Sinking length ℓ_v [mm]	ℓ_{tot} [mm]	Anchorage length ℓ [mm]	Drill-hole diameter d_h [mm]	Slenderness ratio $\lambda = \ell/d_h$
M12	55	12	9.8	60	580	105	14	7.5
					650	140		10.0
					720	175		12.5
M20	95	20	17	100	980	175	22	7.96
					1070	220		10.0
					1180	275		12.5

A.2 Test results

Rods M12 parallel to the grain

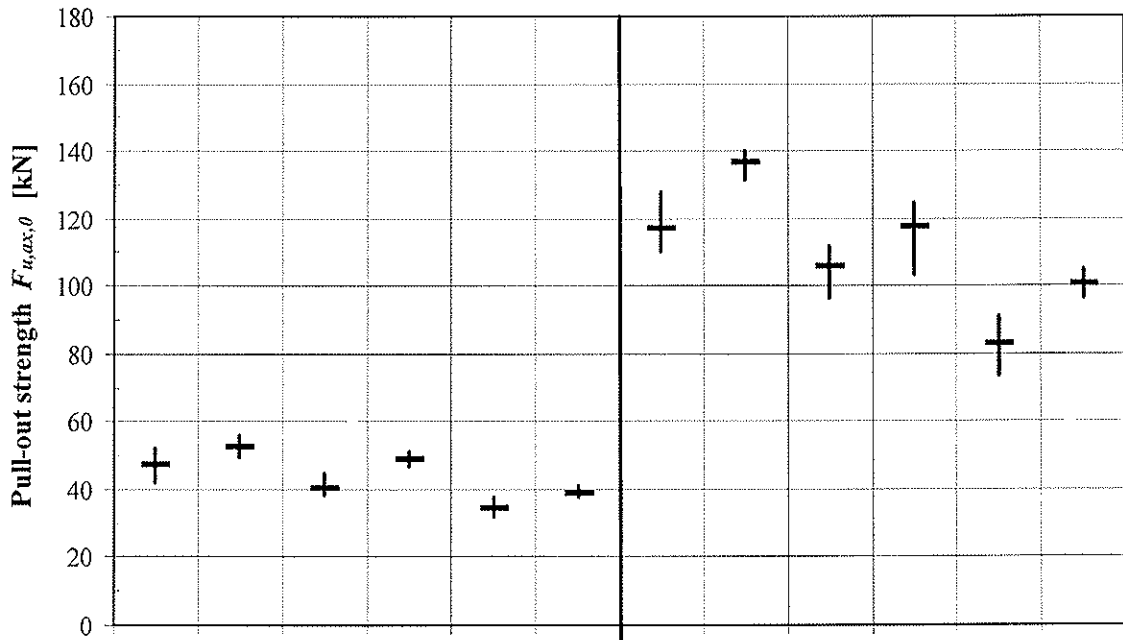
Rods M20 parallel to the grain

Type of specimen	Ind.	Density r_0 [kg/m ³]	ν [%]	F_w [kN]	$F_{u,480}$ ¹⁾ [kN]	$w(F_w)$ [mm]	f_v [N/mm ²]	$f_{v,480}$ ¹⁾ [N/mm ²]	Splits Cracks
M12-0°-175-LD	a1L	357	12.0	46.7	54.1	3.32	6.07	7.03	Cracks
M12-0°-175-LD	b1L	353	12.0	48.1	56.1	3.48	6.25	7.28	Splits
M12-0°-175-LD	c1L	378	11.5	42.2	47.6	2.96	5.49	6.18	Cracks
M12-0°-175-LD	d1L	357	11.6	52.0	60.3	4.06	6.76	7.83	Splits
Mean		361		47.3	54.5		6.14	7.08	
M12-0°-175-HD	a1S	486	13.1	52.4	52.0	3.65	6.80	6.76	-
M12-0°-175-HD	b1S	482	12.5	53.2	53.1	3.78	6.91	6.90	Splits
M12-0°-175-HD	c1S	507	12.9	49.5	48.1	3.22	6.43	6.26	Splits
M12-0°-175-HD	d1S	495	13.0	55.9	55.1	4.19	7.26	7.15	Splits
Mean		493		52.7	52.1		6.85	6.76	
M12-0°-140-LD	a2L	357	11.8	44.5	51.6	3.01	7.23	8.38	-
M12-0°-140-LD	b2L	358	11.8	38.2	44.2	2.44	6.20	7.18	-
M12-0°-140-LD	c2L	378	11.9	39.0	43.9	2.71	6.33	7.13	-
M12-0°-140-LD	d2L	388	11.8	39.6	44.1	2.70	6.43	7.16	-
Mean		370		40.3	45.9		6.55	7.45	
M12-0°-140-HD	a2S	486	12.9	46.8	46.5	2.95	7.60	7.56	-
M12-0°-140-HD	b2S	481	12.6	51.2	51.1	3.46	8.31	8.30	-
M12-0°-140-HD	c2S	507	12.5	49.0	47.6	3.31	7.95	7.74	Splits
M12-0°-140-HD	d2S	495	12.0	48.8	48.1	3.55	7.93	7.81	Splits
Mean		492		48.9	48.3		7.95	7.85	
M12-0°-105-LD	a3L	357	12.0	37.8	43.8	2.47	8.19	9.49	Splits
M12-0°-105-LD	b3L	383	11.5	33.4	37.4	2.32	7.23	8.09	-
M12-0°-105-LD	c3L	375	11.5	32.2	36.4	2.07	6.97	7.89	-
M12-0°-105-LD	d3L	380	11.2	35.4	39.8	2.48	7.67	8.62	Splits
Mean		374		34.7	39.3		7.51	8.52	
M12-0°-105-HD	a3S	506	13.9	38.3	37.3	2.54	8.30	8.09	-
M12-0°-105-HD	b3S	490	13.6	38.4	38.0	2.40	8.32	8.23	Cracks
M12-0°-105-HD	c3S	508	13.2	37.8	36.7	2.44	8.18	7.95	Cracks
M12-0°-105-HD	d3S	481	13.4	41.2	41.2	2.90	8.93	8.92	Cracks
Mean		496		38.9	38.3		8.43	8.29	

Type of specimen	Ind.	Density r_0 [kg/m ³]	ν [%]	F_w [kN]	$F_{u,480}$ ¹⁾ [kN]	$w(F_w)$ [mm]	f_v [N/mm ²]	$f_{v,480}$ ¹⁾ [N/mm ²]	Splits Cracks
M20-0°-275-LD	A1L	357	11.5	113.0	131.0	3.94	5.94	6.89	Cracks
M20-0°-275-LD	B1L	353	11.3	127.6	148.8	4.42	6.72	7.83	-
M20-0°-275-LD	C1L	375	11.5	118.7	134.2	4.07	6.24	7.06	Splits
M20-0°-275-LD	D1L	358	11.4	110.4	127.8	3.68	5.81	6.72	-
Mean		361		117.4	135.4		6.18	7.13	
M20-0°-275-HD	A1S	486	12.8	137.7	136.9	4.39	7.25	7.20	-
M20-0°-275-HD	B1S	490	12.5	137.8	136.4	4.29	7.25	7.18	Cracks
M20-0°-275-HD	C1S	507	12.5	131.5	127.7	4.24	6.91	6.72	Cracks
M20-0°-275-HD	D1S	490	12.9	139.9	138.5	4.70	7.36	7.29	Splits
Mean		493		136.7	134.8		7.19	7.09	
M20-0°-220-LD	A2L	357	11.3	106.4	123.4	3.33	7.00	8.12	-
M20-0°-220-LD	B2L	353	11.4	111.7	130.2	3.59	7.34	8.56	Splits
M20-0°-220-LD	C2L	375	11.5	108.6	122.8	3.70	7.14	8.08	Cracks
M20-0°-220-LD	D2L	358	11.3	96.3	111.5	3.11	6.33	7.33	Cracks
Mean		361		105.7	122.0		6.95	8.02	
M20-0°-220-HD	A2S	486	12.6	119.2	118.5	3.60	7.84	7.79	Cracks
M20-0°-220-HD	B2S	490	13.0	103.6	102.5	3.10	6.81	6.74	Splits
M20-0°-220-HD	C2S	507	12.6	124.8	121.5	3.59	8.21	7.99	Cracks
M20-0°-220-HD	D2S	490	12.8	123.7	122.4	4.02	8.13	8.05	-
Mean		493		117.8	116.2		7.75	7.64	
M20-0°-175-LD	A3L	357	11.2	81.0	93.9	2.48	6.69	7.76	-
M20-0°-175-LD	B3L	353	10.8	86.4	100.8	2.75	7.14	8.33	-
M20-0°-175-LD	C3L	375	11.7	91.1	103.1	2.85	7.53	8.52	Cracks
M20-0°-175-LD	D3L	358	11.6	73.6	85.2	2.33	6.08	7.04	-
Mean		361		83.0	95.8		6.86	7.92	
M20-0°-175-HD	A3S	486	13.4	104.7	104.0	3.05	8.65	8.60	-
M20-0°-175-HD	B3S	490	12.6	100.5	99.5	2.98	8.31	8.23	Splits
M20-0°-175-HD	C3S	507	12.8	96.4	93.8	2.81	7.97	7.75	-
M20-0°-175-HD	D3S	490	12.6	102.0	100.9	3.06	8.43	8.34	-
Mean		493		100.9	99.5		8.34	8.23	

¹⁾ Test values adjusted to a density base of $r_0 = 480 \text{ kg/m}^3$.

LD = Low density HD = High density



Diameter	M12						M20					
Rod-to grain angle	0°						0°					
Anchorage length	175 mm		140 mm		105 mm		275 mm		220 mm		175 mm	
Density	Low	High	Low	High	Low	High	Low	High	Low	High	Low	High

Figure: 6: Rods set parallel to the grain, test results: Mean value and span Min-Max

Rods M12 perpendicular to the grain

Rods M20 perpendicular to the grain

Type of specimen	Ind.	Density r_0 ¹⁾ [kg/m ³]	μ [%]	F_u [kN]	$F_{u,480}$ ⁴⁾ [kN]	$w(F_u)$ [mm]	f_v [N/mm ²]	$f_{v,480}$ ⁴⁾ [N/mm ²]
M12-90°-175-LD	q1L			65.5	70.3	11.29	8.51	9.13
M12-90°-175-LD	r1L			65.6	70.4	9.68	8.52	9.14
M12-90°-175-LD	s1L	362	12	65.8	70.6	9.52	8.55	9.18
M12-90°-175-LD	t1L			-	-	-	-	-
M12-90°-175-LD	u1L			-	-	-	-	-
Mean				65.6	70.4	-	8.53	9.15
M12-90°-175-LD	q1S			-	-	-	-	-
M12-90°-175-LD	r1S			-	-	-	-	-
M12-90°-175-LD	s1S	490	12	-	-	-	-	-
M12-90°-175-LD	t1S			-	-	-	-	-
M12-90°-175-LD	u1S			-	-	-	-	-
Mean				-	-	-	-	-
M12-90°-140-LD	u2L			55.8	59.8	4.36	9.06	9.71
M12-90°-140-LD	t2L			57.1	61.2	3.99	9.28	9.95
M12-90°-140-LD	s2L	363	12	60.1	64.4	5.03	9.75	10.5
M12-90°-140-LD	r2L			63.7	68.3	6.15	10.3	11.1
M12-90°-140-LD	q2L			59.2	63.5	4.45	9.62	10.3
Mean				59.2	63.5	-	9.61	10.3
M12-90°-140-HD	q2S			61.5	61.1	5.48	9.98	9.93
M12-90°-140-HD	r2S			62.8	62.4	5.46	10.2	10.1
M12-90°-140-HD	s2S	491	12	62.4	62.1	5.89	10.1	10.1
M12-90°-140-HD	t2S			64.7	64.3	7.33	10.5	10.4
M12-90°-140-HD	u2S			64.1	63.8	7.03	10.4	10.4
Mean				63.1	62.7	-	10.2	10.2
M12-90°-105-LD	u3L			48.2	51.5	3.66	10.4	11.2
M12-90°-105-LD	t3L			45.7	48.9	3.35	9.90	10.6
M12-90°-105-LD	s3L	367	12	43.5	46.5	3.22	9.42	10.1
M12-90°-105-LD	r3L			41.7	44.6	3.30	9.04	9.66
M12-90°-105-LD	q3L			43.4	46.4	3.51	9.39	10.0
Mean				44.5	47.6	-	9.64	10.3
M12-90°-105-HD	q3S			50.6	50.3	3.71	11.0	10.9
M12-90°-105-HD	r3S			47.2	46.9	3.71	10.2	10.2
M12-90°-105-HD	s3S	492	12	48.6	48.3	3.51	10.5	10.5
M12-90°-105-HD	t3S			49.0	48.7	3.96	10.6	10.5
M12-90°-105-HD	u3S			49.1	48.8	3.50	10.6	10.6
Mean				48.9	48.6	-	10.6	10.5

Type of specimen	Ind.	Density r_0 ¹⁾ [kg/m ³]	μ [%]	F_u [kN]	$F_{u,480}$ ⁴⁾ [kN]	$w(F_u)$ [mm]	f_v [N/mm ²]	$f_{v,480}$ ⁴⁾ [N/mm ²]
M20-90°-275-LD	R1L			146.4	156.0	6.34	7.70	8.21
M20-90°-275-LD	S1L	372	12	147.2	156.9	6.07	7.75	8.25
M20-90°-275-LD	T1L			143.8	153.3	6.58	7.57	8.06
Mean				145.8	155.4	-	7.67	8.18
M20-90°-275-HD	R1S			165.2	164.1	7.35	8.69	8.63
M20-90°-275-HD	S1S	493	12	163.3	162.2	7.06	8.59	8.53
M20-90°-275-HD	T1S			156.7	155.7	6.88	8.25	8.19
Mean				161.7	160.7	-	8.51	8.45
M20-90°-220-LD	R2L			123.4	131.9	5.47	8.12	8.67
M20-90°-220-LD	S2L	368	12	125.8	134.5	5.45	8.27	8.84
M20-90°-220-LD	T2L			125.4	134.0	5.24	8.25	8.81
Mean				124.9	133.4	-	8.21	8.78
M20-90°-220-HD	R2S			143.7	142.6	6.18	9.45	9.38
M20-90°-220-HD	S2S	495	12	136.5	135.5	5.65	8.98	8.91
M20-90°-220-HD	T2S			132.8	131.8	5.74	8.73	8.67
Mean				137.7	136.6	-	9.06	8.99
M20-90°-175-LD	R3L			117.1	125.3	4.96	9.68	10.4
M20-90°-175-LD	R3L	366	12	114.4	122.4	4.98	9.46	10.1
M20-90°-175-LD	T3L			112.6	120.5	4.95	9.31	9.96
Mean				114.7	122.7	-	9.48	10.1
M20-90°-175-HD	R3S			123.3	122.5	5.53	10.2	10.1
M20-90°-175-HD	S3S	492	12	117.6	116.8	4.96	9.72	9.66
M20-90°-175-HD	T3S			121.7	121.0	5.22	10.1	10.0
Mean				120.8	120.1	-	9.99	9.93

¹⁾ Only lamellas within the anchorage zone of the rods were considered.

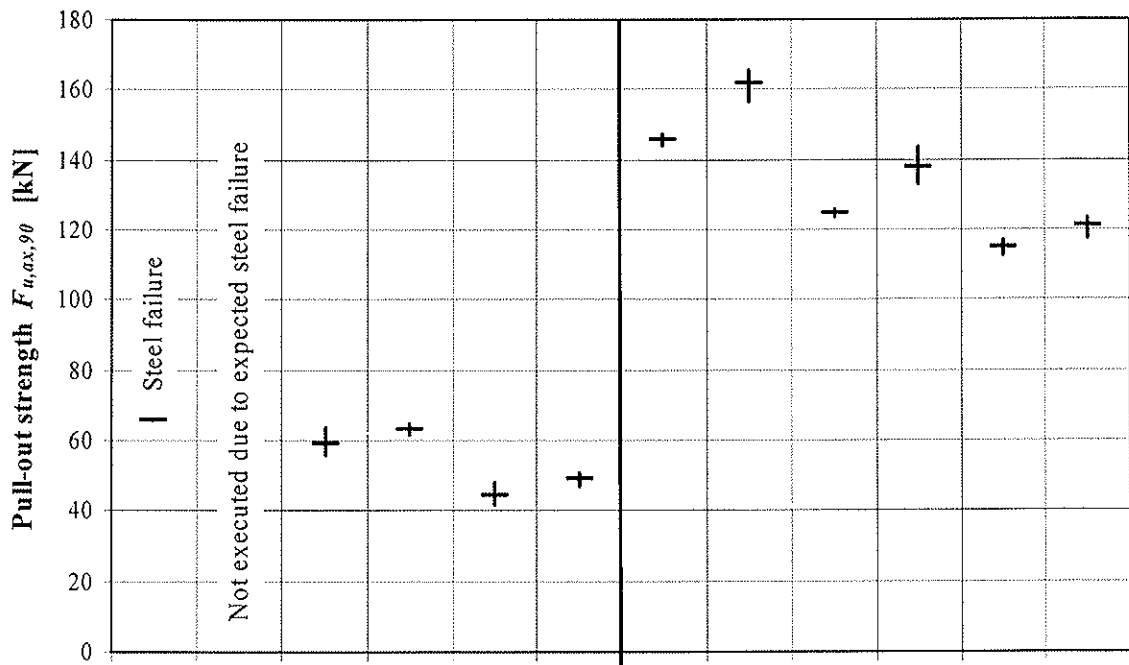
²⁾ Steel failure

³⁾ Not executed due to expected steel failure.

⁴⁾ Test values adjusted to a density base of $r_0 = 480 \text{ kg/m}^3$.

LD = Low density

HD = High density



Diameter	M12						M20					
Rod-to grain angle	90°											
Anchorage length	175 mm		140 mm		105 mm		275 mm		220 mm		175 mm	
Density	Low	High	Low	High	Low	High	Low	High	Low	High	Low	High

Figure 7: Rods set perpendicular to the grain, test results: Mean value and span Min-Max

INTERNATIONAL COUNCIL FOR RESEARCH AND INNOVATION
IN BUILDING AND CONSTRUCTION

WORKING COMMISSION W18 - TIMBER STRUCTURES

GLUED IN RODS IN LOAD BEARING TIMBER STRUCTURES -
STATUS REGARDING EUROPEAN STANDARDS FOR TEST PROCEDURES

B Källander

SP Swedish National Testing and Research Institute

SWEDEN

Presented by B Källander

C Clorius discussed with Källander about PRF and issues related to its ability to bond to steel.
H J Larsen commented about the basis for standardization through the CIB W18 and suggested that more test data should be developed as the CIB W18 group should focus on the evaluation of the test data.
H Blass commented screws can be effectively used in place of the glue-in-rods.

Glued in rods in load bearing timber structures - status regarding European standards for test procedures

Björn Källander

SP Swedish National Testing and Research Institute, Sweden

1 Background

Glued in rods is an efficient method to anchor, reinforce and join structural wood members and has been used in Nordic glulam factories for more than two decades. Rules to provide design values and quality control procedures for the glued in rod connection have been developed.

Glued in rods could be a tool to improve the competitiveness of wood as a structural material. However, the lack of common European rules is a serious hinder to the exploitation of the system, and there is an urgent need to develop European standards covering glued in rods.

1.1 Glued in rods not covered by Eurocode 5

Glued in rods are not covered by Eurocode 5 - Design of timber structures in its present state. Glued in rods were planned to be included in the coming prEN 1995-2 Eurocode 5 Part 2: Bridges and the second draft of prEN 1995-2 of February 21 2003 included an informative Annex C covering bonded in steel rods. However, TC 250 WG5 has decided to remove Annex C from the final drafts.

The decision to omit glued in rods from Part 2 will lead to a delay of at least 5 years before a European standard is set, since glued in rods cannot be included in Eurocode 5 before next time it is revised. The use of glued in rods will continue to rely on different national approval systems.

1.2 Example of a national product approval

Glued in rods have been used for approximately 30 years in the Nordic countries for joining and anchoring of glulam members. The system has primarily been used for short term loads such as wind loads rather than sustained loads. From originally having been made with PRF adhesives and threaded rods screwed into holes of slightly smaller diameter than the rods, it is now made with Epoxy adhesives and holes larger than the rod.

Choice of adhesives, design of the connection, production method and quality control systems are defined by the Swedish national type approval number 1396/78. The system specifies which adhesive is used, material and preparation of the threaded rod, how to drill the holes and how to mix and insert the adhesive in the holes prior to entering the rods. Two methods for internal quality control are allowed: either proof loading each rod to 80

% of the design load or producing separate test samples for destructive testing. Of the two methods, the latter is dominating due to practical difficulties to apply load to groups of rods. A third party monitors the internal quality control, making destructive testing of separate samples.

The long experience of glued in rods has shown that it is a safe and reliable method. So far (July 2004) no failures have been reported to SP Swedish National Testing and Research Institute.

1.3 Principle requirements for an adhesive for glued in rods

An adhesive for any load bearing purposes shall be approved after it is shown that it meets MINIMUM requirements. This is true about adhesives for fingerjoints, for glulam, for plywood and all other structural wood products. It is also true for glued in rods.

An adhesive for glued in rods needs to fulfil four requirements in addition to the requirements for a normal wood to wood adhesive:

- 1) The adhesive shall bond to the rod as well as wood.
- 2) The adhesive shall handle swelling and shrinking of the wood around the rod.
- 3) The adhesive shall handle varying bondline thickness, as the rod not is centered in the hole.
- 4) The adhesive shall bridge the different stiffness properties of the steel rod and the wood.

Also, since the adhesives that presently are used for glued in rods in Europe not are phenolic or aminoplastic, additional tests will be needed to determine creep properties and capability to withstand elevated temperatures.

1.3.1 Requirements based on proposed Eurocode 5 Part 2 Annex C

The now omitted Annex C specified basic requirements for glued in rod connections, requirements that could serve as basis for the development for test procedures and requirements for the adhesive as well as joints. The primary requirements were:

- 1) Annex C limited the use bonded in rods to structures in service class 1 and 2, which in turn sets limits for wood moisture content to 18 % and ambient service temperature to 50°C.
- 2) Annex C defined the rods as threaded or deformed bars, with a note stating that the durability of adhesion to smooth steel surfaces is not well known, and that the adhesion can be influenced negatively by for instance corrosion. This could be interpreted as that the glued in rod connection should not be dependent on adhesion to the rod, it should be safe also if the adhesive has reduced bonding to the steel.
- 3) Annex C required that "It should be verified that the properties of the adhesive and its bond to steel and wood are reliable during the lifetime of the structure within the temperature and moisture ranges envisaged. This requirement could be interpreted as the adhesive shall produce a durable bond to steel as well as to wood, and that adhesives that acts like a cast "nut" inwhich the bolt acts like a screw not is allowed. However, such an interpretaion is somewhat contradicted by the earlier requirement in 2).
- 4) Annex C states that the load carrying capacity of the joint should be limited by the rod, not by the adhesive, its bond to wood or steel, or the strength of the wood. This opens up for systems where for instance weakend zones of the rod are used to reduce its strength,

aiming at a ductile failure in the rod (as in the "GSA-system" studied by Steiger et al, 2004) rather than risking a brittle failure in the bondline or wood.

5) Annex C requires that it should be verified that the thickness of the bond layer is without remarkable influence on the deformation of the joint. This relatively vague requirement could limit the possibility to use adhesives with elastic properties to bridge the differences in stiffness between wood and steel.

6) Annex C stated minimum allowed anchorage length for the rods and characteristic shear strength values for the wood around the rod depending on anchorage length, rod and hole diameter. The minimum anchorage lengths should lead to the preferable ductile failure in the rod also without the weakened rod system.

2 Status of CEN standardisation for glued in rod adhesives

European standardisation is aiming at a three divided system covering glued in rods:

- TC250 Structural Eurocodes shall provide basic requirements and design criteria for the glued in rod connection,
- TC124 Timber structures shall provide methods for production control, and
- TC193 Adhesives shall provide requirements and test procedures for the adhesives to be used.

CEN/TC250/SC5 has taken out glued in rods from Eurocode 5 Part 2, and thus interrupted the preparation of basic requirements and design criteria of glued in rod connections. There is an urgent need to reinitiate such standardisation for the glued in rod connection in order to prepare supportive and complementary documents to the drafts being prepared by TC193/SC1/WG6 and WG11.

CEN/TC124/WG3 has concentrated its efforts on preparation of the harmonized European standard for glulam. TC124 has presently no working group aimed at glued in rods. It is therefore an urgent need to initiate such standardisation.

CEN/TC193/SC1 Wood adhesives has organized two Working Groups in connection to glued in rods, WG6 Adhesives for glued in rods in timber structures and WG11 Adhesives for on-site assembling or restoration of timber structures. WG6 develops a proposal for testing procedures and requirements for adhesives for glued in rods, aimed at adhesives for production under factory conditions. The parallel WG 11 is working on acceptance criteria for adhesives to be used for bonding on the building site.

2.1 Present status within WG6 Adhesives for glued in rods

The work within WG6 is primarily based on the results from the GIROD project. As intended by CEN, the proposed test methods for adhesives developed by GIROD WG2 (Bengtsson and Johansson, 2001) has been brought forward as proposed test methods.

However, within the group there has also been presented an alternative test procedure based on modifications of EN302-1 and EN 302-2 in combination with test procedures used in GIROD WP5 (Aicher, 2002). The alternative test procedure aims not only at determining if an adhesive is suitable for glued in rods, but shall also provide basis for determining design criteria for the glued in rod connection.

In addition to the alternative test procedure proposed, the need for test methods for elevated temperatures are being discussed. Although it has been clearly shown that the pull-out strength of glued in rods is reduced at elevated temperatures (Mischler and Frangi, 2001) it is not clear how high temperatures can be expected in the interior of a large wood member. Fire exposure tests on glulam have shown internal temperatures remaining low (50 °C) for prolonged periods during fire exposure (Källander and Lind, 2001).

Presently the work within WG6 has been stalled as the group is waiting for results from several ongoing studies.

2.2 Present status within WG11 Adhesives for on-site

The work in WG11 is presently primarily aimed at developing procedures for acceptance of adhesives on the building site and for quality control of the glued joint. Although primarily aimed at developing standards for adhesive approval, the application on-site has forced WG11 to also include the actual joint or product in the work, which actually could be seen as part of the work of TC124 as well as TC250.

Three methods for on site testing are discussed:

Method 1) Control of mixing of adhesive by means of measuring the temperature increase during curing of adhesive in a plastic cup, with possible compression testing of the cured adhesive added. The proposed method is now being evaluated by a round robin test (Document WG11: N20).

Method 2) Control of shear strength of the bondline and wood adjacent to the bondline. By gluing and shear testing of separate samples cut from the wood to be bonded, the shear strength of the bondline and the material bonded are determined (Document WG11: N21 and Pizzo et al, 2003).

3) Control of pull out strength by proof loading. Although proof loading could be a preferable method for on site quality control, it is often not possible to do due to the local circumstances (Document WG11: N22).

3 Proposed methods for approval of glued in rod adhesives

The system proposed within WG6 for approval of adhesives is based on short term shear testing of glued samples after climatic treatment and creep rupture testing in elevated temperatures. Two different test procedures have been proposed, the original one based on the methods for evaluation of adhesives developed in GIROD WP2 and one alternative procedure based on test procedures used to determine creep properties in GIROD WP5.

In addition to these it is possible that tests showing that the adhesive can cope with elevated temperatures need to be included (for instance during fire).

3.1 Original test procedure as proposed by GIROD WP2

The GIROD project Work Package 2 (WP2) proposed a system for approval of adhesives entirely based on testing of small samples of threaded steel rods glued into beech, see Figure 1.

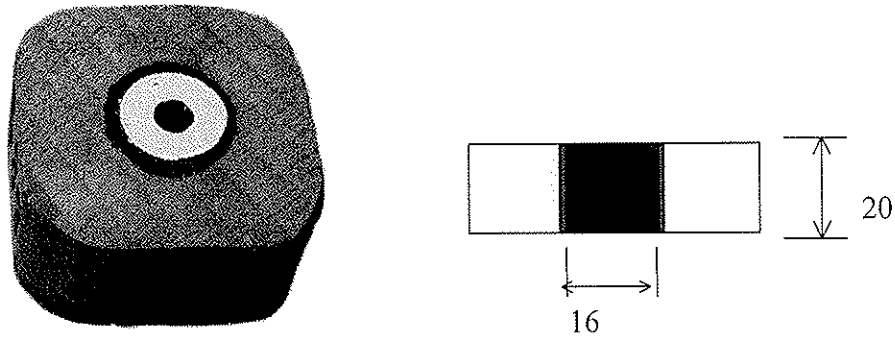


Figure 1. Samples for adhesive evaluation according to GIROD WP2.

The samples in Figure 1 are tested for shear strength after climatic treatment and creep rupture tested at elevated temperature. The proposed system from WP2 follows the established European principle to separate the approval of adhesives from the approval of the bonded product.

3.1.1 Shear testing of samples after climatic treatment

The small samples from Figure 1 are treated according to climates defined in EN 302-1. The samples are treated according to climatic cycle A1 (conditioned in 20 °C /65 % RH), A4 (Boiled 6 h, cooled in water 2 h and tested wet) and A5 (Boiled, cooled and reconditioned for 7 days before testing). Samples are tested in compression.

The results from GIROD WP2 show that the proposed test procedure is capable of differentiating between different adhesives types. The shear tests after climatic treatment show the ability of the adhesive to cope with varying bondline thickness as well as swelling and shrinking of the material. The test is also efficient in order to determine the ability of the adhesive to bond to the rod as adhesives not bonding to the rod will show severe reductions in shear strength after climatic treatment.

Adhesives that fail tests on the small samples also show poor results in the full size members.

3.1.2 Creep rupture testing at elevated temperature

Creep rupture test at 50 °C determines that the adhesive has acceptable creep properties at the upper temperature limit of Service Class 2. The creep rupture test is made on glued in rod samples according to a similar method as in ASTM D4680, see Figure 2.

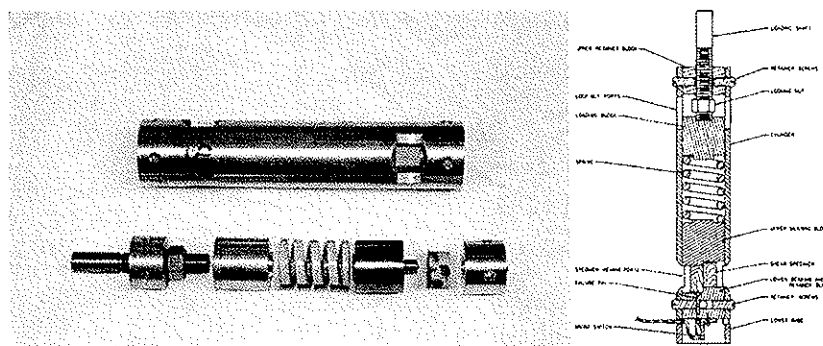


Figure 2. Test rig based on ASTM D4680 for creep rupture test of GIROD WP2 samples.

The samples are tested under constant load in compression at different load levels and the median time to failure is determined at each load. From the median times to failure, a prediction is made of the load corresponding to 10 000 h time to failure, see Figure 3.

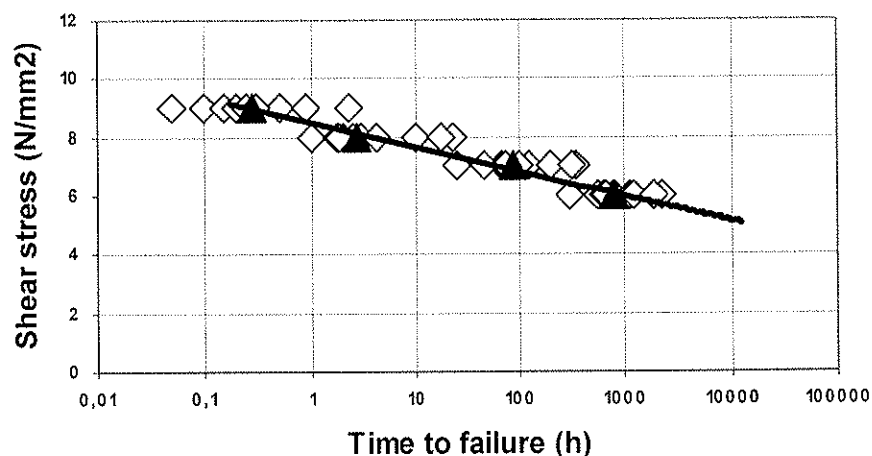


Figure 3. Prediction of load level corresponding to 10 000 h time to failure.

3.1.3 Advantages and disadvantages of GIROD WP2 test procedure

The test procedure according to GIROD WP2 has three major advantages:

- 1) The test methods have been evaluated and the results compared to tests on full size glued in members within the GIROD project.
- 2) It is relatively fast. A creep rupture test requires approximately 6 weeks testing time.
- 3) It does not require extensive investments in heavy testing equipment and the rigs needed can be used in any normally equipped testing facility. A complete set of 40 test rigs for creep rupture testing can be bought at a cost of approximately € 10 000.

The disadvantages are related to the simplicity of the procedure.

- 1) The test procedure is aimed at evaluating adhesives for glued in threaded steel rods, and it is questionable if the method can be applied to adhesives for use with for instance steel plates or glass fibre rods.
- 2) The simple test sample does not produce similar stress distribution as a bondline in a real glued in rod. The compression test of a short test sample will not show the same stress distribution as a longer rod tested in tension. However, this is also the principal case with other established European shear test methods such as for instance EN302-1.

3.2 Alternative test procedure based on GIROD WP5

An alternative test procedure based on GIROD WP5 has been proposed by Simon Aicher of FMFA. The test procedure is based on tests of glued samples made from wood and from steel after climatic treatment in combination with pull out tests and duration of load tests of full size glued in rods.

The proposal is based on the principle that the basic properties of the adhesives are studied to determine the adhesives ability to handle thick gulines between steel and wood, and after this has been done test a large specimen of glued in rod to determine the capability of the adhesive to cope with swelling, shrinking and sustained load.

3.2.1 Short term test of wood and steel samples

Test samples are glued with wood and steel to show the ability of the adhesive to adhere to both materials. Samples similar to EN 302-1 made with bondline thickness up to 4 mm are used. Samples are exposed to climatic treatment similar to EN 302-1 and tested in shear.

A delamination test according to principle in EN 302-2 is used with special samples made with 4 mm bondline thickness added.

3.2.2 Creep test of full size glued in rod samples

Full size glued in rod samples are produced with spruce and loaded with a cantilever system. The samples are stored in a cyclic climate alternating between 25 °C / 45 % RH and 55 °C / 12 % RH for a period of 6 months (or possibly 12 months).

3.2.3 Thermo mechanical test

In addition to the tests above, a thermo mechanical test is suggested for determination of glass transition temperature. Method to be used and requirements are yet to be determined.

3.2.4 Advantages and disadvantages of the alternative test procedure

The two primary advantages of the alternative test procedure are:

- 1) Separate testing of the ability of the adhesive to bond to wood as well as to steel makes the test more universal as compared to testing of a small sample of glued in threaded rod. The alternative test procedure could thus be possible to modify for testing adhesives for other material combinations and / or geometries.
- 2) Testing of full size members of rods glued into spruce wood could lead to a test more closely resembling the stress distribution present in a glued in rod connection.

The primary drawbacks are related to the constant load test.

- 1) It has not been shown that the test procedure actually tests the adhesive. The size of the spruce wood members in combination with the relatively short climatic cycle could lead to the test actually being a creep test for wood rather than a test of adhesives.
- 2) Basic test procedure data as variety, accuracy and repeatability of the test method are not verified. Before this test procedure can be implemented, substantial efforts are required to determine such data.
- 3) The test procedure requires a large climate chamber capable of alternating between two climates, 25°C/45%RH and 55°C/12%RH. The alternating climate makes it impossible to use climate chambers operating at constant climate, and hence it is necessary to use a separate chamber for the glued in rod test. Test rigs and test cabinet big enough to do two parallel tests requires an investment of approximately €160 000.

3.3 Discussion regarding the two proposed test procedures

A key issue regarding the choice of test procedure is the actual purpose of the test, which in this case is to qualify or disqualify an adhesive for use with glued in rods.

An adhesive shall be approved if it is shown that it has properties that will produce a safe and durable joint between the glued in rod and the wood material.

Both of the two proposed test procedures will be capable of selecting adhesives that will provide such safe and durable joints. The original test procedure developed in GIROD WP2 is presently in a state where it on a short time scale can be sent out for public enquiry. A well-defined test procedure and requirements for approval based on results from the GIROD project have been proposed. The alternative test procedure has presently only been presented orally and a fixed test procedure and a proposal for requirements are yet to be presented. Before such an alternative test procedure can be implemented, possibly several years of studies will be required.

A choice between the two test procedures should be based on an evaluation if the additional information provided by the alternative test procedure motivates the longer test period, the higher cost of the test and the delay of a European standard that will follow if the alternative test procedure is selected.

A principal issue is whether it is suitable that a test procedure for approval of adhesives is designed to also provide design values for the glued in rod joint. Such an approach could lead to the development of different design values for glued in rods depending on the choice of adhesive. Such a development could theoretically be beneficial in order to maximize the load carrying capacity of a specific glued in rod connection, but would more likely lead to confusion and a serious risk for mixup between allowed loads for a certain joint design.

When adhesives are tested for approval of wood-to-wood bonding in load bearing structures, the test and approval of the adhesives are clearly separated from the load bearing structure. The European standards EN301 and EN302 specifies requirements and testing procedures for adhesives that use test samples and test procedures that have very little resemblance to the actual loads or climates that the final wood structure will face. The adhesive is approved as it is shown that it is capable of resisting severe climate conditions and loads, but it is clearly not tested to show how it actually performs in the final structure. A similar approach is used in for instance ASTM D2559.

By combining the approval of the adhesive with evaluation of the glued in rod design as in the alternative test procedure, a relatively simple task of determining that an adhesive meets minimum requirements is mixed with a much more complicated task of evaluating an entire joint. As in the tests described by Steiger et al, 2004, the results of the proposed method would thus be limited to the actual rod connection design, the test would provide dimensional criteria for a specific glued in rod design but not for other rods or materials.

An advantage for the alternative test procedure is that it separates the bonding to the rod material from effects of gluline thickness and reactions to swelling and shrinkage in the short term tests. This could make it suitable also for evaluation of adhesives intended for gluing in of other materials as well as geometries. The WP2 procedure combines the effects above in the testing of specified small samples of threaded rods glued into beech. However, at the moment there are no tests reported to show how such tests should be correlated to the performance of larger samples or longer periods, or how different adhesive types react to the tests. Before such an approach could be made, it would be necessary to perform extensive tests on different types of adhesives in order to establish proper test procedures and requirement levels. Although preferable in a longer time frame, presently it would lead to further delays of the standardisation process if such an approach would be used.

The GIROD WP2 test procedure was developed solely for approval testing of adhesives for threaded or deformed steel rods glued in under factory conditions. The test procedure was designed to determine that an adhesive is good enough for this specific purpose.

Although it has several drawbacks, it is a fast and cheap test procedure that is ready to be implemented. A possible way forward would be to implement the test procedure of WP2 and later, as new test results are made available, replace it with a more advanced procedure designed for gluing in of different materials as well as geometries.

4 Conclusions

There is an urgent need for European standards covering glued in rods in load bearing wooden components. Standards are needed for approval of adhesives, design and calculation of joint properties as well as for quality control of the glued in rod connection.

The exclusion of glued in rods from Eurocode 5 Part 2 has made it necessary to once again initiate the development of European standards for basic requirements and design criteria for glued in rods. At the same time there is an urgent need to initiate standardisation of production and production control of glued in rods.

A proposal for European standards for testing procedures and requirements for the adhesives used for glued in rods is being prepared by CEN/TC193/SC1/WG6. The work on the proposal is currently stalled due to an alternative test procedure being proposed.

It is recommended that the original test procedure developed within GIROD WP2 shall be used to provide a European standard for approval of adhesives intended for gluing in threaded or deformed steel rods under factory conditions. The GIROD WP2 test procedure is aimed at determining that an adhesive fulfils minimum criteria for such use. The procedure requires approximately 6 weeks testing and can be made at relatively low cost.

A standard based on GIROD WP2 could later be replaced by a more general test procedure suitable also for approval of adhesives for on site bonding, bonding of other materials as well as bonding of other geometries.

5 Literature

Aicher, Simon. Presentation of proposed test procedure at WG6 meeting at FMPA. Stuttgart, 2002.

Bengtsson, Charlotte and Johansson, Carl-Johan. GIROD - Glued in rods for timber structures. Proceedings. CIB W18, Venice 2001.

Bengtsson, Charlotte and Johansson, Carl-Johan. GIROD - Glued In Rods for Timber Structures SP-Report 2002-26. Borås, 2002.

Källander, Björn and Lind, Per. Strength properties of wood adhesives after exposure to fire. SP Report 2001:35, Borås 2001

Mischler, Adrian and Frangi, Andreas. Pull-out tests on glued-in rods at high temperatures. Proceedings. CIB W18, Venice, 2001.

Pizzo, B. et al. Measuring the shear strength ratio of glued joints within the same specimen. Holz als Roh und W. 61 (2003) 273-280.

Steiger, R. Gehri, E. and Widmann, R. Influence of timber density, rod-to-grain angle (0° and 90 °C), diameter and length on the pull-out strength of single, axially loaded steel rods with a metric screw-thread bonded in glulam elements. Proceedings. CIB W18, Edinburgh, 2004.

Swedish national product approval Typpgodkännandebevis 1396/78. Swedish Institute for Technical Approval in Construction. Borås, 1999. Document CEN/TC193/SC1/WG6: N18. Minutes and resolutions of the third meeting in Stuttgart 2002-10-22

Document CEN/TC193/SC1/WG6: N21. Minutes and resolutions of the 4th meeting in Paris 2003-07-28

Document CEN/TC193/SC1/WG11: N20. Adhesives for on-site assembling or restoration of timber structures. On site acceptance testing. Part 1: Sampling and measurement of the adhesives cure schedule.

Document CEN/TC193/SC1/WG11: N21. Adhesives for on-site assembling or restoration of timber structures. On site acceptance testing. Part 2: Verification of the adhesive joints shear strength.

Document CEN/TC193/SC1/WG11: N22. Adhesives for on-site assembling or restoration of timber structures. On site acceptance testing. Part 3: Verification of the adhesive bond strength using tensile proof-loading.

Document CEN/TC250/SC5:N197. prEN 1995-2 Eurocode 5 - Design of timber structures. Part 2: Bridges. Draft 21 February 2003.

INTERNATIONAL COUNCIL FOR RESEARCH AND INNOVATION
IN BUILDING AND CONSTRUCTION

WORKING COMMISSION W18 - TIMBER STRUCTURES

FRENCH DATA CONCERNING GLUED-IN RODS

C Faye

L Le Magorou

CTBA

P Morlier

J Surleau

LRBB

FRANCE

Presented by F Rouger

H Blass asked about the glass transition temperature of the glue T_g . Rouger answered that it was about 50 C and stated that some adhesive with higher T_g can be found.

H Blass asked whether the rods were protruding through the timber in the FEM calculations. Rouger answered that even if the rod were completely covered the same conclusion would be obtained.

P Glos questioned the validity of the temperature model because the model predicted that it took 5 hr for the surface of the wood to reach ambient temperature. It seemed much too slow from his experience. Rouger answered that this is a convection problem and the temperature of the glue line was the main issue. Rouger further clarified that the timber cover to the glue line was 4 cm.

M Ansell commented that room temperature cured epoxy tended to have low T_g and epoxy with high T_g needed to be heated up.

E Karacabeyli asked about the difference between the two DOL models and commented that the DOL factor for the 10 years loading is 0.5. Rouger answered that the difference of threshold level may be the issue.

P Glos noted that there was no moisture effect and suggested that if wood failure was observed then moisture effect should be present. J W van de Kuilen commented that the stress level was related to the short term strength at the respective moisture conditions and therefore masking the moisture effect.

B Källander commented that T_g is more a theoretical measure and one would not know the real characteristic based on T_g . Also high T_g adhesives are available but creep may be an issue with these adhesives. Rouger responded that the short term specimen test results provided the relation between T_g and properties.

J Köhler commented that the stress ratio used in DOL study depended on the equal rank assumption therefore small sample size can lead to errors.

M Ansell commented on the DSC analysis and T_g and that glueline thickness might have been an issue.

P Glos received clarification that the sample size was 10 specimens per series.

French data concerning glued-in rods

Carole Faye, Laurent Le Magorou - CTBA, France

Pierre Morlier, Juliette Surleau - LRBB, France

1 French Professional Guide for Glued-in Rods

French Professional Guide entitled 'Guide professionnel - Assemblages bois: tiges ou goujons collés de grandes dimensions' was published in 1999.

It contains (in 40 pages) the following topics:

- description of the glued-in rod technology,
- specifications and mechanical requirements for wood, adhesives and rods used for this technology,
- spacing rules between rods and between rods and timber edge for axial and lateral load,
- design rules for glued-in rods parallel or perpendicular to the grain and axially loaded,
- design rules for glued-in rods parallel or perpendicular to the grain and laterally loaded,
- rules for glued-in rod production,
- constructive dispositions.

But, in France, the use of glued-in rods in building constructions is limited because:

- there is no evaluating adhesive method for glued-in rod technology,
- there is no production control test method,
- and there is no knowledge on long term behaviour on this technology.

So, a national research project (2002-2004) is carrying out in collaboration between CTBA, LRBB and the French Glued laminated Timber Syndicate to provide the knowledge required to elaborate these documents.

The main works of the national project are:

- short and long term tests on full size specimen,
- short term and long term tests on small pieces,
- development of finite element model to describe mechanical behaviour including temperature and moisture content evolution into glued-in rods specimen submitted to natural temperature variations.

Two commercial adhesives are tested:

- a two-components Epoxy named Mastifix from Rénoantic S. A. ,
- a two-components CR 421 from Prubond.

For all experiments of the national project:

- specimen are tested in axial load with rods glued parallel to the grain,
- GL24 wood quality with 12 mm threaded rod was used (chosen by glued laminated producers),
- spacing rules between rods and between rods and timber edge for axial and lateral load was the one specified in the French Guide,
- specimen manufacturing was made by glued laminated producers according to production rules given by adhesives producers.

In this paper, only results concerning Epoxy Mastifix are presented.

Additional short term tests on full size specimen with GL24, with 16 mm threaded rod, with the same Epoxy Mastifix, performed for three loading configurations :

- axial load with rods glued parallel to the grain,
- axial load with rods glued perpendicular to the grain,
- axial load with rods glued with a slope of 45° to the grain,

are presented.

These tests were financed by **Simonin and Fargeot** Societies, French glued laminated producers.

2 Instantaneous mechanical behaviour

2.1 Experimental results on axial loads with rods glued parallel to the grain on full size specimen

For axial load configuration, minimum distance rules are given in figure 1.

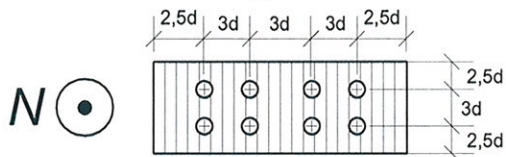


Figure 1: distance rules for axial load with rods glued parallel to the grain (d =rod diameter).

Four experiments series (S1, S2, S3, S4) in pure tension (cf. figure 3) were performed for different geometrical configurations.



Figure 2: failure mode for axial load

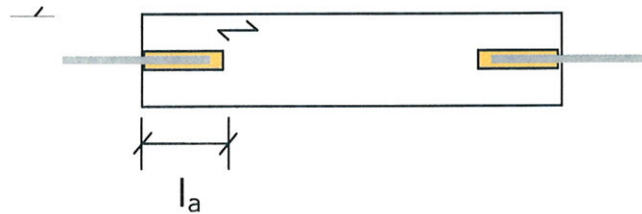


Figure 3 : tension specimen geometry

Two additional test series (S5 and S6) in four point bending (cf. figure 4) were performed respectively for two moisture contents of wood (12% et 20%).

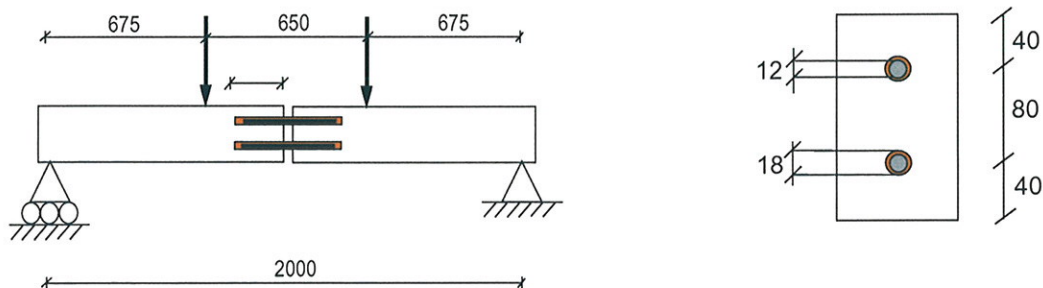


Figure 4: bending specimen geometry and load configuration.

Load capacity values, geometrical parameters for the 6 series and comparison with design rules are presented in table 1.

For series 5 and 6, values on the table 1 correspond to load capacity for **one rod**.

Failure modes are identical for the 6 series: failures occur in the wood in shear, an entire cylinder composed of rod covered by adhesive and wood is pulled out (cf. figure 2).

	Series 1	Series 2	Series 3	Series 4	Series 5	Series 6
Moisture content (%)	12	16	16	16	13	22
Load type	tension	tension	tension	tension	bending	bending
Nb of Specimens	10	5	10	5	10	10
l_a (mm)	210	200	300	400	210	210
d_{rod} (mm)	12	16	16	16	12	12
d_{hole} (mm)	18	22	22	22	18	18
Experimental load (kN)						
Average Value	65.8	81.2	103	114	65.6	61.3
COV	9.2	9.6	13	10	10.5	7
*Characteristic value $F_{ax, k}$	53.9	64.1	76.7	88.6	52	52.7
Rule 1: French Rule (kN)						
Characteristic value $R1_{ax, k}$	38.2	48.7	61	71.2		
$F_{ax, k} \setminus R1_{ax, k}$	1.41	1.31	1.25	1.24		
Rule 2: Adjusted Rule (kN) with $d=d_{hole}$						
Characteristic value $R2_{ax, k}$	52.7	61.8	76.3	88.1		
$F_{ax, k} \setminus R2_{ax, k}$	1.02	1.05	1.01	1.01		
Rule 3: PrEN 1995, part 2 Rule(kN)						
Characteristic value $R3_{ax, k}$	39.8	53.9	68.8	77		
$F_{ax, k} \setminus R3_{ax, k}$	1.35	1.19	1.11	1.15		

Table 1 : experimental series for GL24 beams with the Epoxy Mastifix and comparison with design rules.

**Load capacity characteristic values are calculated according the EN 14358 standing.*

Comparison between load capacity values of series 1 and 5 shows that bending tests are representative of tension ones. So long term tests will be performed in bending and series 5 will be the reference tests for the determination of long term stress level.

Results on series 6 show that load capacity average value decreases when moisture content increases. Characteristic values remain unchanged.

Comparison between design rules and experimental values shows that design Rules 1 and 3 are conservative.

For Epoxy Mastifix, specified adjusted rule is proposed in Rule 2.

Rule 1: French rules - 1999, according to RIBERHOLT's formulation

$$P_{f,k} = 85 f_{v,k} d \sqrt{l_c} \quad \text{with } l_a > 17,5d \quad d = d_{rod} \text{ in mm} \quad l_c = l_a - 1,5d \text{ en mm}$$

$f_{v,k}$ characteristic shear strength of wood, $f_{v,k}=2,7 \text{ MPa}$

Rule 2: Adjusted Rule according Rule 1 for Epoxy Mastifix

$$P_{f,k} = 104 f_{v,k} d l_c^{0,45} \quad \text{with } l_a > 17,5d \quad d = d_{hole} \text{ in mm} \quad l_c = l_a - 1,5d \text{ en mm}$$

$f_{v,k}$ characteristic shear strength of wood, $f_{v,k}=2,7 \text{ MPa}$

Rule 3: draft prEN 1995, part 2 Bridges - 2003, according to GUSTAFSSON's formulation

$$P_{f,k} = \pi d_{equ} l_a f_{ax,k} \frac{\tanh \omega}{\omega} \quad \text{where : } \omega = \frac{0,016 l_a}{\sqrt{d_{rod}}} \quad d_{equ} \text{ (mm)} = \text{minimum} (d_{hole}, 1,15 d_{rod})$$

$f_{ax,k} = 5,5 \text{ MPa}$

2.2 Experimental results on axial loads with rods glued perpendicular to the grain and with a slope of 45° to the grain

Two additional series (S7 and S8) were performed on axial loads but with rods glued perpendicular to the grain and with a slope of 45° to the grain.

For axial loads with rods glued perpendicular to the grain configuration, minimum distance rules are given in figure 5.

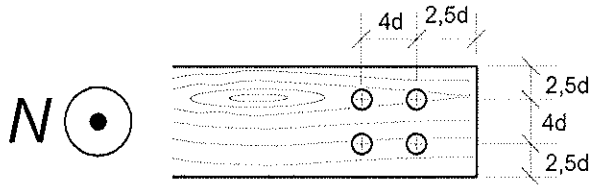


Figure 5: distance rules for axial load with rods glued perpendicular to the grain (d =rod diameter).

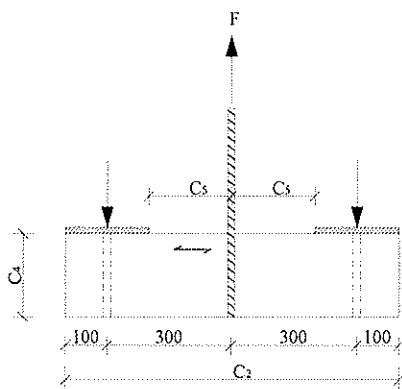


Figure 6 : test for axial load with rods perpendicular to the grain ($C4=200 \text{ mm}$, $C3=80 \text{ mm}$).

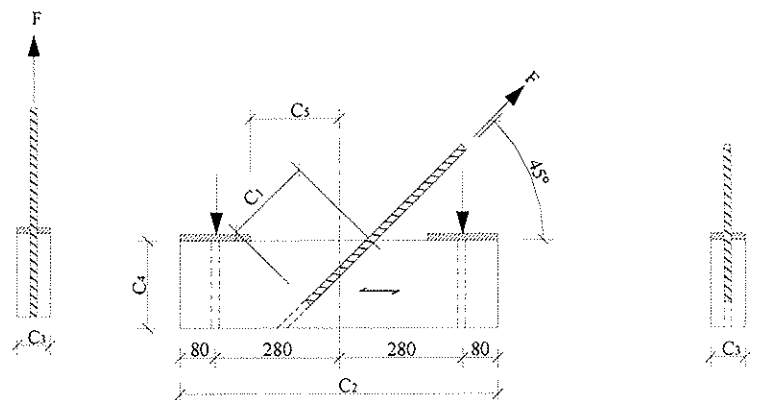


Figure 7 : test for axial load with rods with a 45° slope to the grain ($C3=80 \text{ mm}$, $C4=C1=200 \text{ mm}$).

	Series 7	Series 8
Moisture content (%)	12	12
Load type	Tension Perpendicular to the grain	Tension With a 45° slope
Number of Specimens	5	5
l_a (mm)	200	200
d_{rod} (mm)	16	16
d_{hole} (mm)	22	22
Experimental load (kN)		
Average Value	89.6	80.3
COV	6	10
*Characteristic value	76.6	63.4

*Table 2 : experimental series for GL24 beams with the Epoxy Mastifix . *Load capacity characteristic values are calculated according the EN 14358 standing.*

As expected, strength for rods glued perpendicular to the grain (cf. table 2) is higher than for rods parallel to the grain.

For these 2 load configurations, French guide Rule is also Rule 1 so French guide remains conservative.

3 Duration of load tests on full size glued-in rod specimens

Long term tests were performed in bending according to specimen geometry and load configuration shown in figure 4. Four point bending set-up are shown on Figure 8. Load is applied by air pressure jack and central deflection is measured by a potentiometric gauge. During GIROD program, different stress levels were tested: 70% was considered as low and 80% as high.

For our study, we suggested to keep constant a 75% average stress level in order to obtain failures within 3 months. Reference tests are Series 5 and 6.

Experimental results analysis is made according to the twin sample method with a ranking due to Madsen.



Figure 8: experimental set up for Duration Of Load tests

Long term tests, presented in this paper, are at constant Moisture Content (12% or 20%). After conditioning specimens at the targeted Moisture Content, they were covered by a plastic film to avoid humidity transfer with the external air and specimen were loaded in outdoor conditions, under shelter.

A long term tests series with 22 specimens (eleven at 12% MC, eleven at 20%MC) were carried out.

By matching strength of Series 5 and 6 (if a uniform strength coefficient of 1.07 is applied to specimens at 20% MC), we obtain the reference cumulative distribution of strength (cf. Figure 9), modelled by a two parameter Weibull law

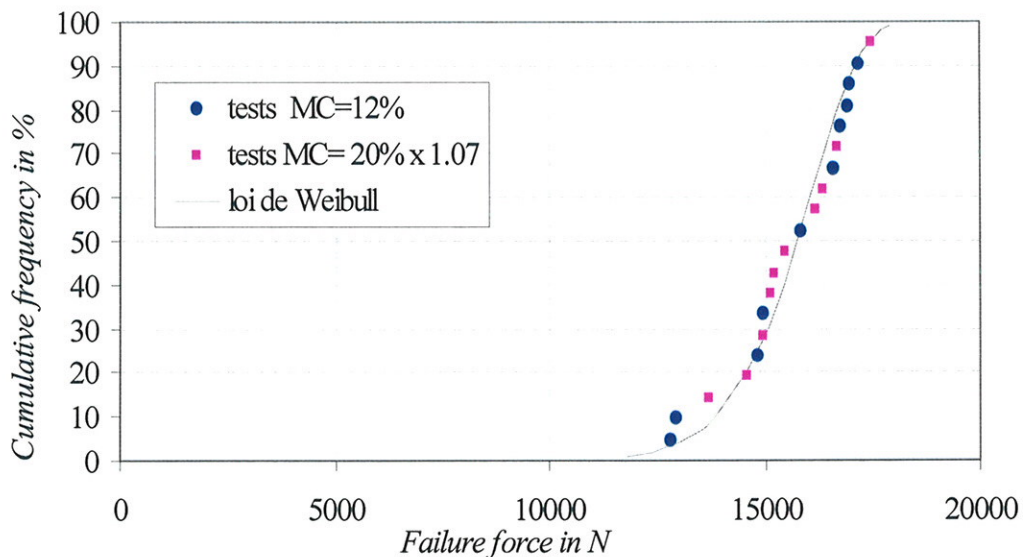


Figure 9: view of general short term bending tests results.

For the DOL experiments, all specimens are loaded at 75% of the average reference strength with a sustained pressure; four specimens prematurely broke during this loading and the test is stopped after the failure of 11 specimens.

Figure 10 illustrates the mode of failure by shear at the interface adhesive/wood.



Figure 10: Failure by pull-out of rod and adhesive together

The ranking method consists in the calculation of the stress level for each specimen: the i^{th} long term failure is associated with an assumed strength corresponding to the i^{th} resistance of the reference distribution (Figure 9).

The 11 long term failure are finally represented on Figure 11 together with the MADISON curve, the best fitting to a Gerhards model, the best fitting to a Barrett and Foschi 2nd model (these models are described in MORLIER and al [1994]).

For a load applied during 10 years, reduction coefficient strength is $k_{dol}=0.73$ with Barrett and Foschi model II and $k_{dol}=0.56$ with Gerhards models.

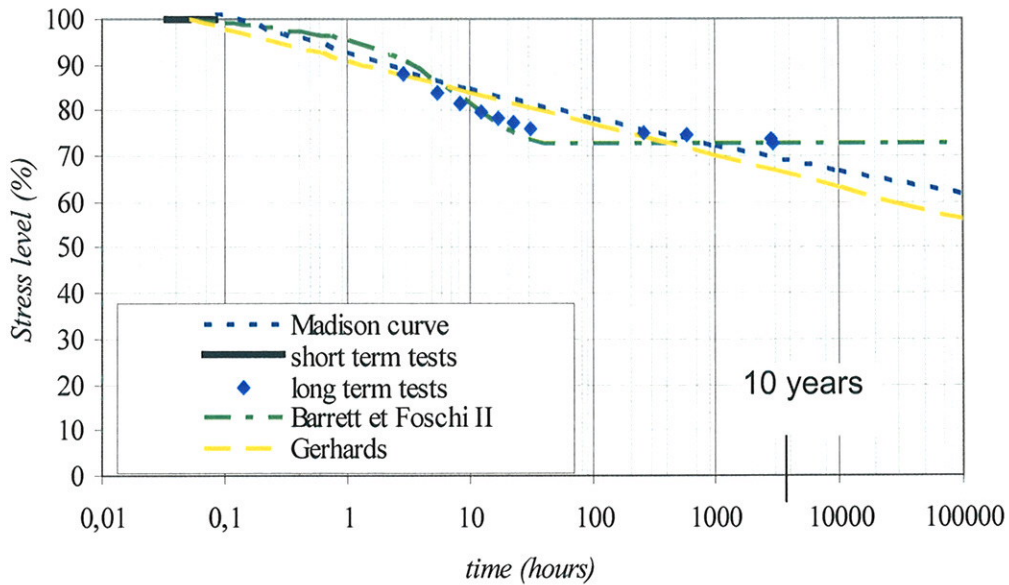


Figure 11: Duration Of Load representation by ranking.

It is clear that the DOL results for glued-in rods are very near from the Madison curve which is approximated in EC5 for glulam in bending: this conclusion was already given in GIROD program.

Those results were obtained for constant Moisture Content but tests are now running with uncovered specimens in outdoor conditions.

The 7 surviving specimens were broken in short term experiments immediately after unloading. Results are presented on Figure 12 according to a representation suggested by MADSEN.

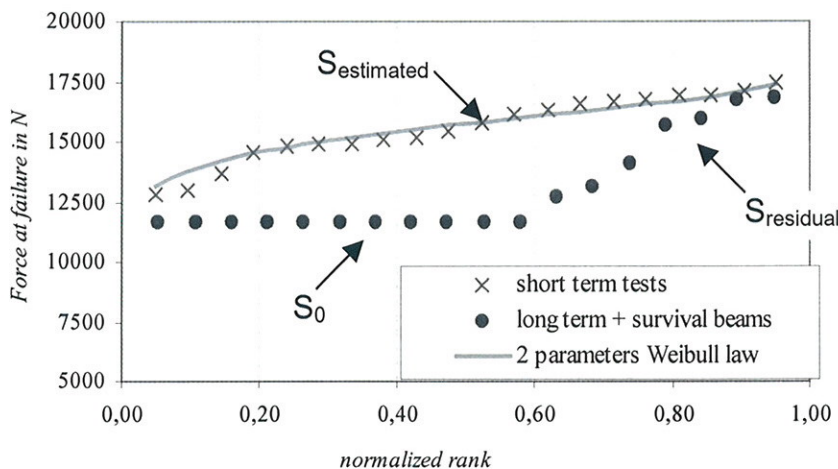


Figure 12: Madsen's representation of the residual strength of surviving specimens

Table 3 gives the results of an estimation of the damage parameter α by:

$$\alpha = \frac{(S_{estimated} - S_0) - (S_{residual} - S_0)}{S_{estimated} - S_0}$$

where:

- S_0 is the sustained load during the DOL experiment,
- $S_{estimated}$ is the strength estimated from Figure 8,
- $S_{residual}$ is the strength obtained by a short term test immediately after DOL experiment.

	Stress level %	Damage parameter α
1	72	0,75
2	72	0,67
3	71	0,48
4	70	0,19
5	69	0,06
6	68	0,05
7	67	0,09

Table 3: damage assessment with α parameter

When the actual stress level is lower than 70%, there is no damage after a 3 month constant loading in glued in rods connection.

4 Duration of load tests on small pieces

The aim of this task is to show that duration of load on structural pieces can be explained by duration of load results on small pieces. This will allow to perform tests only on small pieces in the evaluating adhesive method.

So, short term and long term tests have been performed on small specimens represented on the Figure 13.

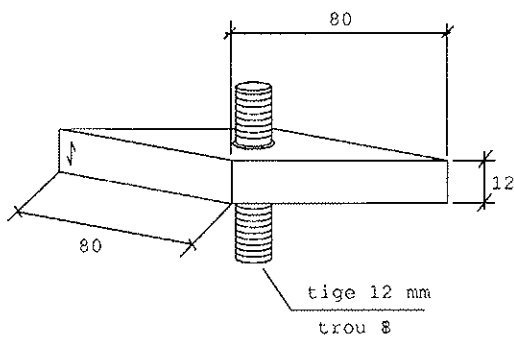


Figure 13: small specimen geometry

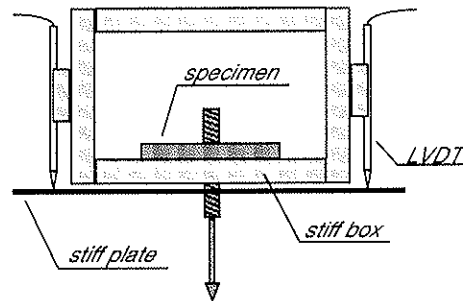


Figure 14: experiment set-up

Local joints is placed in a drilled box (presented Figure 14) and a traction force pull-out the rod and adhesive cylinder. This is the way to obtain a reference force allowing us to start DOL tests on small specimens.



Figure 15: long term experiment set-up for small specimen

Long term tests on small species are currently carried out on eleven tension rigs (Figure 15).

First experimental results on small pieces with structural ones, presented in Figure 16, show that duration of load in constant climate seems close.

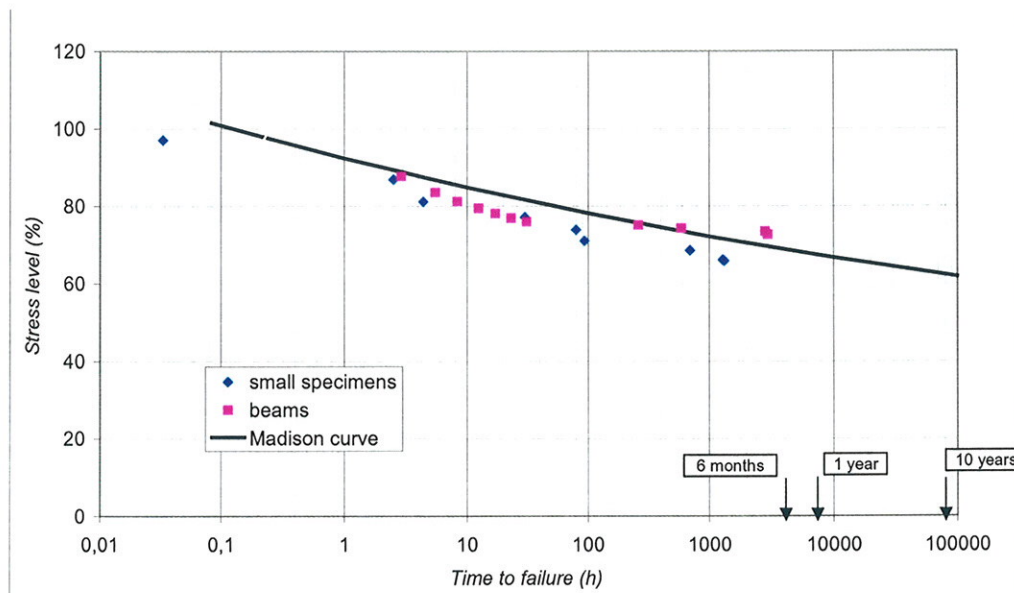


Figure 16: DOL on small pieces and structural beams.

5 Effect of temperature

Destructive compressive tests on cylindrical rods of cured adhesive have been carried out to determine glass transition temperature.

The glass temperature T_g is defined as the temperature of the inflection point (cf. figure 17). The T_g experimental value was $63,4^\circ\text{C}$ for the Mastifix adhesive .

Using a DSC method, T_g was evaluated at 66°C .

The required value established by WG6 and WG11 European Work Group (CEN/TC 193) is 60°C (but supposed to be 55°C in future).

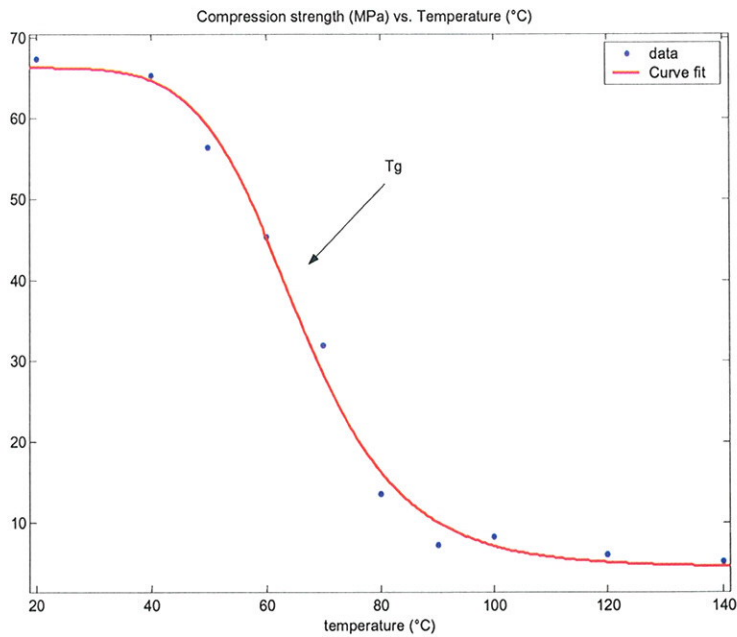


Figure 17 : Compressive strength of cylindrical rods ($\phi=30$ mm, $h=40$ mm) of cured adhesive.

As shown in figure 18, adhesive temperature in interface wood/rod can reach ambient temperature with a delay of 4 or 5 hours (for cross section of 80×160 mm²). These values are simulated by finite element approach.

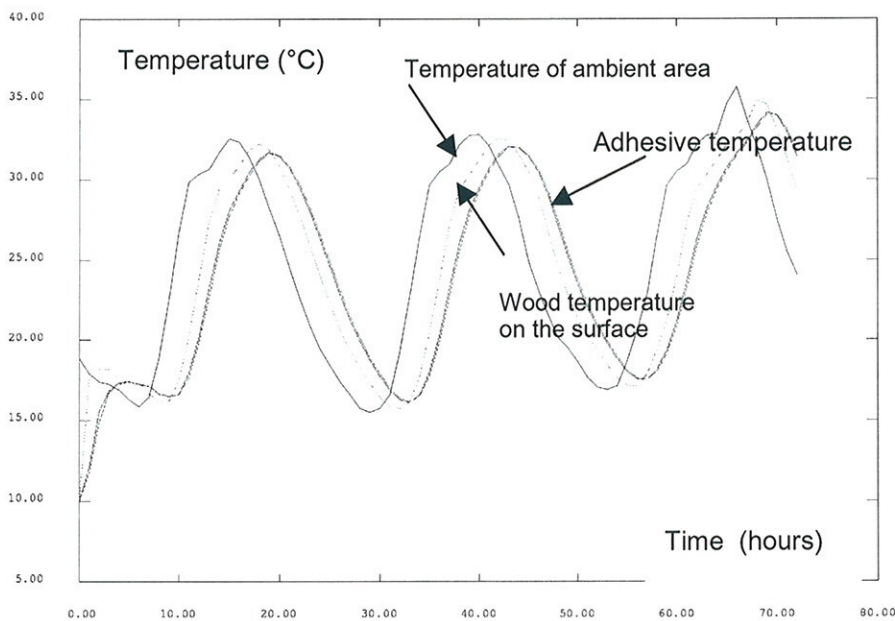


Figure 18: adhesive in the interface and ambient temperatures evolutions during 3 summer days.

Then, to study temperature influence on the connection strength, mechanical tests on small pieces (cf. figures 13 and 14) are currently carried out.

For different temperatures between 20°C and 120°C, small pieces will be loaded in axial direction with rods glued parallel to the grain until failure.

6 Conclusion

Step I of evaluating adhesive method consists on the same tests than Series 3. The required value are given by the Rule 1.

To optimise design rule of glued-in-Rod connections, additional tests like series 3, 4 , 6 and 7 must be done.

If correspondence between DOL small pieces and structural specimen is establish, **Step II of evaluating adhesive method** will consist on short term and long term tests on small species, to evaluate the duration of load of the glued-in-rods connection.

Step III of evaluating adhesive method corresponds to transition temperature determination of the evaluated adhesive.

INTERNATIONAL COUNCIL FOR RESEARCH AND INNOVATION
IN BUILDING AND CONSTRUCTION

WORKING COMMISSION W18 - TIMBER STRUCTURES

ENHANCEMENT OF DOWEL-TYPE FASTENERS BY GLUED CONNECTORS

C O Clorius

A Højman

Department of Civil Engineering, Technical University of Denmark

DENMARK

Presented by C Clorius

Clorius provided clarification that the embedment strength of the steel plate was $\frac{1}{2}$ of the ultimate strength according to Euro Code 3, the fasteners were dowels not bolts, and there were no slippage problems.

Enhancement of Dowel-Type Fasteners by Glued Connectors

C. O. Clorius and A. Højman

Department of Civil Engineering, Technical University of Denmark

Abstract

For the application in a specific case a double-shear dowel-type connection with side glued steel plates were developed and tested. The side-glued steel plates act as single-sided connectors, thus both enhancing the embedment strength and preventing premature wood splitting failure. The tested connection showed approximately three times larger load bearing capacity and approximately two times larger slip modulus when tested according to (EN 26891 1993) and compared to non-reinforced but otherwise similar connection. Variation to dowel material and enhancement has been made covering two steel grades and two steel plate thicknesses. For the comparison with more common connector enhancements test similar to those laid forward in (Blaß, Schmidt & Werner 2001) are presented.

The compliance of the experimental strength and stiffness values with the general principles of (prEN 1995-1-1 2003) is shown and a design rule for fastener enhancement by glued-steel plates based on the general yield-theory is proposed.

1 Background

In a large full scale test of a 200 dowel connection with 4 slotted in steel plates a load application joint was needed. The design restrictions were the "usual": A cheap, compact, joint design that were strong, stiff, easy to manufacture and did not suffer for premature splitting was needed.

Though very specific in history, the design restrictions seems to be "universal". The reported design is by no means original, the design just combines known methods that is, something glued to the side of the wood member preventing splitting and something strong and stiff at the surface enhancing the embedment performance of the wood. Hence, the results laid forward cannot surprise the reader familiar with the effects of connectors and glass fibre reinforcement. However, the success of the application of the design, briefly reported in an *Post Scriptum*, does question the practice of slotted in steel plates and dowels so widely used.

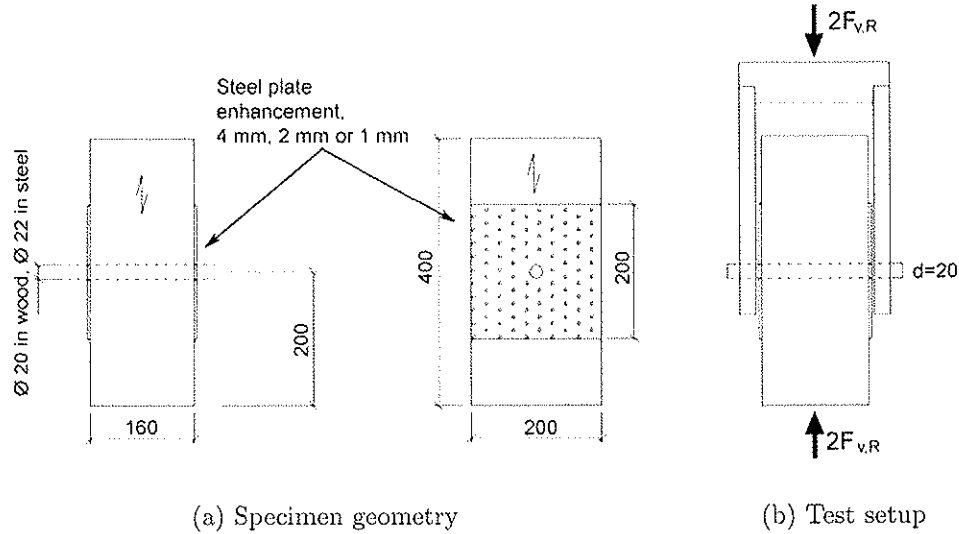


Figure 1: Specimen design and test setup, measures in mm.

Side enhancement	No. with S460 dowels	No. with CrNi dowels	Acronym
Non-enhanced plain design	3	3	Plain-S460/Plain-CrNi
Pressed 1 mm tooth plate		3	Pr-t1-CrNi
Epoxy glued 1 mm tooth plate		3	Gl-t1-CrNi
Epoxy glued 2 mm steel plate		3	Gl-t2-CrNi
Epoxy glued 4 mm steel plate	3	3	Gl-t4-S460/Gl-t4-CrNi

Table 1: Material combinations and number of specimens tested at each combination.

2 Material and method

2.1 Specimen and test method

The test specimens were symmetrical double shear connections with single dowels loaded in the grain direction and an overall geometry as shown in Figure 1(a). The wood was GL30h (*Picea abies*) and three different types of side enhancements were used according to the data given in Table 1. The thin 1 mm plates were of slightly different geometry than indicated in Figure 1(a). The enhancement plates were glued to side with a standard two component epoxy, except for one specimen type where tooth plates (punched metal fasteners) was used without glue. The dowel material were either mild steel (S460) or high strength steel (CrNi). The side-members were thick steel plates, complying with the definition in (prEN 1995-1-1 2003). Tests were performed in accordance with the guidelines of (EN 26891 1993) in a set-up as shown in Figure 1.

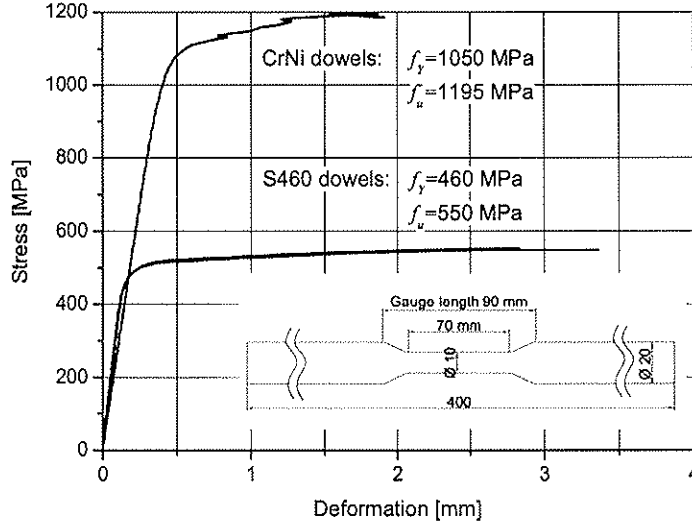


Figure 2: Determination of f_y and f_u for the two dowel materials according to (EN 10002-1 2002).

3 Results and discussion

3.1 Material and derived parameters

Specimens were cut from glulam GL30h with a mean density of $\rho_{12} = 463 \text{ kg/m}^3$ (COV 3%); determined after conditioning to equilibrium with $RH 65\% \pm 2\%$ at $20^\circ \text{ C} \pm 2^\circ \text{ C}$. In accordance with (prEN 1995-1-1 2003) the mean embedment strength parallel to grain can be assessed to:

$$f_{h,0} = 0.082(1 - 0.01d)\rho_{12} = 30.4 \text{ MPa} \quad (1)$$

Where $d = 20 \text{ mm}$ is the dowel diameter. The characteristic of the dowel material were determined in a tension test following (EN 10002-1 2002), results are given in Figure 2. By use of the ultimate tension strength, f_u , the perfect mean perfect plastic bending capacity of the dowels can be assessed by use of the guidelines given in (prEN 1995-1-1 2003):

$$M_y = 0.3 f_u d^{2.6} = \begin{cases} 398.3 \cdot 10^3 \text{ Nmm} & \text{for S460 dowels} \\ 865.3 \cdot 10^3 \text{ Nmm} & \text{for CrNi dowels} \end{cases} \quad (2)$$

Only the steel quality for the 4 mm plates have been determined in a tension test, result given in Figure 3. However it is assumed that the test is representative also for the used 2 mm and 1 mm plates. In accordance with (ENV 1993-1-1 1998) the embedment strength of the steel plates in the configuration used can be determined to:

$$f_{h,s} = 2.5 f_u = 1088 \text{ MPa} \quad (3)$$

When using (3) to determine the embedment strength of the steel-plates it is tacitly assumed that the small holes in the punched plates does not influence the strength.

3.2 Perfect plastic strength

The perfect plastic load-carrying capacity, F_y determined according to the theory of Johansen (1941) and (Johansen 1949) is readily derived for the specific specimen design.

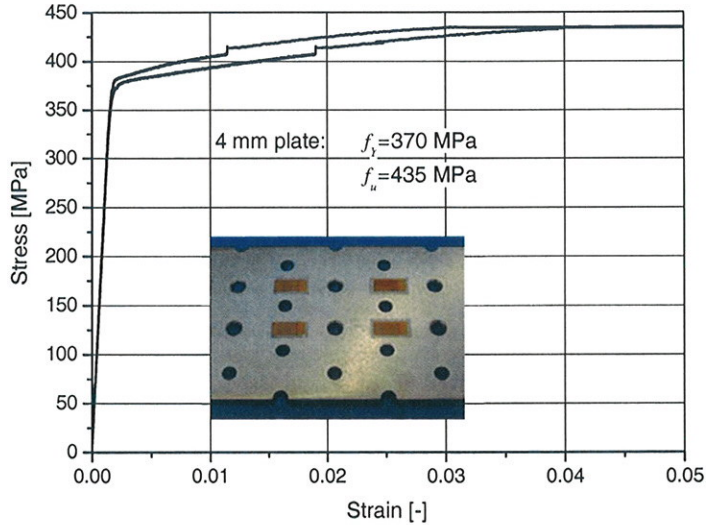


Figure 3: Determination of f_y and f_u for 4 mm glued connector plates.

The outer members of the double shear connection are thick steel plates why only mode I and mode III failures are relevant. In equation (4) the notation is similar to the one used in (prEN 1995-1-1 2003), and subscript s refer to the connector-plate properties.

$$F_y = \min \begin{cases} (0.5 f_{h,2} t_2 + f_{h,s} t_s) d & \text{Mode I} \\ \left(\left(\frac{f_{h,s}}{f_{h,2}} - 1 \right) t_s + \sqrt{\frac{4M_y}{f_{h,2} d} + \left(1 - \frac{f_{h,s}}{f_{h,2}} \right) t_s^2} \right) f_{h,2} d & \text{Mode III} \end{cases} \quad (4)$$

For $f_{h,s} = f_{h,2}$ or $t_s \rightarrow 0$ the influence of the steel-plate connector vanishes and the formulas (4) becomes similar to those given in Eurocode 5 (prEN 1995-1-1 2003, eq. (8.3)), with the only exception that for mode III EC5 allows for additional 10% load bearing capacity. Though additional load carrying due to rope effect has not been included in (4) some effect of axial forces in the dowels might have been present in the tests. The load capacity formula (4) is also given by Blaß et al. (2001) where many more configurations of side enhanced connections are included. The result of applying the perfect plastic formula (4) to the tested connection using the previously given material parameters are listed in Table 2.

3.3 Connection test results

Examples of load-displacement curves for the tested specimens are given in Figures 4 and 5. The influence of dowel material is studied in Figure 4, and the gross observation is that for the plain non-enhanced connections the dowel quality is of no importance for the strength, whereas the 4 mm enhanced connections show variation with dowel quality. The influence of thickness of the enhancement is studied in Figure 5 and an increase in strength and stiffness is seen in the whole range of plate thicknesses. Table 2 gives the the perfect plastic load carrying capacity and the experimental mean values of the following quantities:

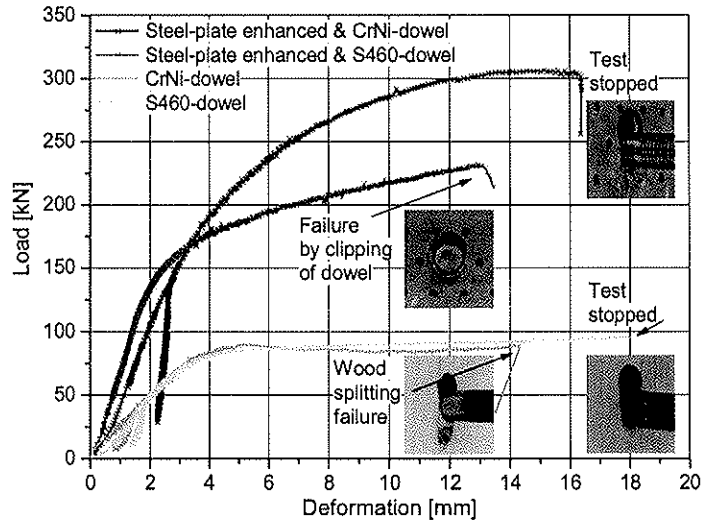


Figure 4: Load-deformation characteristics of four variants of a double shear dowel-type connection with $d=20$ mm dowel of two different steel-grades, respectively with and without glued 4 mm steel-plate embedment enhancement.

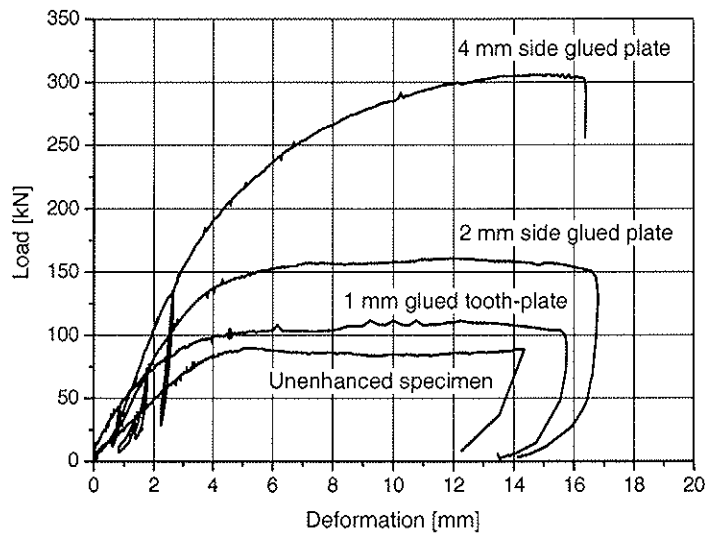


Figure 5: Load-deformation characteristics of four variants of a double shear dowel-type connection with $d=20$ mm CrNi-dowel and four different thicknesses of the side-glued steel-plate embedment enhancement.

- F_{max} The maximum strength determined in accordance with (EN 26891 1993), i.e. maximum load reached before a total slip, ν , of 15 mm.
- $\nu_{F_{max}}$ The slip measured at F_{max} .
- k_s The slip modulus determined by regression of the initial loading ramp in the interval $0.1 F_{est} - 0.4 F_{est}$. Observe that the experimental mean value of k_s corresponds to K_{ser} of (prEN 1995-1-1 2003), the latter assessable for dowels by $K_{ser} = \rho_{12}^{1.5} d/23$.
- k_e The elastic slip modulus determined by regression of data in the load interval $0.1 F_{est} - 0.4 F_{est}$ in the unloading cycle prescribed by the standard.

Type	F_y [kN]		Observed failure mode	F_{max} [kN]	$\nu_{F_{max}}$ [mm]	k_s [kN/mm]	k_e [kN/mm]
	Mode I	Mode III					
Plain-S460	(48.7)	31.1	III	48.2	15	22	41
Plain-CrNi	(48.7)	45.9	I & splitting	44.7	6	11	30
Pr-t1-CrNi	(70.4)	67.5	I & splitting	56.5	10	20	85
Gl-t1-CrNi	(70.4)	67.5	I	55.9	12	21	88
Gl-t2-CrNi	(92.2)	87.6	I	78.9	12	22	99
Gl-t4-S460	(135.7)	112.2	III & dowel clip	115.5	(12)	43	186
Gl-t4-CrNi	(135.7)	128.2	I	150.8	15	34	182

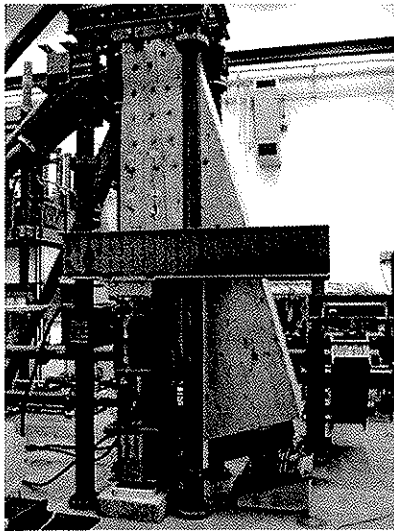
Table 2: Result summary for tested specimens - mean values pr. shear plane.

The following comments apply to the results given:

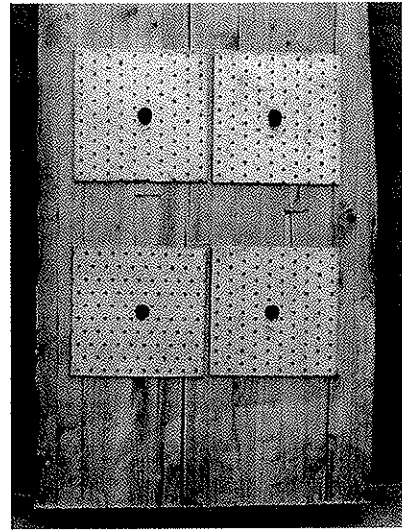
Plain-S460	The observed mode III failure strength is larger than the perfect plastic strength – probably due to the rope effect.
Plain-CrNi	Observed strength corresponds to perfect plastic strength, the insignificant difference between two plastic modes explains failure mode.
Both Plain	The high strength CrNi dowel is indeed a "stout" dowel and premature splitting is anticipated and explains the higher strength met when using the "slender" S460 dowel. Rope effect met in Plain-S460 may explain higher stiffness compared to the Plain-CrNi, the k_s of the latter corresponds to estimated $K_{ser} = \rho_{12}^{1.5} d / 23 = 8.7$ kN/mm.
Both t1-CrNi	Except less tendency to splitting there is not observed any effect of gluing compared to mechanically fastening of side plate. The perfect plastic model overestimates the strength by 20%. However, this can be a consequence of a poorer steel quality for the 1 mm plates.
Gl-t2-CrNi	Perfect plastic capacity of connection overestimated by 10%.
Gl-t4-S460	Modelled and observed strength corresponds, however failure is due to clipping of dowel.
Gl-t4-CrNi	The observed experimental capacity exceeds the maximum perfect plastic capacity by 10%, this is spurious.
all	The increase of the slip modulus k_s with increased plate thickness is lower than the strength increase. The ratio between k_e and k_s is in the order 2.3 for the non-enhanced and in the order 4.5 for the enhanced. The ratio is generally the effect of initial permanent plastic/viscous deformations met in the initial loading not being present in second loading, the higher for the enhanced connections is probably due to second loading primarily utilizing elastic properties of the steel plates.

4 Post scriptum

Figures 6 and 7 shows the application of the glued steel plate enhanced dowels type fasteners. The cross section of the large specimen seen in Figure 6 failed in tension/bending due to severe cross section reduction – also incurred by the slots. However, after failure the load application joint seen in Figure 7 remained undamaged, and the CrNi dowels could be removed by hand after having transferred 250 kN each.

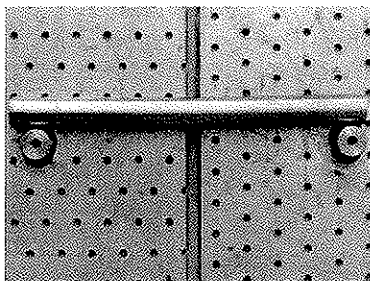


(a) Mounted specimen

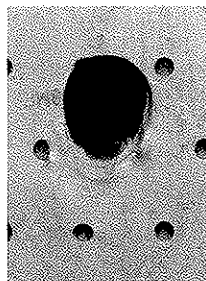


(b) Tension force transferrer after testing

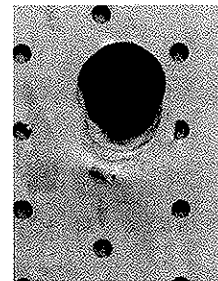
Figure 6: Large test specimen containing a connection with 100 dowels and 2 slotted in steel plates, load application were provided by 4 CrNi dowels and 4 mm glued steel plate enhancement.



(a) Dowel bending



(b) Embedment



(c) Embedment

Figure 7: Dowel and embedment after loading with approx 250 kN pr. dowel.

5 Concluding remarks

The reported tests give reason to the following statements:

- The short term strength of dowel type joints is significantly increased with thick stiff glued connectors, and premature splitting is efficiently prevented.
- The short term strength of dowel type joints with thick stiff glued connectors can safely be calculated by the perfect plastic model, i.e. the general rule for connectors in Eurocode 5.
- The long term behavior of the glue interface – moisture induced wood strain and resulting fatigue – needs to be investigated before application.
- The use of glued connectors is a means for safe enhancement the joint performance compared to the often seen unsafe strategy where optimization is made by including more slotted in plates consequently weakening the cross section.

References

- Blaß, H. J., Schmidt, M. & Werner, H. (2001), 'Verstärkung von verbindungen', *Bauen mit Holz* **01**(9), 40–48.
- EN 10002-1 (2002), Metallic materials. Tensile testing. Part 1: Method of test at ambient temperature, Standard, CEN.
- EN 26891 (1993), Timber structures – Test methods – Joints made with mechanical fasteners – General principles for the determination of strength and deformation characteristics, Standard, CEN.
- ENV 1993-1-1 (1998), Eurocode 3 – Design of steel structures – Part 1-1: General – Common rules and rules for buildings, Code, CEN.
- Johansen, K. W. (1941), 'Forsøg med træforbindelser (in Danish)', *Bygningsstatistiske meddelelser*.
- Johansen, K. W. (1949), 'Theory of timber connections', *International Association of Bridge and Structural Engineering Publication* **9**, 249–262.
- prEN 1995-1-1 (2003), Eurocode 5 – Design of timber structures – Part 1-1: General – Common rules and rules for buildings, Code, final draft, stage 49, CEN.

INTERNATIONAL COUNCIL FOR RESEARCH AND INNOVATION
IN BUILDING AND CONSTRUCTION

WORKING COMMISSION W18 - TIMBER STRUCTURES

REVIEW OF PROBABILITY DATA FOR TIMBER CONNECTIONS WITH
DOWEL-TYPE FASTENERS

A Leijten
Delft University of Technology
THE NETHERLANDS

J Köhler
Swiss Federal Institute of Technology, Zürich
SWITZERLAND

A Jorissen
Dept. of Building Science, Eindhoven
THE NETHERLANDS

Presented by J Köhler

F Lam commented that the beta values might be lower if individual data sets were considered.

K Crews commented that single fasteners as dowels were considered and group behaviour should also be studied.

Review of probability data for timber connections with dowel-type fasteners

Ad Leijten,
Delft University of Technology, the Netherlands

Jochen Köhler,
Swiss Federal Institute of Technology, Zurich, Switzerland

André Jorissen,
Dept. of Building Science, Eindhoven, the Netherlands

1 Introduction

In the European design standard, Eurocode 5 (EN1995-1-1) the Johansen model is presented to predict the strength of connections with dowel-type fasteners. This model contains besides a number of geometrical parameters two material parameters; the embedment strength of the timber and the yield moment of the fastener. This study focuses on the main influencing independent parameters of the embedment strength being; the timber density and diameter of the fastener. The embedment strength expressions in Eurocode 5 are based on a comprehensive study by Whale and Smith (1986b) and Ehlbeck and Werner (1992). The influence of the timber density and the fastener diameter was derived using regression analyses. Expressions for the lower 5%-Fractile value were assumed to be the same as for the mean value. This was achieved by simply exchanging in the regression formula the mean value of the density by the lower 5%-Fractile value of the density.

In the present study embedment test results from the above-mentioned research and test data from later investigations are considered to create a probabilistic framework for the prediction of the embedding strength. The presented framework is applied in a reliability analysis of a simple dowel connection. The lower 5%-Fractile of the embedding strength is introduced to characterize the evaluated probability distribution of the embedding strength. This information can be used to be incorporated in probabilistic design codes to feed design models of timber connections.

2 Parallel and perpendicular to grain embedment test results

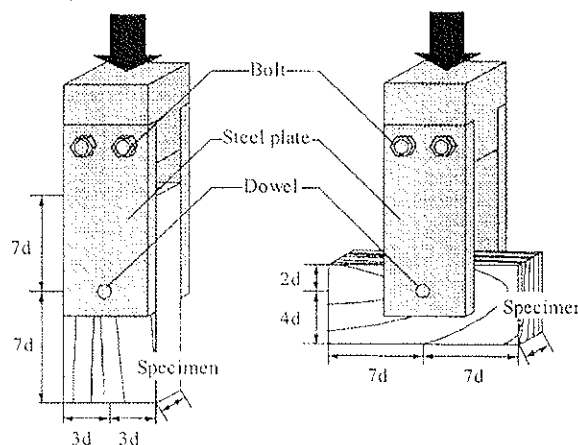


Figure 1: Embedment test according to EN 383 taken from Sawata and Yasumura (2002)
Left: Parallel to grain Right: perpendicular to grain

In the past many embedment tests have been reported. For the purpose of this study only results are evaluated that follow the procedure and definition of the embedment strength laid down in EN 383. The standardised test set-up for parallel to grain tests as well as perpendicular to grain is given in Figure 1. This standard defines the embedment strength as the highest embedment stress within 5mm displacement for both parallel and perpendicular to grain tests. For the parallel to grain test the maximum load is usually reached within 2 or 3 mm displacement and the load-displacement curves show a typical linear and full plastic branch. The fibres directly underneath the dowel buckle locally. For the perpendicular to grain test the physical failure mechanism is completely different. The fibres are loaded perpendicular to the grain and due a chord or cable effect of the fibres a hardening branch appears in the load displacement diagram, Figure 2.

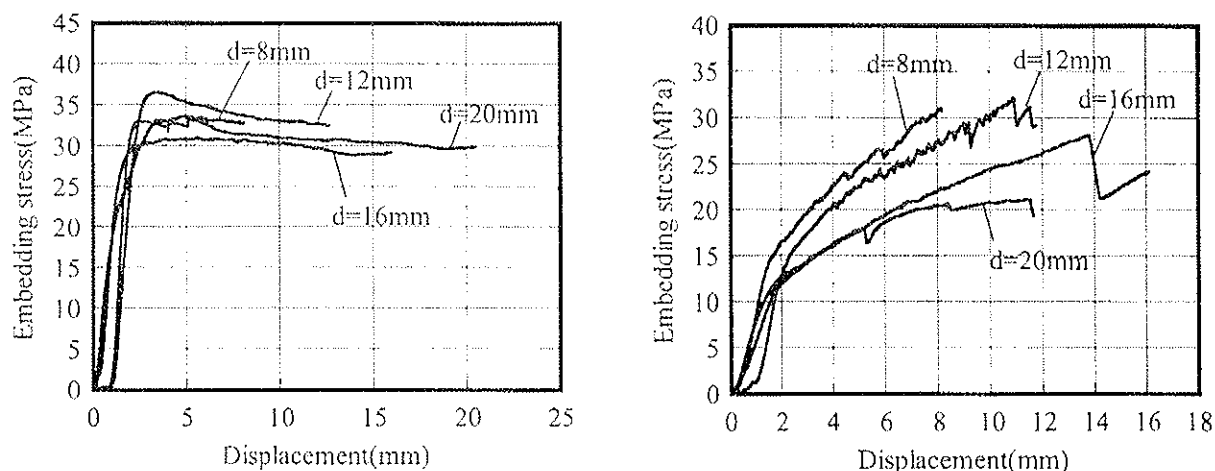


Figure 2: Difference in load-displacement behaviour parallel and perpendicular to grain test. (Taken from Sawata and Yasumura (2002))

The hardening is dependent of the diameter of the fastener. After some initial testing Whale and Smith (1986b) defined the embedment strength for both nails and dowels as the embedment stress at 2,1mm displacement in both directions. Sawata and Yasumura (2002) demonstrated this 2,1 mm limit result in conservative values for perpendicular to grain embedment for dowel fasteners.

3 The Databases

To enable comparison databases are reviewed and are brought in line if necessary with requirements of EN383. Data from the following sources were considered and evaluated:

- Whale and Smith (1985a,b). The test specimens comprised many wood species and at least 40 tests per wood species per fastener diameter, Table 1. Perpendicular to the grain data related to dowel fasteners >8mm were ignored because of reasons given above. To comply with the standard reference climatic conditions the density of all specimens was modified using the method given by W.T. Simpson (1993).
- Ehlbeck and Werner (1992) confined their research to deciduous wood species. In his PhD-thesis Werner (1993) presents an overview of the parameters that influences the strength of connections with dowel type fasteners.
- Vreeswijk (2003) focused mainly on high-density wood species (11 tests Spruce).
- Mischler (not published) performed embedment tests exclusively with Spruce specimens focusing on small pre-drilled holes for 5 and 7mm diameter.
- Sawata and Yasumura (2002) made a comprehensive survey using Japanese pine exclusively. An equal number of experiments per dowel diameter (8, 12, 16 and 20 mm) parallel and perpendicular to the grain make this database very well balanced.

Table 1: Wood species and number of embedment tests

Whale & Smith (1985a.b)	Ehlbeck & Werner (1992)	Vreeswijk (2003)	Mischler (not publ.)	Sawata & Yasumura (2003)
Sitka Spruce n = 357	Beech n = 55	Spruce n = 11	Spruce n = 130	Pine n = 1009
Scots Pine n = 160	Oak n = 20	Oak n = 10	-	-
European redw. n = 357	Teak n = 5	Massaranduba n = 10	-	-
Spruce Pine Fir n = 160	Merbau n = 19	Angelim Vermelho n = 12	-	-
Keruing n = 180	Afzelia n = 20	Azobé n = 10	-	-
Greenhart n = 180	Bongossi n = 35	Cumarú n = 10	-	-

In Table 2 a general overview of the data is given. Since Whale and Smith (1986b) showed no significant difference between the results in tension and compression parallel to grain these data sub sets were combined. A summary of the mean and standard deviation of the specimen densities per wood species is given in Table 3.

Table 2: Review of source and sample size of the database.

NAILS (not-drilled)				
Source	Parallel to grain		Perp. to grain compression	Total
	tension	compression		
Whale and Smith (1985a)	400	120	400	920
Whale and Smith (1985b)				
Nails	520		400	920
DOWELS				
Whale and Smith (1985a)	360	120	360	840
Whale and Smith (1985b)				
Ehlbeck and Werner (1992)	79	45	30	154
Sawata and Yasumura (2003)	-	503	506	1009
Mischler (not published)	-	80	50	130
Vreeswijk (2003)	-	62	-	62
Total Dowels	1249		946	2195
Total Nails + Dowels	1769		1346	3115

Table 3: Overview of the density per wood species

Coniferous	n	density			Deciduous	n	density		
		mean	st.d	COV			mean	st.d	COV
Sitka Spruce	357	393	39.1	10	Keruing	200	707	60.9	9
Scots Pine	119	458	59.0	13	Greenhart	120	905	35.9	4
European Redwood	358	460	46.6	10	Beech	56	717	33.1	5
European Whitewood	119	390	41.6	11	Teak	5	652	9.7	1
Spruce Pine Fir	119	411	36.8	9	Oak	30	718	36.7	5
Picea (Japan)	1009	398	44.2	11	Merbau	19	802	36.5	5
Spruce	151	446	51.7	12	Afzelia	20	714	24.0	3
					Bongossi	35	1086	56.3	5
					Massaranduba	10	972	27.3	3
					Angelim Vermelho	11	1104	40.0	4
					Azobe	10	1072	11.2	1
					Cumarú	10	1142	18.7	2

In Figure 3 the density distribution of all the specimens of all wood species excluding the Japanese species, *Picea Jezoensis*, is presented. The large number of coniferous wood distinguishes itself clearly from the other deciduous species. The density range of the deciduous wood species is much wider than the coniferous and apparently is well represented around 700, 900 and 1100 kg/m³. The density distribution play a role in the assumptions for the regression analysis applied below.

4 Data analysis

The data bases are grouped according to failure mechanism and information which is always available in design. Therefore, eight groups were identified, namely, coniferous or deciduous wood species with nails or dowels loaded parallel or perpendicular to the grain. By testing if the sub data sets per group are statically similar it was observed that considerable differences exist. For that reason the use of multivariate models for the analysis of the groups is not possible. However, it is assumed that the sum of a sufficiently large number of sub data sets belonging to one group is normal distributed and a regression model derived from the entire combined group can be applied. The best fit was found for the following expression:

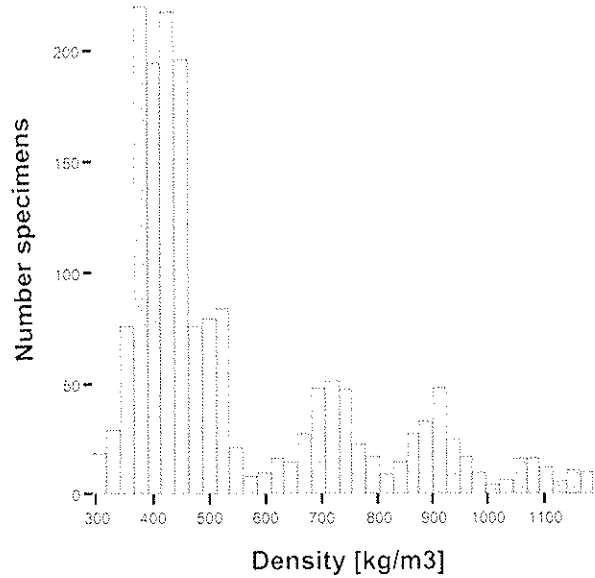


Figure 3: Density histogram

$$f_h = A\rho^B d^C \quad (1)$$

where

- f_h is the embedment strength,
 - ρ is the timber density and
 - d is the diameter of the fastener.
- A , B and C are model parameters.

Considering the natural logarithms of the material properties involved a simple linear equation can be written and multiple linear regression analysis can be utilized to estimate the model parameters.

4.1 Regression Analysis

The regression analysis takes basis in n simultaneous observations of the embedment strength $f_h = (f_{h,1}, f_{h,2}, \dots, f_{h,n})^T$ as the dependent material property and the density $\rho = (\rho_1, \rho_2, \dots, \rho_n)^T$ and the diameter of the fastener $d = (d_1, d_2, \dots, d_n)^T$ as indicative properties. Assuming that at least locally a linear relationship between the natural logarithm $\ln(f_h) = f_h^*$, $\ln(\rho) = \rho^*$ and $\ln(d) = d^*$ exist the regression may be performed on the basis of

$$f_h^* = A^* + B\rho^* + Cd^* + \varepsilon \quad (2)$$

where $A^* = \ln(A)$, B and C are the regression coefficients and where ε is an error term. Assuming that the error term ε is normal distributed with zero mean and unknown standard deviation σ_ε , the maximum likelihood method, see e.g. Lindley (1965) may be used to estimate the mean values and covariance matrix for the parameters A^* , B , C , σ_ε .

The multi linear regression analysis results are summarized in Table 5 for nails (pre-drilled) and for dowels. Regarding Table 5 it should be noted that the Japanese data (n=1009) is very dominating for the coniferous wood species. Comparison with the European coniferous wood species shows significant differences. For this reason additional columns are provided in Table 5 including and excluding the Japanese data as shown at the bottom of the table.

Table 5: Regression parameters for (pre-drilled) Nails and Dowels

$\ln(f_h [MPa]) = A^* + B \ln(\rho [kg/m^3]) + C \ln(d [mm]) + \varepsilon$; $\mu \hat{=}$ mean, $\sigma \hat{=}$ standard deviation

Correlation coefficients as $r_{x,y} = \frac{Cov(x,y)}{\sigma_x \sigma_y}$

	Nails				Dowels					
	n = 397	n = 319	n = 120	n = 80	n = 940	n = 448	n = 503	n = 503	n = 285	n = 30
	Coniferous		Deciduous		Coniferous				Deciduous	
		⊥		⊥	¹	²	³	⊥ ³		⊥
μ_{A^*}	-4.563	-3.086	-5.533	-7.905	-0.938	-2.334	-1.247	-2.655	-2.441	-2.245
σ_{A^*}	0.440	0.391	0.513	0.533	0.200	0.232	0.197	0.311	0.296	0.655
μ_B	1.345	1.148	1.507	1.887	0.808	1.066	0.837	1.111	1.091	1.128
σ_B	0.072	0.064	0.077	0.079	0.032	0.038	0.033	0.052	0.044	0.097
μ_C	-0.273	-0.420	-0.181	-0.418	-0.157	-0.253	-0.081	-0.420	-0.253	-0.455
σ_C	0.030	0.027	0.037	0.039	0.011	0.012	0.013	0.021	0.018	0.038
μ_{σ_ε}	0.175	0.141	0.119	0.101	0.126	0.107	0.080	0.129	0.129	0.112
$\sigma_{\sigma_\varepsilon}$	0.004	0.004	0.005	0.006	0.002	0.003	0.002	0.003	0.004	0.010
r_{A^*B}	-0.995	-0.995	-0.994	-0.994	-0.989	-0.991	-0.984	-0.984	-0.986	-0.987
r_{BC}	0.085	0.039	0.006	0.004	0.097	0.105	-0.092	-0.130	-0.115	-0.129
r_{A^*C}	-0.182	-0.138	-0.115	-0.113	-0.244	-0.235	-0.085	-0.050	-0.049	-0.030

¹ including Japanese Data; ² excluding Japanese Data; ³ only Japanese Data

4.2 Prediction of the embedding strength

Using the information from the regression analysis, the probability distribution function of the embedding strength can be estimated for given distribution function of the timber density and given diameter of the fastener. The probability distribution function of the embedding strength can be written as follows:

$$F(x) = P\left(\exp\left(A^* + B \ln(\rho) + C \ln(d) + \varepsilon\right) \leq x\right) \quad (3)$$

Where A^* , B , C are the random model parameters, ρ is the random density, ε is the error term and d is the known diameter of the fastener.

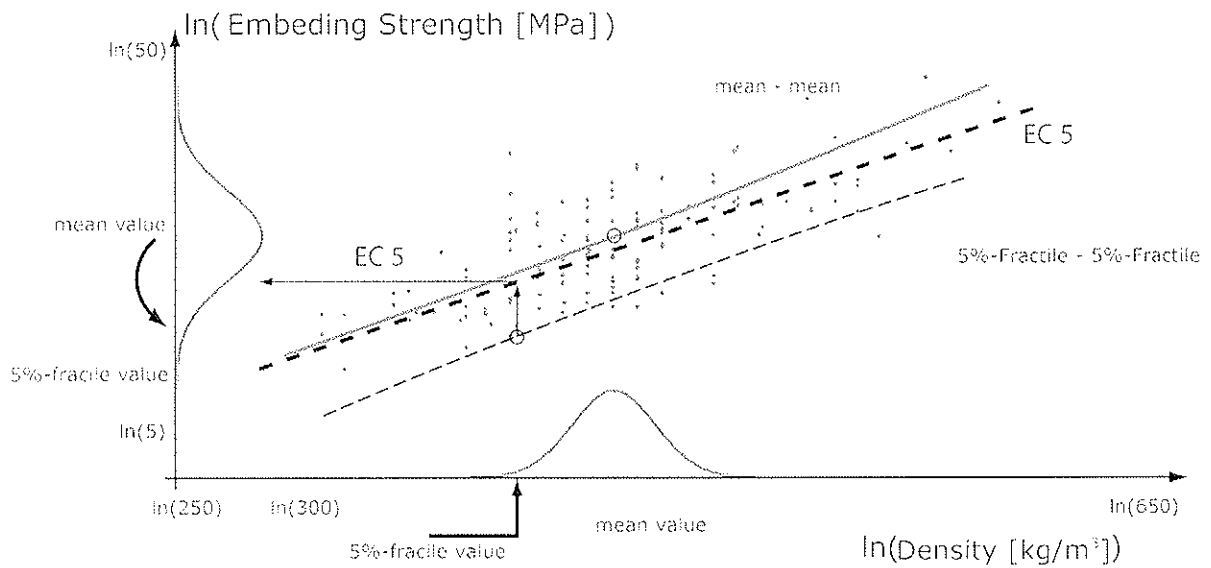


Figure 4: Logarithm of embedding strength over logarithm of density for a given diameter of the fastener. Scheme for the estimation of 5%-values.

For practical use it is often convenient to take the 5%-Fractile values of density to estimate the 5%-Fractile value of the embedding strength directly for a given fastener diameter. Figure 4 shows how such an estimate can be deduced. The coefficients of variation of the density is assumed to be 10% and constant along the $(\ln)x$ -axis. Therefore the distribution function for the density can be specified for given 5%-fractile value of the density. For given density distribution the 5%-fractile value of the embedding strength, $f_{h,0.05}$ can be estimated by solving the following equation:

$$P\left(\exp\left(A^* + B \ln(\rho) + C \ln(d) + \varepsilon\right) \leq f_{h,0.05}\right) = 0.05 \quad (4)$$

Equation (4) can be solved e.g. by using the first order reliability method (FORM). The Eurocode 5 adopted approach takes a vertical line from the point of the lower 5%-Fractile of density and the intersection with the mean regression curve gives the lower 5%-Fractile of the embedment strength. The mean regression curve in EC5 is given with $f_h = 0.082(1 - 0.01 d)\rho$ and is shown in Figure 4 as a means of comparison.

5 Example – Reliability analysis of a simple dowel connection

In the following Example a simple dowel connection is considered. The connection is designed according to EC5. The failure probability of the connection is calculated using the probability distribution for the embedding strength as evaluated above.

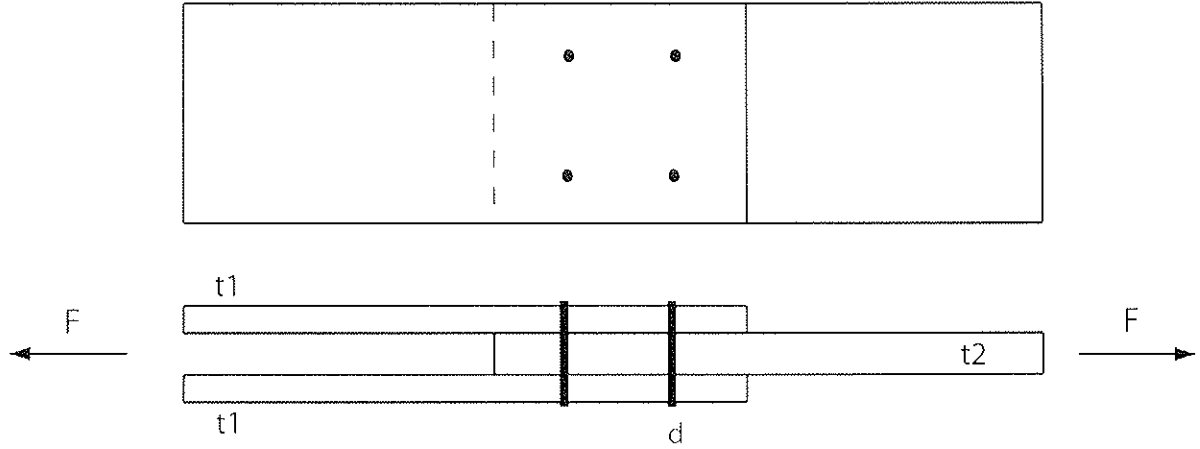


Figure 6: A simple connection with dowels.

A simple double shear timber connection is considered. It is loaded with the force F which is a combination of dead load and live load. The following variables are considered for design:

Table 6: Properties for design

Thickness of middle board [mm]	t_2	100
Thickness of outside boards [mm]	t_1	60
Dowel diameter [mm]	d	12
5%frac-value of density [kg/m^3]	ρ_k	380
5%frac-value of yield stress [MPa]	$f_{v,k}$	360
50%frac-value of dead load [kN]	G_k	10
98%frac-value of live load [kN]	Q_k	12

According to EC 5 the required number of fastener shear planes is evaluated:

$$F_d = 1.35 G_k + 1.5 Q_k \quad (a)$$

$$f_{h,0,k,1+2} = 0.082(1 - 0.01 d) \rho_k \quad (b)$$

$$M_{v,k} = 0.3 f_{v,k} d^{2.6} \quad (c) \quad (5)$$

$$\beta = \frac{f_{h,k,2}}{f_{h,k,1}} = 1 \quad (d)$$

$$F_{v, RK} = \min \begin{cases} f_{h,1,k} t_1 d & \text{(g)} \\ 0,5 f_{h,1,k} t_2 d \beta & \text{(h)} \\ 1,05 \frac{f_{h,1,k} t_1 d}{2 + \beta} \left[\sqrt{2\beta(1 + \beta) + \frac{4\beta(2 + \beta)M_{y,k}}{f_{h,1,k} d t_1^2}} - \beta \right] & \text{(j)} \\ 1,15 \sqrt{\frac{2\beta}{1 + \beta}} \sqrt{2M_{y,k} f_{h,1,k} d} & \text{(k)} \end{cases} \quad (6)$$

$$n_{req} = \frac{F_d}{R_d} = \frac{F_d}{F_{v, RK} \frac{k_{mod}}{\gamma_M}} \quad (7)$$

n_{req} is equivalent to the design variable in the reliability analysis. The following random variables are introduced:

Table 7: Stochastic Models (Reference period for loads: 1 year)

		Type	mean	stdev	COV	Char. Value
model uncertainty	X	Lognormal	1	0.1	0.1	-
density $[kg/m^3]$	ρ	Normal	455	45.5	0.1	380
yield stress $[MPa]$	f_y	Log-normal	391	19.5	0.05	360
dead load $[kN]$	G	Normal	20	2	0.1	20
live load $[kN]$	Q	Gumbel	11.8	4.71	0.4	24

The different failure modes of the Johansen equations are considered as four (g-k) components in a serial system.

The limit state functions are:

$$g_i = n_{req} F_{v, RK, i} X - G - Q \quad \text{with } i = 1, 2, 3, 4 \quad (8)$$

with

$$\begin{cases} F_{v, RK, 1} = f_{h,1} t_1 d & \text{(g)} \\ F_{v, RK, 2} = 0,5 f_{h,1} t_2 d \beta & \text{(h)} \\ F_{v, RK, 3} = 1,05 \frac{f_{h,1} t_1 d}{2 + \beta} \left[\sqrt{2\beta(1 + \beta) + \frac{4\beta(2 + \beta)M_y}{f_{h,1} d t_1^2}} - \beta \right] & \text{(j)} \\ F_{v, RK, 4} = 1,15 \sqrt{\frac{2\beta}{1 + \beta}} \sqrt{2M_y f_{h,1} d} & \text{(k)} \end{cases} \quad (9)$$

$f_{h,1}$, β and M_y are now considered as random variables. The estimation of the probability distribution function of the embedding strength is performed like described above. (Equation 3)

The parameters for the regression are taken from group ‘coniferous, dowels, parallel’ without Japanese data, Table 5, and are summarized in Table 8.

Table 8: Regression Parameters

Parameter	Type	Mean	stDev
A	Normal	-2.33	0.23
B	Normal	1.07	0.04
C	Normal	-0.25	0.012
ε	Normal	0	0.11

Correlation Coefficients

	A	B	C	ε
A	1	-0.99	-0.24	0
B	-0.99	1	0.11	0
C	-0.24	0.11	1	0
ε	0	0	0	1

Based on the 5%-fractile value of the density the mean value of the density is estimated assuming that the density is normal distributed with a known coefficient of variation. With the distribution function of the density and the knowledge about the diameter of the fastener the distribution function of the embedding strength can be estimated using Equation (3). The assumed coefficient of variation of the density is 0.1...0.2.

A reliability analysis using First Order reliability Method (FORM), see e.g. Madsen et al. (1986) gives the following results:

Table 9: Results: Reliability Index (β -Index) and probability of failure P_f for a dowel connection designed according EC5 (reference period: 1 year).

COV	0.1	0.12	0.14	0.16	0.18	0.2
β -Index	5.235	5.233	5.090	4.749	4.353	3.989
P_f	8.25E-08	8.34E-08	1.79E-07	1.02E-06	6.71E-06	3.32E-05

Even with an assumed COV for the density of 0.18 the reliability index is in an acceptable region. E.g. in the JCSS - Probabilistic Model Code (2001) a β -Index around 4.2 is proposed.

It should be considered that in many cases the actual number of shear planes is higher than given by equation (7) because the number of fasteners is always an integer value. Therefore, the beta values in Table 9 are lower bound values for the reliability index.

6 Conclusions regarding the results

From the evaluation of the analyses results it can be concluded that:

- Caused by differences in definition of the embedment strength perpendicular to grain a large portion of the available database was unsuitable for evaluation.
- A framework for the evaluation of the probability distribution of the embedding strength is presented for given 5%-Fractile value of the density and the diameter of the fastener is presented. In doing so it is distinguished between timber family, loading direction and fastener type.
- The 5%-Fractile value of the probability distribution is quantified to characterize the distribution.
- Applying the method in a reliability analysis with a simple connection, acceptable results for the failure probability can be obtained.

7 Acknowledgement

The authors would like to thank Prof. M. Faber (ETH) for the spontaneous co-operation in the realization of this study. Furthermore, the EC sponsored COST Action E24 is acknowledged

providing financial support of this short scientific mission. This study could only be accomplished by the grateful contributions of the researchers that carried out and reported the experiments. In particular Prof. Ian Smith from the University of New Brunswick, Canada, is mentioned who retrieved half of the TRADA database that was almost lost. Furthermore, Luke Whale of Timber Solve UK, Hans Blass for sending the research report of Ehlbeck and Werner, Karlsruhe Technical University Germany, as well as Kei Sawata and Motoi Yasumura of Shizuoka University, Japan, who granted us the use of their extensive data base.

8 Literature references

- Ehlbeck, J. and Werner, H., 1992, Coniferous and deciduous embedding strength for dowel-type fasteners, *In: Proceedings of CIB-W18*, Paper 25-7-2.
- Faber M.H., Köhler J. and Sorensen, J.D. (2004) *Probabilistic Modelling of Graded Timber Material Properties*, Journal of Structural Safety, Volume 26, Issue 3, Pages 295-309, July 2004.
- Joint Committee on Structural Safety. 2001. Probabilistic Model Code, Internet Publication: www.jcss.ethz.ch.
- Leijten and Köhler (2004), STSM report COST action E24.
- Lindley, D. V. (1965). "Introduction to Probability & Statistics" Cambridge University Press.
- Madsen, H.O. and Krenk, S. and Lind, N.C. (1986). *Methods of Structural Safety*, Prentice-Hall.
- Sawata, K., Yasumura, M. 2002, Determination of embedding strength of wood for dowel-type fasteners, Journal of Wood Science, 48:138-146, 2002
- Simpson, W. T., 1993, *Specific gravity, moisture content and density relationship for wood*, Gen. Tech. Report. FPL-GTR-76, Madison WI, USA Department of Agriculture, Forest Services, Forest Products Laboratory, 13p.
- Vreeswijk, B., Verbindingen in hardhout, Master Thesis, Faculty of Civil Engineering TU-Delft, 2003.
- Werner, H., 1993, Tragfähigkeit von Holz-Verbindungen mit Stiftförmige Verbindungsmitteln unter Berücksichtigung streuender Einfluß größen, PhD-thesis, Universität Karlsruhe.
- Whale, L. R.J. and Smith, I., Hilson, B.O. 1986c, Behaviour of nailed and bolted joints under short-term lateral load – conclusions from some recent research, *In: Proceedings of CIB-W18*, Paper 19-7-1.
- Whale, L.R.J. and Smith, I., 1986a, *Mechanical joints in structural timberwork*, information for probabilistic design, Annex to research report, CEC-project, TRADA, research report 17/86.
- Whale, L.R.J. and Smith, I., 1986b, The derivation of design clauses for nailed and bolted joints in Eurocode 5, *In: Proceedings of CIB-W18*, Paper 19-7-6.
- Whale, L.R.J. and Smith, I., 1985a, *Mechanical timber joints, embedment tests*, Annex to Final report of DOE-project, April 1983 – September 1985, TRADA
- Whale, L.R.J. and Smith, I., 1985b, *Mechanical timber joints, embedment tests*, Report to DOE-project, April 1983 – September 1985, TRADA

INTERNATIONAL COUNCIL FOR RESEARCH AND INNOVATION
IN BUILDING AND CONSTRUCTION

WORKING COMMISSION W18 - TIMBER STRUCTURES

BEHAVIOUR OF FASTENERS AND GLUE-IN RODS
PRODUCED FROM STAINLESS STEEL

A Kevarinmäki

VTT Building and Transport

FINLAND

Presented by A Kevarinmäki

H J Larsen commented that the test results for specialized products such as self tapping screws are needed. Also ordinary screws might also be problematic and the Eurocode is based on 20 year old data.

J König responded that amendment for Eurocode can be considered and a ready proposal should be prepared.

H Blass commented that the Hanssen formula might not be suitable to be generalized for all proprietary products as issues such as connector diameter need to be carefully studied.

J König responded that limitations can be put in the formula.

J Köhler commented that comparisons with code values should be done in a consistent manner; i.e., characteristic values should not be compared to nominal values.

Behaviour of fasteners and glued-in rods produced from stainless steel

Ari Kevarinmäki

VTT Building and Transport, Finland

1 Introduction

In addition to better durability the use of stainless steel improves the fire resistance of connections. The stainless steel has good fire resistance properties. Unprotected stainless steels have enough capacity in fire resistance class R30 and certain titan stabilised grades also in class R60 without overdesign in normal temperature. So the fire protections and/or groovings of the effective cross-sections of timber members for the connections may be avoided with the use of stainless steel. However, also in normal temperature the design rules of timber fasteners are normally given only for the non-alloy steel. The stainless steel grades have a low 0,2 -yield value (normally 220 N/mm²) but a high tensile strength (even > 800 N/mm²) with the ultimate elongation more than 40 %. The paper summarizes the results of the research done for the verification of the design rules for the stainless steel fasteners in normal temperature. All the tests have been done in VTT Technical Research Centre of Finland and a detailed report will be published in 2005.

2 Yield moment tests of fasteners

The yield moment tests of nails, screws and bolts were done according to the EN 409:1993 with the fasteners bending apparatus shown in figure 2.1. All the test series of stainless steel fasteners included at least 10 parallel tests - most of them 15 and some 30. The yield moment of nails were determined as the bending moment at which the nail has deformed through an angle of 45° at maximum. For screws and bolts the yield moment was determined with a maximum rotation angle $\alpha = 45^\circ/d^{0.7}$ as stated in prEN14592:2002. The variations of determined yield moments were small: 4 % at maximum, when the average was about 2 %.

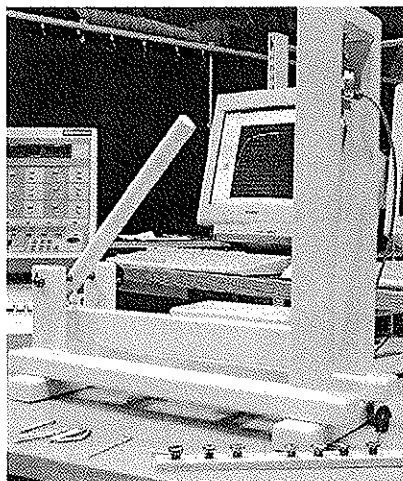
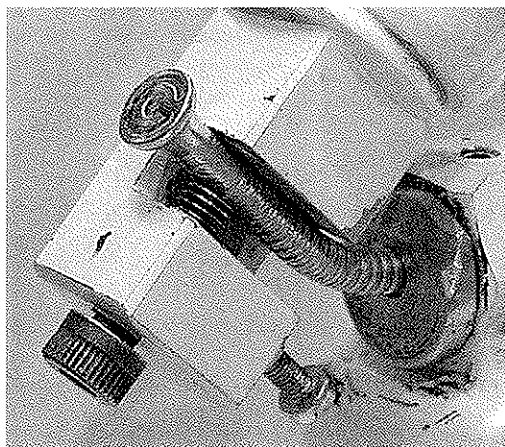


Figure 2.1 *Fasteners bending apparatus.*

The steel grade of all the stainless steel nails was acid proof EN 1.4401. The tensile strength of cold-drawn wire used for the stainless steel nails was either 700 or 750 N/mm² according to the information given by the nail producers. The mean values of test results of stainless steel nails are presented in figure 2.2 with the comparison test series of non-alloy nails. There are also shown the yield moment test results of two series of stainless steel annular ringed shank nails presented by Werner & Siebert, 1991 (marked by symbol W&S). The presented yield moment curves of Eurocode 5 (prEN 1995) have been calculated by the equation of smooth round nails: $M_{y,k} = \frac{f_u}{600} 180d^{2.6}$.

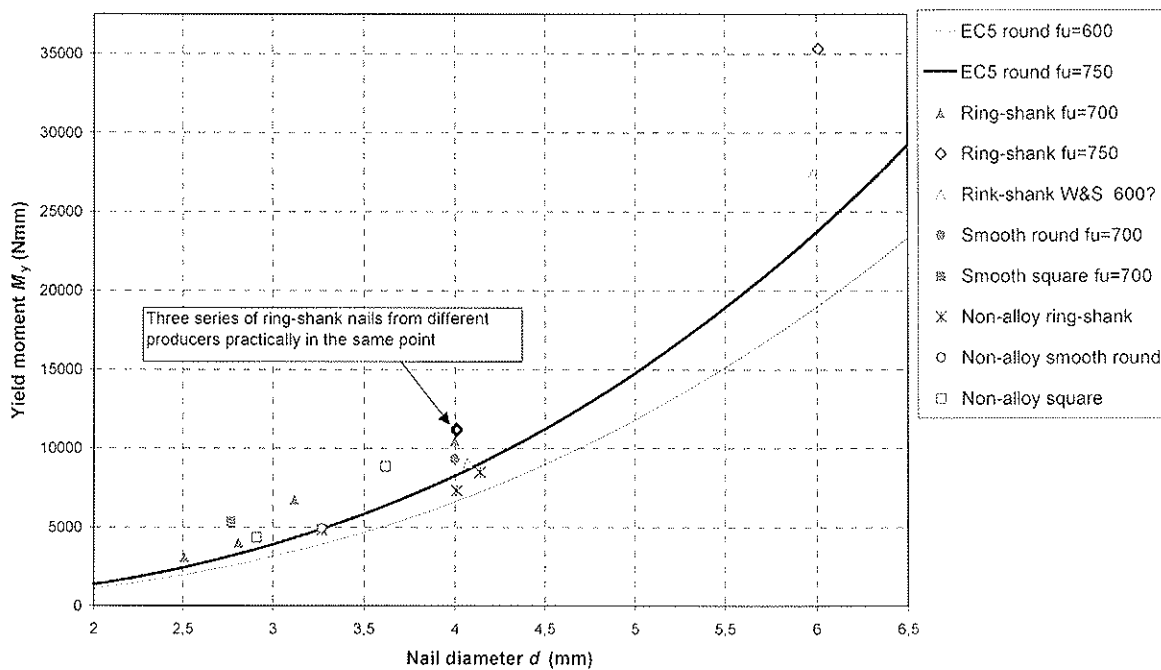


Figure 2.2 Mean values of yield moment tests of stainless steel nails. f_u is the tensile strength of wire used in nail production, for presented non-alloy nails $f_u = 600$ N/mm².

The tests showed clearly better yield moment values for the stainless steel nails than for similar non-alloy nails. The Eurocode equations of yield moments may be safely used for stainless steel nails. However, for full utilization of the nail capacity it is advisable to test the yield moment values for the actual stainless steel nail type and dimension. A significant strengthening of stainless steel material may be occurred in the profiling of nails and the strength increases also in the bending of nails by the strain hardening. In the tension tests of stainless steel annular ringed shank nails of 3,1 mm the tensile strength was up to 1350 N/mm² (wire material 700 N/mm²). The tensile strength of the stainless steel nails of 4,0 mm was at mean value 699 N/mm² for smooth part and 982 N/mm² for the annularly profiled shank of the same nails.

The tested screws and bolts were produced from stainless steel grade A2 (EN 1.4301) or acid proof steel A4 (EN 1.4401) in different strength classes ($f_{u,k} = 500..800$ N/mm²). The mean value of test results of the stainless steel screws and bolts are presented in figures 2.3 and 2.4 with the comparison of the yield moment curves of Eurocode 5 (prEN 1995). For the screws with smooth shank diameter $d \leq 6$ mm, the yield moments have been calculated by the Eurocode equation of smooth round nails. The yield moments of the threaded part of screws have been calculated by using the effective diameter taken as 1,1 times the thread

root diameter. For bolts and lag screws $d > 6$ mm, the comparison curves of yield moments have been calculated as $M_{y,k} = 0,3 f_{u,k} 180 d^{2,6}$.

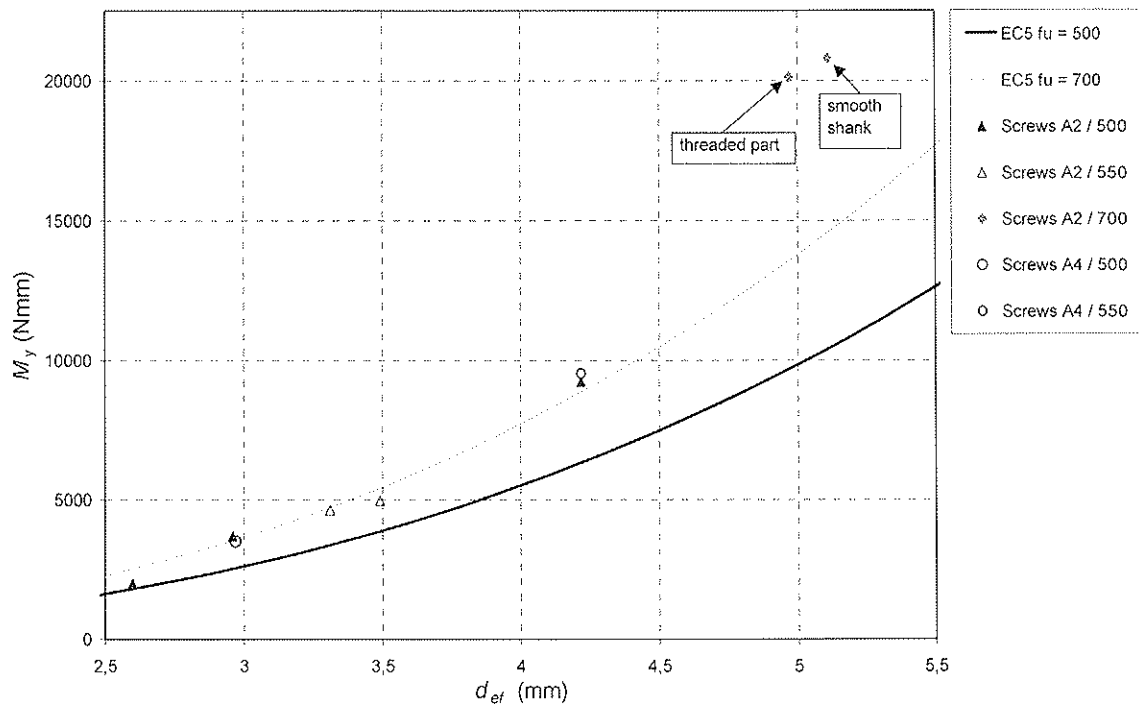


Figure 2.3 Mean values of yield moment tests of stainless steel screws. The effective diameter d_{ef} is the smooth shank diameter or 1,1 times the thread root diameter depending on the testing point.

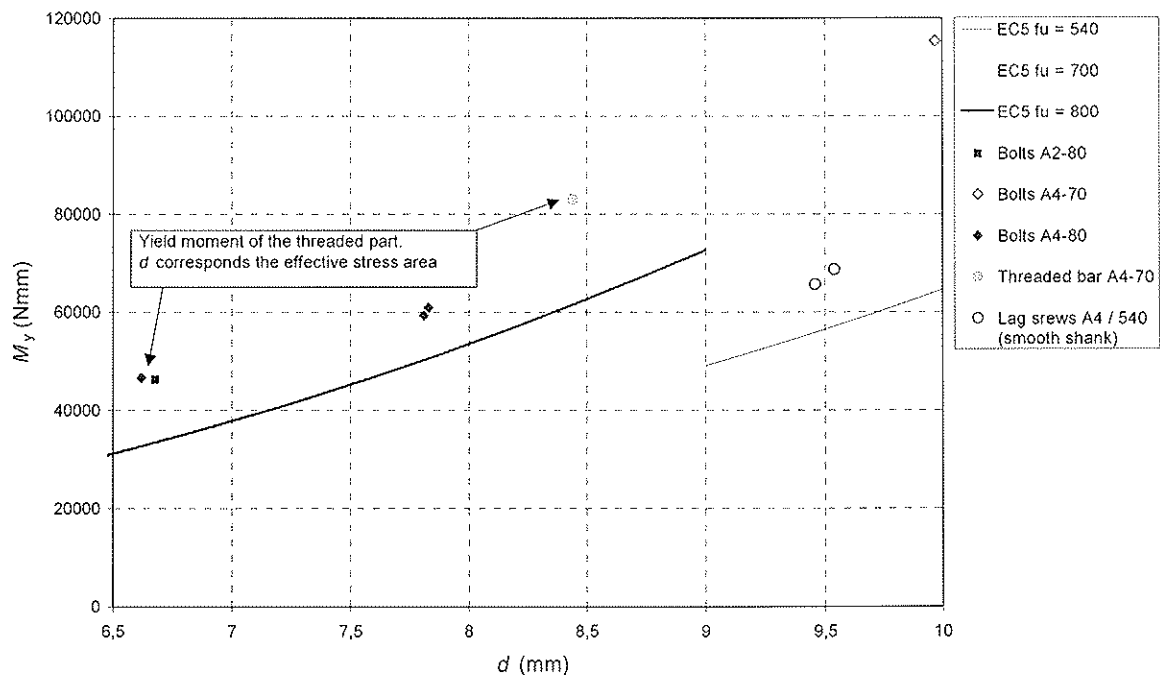


Figure 2.4 Mean values of yield moment tests of stainless steel bolts and lag screws $d \geq 6$ mm. Grade A4-80 is the cold-worked acid proof stainless steel (EN 1.4401) with the tensile strength $f_u = 800$ N/mm².

The tests showed that the Eurocode equations of yield moments may be safely used also for stainless steel screws and bolts. The behaviour of the stainless steel fasteners is very ductile. The load-rotation angle curves of the yield moment tests of the stainless steel screws and bolts were generally clearly increasing at the point where the yield moment values were determined ($\alpha = 45^\circ/d^{0.7}$). This creates an additional safety for the joints of stainless steel fasteners.

3 Withdrawal tests of nails and screws

The withdrawal capacities of five different types and sizes of stainless steel screws and four annular ringed shank nails were tested perpendicular to the grain direction of wood. Also two types of non-alloy nails were tested for comparison. All the stainless steel nails had been made of acid-proof steel grade EN 1.4401 (A4). The screws had steel grade EN 1.4301 (A2) or EN 1.4401 (A4). The screws of test series AR and RR were self-tapping screws. Pre-bored pilot holes were used only with the lag screws of KR-series.

The tests were done according to EN 1382 with sawn timber (spruce) and LVL (Kerto-S). There were 5 similar test specimens in each test series. The sawn timber specimens include two similar fasteners: one in tangential direction and the other in radial direction as presented in EN 1382. The results showed no systematic difference with regard to the two directions normal and tangential to the annular rings. For LVL the tests were done only for fasteners assembled perpendicular to the veneers.

The test series and results are presented in tables 3.1 and 3.2. The used symbols are as follows:

- ρ_{65} is the measured density in moisture content of wood conditioned at RH65,
- l_p is the depth penetration of fastener,
- F_{max} is the mean value of failure load for the test series,
- var is the coefficient of variation of the failure load (= standard deviation/ F_{max}),
- $f_{ax,m}$ is the mean withdrawal parameter calculated according to equation (3.1),
- $f_{ax,Ehl}$ is the withdrawal parameter of nails calculated according to equation (3.2),
- $f_{ax,EC5}$ is the withdrawal parameter of screws calculated according to equation (3.3),
- $F_{ax,EC5}$ is the withdrawal capacity of screws calculated according to equation (3.4),
- $F_{ax,Han}$ is the withdrawal capacity of screws calculated according to equation (3.5) using the measured timber densities ρ_{65} .

Table 3.1 Withdrawal test results of annular ringed shank nails.

test series	nails size (mm)	steel material	timber	ρ_{65} (kg/m ³)	l_p (mm)	F_{max} (N)	var (%)	$f_{ax,m}$ (N/mm ²)	$f_{ax,EHL}$ (N/mm ²)
AA1	4,0x40	EN 1.4401	solid	463	30	1293	10,3	10,8	7,72
AA1-K	4,0x40	EN 1.4401	Kerto-S	540	30	1858	3,7	15,4	10,5
AAS	4,0x40	elect. zincd	solid	464	30	1176	11,3	9,77	7,75
AAS-K	4,0x40	elect. zincd	Kerto-S	539	30	1754	8,3	14,6	10,5
AA2	6,0x60	EN 1.4401	solid	437	40	1852	14,5	7,70	6,87
KN2	2,8x78	EN 1.4401	solid	462	30	600	19,1	7,15	7,68
KN2-K	2,8x78	EN 1.4401	Kerto-S	558	30	1147	12,5	13,7	11,2
KN3	3,1x70	EN 1.4401	solid	436	30	806	11,3	8,58	6,84
KN5	3,1x100	hot zincd	solid	431	30	949	19,4	9,68	6,69

The mean withdrawal parameters have been calculated according to EN 1382

$$f_{ax,m} = \frac{F_{max}}{l_p \cdot d} \quad (3.1)$$

where d is the nominal diameter of the fastener (= outer diameter of threaded part).

Ehbeck and Siebert (1988) have presented for the withdrawal parameter of annular ringed shank nails

$$f_{ax} = 36 \cdot 10^{-6} \cdot \rho^2 \quad (3.2)$$

The tests of nails showed no practical difference between the withdrawal strengths of stainless steel nails and zinc coated non-alloy nails (compare results of AA1 and AAS series). The test results of ring-shank nails corresponded quite well with the equation (3.2). However, there are significant differences between the withdrawal strengths of different nails, depending on the geometry and depth of annular rings (see figure 3.1). So it is recommended, that the withdrawal strength of different nail types and diameters would be tested separately.

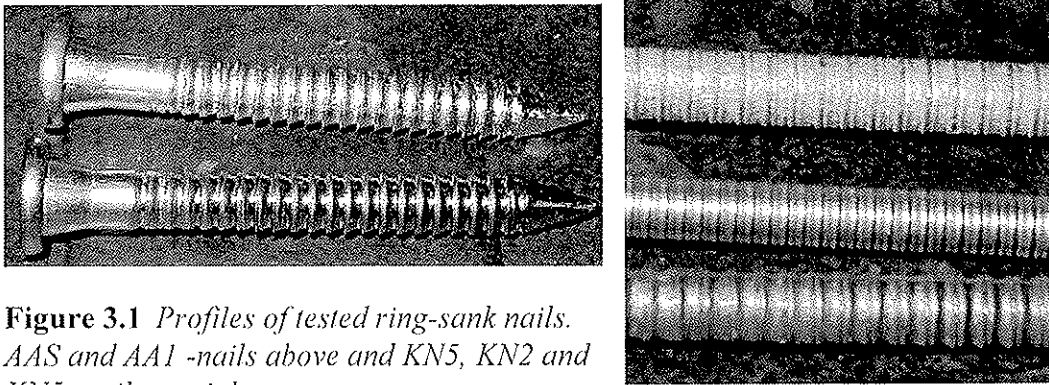


Figure 3.1 Profiles of tested ring-shank nails. AAS and AA1 -nails above and KN5, KN2 and KN5 -nails on right.

Table 3.2 Withdrawal test results of stainless steel screws.

test series	screws size (mm)	steel grade	timber	ρ_{65} (kg/m ³)	l_p (mm)	F_{max} (N)	var (%)	$f_{ax,m}$ (N/mm ²)	$f_{ax,EC5}$ (N/mm ²)	$F_{ax,EC5}$ (N)	$F_{ax,Han}$ (N)
AR	5,0x45	A2	solid	481	30	2920	10,3	19,5	38,0	4516	2210
AR-K	5,0x45	A2	Kerto-S	556	30	2964	4,2	19,8	47,2	5613	2555
RR2	6,0x80	A2	solid	429	30	2859	7,0	15,9	32,0	4260	2271
RR3	4,0x50	A4	solid	461	30	2359	16,0	19,7	35,6	3658	2440
RR7	6x70	A2	solid	454	35	3592	9,1	17,1	34,8	5396	2904
RR7-K	6x70	A2	Kerto-S	546	35	3546	10,9	16,9	45,9	7116	3492
KR1	M10x80	A4	solid	442	46	6140	12,2	13,3	33,5	9273	5849
KR1-K	M10x80	A4	Kerto-S	558	40	5560	8,7	13,9	47,5	11368	6153

Eurocode 5 (prEN 1995-1-1:2003) gives for the withdrawal strength perpendicular to the grain

$$f_{ax} = 3,6 \cdot 10^{-3} \cdot \rho^{1,5} \quad (3.3)$$

and for the withdrawal capacity of the screw

$$F_{ax} = (\pi \cdot d \cdot l_{ef})^{0,8} f_{ax} \quad (3.4)$$

where d is the outer diameter of screw measured on the threaded part and l_{ef} is the pointside penetration length of threaded part minus one screw diameter.

It shall be noted that the withdrawal parameter of equations (3.3) and (3.1) are meaning different matter. However, the draft of fastener standard prEN 14592:2002 states that the withdrawal parameter of screws used in eq. (3.4) may be tested and determined according to EN 1382 (eq. 3.1). This inconsistency between these three standards shall be corrected.

Hansen (2002) has tested the withdrawal strength of self-tapping screws made of non-alloy steel. Hansen presents for the withdrawal capacity of self-tapping screws equation

$$F_{ax} = \pi \cdot d \cdot l_{ef} \cdot 0,0117\rho \quad (3.5)$$

where d and l_{ef} are defined as in equation (3.4). It may be also modified to the general form

$$F_{ax,\alpha,k} = \frac{f_{ax,k} \cdot d \cdot l_{ef}}{\sin^2 \alpha + 1,5 \cos^2 \alpha} \quad (3.6)$$

where $f_{ax,k} = 0,037\rho_k \quad (3.7)$

The withdrawal test results of stainless steel screws corresponded well to the Hansen's (2002) results with non-alloy self-tapping screws. Eurocode 5 gives clearly too high withdrawal capacities for screws - the calculated capacities are roughly 2-times higher than the test results, see table 3.2. The clear overestimation of withdrawal capacity of Eurocode 5 has been stated also with inclined screws $\alpha = 45^\circ$ (Kevarinmäki 2002).

4 Load bearing tests of dowel type joints

The behaviour of the whole joints was checked by the load bearing tests of stainless steel plate to timber joints with stainless fasteners. The tests were done with nailed, screwed and bolted joints according to EN 1380:1999. The nails and screws had a conical (tapered) shape under the head, so the fasteners had a tight fitting in the holes of steel plates. The structure of test specimens is shown in figure 4.1 and the test variables in table 4.1. There were three similar test specimens in each test series and each test specimen included two similar joints. The joints were tested to failure in tension.

Table 4.1 Test series and test results of steel-to-timber joint test specimens. t_s is thickness of stainless steel plate (EN 1.4571). $F_{R,m}$ is the calculated joint capacity. For test series with thin steel plate ($t_s = 2$ mm), the joint capacity has been calculated also with the equations of thick steel plates ($t=4$).

test series	fastener type	size (mm)	n	grade / $f_{u,k}$	timber	ρ_{05} (kg/m ³)	t_s (mm)	F_{max} (kN)	var (%)	$F_{R,m}$ $t=2$ (kN)	$F_{R,m}$ $t=4$ (kN)
V1	nail	4,0x50	4+4	A4 / 750	C30	417	2	24,2	5,9	14,6	19,6
K1	nail	4,0x50	4+4	A4 / 750	Kerto-S	534	4	32,1	1,0	-	24,6
V2	nail	4,0x60	4+4	A4 / 750	C30	405	4	25,5	2,3	-	21,2
V3	screw	5,0x40	4+4	A2 / 550	C40	447	2	24,6	10,2	12,0	16,8
V4	bolt	M8x110	4	A4 -80/ 800	C40	431	4	77,3	1,6		63,7

In all the cases the fasteners yielded clearly before the failure of joints. The nails and screws had the first yield point in the near by head and the longest nails had also a clear second plastic hinge (see figure 4.2). The capacities of tested joints were calculated

according to Eurocode 5 (prEN 1995-1-1:2003) with the measured mean values as the material parameters: density, yield moment and withdrawal strength. The comparison presented in table 4.1 shows that the calculated capacities were exceeded and Eurocode 5 may be safely used for the design of joints with stainless steel fasteners. The test results of specimens with thin steel plates ($t_s = 2$ mm) showed also that the joint capacities may be calculated by the equations for a thick steel plate if the nails or screws have a conical head, alike as Ehlbeck & Görlacher (1982) have shown for the non-alloy nails with the conical heads.

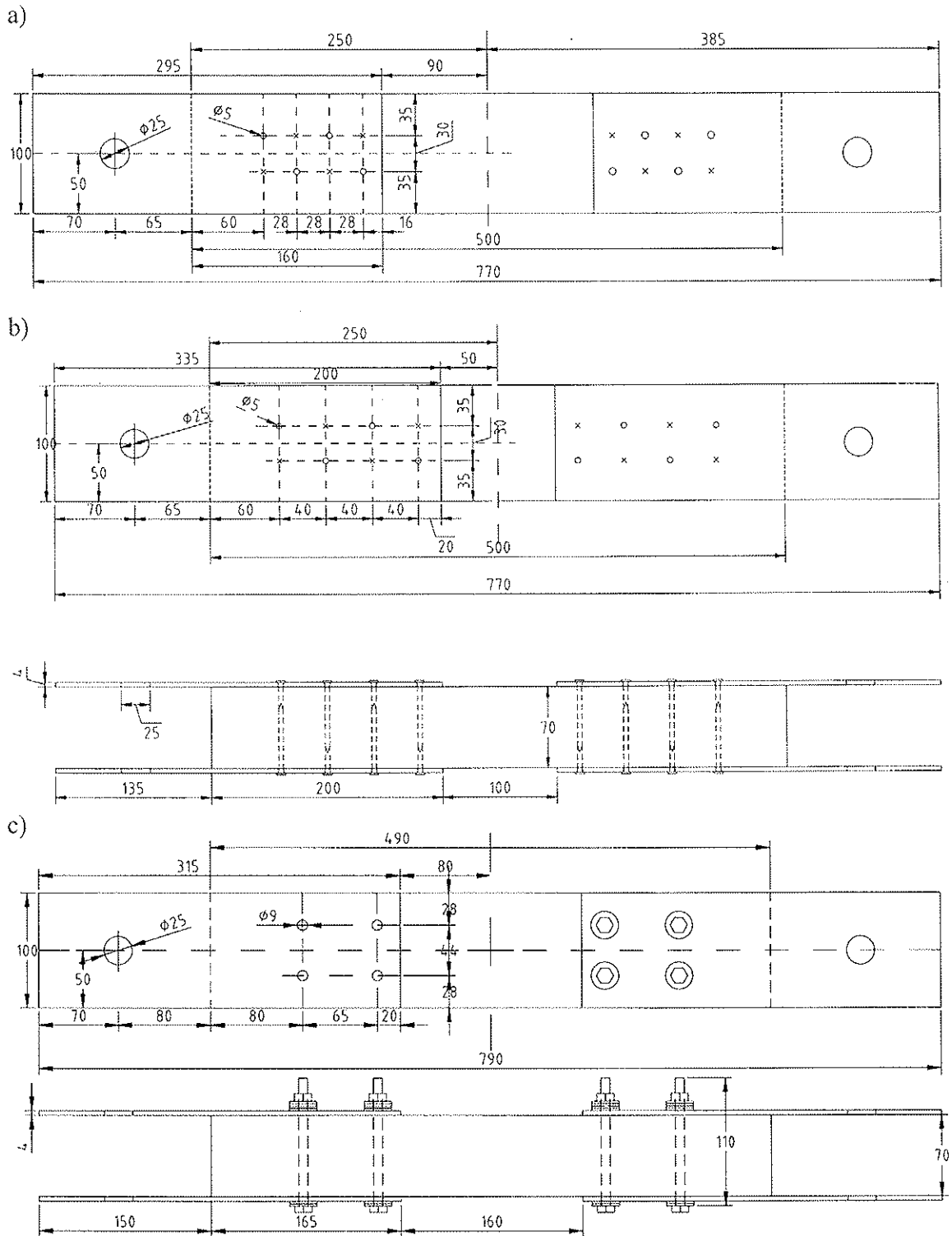


Figure 4.1 Structure of joint test specimens.

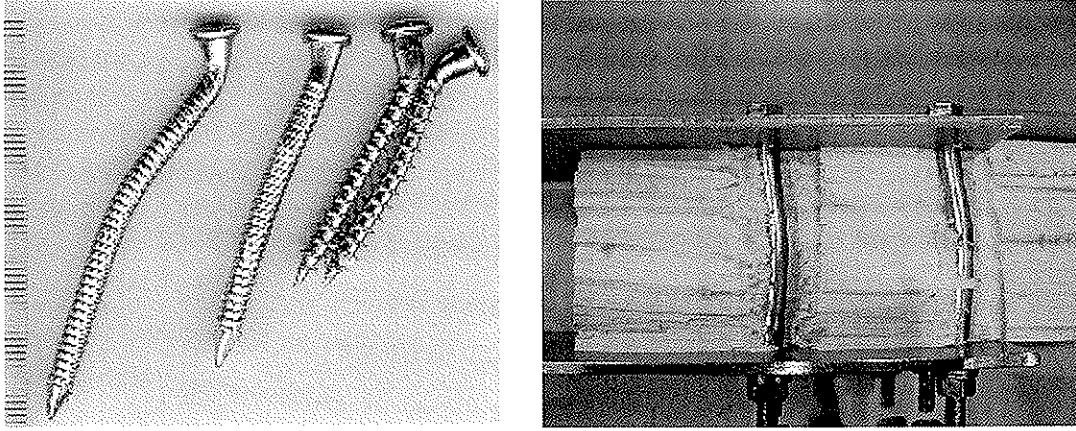


Figure 4.2 Fasteners after testing of joints.

5 Anchorage strength of glued-in rods

The anchorage strength of glued-in stainless steel rods was tested with different anchorage lengths and diameter of rods by the joints of one rod. The glued-in rods were made of hot rolled ribbed stainless steel reinforcing bars used in concrete structures. The material grade of the austenitic steel was EN 1.4306 (AISI 304 L). One reference test series was done also with non-alloy reinforcing steel bars ($f_{y,k} = 500 \text{ N/mm}^2$).

The rods with a diameter (d) of 16 and 20 mm were glued with epoxy adhesive into spacious holes ($D = 20$ and 25 mm) drilled in the glulam beams. The direction angle α with the grain direction was 90° , see figure 5.1. The average density of used glulam was $\rho_\omega = 493 \text{ kg/m}^3$ and the moisture content $\omega = 13 \%$. The tests were done with three different anchorage lengths (l_a) for 16 mm rods and with two lengths for 20 mm rods. The rods were loaded in tension and the slip between the rod and surface of glulam was measured. There were three similar test specimens for each test series. The test variables and the mean value of test results are presented in table 5.1.

The average anchorage strengths has been calculated for the bore area of the hole:

$$f_{a,m} = \frac{F_{\max}}{\pi \cdot D \cdot l_a} \quad (5.1)$$

where F_{\max} is the mean value of failure loads.

For the comparison, the characteristic anchorage strengths were calculated both with the design method presented by Jorma Kangas (Kangas, 1994) and the equation proposed to Eurocode 5 (draft prEN 1995-2, 2003-05-28). According to Kangas in all direction angles $\alpha \geq 15^\circ$

$$f_{a,k} = 6,5 \cdot (1 - l_a / 100d) \quad [\text{N/mm}^2] \quad (5.2)$$

The Working Draft for Eurocode 5 (draft prEN 1995-2, 2003-05-28) gave for the anchorage strength of glued-in rods in all grain directions

$$f_{a,k} = 5,5 \cdot \frac{\tanh \omega}{\omega} (1 - l_a / 100d) \quad [\text{N/mm}^2] \quad (5.3)$$

$$\text{where } \omega = \frac{0,016 \cdot l_a}{\sqrt{D}} \quad (5.4)$$

Note: all the design rules of glued-in rods have been removed from the present final draft of prEN 1995-2.

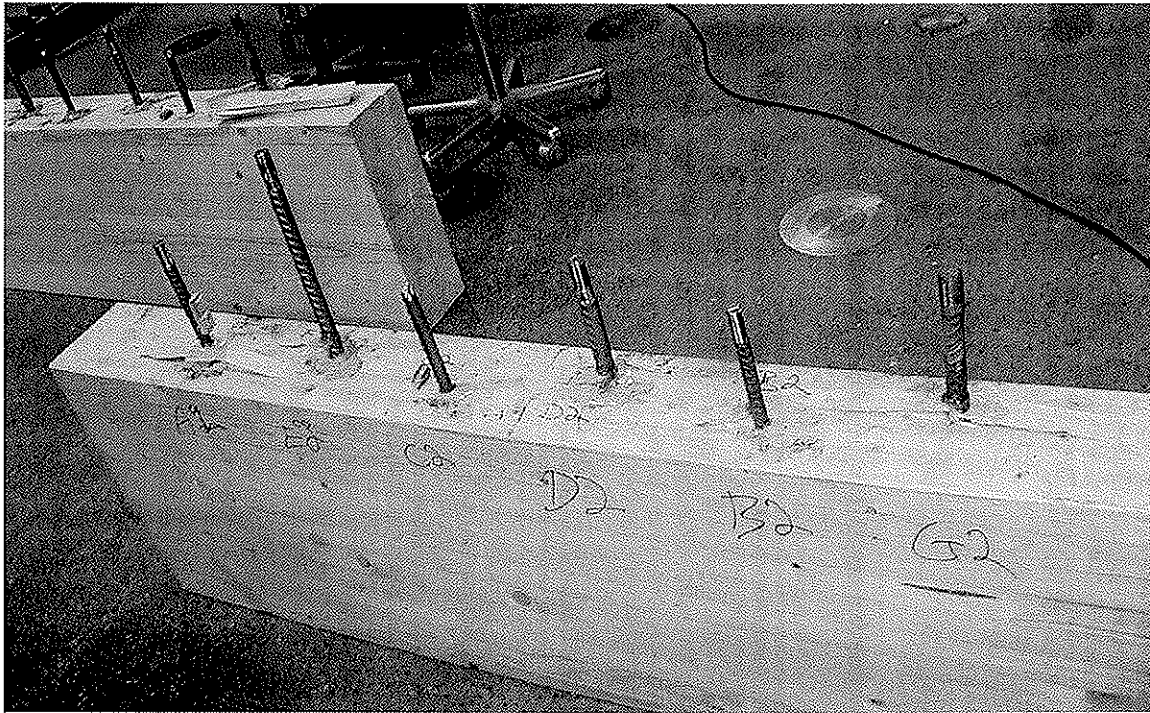


Figure 5.1 Test specimen after anchorage tests of glued-in rods.

Table 5.1 Anchorage tests results of glued-in rods. δ_{max} is slip of rod at failure load F_{max} . $f_{t,m}$ is tension stress of rod at failure load. $f_{a,k}$ is characteristic anchorage strength calculated according to equation (5.2) and (5.3).

test series	material	d (mm)	D (mm)	l_a (mm)	δ_{max} (mm)	F_{max} (kN)	var (%)	$f_{t,m}$ (N/mm ²)	$f_{a,m}$ (N/mm ²)	$f_{a,k}$ (5.2) (N/mm ²)	$f_{a,k}$ (5.3) (N/mm ²)
A	EN 1.4306	16	20	240	1,23	98,4	5,8	489	6,53	5,53	4,46
B	EN 1.4306	16	20	360	2,00	142,5	6,0	709	6,30	5,04	3,67
C	EN 1.4306	16	20	480	2,02	166,0 *)	2,6	826	5,51	4,55	3,00
D	EN 1.4306	20	25	300	2,52	141,1	12,9	449	5,99	5,53	4,26
E	EN 1.4306	20	25	480	3,81	203,6	5,4	648	5,40	4,94	3,26
G	non-alloy	20	25	300	1,32	142,4	9,3	453	6,04	5,53	4,26

*) Tension failure of steel rods. Anchorage failure in all other test series.

According to the test results, the anchorage strength of glued-in rods made of stainless steel reinforcing bars is the same as with the non-alloy steel rods. The high tension strength of stainless steel bars may be utilised even up to 800 Mpa by using long anchorage lengths.

The anchorage capacities of all test series corresponded well with the values calculated by the equation (5.2) presented by Kangas (1994). The length effect was in accordance with the equation (5.2) also in the case of the longest anchorage length (30d). In equation (5.3) the anchorage length effect is clearly too conservative.

6 Conclusions

The main result of the research was that the ultimate tensile strength of stainless steel may be fully utilized in the design of the connections of timber structures. The Eurocode equations of yield moments (prEN 1995-1-1:2003) may be safely used for stainless steel fasteners with the ultimate tensile strength of stainless steel. However, for full utilization of the stainless steel fastener capacity, it is advisable to use the tested yield moment values for the actual fastener type and dimension. The stainless steel material may be significantly strengthened in the manufacturing of certain type of stainless fasteners (e.g. threaded nails). Also the strain hardening occurred in the bending of the stainless fasteners may be utilized by using the tested yield moment values. The high ductility and strain hardening of stainless steel fasteners improve the capacity and behaviour of the connections of timber structures.

The withdrawal strength of stainless nails and screws is practically the same as with similar non-alloy fasteners, although the edges of fasteners profiles are generally slightly more round with stainless fasteners. However, the present new version of Eurocode 5 (prEN 1995-1-1:2003) gives about two times too high withdrawal capacity values for the common self-tapping screws loaded perpendicular to the grain. It is also in conflict with the testing and product standards (EN 1382:1999 and prEN 14592:2002). The withdrawal capacity presented for the self-tapping screws by Hansen (2002) is proposed for the correction of Eurocode 5, see equations (3.6) and (3.7).

The anchorage strength of glued-in rods made of stainless steel reinforcing bars is the same as with the non-alloy steel rods and it may be calculated according to the equation (5.2) presented by Kangas (1994). The full anchorage strength of glued-in ribbed stainless steel rods is reached even with the tension stress value of 800 N/mm^2 .

7 References

- Ehlbeck, J. & Görlacher, R., 1982, Mindestnagelabstände bei Stahlblech-Holznagelung. Research Report, Versuchsanstalt für Stahl, Holz und Steine, Universität Karlsruhe, Germany.
- Ehlbeck, J., & Siebert, W., 1988, Axially loaded nails - Proposals for a supplement to the CIB-Code. Proceedings CIB-W18 Parksville, Vancouver Island, Canada.
- Hansen, K.F, 2002, Mechanical properties of self-tapping screws and nails in wood. Can. Journal of Civil Eng. 29: 725-733.
- Kangas, J., 1994, Joints of glulam structures based on glued-in ribbed steel rods. VTT Publication 196. Espoo, Finland.
- Kevarinmäki, A., 2002, Joints with Inclined Screws. Proceedings CIB-W18 Kyoto, Japan.
- Werner, H. & Siebert, W., 1991, Neu Untersuchungen mit Nägeln für den Holzbau. Holz als Roh- und Werkstoff. 49: 191-198.

INTERNATIONAL COUNCIL FOR RESEARCH AND INNOVATION
IN BUILDING AND CONSTRUCTION

WORKING COMMISSION W18 - TIMBER STRUCTURES

DOWEL JOINTS IN ENGINEERED WOOD PRODUCTS:
ASSESSMENT OF SIMPLE FRACTURE MECHANICS MODELS

M Snow

I Smith

A Asiz

University of New Brunswick

CANADA

Presented by A Asiz

A Jorissen questioned the test configuration of 88mm by 300 mm (height by length) because the load path for a different configuration can be very different. Asiz responded that the test configuration was ASTM based. Asiz also acknowledged that Eqn 4 was theoretical not empirical.

Dowel joints in Engineered Wood Products: Assessment of simple fracture mechanics models

Monica Snow, Ian Smith, Andi Asiz
University of New Brunswick, Canada

1 Introduction

Tests are in progress at UNB to determine failure loads and mechanisms for connections where bolts load engineered wood products (EWP). The EWP being studied is Laminated Strand Lumber (LSL).

Simple fracture mechanics models are used to analyze LSL as well as solid wood (control condition) to investigate whether existing models are appropriate for these materials. Analysis examined whether or not simple 'change in compliance based' fracture mechanics models can predict observed failures to an acceptable accuracy. Models considered include those proposed during previous CIB-W18 meetings. It is concluded that for simple arrangements Linear Elastic Fracture Mechanics (LEFM) models can yield good predictions. However, this provided no certainty of accuracy for other, more complex, joints.

2 Experimental Program

2.1 Single dowel joint tests

LSL is a structural composite lumber product manufactured by Trus Joist, A Weyerhaeuser Business and known by its trade name TimberStrand®. It is formed from sliced wood strands that are aligned in a direction parallel with the length of the member and bonded together with isocyanate-based adhesives. Such products are used primarily in light-frame construction.

LSL specimens used for testing were cut from material produced at the Chavies, Kentucky USA plant. The species composition of this material was primarily Yellow Poplar [*Liriodendron tulipifera* L.] and had an assigned grade of 2250Fb-1.5E. The solid wood species was Eastern White Pine [*Pinus strobus* L.]

Double shear joints were tested wherein a single 19 mm ($\frac{3}{4}$ ") diameter dowel loaded LSL or solid wood main member perpendicular to the strongest axis of material symmetry, i.e. loading solid wood normal to the grain direction and LSL normal to the strand direction, Figure 1. The central member was 44.5 mm ($1\frac{3}{4}$ "), which insured negligible bolt bending and maximized the likelihood of fracturing/brittle failure. The side members were made of 33 mm ($1\frac{1}{4}$ ") thick high strength transparent polycarbonate material, GE Lexan®, instead of the more usual steel to enable visual recording of the behavior of the wood-connection system under applied load. Tests followed protocol specified in the ASTM D5652-95 (2000) "Standard Test Methods for Bolted Connections in Wood and Wood-Based Products" [1].

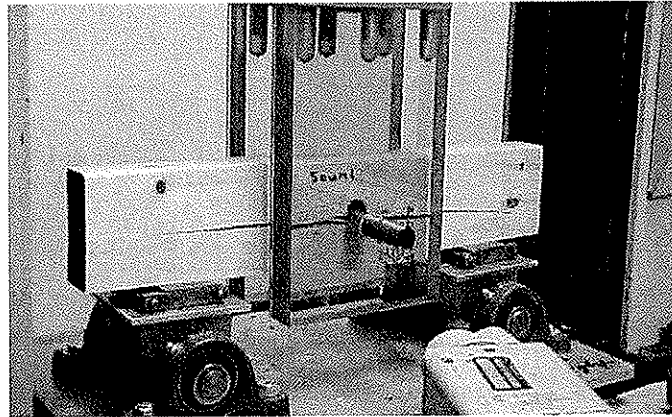


Figure 1: Test Set-up with Solid Wood Centre Member

Test results for strength of single dowel joints for LSL and solid wood are summarized in Table 1. These include mean values (kN) of applied load corresponding to the appearance of the first surface cracks of 10 mm in length, yield point, and ultimate strength.

Table 1: Specimen Strength

	Load - 1st Crack (kN)		Yield Strength *(kN)		Ultimate Strength (kN)	
	Pine	LSL	Pine	LSL	Pine	LSL
Mean (kN)	7.5	26.7	7.8	21.9	8.6	28.4
Standard Deviation (kN)	0.7	4.3	0.7	4.3	0.9	3.1
Coefficient of Variation (%)	10%	16%	9%	20%	10%	11%

* as defined by ASTM D5652-95(2000):

Figure 2 shows typical load-crosshead displacement curves. The initial concavity of each response is due to take-up of slack in the dowel hole. There was little practical difference in initial stiffness for LSL and solid wood once the dowel bedded down, but clearly there were some differences in ultimate load and failure characteristics.

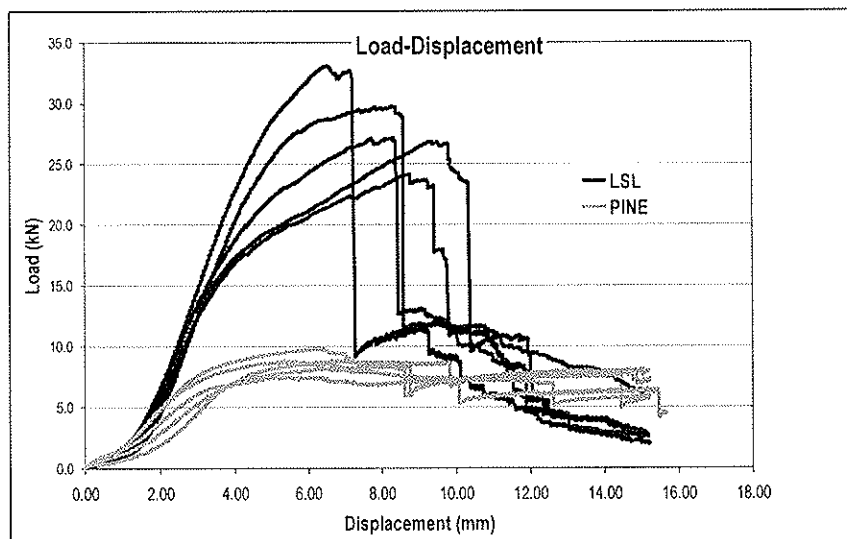


Figure 2: Load-Crosshead Displacement Curves

Failures for both wood materials tested were always due to fracturing of the main member as observed and digitally imaged through the side members. Selection of boundary conditions and fracture toughening control whether crack growth is inherently stable or inherently unstable. In this study, the arrangement, Figure 1, could be either inherently stable or unstable in the absence of toughening. Thus crack growth and failure may not coincide. Figures 3 and 4 illustrate fracturing at ultimate load.

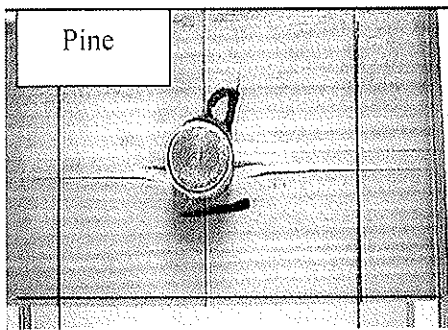


Figure 3: Pine specimen at Ultimate Load

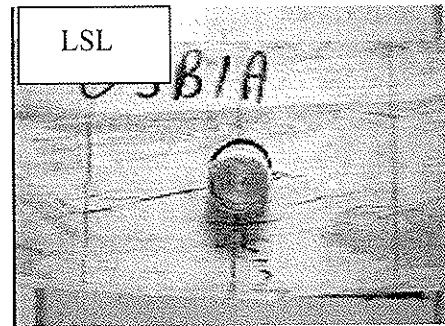


Figure 4: LSL specimen at Ultimate Load

Results indicate that LSL failure characteristics are very different from solid wood. Pine specimens had the lower yield and ultimate strength and showed apparent ductility beyond the ultimate loading. First visible (> 10 mm long) cracks in pine specimens occurred between 92 and 100% of the yield load, with bearing failure and splits associated with cracks greater than 50 mm. When LSL specimens reached an apparent first yield condition (yield point), minimal splitting and crushing had occurred. At or near ultimate load, brittle fracture of the material occurred with a near instantaneous large decrease in residual carrying capacity of the material. Failure was distinguishable as a tension fracture at the extreme bottom fibres, which propagated upward to the dowel hole perpendicular to the member axis. In essence LSL specimens failed due to excessive bending moment in the central member. This reflects that there is much cross-lamination of strands and macro homogenisation that greatly toughens LSL against fracturing at the hole. It is apparent that when using an ASTM D5652-95(2000) [1], or similar test arrangement there is no guarantee of what the failure mode will be nor of whether stability is due to the choice of geometric variables or intrinsic fracture toughness.

2.2 Material property tests

Because of limited published test results relating to material properties of LSL, especially with regards to fracture behaviour, subsidiary tests for LSL were conducted to determine mechanical and physical properties. Results of the mechanical property testing, including Modulus of Elasticity (E_i), Modulus of Rigidity (G_{ij}) and Poisson ratios (ν_{ij}) are summarized in Table 2. No tests for mechanical properties for solid wood were carried out. Published values were used in subsequent modeling. These values are summarized in Table 3 [2].

Table 2: LSL mechanical properties

Mechanical Property	Values	COV
Density, ρ	640 kg/m ³	7%
E_x	6400 Mpa	20%
E_y	810 Mpa	23%
ν_{xy}	0.360	67%
G_{xy}	101 MPa	12%

Table 3: Pine mechanical properties

Mechanical Property	Values
Density, ρ	380 kg/m ³
E_x	10,100 Mpa
E_y	79 Mpa
ν_{xy}	0.360
G_{xy}	525 MPa

Fracture testing of LSL for both Mode I and Mode II fracture was also conducted. For both Mode I and Mode II, three test sets were employed; a set for three different notch lengths, with six replicates for each set. Compact specimen arrangements were used for Mode I and II fracture testing as shown in Figures 5 and 6. Specimens for Mode I compact tension tests were 155mm in length, with notch lengths of 65mm, 70mm, and 75mm. Compact shear specimens for Mode II tests were 70mm long with 2 parallel notch lengths of 35mm, 45mm, and 55mm.

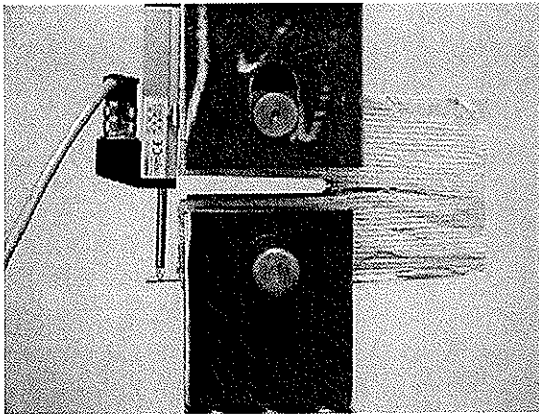


Figure 5: Mode I Fracture Test Set-up

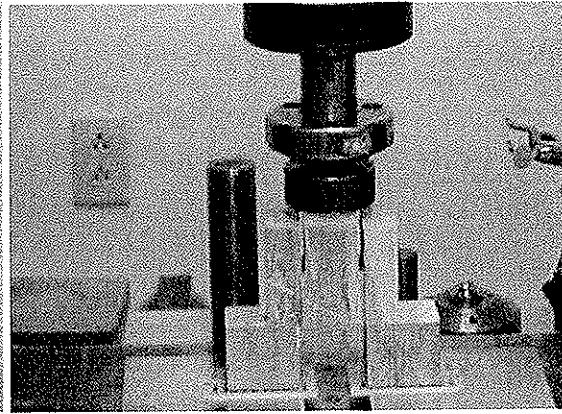


Figure 6: Mode II Fracture Test Set-up

Characteristic fracture behavior for LSL in Mode I is shown in Figure 7 and in Mode II in Figure 8. Typical load-displacement curves for the fracture tests are presented in Figure 9 for Mode I and in Figure 10 for Mode II.

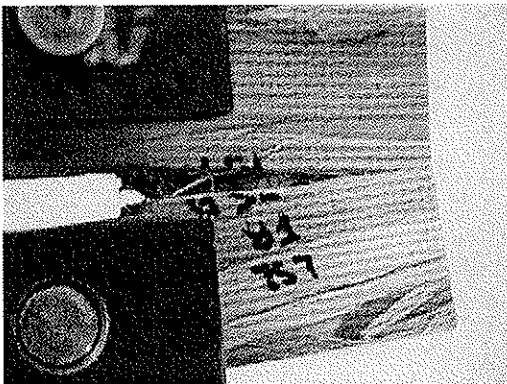


Figure 7: Mode I Fracture

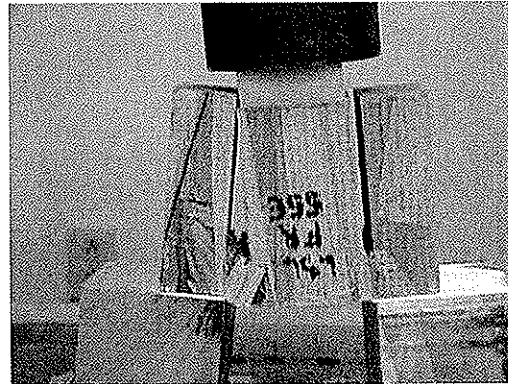


Figure 8: Mode II Fracture

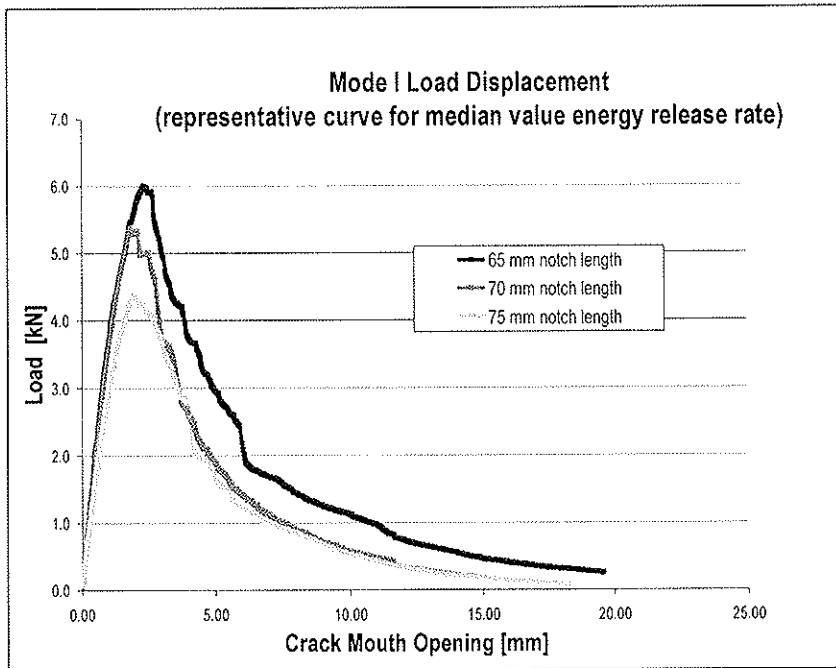


Figure 9: Mode I Load Displacement Curve

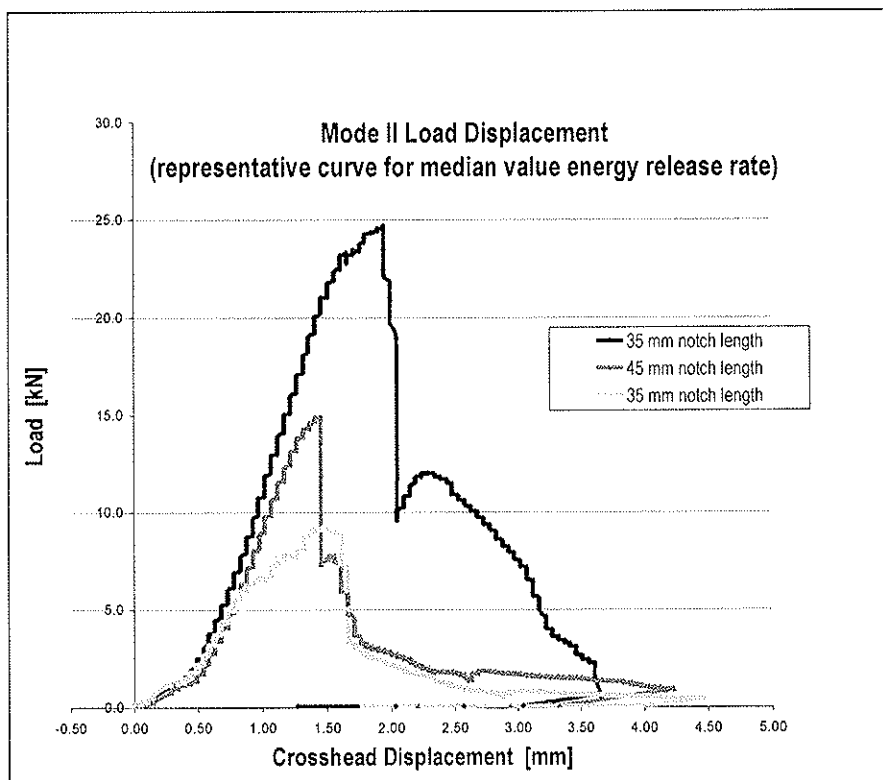


Figure 10: Mode II Load Displacement Curves

Fracture test results for LSL are presented in Table 4. The energy release rates (G_{ic}) are based on the fracture tests ($i = I$ and II). K_{ic} values were determined using these rates, the mechanical properties of LSL and the relationship between G_{ic} and K_{ic} for anisotropic materials expressed in the following equation [3].

$$G_{ic} = \sqrt{\left(\frac{a_{11} a_{22}}{2}\right) \left(\sqrt{\frac{a_{11}}{a_{22}} + \frac{2a_{12} + a_{66}}{2a_{22}}}\right)} K_{ic}^2 \quad (1)$$

$$\text{where } \begin{Bmatrix} \varepsilon_1 \\ \varepsilon_2 \\ \varepsilon_3 \end{Bmatrix} = \begin{bmatrix} a_{11} & a_{12} & 0 \\ a_{21} & a_{22} & 0 \\ 0 & 0 & a_{66} \end{bmatrix} \begin{Bmatrix} \sigma_1 \\ \sigma_2 \\ \sigma_3 \end{Bmatrix} \text{ with } \begin{bmatrix} a_{11} & a_{12} & 0 \\ a_{21} & a_{22} & 0 \\ 0 & 0 & a_{66} \end{bmatrix} = \begin{bmatrix} \frac{1}{E_x} & \frac{\nu_{xy}}{E_x} & 0 \\ \frac{\nu_{yx}}{E_y} & \frac{1}{E_y} & 0 \\ 0 & 0 & \frac{1}{G_{xy}} \end{bmatrix}$$

Table 4: LSL Fracture Results

Fracture Mode	G_{ic} , Energy Release Rate (kN/m)	K_{ic} , Stress Intensity Factor (kN-m ^{-3/2})
Mode I	7.8	6480
Mode II	11.0	7720

3 Fracture Mechanics Modeling

3.1 Finite element model of the main member

The single dowel joint geometry used for finite element modeling is shown in Figure 11. Two symmetric sharp-cracks were assumed to exist near the dowel hole. The crack was positioned at the middle edge of the dowel hole. In this study, several different crack lengths were examined. Because of the symmetry of geometry and loading, only half of the dowel joint was analysed. Since the dowel stiffness is large compared to wood or LSL stiffness, 2D plane stress conditions were assumed. Numerical analysis was performed using commercial finite element software ABAQUS version 6-4.1. The study was limited to small strain analysis.

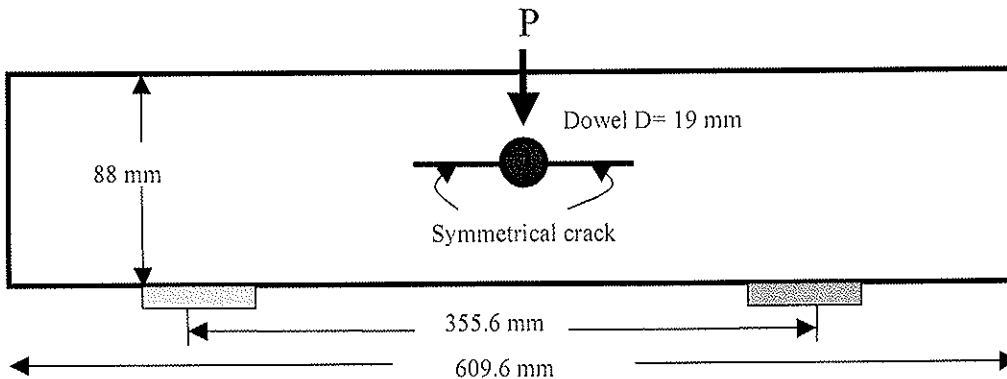


Figure 11: Geometry of dowel joints in EWP

Due to the symmetry only a half system needed to be analyzed. Figure 12 is representative of the finite element mesh for the main member and the dowel joints, showing the detailed mesh in the vicinity of the crack tip. The mesh was changed for each crack length to give the same level of mesh refinement around the crack tip region. The total number of degrees of freedom used varies between 15,000 and 20,000. Elements used for the mesh configuration include eight-node isoparametric elements (CPS8) for wood and four-node isoparametric elements (CPS4) for the steel dowel. In the vicinity of the crack tip, sixteen quarter-point-singular isoparametric elements were used to better approximate the stress 'singularity'. At the connection, contact surfaces were created between wood and dowel assuming a no slip condition between them. Conditions at the connection also include the assumption that the dowel is a perfect fit with the dowel hole. A load of 1 kN (0.5 kN for the half model shown) was applied at the dowel. Cracks of 11 mm, 25.4 mm, 38.1 mm, 59.1 mm, and 128 mm in length were modeled.

LSL and solid wood (pine) are modeled as linear elastic orthotropic materials with the mechanical properties given in Tables 2 and 3, respectively. While the steel dowel is modeled as an isotropic material with modulus of elasticity and Poisson's ratio of 200 GPa and 0.30, respectively.

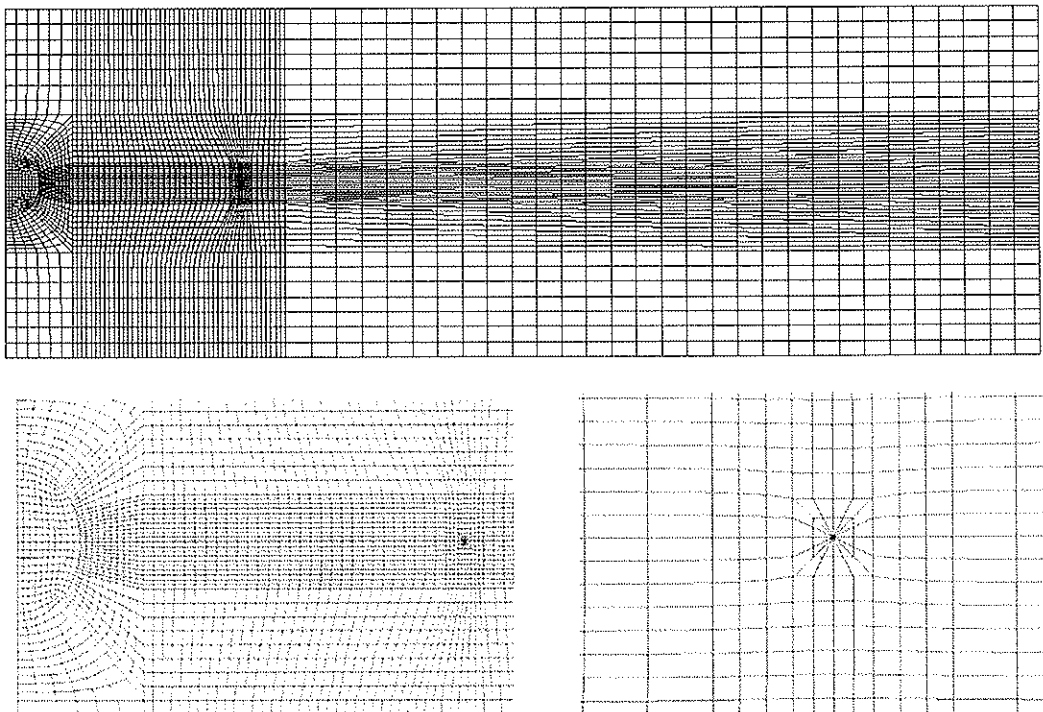


Figure 12: Finite element mesh and its detail at the crack tip

3.2 Numerical assessment

In this study, the stress intensity factor was calculated using the domain J -integral method via routine library available in ABAQUS [3]. The J -integral method is usually used in rate-independent quasi-static fracture analysis to characterise the energy release rate associated

with crack growth. J values can be related to the stress intensity factors if the material has a linear response, i.e. LEFM. The J -integral should be independent of the domain (path) used. In this study, three-contour integral has path independence J values. A variation of less than $\pm 5\%$ was found for all models indicating that there is no need for mesh refinement around the crack tip. For illustration, the deformed shapes of dowel joint with various crack lengths are shown in Figure 13.

The calculated stress intensity factors *versus* crack lengths (11mm, 25.4mm, 38.1mm, 59.7 mm, and 128 mm) both for LSL and solid wood (pine) are presented in Figures 14 and 15, respectively. According to the models, the opening-mode (Mode I) dominates the fracture process compared with the shearing-mode (Mode II) for LSL. However, when the crack is longer the shearing-mode has a stronger influence on fracture behaviour. This is in contrast to solid wood (pine) where shearing mode dominates the fracture process after crack length reaches about 30 mm.

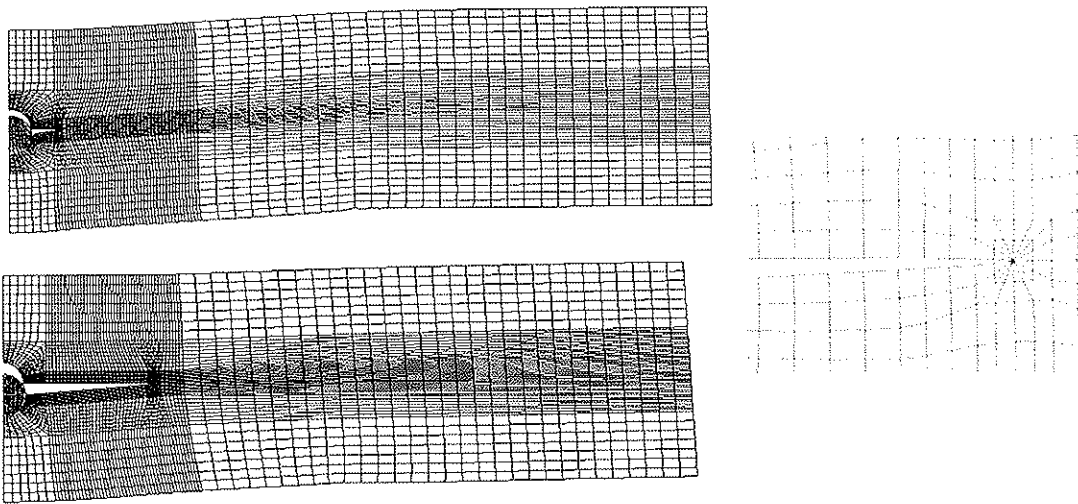


Figure 13: Deformed shapes of the dowel joints for various crack lengths

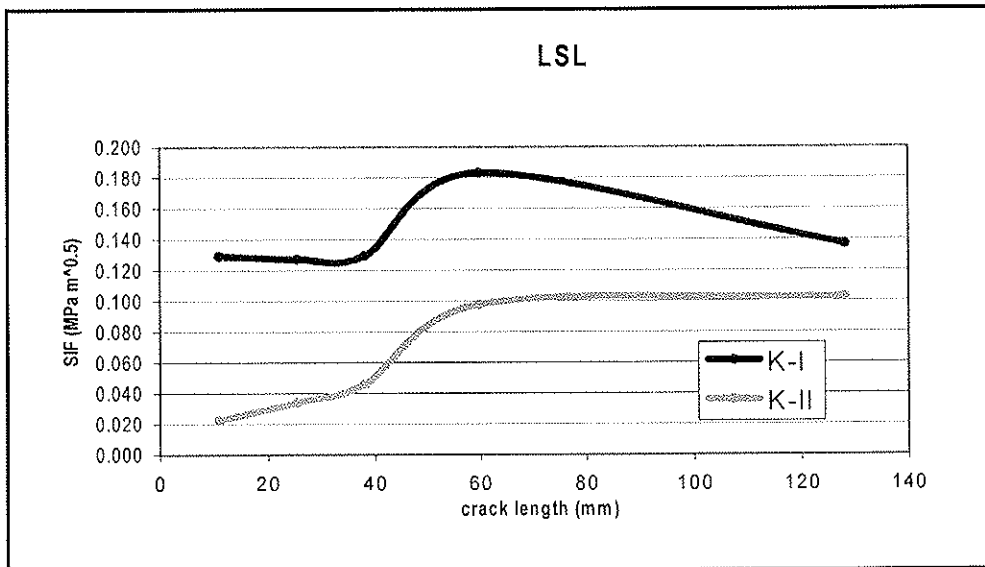


Figure 14: Stress intensity factors for LSL

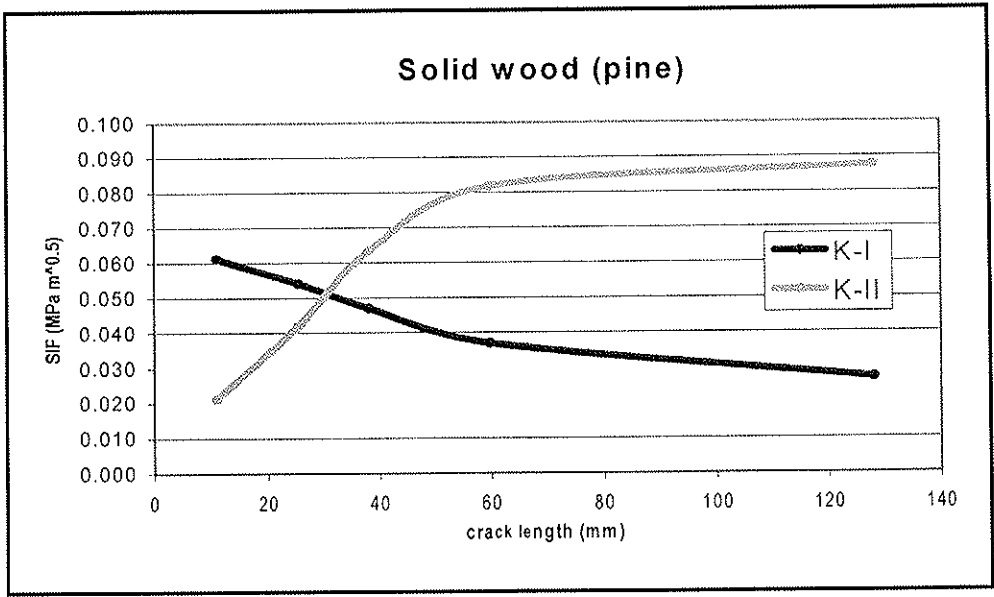


Figure 15: Stress intensity factors for solid wood

At the observed ultimate load (see Table 1), the stress intensity factors for various crack lengths can be examined based on the fracture criterion of Wu [5], i.e.

$$\frac{K_I}{K_{IC}} + \left(\frac{K_{II}}{K_{IIC}} \right)^2 = 1 \tag{2}$$

where K_{IC} and K_{IIC} are the critical stress intensity factors for opening and shearing modes, respectively. The values for LSL are obtained from the fracture testing discussed previously (see Table 4), while the values for solid wood (pine) was obtained from the literature [6]. Since no data was available for values of K_{IIC} for solid wood (pine), a ratio of 4 was assumed between K_{IC} and K_{IIC} . In the equation (2), the values for K_I and K_{II} are determined from the stress intensity factors values calculated before based on the unit load applied assuming linear material response. The results are presented in Tables 5. Crack propagation load versus crack length is plotted in Figure 16.

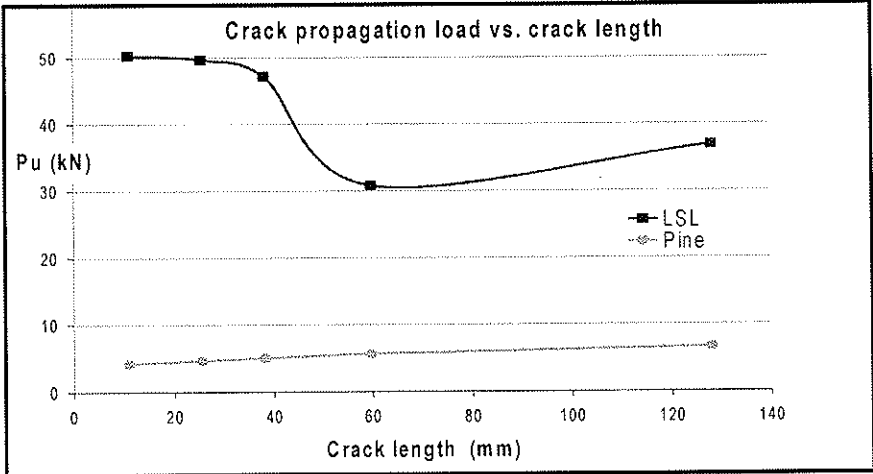


Figure 16: Crack propagation load vs. crack length for LSL and pine

Results indicate that for LSL all Wu's criterion values are less than 1.0. This implies that the dowel joint in LSL was not expected to fail even at longer crack lengths. This is contrary to test results where the crack propagates from the bottom side of the dowel mimicking the failure process of a three-point bending test. It can be concluded for LSL that the analysis of only a symmetrical crack positioned at the middle of the dowel hole is inconsistent with experimental results. The result obtained in LSL is in contrast with that in solid wood. For solid wood, a small crack (about 10mm) leads to unstable crack propagation.

Table 5: K_I , K_{II} , and Wu criterion values at the ultimate load for LSL and solid wood (pine)

Crack lengths (mm)	LSL: Load at $\frac{1}{2} P_p = 14.2$ kN			Pine: Load at $\frac{1}{2} P_p = 4.3$ kN		
	K_I (kN-m ^{-3/2})	K_{II} (kN-m ^{-3/2})	Wu's criterion	K_I (kN-m ^{-3/2})	K_{II} (kN-m ^{-3/2})	Wu's criterion
11.0	1860	328	0.29	263	92	1.02
25.4	1833	492	0.29	232	180	0.92
38.1	1866	666	0.30	202	272	0.84
59.7	2638	1408	0.44	159	352	0.72
128	1972	1477	0.34	116	376	0.58

3.3 Closed form analysis

Assessment of splitting strength of LSL and solid wood was carried out using equations presented by van der Put [7] and Jensen et al [8]. The equations are as follows:

Van der Put:
$$\frac{V_f}{b\sqrt{h}} = \sqrt{GG_f} \sqrt{\frac{\alpha}{0.6(1-\alpha)}} \quad (3)$$

where α defines the location of the dowel with respect to the loaded edge and the height of the beam,
 b is the width of the beam,
 h is the height of the beam,
 G is the shear modulus of the material,
 G_f is the fracture energy perpendicular-to-grain, and
 V_f is the maximum shear force at fracture.

Jensen et al:
$$P_p = \mu P_{p,LEFM} = \mu b \sqrt{\frac{20}{3} GG_f h_e} \quad (4)$$

with $\mu = \sqrt{\frac{2\zeta+1}{\zeta+1}}$ and $\zeta = \frac{5}{\sqrt{3}} \frac{G}{E} \sqrt{\frac{2EG_f}{h_e f_t^2}}$

where b is the width of the beam,
 h_e is distance from the closest dowel to the loaded edge,
 G is the shear modulus of the material,
 G_f is the fracture energy perpendicular-to-grain,
 E is the Modulus of Elasticity,
 f_t is the tensile strength parallel-to-grain,
 $P_{p,LEFM}$ is the failure load as a LEFM solution, and
 P_p is the failure load

A comparison of the experimental and calculated values for splitting failure loads of the beam is presented in Table 6.

Table 6: Comparison of ultimate load for LSL and solid wood (pine)

	LSL: Failure (ultimate) load P_p (kN)	Pine: Failure (ultimate) load P_p (kN)
Experimental	28.4	8.6
Van der Put ($P_p = 2V_f$)	29.9	7.4
Jensen et al	22.5	7.3

Results of the closed form analysis indicate a good fit to the test results; however, the implication that it explains splitting behaviour should not be extrapolated from this analysis.

In effect the simple equation suffers from the same flaw as the FE analysis for LSL in that it fails to recognize the critical failure mechanisms for LSL (3-point bending). Whereas the equations derived by van der Put and Jensen are based on the premise that the splitting will initiate and propagate from the high stress area of the joint; in fact, the splitting initiates at the extreme fibre of the tension side of the LSL beam and propagates upwards to the dowel location.

4 Conclusion

According to finite element modeling of LSL for the particular test set-up used in the experimental program, material resistance to Mode I, crack mouth-opening fracture dominates the failure process. Application of Wu's criterion indicates that crack propagation never becomes unstable for LSL and implies that the dowel joint is not expected to fail, even at longer crack lengths. Analysis does not account for the failure mechanism observed during testing where tension fracture initiated at the extreme fibre and then propagated upwards to the dowel hole, perpendicular to the main member.

Finite element modeling of pine indicates that Mode I, crack mouth-opening fracture dominates failure to a crack length of about 30mm. According to Wu's criterion, pine will exhibit unstable crack propagation at about 10mm.

Test results are in reasonable agreement with the European fracture models proposed by van der Put and Jensen for the particular single dowel joint arrangement studied, but caution must be used in extrapolating these findings for other joint configurations or loading conditions.

5 References

- [1] American Society for Testing and Materials (ASTM). 2000. Standard Test Methods for Bolted Connections in Wood and Wood Base Products, Designation D 5652-95(2000), ASTM, West Conshohocken, PA.
- [2] Forest Products Laboratory (FPL). 1999. Wood Handbook: Wood as an Engineering Material; General Technical Report FPL-GTR-113. Forest Products Society and United States Department of Agriculture, Washington, DC, USA. 1999.

- [3] Hibbit, Karlsson & Sorenson. 2003. ABAQUS/Standards version 6.4-1: User's Manual, Pawtucket, Rhode Island, USA.
- [4] Sih, G. C., P. C. Paris and G. R. Irwin. 1965. On cracks in rectilinearly anisotropic bodies, *International Journal of Fracture Mechanics*, 1: 189-203.
- [5] Wu, E. M. 1967. Application of fracture mechanics to anisotropic plate, *Journal of Applied Mechanics*, Vol. 34 (4): 967-974.
- [6] Patton-Mallory, M. and S. Cramer. 1987. Fracture mechanics: a tool for predicting wood component strength, *Forest Products Journal*, ASCE, Vol. 123 (8): 1054-1062.
- [7] van der Put, T.A.C.M. 2000. Evaluation of perpendicular to grain failure of beams caused by concentrated loads of joints. CIB-W18, paper 33-7-7, Delft, the Netherlands.
- [8] Jensen, J., P. Gustafsson, and H. Larsen. 2003. A tensile fracture model for joints with rods or dowels loaded perpendicular-to-grain. CIB-W18 paper 36-7-9, Colorado, USA.

INTERNATIONAL COUNCIL FOR RESEARCH AND INNOVATION
IN BUILDING AND CONSTRUCTION

WORKING COMMISSION W18 - TIMBER STRUCTURES

NUMERICAL MODELLING OF TIMBER AND CONNECTION ELEMENTS
USED IN TIMBER-CONCRETE-COMPOSITE CONSTRUCTIONS

M Grosse

K Rautenstrauch

Bauhaus-University Weimar

GERMANY

Presented by M Grosse

J W van de Kuilen asked about the connect element and the friction value. Grosse responded that surface elements were used and the friction value was approximately 0.5 to 0.6.

J Köhler asked about the material properties. Grosse responded that the material properties were based on literature and there were 16 values.

J Zhang asked about load reversal and Grosse clarified that short term experiments were considered without load reversal.

Numerical modelling of timber and connection elements used in timber-concrete-composite constructions

Dipl. -Ing. Marco Grosse
Prof. Dr. -Ing. Karl Rautenstrauch
Bauhaus-University Weimar, Germany

1 Introduction

Experiments are an important basis of civil engineering. Experimental tests are needed to define physical properties of building materials as well as to make reliable statements concerning the structural safety of components considering scattering influences. It has to be noticed, that limited information can be gained from test with conventional measurement techniques. Most often only the applied load, deflections of few points relative to a reference and integral strains at some sections can be determined. In spite of the enormous effort in applying measurement techniques, the flux of forces within the member can not be determined directly. It can only be interpreted with an engineering understanding of the measuring data and the responses of a structure. Furthermore, the information won from the experimental test only apply to the fixed boundary conditions and are not transferable to real installation conditions without limitations. They are two alternatives that improve the meaningfulness of tests:

1. *Increasing the concentration of measuring points:* This can not be realized with classic mechanical or electronic measurement techniques. Concentration of the measuring points is easily possible using contactless methods, such as the close-range-photogrammetry.
2. *Accompanying numeric simulation of the tests:* The distribution of forces, stresses and strains across the member can be calculated and visualized by verifying a mathematical model based on the experimental results. In the model it doesn't cause any difficulties to vary boundary conditions and material properties. With this procedure it is possible to improve the test programme and also to optimize the examined member.

At the Chair of Timber and Masonry Engineering we pursue both approaches. In the context of research projects we are developing a new photogrammetric system, which is suitable for timber elements taken into account the special requirements of the material. This system is introduced in paper 37-19-2 and some applications and results are shown. This paper deals with the numeric simulation of timber and timber-concrete-composite elements, with a special concern to introduce the developed constitutive material model for wood. Our research in this area is promoted by the *DFG* (German Research Foundation).

2 Non-linear computational approach

The ultimate resistance and the load carrying reserves in the post-critical range besides the linear-elastic load-deflection-relationship at service-load are determined in experimental tests. Therefore it is no longer sufficient for numeric simulations to describe the material

only with the linear-elastic theory. The degradation of strength is depending on type and direction of loading, and has to be included to characterise the load carrying behaviour and to compute failure mechanisms above the service-load range.

For this reason constitutive material models for timber and concrete based on the plasticity theory were implemented in the FEM-program ANSYS. The mathematical model is based on the classic continuum mechanics. Therefore the mechanical properties of the material and the resulting damages are spread over a certain area. With this approach a crack is not described discretely but by its effect on the stress-deformation behaviour (see chapter 3.2.1). The real crack opening is averaged in form of plastic strains along an element.

At first only the short-time carrying behaviour using the material model is examined and rheologic and hygroscopic properties need not to be considered. Under this assumption the nonlinear mechanical behaviour can be represented based on time-independent plasticity. Material strains resulting from loading are reduced to an elastic part and an irreversible immediately appearing part (equation 1). The underlying theory permits an expansion of the irreversible portion of the deformation, therefore behaviour depend on time and moisture content like creep and shrinkage can be implemented in future research.

$$\begin{aligned} \{\varepsilon_{tot}\} &= \{\varepsilon_{el}\} + \{\varepsilon_{pl}\} \\ \{\varepsilon_{tot}\}^T &= \{\varepsilon_x, \varepsilon_y, \varepsilon_z, \gamma_{xy}, \gamma_{yz}, \gamma_{xz}\} \end{aligned} \quad (1)$$

According to the plasticity theory there are three principle relations describing mathematically the strength behaviour of materials:

- The material behaves linear-elastically until reaching the *yield criterion*.
- Exceeding this limit the residual strength is calculated according to the *hardening rule* dependent on the plastic strain (strain softening).
- Stress states above this residual strength are not allowed and have to be traced back to permitted values. Plastic strains arise due to this reduction according to the defined *flow rule*. This algorithm causes an iterative procedure.

3 The material model for wood

3.1 Assumptions and restrictions

Wood is an inhomogeneous, anisotropic and strongly porous material. Its mechanical properties are primarily affected by density, species and moisture content of wood. The developed material model presented in this paper is without restrictions only valid for softwood due to the implemented failure mechanisms. It is formulated depending on initial parameters, to enable an approximation of real stress-strain curves. An adaptation to different climatic conditions is also possible. Wood is also riddled by many macroscopic defects like knots, shakes and fibre deviations that very adversely influence the quality of the material. In the material model, however, such defects are neglected and a defect-free material is assumed.

In addition, orthotropic behaviour can be assumed regarding to the natural axes of wood, which describe a cylindrical coordinate system. Not only the elastic constants but also the fracture toughness, failure mechanisms and strength degradation vary widely with the natural axes longitudinal to the trunk (L), radial (R) and tangential (T) to the annual rings. In principle wood fails in a brittle failure at tension or shear but shows a ductile behaviour when loaded in compression. These special features of wood will be considered by the three dimensional material model.

3.2 Hardening rule

3.2.1 Strength reduction due to tension or shear loading

In *tension loading perpendicular to the grain*, the longitudinal crack propagation is predefined by the fibre direction. The failure is marked by a brittle fracture with a clear crack formation. Only a small process zone forms, the damage does not spread outside the crack line. At microscopic-scale it can be recognized that cells are arranged in a line in radial direction, but alongside the annual rings they are shifted against each other. Due to this anatomical construction there is a separation plane in the LR-plane. Therefore a fibre separation mainly in the middle lamella can be observed during crack formation [5]. In the LT-plane the crack proceeds mainly through the cell walls of adjacent fibres. Both of these failure mechanisms lead to brittle failure. The ultimate strengths are within the same range, but are only about 10% of the tensile strength in fibre direction of defect-free wood.

The crack surface of a *longitudinal tension* fracture is very fibrous. The crack-line intersects the tracheids in spring wood. In the more rigid late wood the fibres are separated [3]. Contrary to the mechanical expectation the crack can also progress partly in force direction along the boundary layer between early and late wood. Only little energy is dissipated as a result of crack growing compared to the strain-energy stored in the member during a test. Therefore it is very difficult to enforce stable crack propagation; even in a displacement-controlled test. For these reasons fracture-mechanical experiments for this mode are extensive and difficult to perform and sparsely documented in literature [12, chapter 2] [13].

Shearing represents a condition in which the principle-stress trajectories course at 45° to the treated plane. This explains, why shear failure is very similar to tension failure. Shear failure in the RT-plane, as a result of τ_{LR} or τ_{LT} , is excluded. Only longitudinal shear sliding can be observed. The interface between late and early wood represents the weakest plane in timber. If the crack can spread freely, it will follow this interface. So it is incidental that rolling-shear failures due to τ_{RT} and τ_{TR} have to be distinguished.

The strength-reduction as result of shear or tension failure respectively is described by an exponential function in dependence of fracture-energy G^F dissipated during crack formation. In addition the formulation has to take into account the mesh used in the numeric model, e.g. by inclusion of the crack-band width h [2]. Otherwise the rate of strength-reduction is mesh-dependent. With increasing element size the computed elongation and the area below the work-diagram would increase (more energy dispersed). By adoption of a softening-function Ω for example for tangential tension-loading it follows:

$$f_{T,t,\kappa}(\kappa_2) = f_{T,t} * \Omega_{fT,t}(\kappa_2) \quad (2)$$

$$\Omega_{fT,t}(\kappa_2) = e^{-\left(\frac{h * f_{T,t}}{G_{T,t}^F} * \kappa_2\right)} \quad (3)$$

The degradation-parameter κ is a measure for plastic strains. It also considers the interaction between failure modes, in this case between tension perpendicular to grain, longitudinal shear and rolling shear in the LR-plane, and leads to a synchronous strength-degradation:

$$\kappa_2 = \sqrt{\varepsilon_{pl,T,t}^2 + \varepsilon_{pl,TL,s}^2 + \varepsilon_{pl,TR,s}^2} \quad (4)$$

In the case of pure tangential tension equation 3 limits a surface of:

$$\int_{\kappa_2=0}^{\infty} \Omega_{fT,t} d\kappa_2 = \frac{G_{T,t}^F}{h * f_{T,t}} \quad (5)$$

Transferred to a stress-crack opening-relationship this approach describes a surface below the function corresponding to the fracture-energy $G_{T,t}^F$. Often the stress is associated with the normalized deformation u/l , as shown in figure 1 for the results of *Poulsen's* tension-test [15]. Then the simulated curve limits a surface corresponding to the specific strain energy U_{el} in the elastic-range. The fracture energy related to the origin length is the result within the post-critical stage (figure 1(c)).

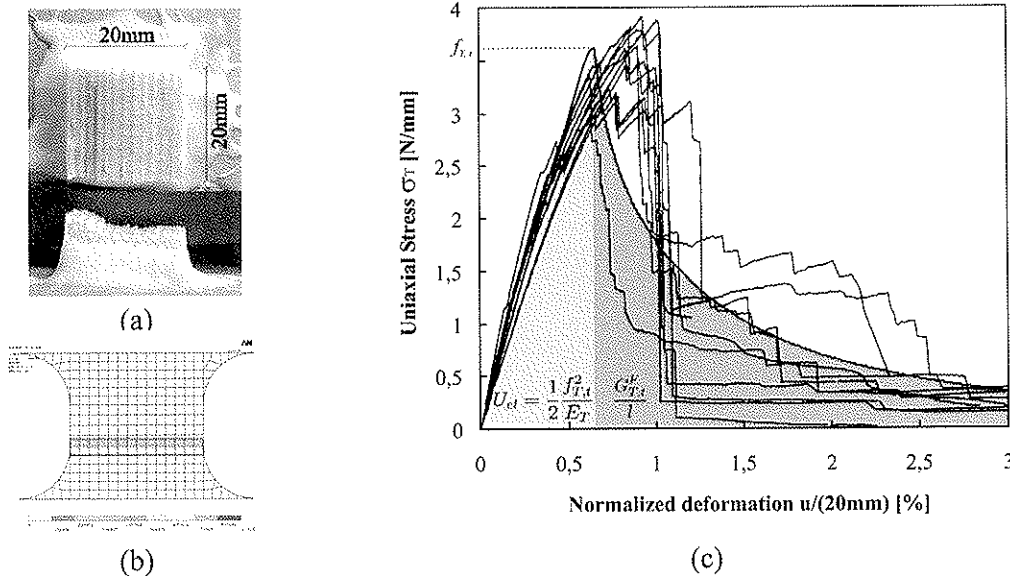


Figure 1: Transverse tensile test according to *Poulsen* [15]: (a) failed specimen (b) computed plastic strains for $u/20 = 3.0\%$ (c) test results and simulated strength-reduction

3.2.2 Strength degradation due to compression

The strength-degradation as a result of *longitudinal compression* can be divided into five stages (figure 2(a)):

Stage I: A linear elastically response can be assumed for wood for moderate longitudinal compressive strain. *Stage II:* Above the proportional limit the compressive strength is primarily affected by crumpling of the fibres. *Poulsen* names this non-linear transition up to the maximum load as "incipient kinking" [15]. The results of own experiments show that the deformations in this stage are almost evenly distributed over the entire specimen length (see chapter 5). *Stage III:* The compressive strength is limited by localised buckling of the fibres. A macroscopically recognizable kink-band under a small angle to the fibre forms [11][16]. A strength reduction is observed within this range of "transient kinking". The kink band will be compressed as expected. But an additionally shear-distortion occurs in consequence of lateral buckling of the fibres. The member parts are shifted against each other perpendicularly to the load or grain direction respectively. *Stage IV:* In the following phase of "steady-state kinking" adjacent material is pushed into the kink band. A relatively constant level of the residual strength results. Perpendicular tensile stresses develop between the fibres when they kink differently within this band and the member can crack lengthwise. *Stage V:* *Adalian* und *Morlier* proved a further phase within very large compressive deformations characterized by an immense hardening of the material [1].

For the mathematical description of the strength-development interpolation values need to be defined, based on the stress-strain-relationship that is schematically given in figure 2(a).

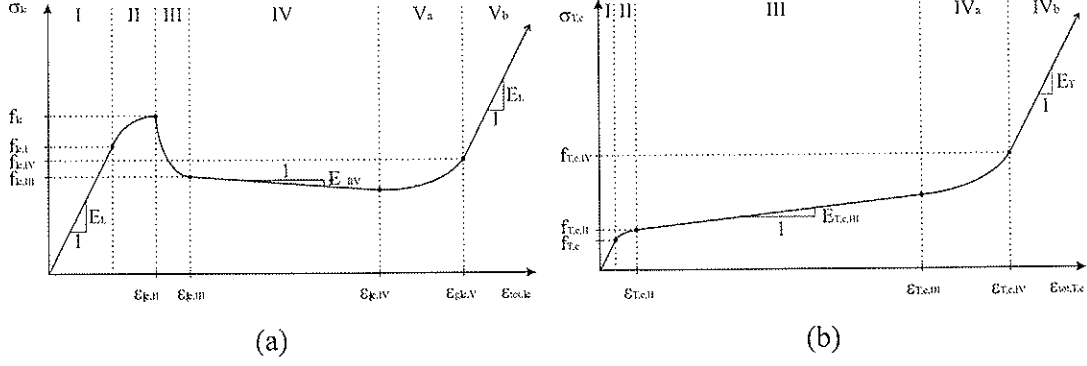


Figure 2: Numerically implemented strength development at compression: (a) longitudinal (b) perpendicular to the grain

These parameters are converted into internal variables. The strength can be computed using the sectional defined degradation-function $\Omega_{fL,c}$, which depends itself on the parameter κ_1 . Owing to shortage of space the individual equations can't be specified in this paper, but this means in principle:

$$\begin{aligned}
 f_{L,c,\kappa}(\kappa_1) &= f_{L,c} * \Omega_{fL,c} \\
 \Omega_{fL,c} &= f_i(\kappa_1) \quad (i = II, III, IV, Va, Vb) \\
 \kappa_1 &= \epsilon_{pl,L} \quad (\text{for } \epsilon_{pl,L} < 0)
 \end{aligned} \tag{6}$$

During transient kinking (stage III) the entire deformation forced upon the member takes place inside the kink band. Therefore $\epsilon_{gL,c,III}$ is not an absolute measure of strain. Otherwise the rate of strength-reduction would be dependent on the element size, as described in section 3.2.1. The degradation-function $\Omega_{fL,c}$ and thus the parameter $\epsilon_{gL,c,III}$ have to be described in dependence of the energy dissipated within fibre kinking. To characterize this fracture energy was another reason for conducting the compression tests introduced in chapter 5. Regrettably the test results are currently not evaluated exhaustive and the numeric implementation still has to be completed.

For *compression perpendicular to the grain*, the failure is also characterized as ductile. The stress-strain-diagrams in radial and tangential directions (figure 2(b)) are very similar [8]. Failure is originated by kinking of the cell walls parallel to the load as result of radial compression [14][8] and flexural failure of cell walls perpendicular to load due to tangential compression [8]. Again the damage spreads in a band [19]. In the case of radial loading a slightly strength-drop can be registered after reaching the maximum. This marginal deviation from the behaviour in tangential direction was neglected during the numeric implementation. Compression failure shows an almost linear, slightly rising trend of the strength in the post-critical range. Again, at large deformations an immense hardening arises due to compression perpendicular. The strength development was realised numerically by formulating the degradation-function in sections. For the computation a separate input of the parameters for radial and tangential direction is necessary, see figure 2(b).

3.3 The yield criterion

The yield criterion determines the stress-level where non-linear behaviour starts and irreversible portions of deformation are computed. It corresponds to the yield stress in the case of a uni-axial loading. For multi-axial stresses the interactions between the individual components of the stress vector $\{\sigma\}$ have to be considered, whereby an earlier failure is possible.

The yield criterion F is to be defined depending on the stress-state σ and the degradation-parameter κ :

$$F(\sigma, \kappa) = 0 \quad (7)$$

Many researchers worked on the formulation of possible failure criteria for wood. A very good summary is given by *Edlund* [7]. For anisotropic materials like wood a formulation based on the general strength theory by *Tsai/Wu* is usually used [23]. A good adjustment to experimental results is possible by considering higher-order interaction terms of the strength-criterion formulated as tensor polynomial. Such a regression equation following the work of *Hemmer* [9] was implemented as a generalized yield criterion in ANSYS in the context of our research project already some time ago.

However, using a universal yield criterion like *Tsai/Wu*, it is not possible, to include material-specific failure mechanisms and resulting strength-degradation in the post-critical range in dependence of type and direction of loading. According to the classical theory of plasticity there are only two possibilities to describe the change of the yield surface. It can be expanded in size (isotropic work hardening) or translated in space (kinematic hardening) following a hardening rule, which is a function of plastic strain respectively. An uneven modification, changing the shape, is not possible. To describe complex, anisotropic material behaviour with the help of plasticity another approach was established in numeric analysis. Different failure mechanisms are taken into account by several separate yield criteria [18]. Only with this approach it is possible to characterise and simulate independently from each other the strength degradations related to the mode and direction of loading, described for wood in detail in the previous section.

The developed material model for softwood is based predominantly on the maximum-stress criterion. *Stuessi* suggested such a formulation for wood in 1946 [22]. The individual, plan surfaces of this criterion can be described in principle using the following equation:

$$F_i = \sigma_i - \Omega * f_i = 0 \quad (8)$$

with:

- σ_i = component of the stress vector
- Ω = degradation-function
- f_i = respective tensile, compression or shear strength

However, interactions between transverse tension, longitudinal sliding shear and rolling shear in the LT- and in the LR-plane respectively were shown as result of different test programs [6][9][10][20]. The mechanical background of these interactions is described in section 3.2.1. Furthermore the increase of the longitudinal shear strength in LR-plane during simultaneously transverse compression $\sigma_{T,c}$ needs to be taken into account, e.g. documented by *Keenan* [10]. These three stress-interactions are considered in the proposed material model. The implemented multi-surface yield criterion is illustrated in figure 3 for the particular case of plane stress in the LR- and LT-plane respectively.

3.4 The flow rule

Linear elastically behaviour is present as long as the condition $F(\sigma, \kappa) < 0$ is valid. Otherwise the proportional limit is exceeded and plastic strains occur. The plastic strain increment is computed with the help of the flow rule, which is given by:

$$d\varepsilon_{pl} = d\lambda * \frac{\delta Q}{\delta \sigma} \quad (9)$$

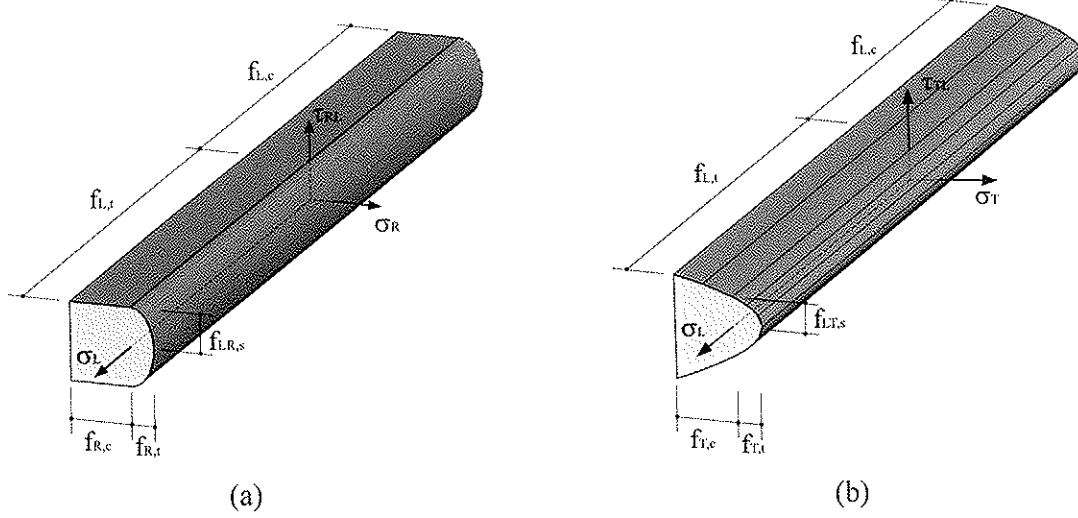


Figure 3: Multi-surface yield criterion for softwood, illustrated for plane stress: (a) in LR-plane (b) in LT-plane

With increasing deformation all further stress-states must lie on the yield surface. This postulation in the form of the plastic consistency condition can be deduced mathematically to:

$$dF = \left\{ \frac{\delta F}{\delta \sigma} \right\}^T * \{d\sigma\} + \left\{ \frac{\delta F}{\delta \kappa} \right\}^T * \{d\kappa\} = 0 \quad (10)$$

The direction of plastic strain increase results from the partial derivation of the plastic potential Q to the components of the stress vector $\{\sigma\}$. Because not enough validated test results are available to determine the plastic potential of wood for all failure modes, in principle associated flow rules are used in the material model:

$$Q(\sigma, \kappa) = F(\sigma, \kappa) \quad (11)$$

Exceeding a maximum-stress criterion, only plastic strains are computed toward the respective stress component by means of this attempt. But the material model is still to be expanded by formulating a non-associated flow rule for the case of longitudinal compression ($Q(\sigma, \kappa) \neq F(\sigma, \kappa)$), in order to represent the distortion of the kink band.

The amount of the plastic strain increment is determined in equation 9 by the plastic multiplier $d\lambda$. Its computation can be deduced from equation 10:

$$d\lambda = \frac{\left\{ \frac{\delta F}{\delta \sigma} \right\}^T * D * d\varepsilon}{\left\{ \frac{\delta F}{\delta \sigma} \right\}^T * D * \frac{\delta Q}{\delta \sigma} + H} \quad (12)$$

mit $H = -\frac{\delta F}{\delta \kappa} * \frac{d\kappa}{d\lambda}$ (hardening modul)

The interaction between several yield criteria has to be taken into account for discontinuous transition using multi-surface plasticity. Thus the plastic multipliers have to be determined from a set of equations similar to equation 12. An iterative procedure is needed to include strength degradations. The return-mapping-algorithm is used, which was implemented in ANSYS by *Schlegel* [17].

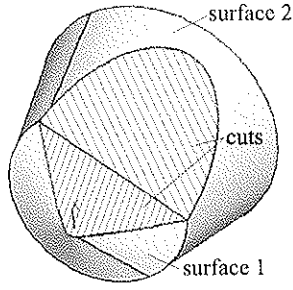


Figure 4: Singular *Drucker-Prager* yield surface [17]

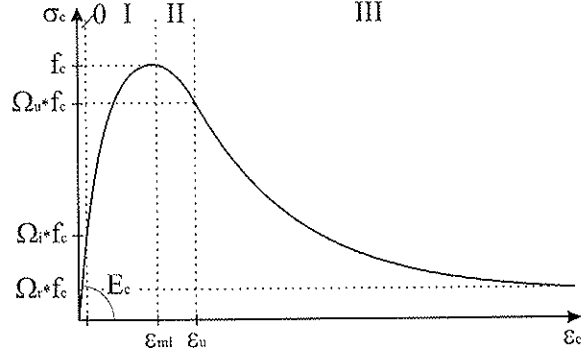


Figure 5: Implemented strength development for concrete in the case of multi-axial compression and interaction of compression and tension [17]

4 The material model for concrete

To model composite structures a material model for concrete is necessary. Contrary to wood, concrete or other mineral top layers are almost isotropic and homogeneous materials. Thus the definition of the failure condition has to be independent of the choice of the reference coordinate system. A formulation of the yield criterion depending on the principal stresses or the invariants of the stress vector is recommended [4]. Also concrete proves to be quite ductile under compression. Tension failure is characterized by cracking, whereby brittle softening occurs.

The implemented material model is based on a singular *Drucker-Prager* criterion, which was extended by *Schlegel* for modelling of mortar [17]. The failure condition is represented by two yield surfaces. The first yield surface limits the tensile strength and the second characterizes compression failure. The surfaces describe tapered cones, which are arranged rotation-symmetrically to the hydrostatic axis, see figure 4. The conventional *Drucker-Prager* criterion, represented by the second surface, can be formulated dependent on engineering strengths, but it is usually defined as:

$$F = 3\beta\sigma_m + \left[\frac{1}{2} \{s\}^T \{s\} \right]^{\frac{1}{2}} - \sigma_y \quad (13)$$

with:

$$\sigma_m = \frac{1}{3}(\sigma_x + \sigma_y + \sigma_z) \quad \text{the mean or hydrostatic stress}$$

$$\{s\} = \sigma - \sigma_m [1 \ 1 \ 1 \ 0 \ 0 \ 0]^T \quad \text{the deviatoric stress vector}$$

$$\beta = \frac{2 \sin \phi}{\sqrt{3}(3 - \sin \phi)} \quad \text{a material constant}$$

$$\sigma_y = \frac{6c \cos \phi}{\sqrt{3}(3 - \sin \phi)} \quad \text{the yield parameter}$$

$$\phi = \text{the input angle of internal friction}$$

$$c = \text{the input cohesion value}$$

Within the tension range ($\sigma_m > 0$) the formation of cracks after exceeding the yield criterion is accommodated by an exponential degradation of the tensile strength, like described for wood. In the case of multi-axial compression and interaction of compression and ten-

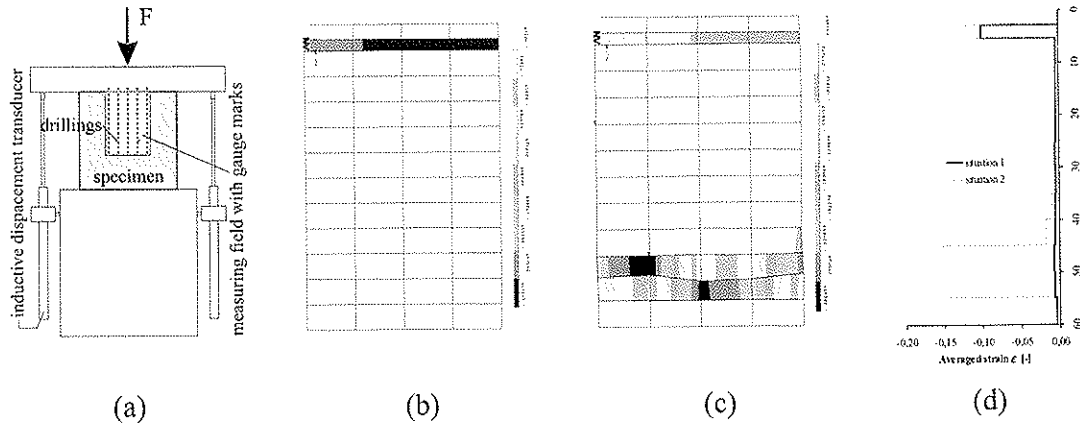


Figure 6: Compression test using close-range-photogrammetry: (a) test set-up; visualized strain-distribution between measuring points using ANSYS (b) situation 1: at maximum load and (c) situation 2: end of transient kinking; (d) averaged strains along measuring field

sion the strength degradation is formulated in sections [17]. For their definition interpolation values on the stress-strain-relationship have to be found, see figure 5.

5 Modelling of contact problems in timber engineering

The structural response of contact connections like step-joints or connection elements in timber-concrete-composite structures, such as notches, flat-steel-locks or studs welded on a cantilever, is always computed too rigid without additional simulation considerations. This is explained by the fact that the load concentrates first in the more rigid latewood within the range of the contact-joint. A transition zone results, in which the stress is distributed over the entire volume. These fibres are substantially more stressed than the early-wood fibres. The consequence is a premature failure, where the fibres are crumpled and the contact area is smoothed.

To examine the contact problem in detail, compression tests were carried out with loads completely and partially distributed on an area, see figure 6(a). At the same time the failure mechanism at compression parallel to the grain was examined more exactly, as already noted in chapter 3.2.2. These tests could only be realized using close-range photogrammetry. In the lower range of loading an excessive increase of deformations within the area between the first two rows of gauge marks can be clearly recognized (figures 6 and 7) in spite of the contact joint remaining closed by clamping the specimen with approx. 350 N. The stiffness in this zone is also considerably less within the service load range, see figure 7.

Shortly before reaching the maximum capacity a strong non-linearity is noted in the kink band, due to the stress concentrations at the drillings. But a clear deviation from the linearity is recognizable also in the undisturbed zones, where no fibre kinking occurs (figure 7). After reaching the maximum capacity the complete deformation takes place in the area of the kink band.

The effect of this phenomenon on the rise of the load-deformation relation can be taken into account numerically by two approaches. Commonly contact elements are used for modelling the joint. Their normal stiffness and initial gap can be adjusted, to fit the modulus of displacement determined in the shear tests. The second approach is to update the modulus of elasticity or material behaviour respectively of the elements placed below the joint.

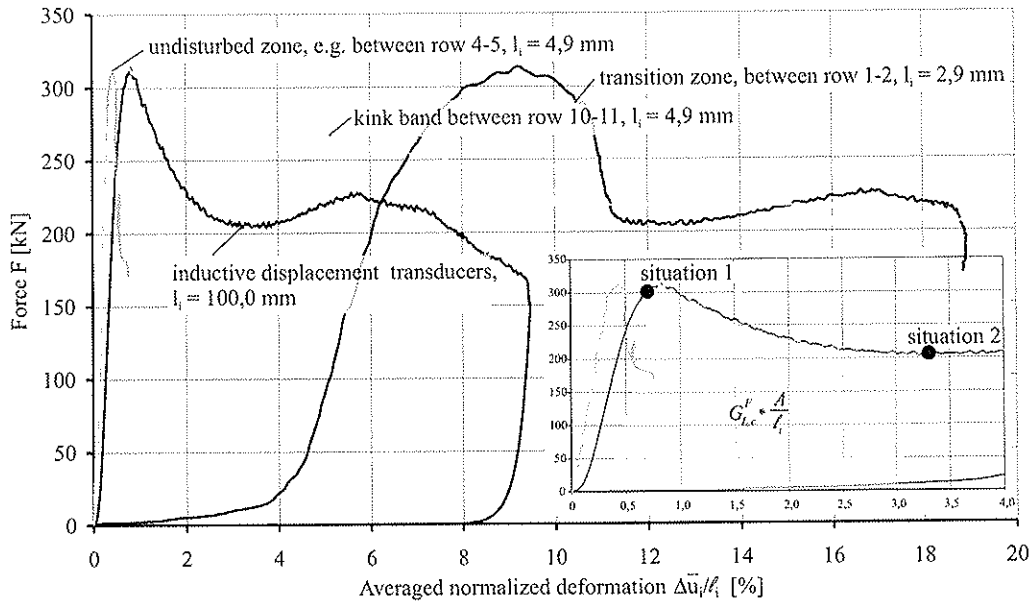


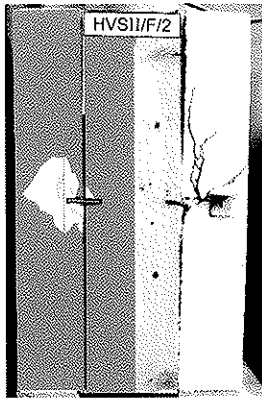
Figure 7: Load-deformation-curves determined between several measuring points of a representative specimen

6 Modelling of composite connection elements

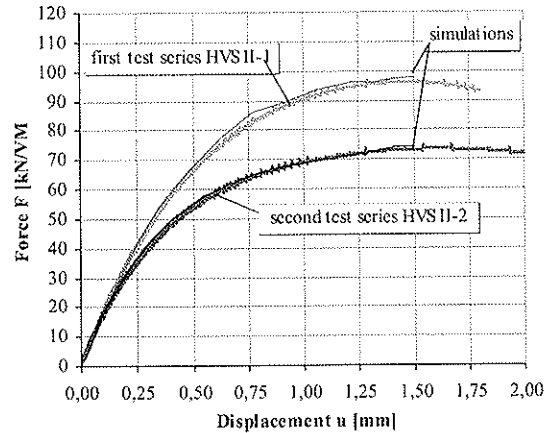
With the implemented material models for timber and concrete it is possible to simulate the load carrying behaviour and the failure mechanisms of timber-concrete-composite structures. Some examples show the efficiency of such models. The simulated damages, characterized by plastic strains, are compared to the real failure modes.

Connections with flat-steel-locks: Both, the cracking of concrete and the plastification of wood within the joint can be simulated very well using a FE-model, see figure 8(a). Two specimen series were tested, the first with high concrete quality ($f_{cm}=41 \text{ N/mm}^2$), the second with low quality ($f_{cm}=24 \text{ N/mm}^2$). The experimentally determined load-deformation curve of both series (averaged regression curves) and the curve computed with the appropriate material parameters are presented in figure 8(b). The carrying behaviour of the flat-steel-locks was simulated very well; and the influence of the concrete quality was examined numerically using the mechanic properties for the concrete strength classes according to standard DIN ENV 206. The combination of experimental and numerical investigations provides the basis for the maximum resistance of this connection specified in the technical approval document Z-9.1-473.

Connections with notches: Connections with notches are frequently used in timber-concrete-composite slabs and some design recommendations for them are made in standard EC 5 part 1-2. We examined the effect of different flank gradients experimentally as well as numerically. It can be stated, that both the maximum load and the load carrying behaviour are not affected by the flank-gradient in the push-out-test. In this experimental set-up compressive struts develop directly between the loading points and the support. The compressive strength of the concrete determine the maximum load, given a sufficient length of timber in front of the step joint, and the effect of actions is approximately identical for all connection variations.

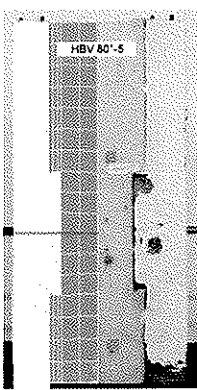


(a)



(b)

Figure 8: Push-out-test with flat-steel-locks: (a) real and simulated damage (b) experimentally determined and computed load-deformation curve



(a)



(b)



(c)



(d)



(e)

Figure 9: Push-out-test with connections using notches: (a) specimen with damage and FE-Modell (b) computed distribution of principal compressive stress; and simulated failure in form of intensity of plastic strains for specimens with a flank gradient of (c) 80° (d) 90° (e) 100°

Connections with studs welded on a cantilever: This type of connections is particularly suitable for application in timber-concrete-composite bridges due to the high rigidity and load-bearing capacity [21]. Again, the load carrying behaviour could be simulated very well. The failure was to be attributed to shearing of the headed stud. But the connections are not used equally in this shear-test arrangement. The bottom fastener will be stressed exceeding, see figure 10(c), and fails prematurely, figure 10(b).

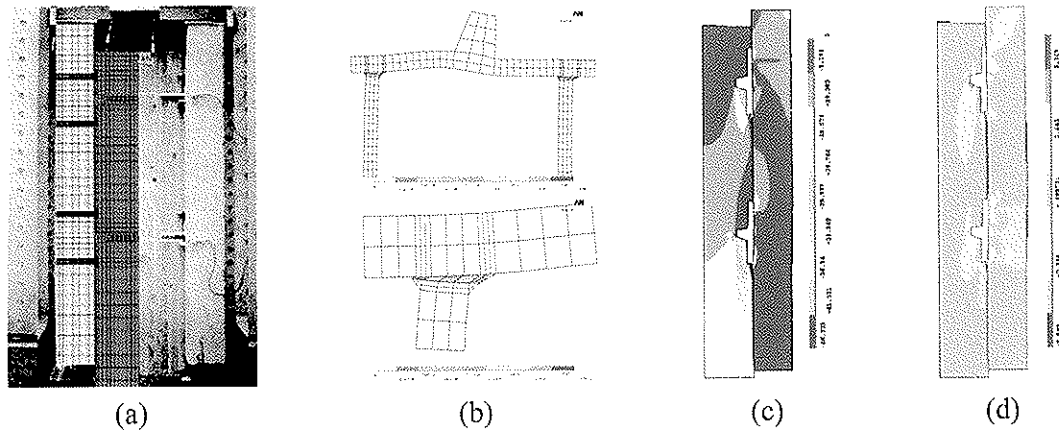


Figure 10: Connections with studs welded on a cantilever: test set-up according to Steurer [21] and FE-model (b) simulated failure of the stud from the bottom connection (c) computed distribution of principal compressive stress and (d) shear stress

7 Summary

A constitutive material model for softwood, based on time-independent multi-surface plasticity was introduced in the paper. This model is able to represent the effects of all nine material-specific micro-mechanical failure modes, mostly arising independently, on the stress-deformation-relationship of wood. Furthermore a compression test was presented; determining the structural response to longitudinal compression and investigating the behaviour of contact connections and the fracture energy dissipated during kink-band formation. In addition a material model for concrete, needed to simulate the load carrying behaviour of timber-concrete-composite structures was introduced. The efficiency of FE-simulations using these material-models was demonstrated by three examples.

References

- [1] Adalian, C.; Morlier, P. Wood model. *Holz als Roh- und Werkstoff*, 60:433–439, 2002.
- [2] Bazant, Z.P.; Oh, B.H. Crack band theory for fracture of concrete. *Materiaux et Constructions*, 16(93):155–177, 1983.
- [3] Bodig, Jozsef; Jayne, Benjamin A. *Mechanics of Wood and Wood Composites*. Krieger Publishing Company, Malabar, Florida, 1993.
- [4] Chen, Wai-Fah; Saleeb, Atef F. *Constitutive equations for engineering materials*. John Wiley and Sons, 1981.
- [5] Dill-Langer, G.; Lütze, S.; Aicher, S. Microfracture in wood monitored by confocal laser. *Wood Science and Technology*, 36:487–499, 2002.
- [6] Eberhardsteiner, J. *Mechanisches Verhalten von Fichtenholz, Experimentelle Bestimmung der biaxialen Festigkeitseigenschaften*. Springer-Verlag, Wien, 2002.
- [7] Edlund, Bo. Bruchhypothesen für orthotropes material. In *Ingenieurgeologie in Forschung und Praxis*, pages 17–22. Bruder-Verlag, Karlsruhe, 1982.
- [8] Gibson, L.J.; Ashby, M.F. *Cellular solids, Structure and properties*. Cambridge University Press, Cambridge, 1997.
- [9] Hemmer, K. *Versagensarten des Holzes der Weisstanne (abies alba) unter mehrachsiger Beanspruchung*. Dissertation, Karlsruhe, 1984.

- [10] Kennan, F.J. *The shear strength of glued laminated timber beams*. Dissertation, University of Toronto, 1978.
- [11] Kucera, L.J.; Bariska, M. On the fracture morphology in wood part.2. *Wood Science and Technology*, (19):19–34, 1985.
- [12] Mark, Richard E. *Cell wall mechanics of tracheides*. Yale University Press, 1967.
- [13] Mindes, S. The fracture of wood in tension parallel to the grain. *Canadian Journal of Civil Engineering*, 4(4):412–416, 1977.
- [14] Müller, Ulrich. *Analyse der mechanischen Eigenschaften von Massivholz unter Berücksichtigung der Zellstruktur*. Dissertation, Universität für Bodenkultur (BOKU), Wien, 2003.
- [15] Poulsen, Johannes Sand. *Compression in clear wood*. Doctoral thesis, Department of Structural Engineering and Materials, Technical Univ. of Denmark.
- [16] Poulsen, J.S.; Moran, P.M.; Shih, C.F.; Byskov, E. Kink band initiation and band broadening in clear wood under compressive loading. *Mechanics of materials*, (25):67–77, 1997.
- [17] Roger Schlegel. *Numerische Berechnung von Mauerwerkstrukturen in homogenen und diskreten Modellierungsstrategien*. Dissertation, Bauhaus-Universität Weimar, eingereicht 2004.
- [18] Simo, J.C.; Kennedy, J.G.; Govindjee, S. Non-smooth multisurface plasticity and viskoplasticity. loading/unloading conditions and numerical algorithms. *International Journal for Numerical Methods in Engineering*, 26:2161–2185, 1988.
- [19] Smith, Ian ; Landis, Eric ; Gong, Meng. *Fracture and fatigue in wood*. John Wiley and Sohns, 2003.
- [20] Spengler, R. Festigkeitsverhalten von Brettelelementen aus Fichte unter zweiachsiger Beanspruchung: Ergebnisse aus experimentellen Untersuchungen. Technical report, Technische Universität München, Bauingenieurwesen 2, 1986.
- [21] Anton Steurer. Holz/Beton-Verbund im Brückenbau: Die Crestawald-Brücke bei Sufers. In *31. SAH-Fortbildungskurs: Tragende Verbundkonstruktionen mit Holz*, pages 245–285. Schweizerische Arbeitsgemeinschaft für Holzforschung (SAH), November 1999.
- [22] Stüssi, F. Holzfestigkeit bei Beanspruchung schräg zur Faser. *Schweizerische Bauzeitung*, (20):251–252, November 1946.
- [23] Tsai, S. W.; Wu, E. M. A general theory of strength for anisotropic materials. *Journal of Composite Materials*, (5):58–80, 1971.

INTERNATIONAL COUNCIL FOR RESEARCH AND INNOVATION
IN BUILDING AND CONSTRUCTION

WORKING COMMISSION W18 - TIMBER STRUCTURES

DESIGN OF RIM BOARDS FOR USE WITH I-JOIST FRAMING SYSTEMS

B Yeh

T G Williamson

APA - The Engineered Wood Association

UNITED STATES

Presented by T Williamson

E Karacabeyli asked about the durability of this product. Williamson responded that this is a building envelope issue and not a structural product issue for this standard.

H Blass asked whether there was an OSB production standard in North America. Williamson clarified that OSB production standard in North America is available.

General discussions followed on what type of data is available, EN 300, and perforation would be okay within recommended range.

Williamson extended an invitation to the 9th WCTE 2006 in Oregon.

Design of Rim Boards for Use with I-Joist Framing Systems

Borjen Yeh, Ph.D., P.E.
Thomas G. Williamson, P.E.
APA - The Engineered Wood Association, U.S.A.

Abstract

The fastest growing glued engineered wood composite in North America is pre-fabricated wood I-joists. I-joists now represent approximately 45% of the residential raised floor construction market in North America. This translates to over 300 million lineal meters (1 billion lineal feet) of I-joists being used annually in North America. A key structural component for the I-joist floor system is the rim board, which serves as a closure panel, as an element to transfer vertical loads, and as a lateral load resisting element. In traditional sawn lumber construction, the rim board is typically a sawn lumber joist. However, sawn lumber joists are not satisfactory for use with I-joist framing due to differential shrinkage and other considerations. As such, rim boards used with I-joist framing are other engineered wood composites including primarily oriented strand board (OSB), laminated veneer lumber (LVL), plywood, oriented strand lumber (OSL), and laminated strand lumber (LSL).

Since rim boards represent an essentially unregulated building component in North America, APA - The Engineered Wood Association determined there was a need to develop qualification and acceptance criteria for rim boards given the wide range of products that could be used as rim boards. This paper describes the development of the *Performance Standard for APA EWS Rim Boards*, PRR-401, and the test procedures that have evolved as industry standards. Also discussed are design recommendations developed by APA for transmitting lateral forces between floors and between floors and foundations using rim boards. Fire-rated rim board assemblies are also presented. Lastly, this paper describes the limitations on holes in rim boards as is common in residential construction.

1. Introduction

Prefabricated wood I-joists have been used in North American residential construction for more than 35 years. The total production volume for I-joists grew phenomenally from 39.6 million lineal meters (130 million lineal feet) in 1989 to 326 million lineal meters (1.07 billion lineal feet) in 2003. A vast majority of these I-joists, approximately 80%, have been used in new residential floor construction. This represents a market share of approximately 45% in 2003 [1], which exceeds the market share of solid-sawn lumber floor joists.

A key structural component of the I-joist floor system is the rim board, which is a wood component that fills the space between the sill plate and bottom plate of a wall or, in second floor construction, between the top plate and bottom plate of two wall sections. The rim board matches the depth of the framing members between floors or between the floor and foundation to perform one or a combination of the following functions:

- To transfer all vertical loads from above to below at the rim board location
- To provide diaphragm attachment for floor sheathing to the top edge of rim board
- To transfer lateral loads from the diaphragm to the wall plate below
- To provide lateral support for the floor joists through the attachment to the joists
- To provide closure for ends of floor joists
- To provide attachment base for siding and/or exterior deck ledger

While lumber has been traditionally used as rim boards with sawn lumber floor systems, its depth dimension is not compatible with typical I-joist depths. Additionally, since the sawn lumber rim boards have different shrinkage or swelling characteristics than I-joists when exposed to moisture changes, it is always problematic to maintain dimensional compatibility when an I-joist floor system is mixed with sawn lumber rim boards. With the increasing use of wood I-joists, a demand for compatible engineered wood rim boards has resulted. After years of research and development, APA published the *Performance Standard for APA EWS Rim Boards*, PRR-401 [2], in 1997. Most of the product evaluation methods given in PRR-401 were subsequently incorporated into the *Acceptance Criteria for Wood-Based Rim Board Products*, AC124 [3], by the then ICBO Evaluation Service (ICBO-ES). Since then, the total production volume for rim boards, mostly oriented strand board (OSB) and laminated strand lumber (LSL), has grown from approximately 3.2 million square meters (35 million square feet) in 1997 to 5.4 million square meters (59 million square feet) on a 25-mm (1-inch) thickness basis [4]. The standard sizes for rim board products certified by APA is 25 to 32 mm (1 to 1-1/4 inches) in thickness, 241 to 610 mm (9-1/2 to 24 inches) in depth, and 2.4 to 7.3 m (8 to 24 feet) in length.

2. Evaluation Methods

As an engineered wood product, the rim board should be manufactured in accordance with a recognized product standard, such as the *Voluntary Product Standards PS1* [5] or *PS2* [6] in the U.S., or *Construction Sheathing CSA-0325* [7] in Canada, for wood structural panel products. Since the rim board functionalities, as mentioned above, are beyond typical sheathing applications, additional product evaluation is required per APA PRR-401 and ICBO-ES AC124. This includes horizontal load transfer capacity, uniform vertical load capacity, concentrated vertical load capacity, and lag screw lateral resistance (for attachment of deck ledgers). The durability of rim boards is addressed by the lateral nail durability and thickness swell tests. In addition, edgewise-bending properties for rim boards are required to be evaluated in PRR-401 so that the rim board products may be used to span over an opening of 1.2 m (4 feet) or less as a bending member. Due to the space limitation in this paper, the following paragraphs briefly describe these test methods.

The horizontal load transfer capacity is evaluated using ten replicates of 91-cm (3-ft) long and 30-cm (1-ft) wide rim board assemblies, as shown in Figure 1. Each assembly represents a section of floor where the lateral loads are transferred through the rim board and floor joists using the minimum nailing schedule prescribed in the International Building Code [8]. As several nail types, including toe nails (rim board to sill plate), face nails (rim board to joist and sheathing to joist flange), slanted nails (joist to sill plate), and edge nails (sheathing to rim board), are part of the lateral load transfer mechanism, the only rational option for evaluating the lateral load transfer capacity is through the assembly test. It should be noted that due to the difficulty in nailing the sheathing into the

edge of rim board when the rim board thickness is too small, the industry has adopted a minimum rim board thickness of 25 mm (1 inch) to reduce the likelihood of missing edge-nail connections. Overall, due to the fact that the core density of OSB is generally lower than the face, the predominant failure mode for OSB rim boards is the edge nailing between sheathing and rim board.

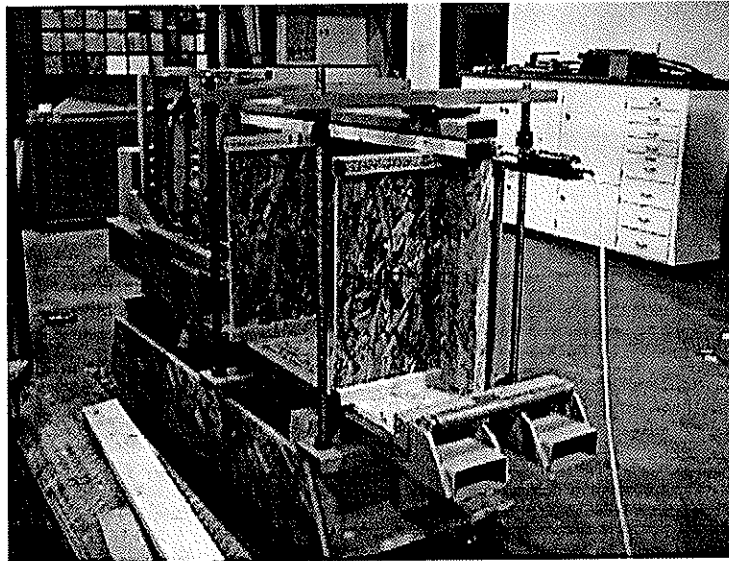


Figure 1. Test setup for horizontal load transfer capacity

The uniform vertical load capacity of rim board is evaluated using the rim board as a stand-alone column. The uniform vertical load capacity determined from these column tests is compared with the theoretical column buckling capacity. The uniform vertical load capacity is published based on the lower of the empirical and theoretical values. The concentrated vertical load capacity is tested in a similar manner and the mean test value from 10 tests is required to be at least 46.7 kN (10,500 lbf), which is equivalent to an allowable load of 15.6 kN (3,500 lbf), based on the provisions of the conventional construction practices prescribed in the International Building Code [8].

The lag screw tests are intended to provide a design value for the attachment of deck ledger to siding and rim board. In the U.S., the attachment typically consists of lag screws of 12.7 mm (1/2 inch) in diameter. However, due to the lag screw penetration being limited to the rim board thickness, which is below the minimum penetration of 4 times the fastener diameter, performance tests are required, as shown in Figure 2. The predominant failure mode for OSB rim boards is the fastener rotation and crushing of wood (referenced to as a Mode II failure).

Since rim boards are limited to dry service conditions, such as with most protected framing members where the average equilibrium maximum moisture content for solid-sawn lumber is less than 16%, the durability of rim boards is addressed by conducting lateral nail durability and thickness swell tests. The lateral nail durability tests are performed in the same manner as the lateral load transfer capacity tests (see Figure 1) with the exception that the rim board used in the assembly is pre-conditioned by a 24-hour water soak in accordance with Method B of ASTM D1037 [9] and the assembly is assembled while the rim board is still wet. The whole assembly is then re-dried to room conditions before the mechanical test is conducted. This is intended to simulate the conditions when the rim board is installed wet due to a rain delay in construction and

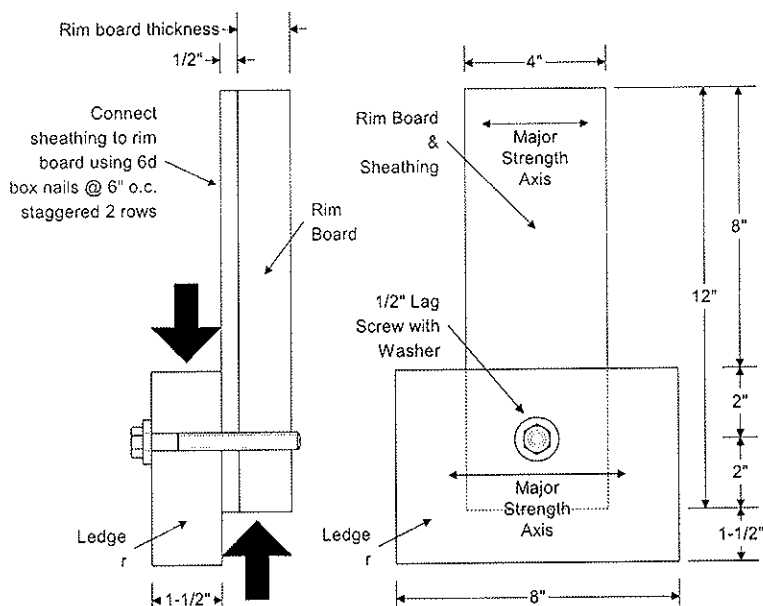


Figure 2. Test setup for lag screw lateral resistance

subsequently re-dried after the building is closed in. The mean lateral load transfer capacity obtained from the lateral nail durability tests cannot be less than 75% of the mean capacity determined from the control (dry). In addition, the mean thickness swell of rim boards based on the 24-hour water soak cannot exceed 10% and no individual value shall exceed 12%.

The edgewise-bending properties of rim boards are evaluated in accordance with the principles of ASTM D5456 [10]. For quality assurance purposes, PRR-401 requires rim board products to meet the process control requirements in accordance with typical structural panel production. In addition, thickness swell, internal bond, and density of rim boards are required to meet the control values established during qualification.

3. Design Values

Tables 1 and 2 show the characteristic properties for 2 generic rim board products certified by APA. These 2 classes of rim boards have been widely used and accepted in North America since 1997. It should be noted that there are some additional proprietary rim board products that reflect different design values evaluated in accordance with AC124 and recognized in a code-compliance report.

4. Design Considerations

4.1 Connection requirements

The design values given in Tables 1 and 2 are based on the results of performance tests. As a result, the rim board design and installation must be based on the following connection requirements, which are part of the performance tests:

Table 1. Required Mean Test Values^(a) for *APA EWS* Rim Boards

Grade	$t_{min}^{(b)}$ (mm)	$H^{(c)}$	$V^{(d)}$			$Z^{(e)}$	$P^{(f)}$
		(kN/m)	(kN/m)			(kN)	(kN)
		Depth (d) Limitation (cm)					
		$d \leq 61$	$d \leq 41$	$41 < d \leq 61$	$d \leq 61$	$41 < d \leq 61$	
Rim Board	25	7.4	144	72	5.3	47	
	29	7.4	193	131	6.2	47	
Rim Board Plus	25	N/A ^(g)					
	29	8.2	212	140	6.2	47	

^(a) The tabulated values are the average test values.

^(b) Minimum thickness.

^(c) Mean test value for the horizontal load transfer capacity.

^(d) Mean test value for the vertical load capacity.

^(e) Mean test value for the lateral resistance of a 12.7-mm diameter lag screw.

^(f) Mean test value for the concentrated load capacity, which is required only when the rim board exceeds 41 cm in depth.

^(g) The minimum thickness for *APA EWS* Rim Board Plus is 29 mm.

Table 2. Required Edgewise Bending Values for *APA EWS* Rim Boards^(a)

Grade	$f_{be}^{(b)}$ (MPa)	$E_c^{(c)}$ (MPa)	$f_{ve}^{(d)}$ (Mpa)	$f_{cLe}^{(e)}$ (MPa)
Rim Board or Rim Board Plus	14.3	3,999	5.9	6.3

^(a) The tabulated values are test values.

^(b) Characteristic (5th percentile with 75% confidence) edgewise bending strength.

^(c) Characteristic (mean) edgewise apparent modulus of elasticity.

^(d) Characteristic (5th percentile with 75% confidence) edgewise shear strength.

^(e) Characteristic (mean) edgewise compressive strength perpendicular to grain at 0.04-in. deformation.

a) Floor sheathing to Rim Board – Use 64-mm (2-1/2-inch) long common nails at 150 mm (6 inches) o.c. It should be noted that the horizontal load transfer capacity is not necessarily increased with decreased nail spacing. This is because the tendency to split at the edge-nailed joint is greater with decreasing nail spacing, which will offset the increased joint strength due to the increased number of nails for a given rim board length. To avoid excessive splitting, the nail spacing shall not be less than 75 mm (3 inches). For the same reason, the 89-mm (3-1/2-inch) long common nails used to connect the bottom plate of a wall to the rim board through the sheathing do not increase nor reduce the horizontal load transfer capacity of the rim board provided that the 64-mm (2-1/2-inch) long common nail spacing (sheathing-rim board) is 150 mm (6 inches) o.c. and the 89-mm (3-1/2-inch) long common nail spacing (bottom plate-sheathing-rim board) is in accordance with the prescriptive requirements of the International Building Code [8].

b) Rim Board to I-Joist – Use two 64-mm (2-1/2-inch) long common nails, one each into the top and bottom flanges. This is typical for rim board having a thickness up to 29 mm (1-1/8 inches). A larger nail size may be required by the I-joist manufacturer or for thicker rim board products.

c) Rim Board to Sill Plate – Toenail using 64-mm (2-1/2-inch) long common nails at 150 mm (6 inches) o.c.

d) Attachment of Lumber Ledgers to Rim Board – Use 12.7-mm (1/2-inch) diameter lag screws with a minimum nominal length of 100 mm (4 inches) or use 12.7-mm (1/2-inch) diameter through-bolts with washers and nuts. Note that the lag screw should be inserted in a lead hole by turning with a wrench, not by driving with a hammer. Over-torquing can significantly reduce the lateral resistance of the lag screw and should therefore be avoided.

e) Lateral Resistance of Nails Applied to The Faces of Rim Board – Calculate the lateral nail resistance based on the procedures given in the applicable code using an equivalent specific gravity of 0.50 for OSB rim boards. If the rim boards are made of structural composite lumber (SCL), refer to the equivalent specific gravity published by the SCL manufacturer.

4.2 Rim boards spanning over opening

Rim boards may be used to span openings up to 1.2 m (4 feet) in length, depending on the applied loads at the opening. In some instances, the rim board may not have sufficient edgewise-bending capacity to resist the applied loads to the same level as the uniform vertical load capacity given in Table 2, which is based on a fully supported rim board. If there is not sufficient edgewise-bending capacity, a built-up (multiple pieces of) rim board may be considered for providing adequate edgewise-bending capacity. When spanning openings, rim board end (butt) joints shall not occur over the opening.

4.3 Holes in rim board

Based on experience with similar products, the maximum allowable hole size for rim boards is limited to 2/3 of the rim board depth as shown below. Based on the test results of an APA research study [11], the length of any rim board segment containing a hole is required to be at least 8 times the hole size to allow for stress re-distribution around the hole, while maintaining an adequate factor of safety.

Table 3. Maximum allowable hole size and minimum rim board length

Rim board depth (cm)	Maximum allowable hole size ^{(a)(b)} (cm)	Minimum Rim Board length ^(c) (cm) for the maximum allowable hole size
24	16	127
30	20	157
36	24	188
41	27	213

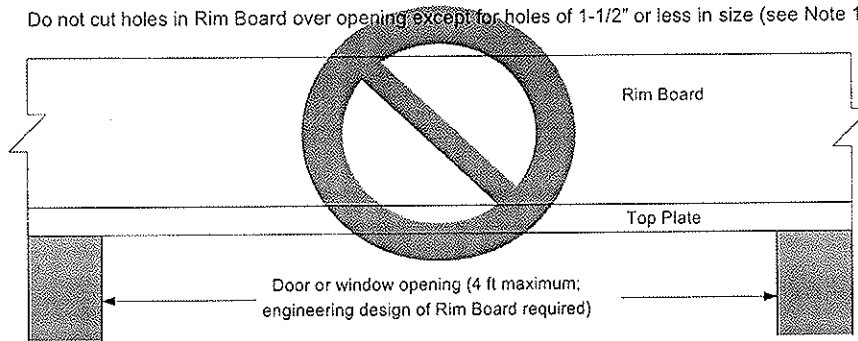
^(a) These hole provisions do not apply to rim board installed over openings, such as doors or windows.

^(b) The diameter of a round hole or the longer dimension of a rectangular hole.

^(c) The length of rim board per wall line. For multiple holes, the minimum rim board length shall be 8 times the sum of all hole sizes.

a) Holes should not occur in rim board installed over openings, such as doors or windows, where the rim board is not fully supported, except that holes of 38 mm (1-1/2 inches) or less in size are permitted provided they are positioned at the mid-depth and in the middle 1/3 of the span.

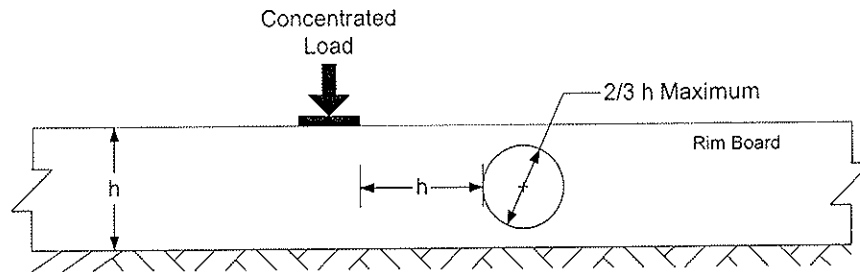
Do not cut holes in Rim Board over opening except for holes of 1-1/2" or less in size (see Note 1).



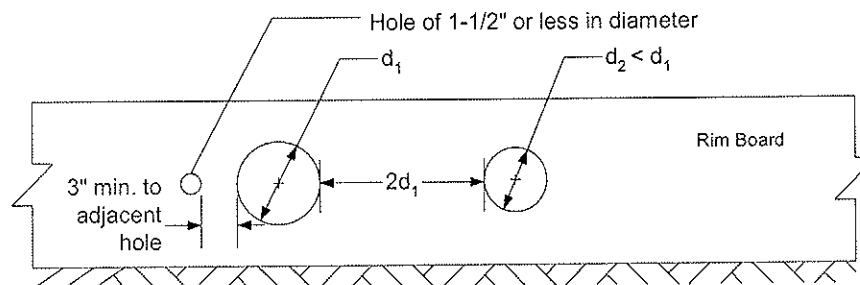
b) Field-cut holes should be vertically centered in the rim board and at least one hole diameter or 15 cm (6 inches), whichever is less, clear distance away from the end of the wall line. Holes should never be placed such that they interfere with the attachment of the rim board to the ends of the floor joist, or any other code-required nailing.

c) While round holes are preferred, rectangular holes may be used, provided that the corners are not over-cut. Slightly rounding corners or pre-drilling corners with a 25-mm (1-inch) diameter bit are recommended.

d) When concentrated loads are present on the rim board (loads not supported by other vertical-load-carrying members such as squash blocks), holes should not be placed in the rim board within a distance equal to the depth of the rim board from the area of loading.



e) For multiple holes, the clear spacing between holes should be at least two times the diameter of the larger hole, or twice the length of the longest side of the longest rectangular hole. This minimum hole spacing does not apply to holes of 38 mm (1-1/2 inches) or less in diameter, which can be placed anywhere in the rim board except that the clear distance to the adjacent hole should be 76 mm (3 inches) minimum.



4.4 Fire-rated rim board assemblies

In the U.S. building codes, fire resistant or fire-rated assemblies are required in certain locations, occupancies, and types of buildings to slow or prevent the spread of fire. When fire-rated walls and/or floor/ceiling assemblies are required, a fire barrier over the walls is typically required to prevent flames from escaping the confinement provided by the wall or ceiling assembly. Rim boards in continuous length can be used as an effective fire barrier. Based on a study commissioned by APA and conducted by the Forest Products Laboratory, U.S. Department of Agriculture [12], several 1-hour and 2-hour fire-rated assemblies, both with load transfer (the load carried by the fire-exposed rim board is assumed to transfer to the adjacent rim board when the fire-exposed rim board fails) and without load transfer. Figure 3 shows the 1-hour fire-rated rim board assemblies with load transfer. For a complete list of fire-rated rim board assemblies, please refer to APA Data File D350, *APA Rim Board in Fire Rated Assemblies* [13], at the APA web site (<http://www.apawood.org>).

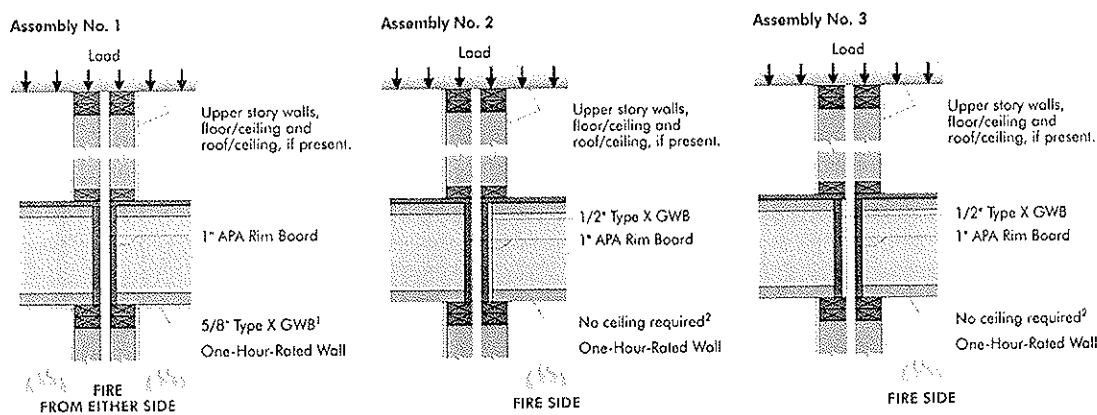


Figure 3. One-hour fire-rated rim board assemblies with load transfer

4.5 High lateral load transfer

When rim boards are used in applications where a high lateral load transfer capacity is required, the following options are available. For additional design information, please refer to APA Data File EWS Y250, *Shear Transfer at Engineered Wood Floors* [14], at the APA web site (<http://www.apawood.org>).

- a) Use commercially available specialty metal connectors made by connector manufacturers between the rim board and framing or sole plate, as shown in Figure 4. These types of connectors are installed using face nailing into the rim board, thereby increasing the lateral load transfer capacity of the rim board assembly.

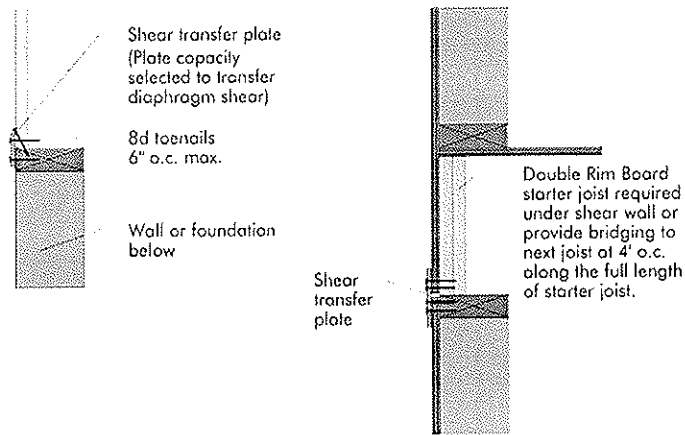


Figure 4. High lateral load transfer using metal connectors

b) Use nailed connections with face nailing into the rim board or additional lumber blocking, as shown in Figure 5.

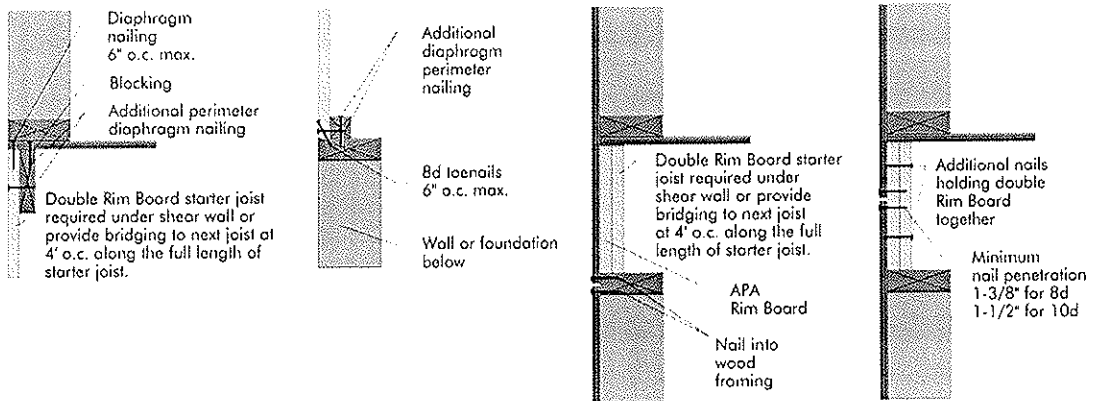


Figure 5. High lateral load transfer using metal connectors

5. Conclusions

Rim boards are an integral part of engineered wood systems because they transfer both lateral and vertical forces, and provides lateral support for the floor joists. Due to their multiple functionalities, rim boards should be properly manufactured, evaluated, designed, and constructed to ensure that the design loads are successfully transferred through rim boards. With the increasing demand for I-joist floor systems, it is expected that engineered rim boards will play a critical role in future building construction. This paper provides some information for proper design and construction of rim boards.

6. References

1. APA - The Engineered Wood Association. 2004. *Regional Production and Market Outlook for Structural Panels and Engineered Wood Products 2004 - 2009*, APA Economics Report E70. Tacoma, WA.
2. APA - The Engineered Wood Association. 2002. *Performance Standard for APA EWS Rim Boards*, PRR-401. Tacoma, WA.
3. ICBO Evaluation Service, Inc. 2000. *Acceptance Criteria for Wood-Based Rim Board Products*, AC124. Whittier, CA.
4. APA - The Engineered Wood Association. 2003. *Residential Construction 2002: Structural Panels and Engineered Wood Products*, APA Market Research M17. Tacoma, WA.
5. National Institute of Standards and Technology. 1995. *Voluntary Product Standard PS 1-95 Construction and Industrial Plywood*. Gaithersburg, MD.
6. National Institute of Standards and Technology. 1992. *Voluntary Product Standard PS2-92 Performance Standard for Wood-Based Structural-Use Panels*. Gaithersburg, MD.
7. Canadian Standards Association. 1991. *Construction Sheathing*. CAN/CSA-O325-M91. Rexdale (Toronto), Ontario, Canada.
8. International Code Council. 2003. *International Building Code*. Country Club Hills, IL.
9. ASTM International. 2003. *Standard Test Methods for Evaluating Properties of Wood-Base Fiber and Particle Panel Materials*. ASTM D1037. Annual Book of ASTM Standards. West Conshohocken, PA.
10. ASTM International. 2003. *Standard Specification for Evaluation of Structural Composite Lumber Products*. ASTM D5456. Annual Book of ASTM Standards. West Conshohocken, PA.
11. White, R.H. 2003. *Fire Resistance of Engineered Wood Rim Board Products*. Research Paper FPL-RP-610. Forest Products Laboratory, USDA. Madison, WI.
12. APA - The Engineered Wood Association. 2003. *Holes in Rim Board Used in Conventional Construction*, Data presented at the I-Joist/LVL Technical Advisory Committee Meeting held in Reno, NV, on March 30, 2003.
13. APA - The Engineered Wood Association. 2003. *APA Rim Board in Fire Rated Assemblies*, APA Data File D350. Tacoma, WA.
14. APA - The Engineered Wood Association. 2003. *Shear Transfer at Engineered Wood Floor*, APA Data File EWS Y250. Tacoma, WA.

INTERNATIONAL COUNCIL FOR RESEARCH AND INNOVATION
IN BUILDING AND CONSTRUCTION

WORKING COMMISSION W18 - TIMBER STRUCTURES

DEVELOPMENT OF STRUCTURAL LVL FROM TROPICAL WOOD
AND EVALUATION OF THEIR PERFORMANCE FOR THE
STRUCTURAL COMPONENTS OF WOODEN HOUSES
PART-1. APPLICATION OF TROPICAL LVL TO A ROOF TRUSS

Kohei Komatsu

Research Institute for Sustainable Humanosphere, Kyoto University
JAPAN

Yakni Idris

Civil Engineering Dept, University of Sriwijaya, Palembang

Sutadji Yuwasdiki

Anita Firmanti

Research Institute for Human Settlement, Bandung,

Bambang Subiyakto

Research Center for Bio-Material Science, Chibinon

INDONESIA

Presented by K Komatsu

H Blass noted that only the bottom chord of the truss was loaded and commented that as roof truss upper chord loading would be more appropriate. Komatsu agreed and explained that constraints of test equipment limited the load applications to the lower chord only.

P Glos asked for more information on the LVL material used including thickness and bending strength. Komatsu responded the veneer thickness was 1.2 mm and bending and in-plane shear tests of the LVL were also performed but the data is available in different paper.

P Ross questioned why press metal plates not used and as a triangulated truss system why was a less sophisticated approach not used. Komatsu answered that the structural design method was of secondary interest as this is a new material under development; therefore, non-linear FEM was used to get more accurate information.

R Steiger asked whether FEM was used because of geometric nonlinearity. Komatsu responded that its use was academic reason and if the material was already available in the market less sophisticated method would be chosen.

Development of Structural LVL from Tropical Wood and Evaluation of Their Performance for the Structural Components of Wooden Houses

Part-1. Application of Tropical LVL to a Roof Truss

By

Kohei Komatsu¹, Yakni Idris², Sutadji Yuwasdiki³, Bambang Subiyakto⁴ and Anita Firmanti³:

- 1: Research Institute for Sustainable Humanosphere (previous name: Wood Research Institute), Kyoto University, Uji, Japan
- 2: Civil Engineering Dept, University of Sriwijaya, Palembang, Indonesia.
- 3: Research Institute for Human Settlement, Bandung, Indonesia
- 4: Research Center for Bio-Material Science, Chibinon, Indonesia

Abstract

A structural design of roof truss and evaluation of its structural performance as a target for utilizing tropical LVL was done. Simple structure, which can be built-up on-site using minimum number of bolts so as economical as possible, were our development concept. In accordance with this concept, a roof truss of 4.5m span length was designed using only M12 bolts and uniform dimension's LVL for all members. Vertical two points loading tests were done to evaluate performance as a roof truss. Experimental measurements on the mid-span deflections, strain distributions in members and load-slip relationships at heel joints were compared with those obtained from nonlinear FEM analyses. Basic mechanical properties of LVL members as well as bolted joints properties were also evaluated experimentally and these data were utilized for calculating the theoretical equations. Fairly good agreements between experiments and FEM analyses were obtained. From these research activities, it was confirmed that the bolted LVL roof truss developed in this research project had reasonable economical merit and structural safety.

1. Introduction

Laminated veneer lumber (LVL) seems to be one of the most effective re-constituted wood based material ever developed in the field of forest products industries, because it can utilize relatively small diameter logs, mixed species and can be produced by making use of both equipments and knowledge for plywood industry in some extents.

In Indonesia, production of LVL is growing year by year as a main forest product, which is alternative of plywood product, as LVL can be easily produced using plywood production technique. Its use in Indonesia, however, is still limited and the most products are being exported to Japan for furniture or non-structural use.

While in Japan, LVL is now considered as one of the basic engineered wood products, which is used for such parts as long span girders, beam & column members of portal frame where higher reliability is required. To meet with this requirement, we have started a cooperative research project to evaluate the structural performance of LVL that is being produced in Indonesia using mixed species veneers taken from plantation grown tropical hardwood and rubber wood.

In this article, we would like to introduce a R&D for evaluating structural performance of simple roof truss made of tropical LVL as the part of JSPS (Japan Society for the Promotion of Science) – LIPI (Lembaga Ilmu Pengetahuan Indonesia: Indonesian Institute of Sciences) Core University Program taken by the authors.

2. Experiments

2.1 Concept of Roof Truss

In developing a roof truss, we paid care to make the structure as simple as possible to be built up on-site by using materials having same cross section and minimum number of bolts. All members used in this roof truss had a uniform cross section of 45 mm x 90 mm, which is being used as the diagonal bracing material in shear walls of Japanese conventional wooden dwelling houses. From the points of easy built-up and restructuring process without using special equipments, only M12 bolts of 12 mm diameter were used for constituting roof truss with large diameter washers. Figure 1 shows a roof truss designed in accordance with the concept mentioned above.

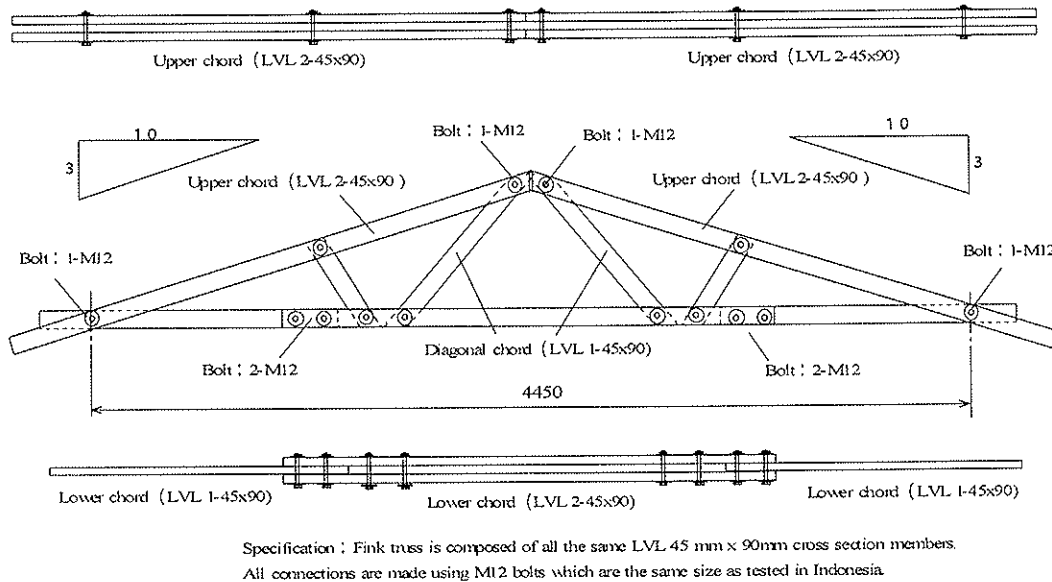


Figure 1 Structure of roof truss

2.2 Physical Properties of LVL Used

All Laminated Veneer Lumbers were manufactured from a mixture of *Paraserianthes falcataria* (Falcataria) and *Hevea brasiliensis* (rubber wood) veneers. This LVL is a new product developed by a joint venture between Uni-Cooperation (Japan) and HASCO Group Company in Jambi Sumatera Island, Indonesia. Falcataria and rubber wood was used 1:1 in the LVL. All the plies were laminated parallel to the length. Both Falcataria, a fast-growing forest plantation species, and rubber wood, an agricultural by-product, are tropical timber species. Photographs 1 and 2 show standing trees of Falcataria and cutout logs in Sumatera Island, Indonesia.



Photo.1 Standing trees of Falcataria

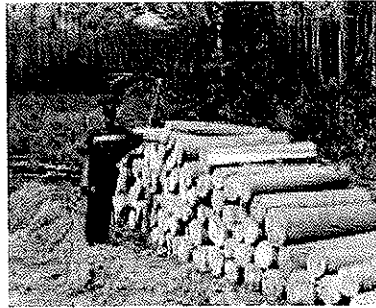


Photo.2 Cutout logs

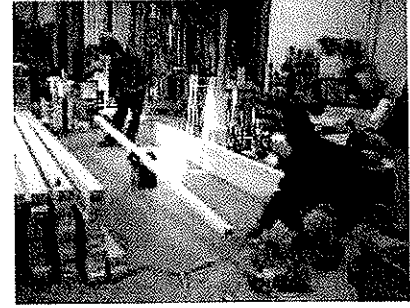


Photo.3 Measuring MOE by FFT.

The size of LVL was 45 mm in thickness, 90 mm in width and 3000 mm in length. Modulus of elasticity (MOE) of each LVL piece brought into experimental hall in Kyoto University, Japan were all measured by using handy-type FFT analyzer (Ono-Sokki Co.Ltd.) before processing and assembly. Photograph 3 shows feature how handy-type FFT analyzer was used for measuring MOE of each test piece. Table 1 shows physical properties of LVL used for the roof truss specimens.

Table 1 Physical properties of LVL used	Mean value	Std. dev.	CV (%)	N
MOE (kN/mm ²)	10.6	0.51	4.8	27
Density (kg/m ³)	525	8.7	1.7	27

2.3 Tests on Bolted Joints of LVL

In order to obtain a series of supplemental data for analyzing truss behaviors under vertical loads, tests on bolted joint of LVL were also conducted by using the materials taken from the undamaged parts of truss specimens after the all destructive tests on roof trusses were completed.

Tests on bolted joints were done in parallel as well as in perpendicular to the main member's longitudinal direction by applying tensile force for making sure of clear failure loads and failure mode. Photographs 4 and 5 show test on bolted joints of LVL. Tensile load was applied by using an oil jack of 150 kN capacity and relative slip displacements between main member and two side members were measured using two set of displacement measuring devices whose capacity was 10000 micro-strain at 50 mm elongation.



Photo.4 Test on bolted joint in parallel to the grain.

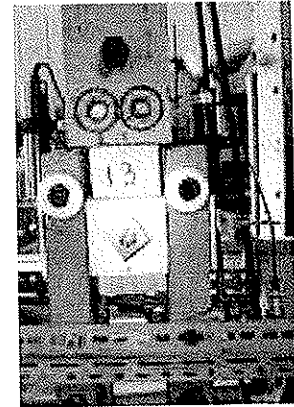


Photo.5 Test on bolted joint in perpendicular to the grain.

2.3 Tests Set-Up for Vertical Two-Points Loading on Bolted LVL Trusses

Figure 2 and photo.6 show a test set-up for vertical two-points loading on bolted LVL trusses. A servo-actuator of 1000kN capacity was used for applying vertical monotonic load. A load-cell having 2000 micro-strain capacity at 1000 kN was used for measuring applied load. While vertical deflection at mid-span and two loading points were measured using wire-type large deflection measuring devices whose capacity was 5000 micro-strain at 500 mm deflection. Relative displacements at each nodal point in the truss were measured using high precise measuring devices whose capacity was 10000 micro-strain at 50 mm elongation. Strains at mid-point of each truss members were measured by gluing paper-base strain gauges of 20 mm in length. In the experiment, three replications of truss specimens were prepared and tested until final destruction.

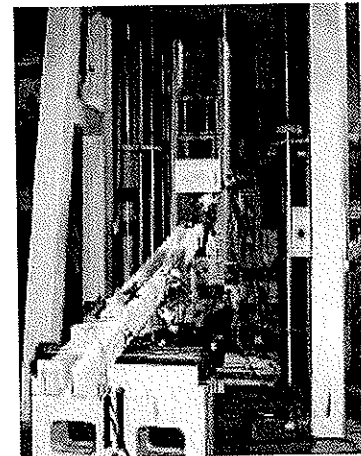


Photo. 6 Test set-up for vertical two-points loading on bolted LVL trusses.

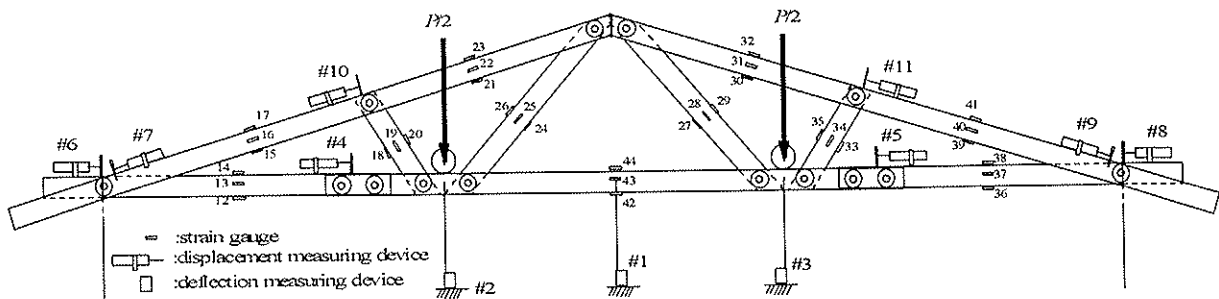


Fig.2 Test set-up for vertical two-points loading on bolted LVL trusses.

3. Nonlinear FEM Analyses

In this article, truss members were represented as an elastic 2D beam element, while joint part, which is shared with two nodal points, i.e. node-I belonging in elemnt-2 and node-J belonging in element-1 as defined in Fig.3 was represented as the nonlinear "joint element"[3].

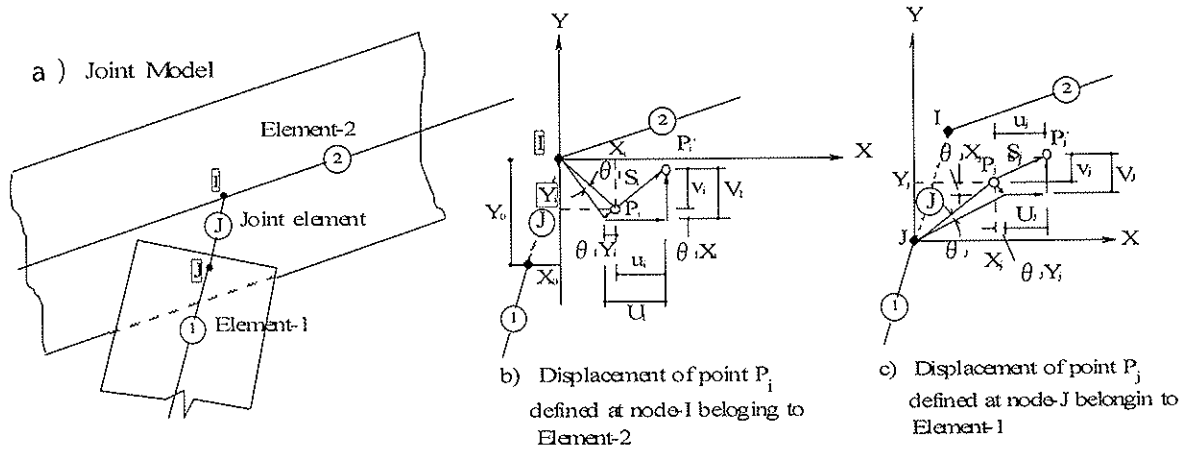


Fig.3 Concept of "joint element" for the nonlinear semi-rigid FEM analysis.

Slip displacement of individual fastener is defined as the relative displacement of point P_i and point P_j as shown in Fig.3. X,Y component of slip S_j are;

$$\begin{aligned} S_{xj} &= u_j - u_i = (U_j + Y_j \theta_j) - (U_i + Y_i \theta_i) \\ S_{yj} &= v_j - v_i = (V_j - X_j \theta_j) - (V_i - X_i \theta_i) \end{aligned} \quad \dots (1)$$

Actual slip of j-th fastener $S_{\phi j}$ occurs toward the direction of ϕ and expressed as equation (2).

$$\begin{aligned} S_{\phi j} &= \sqrt{S_{xj}^2 + S_{yj}^2} \quad \dots (2) \\ \phi &= \tan^{-1}(S_{yj} / S_{xj}) \end{aligned}$$

The total strain energy stored in the "joint element" is a summation of each strain energy due to individual fastener;

$$U_e = \sum_{j=1}^n \left\{ \int P_{\phi j}(S_{\phi j}) ds \right\} \dots (3)$$

Here, $P_{\phi j}$ is a reaction force of j-th fastener corresponding to the slip $S_{\phi j}$, and this relationship might be able to be represented by using a 3-parameters exponential equation (4) which was first introduced by Norén [1] then generalized by Foschi [2] for characterizing nonlinear load-slip behavior of nailed joint.

$$P_{\phi j} = \left(P_{0-\phi j} + K_{u-\phi j} S_{\phi j} \right) \left\{ 1 - \exp \left(\frac{-K_{s-\phi j}}{P_{0-\phi j}} S_{\phi j} \right) \right\} \quad \dots (4)$$

where,

$P_{0-\phi j}$ is the intercept of load axis.

$K_{u-\phi j}$ is the secondary slope of load P - slip S relationship.

$K_{s-\phi j}$ is the initial slope of $P - S$ relationship

The stiffness matrix of the "joint element" could be formulated [3] by taking step-wise linear approximation into nonlinear analysis. Consequently, the incremental strain energy ΔU_e is expressed as equation (5).

$$\begin{aligned} \Delta U_e &= \sum_{j=1}^n \left\{ \int \Delta P_{\phi_j} (\Delta S_{\phi_j}) ds \right\} \cong \sum \left(\int K_{\phi_j} \Delta S_{\phi_j} ds \right) \dots (5) \\ &= \frac{1}{2} \sum \left(K_{\phi_j} \Delta S_{\phi_j}^2 \right) = \frac{1}{2} \sum \left(K_{\phi_j} \Delta S_{X_j}^2 + K_{\phi_j} \Delta S_{Y_j}^2 \right) \end{aligned}$$

Employing Castigliano's theorem into equation (5), an incremental nodal forces vector $\{\Delta F\}$ was obtained in equation (6).

$$\begin{aligned} \{\Delta F\} &= \{\Delta N_I, \Delta Q_I, \Delta M_I, \Delta N_J, \Delta Q_J, \Delta M_J\}^T \\ &= \left\{ \frac{\partial \Delta U_e}{\partial \Delta U_I}, \frac{\partial \Delta U_e}{\partial \Delta V_I}, \frac{\partial \Delta U_e}{\partial \Delta \theta_I}, \frac{\partial \Delta U_e}{\partial \Delta U_J}, \frac{\partial \Delta U_e}{\partial \Delta V_J}, \frac{\partial \Delta U_e}{\partial \Delta \theta_J} \right\}^T \dots (6) \end{aligned}$$

From the relationship of $\{\Delta F\} = [K]\{\Delta \delta\}$, stiffness matrices $[K]$ of the "joint element" could be obtained in equation (7).

$$[K] = \begin{bmatrix} K1 & 0 & K2 & -K1 & 0 & -K3 \\ & K1 & -K4 & 0 & -K1 & K5 \\ & & K5 & -K2 & K4 & -K7 \\ & & & K1 & 0 & K3 \\ & & & & K1 & -K5 \\ & & & & & K8 \end{bmatrix} \dots (7)$$

where,

$$\begin{aligned} K1 &= \sum K_{\phi_j}, \quad K2 = \sum K_{\phi_j} Y_i, \quad K3 = \sum K_{\phi_j} Y_j, \quad K4 = \sum K_{\phi_j} X_i, \quad K5 = \sum K_{\phi_j} X_j \\ K6 &= \sum K_{\phi_j} X_i^2 + \sum K_{\phi_j} Y_i^2, \quad K7 = \sum K_{\phi_j} X_i X_j + \sum K_{\phi_j} Y_i Y_j, \quad K8 = \sum K_{\phi_j} X_j^2 + \sum K_{\phi_j} Y_j^2 \dots (8) \end{aligned}$$

here, K_{ϕ_j} is defined as a tangential slip modulus of j-th fastener in ϕ direction as equation (9), and X_j, Y_j are x,y coordinate of each fastener defined in the joint element.

$$K_{\phi_j} = dP_{\phi_j} / dS_{\phi_j} \cong \Delta P_{\phi_j} / \Delta S_{\phi_j} \dots (9)$$

Once the incremental stiffness matrices of the joint element is determined ostensively as in equations (7), (8), any frame structures having nonlinear semi-rigid joints can be solved by employing a conventional FEM program incorporating some modification for non-linear calculation scheme. The authors used the Newton-Raphson method for this non-linear calculation scheme. In the case of roof truss tested, a nonlinear semi-rigid model shown in Fig.4 represented actual truss structure.

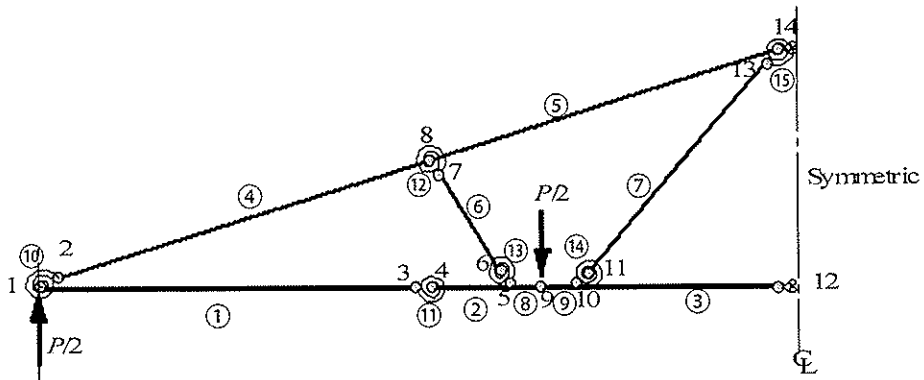


Fig.4 FEM model of the roof truss by using joint element concept.

4. Results

4.1 Mid-Span Deflection

Figure 5 shows comparisons between observed load-mid-span deflection relationships and calculated one.

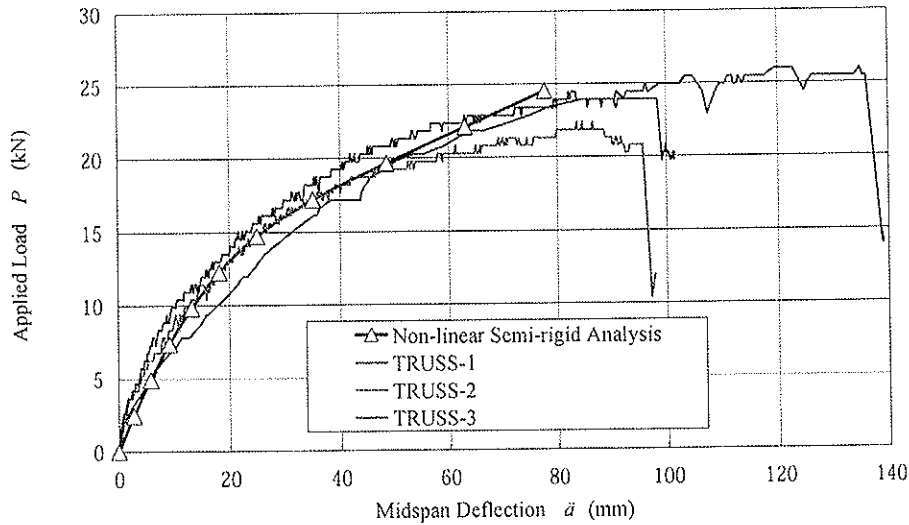


Fig.5 Load (P) – mid-span deflection (δ) relationships.

4.2 Slip Behavior at Heel Joints

Generally speaking, design of the heel joints is most important for wooden fink truss, as the joint becomes most critical point both in deflection and strength of fink truss. The relative slip displacement S_{12} at the heel joint of the truss analyzed by nonlinear FEM was defined in equation (10).

$$S_{12} = \sqrt{(u_1 - u_2)^2 + (v_1 - v_2)^2} \dots (10)$$

where,

u_1, u_2 : nodal displacements at node-1 and node-2 corresponding to the axial force (refer to Fig.4).

v_1, v_2 : nodal displacements at node-1 and node-2 corresponding to the shear force (refer to Fig.4).

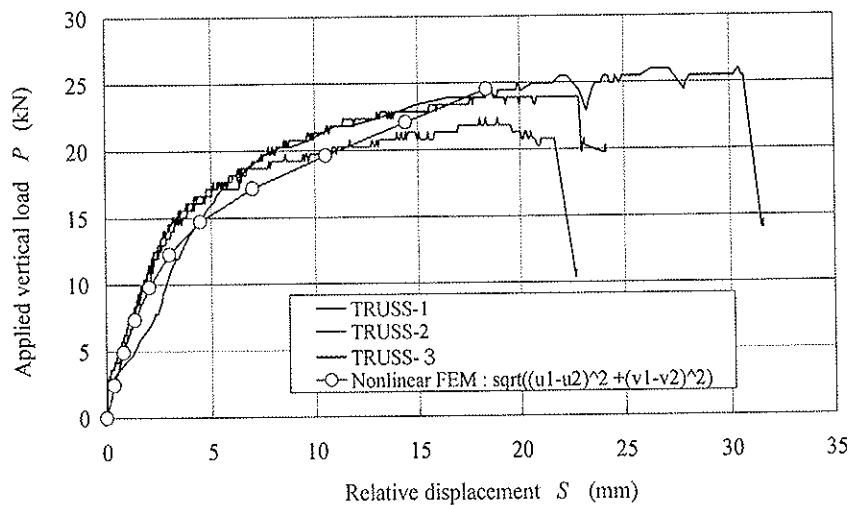


Fig.6 Load (P) – heel joint slip (S) relationships.

While, observed relative slip displacement S_{heel} at the heel joints tested was assumed as the equation (11) that means an average value of four measuring devices defined in Fig.2

$$S_{heel} = (\#6 + \#7 + \#8 + \#9) / 4 \dots (11)$$

where,

#6, #7, #8 and #9 : relative displacements measured at each locations (refer to Fig.2).

Figure 6 shows comparisons between observed load (P) – heel joint slip (S) relationships and calculated one.

4.3 Stresses in Members

Figure 7 shows comparisons between observed stresses (measured strain x mean MOE=10.6GPa) and calculated ones at center of bottom chord in the loading levels of 10 kN and 20 kN.

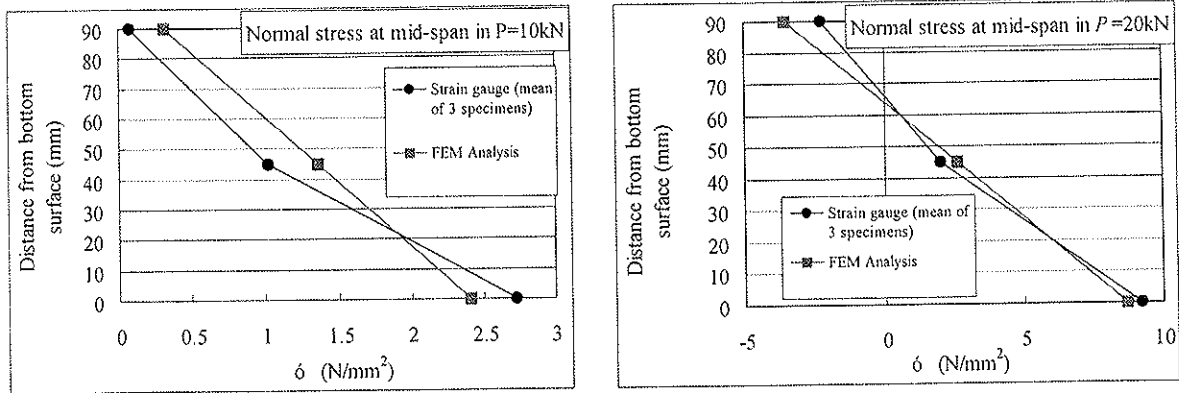


Fig.7 Comparisons between observed stresses vs. calculated ones at mid-span.

Figure 8 shows comparisons between observed stresses (measured strain x mean MOE=10.6GPa) and calculated ones at element-1 and element-4 in the loading levels of 15 kN.

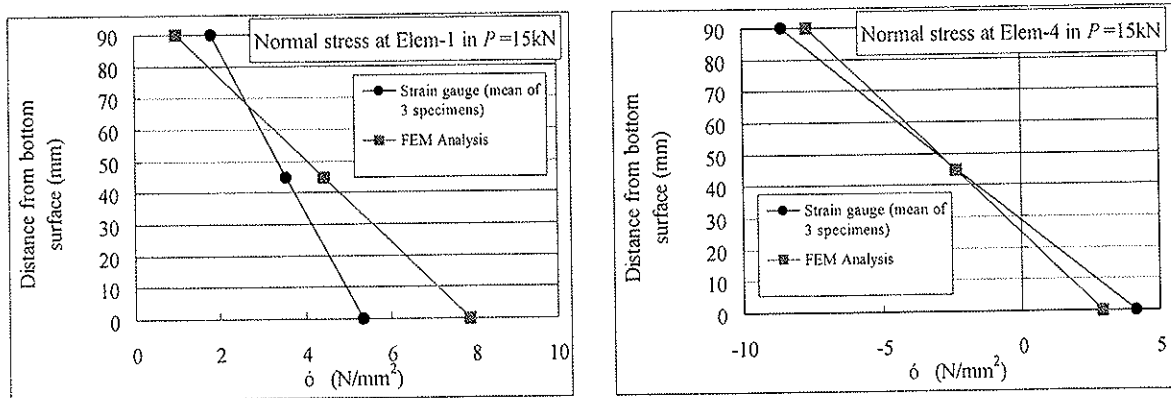


Fig.8 Comparisons between observed stresses vs. calculated ones at element-1 and 4.

4.4 Results of Bolted Joints

Figure 9 shows load-slip relationship obtained from the tests on the bolted joints of LVL.

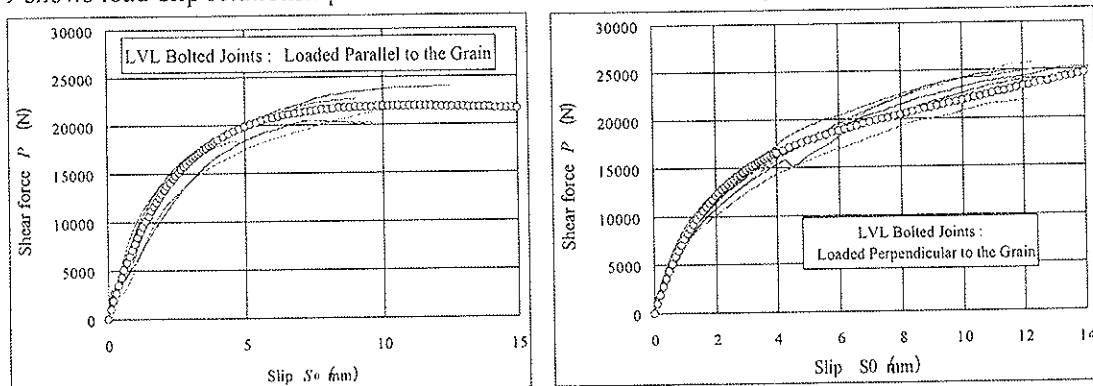


Fig.9 load-slip relationship obtained from the tests on the bolted joints of LVL.

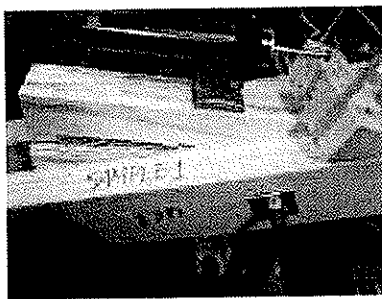
The circular plots in Fig.9 indicate the best-fitted 3-parameters exponential plots, with which the nonlinear FEM analyses were done. The 3-parameters obtained in these experiments are shown in Table 2.

Table 2 Best fitted 3-parameters obtained from tests on the bolted joints of LVL.

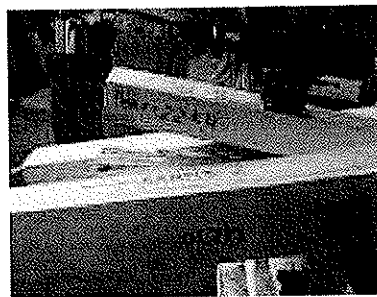
Parallel to the grain loading			Perpendicular to the grain loading		
P_0 (N)	K_{u0} (N/mm)	K_{s0} (N/mm)	P_{90} (N)	K_{u90} (N/mm)	K_{s90} (N/mm)
22000	-50	10000	12500	950	11000

4.4 Failure Phenomena of Trusses

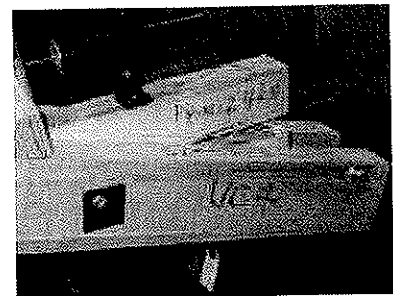
Photographs 7-a), b) and c) show typical failure phenomena observed on the test specimens. As can be seen from these photographs, it is clear that the splitting failure at the heel joint was the most critical fracture criterion for this type of wooden truss.



a) Truss-1



b) Truss-2



c) Truss-3

Photos. 7 Typical splitting failures at the heel joint.

5. Conclusions

A roof truss (fink truss) of 4.5m span length was made of 45 mm x 90 mm cross section tropical LVL for all members by using M12 bolts as the fasteners. Vertical two points loading tests were done to evaluate performance for the roof truss. Mid-span deflections, strain distributions in members and load-slip relationships at heel joints were carefully observed and those data were compared with those obtained from nonlinear FEM analyses.

Fairly good agreements between observed values and FEM analyses were obtained. From these results, it was confirmed that the bolted roof truss made of tropical LVL developed in this project had reasonable economical merit and that FEM analyses gave satisfactory predictions for the structural performance of roof truss made of tropical LVL.

References

- [1] B. Norén : "Nailed Joint-A Contribution to the Theoretical Analysis of Yield and Strength", Medd. 123B, Swedish Forest Products Research Laboratory, Stockholm, 1962.
- [2] R.O. Foschi : "Load-slip characteristics of Nails", Wood Science, 7(1), p.69-68, 1974.
- [3] Kohei Komatsu, Fumio Kamiya and Yoshihiko Hirasima : Full-Size Test and Analysis on Glulam Two Storied Portal Frames, Proceedings of the 1988 International Conference on Timber Engineering, Vol.2, 205-220, Seattle, (1988).

Acknowledgements

The authors would like to express their sincere thanks to the financial support from JSPS and also to the kind supports from Mr.Yokoo of Uni-Wood Cooperation.

INTERNATIONAL COUNCIL FOR RESEARCH AND INNOVATION
IN BUILDING AND CONSTRUCTION

WORKING COMMISSION W18 - TIMBER STRUCTURES

REINFORCEMENT OF LVL BEAMS WITH BONDED-IN PLATES AND RODS -
EFFECT OF PLACEMENT OF STEEL AND FRP REINFORCEMENTS
ON BEAM STRENGTH AND STIFFNESS

P Alam

Åbo Akademi Universitet
FINLAND

M P Ansell

University of Bath

D Smedley

Rotafix Ltd.

UNITED KINGDOM

Presented by M Ansell

F Lam, H J Larsen and Ansell discussed the practicality of these reinforced beams including cost and possible change of failure mode. It was agreed that these beams can be effectively used in repair of structures. 90% of this type of product will be used in repair work.

M Ballerini commented an Italian company has a commercial product available intended for repair and restoration project.

P Glos commented why is there a need for so much repair.

Y H Chui asked about the method of stress strain curve of the adhesive. Ansell replied that it was obtained from experimental tensile and compressive tests on small specimens.

Reinforcement of LVL beams with bonded-in plates and rods - effect of placement of steel and FRP reinforcements on beam strength and stiffness

Parvez Alam

Åbo Akademi Universitet, Finland

Martin P. Ansell

University of Bath, UK

Dave Smedley

Rotafix Ltd., UK

1 Introduction

Two metre long laminated veneer lumber (LVL) structural beams were reinforced using four different geometrical configurations of reinforcement (Phases I, II, III and IV). Each configuration was reinforced using either grade 43 mild steel or one of three different types of pultruded fibre reinforced plastic (FRP) composite. The objective of the research is to determine the reinforcement capabilities of different reinforcing plates and rods as a function of (a) the reinforcing materials, (b) the geometrical configurations of the four phases of reinforcement and (c) the volume fraction of reinforcement. Objectives (a) and (b) were reached by laboratory testing of reinforced beams for all four types of reinforcement and objective (c) was achieved by numerical simulations for the four phases of steel reinforcement. The paper concludes with design recommendations based on density and cost considerations for all of the experimentally tested reinforced beams.

2 Materials and manufacture of composite beams

Four different materials were used for reinforcing LVL (Kerto S). These included grade 43 mild steel grit blasted to SA 2.5 (Swedish standard for steel surfaces), carbon fibre reinforced vinyl ester thermoset (CFRP), glass fibre reinforced vinyl ester thermoset (GFRP) and glass fibre reinforced polyurethane thermoplastic (FULCRUM). The FRP plates and rods were all pultruded and were bonded into the LVL beams using Rotafix CB10TSS, a low modulus thixotropic epoxy adhesive. Four different beam series were evaluated. Phase I had a full depth flitch configuration. Phases II, III and IV incorporated various geometrical arrangements where rods and plates were bonded into routed slots machined into the top and bottom surfaces of the LVL beams. Figure 1 shows cross sectional schematics for each of the composite beam configurations. The reinforcement volume fractions differed between the reinforcing materials as well as the configurations. The volume fractions used were based upon the commercial availability of the particular materials and hence bear more relevance to practical usage. The cross sectional dimensions of the two metre long composite elements are given in Table 1.

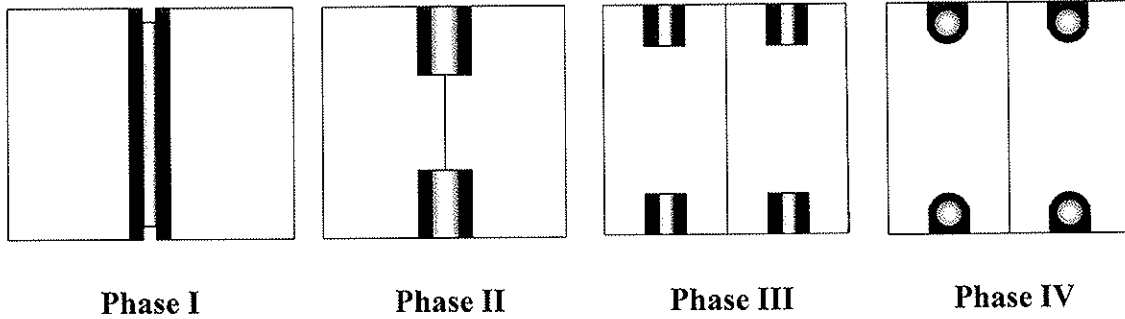


Figure 1 Composite beam reinforcement configurations for phases I, II, III and IV.

	Phase I		Phase II		Phase III		Phase IV	
	Depth /mm	Width /mm	Depth /mm	Width /mm	Depth /mm	Width /mm	Depth /mm or shape	Diameter or Width /mm
LVL	110	51×2	110	51×2	110	51×2	110	51×2
STEEL	100	6	40×2	5	20×4	5	Round	10
GFRP	100	4	40×2	4	20×4	4	Round	10
CFRP	100	1.5	40×2	1.5	20×4	1.5	Round	10
FULCRUM	100	1.2×3	40×2	1.2×3	20×4	1.2×2	Square	10

Table 1 Cross sectional dimensions for composite elements used in each phase.

3 Experimental test conditions

Two metre long composite beams were subjected to loading under conditions of four-point bending (BS EN 408:1995) with 600mm between adjacent rollers at a crosshead rate of 2mm.min⁻¹. The beams were tested under service class 2 conditions and the LVL retained a moisture content of approximately 12%. An LVDT displacement transducer attached to the moving crosshead was used to monitor the centre point deflection and hence surface strain.

4 Flexural properties of the reinforced beams

The median flexural modulus and flexural strength values for all tested beams are plotted in Figures 2 and 3 respectively. Error bars indicate the upper and lower boundaries of the sample range and the table in each figure shows in brackets the percentage difference from the properties of unreinforced LVL (flexural modulus of 14 GPa and edgewise flexural strength of 51 MPa). Comparing flexural properties for phase I-IV beams within each reinforcement series shows that the geometrical location of the reinforcement within a composite beam is very critical. A smaller volume of reinforcement situated strategically away from the neutral axis inside routed-out grooves gives flexural strength and stiffness properties that are as good as if not better than, full depth flitch plates. This is true for each of the reinforcing materials used.

It is difficult however to compare the experimentally determined flexural properties between the different reinforcement types because the reinforcements have different dimensions and hence, volume fractions. The transformed section method is therefore used to compare the strength values. The transformed strengths are calculated by theoretically transforming, by taking ratios of moduli, the area fractions of the reinforcement and adhesive to equivalent areas of LVL. Figure 4 shows the median values for the transformed

flexural strengths and the range of values, indicated by error bars. Individual values and their percentage difference from unreinforced LVL are listed in an accompanying table.

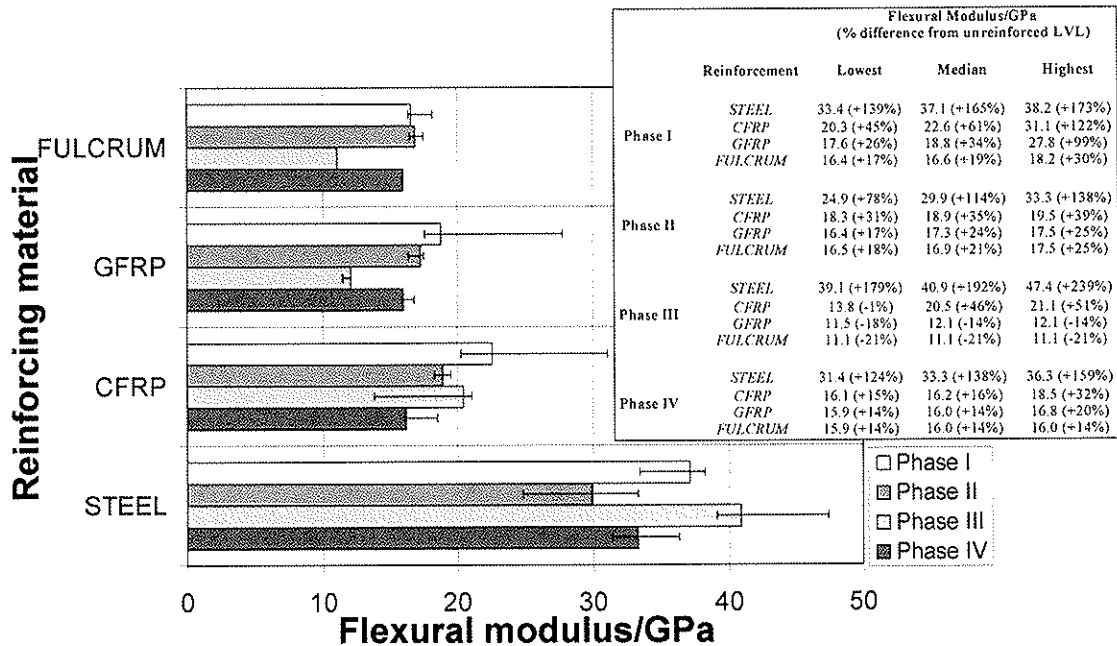


Figure 2 Median values for the flexural modulus for all tested beams with error bars indicating the upper and lower ranges. An accompanying table also shows the individual values and their percentage differences from unreinforced LVL.

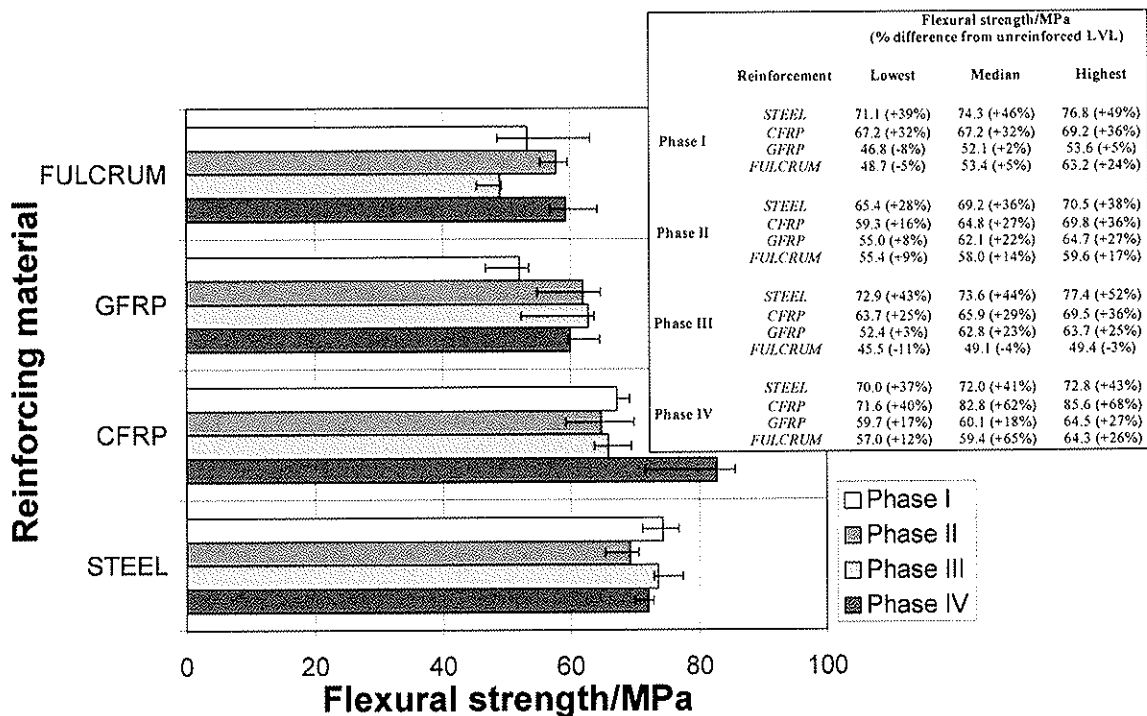


Figure 3 Median values for the flexural strength for all tested beams with error bars indicating the upper and lower ranges. An accompanying table also shows the individual values and their percentage differences from unreinforced LVL.

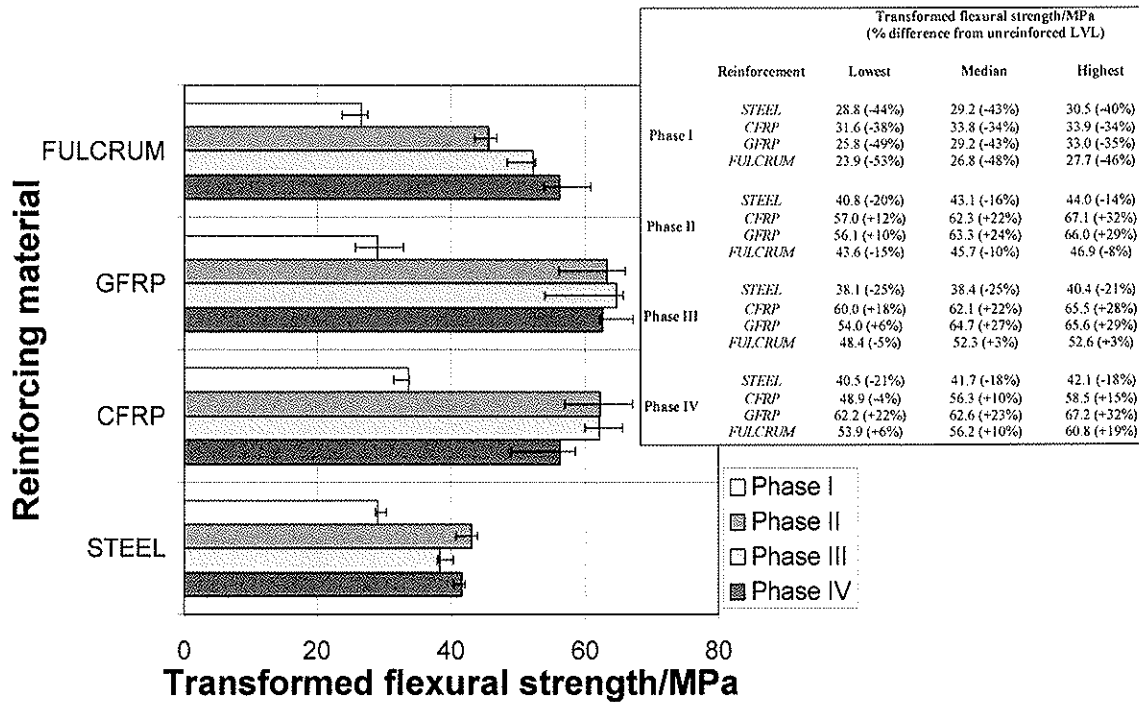


Figure 4 Median values for the transformed flexural strength for all tested beams with error bars indicating the upper and lower ranges. An accompanying table also shows the individual values and their percentage differences from unreinforced LVL.

Using the transformed method of analysis for flexural strength to compare both the phase I-IV beam configurations as well as the reinforcing materials, it can be said that the lower modulus reinforcements (GFRP and FULCRUM) often perform as well and sometimes better than the higher modulus reinforcements (CFRP and G43 mild steel). Within each reinforcement series, the phase II, III and IV beams also are seen to yield higher strength properties than phase I beams, but their strengths are quite similar. If the phase I-IV reinforcements were assigned equal volume fractions and then compared, the strength differential between reinforcement phases could be assessed.

5 Numerical analysis of steel-LVL composite beams

Having ascertained the mechanical properties of the composite beams experimentally, attention now turns to predicting the mechanical properties of composite beams. In particular, the flexural modulus and the limit of proportionality (or yield strength) of steel-LVL composite beams in the phase I-IV configurations will be predicted using the finite element method. The prediction of the limit of proportionality is essential since the principal aim when designing timber structures is to prevent the structure from entering a state where deformation within the structure is non-recoverable.

5.1 Methodological approach to non-linear modelling

The composite beams showed material and geometrical symmetry about a vertical axis in the centre of the cross section and the half beam cross sections were built using the dimensions shown in Figure 5. The beams were subsequently discretised using 1st order

finite elements. The non-linear stress-strain relationships input for grade 43 mild steel reinforcement and for the CB10TSS epoxy adhesive are shown in Figures 6 (a) and (b) respectively. Both the steel and the adhesive are assumed isotropic and begin straining plastically at a critical yield stress σ_v , calculated according to the von Mises principle, $\sigma_v = \sqrt{(\sigma_1 - \sigma_2)^2 + (\sigma_2 - \sigma_3)^2 + (\sigma_3 - \sigma_1)^2}$. The steel work hardens beyond yielding whereas the adhesive is assumed to experience perfect plasticity beyond yield.

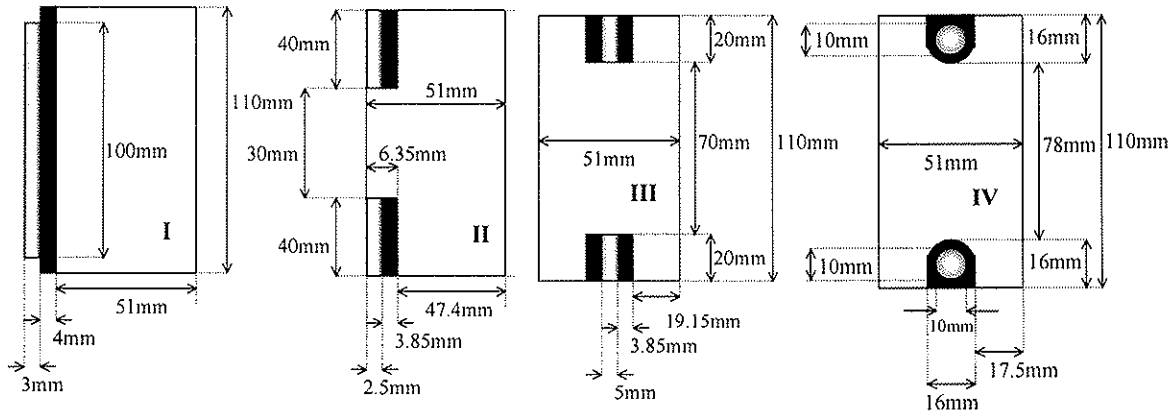


Figure 5 Cross sectional dimensions of phase I, II, III and IV models respectively

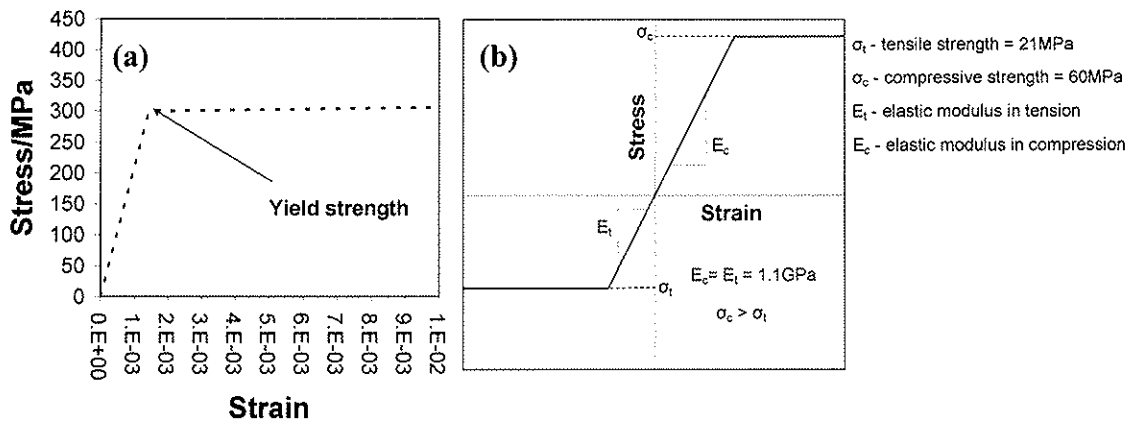


Figure 6 Stress-strain approximations for mild steel (a) and CB10TSS epoxy adhesive (b)

The Shih and Lee (1978) modification of Hill's (1948) potential was used to approximate the non-linear stress-strain behaviour of the LVL to three orthogonal axes of anisotropic symmetry. The Shih and Lee modification allows little room for the high tensile-compressive yield stress differential that is present in LVL, which can be a potential problem for flexural members that experience both stress states on either side of the neutral axis. The problem was overcome by linearly interpolating between the data predictions of two models, one possessing the tensile characteristics of LVL and the other with the compressive characteristics. The major assumptions therefore are that the axis of neutrality is located precisely at half the depth of the beam and that there is an equal contribution to deformation from both the tensile and compressive characteristics of the LVL. The bi-linear approximations for normal and shear stresses are provided in Figures 7 and 8 respectively.

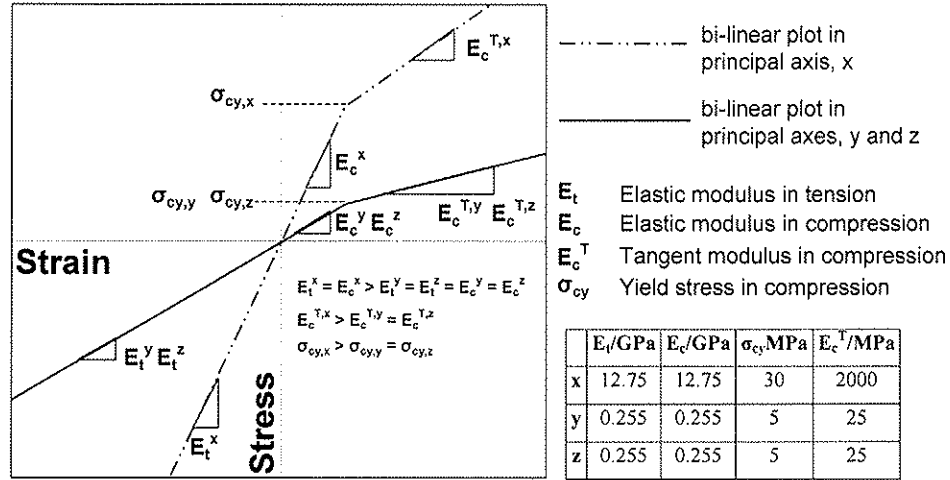


Figure 7 Stress-strain approximations and related values for LVL in each principal axis

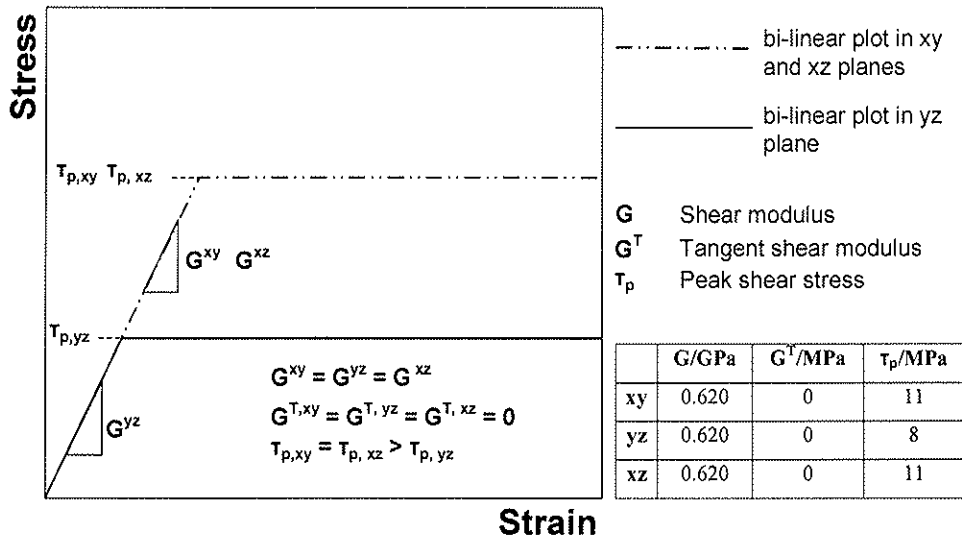


Figure 8 Shear stress- shear strain approximations and related values for LVL

5.2 Modelling the effects of reinforcement volume fraction for steel

Computational simulations were carried out for five different reinforcement volume fractions for each of the phases I-IV steel-LVL composite beams. The widths of phases I-III steel plates and the diameter of phase IV steel rods were adjusted to yield reinforcement volume fractions of 1%, 2%, 2.8%, 4% and 5%. The predictions for the flexural modulus and the yield strength are shown in Figures 9 and 10 respectively.

A mathematical relationship is applied to the finite element predictions as it relieves the requirement for repetitive computational simulations that will cater for every real dependent variable within a particular real independent variable range. The relationship therefore assumed for the flexural modulus as a function of the reinforcement volume fraction, x , occurs when $f : x \mapsto ax^b, x \in \mathbb{R}, 1 \leq x \leq 5$ where a and b are constants particular to each composite phase. The assumed relationship for the yield strength as a function of the reinforcement volume fraction, x , occurs when $f : x \mapsto cx + d, x \in \mathbb{R}, 1 \leq x \leq 5$ where c

and d are constants particular to each composite phase. These mathematical relationships were chosen as they generally yielded high coefficients of determination, R^2 , as is shown in each graph.

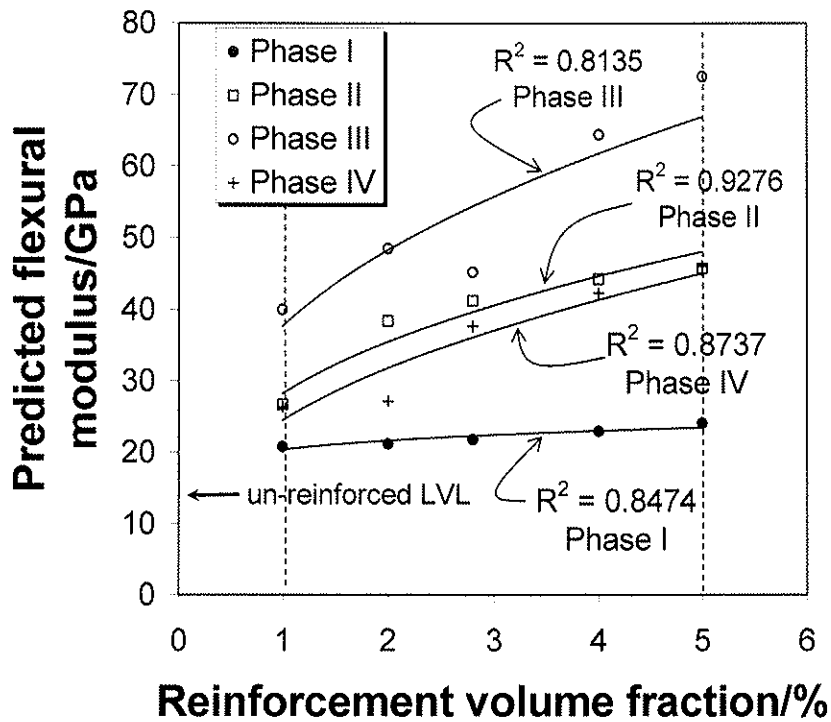


Figure 9 Theoretical flexural modulus as a function of the reinforcement volume fraction for phase I-IV steel-LVL composite beams

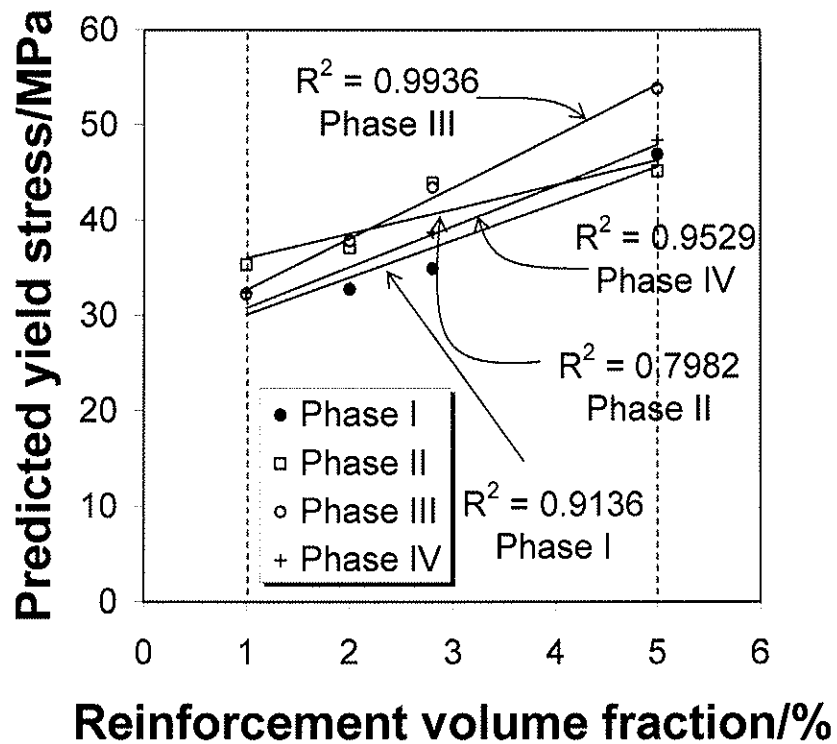


Figure 10 Theoretical yield strength as a function of the reinforcement volume fraction for phase I-IV steel-LVL composite beams

Examination of Figures 9 and 10 demonstrates that the effect of reinforcement volume fraction on the flexural modulus is non-linear. This finding agrees with the experimental and theoretical findings of Dorey and Cheng (1996) and Gilfillan *et al* (2001). Furthermore, the importance of the reinforcement geometry and its configuration within the LVL beam is unambiguous from the results of the numerical simulations. Superior flexural modulus and yield strength values are predicted as occurring in the phase III configuration (small vertical laminates grooved into the tension and compression faces of the LVL). This geometry is predicted to be better also than the phase IV reinforcing rods, which are also grooved into the tension and compression faces of the LVL. The geometry of the reinforcing plates is such that a greater percentage of the reinforcement is positioned nearer to the outermost fibres. Contrarily, reinforcing rods are thickest at a distance of at least the rod radius from its edge. Therefore rods are a less effective reinforcement geometry than plates at the beam surface assuming that the reinforcement volume fractions remain constant for the sake of comparison.

The general trends between reinforcement phases I-IV are the same for the flexural modulus and the yield stress. Phase II yield stresses however, Figure 10, show a slight deviation from the general trend observed for phases I-IV.

6 Design considerations

In section 5, finite element simulations demonstrated that vertical plates situated at the outmost fibres of the beam are more effective for reinforcing LVL beams than deeper plate inserts or rods of the same volume fraction. If a designer therefore wishes to maximise the mechanical performance of a composite beam as a function of reinforcement volume fraction, it is suggested that small plate inserts are placed into grooves at the outermost tension and compression fibres of the beams.

If the designer however wishes to maximise the flexural properties whilst minimising the cost and the density, plate reinforcements may not be ideal. Figures 11 and 12 show plots of the experimental (from section 4) flexural moduli and strengths respectively, plotted as a function of the product of the average density of the whole beam and the cost of the reinforcement. Firstly, phase IV (rod reinforcements) are the optimal reinforcement geometry within each material reinforcement series. The phase IV beams have respectable flexural properties and yet have the lowest cost-density product. Furthermore, when comparing the different material reinforcements, the steel rod reinforcements in LVL are very clearly superior to the pultruded fibre reinforced composites as they have the lowest cost-density product yet have very favourable strength and stiffness properties.

Steel reinforcements do however have certain drawbacks. One is that they are more susceptible to degradation within the LVL. This can have negative effects not only as the efficiency of the reinforcement deteriorates, but also as the corrosion products of steel chemically deteriorate wood (Thompson, 1982) and also occupy four times as much volume as the steel itself (Marshall *et al*, 1998). The overall consequence, therefore, is that rusting steel can seriously damage the host timber. For this reason, FRP reinforcements are often preferred and when examining the plots with respect to the different FRP reinforcements, the lower modulus GFRP and FULCRUM reinforcements are preferred to the CFRP because they enhance the strength and stiffness to a similar extent and yet they are a good deal cheaper.

In conclusion, it can be said that design considerations are dependant upon the design objectives. If the aim is only to enhance the mechanical performance, then finite element

models for steel show that small plate reinforcements located at the outmost fibres of the beam are superior to rods and full depth plates when equal volume fractions of reinforcement are used. If the aim is to minimise the cost and density whilst maximising the mechanical properties, then rods are the superior geometry as they yield respectable mechanical properties at a fraction of the cost. Steel rod reinforcements are by far the better choice of material if rusting can be eliminated and in cases where FRP reinforcements need to be used, the lower cost, lower modulus FRP composites (GFRP and FULCRUM) are preferable to CFRP.

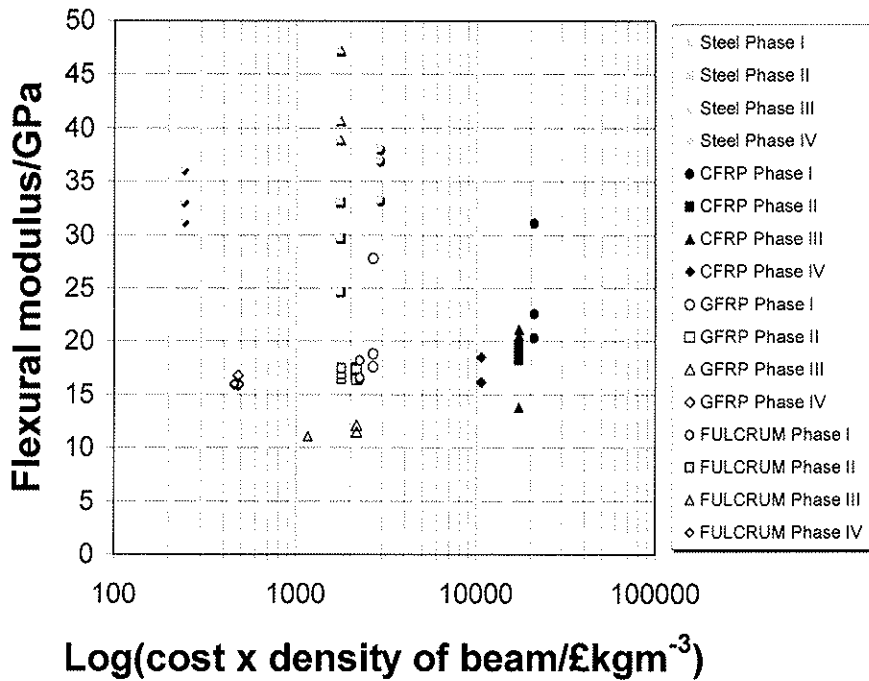


Figure 11 Flexural modulus plotted as a function of the cost of the reinforcement \times averaged density of each composite beam.

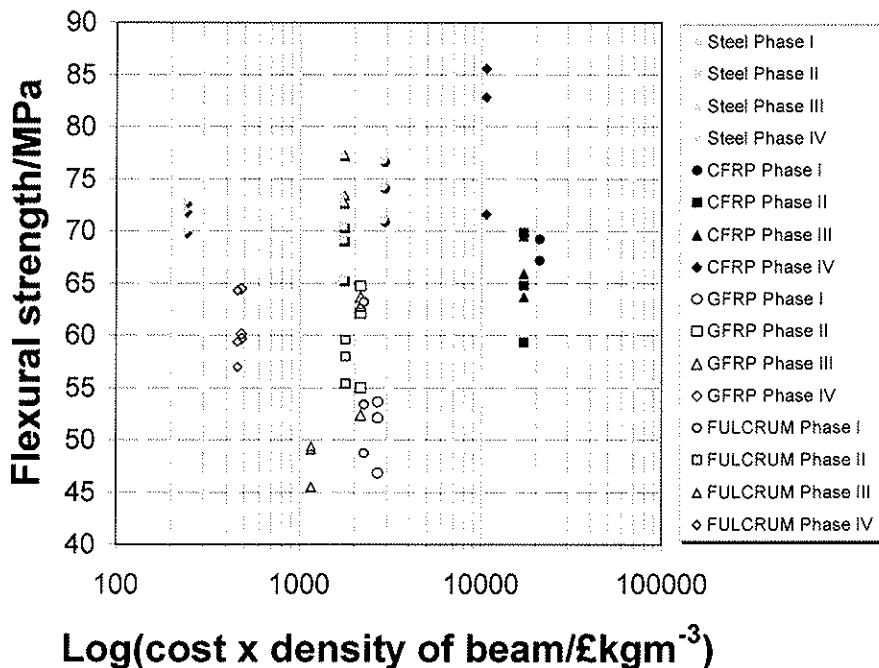


Figure 12 Flexural strength plotted as a function of the cost of the reinforcement \times averaged density of each composite beam.

7 Conclusions

- Grade 43 mild steel and FRP reinforcements were tested in four phases with different geometrical configurations.
- Examination of the flexural strength and stiffness data showed that smaller volumes of plate and rod reinforcement at the outermost tension and compression fibres of the beam are as effective as full depth flitch plates for improving mechanical properties.
- Using the transformed section approach, it was found that lower modulus reinforcements such as GFRP and FULCRUM are as effective as higher modulus reinforcements such as mild steel and CFRP for improving the mechanical performance of reinforced LVL beams.
- Non-linear finite element models were developed for phases I-IV steel-LVL beams to predict the flexural modulus and the yield strength as a function of the reinforcement volume fraction.
- Finite element predictions for steel reinforcement showed that better flexural properties are attainable by locating small plates at the outermost fibres than similarly located rod reinforcements with equal volume fractions.
- Design recommendations regarding the geometrical arrangements of composite components and of reinforcing materials have been discussed with respect to enhancement of mechanical properties, volume fraction, density and cost. Design recommendations are based on both numerical and experimental findings.
- Low cost, low modulus reinforcements strategically located within LVL beams have a great deal of potential for use in practical reinforcement of structural timber.

8 References

- Dorey, A. B. & Cheng, J. J. R.** (1996); Development of a composite glued laminated timber; A Canadian Forest Service & Land and Forest Service Publication.
- Gilfillan, R., Gilbert, S. & Patrick, G** (2001); The improved performance of home-grown timber glulam beams using fibre reinforcement; Journal of the Institute of Wood Science, Vol. 15 No. 6 pp. 307-317.
- Hill, R.** (1949); A theory on the yielding and plastic flow of anisotropic metals; Proceedings of the Royal Society A, Vol. 193 pp. 281-297.
- Marshall, D., Worthing, D. & Heath, R.** (1998); Understanding housing defects; Interprint Limited.
- Shih, C. F. & Lee, D.** (1978); Further developments in anisotropic plasticity; Journal of Engineering Materials and Technology, Vol. 100 pp. 294-302.
- Thompson, W. S.** (1982); Adverse environments and related design considerations – chemical effects; Proceedings of “Structural uses of wood in adverse environments”, Pub. Van Nostrand Reinhold, pp.117-130.

9 Acknowledgement

The authors thank the Engineering and Physical Sciences Research Council for funding a research studentship at the University of Bath and Stan Bowen for preparing the beams.

INTERNATIONAL COUNCIL FOR RESEARCH AND INNOVATION
IN BUILDING AND CONSTRUCTION

WORKING COMMISSION W18 - TIMBER STRUCTURES

ESTIMATING 3D BEHAVIOUR OF CONVENTIONAL TIMBER
STRUCTURES WITH SHEAR WALLS BY PSEUDO-DYNAMIC TESTS

M Yasumura
Shizuoka University

M Uesugi
Miyazaki Prefecture Wood Utilization Technical Center

JAPAN

L Davenne
Laboratoire de la Mécanique et Technologie

FRANCE

Presented by M Yasumura

P Quenneville asked whether more tests on different aspect ratios be conducted. Yasumura answered no as the model can be used to predict the response of such systems.

E Karacabeyli observed that the diaphragm without blocking had no nails on the perimeter. Yasumura responded that he wanted to study the more extreme cases for comparison therefore a very flexible system was chosen.

A discussion took place on the assumption of stiffness of the diaphragm between F Lam, A Cecotti and Yasumura. It was agreed that the assumed values gave good results. As the response of pseudo dynamic tests is dependent on the assumed stiffness, refinements to the model could be taken.

Estimating 3D behaviour of conventional timber structures with shear walls by pseudo-dynamic tests

Motoi YASUMURA

Shizuoka University, Japan

Motoi UESUGI

Miyazaki Prefecture Wood Utilization Technical Center, Japan

Luc DAVENNE

Laboratoire de Mécanique et Technologie, France

1 Abstract

One of the most important causes of the seismic damage of timber buildings is the unbalance of the lateral resistance of shear walls and the lack of the shear stiffness of the horizontal diaphragm. These damages were often observed during the 1995 Hyogoken-Nanbu Earthquake on conventional commercial buildings that had large openings in front of the building. The objective of this research is to analyse the influence of the unbalance of the lateral resistance of shear walls and the shear stiffness of the horizontal diaphragm on 3D dynamic behaviour of the structures by pseudo-dynamic tests. The specimens were conventional post and beam timber structures with shear walls of 3m width, 3m depth and 3m height. Specimens had 7.5mm plywood sheathed shear walls and a horizontal diaphragm sheathed with 24mm thick plywood. There were two types of horizontal diaphragms, i.e., the rigid diaphragm in which all the perimeters of plywood sheathings were nailed and the semi-rigid one that were only nailed in transversal direction. Four specimens with different combination of shear walls and diaphragms were prepared. Specimens WW-R and WW-S had shear walls with window opening in both loading direction and rigid and semi-rigid diaphragms, respectively. Specimens WS-R and WS-S had shear walls with opening and slit openings in loading direction and rigid and semi-rigid diaphragms, respectively. Both frames perpendicular to the loading direction were sheathed with plywood without openings. The lateral loads were applied to one side of the top of the specimen to give the eccentric loading. The lateral load based on the accerelogram of El Centro NS scaled up to 0.4G. The mass was assumed to be 10t. The test results were compared with the simulation with the lumped mass 3D model. It was shown that the model predicted quite well the earthquake response of 3D structures and useful for the parameter studies to estimate 3D behaviour of timber structures.

2 Introduction

In the previous paper of the 36th CIB-W18 meeting, it was shown that the pseudo-dynamic test was one of the most efficient methods to predict the seismic performance of timber

structures¹⁾. It is well known that one of the major causes of the damages of timber structures by earthquakes is the lack of the balance of the lateral stiffness of shear walls that causes the torsional deformation of the horizontal diaphragm and the concentration of the deformation in a weak part of the structure. This happens especially in commercial buildings that have large openings in front of the building and the houses having garages in the first story as was observed in 1989 Loma Prieta Earthquake. This damage is typical in Japanese conventional wooden buildings whose horizontal diaphragm is not rigid enough to transfer the shear forces to the adjacent shear walls as was frequently observed in 1995 Hyogo-ken Nanbu Earthquake²⁾. Thus the new building codes require to check the shear stiffness of the horizontal diaphragms based on the distance between the shear walls facing each other. This design procedure is based on the static design on particular cases, and more detailed study should be done to estimate the effects of horizontal diaphragms on 3D behaviour of the structure more precisely. Thus some dynamic parametric studies will be necessary to estimate 3D behaviour of the conventional timber structures.

Recently the floor system sheathed with the structural panel such as plywood is more frequently used for the horizontal diaphragms of Japanese conventional buildings to obtain higher shear stiffness. Thick panels of 24 to 35mm thickness are often used for subfloor to simplify the floor structures. In this study pseudo-dynamic tests were conducted on 3D structural model of conventional post and beam structures with plywood-sheathed shear walls and the horizontal diaphragm with 24mm thick plywood subfloor. The test results were compared with the dynamic analysis with the lumped mass 3D model. This model predicting quite well the earthquake response of 3D structures may be useful for conducting the parameter studies to estimate 3D behaviour of timber structures.

3 Specimens

Figure 1 shows the general description of the specimen and the test set-up. The specimens had one story conventional post and beam frames of 3m width, 3m depth and 3m height. Plywood sheathings were nailed on four faces of the structure.

The specimens consisted of 105-by-105mm posts and sills and 105-by-210mm beam of spruce (*Picea* spp.) glued laminated timber. Posts placed at every 1000mm were connected to the sill and the beam with a steel pipe of 26.5mm diameter and hold down connections (HD-B15). One hold down connection was attached at the foot and top of the posts. Sills were attached tightly to steel base frame with the bolts of 16mm diameters. Seven and a half millimeters thick lauan plywood JAS Grade I was nailed on one

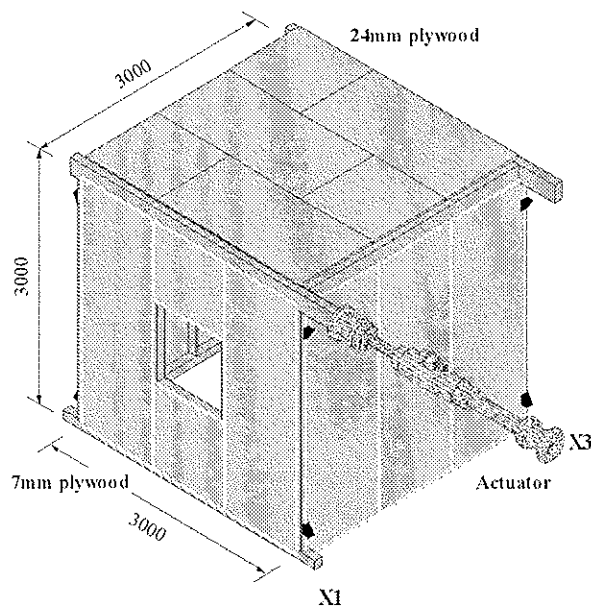


Fig.1 3D specimen and test set-up

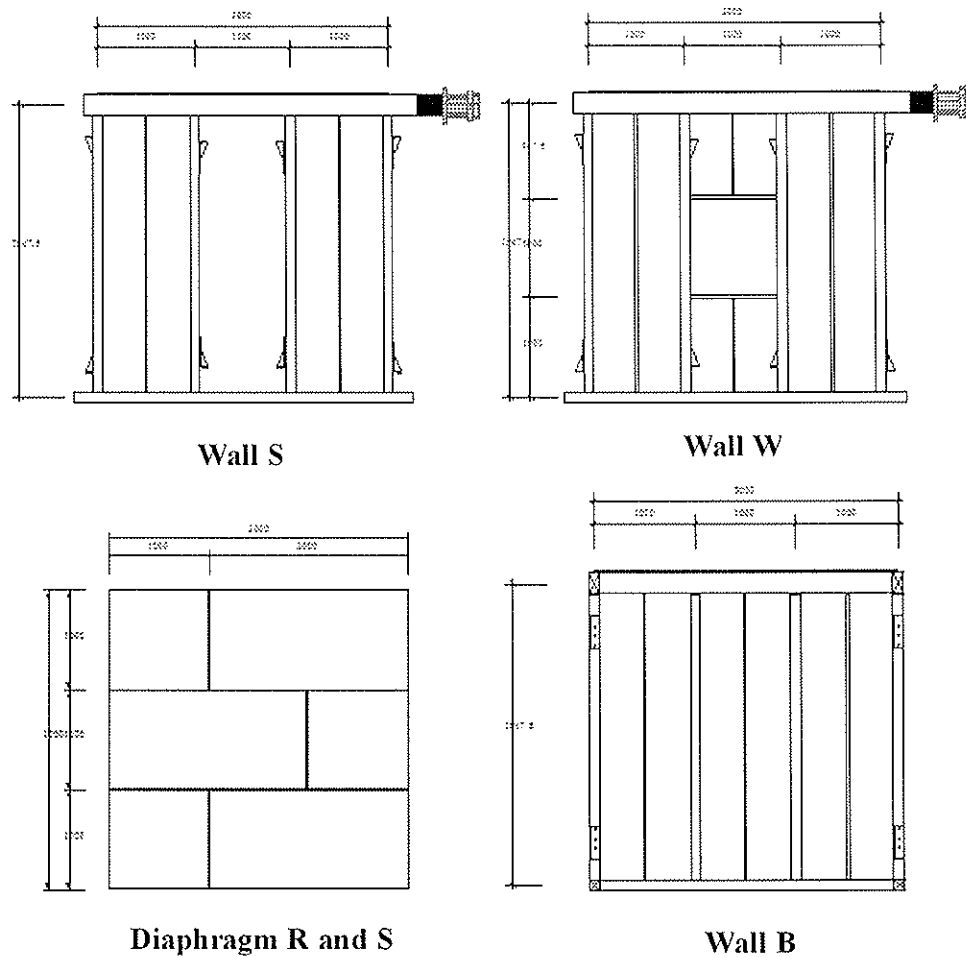


Fig.2 Vertical frames of Wall W, S, B and horizontal diaphragm R and S

side of the frame with N50 common nails at the interval of 150mm. The wall panels of the loading direction (X) had an opening of two different configurations at the center of the wall. The details of wall panels and floor are shown in Fig.2. Wall panel (W) had an opening of 1000mm width and 1000mm

height, wall panel (S) had an opening of 1000mm width continuing from the sill to the top beam. The wall panels of the perpendicular direction (Y) had no openings (B).

Horizontal diaphragms consisted of 105-by 105mm beams placed at every 1000mm on which 24mm thick Sugi plywood (JAS Grade II) was nailed on the floor framings at the

Table 1 Shear walls used for 3D specimens

Specimen	Loading plane(X1)	Unloading plane(X3)	Horizontal diaphragm
WW-R	W	W	R
WS-R	W	S	R
WW-S	W	W	S
WS-S	W	S	S

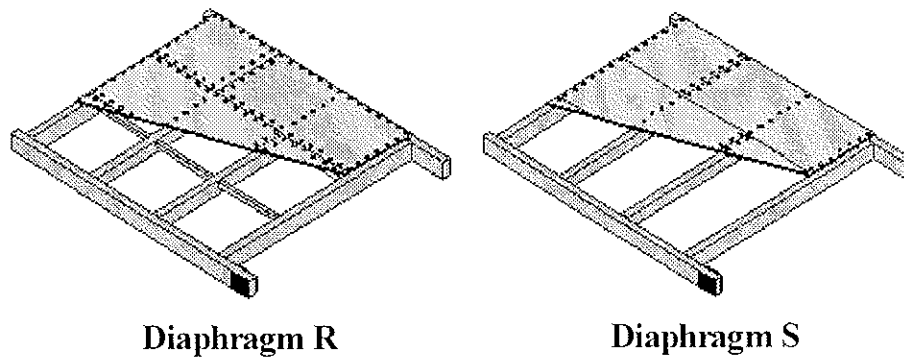


Fig.3 Floor framing and nail patterns of the horizontal diaphragm R and S

interval of 150mm with N75 nails. There were two kinds of diaphragms as shown in Fig.3. One had 45-by 45mm spruce blocking at the joints of plywood, and all the perimeters of the sheet material were nailed. The other had the tongue and groove at the joints of plywood and had no blocking and nail joints. We call the former “rigid floor (R)” and the later “flexible floor (S)”.

The specimens had the vertical diaphragm of the combination of the wall panels as shown in Table 1. Specimen WW had a wall panel with a window opening (W) in X1 and X3, and specimen WS had a wall panel with a window opening (W) in X1 and a wall panel with a slit opening in X3. Both the specimens with rigid floor (WW-R, WS-R) and flexible floor (WW-S, WS-S) were prepared.

4 Test methods

The lateral loads were applied at the top of one side of the first story as shown in Fig.1 to give the eccentric load. Computer-on-line system (*Saginomiya ATC-20*) was used for the pseudo-dynamic tests. The mass of 10t was assumed taking into account of the wall coefficient of plywood-sheathed shear walls of 2.5. The accelerogram used for the pseudo-dynamic tests and dynamic analysis was the NS components of the 1940 El Centro NS linearly scaled up to have the maximum acceleration of 0.4G. Horizontal displacements in X and Y directions at the top of the specimen and the vertical displacements of each post were measured by electric transducers. The stress of the bolts connecting the hold-down was also measured to obtain the tensile force at the bottom of the posts.

The reversed cyclic lateral loading tests³⁾ were conducted separately on the shear walls and horizontal diaphragms used for 3D structures.

5 Results and discussions

5.1 Modeling of shear walls

The same hysteretical model as used in the previous study^{1,4)} was used for the analysis. The outline of the model is shown in Fig.4.

5.2 Modeling of horizontal diaphragm

Figure 5 shows the load-displacement relationships of the horizontal diaphragms. They show that the initial stiffness and the strength of the rigid diaphragm with blocking was approximately three times higher than those of the flexible one without blocking, and the nail joints between the sheets material played an important roll to transfer the shear force while the tange and groove joints was not efficient if some adhesives or mechanical joints were not applied. The initial shear stiffness for these diaphragms was obtained as follows.

$$G_f = k_0 \cdot \frac{H}{L} \quad (1)$$

Where G_f and k_0 are the shear stiffness and the initial stiffness of the diaphragm, and L and H are the width (3m) and the depth (3m) of the diaphragm, respectively.

The values of k_0 for the rigid (R) and flexible (S) diaphragms were determined as 1240N/mm and 400N/mm, respectively, from the experiments.

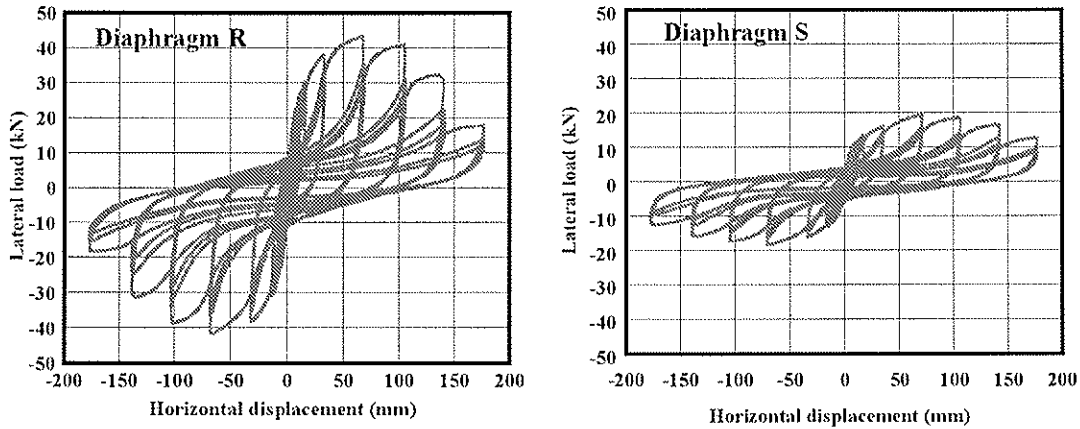


Fig 5 Load-displacement relationships of horizontal diaphragms

5.3 Modeling of structure

3D model as shown in Fig.6 was assumed for the analysis. The model consists of four masses of m_1 to m_4 supported by four non-linear springs representative of four vertical diaphragms and connected each other by the horizontal diaphragm. It is assumed that the horizontal diaphragm deforms as parallelogram and has linear shear stiffness of G_f . The stiffness matrix for the horizontal diaphragm K_f is expressed as follows;

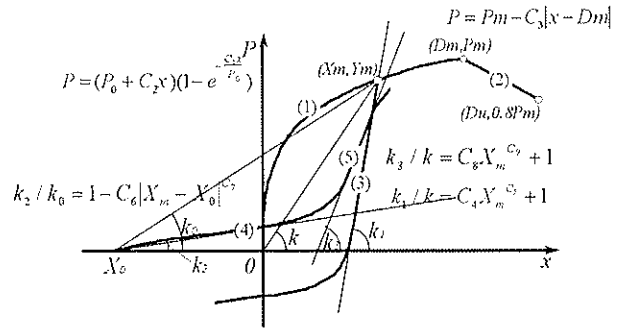


Fig 4 Hysteretical model of shear walls

$$K_f = G_f \begin{bmatrix} \frac{L}{H} & -\frac{L}{H} & 1 & -1 \\ -\frac{L}{H} & \frac{L}{H} & -1 & 1 \\ 1 & -1 & \frac{H}{L} & -\frac{H}{L} \\ -1 & 1 & -\frac{H}{L} & \frac{H}{L} \end{bmatrix} \quad (2)$$

where, G_f is the shear stiffness of diaphragm, L and H are the length and depth of the diaphragm, respectively.

5.4 Comparison of simulation with experimental results

Figure 7 shows the horizontal displacement responses of X1 and X3 walls in pseudo-dynamic tests and simulation. It shows that there are few differences of the response of the X1 wall between the specimen having rigid horizontal diaphragm and the flexible one. The displacement response of X3 walls with rigid diaphragm is approximately twice as large as those with flexible diaphragm. In any case the simulation predicted quite well the response. Figure 8 shows the deformation of the horizontal diaphragm in pseudo-dynamic tests and the simulation at the peak of 2.2sec. The horizontal displacements in X and Y directions are magnified by ten. It shows that the deformation of the specimen with rigid diaphragm is mostly rotation and the shear deformation of the diaphragm is very small and approximately 1/200 and 1/330rad. in WW-R and WS-R, respectively. The deformation of the specimen with flexible diaphragm is mostly the shear deformation of the diaphragm, approximately 1/68 and 1/84rad. in WW-S and WS-S and the rotation of the diaphragm is very small. This shows that the lateral forces are mainly transferred by the horizontal diaphragm and the perpendicular walls in the case of the specimen with the rigid diaphragm. In the case of the specimens with the flexible diaphragm, lateral forces are not fully transferred to the opposite shear walls nor perpendicular shear walls because of the shear deformation of the horizontal diaphragm. It is notable that although the torsional deformation of the structure and the shear deformation of the horizontal diaphragms are different, there are few differences in the maximum response of X1 walls between the specimens with rigid diaphragm and the flexible one, and that of X3 walls were about a half and a quarter as large as that of X1 in the case of the walls with rigid and flexible horizontal diaphragms, respectively.

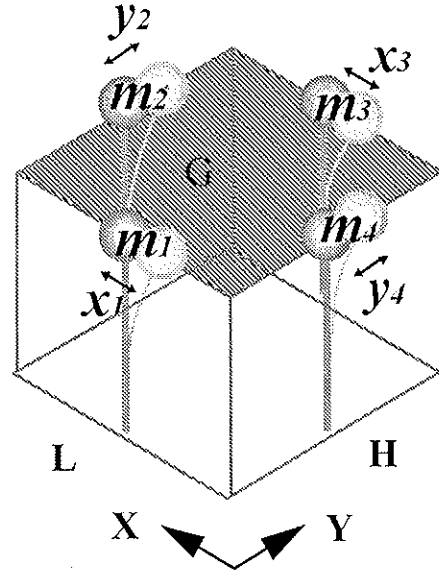


Fig.6 3D lumped mass model

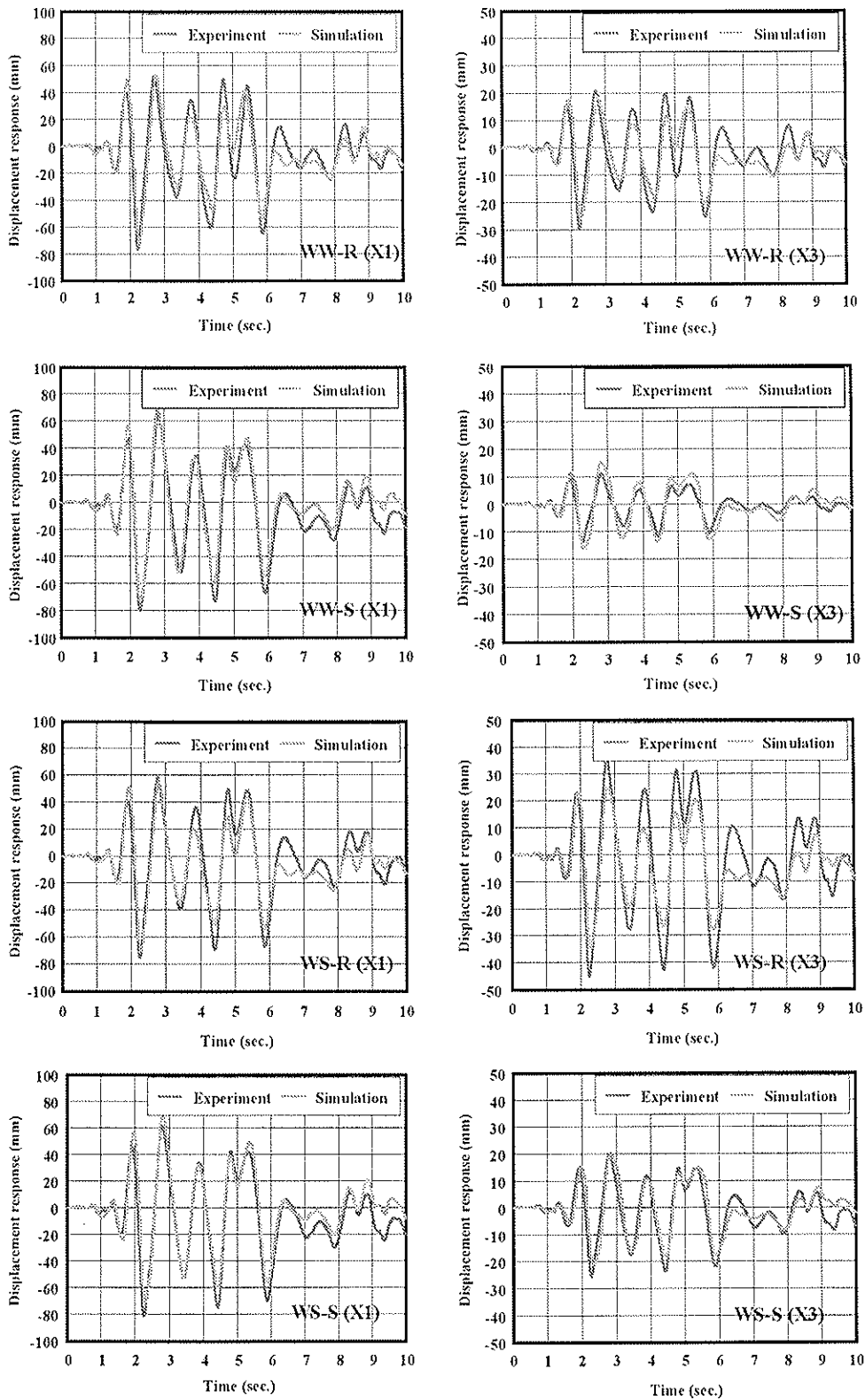


Fig.7 Comparison of the simulated displacement response in X1 and X3 walls with the experimental results.

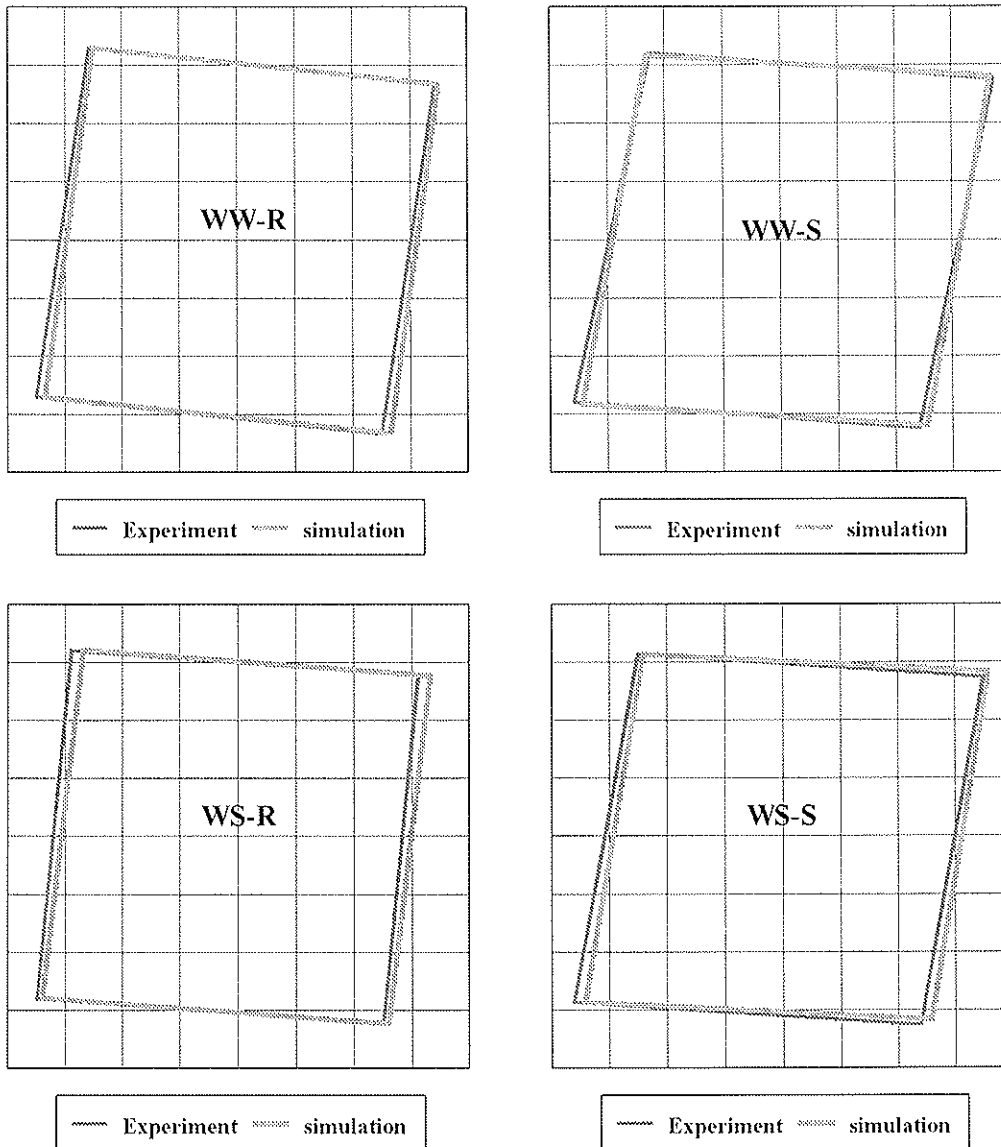


Fig.8 Shear deformation of the horizontal diaphragms by the simulation and the pseudo-dynamic tests. The deformation in X and Y directions are magnified by ten.

6 Conclusions

Summarizing the results mentioned above, the following conclusions are led.

- 1) The initial shear stiffness and the strength of the rigid diaphragm with blocking was approximately three times higher than those of the flexible one without blocking, and the nail joints between the sheets material played an important roll to transfer the shear

force while the tongue and groove joints was not efficient if some adhesives or mechanical joints were not applied.

- 2) There are few differences of the displacement response at the top of the wall in loading side (X1) between the specimen having rigid horizontal diaphragm and the flexible one. The displacement response at the top of the wall in unloading side (X3) with rigid diaphragm is approximately twice as large as those with flexible diaphragm.
- 3) The deformation of the specimen with rigid diaphragm is mostly rotation and the shear deformation of the diaphragm is very small. The deformation of the specimen with flexible diaphragm is mostly the shear deformation of the diaphragm and the rotation of the diaphragm is smaller than that with rigid diaphragm.
- 4) The simulation predicted quite well the earthquake response of the structures. The lumped mass 3D model proposed in this study is suitable for conducting a parameter study on 3D dynamic behaviour of timber structures.

7 Acknowledgements

The research was supported by the Grants-in-Aid for Scientific Research “Category C” of Monbu Kagakusho and JSPS. The author thanks Mr. Yasui and Mr. Kamada, graduate students of Shizuoka University for their help to conduct the tests and analysis of test data.

8 References

- 1) Yasumura, M. (2003) Pseudo-dynamic tests on conventional timber structures with shear walls, Proc. of the 36th CIB-W18 meeting, paper 36-15-4
- 2) Yasumura, M., Yamaguchi, N., Nakajima, S. (1996) Damage of wooden buildings caused by the 1995 Hyogo-ken Nanbu Earthquake, Proc. of the 29th CIB-W18 meeting, paper 29-15-2
- 3) ISO 16670 (2004) Timber structures – Joints made with mechanical fasteners – Quasi-static reversed-cyclic test method
- 4) Yasumura, M. (2001) Evaluation of damping capacity of timber structures for seismic design, Proc. of the 34th CIB-W18, paper 34-15-3

INTERNATIONAL COUNCIL FOR RESEARCH AND INNOVATION
IN BUILDING AND CONSTRUCTION

WORKING COMMISSION W18 - TIMBER STRUCTURES

TESTING OF RACKING BEHAVIOR OF MASSIVE WOODEN WALL PANELS

B Dujic

University of Ljubljana, Faculty of Civil and Geodetic Engineering

J Pucelj

RIKO HIŠE Ltd., Ribnica

R Zarnic

University of Ljubljana, Faculty of Civil and Geodetic Engineering

SLOVENIA

Presented by B Dujic

C Clorius commented that new anchorage system is available.

A Cecotti commented that AC24 protocol for steel connection and European document and ISO standards for joints are available.

P Quenneville asked with such a rigid system whether tests should focus on the connection only. Dujic responded that the diagonal deformations of the wall were also measured. P Quenneville suggested that as the rigidity of the wall is now known further information on design should be based on connection behaviour.

Testing of Racking Behavior of Massive Wooden Wall Panels

Bruno Dujic

University of Ljubljana, Faculty of Civil and Geodetic Engineering, Slovenia

Janez Pucelj

RIKO HIŠE Ltd., Ribnica, Slovenia

Roko Zarnic

University of Ljubljana, Faculty of Civil and Geodetic Engineering, Slovenia

Abstract

Massive wooden wall panels (SPF glued lamellate panel of size 244/244 cm), produced by Slovenian company RIKO HIŠE Ltd., were tested by monotonous and cyclic horizontal load in combination with constant vertical load. Monotonous horizontal load was applied following the EN 594 protocol. Testing by cyclic load followed the ATC-24 protocol for the testing of steel components. This protocol was applied because the main purpose of testing was to study the behavior of steel anchors. The influence of anchoring systems on shear stiffness and strength of timber wall panels was studied. The tested wooden panels have relatively high stiffness and load-bearing capacity. Therefore, the critical elements that govern the wooden shear cantilever response to earthquake excitations are anchors connecting panels with building foundation. The test results provided the basic data on stiffness and strength of the tested anchor systems that influence the entire racking response of massive shear cantilever wall panels. These experimentally obtained mechanical properties make possible the seismic design of prefabricated system according to EC8.

1 Introduction

The new generations of lightweight, prefabricated structures have recently become popular in the European market. The new trends in structural design bring multi-storey timber structures and business buildings in focus of investors. Special attention is paid to buildings located in earthquake prone areas of Central and South Europe. Therefore, the appropriate structural upgrade should be implemented in the existing structural systems to increase their seismic resistance. Slovenian companies are well established in the North European market where earthquake is not the major issue in structural design. The new European directives and standards (Construction Product Directive, Eurocodes) are demanding regarding the seismic resistance of structures constructed in Central Europe (Italy, Slovenia) and South Europe (Greece, Portugal, Turkey). Therefore, Slovenian industry of prefabricated timber structures should follow these demands if it wishes to respond to the needs of these particular segments of the European market.

The assessment of the response of prefabricated houses constructed from wooden structural elements to accidental actions, such as earthquake or strong wind, is demanding because of specific characteristics of load bearing system and mechanical connectors. Currently a research project is going

on at the Faculty of Civil and Geodetic Engineering at University in Ljubljana, financed by the Slovenian Ministry for Education, Science and Sport and company RIKO HIŠE Ltd. In the scope of the project joint connections, which influence the load bearing capacity of structural system exposed to different actions, will be tested. Within the first phase of research, massive wooden wall panels have been exposed to the monotonous and cyclic horizontal load in combination with constant vertical load. The influence of anchoring systems to shear stiffness and strength of timber wall panels has been studied. The tested type of wooden panels has relatively high stiffness and load-bearing capacity if appropriately tied together and anchored in the base. Experimentally obtained data make possible the reliable design of RIKO house exposed to different actions including earthquake and strong wind. Further development of numerical model of racking behavior of massive wooden wall panels will lead to the development of more accurate design procedure for earthquake resistant massive wooden buildings. The future model will be used for simulation and prediction of behaviour of structural elements and building structure as a whole when exposed to earthquake excitation.

Within the first year of the project the basic massive wood wall panels were tested simultaneously with applied constant vertical and cyclic horizontal load. In addition, comparative tests applying the monotonous horizontal load according to SIST EN 594 were carried out. The influence of anchoring systems to shear stiffness and strength of timber wall panels was evaluated. The existing anchoring system of wall panels was modified following the observed behaviour of the tested specimens. The main data obtained from the test results are: initial stiffness, load carrying capacity, ductility, stiffness degradation at reversed cycles of loading, energy dissipation and failure mechanisms.

2 Description of structural system

The basic construction component of RIKO house is a 100 mm thick solid wood wall made from carefully selected conifer, which is laminated and glued. A modified form of the basic construction component can be applied to the whole building (roof, partition wall, floor). Laminated timber elements contain 1-K-PUR adhesive, which does not contain formaldehyde. Dry wood contains only 10% of moisture. A house is erected from prefabricated large wall elements (walls with insulation, facade, windows and doors), as can be seen from Figure 1.

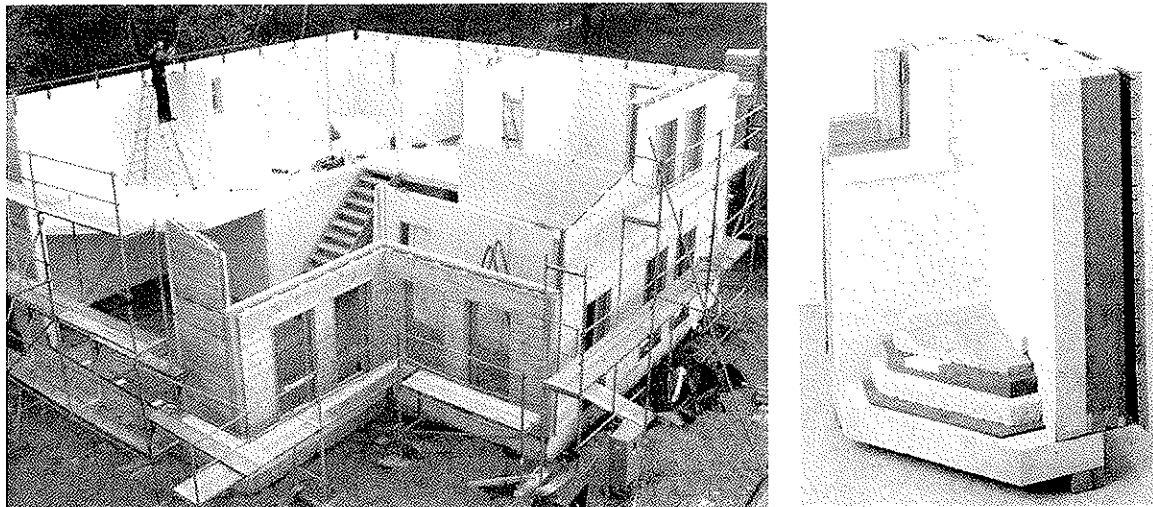


Figure 1: Assemblage of prefabricated large panels system (a) and corner detail of load-bearing construction with interior and exterior finishes (b).

The interior walls are smooth and therefore additional coating with natural materials (natural oils, wax) can be easily applied. From the detail of building corner (Figure 1) it can be seen that the massive spruce wooden wall is located in the interior face of the external wall and is thus protected against extreme weather fluctuations (primarily moisture). The outer face of the wooden wall is

protected by two layers of insulation panels. The first thermal insulation layer of optional thickness between 100 - 220 mm and secondary protective layer of 25 mm are attached (screwed) to the exterior side of the walls. The outer façade wainscot is usually made of larch wood in the form of ventilated façade.

The external massive wooden walls are constructed in the form of single structural element that is anchored to the foundation by means of angle irons fixed to one side of the wooden panel by nails and on the other side to the building foundation by steel anchor bolt. The inner structural system of the building is constructed of the combination of massive wooden walls, single columns and wooden frames with both sides plaster board sheathings (Figure 2a). Most of the horizontal action is carried by external wooden walls. The load carrying capacity and the deformability of massive wooden structure is governed by tensile strength of wood perpendicular to the grain direction, and mechanical properties of fasteners connecting wooden panels and anchorage system.

During the assembly, the wooden panels are placed on several plastic plates approximately 10 mm thick in order to nivelate them. The lower edge of the wooden panel is protected against rising damp by hydro-insulation. The gap between the lower edge of the panel and the foundation is filled by polyurethane foam after fixing of anchors. The entire horizontal force acting to panels is thus carried out only by dowel action of anchors (Figure 2b). Relatively significant horizontal displacements of panel relatively to foundation may develop during the horizontal action of an earthquake or even strong wind. Therefore, the experimental project was launched in order to improve and optimize the existing anchorage system.

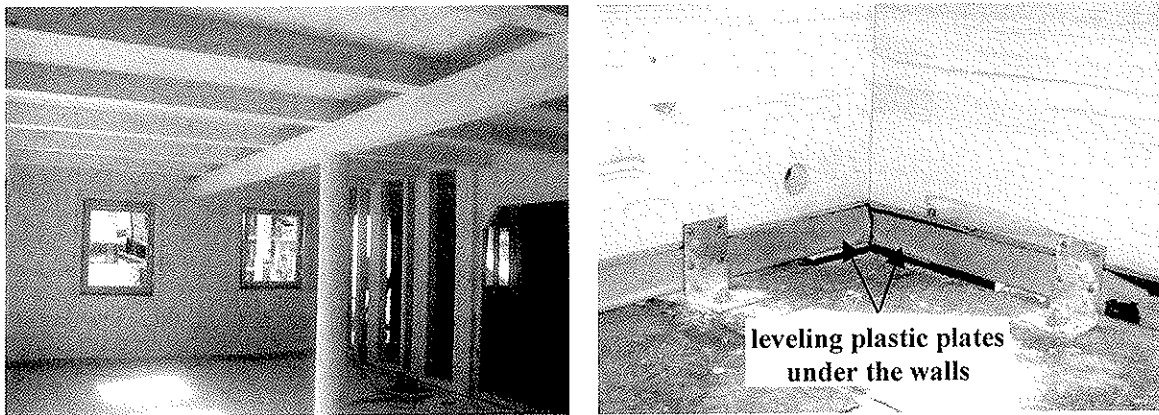


Figure 2: The interior of the load-bearing structure (a) and corner detail of the anchorage system with damp insulation and leveling plastic plates placed along the lower edge of panel (b).

3 Racking tests of massive wall panels

The main goal of the tests was to obtain data on mechanical properties of different wall configurations fixed to the foundation with different anchorage systems. Following the concept of performance based earthquake engineering design, the deformation level of a structure exposed to different load actions should be defined through the combination of experimental and analytical research. Careful design of structural system based on permissible story drift magnitude should result in sufficient resistance of the building exposed to earthquake and strong wind action with occurrence of only limited damages of non-structural parts of the building and no damages of structural system.

The first phase of research was aimed at the development of optimal configuration of panel anchorage. The tests started with anchorage that is currently used, followed by modified anchorage. The modification of anchorage improved its efficiency without significant change of its cost.

3.1 Test set-up of cantilever panels

The construction of set-up enables racking and shear testing of panels exposed to constant vertical load without influencing the movement and the rotation of the specimen free edge. The horizontal load is applied by gradual forcing of displacements along the free edge of the specimen. The set-up facilitates the testing of specimens in the form of cantilever panels turned upside-down and supported along the upper edge by a steel frame structure. The test set-up for combined constant vertical and displacement-controlled horizontal loading is composed of five major parts, marked in Figure 3 by numbers 1 to 5. The pair of lever beams (1) follows the vertical deformation of a specimen, while constant vertical load provided by counterbalance acts on the specimen. The horizontal displacement is applied along the lower horizontal edge of the specimen by a single displacement-controlled actuator (5) that moves the roller beam (3). The beam rolls along the supporting beam (2) that is hinged between the pair of lever beams. The specimen is tested as cantilever panel turned upside-down and supported along the upper edge by the steel frame (4). During the testing, the lower edge of the panel is supported by hinged (2) and horizontally movable mechanism (3), which allows its free horizontal movement and rotation. The set-up is calibrated for vertical and horizontal load.

The measuring of strains of the upper flanges of lever beams in cross section above the lever support enable the control of vertical load acting to the tested specimen. The horizontal action of hydraulic actuator is controlled by data acquisition and actuator control system Röell/Amsler. The capacity of the test set up is 500kN of constant vertical load provided by ballast and 250kN of horizontal load in displacement range of $\pm 200\text{mm}$ provided by Instron hydraulic actuator.

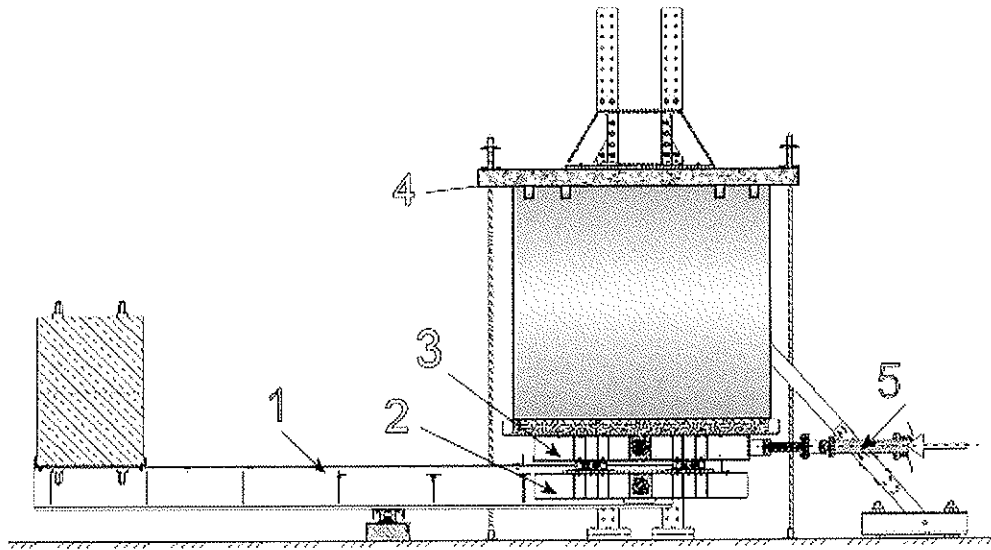


Figure 3: Test set-up for racking testing of shear cantilever panels turned upside-down and along the bottom edge supported by hinged and horizontally movable mechanism.

3.2 Description of test specimens and testing procedures

Altogether, three different anchor configurations were studied. Thus, fifteen tests were carried out applying three different loading protocols for horizontal load in combination with three different magnitudes of constant vertical load. The main characteristics of anchors composed of commercially available components are presented in Table 1 and shown in Figure 4. Anchors are fixed to wooden panel by nails and to concrete foundation by bolt. The first type of anchor listed in Table 1 is the type presently used in practice, the other two anchor types are studied to be eventually used in future.

Table 1: Characteristics of tested anchors.

Type of anchor	Angle iron		Annular nails $\phi 4.0/60\text{mm}$	Type of Fischer anchor bolt	Washer (steel plate) [mm]
	Type	Dimension [mm]			
BMF	6191	90/60/2.5/60	4	FBN 10/15+23	N/A
BMF+plate			4		60/60/10
Würth	W-VAD M12	240/72/2.5/60	6		

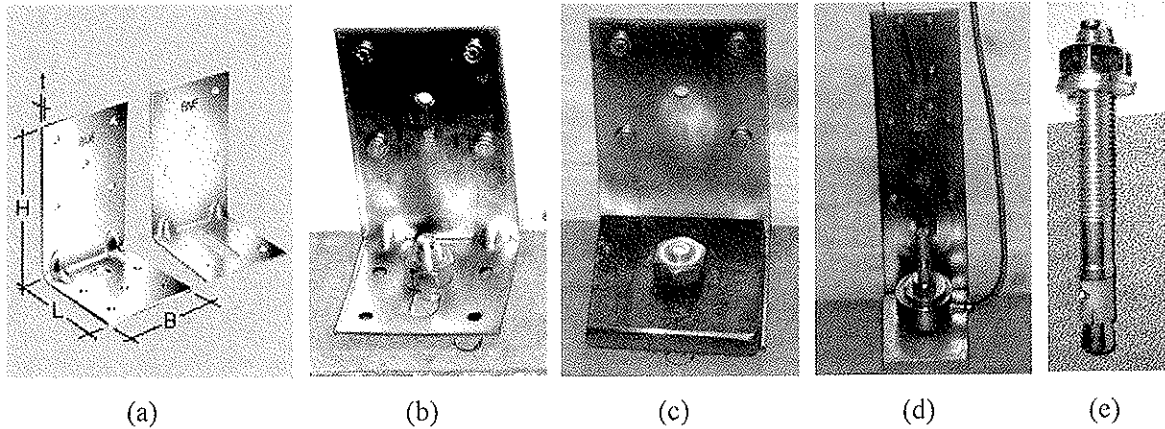


Figure 4: BMF 6191 angle iron (a), BMF anchor in basic configuration (b), modified BMF anchor with steel washer (c), Würth anchor with original steel washer (d) and Fisher anchor bolt (e)

Two types of panel-to-foundation contacts were tested: the first one as built on site having gap along the lower edge of the wooden panel due to levelling with plastic plates as described above (Figure 2B), and the second one with direct contact of wooden panel and concrete foundation along the entire length of the panel. In the case of the second configuration the friction forces acting along the panel-to-concrete edge provide the addition to the dowel strength of anchors. The responses of the tested anchors are presented in Figures 8, 9 and 10. The overview of the tests and the main characteristics of test responses are presented in Table 2.

Figure 5 shows one of the specimens during racking test together with the layout of instruments. The deformation of wooden panel was measured along the vertical edges and in both diagonal directions. Displacements were measured at both horizontal edges of the panel. The displacements measured above the supporting roller beam (Figure 3, element 3) were used to control the test running. Since the tested specimen was turned upside down, this control point is the actual building located at the upper edge of the wall panel. Therefore, in all diagrams and comments this point is named “top displacement”. In addition, the vertical panel-to-foundation dilatation was been measured, as well as strains of angle irons and forces in anchor bolts. Deformations were measured by HBM transducers, strains by strain-gauges, and forces in anchor bolts by high precision ring-shaped dynamometers (Figure 4d and 11c). Acting forces were obtained from hydraulic control system. Protocols for horizontal load were defined according to EN 594 for monotonous and ATC-24 for cyclic loading. It should be mentioned that EN 594 protocol is twofold. The first part of this protocol (test type A from Table 2) aims at the load bearing capacity of anchorage. The second part of the protocol defines the entire test of anchorage including intermediate deloadings and short term constant load actions (test type B from Table 2).

Table 2: The overview of racking tests and main characteristics of the tested panels.

Test			Type of load	Type of anchor	Ultimate Limit State		Failure mode
No.	Name of specimen	Date			Load [kN]	Displacement [mm]	
1	MW1c_m_1	19.2.04	A-V ₁	BMF	41	37	P1
2	MW1c_m_2	20.2.04		BMF+plate	31	15	P2
3	MW1c_m_3	1.3.04	B-V ₁	BMF	35.5	50	P1
4	MW1c_m_4	3.3.04	A-V ₁	BMF+plate	28	22	P2
5	MW1c_m_5	12.3.04	B-V ₁	Würth	37.5	18	
6	MW1c_m_6	15.3.04	B-V ₁		25	19	
7	MW2c_c_1	17.3.04	C-V ₁	BMF	34	24	P1
8	MW2c_c_2	22.3.04		BMF+plate	25	12	P3
9	MW2c_c_3	22.3.04		Würth	32	12	
10	MW2c_c_4	22.3.04			34	13	P2
11	MW3c_m_1	25.3.04	A-V ₁	BMF with plastic plates	32	23	P4
12	MW3c_c_2	26.3.04	C-V ₁		23	28	
13	MW3c_c_3	31.3.04	C-V ₂	BMF	24.5	24	
14	MW3c_c_4	1.4.04	C-V ₃		20.5	24	
15	MW3c_c_5	1.4.04		Würth	25.5	13	P2
Type of test							
A		Definition of ultimate limit state by monotonous test					
B		Test according to EN 594 applying monotonous loading protocol					
C		Definition of hysteresis curve applying cyclic loading					
Intensity of constant vertical load							
V ₁ = 38kN			V ₂ = 24kN			V ₃ = 15kN	
Failure mode of anchorage							
P1		Deformation of angle iron below the anchor washer (Figure 11a)					
P2		Longitudinal tensile failure of wooden panel (Figure 11b,c)					
P3		Tensile failure of anchor along the washer					
P4		Deformation of angle iron					

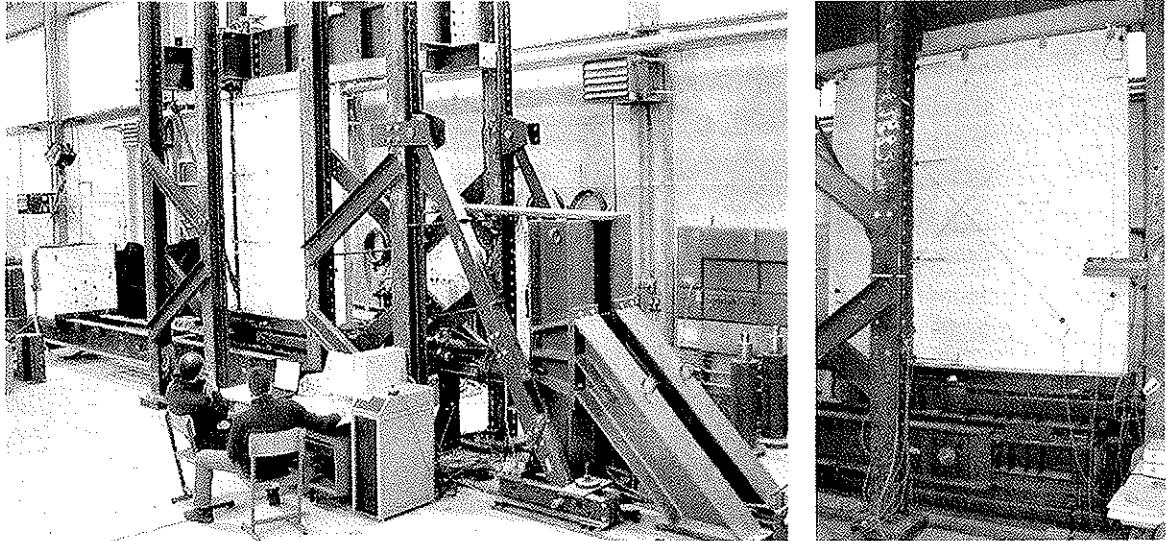


Figure 5: Racking test in lab at UL FGG (a) with instrumentation of massive wooden wall panel (b).

3.3 Influence of anchors on racking strength and stiffness of the wall

The main disadvantage of the currently used anchorage system, where lower edge of wooden panel is laid on plastic plates (Figure 2b and 11b), is its insulation from beneficial influence of friction. Therefore, anchors carry the whole horizontal and racking load by combined dowel and tensile-compressive effect. It results in significant deformation of angle irons. The anchorage will be upgraded by adding tooth-plate below the panel that will be designed to carry horizontal load. Angle irons will thus be loaded only by racking load and reduced deformation and displacing of the entire panel will be achieved. Similar behaviour was simulated during tests where wooden wall was laid on concrete beams and anchored with three different types of anchors (Table 1 and 2). The radical difference was observed in responses of frictionless (Figure 6) and friction exposed (Figure 7) anchored wall.

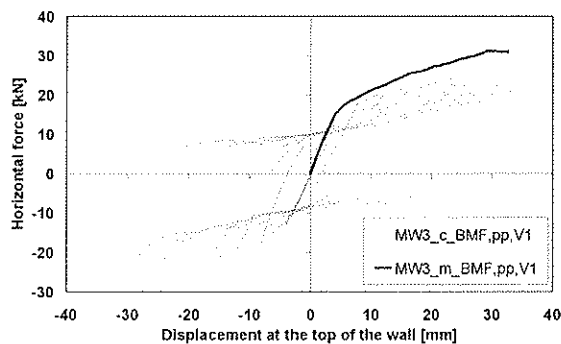


Figure 6: Monotonic and cyclic load-displacement response of shear wall having BMF anchors with levelling plastics plates and loaded with 38kN of vertical load.

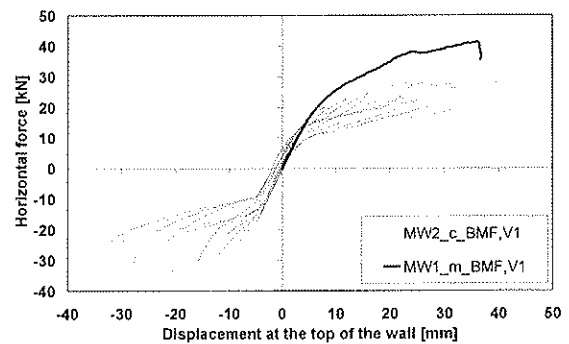


Figure 7: Monotonic and cyclic load-displacement response of shear wall having BMF anchors with active friction and loaded with 38kN of vertical load.

The main characteristic of the behaviour of basic anchorage system configuration with plastic plates was large deformability due to dowel behaviour of anchors, which results in deformation and yielding of angle irons. It leads to significant stiffness degradation that can be clearly seen from the shape of hysteretic curves (Figure 6). The large dissipation of energy is another clearly seen characteristic of the basic configuration. Although dissipation of energy is a desirable property of earthquake exposed

structures, in our case it was associated with large deformations that should be limited according to serviceability requirements. Wooden panels tested without levelling plates, where significant part of the horizontal load was carried by friction, dissipated less energy, but stiffness degradation was negligible. Friction force can be roughly estimated from hysteretic responses where the stiffness changes visibly. In the case presented in Figure 7 the share of friction force is roughly 60% of the ultimate strength of anchorage.

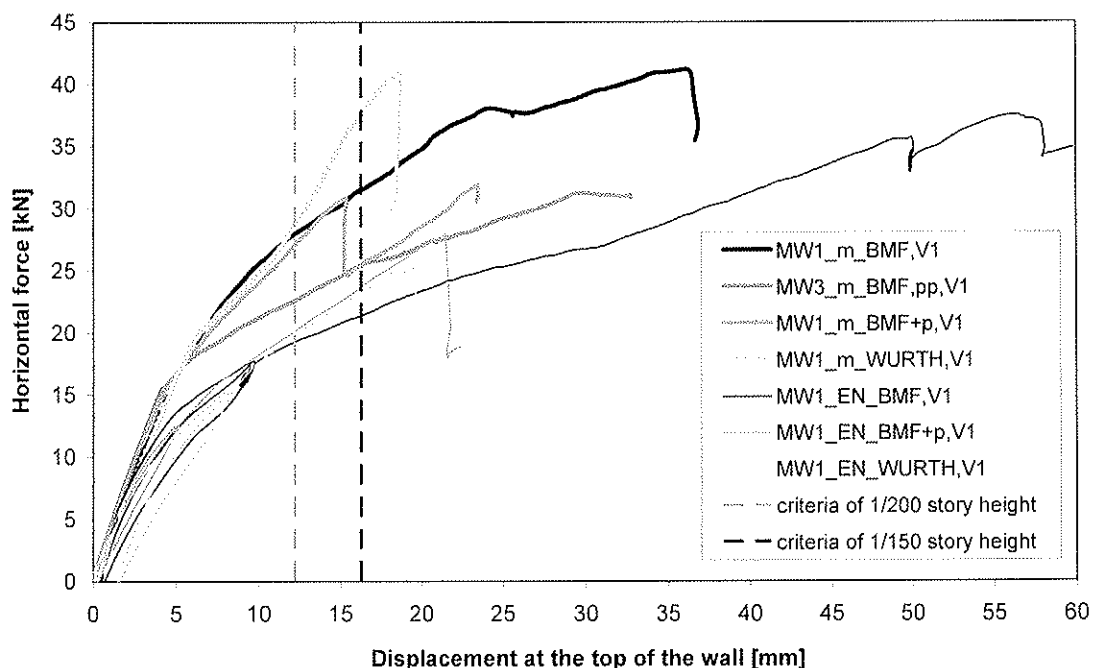


Figure 8: Comparison of response of differently anchored wooden panels exposed to monotonous loading.

The response diagrams of monotonously loaded wall panels having different anchorages are compared in Figure 8. All compared specimens were loaded with constant vertical load of 38kN. The names of specimens explain the type of anchorage and the type of monotonous loading. BMF, BMF+p and Würth stand for the type of anchorage angle iron (see Table 1); “pp” marks the specimen with plastic levelling plates (frictionless specimen), “m” stands for testing with the single run monotonous loading, and “EN” for the monotonous loading with deloadings and stabilized load sections.

Building codes usually limit the story drift of wooden buildings. Therefore in Figure 8 the criteria of 1/150 and 1/200 story height limits are marked to compare the behaviour of the tested anchorage. The story height of the tested panels is 2.44m. Thinner lines of the diagrams present the response of specimens to load protocol defined by European standard EN 594. Thicker lines show the responses of specimens to single run monotonous loading that precede the loading according to protocol EN 594 and give information about load carrying capacity of specimen. Load carrying capacity and stiffness of specimens loaded by EN 594 protocol was significantly lower in comparison to the one achieved by single run monotonous loading. Load reversals and stabilisations exposed the anchors to low cycle fatigue and caused their weakening. The currently used anchorage of RIKO houses is flexible and fails by yielding of angle iron (Figure 11a). The wooden wall has lower stiffness at the observed story drifts than other tested types of specimens. Bilinearity of the diagrams is caused by constant vertical load acting on wooden walls. Therefore, less vertically loaded walls exhibit lower load bearing capacity. Modification of BMF anchorage by washer plate increased the stiffness and strength of anchorage. Washer plate prevented deformation of angle iron and anchorage failure occurred by tensile splitting of wooden panel just above the nailed edge of the angle iron (Figure 11c). Similar behaviour was observed in the case of anchorage by Würth angle iron (Figure 11d). Higher strength capacity of modified BMF and Würth anchorage can be achieved by local strengthening of wooden panel.

The testing of panels with monotonous loading was followed by the testing with cyclic loading according to the ATC-24 protocol. To obtain information about strength degradation and stiffness deterioration, the loadings at the selected deformation levels were repeated three times. In Figure 9 hysteretic curves of four differently anchored specimens loaded with the constant vertical load of the same intensity ($V_1 = 38\text{kN}$) are compared by skeleton curves. In Figure 10 specimens with the same anchorage system (basic BMF anchors) at three different levels of constant vertical load ($V_1 = 38\text{kN}$, $V_2 = 24\text{kN}$ and $V_3 = 15\text{kN}$) are compared. Presented envelopes were calculated as average envelopes of positive and negative branch of skeleton curves obtained by testing. The highest (V_1) and the lowest (V_3) level of vertical load were obtained by structural analysis of five typical layouts of two-story RIKO houses.

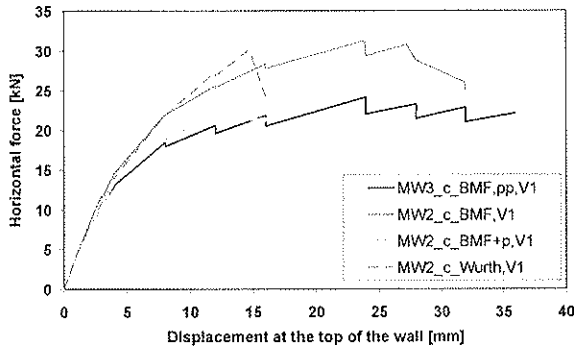


Figure 9: Comparison of hysteretic envelopes of differently anchored wooden panels loaded with constant vertical load of equal intensity (38kN).

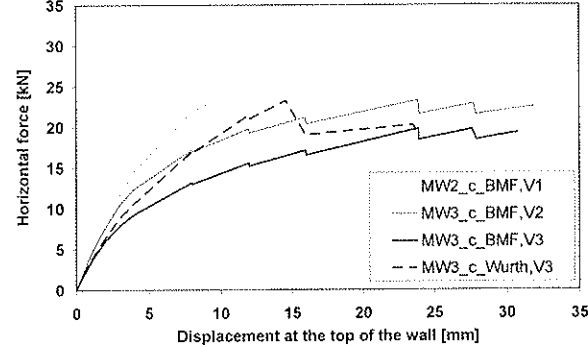


Figure 10: Comparison of hysteretic envelopes of differently anchored wooden panels loaded with constant vertical load of different intensities.

The influence of vertical load intensity is clearly seen from Figure 10, where vertical load directly influenced the load bearing capacity and stiffness of the basic anchorage BMF. The advantage of the modification by adding washer plate is lower sensitivity to the influence of vertical load intensity and thus more even response of differently loaded wall in actual building during an earthquake or strong wind action. In addition, the anchors with washer plate exhibit higher strength and stiffness in comparison to the basic BMF anchor.

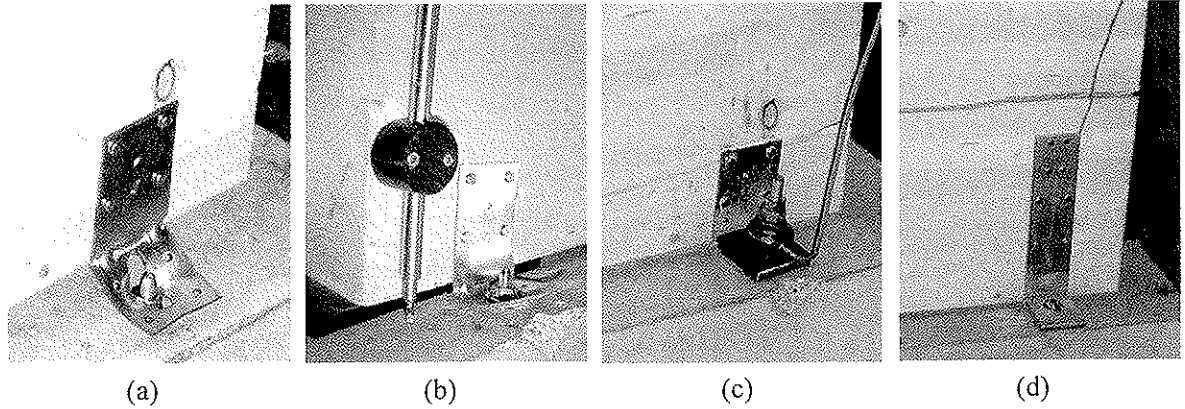


Figure 11: Anchors at attained ultimate limit state: deformed basic BMF angle iron anchoring the wooden panel without levelling plastic plates (a) and with levelling plastic plates (b), tensile splitting of wooden panel above the upper edge of the nailed part of BMF angle iron with washer plate (c) and tensile splitting of wooden panel above the upper edge of the nailed part of Würth angle iron with washer plate (d).

According to the first analysis of the tested anchorage systems, their influence on the response of the entire structure of the observed type of wooden house is of major importance. Due to assembling

technology levelling of panels with plastic plates and insulation of lower edges of panels can not be omitted. That leads to the next step of the modification of anchors with introducing tooth plates that are designed on shear to carry horizontal load. Anchors will be designed on tension-compression to carry racking load. The next step of research will be oriented towards the optimisation of anchorage system introducing tooth-plates.

4 Conclusion

Test results give insight in the possibilities of low cost improvement of wooden wall anchorage systems. By simple modification of anchorage a significant stiffness increase can be achieved, while load bearing capacity is limited by material properties of anchorage components and by local strength of wood panel. The modified anchors have beneficial influence on the response of wooden houses to strong earthquakes meeting the serviceability criteria. The failures of anchorages exposed to large deformations are repairable without involving high costs or labour efforts what makes post earthquake interventions less demanding.

The main conclusions derived from herein presented experimental research are that the racking behaviour of cantilever massive wood walls is very sensitive to the magnitude of vertical load and the type of anchorage system. The test results show that moderate additional investment in slight variation of anchorage system can significantly upgrade the racking resistance of the wall, especially at lower magnitude of the vertical load. By using unsuitable anchoring, the magnitude of vertical load has a beneficial influence on racking strength of the wall.

5 Acknowledgment

The testing program was carried out in the scope of projects funded by the Ministry of Education, Science and Sport of the Republic of Slovenia. The financial contribution of RIKO HIŠE Ltd to the applied research project named “Upgrade of Earthquake Resistance of Timber Structures”- MESS 3311-03-8225135 is gratefully acknowledged.

6 References

- [1] Dujic, B., 2001. “Experimental Supported Modelling of Response of the Timber Frame Wall Panels to Horizontal Cyclic Load”, Ph.D. thesis (in Slovenian), Faculty of Civil and Geodetic Engineering, University of Ljubljana, Slovenia.
- [2] Dujic, B., Zarnic R., 2002. “Influence of Vertical Load on Lateral Resistance of Timber-Framed Walls”, Proceedings of CIB-W18/35-15-4, Kyoto, Japan.
- [3] EN 594:1995, Timber structures - Test methods - Racking strength and stiffness of timber frame wall panels, CEN, European Committee for Standardization, Brussels.
- [4] RILEM TC 109-TSA, 1994. “Timber Structures in Seismic Regions: RILEM State-of-the-Art Report”, Materials and Structures, Vol. 27: 157-184.

INTERNATIONAL COUNCIL FOR RESEARCH AND INNOVATION
IN BUILDING AND CONSTRUCTION

WORKING COMMISSION W18 - TIMBER STRUCTURES

INFLUENCE OF FRAMING JOINTS ON PLASTIC CAPACITY OF
PARTIALLY ANCHORED WOOD-FRAMED SHEAR WALLS

B Källsner

Trätek - Swedish Institute for Wood Technology Research

U A Girhammar

Department of Applied Physics, Umeå University

SWEDEN

Presented by B Källsner

B Dujjič and Källsner discussed the concept of fully vertical shear capacity.

R Steiger commented that in the lower bound plasticity method equilibrium must be fulfilled; however, he felt that the boundary condition should also be considered. Källsner answered that in plastic method deformations were not considered as only the strength of the system was considered.

R Steiger commented that the elastic solution should consider deformation. Källsner agreed.

B J Yeh asked if it is possible that the vertical load contributed to the friction of the test setup. Källsner answered one cannot use friction forces in this case.

H Blass commented that it does not matter whether one anchored the tensile stud or put the vertical load onto the tensile stud. E Karacabeyli further commented on the difference between the fully anchored and partially held down cases with respect to the contribution of vertical load. He further explained that similar approach was developed in the Canadian code. Källsner agreed that it was done independently. H Blass commented that one of the objectives of this work is to obtain a unified approach in the European code.

Influence of framing joints on plastic capacity of partially anchored wood-framed shear walls

Bo Källsner

Träteknik - Swedish Institute for Wood Technology Research, Sweden
School of Technology and Design, Växjö University, Sweden

Ulf Arne Girhammar

Department of Applied Physics, Umeå University, Sweden

Abstract

In this paper a plastic lower bound method is used to study the influence of framing joints (stud-to-rail) on the load-carrying capacity of partially anchored wood-framed shear walls. The calculations show that by considering these, the load-carrying capacity can often be increased by 10 to 15 %.

As a consequence of the calculations an alternative method is presented in which the full vertical shear capacity of the wall is utilised, disregarding that the conditions of equilibrium are not always fulfilled. This method results in a load-carrying capacity that is equal to or slightly higher than the capacity of the more complicated lower bound method. The great advantage of the method is that the load-carrying capacity can be determined in a simple straightforward process without any additional checks of equilibrium conditions.

1 Introduction

1.1 Background

In Eurocode 5 (2003) two methods for design of shear walls are given. In the first method it is assumed that the wall is fully anchored, i. e. the studs loaded in tension are assumed to be fully anchored to the substrate with tie-downs or to be secured against uplift by vertical actions. This method is based on a simple analytical model in which the conditions of force and moment equilibrium are fulfilled. In the second method it is assumed that the bottom rail is anchored to the substrate while the studs are not. This method is mainly empirically based. At several occasions it has been pointed out that the code should incorporate a common analytically based method covering the most frequently structures used.

A method that may serve as a basis for this purpose has been presented in a sequence of three papers: Källsner et al (2001, 2002, 2004). A plastic lower bound method is used in which the studs can be handled as fully or partially anchored with respect to vertical uplift. The method covers static loads and can be applied when mechanical fasteners with plastic or partially plastic characteristics are used. In the calculations performed so far, the framing joints (stud-to-rail) have only been assumed to transfer withdrawal forces (Girhammar et al, 2004). Since the framing joints are often more effective in shear, this situation will be studied here.

1.2 Objective

The overall purpose of the research project is to develop an analytical method for design of wood-framed shear walls in the ultimate limit state that:

- can be used for design of walls with various geometric layout, sheet materials and fasteners
- handles different ways of anchoring the bottom rail and the vertical studs
- is able to consider different load configurations
- results in economical structures
- explains the structural behaviour
- opens up for possibilities to reinforce the structures
- can be transformed into code format.

The purpose of this paper is to investigate the influence of the framing joints on the load-carrying capacity of partially anchored wood-framed shear walls and to give some design recommendations.

2 Plastic lower bound method

2.1 Basic assumptions

For design of partially anchored shear walls a plastic lower bound method (Neal, 1979) is proposed. This means that a force distribution is chosen that fulfils the conditions of force and moment equilibrium for each timber member and sheet. The basic assumptions in Section 2.2 will be identical to those given in Källsner et al (2001, 2002, 2004) and are as follows:

- the sheathing-to-timber joints, referring to the vertical studs and to the top rail, are assumed to transfer shear forces only parallel to the timber members
- the sheathing-to-timber joints, referring to the bottom rail, are assumed to transfer forces both parallel and perpendicular to the bottom rail
- the framing joints are not assumed to transfer any tensile or shear forces
- compressive forces can be transferred via contact between adjacent sheets and in the framing joints.

In Section 2.3 the third assumption above will be replaced by the assumption:

- the framing joints can transfer tensile or shear forces

In order to obtain simple expressions for the racking resistance of the shear walls, the fasteners are assumed to be continuously distributed along the timber members. The load-carrying capacity of the sheathing-to-timber joints is consequently given in force per unit length. In all the examples presented below, it is assumed that the fastener spacing around the perimeter of the sheets is constant.

2.2 Partially anchored shear wall

By a partially anchored wall is meant a wall where the vertical stud on the tension side is not completely anchored to the substrate against uplift.

In order to clarify the structural behaviour of shear walls, the wall configuration according to Figure 1 will first be studied. The wall is subjected to $n+1$ external vertical loads V_0 to V_n and a racking load H . The spacing of the studs is s and the length of the wall is l . This

means that $l=ns$. The width and height of the full format sheets are denoted by b and h , respectively. The bottom rail is assumed to be fully anchored to the substrate. The studs are assumed to have no tie-downs i.e. they are completely free from the bottom rail with respect to tension and shear forces. The forces acting on the wall in the ultimate limit state are assumed to be distributed according to Figure 1. The forces acting along the lower part of the wall are shown in a section immediately above the bottom rail and represent the forces in the sheathing-to-timber joints. These forces are assumed to act either perpendicular or parallel to the bottom rail. The plastic capacity per unit length of these joints is denoted by f_p and it is assumed that plasticity has been attained along the entire bottom rail. The μ factor opens for the possibility of using reduced strength properties when the fastener forces act perpendicular to the edges of the sheets and the frame members. The notation l_{eff} is used to indicate that this part of the total length of the wall is fully effective for horizontal load transfer. The rest of the wall length, $l-l_{eff}$, must be used for anchoring the wall to the substrate.

Further, it is assumed that the plastic shear flow has not been attained along any of the vertical studs. Since the stud furthest to the right is subjected to the highest shear force, this condition can be formulated as

$$\sum_{i=0}^{n-1} V_i + \mu f_p (l - l_{eff}) \leq f_p h \quad (1)$$

Moment equilibrium around the lower right corner of the wall diaphragm gives

$$Hh - \sum_{i=0}^{n-1} V_i (l - l_i) - \mu f_p (l - l_{eff}) \left(\frac{l + l_{eff}}{2} \right) = 0 \quad (2)$$

Force equilibrium in the horizontal direction gives

$$H = f_p l_{eff} \quad (3)$$

We now introduce the non-dimensional parameters

$$\alpha = \frac{l}{h} \quad (4)$$

$$\beta = \frac{\sum_{i=0}^{n-1} \left(\frac{n-i}{n} V_i \right)}{f_p h} \quad (5)$$

The nominator of β is simply equal to the reaction force of the vertical forces V_0 to V_n considering the shear wall as a simply supported beam on the two end studs i.e. corresponding to an equivalent vertical load on the leading stud. The denominator of β is equal to the maximum load that can be transferred between a vertical stud and a sheet, i.e. corresponding to the full plastic capacity. The parameter β must always be less than unity. Using equations (2) - (5) the effective wall length can be calculated as

$$l_{eff} = l \left(\sqrt{1 + \left(\frac{1}{\alpha \mu} \right)^2} + \frac{2\beta}{\alpha \mu} - \frac{1}{\alpha \mu} \right) \quad (6)$$

Vertical force equilibrium gives the reaction force R_n acting on stud n as

$$R_n = \sum_{i=0}^n V_i + \mu f_p (l - l_{eff}) \quad (7)$$

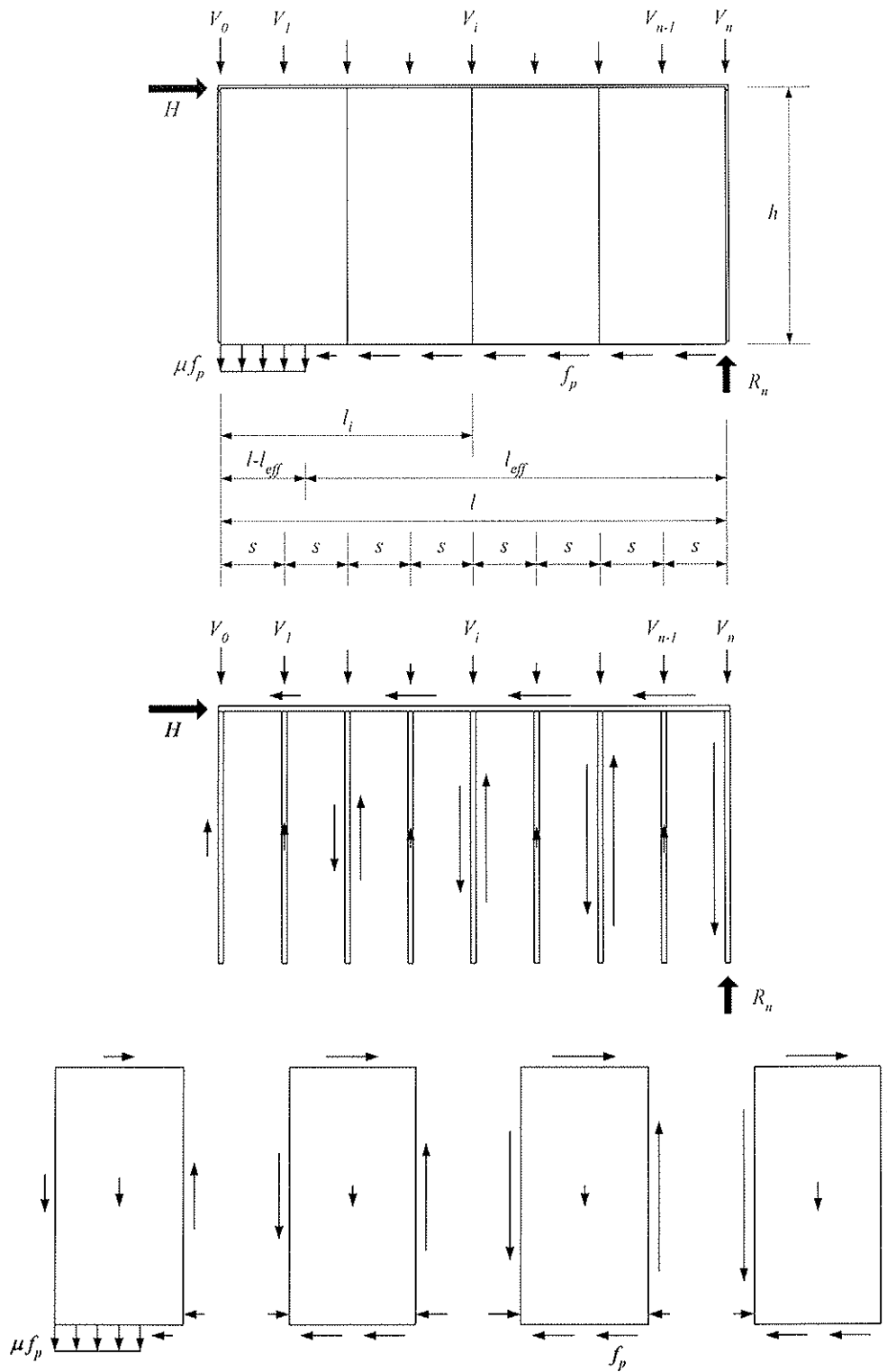


Figure 1. Forces acting on a shear wall with fully anchored bottom rail and no tie-downs. The plastic capacity has not been attained in the sheathing-to-timber joints along any of the vertical studs.

By studying the force and moment equilibrium of the individual sheets in Figure 1, it is obvious that the proposed model will only work if compressive forces are transferred between the adjacent sheets. If contact forces between adjacent sheets are not accepted the

model must be applied on each individual sheet. This will result in a somewhat lower load-carrying capacity for the wall (Källsner et al, 2001).

So far the calculations have been based on condition (1) saying that the plastic shear flow f_p has not been attained along any of the vertical studs. Now we will study the case when this condition is not fulfilled. Consider the wall in Figure 2. We assume that the plastic shear flow f_p has been attained in a vertical section immediately to the right of stud number n , while it has not been attained in a section immediately to the left of the same stud. In this case the wall can be handled as two separate walls as shown in the lower part of Figure 2. We observe that for the left part of the wall, condition (1) is fulfilled. This means that equations (2)-(6) can be applied on the left part of the wall, observing that l now denotes the length of this part. For the right part of the wall the plastic shear flow f_p has been attained along the edges of all sheets. This means that these sheets cannot transfer any more forces and that the external vertical forces V_{n+1} to V_N are transferred via the vertical studs directly to the bottom rail.

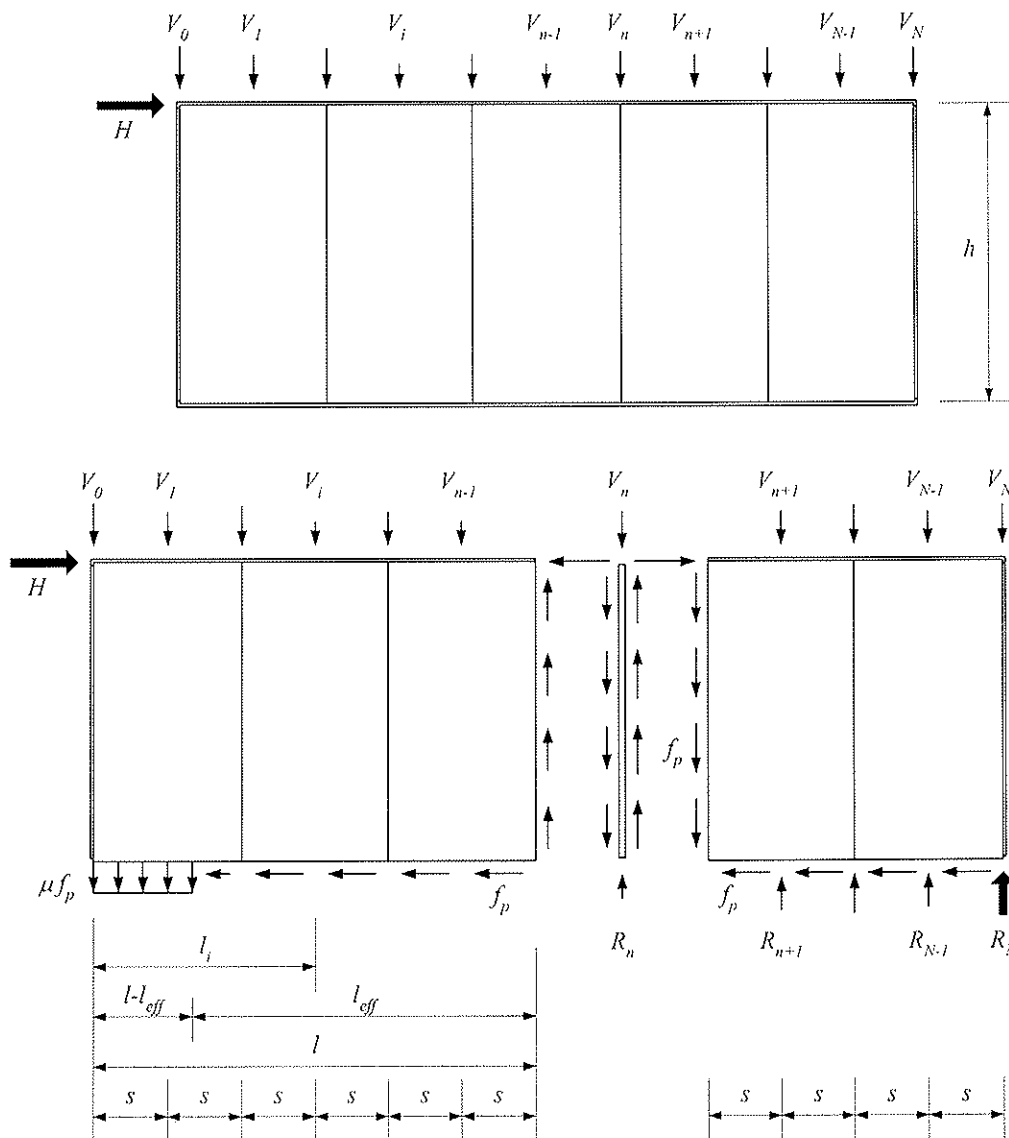


Figure 2. Forces acting on a shear wall with fully anchored bottom rail and no tie-downs. The plastic capacity has been attained in the sheathing-to-timber joints on the right side of vertical stud n .

Since the length of the left part of the wall is $l=ns$ and the length of the right part of the wall is equal to $(N-n)s$ the total effective length L_{eff} becomes

$$L_{eff} = ns \left(\sqrt{1 + \left(\frac{1}{\alpha\mu} \right)^2} + \frac{2\beta}{\alpha\mu} - \frac{1}{\alpha\mu} \right) + (N-n)s \quad (8)$$

Vertical force equilibrium gives the reaction force R_n acting on stud n as

$$R_n = \sum_{i=0}^n V_i + \mu f_p (l - l_{eff}) - f_p h \quad (9)$$

and the reaction force R_N acting on stud N as

$$R_N = V_N + f_p h \quad (10)$$

2.3 Influence of framing joints

2.3.1 Vertical withdrawal in framing joints

A very simple way to consider the influence of the framing joints on the load-carrying capacity of shear walls is to assume that the framing joints can only transfer withdrawal forces between the studs and the bottom rail. The withdrawal forces can then be handled as external vertical loads acting on top of the studs and the load-carrying capacity can be calculated according to the principles given in Section 2.2.

2.3.2 Transfer of horizontal shear forces in framing joints

An alternative way of taking into account the effect of the framing joints is to assume that the framing joints between the studs and the bottom rail can only transfer horizontal shear forces. A question of great importance is: How many of these framing joints that can be used for transfer of shear forces while still fulfilling the equilibrium conditions of all timber members and sheets? Considering the wall configuration shown in Figure 2 it seems reasonable to make a difference between the left and the right part of the wall. In the right part of the wall the sheathing-to-timber joints along the perimeter of the sheets are fully utilised in shear. This means that these joints cannot be used for transfer of horizontal force components to the vertical studs. However, the sheathing-to-timber joints in the centre of these sheets can be used for this purpose. In Figure 3 a possible force distribution is shown where the force is transferred via contact between adjacent sheets. As a good approximation, the influence of the force eccentricity in the stud and the influence of the deviation of the contact force from the lower edge of the sheathing can be neglected.

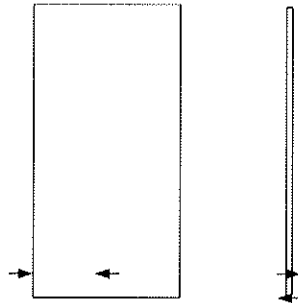


Figure 3. Transferred forces from a framing joint to a vertical stud and a sheet.

For the left part of the wall in Figure 2 it seems reasonable to use all studs except the one furthest to the right for shear transfer.

In order to investigate the influence of the framing joints on the capacity of a shear wall, three load cases must be considered. In these cases we will assume that the total transferred shear force of the framing joints is uniformly distributed along the studied length l of the wall. The plastic capacity of this shear flow will be denoted by $f_{fr,p}$. When the shear flow is lower than the plastic value it will be denoted by f_{fr} . Since l is often only a part of the total length L of the wall, $f_{fr,p}$ will increase when l decreases.

2.3.3 Horizontal shear in framing joints – Case 1

The forces acting on a wall in the ultimate limit state are assumed to be distributed as in Figure 4. The plastic shear flow of the framing joints $f_{fr,p}$ is assumed to act along the bottom rail. As in Section 2.2 it is assumed that the plastic shear flow f_p has not been attained along any of the vertical studs, i. e. condition (1) is fulfilled. It is further assumed that

$$f_{fr,p} l < H \quad (11)$$

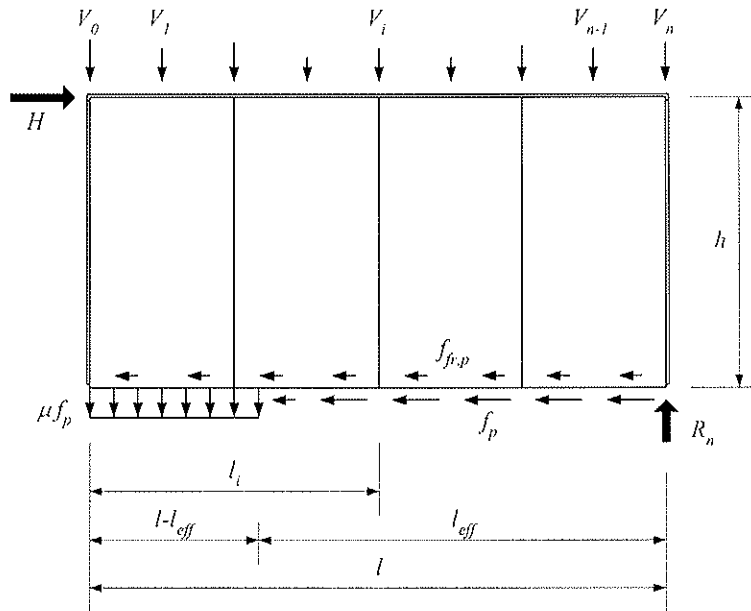


Figure 4. Assumed force distribution in load case 1.

A moment equation around the lower right corner of the wall will result in equation (2). Force equilibrium in the horizontal direction gives

$$H = f_p l_{eff} + f_{fr,p} l \quad (12)$$

Insertion of equation (12) into equation (2) using notation (4) and (5) yields

$$l_{eff} = l \left(\sqrt{1 + \left(\frac{1}{\alpha\mu} \right)^2 + \frac{2\beta}{\alpha\mu} - \frac{2}{\alpha\mu} \frac{f_{fr,p}}{f_p} - \frac{1}{\alpha\mu}} \right) \quad (13)$$

From equation (12) the capacity of the wall can be expressed as

$$\frac{H}{f_p l} = \frac{l_{eff}}{l} + \frac{f_{fr,p}}{f_p} \quad (14)$$

If the ratio $f_{fr,p}/f_p$ is high it is not possible to find any solution of equation (13) that fulfils the conditions given. Consequently, we must assume that the shear flow of the framing joints is lower than the plastic value. This will be done in load cases 2 and 3.

2.3.4 Horizontal shear in framing joints– Case 2

For small wall lengths we may have the situation where the whole length of the sheathing-to-timber joints along the bottom rail is used for the stabilising moment of the vertical forces. This load case is shown in Figure 5 where the plastic shear flow of the framing joints $f_{fr,p}$ is too high in order to fulfil the moment equilibrium and must be replaced by f_{fr} .

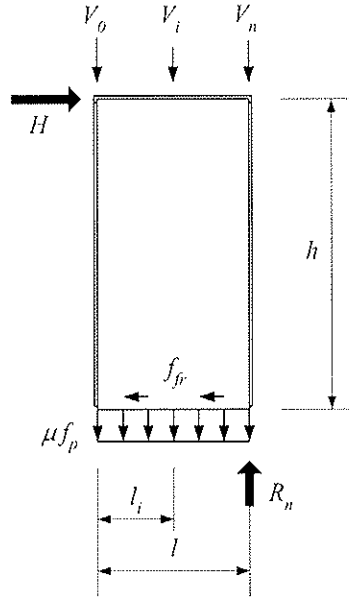


Figure 5. Assumed force distribution in load case 2.

A moment equation around the lower right corner of the wall gives

$$Hh - \sum_{i=0}^{n-1} V_i(l - l_i) - \mu f_p l \frac{l}{2} = 0 \quad (15)$$

and capacity H is obtained as

$$H = \left(\frac{1}{2} \mu \alpha + \beta \right) f_p l \quad (16)$$

A horizontal equilibrium equation gives

$$f_{fr} = \left(\frac{1}{2} \mu \alpha + \beta \right) f_p \quad (17)$$

2.3.5 Horizontal shear in framing joints – Case 3

In Section 2.3.4 it was assumed that the sheathing-to-timber joints were subjected to vertical tension forces along the whole bottom rail. We will now study the case when the sheathing-to-timber joints are only subjected to vertical loads from stud No. 0 to

somewhere between stud No. $n-1$ and stud No. n according to Figure 6. As in Section 2.3.4 it is assumed that the plastic shear flow of the framing joints can not be fully utilised, i. e. we have the shear flow f_{fr} .

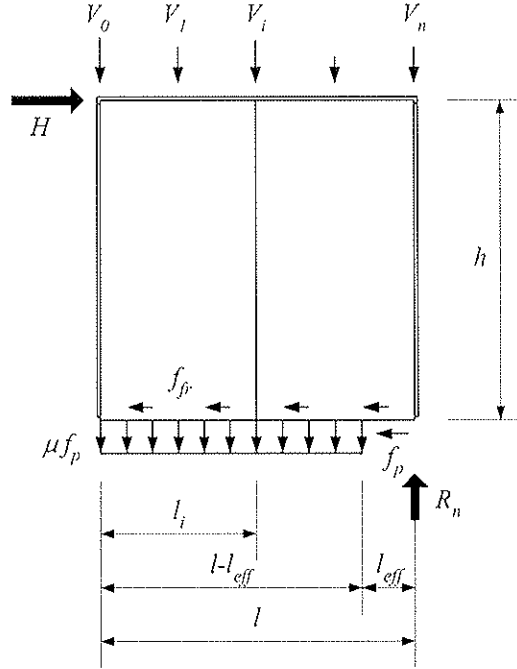


Figure 6. Assumed force distribution in load case 3.

By choosing the length of the tension zone $l-l_{eff}$ so that the full vertical shear capacity of the wall segment is attained immediately to the left of stud No. n we obtain

$$\sum_{i=0}^{n-1} V_i + \mu f_p (l - l_{eff}) = f_p h \quad (18)$$

A moment equation around the lower right corner of the wall will result in equation (2). We now introduce the non-dimensional parameter

$$\kappa = \frac{\sum_{i=0}^{n-1} V_i}{f_p h} \quad (19)$$

and the parameters given by (4) and (5). From equation (18) it is obvious that $\kappa \leq 1$. By inserting l_{eff} from equation (18) into equation (2) we obtain the capacity H of the wall as

$$H = \left(1 + \beta - \kappa - \frac{1}{2\alpha\mu} (1 - \kappa)^2 \right) f_p l \quad (20)$$

A horizontal equilibrium equation gives

$$f_{fr} = \left(\beta - \kappa + \frac{1}{2\alpha\mu} (1 - \kappa^2) \right) f_p \quad (21)$$

2.3.6 Combined withdrawal and shear

It is possible to optimise the capacity of a wall segment with respect to the use of the framing joints as withdrawal or shear elements. Since the increase in capacity is usually fairly small this theory will not be shown here.

3 Model utilising full vertical shear capacity of wall

The method described in Section 2 was based on the assumption that all parts in the wall had to be in equilibrium. In connection with the evaluation of the test results in Section 4 it became obvious that in many cases it is possible to use a very simple procedure for design of shear walls. The drawback of this method is that the conditions of equilibrium are not always fulfilled. However, the deviation in load-carrying capacity obtained with the method is often very small compared to the method in Section 2.

The new method is based on the principle that the vertical shear capacity $f_p h$ of the wall shall be utilised at maximum. This situation has in fact already been studied in Sections 2.3.4 and 2.3.5 but there we always had to fulfil the condition $f_{fr} \leq f_{fr,p}$. In the new method we will disregard this condition, i. e. not consider that the horizontal shear flow from the framing joints along the bottom rail is sometimes too low to fulfil horizontal equilibrium of the wall.

For small wall lengths where the full vertical shear capacity of the wall $f_p h$ is not attained in any section, the horizontal capacity H is given by equation (16).

For large wall lengths where the vertical shear capacity $f_p h$ is attained in a section somewhere between the two end studs according to Figure 7, capacity H can be determined using equation (20) adding the full plastic capacity of the wall to the right of stud n .

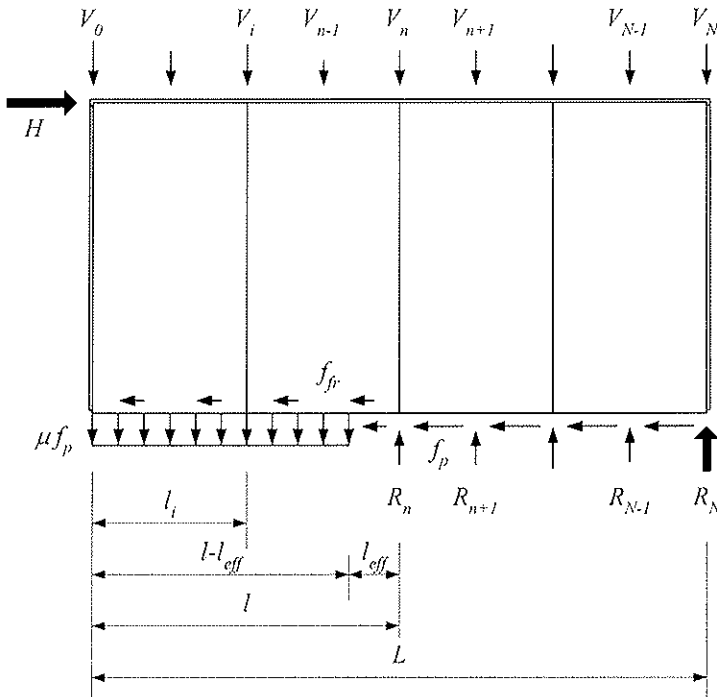


Figure 7. Assumed force distribution in a wall of large length.

An alternative way is to calculate the capacity considering the moment equilibrium of the whole wall around the lower right corner. In this case the vertical forces V_n to V_N shall not be considered, since they are directly transferred via the vertical studs to the substrate. Thus if we use the notations

$$\alpha_L = \frac{L}{h} \quad (22)$$

$$\beta_L = \frac{\sum_{i=0}^{n-1} \left(\frac{N-i}{N} V_i \right)}{f_p h} \quad (23)$$

the capacity H of the total wall may expressed as

$$H = \left(1 + \beta_L - \kappa - \frac{1}{2\alpha_L \mu} (1 - \kappa)^2 \right) f_p L \quad (24)$$

4 Comparison with test results

Results from testing of partially anchored shear walls made of hardboard are reported in Girhammar et al (2004). For each type of wall, the number of tests was 3 or 4. Using test results of fully anchored shear walls, the plastic capacity of the sheathing-to-timber joints was determined to $f_p = 12,5$ kN/m. The withdrawal and shear capacities of single framing joints were determined by testing to 1 kN and 2 kN, respectively. The size of the sheets was 1200x2400 mm and the dimension of the timber members was 45x120 mm. The distances between the fasteners were 100 mm along the perimeter of the sheets and 200 mm along the vertical centre lines of the sheets.

Measured and calculated load-carrying capacities are shown in Figures 7-9 for some different wall and load configurations. The calculated curves are based on four different assumptions: Full vertical shear (Section 3), shear in framing joints (Sections 2.3.2-2.3.5), withdrawal in framing joints (Section 2.3.1) and no framing joints (2.2).

The theoretical curves show that the load-carrying capacity is increased when the influence of the framing joints is considered. Since the framing joints have higher shear strength than withdrawal strength it is not unexpected that it is more favourable to use them for shear transfer.

The theory, based on using the full vertical shear capacity of the wall, results in curves that are close to the ones obtained considering the shear transfer in the framing joints.

The test results shown here seem to be in best agreement with the theory based on full vertical shear.

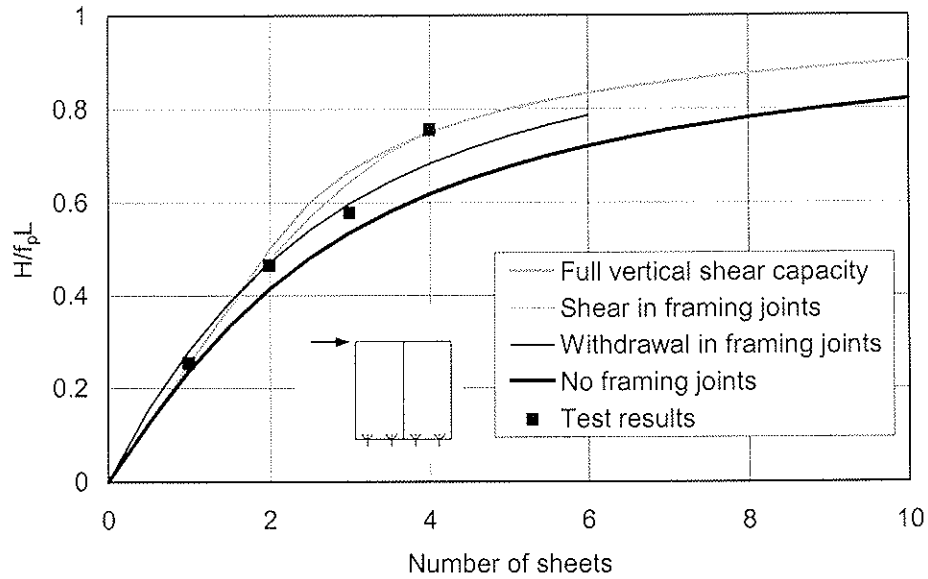


Figure 7. Measured and calculated relative load-carrying capacities of shear walls as function of the number of sheets.

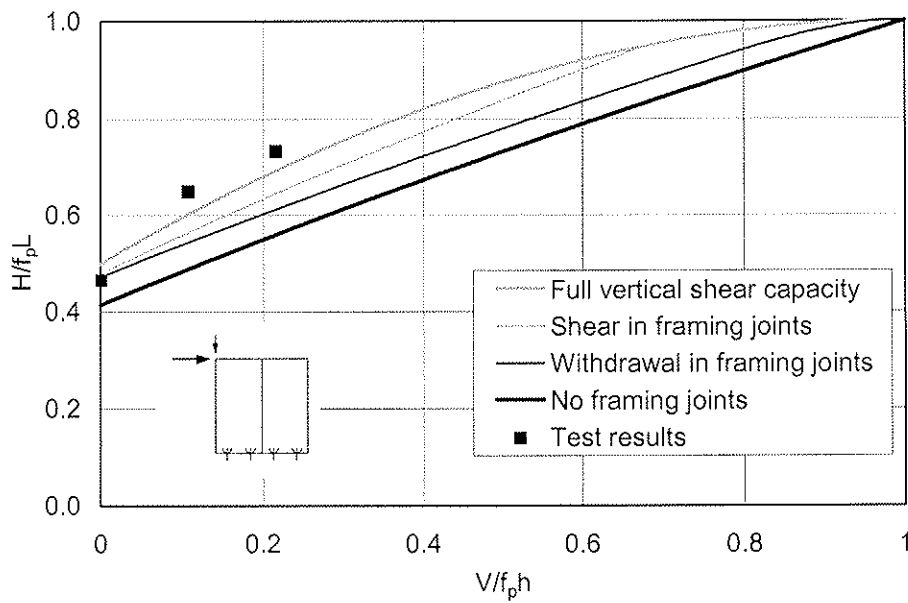


Figure 8. Measured and calculated relative load-carrying capacities of shear walls as function of the applied relative vertical load.

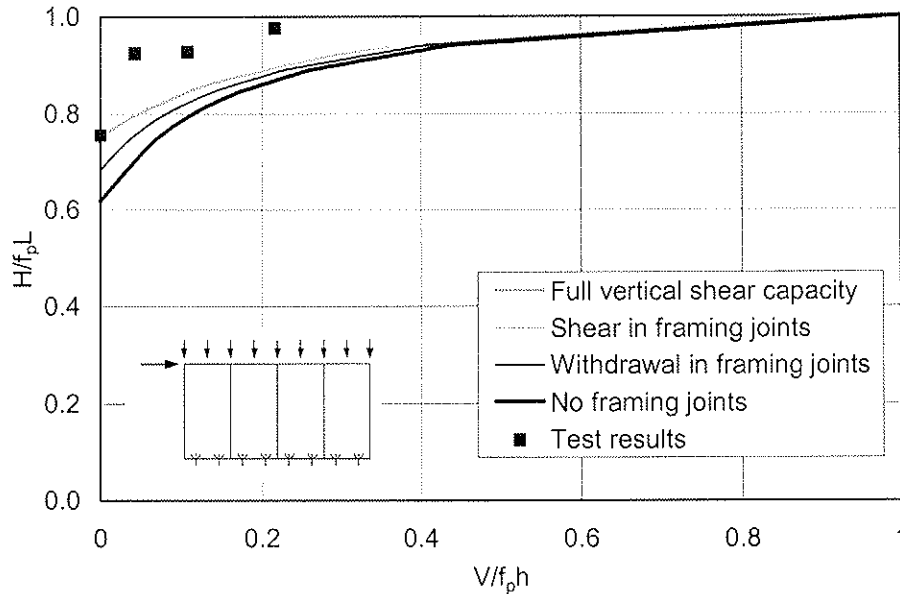


Figure 9. Measured and calculated relative load-carrying capacities of shear walls as function of the applied relative vertical load.

5 Conclusions

A plastic lower bound method is used to study the influence of the framing joints (stud-to-rail) on the load-carrying capacity of partially anchored wood-framed shear walls.

The calculations show that by considering the framing joints, the load-carrying capacity of a shear wall can often be increased by 10 to 15 %.

A very simple design method is demonstrated in which the full vertical shear capacity of the wall is utilised, disregarding that the conditions of equilibrium are not always fulfilled. This method results in a load-carrying capacity that is equal to or slightly higher than the capacity of the more complicated lower bound method. In order to use the method in practice, some requirements should be added concerning the shear strength of the framing joints in relation to the strength of the sheathing-to-timber joints.

References

- prEN 1995-1-1, Eurocode 5 – Design of timber structures – Part 1-1: General – Common rules and rules for buildings, December 2003.
- Girhammar U.A., Källsner B.: Tests on partially anchored wood-framed shear walls. *Proceedings 8th World Conference on Timber Engineering*, Lahti, Finland, June 14-17, 2004.
- Källsner B., Girhammar U.A., Wu L., A Simplified Plastic Model for Design of Partially Anchored Wood-Framed Shear Walls, *Proceedings CIB-W18 Meeting*, Venice, Italy, 2001.
- Källsner B., Girhammar U.A., Wu L., A Plastic Design Model for Partially Anchored Wood-Framed Shear Walls with Openings, *Proceedings CIB-W18 Meeting*, Kyoto, Japan, 2002.
- Källsner B., Girhammar U. A.: A plastic lower bound method for design of wood-framed shear walls. *Proceedings 8th World Conference on Timber Engineering*, Lahti, Finland, June 14-17, 2004.
- Neal B.G., *Plastic Methods of Structural Analysis*, 2nd edition, London, 1978.

INTERNATIONAL COUNCIL FOR RESEARCH AND INNOVATION
IN BUILDING AND CONSTRUCTION

WORKING COMMISSION W18 - TIMBER STRUCTURES

BRACING OF TIMBER MEMBERS IN COMPRESSION

J Munch-Andersen

Danish Building and Urban Research

DENMARK

Presented by J Munch-Andersen

P Quenneville asked whether the bracing members acting only in compression. Andersen answered no as both tension and compression forces can be considered in the bracing members.

Bracing of timber members in compression

Jørgen Munch-Andersen

Danish Building and Urban Research, Denmark

Introduction

Timber members or systems of members in compression often require lateral support at intermediate nodes to prevent stability failure of the beams. The requirements to strength and stiffness of a system that can provide this support are studied. The study was initiated in connection with the preparation of a practical guideline for bracing of trusses in roof structures in accordance with the requirements in the first version from 1998 of a new generation of the Danish Code of Practice for the structural use of timber [1]. This code has rules very similar to those in Eurocode 5 [3]. It appeared that no simple amendments to the traditional way of bracing small and medium-size roof structures for wind load would meet these requirements. However, there is no evidence that increased bracing would be necessary to avoid stability failure during snow load for normal span trusses. For long span trusses (about 20 m) made from 45 mm planks, problems have been seen that justify that sufficient bracing must be ensured.

The basis for the rules in Eurocode 5 were reviewed in order to find arguments for reducing the requirements to a level more in line with experience from practice. It appeared that the rules were not at all conservative for a single member in compression, but for a series of members - like in roof structures - there are system effects that would warrant a significant reduction. A revised version of the Danish code from 2003 [2] includes some of the findings in this paper regarding system effects.

Failure modes

When a timber member with length l is braced laterally at intermediate nodes spaced a apart, the number of sections become $m = l/a$. Such a member in compression can have several failure modes, see Figure 1. The failure can occur between two nodes as in Figure 1a with half wavelength a . It can also take place with longer half wavelengths as in Figure 1b, where the half wavelength is $2a$. A third possibility is failure over the entire length with half wavelength l . The compression force is called N .

In order to prevent the failure mode in Figure 1a, the distance a must be chosen to be so small that the member stiffness and strength is sufficient to ensure that failure will not occur between two nodes. The other failure modes in Figure 1 should be prevented by the bracing system.

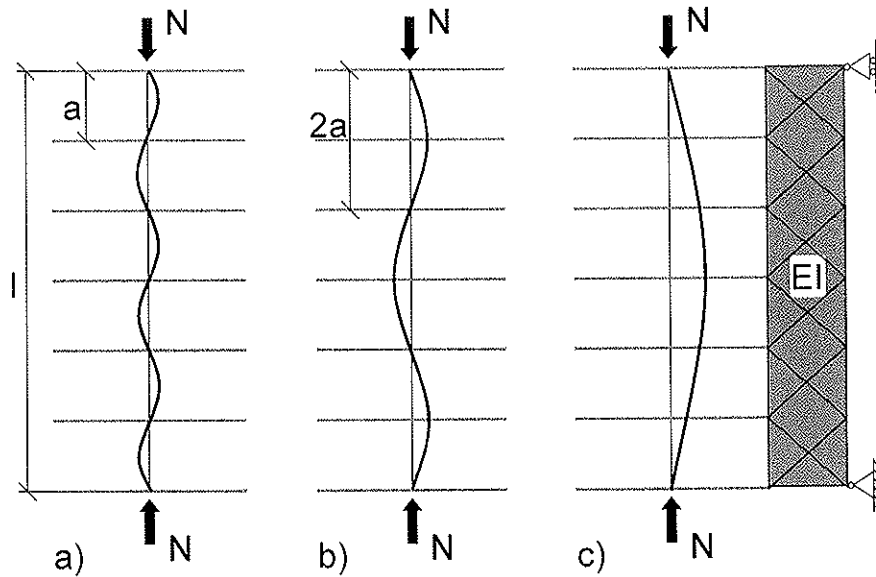


Figure 1. Timber members with compression force N and lateral bracing spaced a apart. The figure shows deflections for failure modes with half wavelengths a , $2a$ and l . Failure with half wavelength larger than a is assumed to be prevented by lateral bracing being connected to a bracing system with the bending stiffness EI .

Requirement to bracing distance a

When checking for the failure mode with half wavelength a , each section between the lateral bracings is traditionally considered as a simply supported column with length a and an initial deflection e_a equal to the maximum value permitted in the grading rules. In the grading rules for columns of structural timber is prescribed that $e_a = a/300$. For a column with several sections, this is only a correct assumption if the permitted initial deflection appears in all sections and with interchanging direction. In this case the forces in the lateral bracing become zero. Because the initial deflections will be more randomly distributed in practise, there will be a certain restraint at the nodes so that the assumption is conservative. The forces in the lateral bracing will then no longer be zero.

Requirement to lateral bracing members

Prevention of the failure mode with half wavelength $2a$ primarily requires that each lateral bracing, including the connection to the timber member and the bracing system, is sufficiently stiff and strong. The requirement will - again a somewhat conservative estimate - be derived for a column spanning two sections, which at the midpoint has the maximum permitted initial deflection e_{2a} for a member with the length $2a$, see Figure 2. The force F , which should be taken up by the bracing member, depends among other things on the stiffness of the bracing, C .

Failure modes with half wavelengths larger than $2a$ will cause smaller requirements to the bracing when it is assumed that the initial deflection is proportional to the half wavelength.

The compression force N causes a moment at the middle of the column equal to $N(e_{2a} + u)$, where u is the elastic deflection. This moment is balanced by the moment from the force in the lateral bracing, which is $\frac{1}{4} F 2a$. (The bending stiffness of the member itself is ignored because its contribution is small when bracing distance a is chosen so that the column can only just withstand N over the length a).

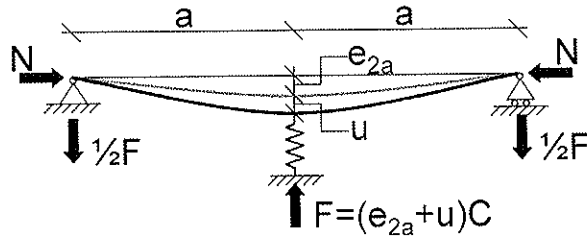


Figure 2. Timber member in compression spanning two sections, each with length a . The member is supported at midpoint by a lateral bracing with stiffness C . The initial deflection at midpoint is e_{2a} , the final elastic deflection is u and F is the force in the bracing when the compression force is N .

According to Hook's law this yields $u = F/C$. This means that equilibrium is obtained if $N(e_{2a} + F/C) = \frac{1}{4} F 2a$, which can be rewritten as

$$F = \frac{e_{2a}}{\frac{a}{2N} - \frac{1}{C}} \quad (1)$$

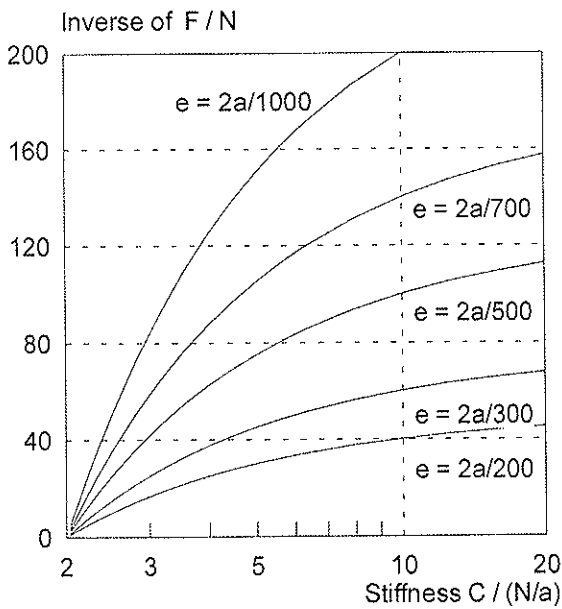


Figure 3. The relation between the stiffness C of the lateral bracing and the force F in the bracing for different values of the initial deflections e .

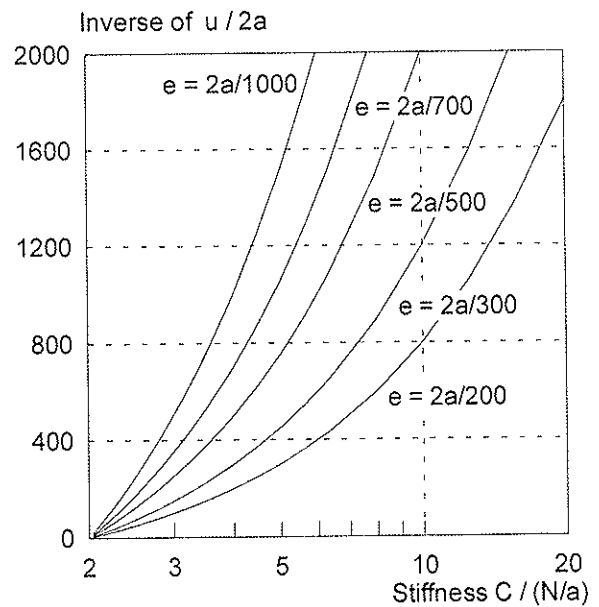


Figure 4. The relation between the stiffness C of the lateral bracing and the deflection u of the bracing for different values of the initial deflections e .

If the stiffness C is large compared with N/a , the second term in the denominator can be ignored. If the initial deflection $e_{2a} = 2a/300$, representing the largest permitted value for structural timber, is inserted into Eq. (1), it is found that $F = N/75$. For laminated timber with $e_{2a} = 2a/500$, the force will be $F = N/125$. If C is not large and for example takes the value $C = 6N/a$, the force increases to $N/50$ for $e_{2a} = 2a/300$. This can also be seen from Figure 3, which shows how the strength requirement increases when the stiffness is reduced. From Figure 4 it can be seen that the elastic deflection for $C = 6N/a$ and $e_{2a} = 2a/300$ becomes $u = 2a/600$.

Requirement to bracing system

Preventing the failure mode with half wavelength l requires sufficient stiffness and strength of the bracing system to which the bracing members are connected, see Figure 1c. The force in each lateral bracing will always be smaller than the force F derived above. The requirements to the bracing system are determined by assuming that the lateral bracing functions as a continuous connection between the timber member and the bracing system. This will be a good approximation when there are many lateral bracings.

It is further assumed that the initial deflection of the member is sine-shaped with the maximum value e_l , which means that when the compression force N is applied, the deflection curve and the moment curve will also be sine-shaped. When the deflection is restrained by the bracing system via the continuous connection, this system will be subjected to a sine-shaped line-load. And a beam with constant stiffness EI subjected to a sine-shaped load will have a sine-shaped deflection curve and moment curve. The maximum values are

$$M_l = \frac{q_l l^2}{\pi^2} \quad \text{and} \quad u_l = \frac{q_l l^4}{\pi^4 EI} \quad (2) \ \& \ (3)$$

Equilibrium requires that $N(e_l + u_l) = M_l$ at the midpoint, which by means of Eq. (2) can be rewritten as

$$q_l = \frac{\pi^2 N(e_l + u_l)}{l^2} \quad (4)$$

If it is assumed that the bracing system is so stiff that u_l is small compared with e_l and $e_l = l/300$, it is found from Eq. (4) that the maximum value of the line-load becomes $q_l \approx N/30l$, which ought to be the minimum value for structural timber. For laminated timber with $e_l = l/500$ the minimum value should be $q_l \approx N/50l$. If the bracing system deforms, the load increases quite significant. If $u_l = l/700$ is assumed, the load for structural timber increases by 43% and for laminated timber by 71%.

If the expression for u_l in Eq. (3) is inserted in Eq. (4), the line-load can be expressed as a function of the stiffness EI of the bracing system. This equation is a parallel to Eq. (1) for the individual bracing member.

$$q_l = \frac{e_l}{\frac{l^2}{\pi^2 N} - \frac{l^4}{\pi^4 EI}} \quad (5)$$

Code requirements

Eurocode 5 [3] has taken the bracing requirements into account. The formulas quoted here refer the recommended and most conservative modification factors in the range within the National Annexes can choose. The Danish code [2] generally applies the least conservative values from the range given in the Eurocode.

Lateral bracing members

The stiffness of the lateral bracing is required to be at least $C = 4N/a$, and the force is taken as $F = N/50$ for structural timber and as $F = N/80$ for laminated timber. From Figure 3 it

can be seen that these forces with the permissible initial deflections correspond to a stiffness of about $C = 6N/a$. With the stiffness required in Eurocode 5, the forces should be about 30% higher.

The stiffness requirement is often expressed as

$$C = 2 \left(1 + \cos \left(\frac{\pi}{m} \right) \right) \frac{N}{a} \quad (6)$$

This expression is derived for elastic supports at the intermediate nodes of a column with m sections, but ignoring the initial deflection at the nodes. When m is not so small, the requirements in Eurocode 5 conform to Eq. (6). This underestimation of C also explains the underestimation of the bracing force F .

Bracing system

Eurocode 5 [3] requires that the bracing system for a single member in compression should be designed for a uniform line-load $q_d = N/30l$ and that the deflection for this load and all other loads acting on the bracing system should be less than $l/500$. The requirements are similar for structural and laminated timber. In the Danish code this requirement is supplemented by the requirement that q_d alone should not cause deflections larger than $l/700$.

The code uses a uniformly distributed load and not a sine-shaped load. In order to compare the code requirements with the equations derived above, it can be shown that if the uniform load is 80% of the maximum load of the sine-shaped load, then the moment and deflection at the midpoint will be almost equal. The code requirement therefore equals $q_l \approx N/24l$. Figure 5 illustrates the relations from Eq. (4) corrected to uniform load. It is seen that if the initial deflection is $l/300$, the load $q_d = N/30l$ corresponds to a deflection u_l less than $l/1000$. If the deflection is allowed to be $l/700$ and $l/500$ respectively, the load increases to $q_d \approx N/27l$ and $q_d \approx N/24l$. For laminated timber with initial deflection $e = l/500$ and permitted deflection $u = l/500$, the load becomes $q_d \approx N/32l$.

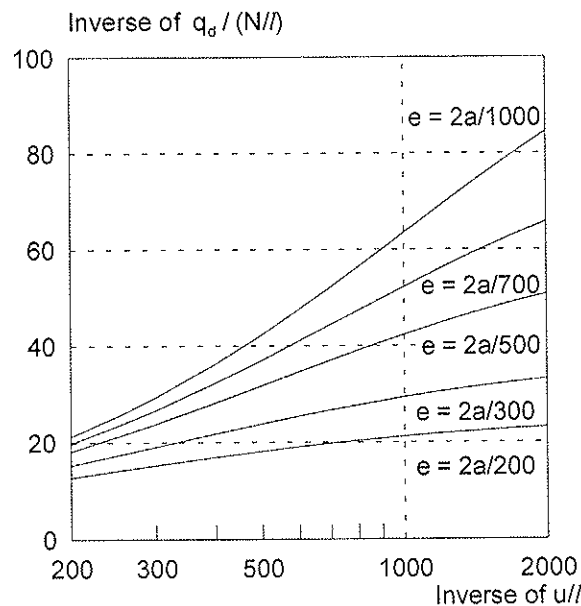


Figure 5. The relation between the deflection u of the bracing system and the uniform load q_d on the bracing system for different values of the initial deflections e .

Bracing of parallel systems of columns

In this section a system of n parallel members in compression is considered, which are connected to a common bracing system via lateral bracing spanning over all n columns. A typical example is the heads of trusses in a roof structure, as shown in Figure 6.

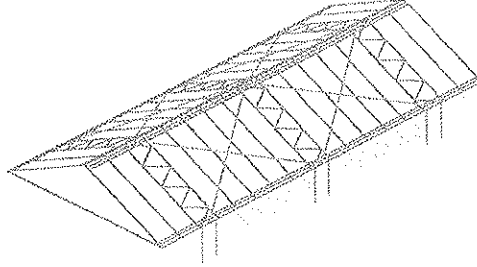


Figure 6. A wide building where the heads of the trusses are braced laterally against stability failure in the roof plane during snow load by the (not shown) battens. The bracing system to which the battens are connected consists of a number of trussed beams between pairs of trusses. For the failure mode with half wavelength l , stringers near ridge and foot of the trusses ensure that reactions at the end of each head can be taken to the ends of the trussed beams, where they will be equalised by the oppositely directed forces in the battens. For other failure modes the resulting force in each batten will be equalised via the trussed beams by oppositely directed forces in other battens.

Common lateral bracing

The connection in each node between timber members and lateral bracing must be able to transfer the force F as determined above by Eq. (1). However, the force in common lateral bracing does not accumulate proportionally with the number of parallel columns, n , because (i) the initial deflection of the n members connected to one bracing will not all have the maximum permitted size and (ii) their direction is randomly distributed so that the bracing forces will eliminate each other. It is therefore assumed that it is sufficient to design a common lateral bracing and its connection to the bracing system for $2F$ or $3F$. This means that ordinary nail connections can still be used for normal roof constructions.

Common bracing system

The line-load on the bracing system from n parallel members will not be proportional with n . It is not unlikely that all the initial deflections over the whole length l has the same direction, but it is not likely that they all have the maximum permitted value. A reasonable design value for the load on a common bracing system might be $2\sqrt{n}q$ instead of nq , where q is the line-load for one column as determined above by Eq. (5). For a roof with 16 trusses this means that the line-load that the bracing system should be designed for is halved.

Systems effect

A common lateral bracing ensures that all columns in a system will obtain the same deflection figure (except deflections between nodes). This means that the effective 5%-fractile of the stiffness modulus of the timber members for failure modes with half wavelength equal to $2a$ or larger will approach the mean value when n is large. This means that there is a significant unused stiffness for local actions.

This can be taken advantage of when using simple bracing systems for smaller roof structures, see Figure 7. This system depends on the truss heads' ability to transfer load over short distances from the battens to the cross bracing. A pragmatic rule included in the revised Danish code [2] is the rule that up to half of the stiffness and strength of the columns can be used to transfer loads locally. This half can be used for $n \geq 16$ and the fraction $n/32$ for smaller n .

This systems effect will also reduce the line-load on the bracing system because the bending stiffness of all the timber members in a system will not be insignificant compared with the necessary stiffness of the bracing system, referred to as EI above.

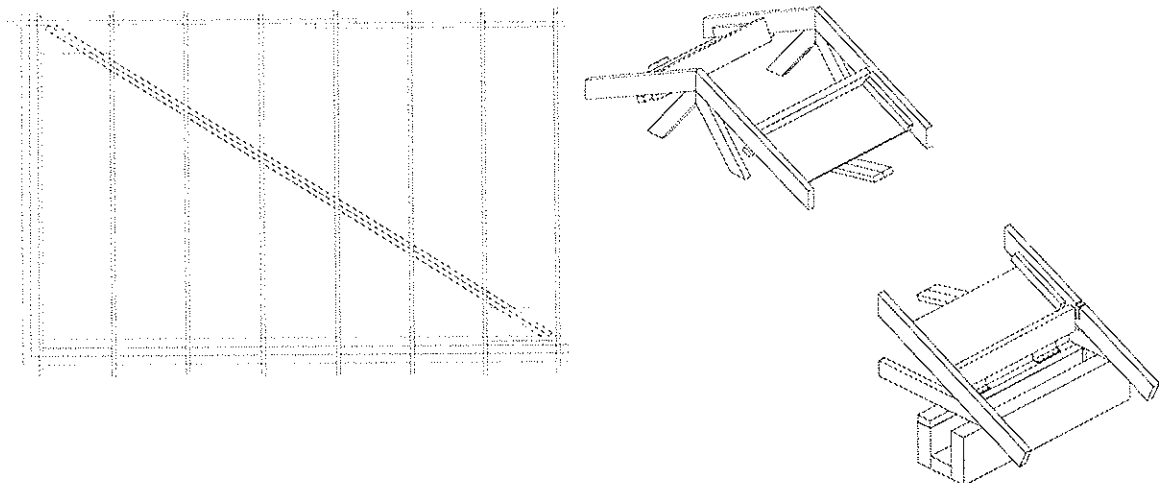


Figure 7. Bracing system for small span trusses based on a cross bracing from ridge to foot. The cross bracing is assembled from two battens and connected to the lower side of the truss heads and to plywood plates at the ends. A stringer near the ridge is also connected to the plywood. At the foot the head beam of the wall serves as stringer. The battens (not shown) function as lateral bracing. The force is transferred to the cross bracing via twisting and bending of the truss head. The twisting of the truss heads is prevented by pieces of planks mounted between two heads, whereas the bending is permissible due to the unused strength from the systems effect.

Conclusions

The bracing requirements for systems of timber members in compression in Eurocode 5 [3] section 9.2.5 are somewhat on the unsafe side, even when the most conservative factors suggested are chosen.

There is a fairly simple relationship between strength and stiffness requirements to the bracing system. The designer could easily be given the possibility of choosing a favourable set for the actual purpose. This could for example be relevant if other performance

requirements call for a smaller deflection than that required for the bracing. Then the load could be reduced as well.

If the requirement to the stiffness of the lateral bracing at intermediate nodes is kept at $C = 4N/a$, the force should be increased from $F = N/50$ to $F = N/37.5$. If the stiffness requirement is increased to $C = 6N/a$, then the present force $F = N/50$ is sufficient.

The present code value for uniform load on the bracing system for one member in compression is $q_d = N/30l$, which corresponds to a maximum deflection of less than $l/1000$. If the load is increased to $q_d = N/24l$, the permitted deflection increases to $l/500$. If other loads - like wind load - increase the deflection, the same deflection requirements should in principle be met, and consequently the stiffness of the bracing system must be increased. Since the load combination factor for wind and snow is small, the practical impact is low.

The reduction of the load, when the initial deflections are smaller, is also significant for the bracing system. Therefore, there should be differentiated requirements for structural timber and laminated timber.

Significant system effects will reduce the accumulated loads both on a common bracing system for several parallel members in compression and on the lateral bracing at intermediate nodes. It is suggested to design the bracing system for $2\sqrt{n}$ times the load q for one member in compression. The accumulated force in the lateral bracing is determined to be only 2 or 3 times the force F determined for one member.

There is also an unused stiffness and strength that can be used to transfer loads locally when simple bracing systems are used for smaller structures.

References

1. Code of Practice for the structural use of timber (DS 413), ver 5.1. Dansk Standard, 1998.
2. Code of Practice for the structural use of timber (DS 413), ver 6.1. Dansk Standard, 2003.
3. Eurocode 5 - Design of timber structures - Part 1-1. General - Common rules and rules for buildings. Final Draft prEN 1995-1-1. CEN, December 2003

INTERNATIONAL COUNCIL FOR RESEARCH AND INNOVATION
IN BUILDING AND CONSTRUCTION

WORKING COMMISSION W18 - TIMBER STRUCTURES

ACCEPTANCE CRITERIA FOR THE USE OF STRUCTURAL
INSULATED PANELS IN HIGH RISK SEISMIC AREAS

B Yeh

T D Skaggs

T G Williamson

Z A Martin

APA - The Engineered Wood Association

UNITED STATES

Presented by B Yeh

F Lam commented that the shake table experience of some of these walls was brittle.

H Blass asked how large were the sip. Yeh answered that they can be up to 8x24 ft or 16x24 ft but 8x8 ft wall sizes were tested.

H Blass commented it needs the presence of splines otherwise they will not work.

B Dujič commented displacement control was used and this system could behave differently after peak load under load control and some of the brittle failures mention by F Lam may be observed. B J Yeh answered that he would like to take a look at the over strength factor.

Y H Chui asked whether dynamic test is considered in the acceptance criteria. B J Yeh answered that this acceptance criteria is in effect today. Length of wall tested is 8 ft and brittle walls may be caught by the ductility criteria.

Discussion took place between F Lam and Yeh on the issue of vertical load going through the sheathing because of possible lacking of vertical studs. B J Yeh answered that this acceptance criteria cover a wide range of loading conditions including vertical and out of plane loading. The issue of cost of testing versus more complicated acceptance criteria was also discussed.

P Glos commented that the paper missed information on the structure of the product tested. Yeh responded that the work takes the code limitation today and demonstrates one has the simulated dynamic behaviour. A Cecotti commented in Eurocode 8 such walls would not be banned but allowed.

Acceptance Criteria for the Use of Structural Insulated Panels in High Risk Seismic Areas

Borjen Yeh, Ph.D., P.E.
Thomas D. Skaggs, Ph.D., P.E.,
Thomas G. Williamson, P.E.
Zeno A. Martin, P.E.
APA - The Engineered Wood Association, U.S.A.

Abstract

One of the fastest growing segments of the US housing construction industry is the use of structural insulated panels or SIPs. These components are also used extensively in commercial construction in the US and other countries. Emphasizing the growing importance of SIPs worldwide is a recent work item initiated by ISO TC 165 in the development of an international standard for the design of SIPs. In the US, SIPs are typically constructed using a foam core with outside layers of oriented strand board (OSB). While it would seem logical that a structural component having double “skins” of OSB would perform well when subjected to high lateral forces, such as those experienced during an earthquake, the US building codes have limited the use of SIPs to low to moderate seismic zones. This limitation is due to the concern that the sealants used in the manufacturing and installation of SIPs may affect their seismic performance.

Since the US building codes do not explicitly cover SIPs, building officials have the authority to accept their use under code-compliance evaluation reports, which are typically published by the ICC Evaluation Service (ICC-ES). These code reports are based on analysis of test data in accordance with ICC-ES AC04, *Acceptance Criteria for Sandwich Panels*. This paper describes efforts by APA - The Engineered Wood Association and the Structural Insulated Panel Association (SIPA) to revise AC04 in gaining recognition for the use of SIPs in high seismic risk zones. APA conducted a series of cyclic load tests using conventional wood framed shear walls and SIP walls. Results of this study confirmed that the SIP walls had equal or better performance than the conventionally framed walls. An analytical procedure for cyclic SIP shearwall tests was developed by APA and was approved by ICC-ES in the revised AC04, which now permits the use of SIPs in high seismic risk zones. To achieve this acceptance, a SIP manufacturer will be required to conduct the aforementioned tests in accordance with the new provisions of AC04.

1. Introduction

Structural Insulated Panels (SIPs) have had a long history of successful performance. The Forest Products Laboratory in Madison, Wisconsin, assembled the first demonstration house using “stress-skin panels” in 1937. Since then, SIPs have illustrated exemplarily structural performance in many parts of the world, including high wind and high seismic risk areas. In fact, it has been reported that SIP structures withstood the 1995 Kobe Japan earthquake (magnitude 7.2) with minimal damage (www.pbspanels.com). In 2003, approximately one percent of the nearly two million housing starts were with SIPs in the US. Although this is a relatively small percentage of the overall market share, it is

important to note that the SIPs market share has nearly doubled since 1997 (APA, 2004). In addition, the Structural Insulated Panel Association (SIPA) in the US is launching a five-year plan to double this again in the next 5 years. The attractive attributes of SIPs have made them popular in areas of the US where stringent energy codes or severe weather fluctuations are coincidental with high seismic risk.

The International Building Code, IBC, (ICC, 2003) has highlighted an issue that affects manufacturers of SIPs in particularly the following section:

2305.3.9 Adhesives. Adhesive attachment of shear wall sheathing is not permitted as a substitute for mechanical fasteners, and shall not be used in shear wall strength calculations alone, or in combination with mechanical fasteners in Seismic Design Category D, E and F.

Since the US building codes do not explicitly cover SIPs, building officials have the authority to accept their use under code-compliance reports, which are typically published by the ICC Evaluation Service (ICC-ES). These reports are based on analysis of test data in accordance with ICC-ES AC04, *Acceptance Criteria for Sandwich Panels*. As expected, the use of SIPs is limited to Seismic Design Categories A, B and C only in accordance with the IBC.

A brief history should be given to the “adhesive ban”. The IBC used the NEHRP Provisions (FEMA, 2001a) as a “resource document”. The Building Seismic Safety Council (BSSC) Technical Subcommittee 7 deliberated on the “adhesive ban” before it was adopted into the NEHRP Provisions based on the consideration that “the current ban on adhesive was imposed for high seismic because of the increased stiffness and associated attracted loads” (BSSC, 2000). However, the restriction was originally based on observations of light framed walls with rigid adhesives between the sheathing and the wood studs. The testing, conducted with rigid construction adhesive, led to impressive increases in wall stiffness and ultimate loads, but failed in a non-ductile mode.

There are two types of “adhesives” that are typically used in SIP assemblies. The first is the adhesive between the oriented strand board (OSB) skins (typical) and the expanded polystyrene core. The second type of “adhesive” is the sealant that is used to prevent air infiltration. The sealants are typically applied to all wood-to-wood connections and wood-to-foam connections. Sealants, depending on their chemical formulation, can provide rigid bonds. After sealants are applied, the SIPs are assembled similar to other light frame wood construction. The panels are typically connected with power driven fasteners into wood top and bottom plates and wood splines.

In order to address the use limitation of SIPs in high seismic risk zones, an analytical procedure for cyclic SIP shearwall tests was developed by APA in 2003 to demonstrate, via cyclic shear wall testing, that SIPs perform similarly to light framed wood walls with wood structural panels. The significance of demonstrating equivalence is light framed wood walls with wood structural panels are code-recognized systems that have historically shown adequate performance in seismic events.

2. Justification for Using Cyclic Testing to Show Equivalence

The 2003 IBC lists seismic design coefficients and factors for approximately 80 different seismic force-resisting systems in Table 1617.6.2. These listed systems range from steel eccentrically braced frames to ordinary plain concrete shear walls. Ranging between these two extremes in terms of seismic performance are light framed wood structural panels shear walls. By code definition, wood structural panels include plywood and OSB. For seismic design following the US building code, there are three listed attributes that are of importance (see Figure 1 for graphical representation of the three attributes):

1. Response modification coefficient, R ,
2. System over-strength factor, Ω_o ,
3. Deflection amplification factor, C_d

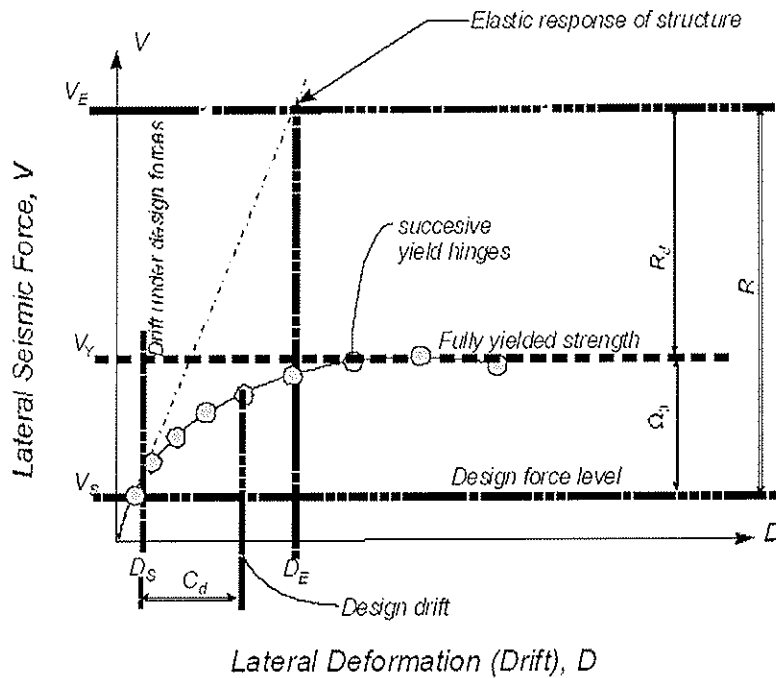


Figure 1. Inelastic force-deformation curve (Originally published as Figure C5.2-1, FEMA, 2001b)

The response modification coefficient, in practice, is the most used factor of the three aforementioned attributes. The response modification coefficient “represents the ratio of the forces that would develop under the specified ground motion if the structure had an entirely linearly elastic response” (FEMA, 2001b). The coefficient, which is always greater than 1.0, is applied to the load side of the equation and effectively reduce the design base shear. This reduction is due to 1.) as the structure begins to perform inelastically, the effective period of the structure is lengthened, which for many structures results in reducing strength demand, and 2.) inelastic behaviour results in a significant amount of energy dissipation (through hysteretic damping). These two combined effects explain the satisfactory performance of structures that should, on paper, have not performed well in a seismic event. The listed values (ICC, 2003) of the response

modification coefficient range from 1.5 (one example is ordinary plain masonry shear walls) to 8 (one example is an eccentrically braced steel frame). For light framed walls with wood structural panels, the response modification coefficient is equal to 6.5. It should be noted that the determination of the response modification coefficient is based on committee decisions; thus, there is no analytical method available currently for deriving the response modification coefficient for an unlisted system in the IBC.

The over-strength factor is used for determining the maximum seismic load effect and represents the ratio of the fully yielded strength of the system to the design strength of the system (See Figure 1). It is also related to the response modification coefficient and the ductility factor. In practice, this value is also based on committee decisions and ranges from 2 to 3 (ICC, 2003). As similar to the response modification coefficient, cyclic test data is typically not used to establish the over-strength factor. For light frame walls with wood structural panels, the over-strength factor is established as 3.0 (ICC, 2003). The IBC effectively requires that a strength level calculation be performed for lateral force resistance systems that could lead to non-ductile failures. The intended purpose of this code provision is to assure that the force demand is delivered to the ductile elements. Examples are the design of shear wall collectors and the design of support for discontinuities in the vertical system (i.e. unstacked shear walls). Note that the IBC exempts some light frame structures for these requirements based on their long history of successful performance when subjected to seismic forces.

The well-recognized definition of the deflection amplification factor is the ratio of anticipated inelastic drift to the elastic deformation calculated under the reduced design forces. The deflection amplification factor takes into account the brittleness of the system. The range of listed deflection amplification factors (ICC, 2003) is $1\frac{1}{4}$ - 5. For light framed wood walls with wood structural panels, the deflection amplification factor is equal to 4. As with the response modification coefficient and the over-strength factor, test data is typically not used to confirm the deflection amplification factor. In practice, the elastic lateral force resistant system deformation is determined by using empirical shear wall deflection equations. These elastic deflection are then “amplified” by the deflection amplification factor and checked against the allowable story drift, which is prescribed as 2.5 percent wall height for most light framed shear walls (Table 1617.3.1, ICC, 2003).

For systems that are not listed under Table 1617.6.2, the following clause is provided in the 2003 IBC (ICC):

1617.6.2 Seismic-force-resisting systems. ... For seismic-force-resisting systems not listed in Table 1617.6.2, analytical and test data shall be submitted that establish the dynamic characteristics and demonstrate the lateral-force resistance and energy dissipation capacity to be equivalent to the structural systems listed in Table 1617.6.2 for equivalent response modification coefficient, R , system over-strength coefficient, Ω_o , and deflection amplification factor, C_d , values ...

Therefore, the purpose of the evaluation procedure listed in section 3 of this paper is to meet the intent of Section 1617.6.2 of the IBC (ICC, 2003). In the past 10 years in the US, there has been an unprecedented amount of cyclic testing of wood shear wall systems. However, there has been little consensus on how these data should be analyzed. The purpose of the evaluation procedure is to compare the dynamic characteristics of a system

(SIPs) that is not listed in the code with a code listed seismic force resisting system (light framed wood walls sheathed with wood structural panels). If the test data demonstrated similar performance characteristics, then one could infer that similar in-service seismic performance would be realized. If this is the case, the limitations of the two systems as well as the seismic design coefficients should be similar.

3. Evaluation Procedure

The evaluation procedure outlined below is based on Appendix A of AC04 (ICC-ES, 2004), which was originally proposed by APA staff to the ICC-ES Evaluation Committee. As previously discussed, the purpose of this evaluation procedure is to permit the use of SIPs in higher seismic design categories. The evaluation procedure, as stated in Appendix A of AC04 “is not intended to determine design capacities, the response modification coefficient, R , the system over-strength factor, Ω_o , or the deflection amplification factor, C_d ”. The purpose of this evaluation procedure is to show that SIP assemblies, with or without sealants, perform similarly to light-frame walls with wood structural panels.

The essence of conducting the comparison tests is to test matched walls as a benchmark. Although completely matching SIP assemblies and conventional light framed wall assemblies is not possible, the matched tests are intended to duplicate as many of the factors as possible. For example, SIPs are typically manufactured with an expanded polystyrene core sandwiched between two sheets of wood structural panels. The matched light frame walls for this test program were sheathed with wood structural panels on both sides of the frame. The same type and number of perimeter fasteners are used to attach the SIP panels into a SIP assembly. The assembly is 2.4m x 2.4m, which is made using two SIP panels or four wood structural panels. Identical tie-down devices are used for both the control (conventional light framed walls) and the SIP assemblies.

3.1 Cyclic Testing

The matched wall tests are conducted following the SEAOSC (1997) test protocol (also known as sequential phase displacement, SPD). If the data is within 15 percent of each other, the results can be combined and the decision point is based on the mean performance. Otherwise, the lowest test value is used. A minimum of three replications is required for each series of tests. In the case of significant variation of test results, the replications can be increased to five, and the decision point may be based on the mean, regardless of variation.

3.2 Data Normalization

Given that the SIP assemblies and the control assemblies may have different design values, the data is normalized by the allowable stress design value. The reason for the different design values is that the SIP systems can have a fundamentally different attachment mechanism than the control assemblies. For example, it is common for individual SIP assemblies to be joined together with a thin (11 mm) wood structural panel spline on each face of the panel.

3.3 Backbone Curve Analysis

The represented backbone curve is the average of the positive and negative cycles of the individual backbone curves. The backbone curve, by definition, is the locus of extremities of the load-displacement hysteresis loops. It represents the peak load from the first cycle of each phase of the cyclic loading. Figure 2 illustrates a hysteresis curve for a conventional light framed wall with the backbone curve overlaid. Figure 3 illustrates a normalized backbone curve (with positive and negative cycles averaged) for three different assemblies. This curve will be further discussed in Section 3.3.4 of this paper.

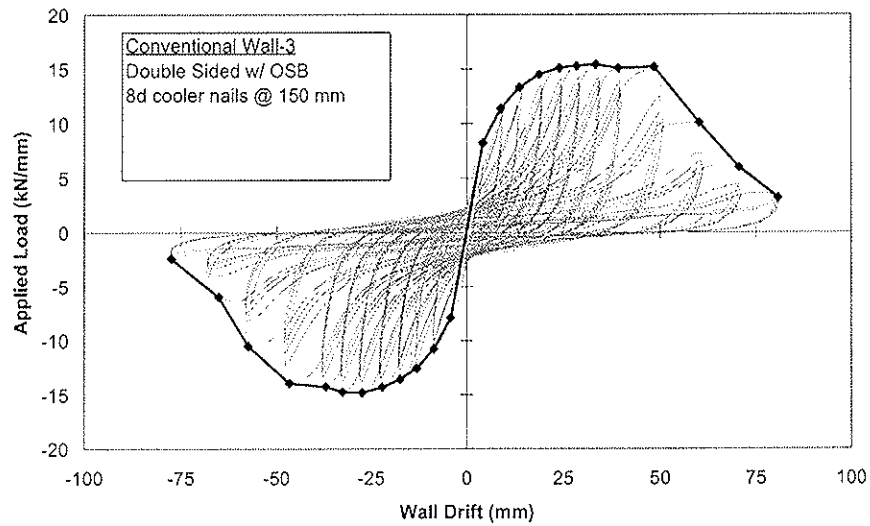


Figure 2. Hysteresis plot of conventional wall (2.4-m wall height) with outer backbone curve overlaid

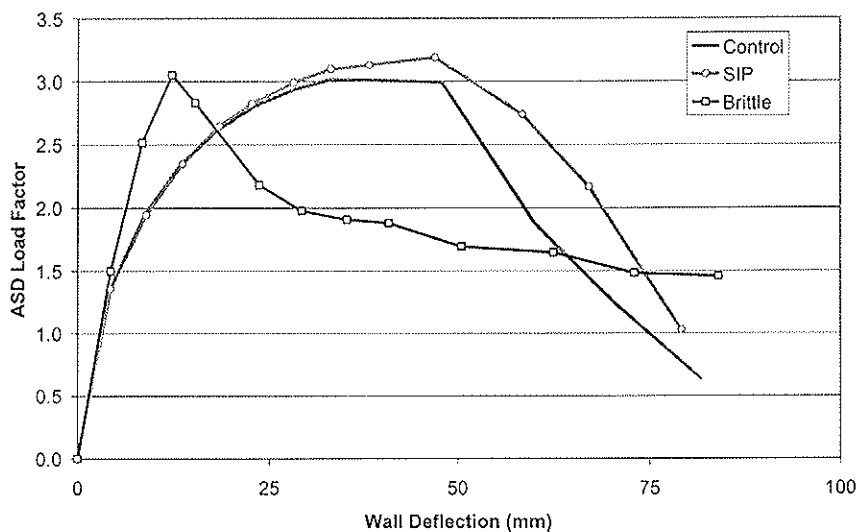


Figure 3. Normalized backbone curves for three different 2.4-m tall assemblies

3.3.1 Ultimate Load Criteria

The normalized ultimate load of the SIP assemblies shall not be less than 90 percent of that for the matched light-framed walls. The importance of the ultimate load is such that a relatively tighter tolerance is required for the ultimate load. In theory, the design value of the assemblies should be based on the ultimate load reduced by a load factor.

3.3.2 Stiffness Criteria

The normalized stiffness, slope of the normalized load versus deflection relationship at normalized load equal to 1.0, for the SIP assemblies shall not be less than 85 percent of that for the matched light-framed walls. Given the authors experience with deflection of wall assemblies as well as the fact that excessive deflection is generally not a life-safety concern, a slightly looser tolerance was specified for stiffness at the allowable stress level.

3.3.3 Deflection at Allowable Story Drift Criteria

The normalized load at the maximum allowable story drift per IBC (2.5 percent wall height, ICC, 2003) for the SIP assemblies shall not be less than 85 percent of that for the matched light-framed walls. As with the stiffness criteria, experience based on extensive assembly testing would indicate that deflection at the allowable story drift could have a large amount of variability. Thus, the tolerance for equivalence was less than the ultimate load criteria.

3.3.4 Application of Backbone Curve Analysis

Figure 3 provides a graphic representation of three backbone curves, including a backbone curve representing the control, a SIP system, and a "Brittle" system. The "Brittle" system was identified before the cyclic testing with expectation that it would fail in a brittle fashion, have little strength after peak load, and fail at a relatively small wall drift. This system was included to demonstrate how the evaluation procedure would identify systems that have significantly different seismic behaviour than light framed walls sheathed with wood structural panels. In terms of the ultimate load criterion, both the SIP assembly and the Brittle assembly exceed the normalized ultimate load of the control. For all practical purposes, the stiffness values at the load factor of 1.0, which represents the stiffness at the allowable stress design value, are identical for all three systems featured in Figure 3. Finally, the normalized load at the allowable story drift of 61 mm is examined. For the SIP assembly, the load at 61 mm exceeds that of the control. For the Brittle system, the load is close to the 85 percent tolerance. However, a closer examination of the backbone curve data is warranted.

3.4 Cumulative Energy Criteria

The area bounded by the normalized hysteresis loops is computed for each cycle of the test protocol. The normalized cumulative energy dissipated by the SIP assemblies shall not be less than 85 percent of that for the normalized matched light-framed walls. Since the current design procedure based on the US building codes does not directly cover cumulative dissipated energy, a looser tolerance than the ultimate load was chosen. Figure 4 demonstrates the application of this criterion for two systems plus the control. Although the SIP system shows a slightly lower normalized cumulative energy for cycles 15 through

approximately 58, the normalized cumulative energy is within 85 percent of the control. As a result, the SIP system is acceptable in terms of cumulative energy dissipated. However, as shown in Figure 4, the Brittle system does not meet the normalized cumulative energy dissipation criterion, which demonstrates the effectiveness of these evaluation procedures for identifying systems that fail in a catastrophic fashion.

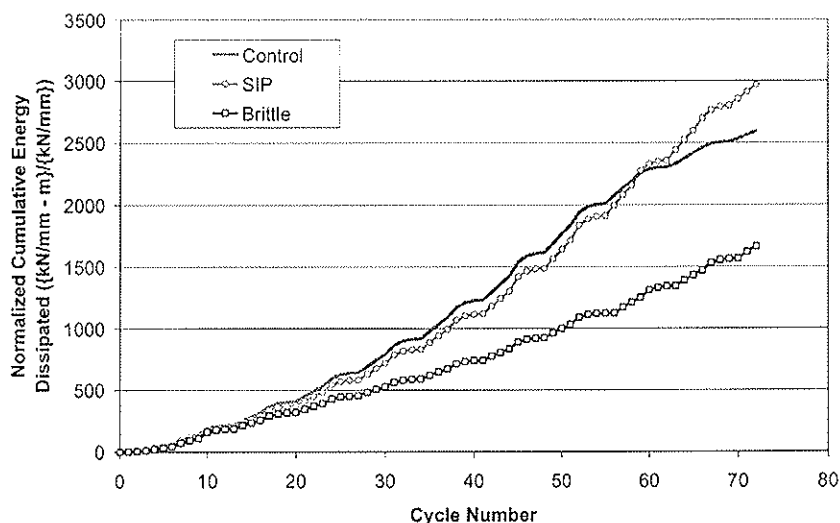


Figure 4. Normalized cumulative energy curves for three different assemblies

3.5 Potential Limitations of Evaluation Procedure

The evaluation methodology adequately identifies equivalent systems in terms of response modification coefficient, which is arguably the most important factor of the published seismic design coefficients. However, it is likely that the proposed criteria will be modified to address the over-strength factor and deflection amplification factor in the future. Figure 5 demonstrates a SIP system (labelled SIP 2) constructed with non-rigid sealants. Note the “humpback” shape of the backbone curve. Based on the testing, it is believed that the humpback shape is related to the non-rigid sealant adding strength and stiffness. The nature of the sealant resulted in a non-catastrophic loss of load. When the sealant bond reached the ultimate shear strength (or shear strain), the remaining resistance was from the mechanical fasteners.

By inspection, it can be noted that SIP 2 meets the backbone curve criteria. Although not shown, SIP 2 also meets the normalized cumulative energy criterion. Given that the peak load is significantly higher than the control, which leads to a significantly higher factor of safety, the inherent over-strength of the SIP 2 assembly is higher than the conventional wall system. This inherent over-strength could be important if the lateral force resistant system is detailed for ductile failures. However, it is possible that the designed collector will not be able to transfer the required load into the ductile element. In terms of deflection amplification, the case is not as clear. Although the peak load is achieved at a relatively small drift (less than 1% drift), the ultimate displacement is significantly higher than the displacement at the peak load. The current literature is not clear on how the

deflection amplification factor would be estimated for a system that exhibits a humpback shape.

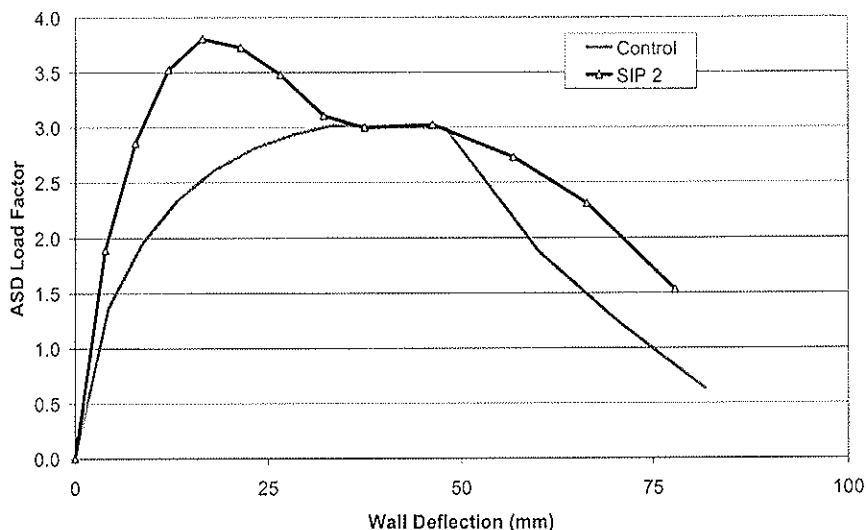


Figure 5. Backbone curve of 2.4-m tall assembly with non-rigid sealants that passes the proposed criteria

4. Conclusions

The aforementioned comparison is based on matched wall tests. The basis for the evaluation is light framed wood walls sheathed with wood structural panels, which are a listed system in terms of seismic design coefficients. Based on cyclic testing of the known system, a normalization technique is used such that data from conventional walls is compared to data collected on SIP assemblies. There are four criteria that are examined:

1. Ultimate Load
2. Stiffness
3. Deflection at allowable story drift, and
4. Normalized cumulative energy dissipation

If the SIP systems demonstrate equivalence to the light framed systems based on the above criteria, it can be considered that the SIP systems have equivalent seismic design coefficients, as given in the 2003 IBC (ICC), for light framed walls sheathed with wood structural panels. Based on limited testing of SIP assemblies with sealants, the assemblies can meet the aforementioned criteria. It should be noted that since the performance of SIP systems is sensitive to fastener type and sealant formulation, additional matched tests may be required with significant changes in sealant formulation and fastener type.

5. References

- APA. 2004. *Regional production & market outlook for structural panels and engineered wood products 2004 - 2009*. APA Economics Report E70. APA - The Engineered Wood Association, Tacoma, WA.
- BSSC. 2000. *Proposal 7-7(2000) changes to 1997 NEHRP provisions*. Building Seismic Safety Council, Washington, DC.
- FEMA. 2001a. *NEHRP recommended provisions for seismic regulations for new buildings and other structures, part 1 – provisions*. FEMA 368. Federal Emergency Management Agency, Washington, DC.
- FEMA. 2001b. *NEHRP recommended provisions for seismic regulations for new buildings and other structures, part 2 – commentary*. FEMA 369. Federal Emergency Management Agency, Washington, DC.
- ICC ES. 2004. *Acceptance criteria for sandwich panels - AC04*. ICC Evaluation Service, Inc., Whittier, CA.
- ICC. 2003. *International building code*. International Code Council. Falls Church, VA.
- SEAOSC. 1997. *Standard method of cyclic (reversed) load test for shear resistance of framed walls for buildings*. Structural Engineers Association of Southern California, Whittier, CA.

INTERNATIONAL COUNCIL FOR RESEARCH AND INNOVATION
IN BUILDING AND CONSTRUCTION

WORKING COMMISSION W18 - TIMBER STRUCTURES

PREDICTING LOAD PATHS IN WOOD SHEARWALLS

Hongyong Mi

Y-H Chui

I Smith

University of New Brunswick

M Mohammad

Forintek Canada Corp

CANADA

Presented by Y Chui

P Quenneville received confirmation that all shear walls in model house were connected the same way.

J M Andersen asked why 4 load cells were needed. Chui answered 4 load cells were needed to catch the up-down action observed.

P Ross asked about the conclusion that the capacity of vertically sheathed wall and the wall with opening behaved similarly. Chui responded that the wall with opening had extra framing around the opening.

H Blass asked about the deformation of the horizontal sheathed shearwalls. Chui responded that the information is available in the paper.

H Blass asked about the gaps between panels in the horizontal sheathed shearwalls. Chui responded that such gaps were maintained per Canadian practice.

E Karacabeyli commented that the conclusions should be limited to the specimens tested and should not be generalized e.g. conclusion on the shearwall with opening.

BJ Yeh received clarification that the horizontal shear wall was unblocked and method of loading used.

T Williamson discussed with Chui the issue of hold down in the unblocked shearwall.

K Crews asked why 3 D load cells were used for a 2 D specimen with in plane loading. Chui answered that out of plane loading will be performed in further studies.

Predicting Load Paths in Wood Shearwalls

Hongyong Mi, Ying-Hei Chui and Ian Smith

University of New Brunswick, Canada

Mohammad Mohammad

Forintek Canada Corp, Canada

ABSTRACT: This paper presents an evaluation of the use of two-dimensional finite element shearwall models to predict load path in a shearwall under lateral and vertical load. Previous modeling attempts focused on predicting load-deformation response of shearwalls. Comparison is made between model predictions and test measurements of shearwall responses. The study shows that ability to accurately predict so-called racking deformations is in itself no guarantee of accurate internal force prediction.

1. INTRODUCTION

With the advancement of electronic technology and computational techniques, finite element based methods have become popular tools for analyzing shearwalls. In the past three decades, numerous shearwall finite element models have been developed (Foschi 1977, Itani and Cheung 1984, Falk and Itani 1989, Dolan 1989, White 1995, Monique and Shenton III 2002). Although good agreement has often been reported between model and experiment derived load versus deformation response, the focus has been on comparison at the overall shearwall system level. That is, comparisons are of selected in-plane boundary deformations of framing members at certain levels of applied racking load. This approach of 'verification' is insufficient to ensure that the model is accurate, because shearwalls are highly redundant structures and many possible internal force flows could produce the same finite number of point boundary displacements. To be fully assured that a model is accurate, it would be necessary to compare model predictions with measured forces in members and at the boundaries. This paper presents a study to evaluate the ability of a commercial finite element model to predict deformation and force responses of shearwalls.

2. DESCRIPTION OF PHYSICAL SHEARWALLS

The finite element program was used to analyse three types of shearwalls shown in Figure 1. Each was 3.66 m in length and 2.44 m in height and matched the basic wall module in a light-frame single storey building at UNB being monitored under the project 'Load paths in wood buildings' (Smith et al 2004). The sheathing panels were oriented vertically in Type A1 and Type A2, and horizontally in Type B. The A2 shearwall had an opening of size 1.83 m \times 0.965 m (length \times height) which is similar to that of a typical window in low-rise residential buildings. Type B had a continuous horizontal unblocked sheathing joint in the middle of the wall.

All shearwalls were built with 38 mm \times 89 mm (1 ½ " \times 3 ½ ") No. 2 or better grade spruce-pine-fir lumber (SPF), with the grade designation corresponding to nomenclature of the Canadian National Lumber Grades Authority. The lumber studs were spaced at 610 mm on centers. Extra studs were added at both sides of the opening to form its edges in Type A2 wall. Top plates of all shearwalls consisted of double members that were

connected to each other by 82 mm (3 1/4") common nails. Oriented strandboard (OSB) of thickness 11 mm (7/16") was used as the sheathing panels, and they were connected to the framing members with 63 mm (2 1/2") common nails. The nail spacing was 150 mm around the edges of panels and 300 mm along intermediate studs for all shearwalls.

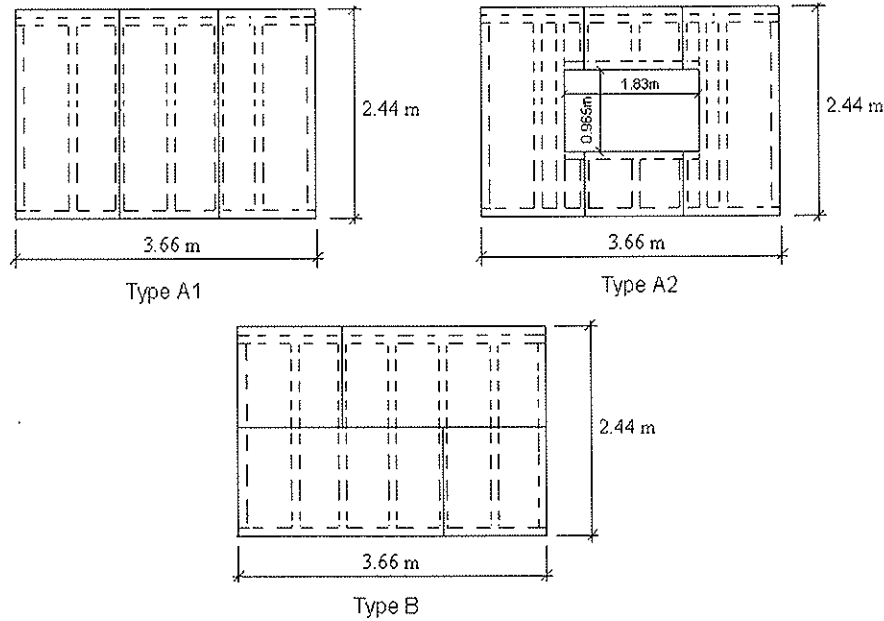
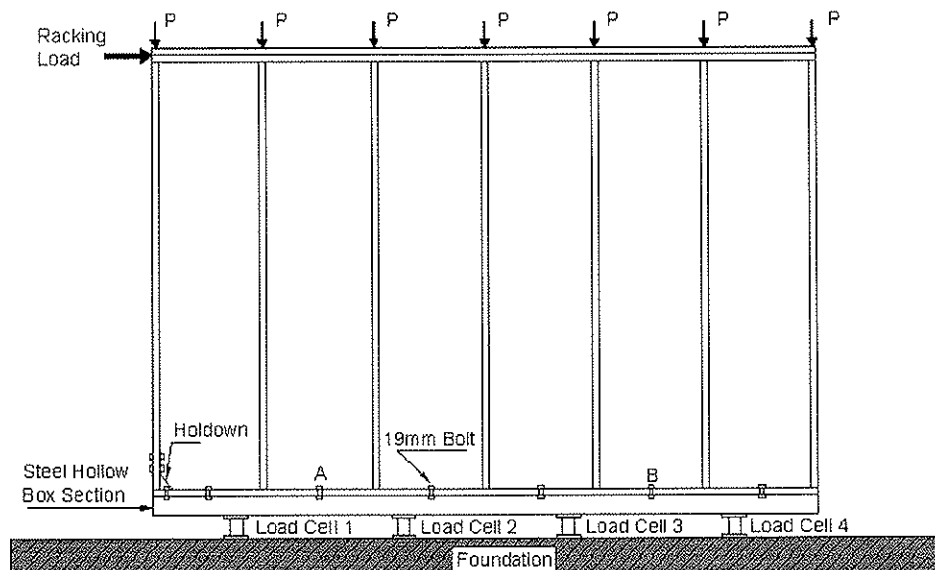


Figure 1 Shearwall Configurations Analysed.

A hold-down was inserted at the end stud closer to the load. The shearwall specimen was connected to the foundation of the test frame via a steel hollow box section and four load cells which measured the forces in vertical and horizontal directions. The construction of the shearwall is shown in Figure 2. Top loads can be applied using a lever system at each stud location. One specimen was tested for wall configurations Type A1 and A2, while three specimens were tested for Type B, each with different vertical top load level.



Note: For Type A2, extra studs are added at both sides of the opening to form its edges as shown in Figure 1, and two connection bolts are omitted at location A and B.

Figure 2 Construction of the Shearwall

3. MODEL DEVELOPMENT

Two-dimensional models were developed in this study using a commercial finite element analysis package SAP2000 (CSI, 2003). They represent the physical structures of the shearwalls as shown in Figures 1 and 2, including the supporting steel hollow box section and load cells. In the models the structural system is divided into member segments (finite elements) that represent sheathing, framing, sheathing-to-framing connections, framing-to-framing connections, shearwall-to-steel hollow box section connections (anchor bolts), the steel hollow box section, the shearwall bottom plate-to-steel hollow box section interface, and the steel hollow box section-to-foundation connections (load cells). The effect of material nonlinearity (e.g., sheathing-to-framing connection and framing-to-framing connection) was considered in the model. The behavior of the shearwall after strength degradation was predicted by using a multi-linear model to define the nonlinear property of the connection. Table 1 summarizes element properties used.

Table 1 Summary of Shearwall Model Input.

Physical Object		Finite Element	Material Property
Framing member	Top Plate	Frame	$E=9500$ MPa, $r=0.3$, $h \times b=76$ mm \times 89 mm
	Bottom Plate, Stud		$E=9500$ MPa, $r=0.3$, $h \times b=38$ mm \times 89 mm
Sheathing		Shell	$E_1=4500$ MPa, $E_2=1300$ MPa, $r_{12}=0.3$, $G_{12}=300$ MPa, $t = 11$ mm
Connection	Sheathing-to-Framing, Framing-to-Framing	Two Joint Link	Determined by connection tests
Boundary Support	Steel Box Channel	Frame	$E=200$ GPa, $r=0.3$, $h=102$ mm, $b=102$ mm, $t_f=6.35$ mm, $t_w=6.35$ mm
	Anchor Bolt	Two Joint Link	$U_1=10$ kN/mm, $U_2=3$ kN/mm, $R_3=1.5$ kN-m/rad
	Hold-dow		$U_1=5$ kN/mm, $U_2=2$ kN/mm, $R_3=1$ kN-m/rad
	Interface		$U_1=10$ kN/mm
	Load Cell	One Joint Link	$U_1=60$ kN/mm, $U_2=6$ kN/mm, $R_3=60$ kN-m/rad

- Note:
- 1, In SAS2000, element property is defined in its local coordinate system. The axes of this system are denoted directions 1, 2, and 3. Their detailed information could be found in the SAP2000 Analysis Manual (SCI 2002).
 - 2, Frame: E =elastic modulus (along the longitudinal axis of framing member); r =Poisson's ratio; h =cross-section height; b =cross-section width; t_f , t_w =flange thickness and web thickness of steel hollow box cross-section.
 - 3, Shell: E_1 , E_2 =elastic modulus in directions 1 and 2 respectively; G_{12} , r_{12} =shear modulus and Poisson's ratio in plane 12 (plane of sheathing).
 - 4, Link: U_1, U_2, R_3 =spring stiffness along directions 1, 2 and about direction 3.

3.1 Framing Members and Sheathing

Framing members of the shearwall included top plate, bottom plate and stud. They were modelled by the frame element which is represented by a straight line connecting two

nodes. These elements are placed in a vertical plane 50 mm away from the shell element which represents the sheathing. This distance accounts for the difference of the locations of the centroid of the framing members to that of the sheathing panels.

The wall sheathing consisted of several pieces of OSB. Models reflected the physical situation in terms of the arrangement of axes of material symmetry and location of edges. As a 3 mm gap existed between panel edges in practice, that gap was reproduced in the models. Four-node quadrilateral shell elements were used to model each sheathing panel adopting approximately 150 x 150 mm as the element size. There were 384 elements for a fully sheathed shearwall (Type A1 and Type B), and 312 elements for a perforated shearwall (Type A2). The nodes of shell elements coincided with the locations of individual nails.

3.2 Connections

Sheathing-to-framing and framing-to-framing connections were incorporated in the shearwall models. They were modelled by the two-node, two-dimensional link elements. Sheathing-to-framing connection link elements consisted of two internal springs shown in Figure 3(a). Use of two springs permitted the link to transfer force in any resultant direction. However framing-to-framing connection link elements comprised three springs shown as Figure 3(b) and permitted transfer of moment as well as force in any resultant direction.

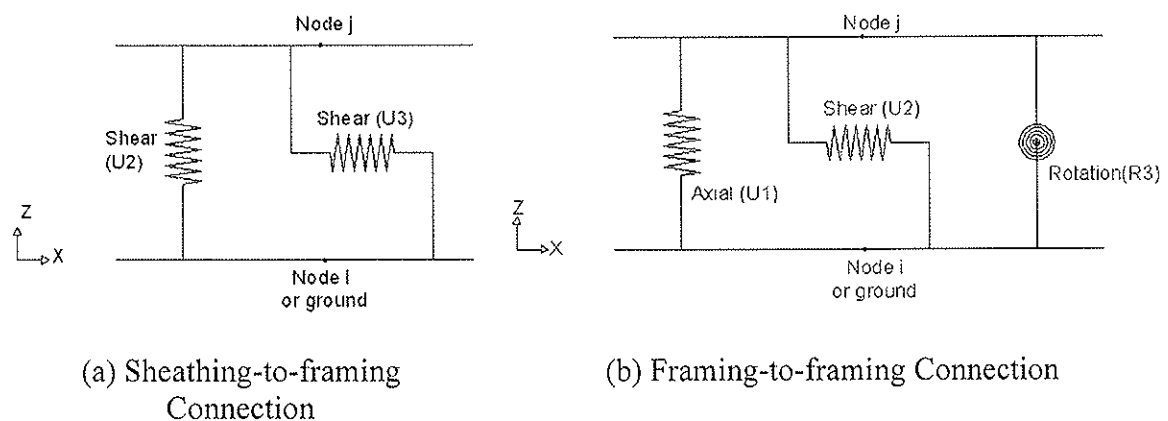


Figure 3 Link Elements

The vertical internal spring (axial-direction) of framing-to-framing connection was assigned a linear stiffness of 10 kN/mm, which is the initial stiffness of load-displacement curve derived from experiments on framing-to-framing connections under withdrawal load. All other springs of the link element representing the connections were defined by a multi-linear response model derived from test data. A typical multi-linear model is shown in Figure 4. This non-parametric multi-linear approach was adopted instead of the usual parametric approach as it was found that calculation breaks down as the analysis reaches the post-peak portion of response.

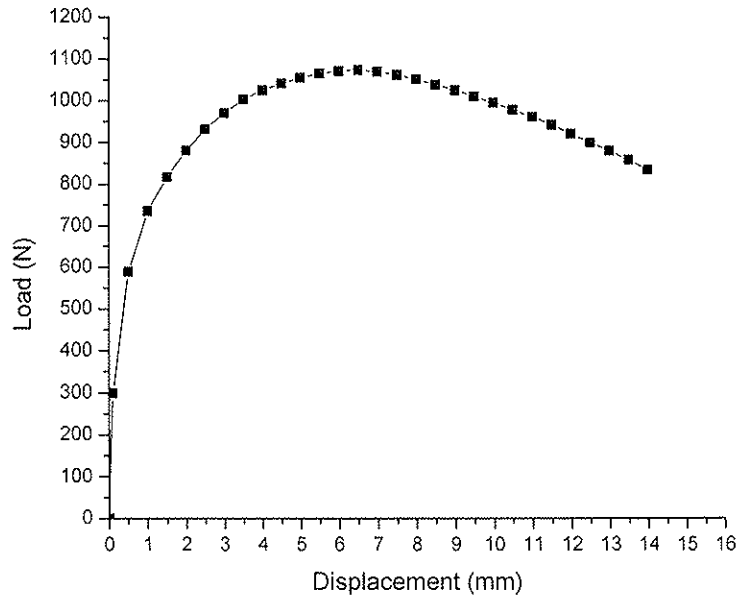


Figure 4 Typical Multi-linear Model used to Define the Connection Response (Sheathing-to-Framing)

3.3 Boundary Conditions

The physical boundary conditions were complex and indeterminate, and reflected characteristics of the steel hollow box section, anchor bolts, the hold-down on the heel corner, and various interface arrangements. Indeterminacy in the system meant that reactions as measured by the supporting load cells did not map directly into the forces under the wall. Thus the support system had to be part of the finite element model. Reaction data, together with boundary displacements, provided a tool for model verification.

The steel hollow box section was modelled by the frame element. The anchor bolts and hold-down were modelled using three-spring link elements, Figure 3(b). Linear responses were assigned to all springs of these link elements, except for the spring of the anchor bolt in the vertical axial direction. A tension-only capability (hook property) was assumed for that spring, Figure 5(a) (CSI, 2002). The force f in the spring is:

$$f = \begin{cases} k(d - open) & \text{if } d - open > 0 \\ 0 & \text{otherwise} \end{cases}$$

where k is the spring stiffness, d the node opening, and $open$ is the initial hook opening, which is greater than or equal to zero.

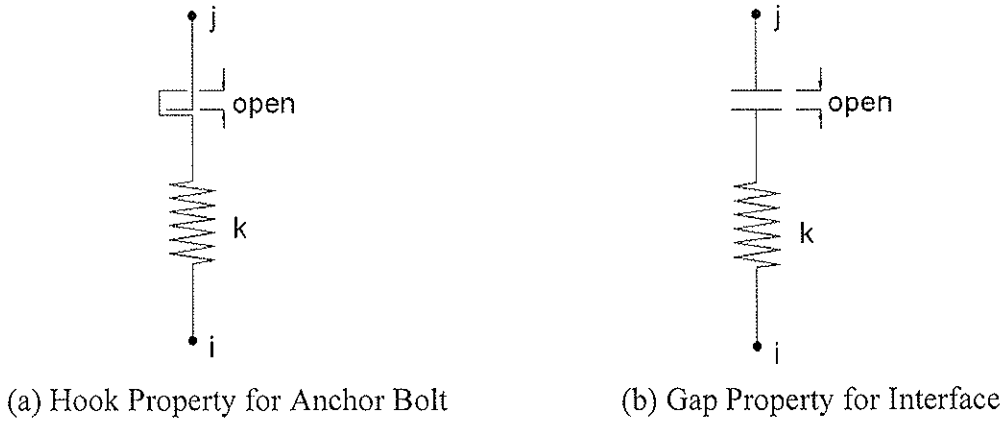


Figure 5 Illustration of Internal Spring Properties in Axial Direction

The interface between the steel hollow box section and wall was modelled by a single spring in the direction of axial deformation. A compression-only capability (gap property) was assigned to the spring, Figure 5(b) (CSI, 2002). The force f in the spring is:

$$f = \begin{cases} k(d + open) & \text{if } d + open < 0 \\ 0 & \text{otherwise} \end{cases}$$

where k is the spring stiffness, d the node opening, and $open$ is the initial gap opening, which is greater than or equal to zero.

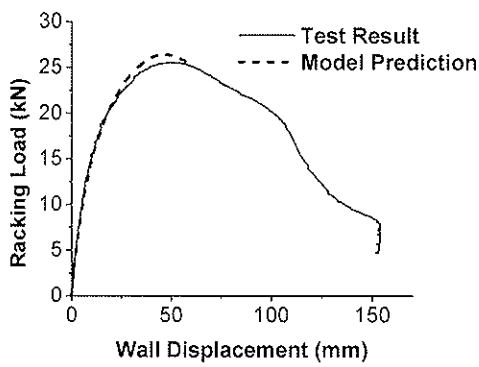
The load cell was modelled using one-joint grounded link element which consists of three internal springs as shown in Figure 3(b). Linear responses were assigned based on testing.

4. MODEL VERIFICATION

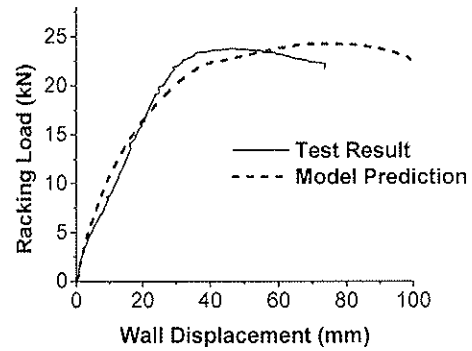
Comparison between the model predictions and experimental results was performed in two aspects: the overall behavior of the shearwall and reaction forces along the foundation. For the shearwalls with configurations of Type A1 and Type A2, the analyses were performed without a top load. For Type B, three cases were run to analyze its behavior: (1) without a top load. (2) with a series of 1.85 kN concentrated top loads to generate about 13 kN dead load in total at the top of the wall. These loads represent the weight of a typical roof. (3) with a series of 4 kN concentrated top loads to create a total of 28 kN dead load. This load is about 60% of the roof weight and snow load for the Fredericton area. The concentrated loads were applied along the wall top plate at the location of each stud.

4.1 Overall System Behavior

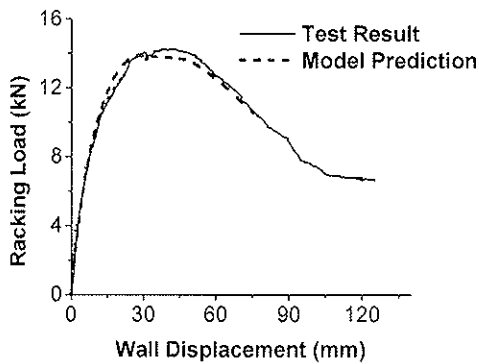
The overall system behavior of the shearwall in this study refers to the racking load and overall system deformation which is the horizontal wall displacement of the upper right-hand corner in Figure 2. It is expressed in the form of racking load versus wall displacement response curve. The model predictions of the shearwalls and corresponding test results are presented in Figure 6.



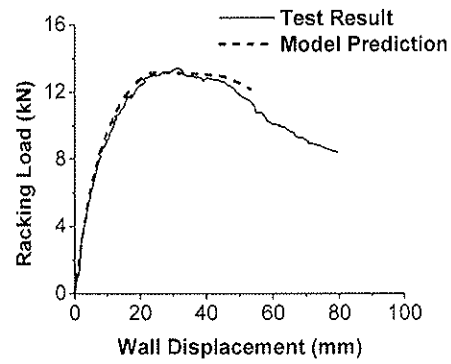
(a) Type A1



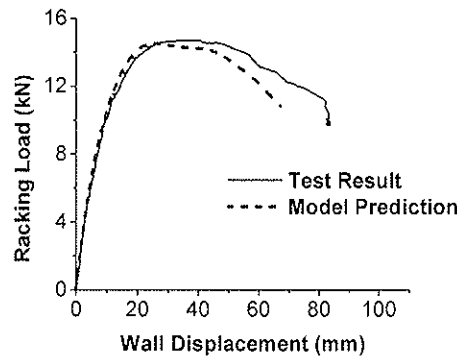
(b) Type A2



(c) Type B without Top Load



(d) Type B with 1.85 kN Top Loads



(e) Type B with 4.0 kN Top Loads

Figure 6 Comparison of Overall System Behavior between Model Predictions and Test Measurements

The overall system behavior verification of shearwall models indicates that the agreement is excellent. The difference between predicted and test maximum load is within 5%. The predicted initial stiffness is, in general, also close to those measured in the tests. The difference between them is less than 12% for all shearwalls except Type A2.

During the test, The A2 specimen was first loaded to about 22 kN before the hold-down was found to be loosened. The load was then released and the hold-down was tightened before the specimen was reloaded again until failure. It is suspected that the pre-loading of 22 kN is the main reason for the relatively large difference between predicted and measured initial stiffness for this specimen.

4.2 Reaction Forces

The model predictions and test results of horizontal and vertical reaction forces are presented in Figure 7 and Figure 8 respectively. They are expressed by the curves of reaction forces versus wall displacement at the upper right-hand corner as shown in Figure 2. For the horizontal reaction force, the test measurement of load cell 4 was not available because of malfunctioning of the sensor in that direction. For the vertical reaction force, the result of Type B with 4 kN top loads was not presented, because its experimental data acquisition system was zeroed after the top load was applied during testing. This was not intended and eliminated the effect of the top load to some extent for the test result while the model prediction was still generated under top loads.

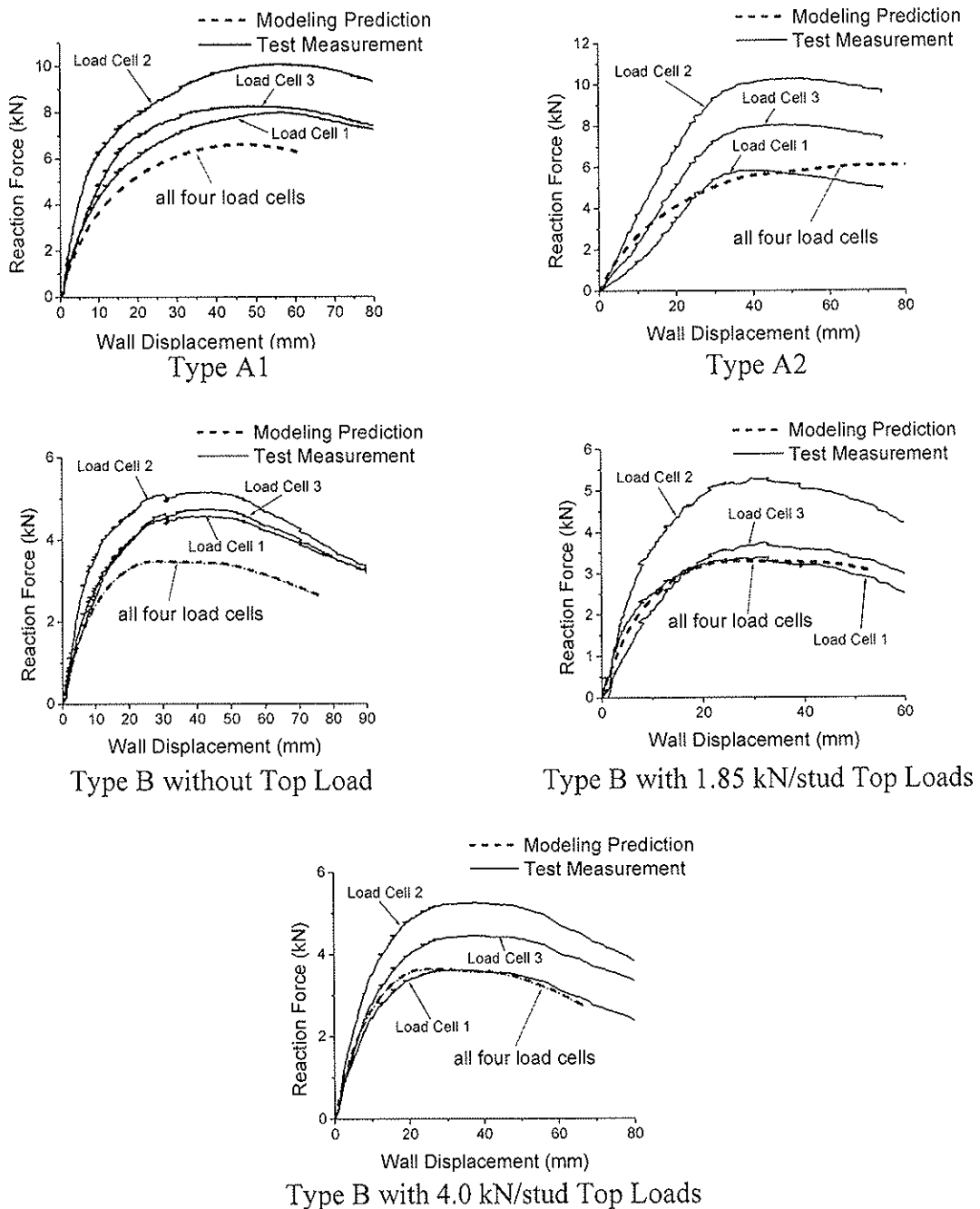


Figure 7 Comparison of Horizontal Reaction Forces between Model Predictions and Test Measurements

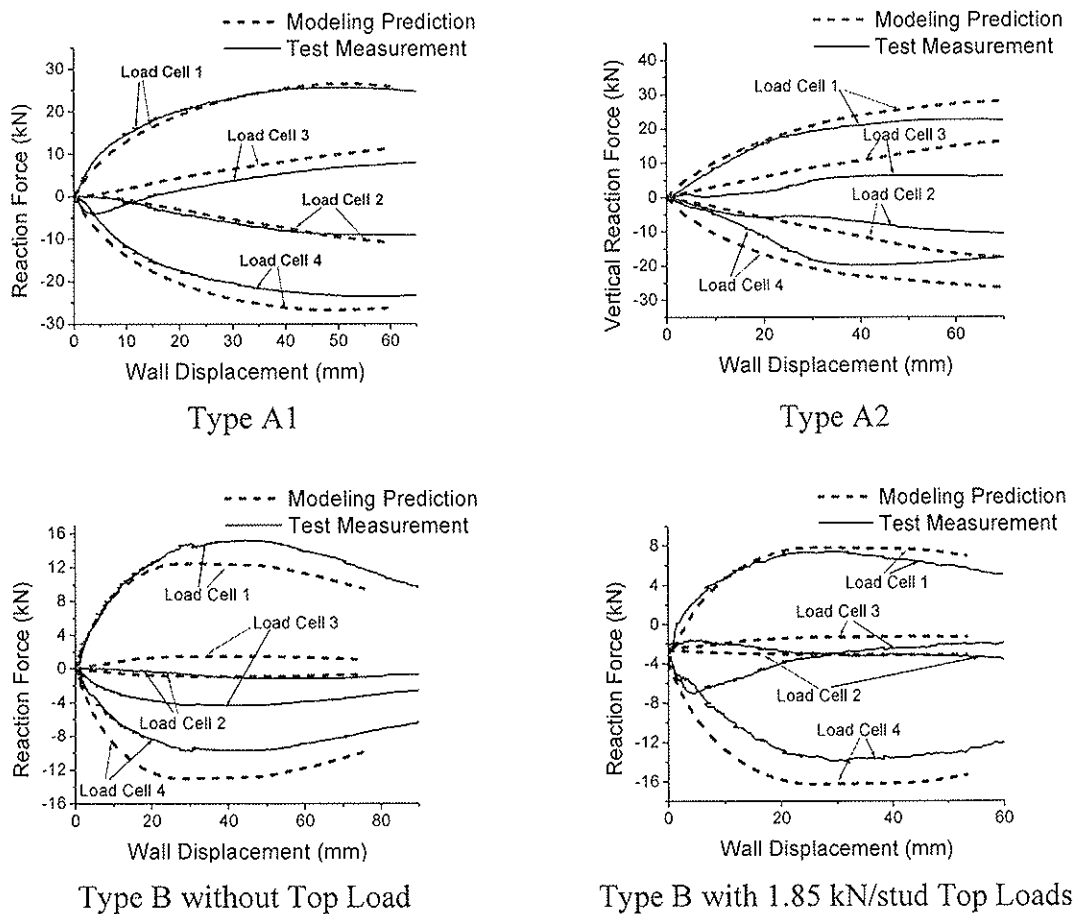


Figure 8 Comparison of Vertical Reaction Forces between Model Predictions and Test Measurements.

According to the model prediction, the horizontal reaction forces at the four load cells are virtually identical, as shown by the overlapped dashed lines in Figure 7. The measured reaction forces are different, and they are always higher than predicted forces. This may be caused by the difference between the model assumption and real support condition. In the shearwall modeling, all load cells were assumed to be identical, but in the actual test specimen these four load cells were not identical. For example, load cells 1, 2 and 3 had a circular cross section, whereas load cell 4 has a square cross section, and there were slight variations in height between the 4 load cells. This discrepancy may also indicate that the steel hollow box section was not as rigid as the model has assumed. All these factors may have contributed to the difference between the model predictions and test results.

The comparison of vertical reaction forces obtained from modeling and testing indicates that a good agreement was achieved. This comparison is shown in Figure 8. It is found that the shearwall models are capable of predicting the general response curve of vertical reaction load. Although the racking load-deformation and vertical force-deformation results presented above are encouraging from the point of view of using finite element method to study load path, the results on the horizontal force predictions indicate that good agreement of load-deformation response does not necessarily guarantee good agreement between predicted and actual forces in members and components. Further research is required to investigate this further.

5. CONCLUSIONS

Finite element models associated with different shearwall configurations were presented. These models can perform non-linear static analysis of the shearwall and are able to model the behavior of shearwalls after strength degradation. Multi-linear curves derived from tests were used to define the properties of sheathing-to-framing and framing-to-framing connections. They are suitable to model the non-linear properties of these connections, and in fact are desirable for modeling the post-peak portion of load-deformation curve. The comparison between the model predictions and test measurements indicates that the agreement of overall system load-deformation behavior is excellent. A reasonably accurate prediction of the vertical force was also achieved. But significant differences between predicted and measured horizontal forces were also found. Research is required to investigate this further. At this stage it cannot be concluded that accurate load-deformation system response implies that accurate member force prediction can be achieved using finite element model.

6. ACKNOWLEDGEMENTS

The authors would like to acknowledge the financial support provided to this study by the Natural Sciences and Engineering Research Council of Canada and Forintek Canada Corp.

7. REFERENCES

- [1] CSI, 2002. SAP2000 Analysis Reference Manual, Computers and Structures, Inc. (CSI), Berkeley, CA, USA.
- [2] CSI, 2003. SAP2000 Nonlinear 8.1.2, Structural Analysis Program, Computers and Structures, Inc. (CSI), Berkeley, CA, USA.
- [3] Dolan, J. D., 1989. The Dynamic Response of Timber Shear Walls, Thesis submitted in partial fulfillment of the requirements for the Degree of Doctor of Philosophy, University of British Columbia, Vancouver, British Columbia, Canada.
- [4] Falk, R. H., and Itani, R. Y., 1989. "Finite Element Modeling of Wood Diaphragms", ASCE Journal of Structural Engineering, Vol. 115, No. 3, p. 543-559.
- [5] Foschi, R. O., 1977. "Analysis of Wood Diaphragms and Trusses: Part I: Diaphragms", Canadian Journal of Civil Engineering, Vol. 4, No. 3, 1977, p. 345-352.
- [6] Itani, R. Y. and Cheung, C. K. 1984. "Nonlinear Analysis of Sheathed Wood Diaphragms", ASCE Journal of Structural Engineering, Vol. 110, No. 9, p. 2137-2147.
- [7] Monique, C. H., and Shenton III, H. W., 2002, "Modeling the Non-Linear Behavior of Wood Frame Shear Walls", 15th ASCE Engineering Mechanics Conference, Columbia University, New York, USA.
- [8] Smith, I., Mohammad, M. and Dick, K., 2004, "Structural monitoring of timber buildings: Overview of work in Canada", 8th World Conference on Timber Engineering, Lahti, Finland, June 14-17, II.469-474.
- [9] White, M. W., 1995. Parametric Study of Timber Shear Walls, Thesis submitted in partial fulfillment of the requirements for the Degree of Doctor of Philosophy, Virginia Polytechnic Institute and State University, Blacksburg, Virginia, USA.

INTERNATIONAL COUNCIL FOR RESEARCH AND INNOVATION
IN BUILDING AND CONSTRUCTION

WORKING COMMISSION W18 - TIMBER STRUCTURES

EFFECTIVE VALUES OF THERMAL PROPERTIES OF TIMBER
AND THERMAL ACTIONS DURING THE DECAY PHASE OF
NATURAL FIRES

J König

Trätec – Swedish Institute for Wood Technology Research

SWEDEN

Presented by J König

B Källander suggested that the possibility of large volume of moisture in the wood escaping in form of water vapor cooled the medium. And he asked about the issue of heat of evaporation. König responded that the water diffused into the wood rather than escaping from the wood. Experimental results are available and some theoretical work is available. The issue of heat of evaporation is considered in the heat capacity.

Effective values of thermal properties of timber and thermal actions during the decay phase of natural fires

Jürgen König
Trätec – Swedish Institute for Wood Technology Research
Box 5609, SE-114 86, Stockholm, Sweden
juergen.koenig@tratek.se

Abstract

For the thermal analysis of structural or non-structural timber members, using conventional simplified heat transfer models, thermal conductivity values of timber are normally calibrated to test results such that they implicitly take into account influences such as mass transport that are not included in the model. Various researchers and designers have used such effective thermal conductivity values, originally determined for standard fire exposure, to evaluate other fire scenarios such as natural fires. This paper discusses in qualitative terms some parameters that govern combustion of wood and their influence on effective conductivity values. Reviewing fire tests of timber slabs under natural fire conditions, it is explained why effective conductivity values, giving correct results for the ISO 834 standard fire scenario, should not be used in other fire scenarios. Therefore, the thermal properties of timber given in EN 1995-1-2 are limited to standard fire exposure. As shown by heat transfer calculations, the effective thermal conductivity of the char layer is strongly dependent on the charring rate and varies therefore during a natural fire scenario. It has also been shown that char oxidation during the decay phase in a natural fire has a significant influence on the temperature development in the timber member, since char surface temperatures exceed the gas temperature in the compartment or furnace. Using increased effective gas temperature as thermal action during the decay phase, and varying conductivity values for the char layer, fairly good agreement could be obtained regarding the temperature development in the timber member and the char depth.

1 Introduction

1.1 Heat transfer in wood exposed to fire

In design by calculation the load-bearing performance of steel and concrete structures exposed to fire is verified by performing a thermal analysis of structural parts and a subsequent structural analysis taking into account the thermo-mechanical material properties. In timber structures, the thermal analysis is normally replaced by determining the char depth and the structural analysis is carried out by replacing the cold strength and stiffness properties of the residual cross-section by reduced properties that are valid in the fire situation, see e.g. the Fire Part of Eurocode 5 (EN 1995-1-2). For advanced calculations, this code also contains thermal and thermo-mechanical properties of timber. Unfortunately, unlike for other materials

such as steel and concrete, the thermal properties of timber are valid only for standard fire exposure. This limitation on the use of advanced calculations is a drawback which prevents the designer to carry out calculations for arbitrary design fires. In this paper, some of the background of the thermal properties given in EN 1995-1-2 is given, and their limitations with regard to different fire scenarios.

In solids heat is transferred by conduction, while heat transfer in gases takes place by radiation and convection. In porous materials heat flux is governed by all three modes of heat transfer. Since wood and charcoal are porous, the temperature development is dependent on all three of them. The physics of heat transfer from a fire compartment into a wood slab forming a boundary of the compartment has been described in several sources, e.g. Kanury (1995), Parker (1995) and Drysdale (1997). For the stage after ignition, the different components of heat flux can be illustrated as shown in Figure 1. The border between wood and the char layer coincides fairly well with the position of the 300-degree isotherm while pyrolysis takes place at different depths (at different temperatures) and at different rates. Apart from conductive heat flux, convective heat flux takes place in the wood due to vaporization of water and its re-condensation in cooler zones, and in the char layer due to reverse flow of cooling pyrolysis gases. Due to the formation of fissures in the char layer, heat transfer is increased due to radiation and convection.

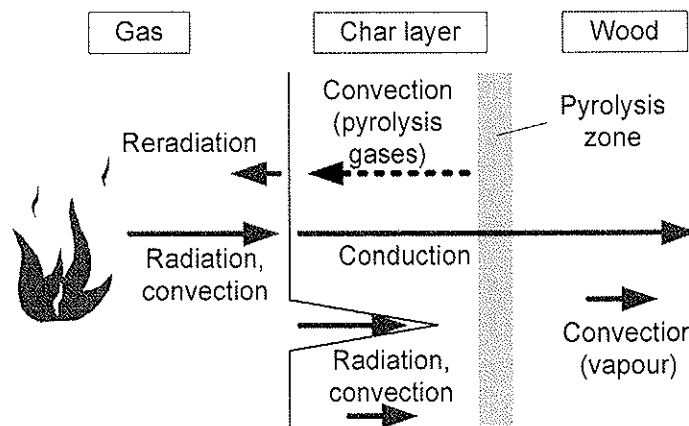


Figure 1 Heat flux components in fire-exposed semi-infinite wood slab

An rigorous analysis of the heat transfer into a wood slab in order to determine the temperature profile in the wood would require a model taking into account mass transport (see e.g. Fredlund, 1988). Unfortunately such models are not developed as easy to use design tools or not yet publicly available, and therefore analyses must be performed using conventional heat transfer models. These heat transfer models and computer codes normally take into account

- conduction in solids;
- radiation in the gas on the fire exposed and ambient side, and in voids;
- convection in the gas at borders between the solid material and the gas;
- the absorption of energy when water is vaporised by introducing a heat sink.

Conductivity values given in different sources vary considerably, see Figure 2 (König et al. 1999, Källsner et al. 2000). There are several reasons: Some may represent physically correct values, obtained from direct measurements, while others may have been determined by

calibration to the results of fire tests. The values by Fredlund (1988) were used in a model that included mass transport.

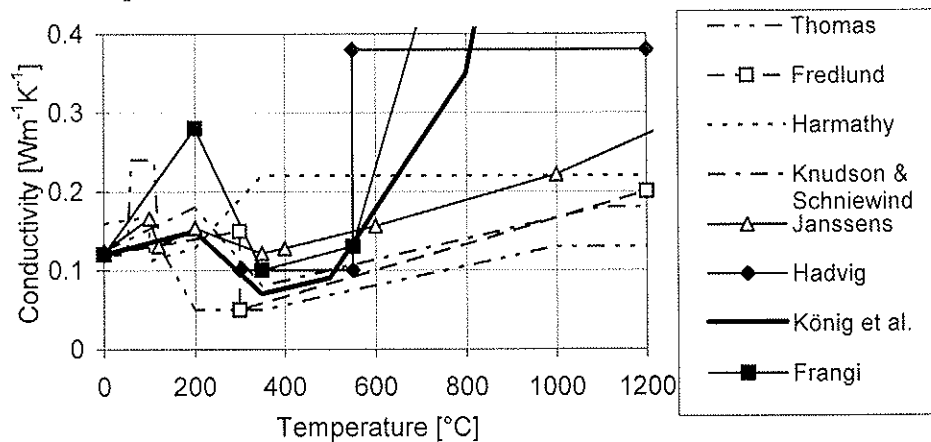


Figure 2 Conductivity vs. temperature of wood and the char layer

The effect of mass transport (e.g. vapour and pyrolysis gases) and the effect of fissures in the charcoal and surface recession of the char layer are often taken into account by applying effective conductivity values rather than the physically correct ones and are normally obtained by calibrating them to test results. When water is vaporised most of the vapour is transferred inwards towards cooler regions of the wood slab until it re-condenses. This energy transport can be modelled by assuming higher conductivity values for temperatures below vaporization temperature, that is about 100°C, and lower conductivity values in the following temperature interval up to about 350°C. This has been done by Thomas (1997), see Figure 2, and similarly by Clancy (2002). The advantage of this manipulation is that the delay of temperature increase beyond 100°C is described in a more realistic way. (This may have consequences when the mechanical resistance is determined, since the temperature around 100°C are significantly sensitive to strength and stiffness reduction of wood.) Apart from this deviation, for wood, i.e. for temperatures below 300°C, most conductivity values shown in Figure 2 are fairly close together. For temperatures greater than 300°C, that is for the char layer, the curves by Hadvig (1981), König et al. (1999) and Frangi (2001) deviate considerably from the others. König et al. (1999) modelled the formation of fissures in the charcoal, starting at about 500°C, and surface recession of the of the char layer by assuming rapidly increasing conductivity values above 500°C. The values by Hadvig (1981) shown in the graph are based on the assumption that the formation of cracks in the char layer takes place at a distance of 6 mm from the char line.

The heat capacity values given by König et al. (1999) were modified in order to fit together with density ratios given by Janssens (1994), see Figure 3, the product of heat capacity c and density ρ are, however, the same. Similarly as above, by modifying Janssens' relationship of density versus temperature, the recession of the surface of the char layer is modelled by assuming that the density of the char-layer decreases linearly to zero between 800 and 1200°C, see Figure 4.

Other authors have modelled the effect of fissures and surface recession of the char layer in a similar way as done König et al., e.g. Povel (2002). Frangi also assumed a heat sink between 200 and 300°C in order to take into account the heat of combustion, similarly as done by Mehaffey et al. (1994). It is, however, highly disputed whether pyrolysis is endothermic or

exothermic (Roberts, 1971); therefore it is neglected by most authors. The introduction of a heat sink to model an endothermic reaction would probably cause higher conductivity values than assumed by König.

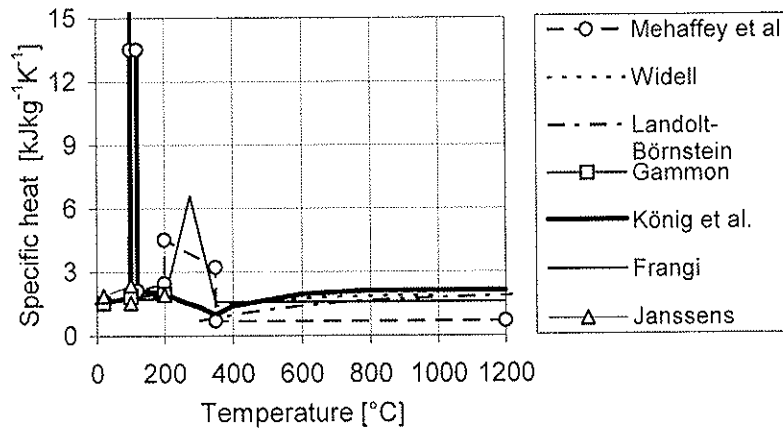


Figure 3 Specific heat values of wood

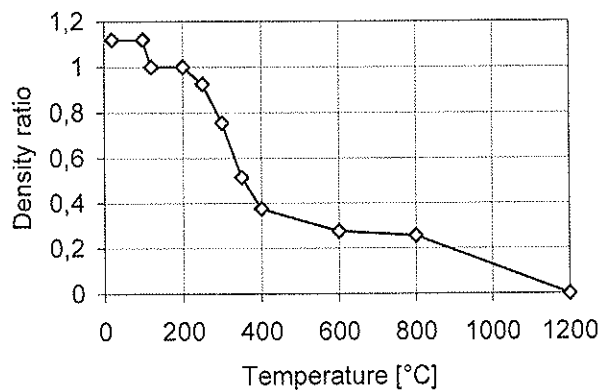


Figure 4 Density of wood/char layer vs. temperature (EN 1995-1-2)

From this discussion can be seen that the choice of thermal properties is strongly dependent on the model used and that there is an interdependence of the properties, mainly conduction and heat capacity: A change of one property can be compensated by another change of the other property.

The values by König et al. (1999), included in the Fire Part of Eurocode 5 (EN-1995-1-2) for application to standard fire scenarios, should only be used when the conventional heat transfer model is applied, that is when mass transport is not explicitly taken into account.

1.2 Reviewing the parametric fire tests by König et al. (1999)

Apart from tests with standard fire exposure, König et al. (1999) also performed six fire tests of timber slabs exposed to natural fires, represented by different parametric fire curves. In three of these tests, C1 to C3, the fire curve corresponded to an opening factor of $0,04 \text{ m}^{0,5}$

and a fire load density of 170 MJ/m^2 related to the total area of the enclosure. In three further tests, C4 to C6, during the heating phase the fire curves corresponded to opening factors of about 0,06 to 0,08. All tests were conducted using a small-scale furnace. The objective of these tests was to verify the charring rates for parametric fire curves given in EN 1995-1-2 which were based on Hadvig (1981) and Toft Hansen et al. (1992). The charring rate during the heating phase is given as

$$\beta_{\text{par}} = k_{\text{par}} \beta_0 \quad (1)$$

where

β_0 is the charring rate for standard fire exposure;

k_{par} is a charring factor dependent on the opening factor O and the absorptivity b of the enclosure.

For the fixed value of the absorptivity given by

$$b = \sqrt{\rho c \lambda} = 1160 \text{ J/m}^2 \text{ s}^{0,5} \text{ K} \quad (2)$$

where ρ is the density, c is the heat capacity and λ is the thermal conductivity of the enclosure, Figure 5 shows the relationship between the opening factor and k_{par} . In this case the opening factor $O = 0,04 \text{ m}^{0,5}$ corresponds to the heating conditions according to the ISO 834 standard fire curve. Correspondingly, for some opening factors, Figure 6 shows the char depth vs. time relationships during the heating phase.

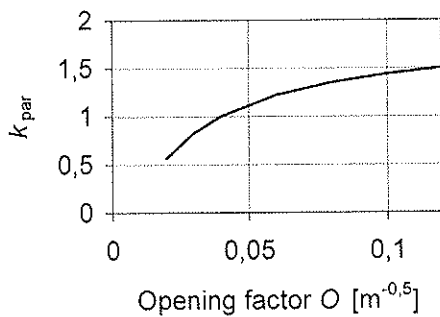


Figure 5 Effect of opening factor on charring factor

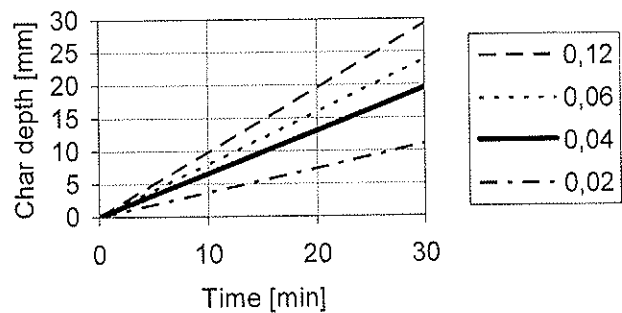


Figure 6 Effect of opening factor on char depth vs. time during heating phase according to EN 1995-1-1

Whereas the experimental results confirm the expressions adopted by EN 1995-1-2, it was seen that, performing heat transfer calculations, the calculated charring rate and char depth was

- *overpredicted during the heating phase for opening factors greater than 0,04, i.e. for a temperature development that is faster than in the standard fire scenario;*
- *underpredicted during the decay phase when temperature is decreasing and the char depth is reaching its maximum value.*

In the following sections results of heat transfer calculations are presented, using the software TCD 5.0 (with Super-Tempcalc).

2 Modelling of the heating phase

For test C4 temperature histories recorded during the heating phase of test C4 are shown in Figure 7 (the position of thermocouples 1 to 6 attached to the surface of the timber and at depths of 6, 18, 30, 42 and 54 mm respectively is shown in Figure 8). The furnace was controlled with a plate thermocouple located 100 mm below the horizontally arranged timber plate. For comparison, the graph also shows the standard fire curve according to ISO 834. Thermocouples were (smooth lines).

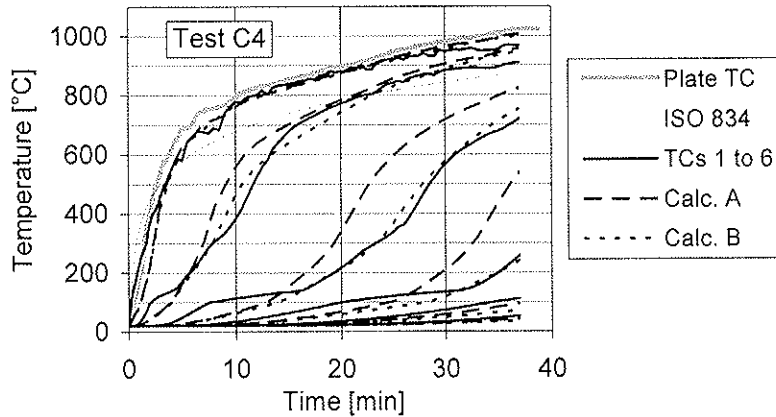


Figure 7 Temperature histories during heating phase of test C4 – Comparison of test results and calculations

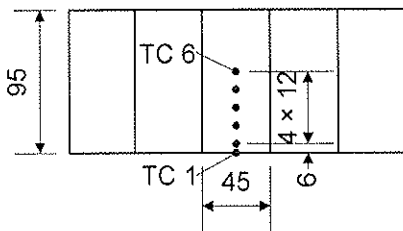


Figure 8 Location of thermocouples

Using the temperature of the plate thermocouple as input thermal action, temperature histories were calculated shown as broken lines. Assuming the thermal conductivity by König et al. (1999), also shown as curve A in Figure 9, the temperature rise at 18 and 30 mm was considerably overpredicted, see the broken lines of Figure 7. Also, the calculated char depth is overpredicted, see Figure 10.

Since the charring rate in the test is greater than the charring rate normally observed for standard fire exposure (which would give a char depth of about 20 mm after 30

minutes) the reverse flow of cooling pyrolysis gases must also be greater. Consequently, the effective conductivity of the char layer, where the reverse flow of cooling gases occurs, must be reduced. Therefore, on a trial and error basis, an alternative relationship B of conductivity and time was chosen with reduced conductivity values in the char layer (where this cooling gas flow occurs) and fitted to the test results. See the dotted lines in Figure 7, 9 and 10.

Similar results (not shown here) were obtained for test C5. For test C6 with a higher gas temperature than in tests C4 and C5, relationship C of Figure 9, implying a further reduction of the effective conductivity of the char layer, gave reasonable agreement with the test results, see Figure 11 and 12.

Vice versa, for fire scenarios with slower heating than during a standard fire exposure, it can be expected that the effective conductivity values of the char layer must be increased, since there is less cooling by pyrolysis gases. In this case, the effective conductivity values valid for standard fire exposure would give non-conservative prediction of the char depth.

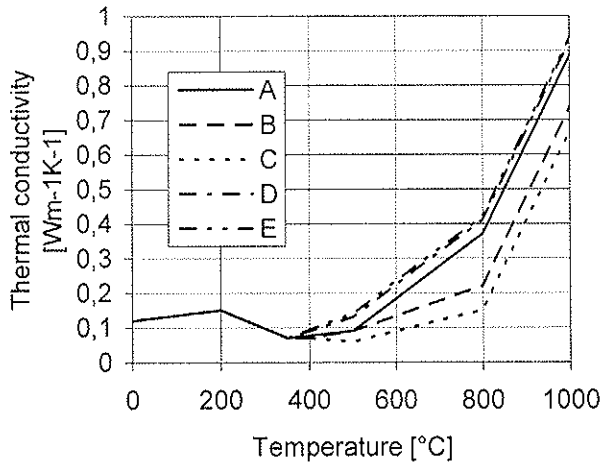


Figure 9 Thermal conductivity values used in the calculations

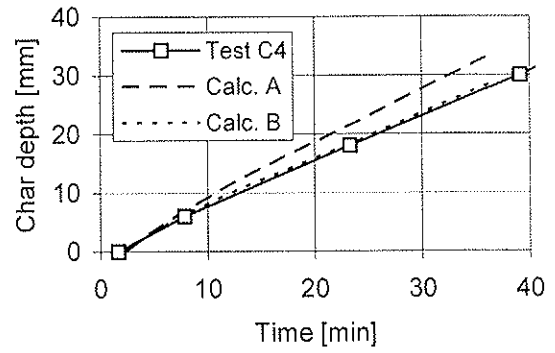


Figure 10 Char depth vs. time during heating phase of test C4 – Comparison of test results and calculations

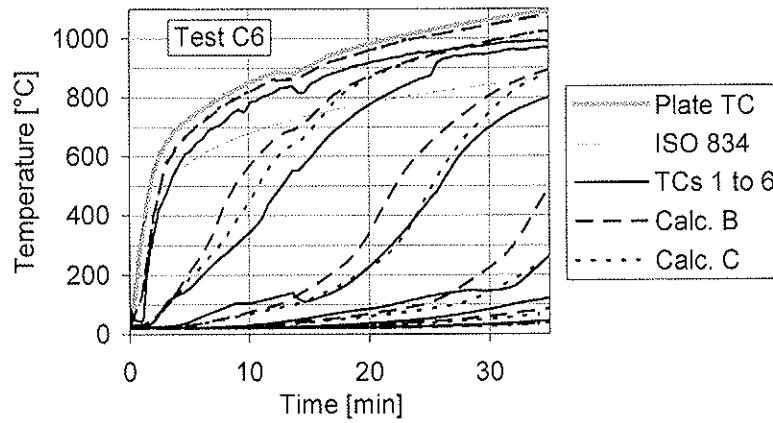


Figure 11 Temperature histories during heating phase of test C6 – Comparison of test results and calculations

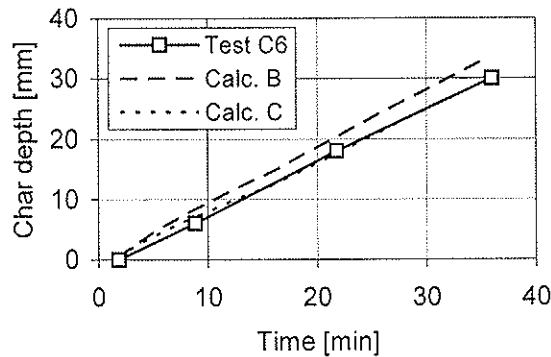


Figure 12 Char depth vs. time during heating phase of test C4 – Comparison of test results and calculations

3 Decay phase

As a consequence of what has been described above, it can be expected that the effective conductivity values of the char layer during the decay phase should increase as the charring rate decreases and finally becomes zero. This measure alone, however, is not sufficient to model heat transfer in a correct way. We will have a look at some typical test results from König et al. (1999) shown in Figure 13 and 14. Having passed the maximum gas temperature in the furnace, during the decay phase, the temperature of, in that order, thermocouples 1 to 4 increase above the gas temperature that was measured with the plate thermocouple. The same can be seen from the temperature profiles shown in Figure 14. The maximum temperature appears to be in the char layer close to its recessing surface and a temperature gradient exists in the gas layer close to the surface.

A reasonable explanation of the occurrence of higher temperatures in the char layer is that glowing combustion starts when increasingly becoming exposed to air (Beyer et al., 1995). Normally, during standard fire exposure, glowing oxidation has no major effect on surface temperature, since “it is unlikely that both glowing combustion of the char and gas-phase combustion can occur simultaneously in the same zone above the surface, since the flow of volatiles through the char will tend to exclude air from direct contact with the char. Therefore, in general, solid-phase char combustion tends to occur after volatilization has largely ended” (Beyer et al., 1995). Char has a rather high heat of oxidation and is susceptible to rapid oxidation at moderate temperatures approximately above 400°C (Ohlemiller, 1995). This statement roughly agrees with Figure 15 showing that the maximum temperature in the char tends to re-approach the gas temperature in the furnace when it decreases below about 400°C. The existence of a temperature gradient in the gas layer close to the char surface is possible since the conditions in the furnace are less turbulent during the decay phase than during the heating phase.

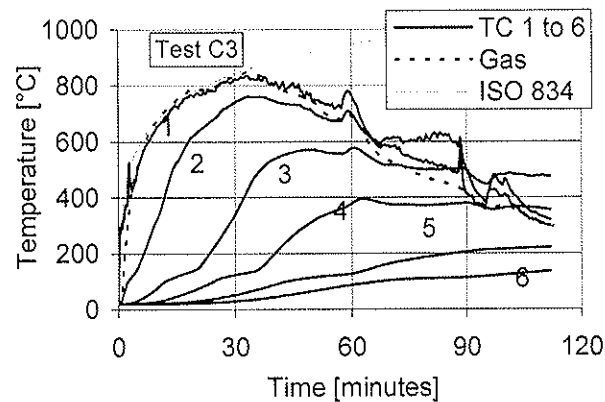


Figure 13 Recorded complete temperature histories for test C3

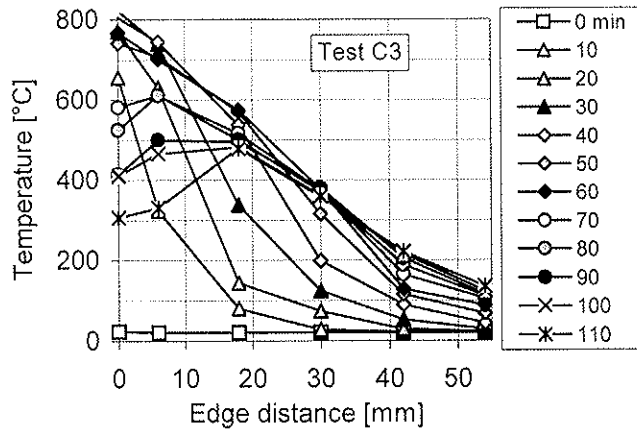


Figure 14 Temperature profiles at specified times

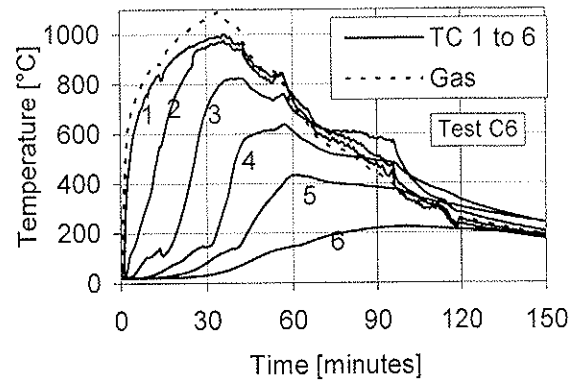


Figure 15 Recorded complete temperature histories for test C6

A heat transfer analysis was carried out, using the temperature recorded by the plate thermocouple as thermal action and the thermal conductivity values according to curve A in Figure 9, that is the same values as given by König et al. (1999) and EN 1995-1-2 (The heat capacity values from the same sources were used in all calculations referred to in this paper). The results show that, during the heating phase, the calculated temperature histories agree fairly well with the test results, while temperature reverses too early in the decay phase (Figure 16). Compared to the test results, the calculated final char depth is too small (Figure 17).

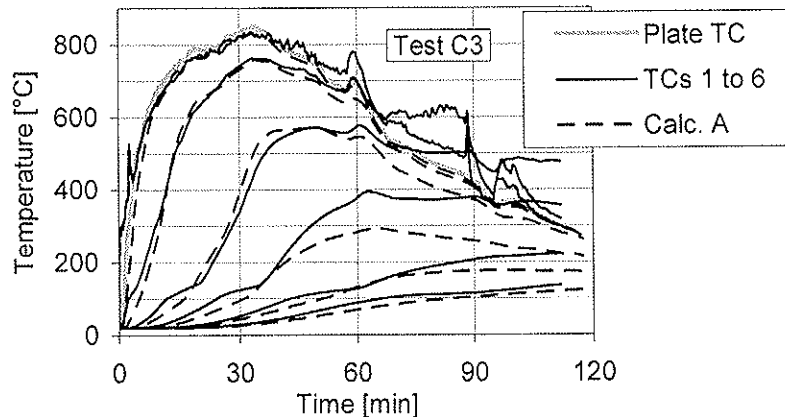


Figure 16 Temperature histories during heating and decay phase of test C3 – Test results and calculation with thermal action as recorded by plate TC

In the next step, during the decay phase, the thermal action fire curve was replaced by a linear curve ending with 400°C at 120 minutes, roughly approximating the maximum temperatures recorded by the thermocouples located at 0, 6, 18 and 30 mm depth. The predicted temperature histories and char depths agreed better with the test results as before (see Figure 17 and 18), however, they were still non-conservative.

In order to reduce this discrepancy, in the following calculations increased conductivity values were used during the decay phase as proposed in the beginning of this section. A

reasonably well fitted results were obtained using curve A for the interval 0 to 37 minutes, curve D for 37 to 45 minutes and curve E for 45 to 112 minutes, see Figure 17 and 19.

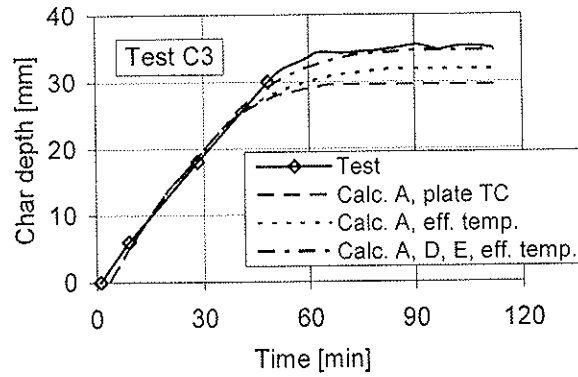


Figure 17 Char depth vs. time of test C4 – Test results and calculations

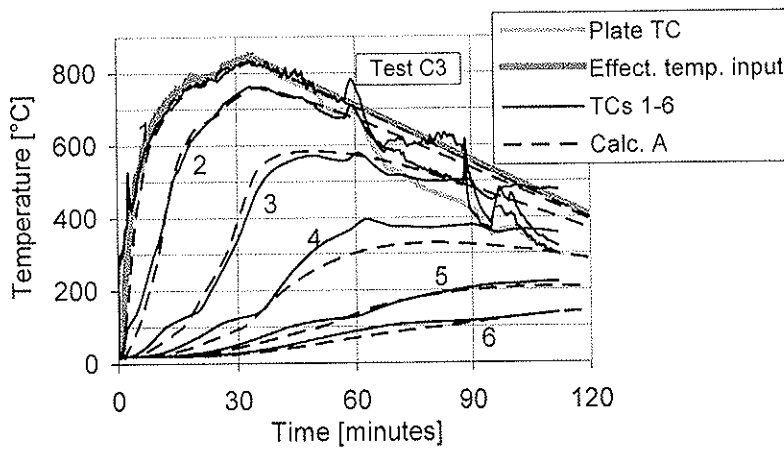


Figure 18 Temperature histories during heating and decay phase of test C3 – Test results and calculation with effective temperature taken as thermal action

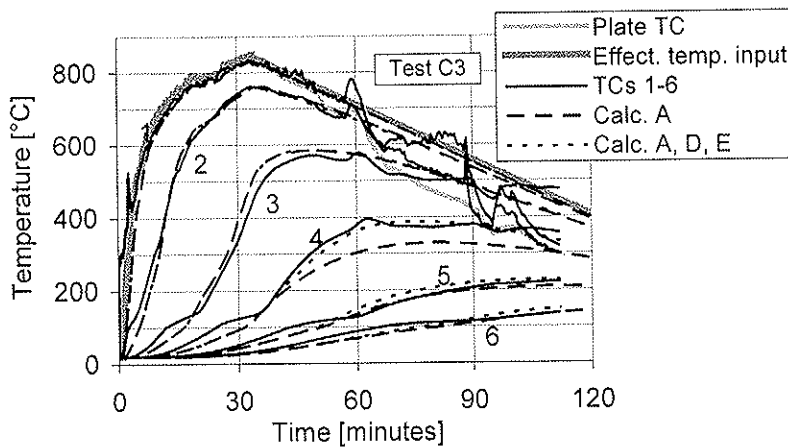


Figure 19 Temperature histories during heating and decay phase of test C3 – Comparison of test results and calculation with effective temperature taken as thermal action and increased conductivity values during decay phase

4 Conclusions

Due to the complex nature of heat transfer in wood and char coal, including phenomena like the formation of fissures in the char layer and the internal convection due to pyrolysis gases and vaporized water, it is necessary to use effective rather than physically correct thermal properties when simplified models are used that do not explicitly take into account mass transport. For timber structures, this need appears to a considerably greater extent than for concrete structures where moisture transport plays a role. The formation of fissures in the char layer due to char contraction has a great influence on the effective conductivity of the char layer.

It has been shown that effective thermal properties that have been verified for standard fire exposure would give incorrect results when applied to other fire scenarios such as parametric fire curves for natural fires. Due to convective cooling due to the reverse flow of pyrolysis gases, the heat flux through the char layer into the wood is delayed. Since this delay is dependent on the rate of charring, the effective conductivity is a function of the charring rate; thus it is also a function of the rate of increase or decrease of temperature.

Char oxidation may occur during the decay phase in natural fires giving rise to char surface temperatures that are considerably above the gas temperature in the furnace or fire compartment. It has been shown that, by assuming effective conductivity values and modified thermal actions using an effective gas temperature in the compartment, good agreement can be obtained between the results from calculations and fire tests.

The present limitation of the use of effective thermal properties should be overcome by deriving them from analytical models that take into account the phenomena described above. Since, for the time being, no such model exists, as an alternative, extensive series of fire tests with various fire scenarios need to be performed. Such fire tests should also be a prerequisite for the validation of models that take into account the relevant parameters governing combustion of wood.

5 Acknowledgement

The investigation described in this paper was funded by Vinnova – Swedish Agency for Innovation Systems.

6 References

- Beyler, C.L. and Hirschler, M.M., 1995, Thermal decomposition of polymers. The SFPE Handbook of Fire Protection Engineering, 2nd edition
- Clancy, P., 2002, A parametric study on the time-to-failure of wood framed walls. Fire Technology, 38, 243-269
- Drysdale, D. D., 1997, Chemistry and physics of fire. National Fire Protection Association, Quincy, Mass.
- EN 1995-1-2:2004 Eurocode 5: Design of timber structures – Part 1-2: General – Structural fire design.
- Frangi, A., 2001, Brandverhalten von Holz-Beton-Verbunddecken. Dissertation, Eidgenössische Technische Hochschule Zürich
- Fredlund, B., 1988, A model for heat and mass transfer in timber structures during fire. Lund

University, Lund

Hadvig, S., 1981, Charring of wood in building fires. Technical University of Denmark, Lyngby

Janssens, M., 1994, Thermo-physical properties for wood pyrolysis models. Pacific Timber Engineering Conference Gold Coast, Australia

Källsner, B. and König, J., 2000, Thermal and mechanical properties of timber and some other materials used in light timber frame construction. Proceedings of CIB W18, Meeting 33, Delft, Paper 33-16-3

Kanury, A. M., 1995, Flaming ignition of solid fuels. The SFPE Handbook of Fire Protection Engineering, 2nd edition

König, J. and Walleij, L., 1999, One-dimensional charring of timber exposed to standard and parametric fires in initially protected and non-protected fire situations. Träteknik – Swedish Institute for Wood Technology Research, Report No. I 9908029

König, J., Norén, J., Bolonius Olsen, F. and Toft Hansen, F., Timber frame assemblies exposed to standard and parametric fires – Part 1: Fire tests

Mehaffey, J. R., Cuerrier, P., Carisse, G., 1994, A model for predicting heat transfer through gypsum board/wood stud walls exposed to fire. Fire and materials, Vol. 18

Ohlemiller, T.J., 1995, Smouldering combustion. The SFPE Handbook of Fire Protection Engineering, 2nd edition

Parker, W. J., 1992, Wood materials. In Barbrauskas, V. and Grayson, S. J. (ed.), Heat release in fires. Elsevier Applied Science, London and New York

Povel, D., 2002, Tragfähigkeit von Holzverbindungen mit stabförmigen Verbindungsmitteln im Brandfall. Dissertation, Technische Universität Berlin

Thomas, G. C., 1997, Fire resistance of light timber framed walls and floors. University of Canterbury, Christchurch, Fire Research Report 97/7

Toft Hansen, F. and Bolonius Olesen, F., 1992. Full-scale tests on loaded glulam beams exposed to natural fires. Department of Building Technology and Struct. Engineering, Aalborg University, Aalborg, Denmark

INTERNATIONAL COUNCIL FOR RESEARCH AND INNOVATION
IN BUILDING AND CONSTRUCTION

WORKING COMMISSION W18 - TIMBER STRUCTURES

FIRE TESTS ON TIMBER CONNECTIONS WITH DOWEL-TYPE FASTENERS

A Frangi

Institute of Structural Engineering, ETH Zürich

A Mischler

University of Applied Science, HSR, Rapperswil

SWITZERLAND

Presented by A Frangi

C Clorius asked how was failure defined and whether deformation criterion was used.

Frangi answered that every failure mode can be observed. It is very difficult to check all of the mode behaviour of the serious damage. Main importance is the loss of cross section.

P Glos asked what additional information was gained from this study as results agreed with previous studies in Germany. Frangi explained that before these tests one did not know the 30 minute rating and now we know the performance of these connections subject to fire more accurately.

P Glos asked whether the German results were referenced. Frangi answered that these tests were done before the German tests but this is the 1st chance that the results were presented and that they were aware of the German results.

Y H Chui asked about the test set up. Frangi answered that the standard ISO test set up was used with the exception that they have to enclose the specimen and they measured the temperature on the surface and made sure that it is standard fire exposure.

J König commented that this work is the most comprehensive set of connection fire test that he has seen. They have the complete set of code reference tests. Test referenced in the Eurocode had only few reference tests so these are weaknesses. Eurocode seemed to be too conservative for this type of dowel connection. He is glad that the improvement due to fire protection agreed well with the Eurocode expression.

A Jorissen expressed surprises at the results of the cover specimen. Frangi explained that in some cases the cover started to fall down quickly leading to variation in the results.

P Glos commented that this would depend on the density of the cover. Frangi answered that more or less the same boards were used and it was just the randomness in the experiment.

R Steiger asked why a reduced load level was used. Frangi responded that 0.3 is the assumed load ratio and other higher levels were reference from the Eurocode.

Fire tests on timber connections with dowel-type fasteners

Andrea Frangi

Institute of Structural Engineering, ETH Zurich, CH-8093 Zurich, Switzerland

Adrian Mischler

University of Applied Science, HSR, CH-8600 Rapperswil, Switzerland

1 Introduction

The present Swiss fire regulations allow the use of combustible materials only for a fire resistance of up to 30 minutes. With the revision of the fire regulations in the year 2005 the fire authorities will allow the use of timber also for the fire resistance class of 60 minutes. This will lead to new markets for timber, particularly for multi-storey buildings.

As the existing design rules for timber connections in fire are only valid for fire resistances up to 30 minutes, a large research project on the fire behaviour of timber connections is currently carried out in Switzerland sponsored by the Swiss Agency for the Environment, Forests and Landscape [1]. The research project aims to enlarge the theoretical and experimental background of the fire behaviour of connections used in modern structural timber engineering. The application of the existing design rules for a fire resistance of 60 minutes will be checked based on the results of experimental tests. Further, new design models for timber connections with fire resistances of 60 minutes will be developed and validated. The design models should be published in a revised SIA Documentation 83 [2], commonly used in Switzerland for fire resistance calculations of timber structures.

From the variety of timber connections, mainly multiple shear steel-to-timber connections with dowels and slotted-in steel plates are studied in the ongoing research project. In recent years, the load-carrying capacity of this type of connection has been thoroughly investigated at the Swiss Federal Institute of Technology of Zurich (ETH) [3,4]. Besides of a high load-carrying capacity and a ductile failure mode, the advantage of this connection is the protection of the slotted-in steel plates against the fire. Therefore a high fire resistance may be achieved.

As experimental tests on timber connections subjected to fire have been recently performed mainly using timber-to-timber connections [5,6,7], the fire behaviour of steel-to-timber connections was experimental analysed with an extensive testing programme. Further, the fire tests were completed by a series of tests at room temperature. The paper describes the main results of the tests conducted on timber connections.

2 Test programme and test parameters

Two different types of connections were tested:

- multiple shear steel-to-timber connections with dowels of diameter 6.3 and 12 mm
- connections with steel side plates and annular ringed shank nails of diameter 4 mm

For the multiple shear steel-to-timber connections with dowels following test parameters were varied:

- load level during the fire tests ($0.3 \cdot F_u$, $0.15 \cdot F_u$ and $0.075 \cdot F_u$ with F_u = load-carrying capacity at room temperature)
- number and configuration of the steel dowels (9x2, 9x3, 3x3 and 4x2)
- timber cover of connection (thickness of outer timber members, edge and end distances)
- diameter of the steel dowels (6.3 mm and 12 mm)

In addition to the unprotected connections some connections were tested protected by timber boards or gypsum plasterboards. For the connections with steel side plates and annular ringed shank nails only the influence of load level during the fire tests as well as the protection of the steel side plates by a fire-proof coat were studied.

Five specimens of each connection type were tested at room temperature. For each connection type and load level two tests were performed under ISO-fire exposure. Table 1 gives an overview of the 30 tests conducted at room temperature and the 26 fire tests.

Table 1 Overview of the experimental tests

connection type	number of tests	test type	load level	remarks
D 01.1	5	room temperature	until failure	9x2 steel dowels diameter dowels: d = 6.3 mm timber cross-section: 200/200 mm
	2	fire test	$0.3 \cdot F_{u,D 01.1}$	
	2	fire test	$0.15 \cdot F_{u,D 01.1}$	
	2	fire test	$0.075 \cdot F_{u,D 01.1}$	
D 01.2	5	room temperature	until failure	9x2 steel dowels diameter dowels: d = 6.3 mm timber cross-section: 280/280 mm
	2	fire test	$0.3 \cdot F_{u,D 01.2}$	
D 01.3	2	fire test	$0.3 \cdot F_{u,D 01.1}$	same as D 01.1, connection protected by 27 mm thick timber boards
D 01.4	2	fire test	$0.3 \cdot F_{u,D 01.1}$	same as D 01.1, connection protected by 15 or 18 mm thick gypsum plasterboards
D 02.1	5	room temperature	until failure	9x3 steel dowels diameter dowels: d = 6.3 mm timber cross-section: 200/200 mm
	2	fire test	$0.3 \cdot F_{u,D 02.1}$	
D 03.1	5	room temperature	until failure	3x3 steel dowels diameter dowels: d = 6.3 mm timber cross-section: 200/200 mm
	2	fire test	$0.3 \cdot F_{u,D 03.1}$	
D 04.1	5	room temperature	until failure	4x2 steel dowels diameter dowels: d = 12 mm timber cross-section: 200/200 mm
	2	fire test	$0.3 \cdot F_{u,D 04.1}$	
N 01.1	5	room temperature	until failure	9x6 nails diameter dowels: d = 4.0 mm timber cross-section: 120/180 mm
	2	fire test	$0.3 \cdot F_{u,N 01.1}$	
	2	fire test	$0.15 \cdot F_{u,N 01.1}$	
N 01.2	2	fire test	$0.3 \cdot F_{u,N 01.1}$	same as N 01.1, steel plates protected by a 2 mm thick fire-proof coat
	2	fire test	$0.15 \cdot F_{u,N 01.1}$	

3 Test specimens

3.1 Material properties

The specimens consisted of glued laminated timber (spruce) grade GL 24h according to EN 1194 [8]. In order to avoid a failure of the timber cross-section, glued laminated timber grade GL 36h according to EN 1194 was used for the specimen D 02.1. For all specimens the moisture content and the density were measured. Table 2 gives an overview of the timber properties of the specimens.

Table 2 Timber properties of the specimens

connection type	test type	moisture	density			density at 12% moisture content		
		mean value [%]	mean value [kg/m ³]	coef. of variation [%]	5% fractile [kg/m ³]	mean value [kg/m ³]	coef. of variation [%]	5% fractile [kg/m ³]
dowelled connection	room temp.	10	452	4.0	423	457	4.1	426
	fire test	10	442	4.9	407	446	4.9	410
nailed connection	room temp.	8.5	432	4.4	401	439	4.4	407
	fire test	9.0	441	3.1	419	447	3.0	425

The characteristic yield strength and tensile strength of the steel plates used was 355 N/mm² and 510 N/mm², respectively. The tensile strength of the steel dowels was determined with 3 tensile tests. The mean tensile strength of the steel dowels with diameter of 6.3 and 12 mm was 598 N/mm² and 636 N/mm², respectively.

3.2 Multiple shear steel-to-timber connections with dowels

The geometry of the multiple shear steel-to-timber connections with dowels and slotted-in steel plates is shown in the following figures. The thickness of the steel plates was 5 mm. The diameter of the steel dowels was 6.3 mm with the exception of the connection D 04.1. For this connection the diameter of the steel dowels was 12 mm.

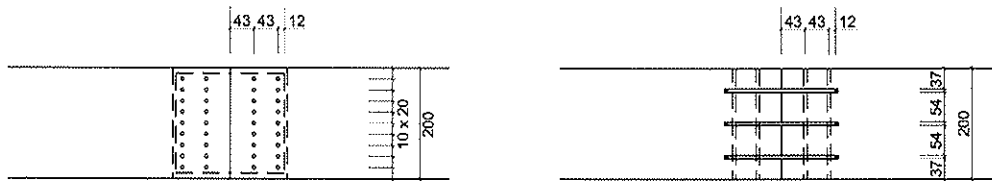


Figure 1 Connection D 01.1, 9x2 steel dowels

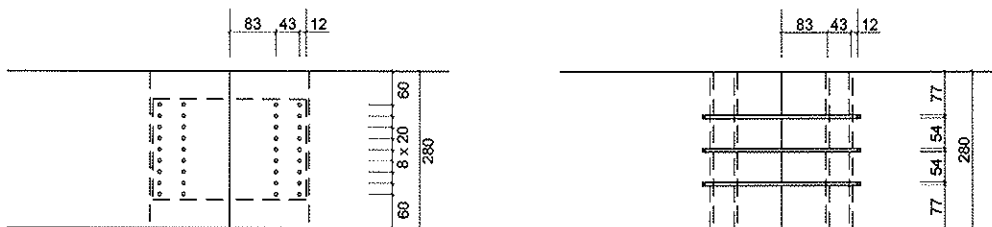


Figure 2 Connection D 01.2, 9x2 steel dowels, timber covers of the connection increased by 40 mm

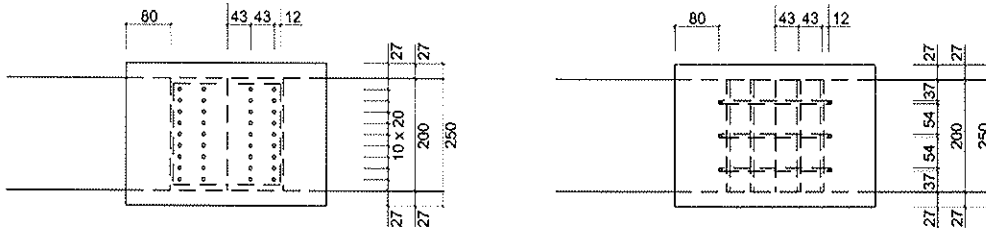


Figure 3 Connection D 01.3, 9x2 steel dowels, connection protected by 27 mm thick timber boards, fixed by galvanised nails 2.0 x 50 mm

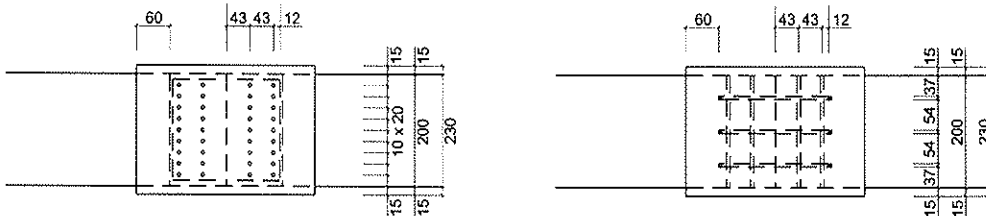


Figure 4 Connection D 01.4, 9x2 steel dowels, connection protected by „Fermacell“ gypsum plasterboards of 15 or 18 mm thickness, fixed according to technical rules of the manufacturers

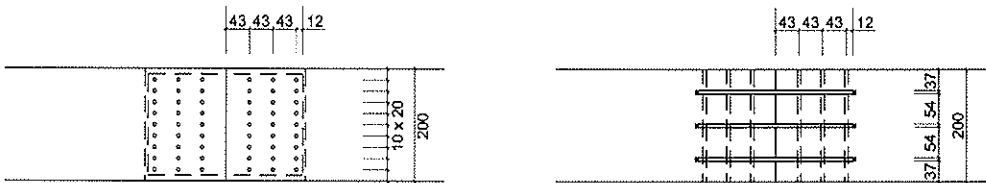


Figure 5 Connection D 02.1, 9x3 steel dowels

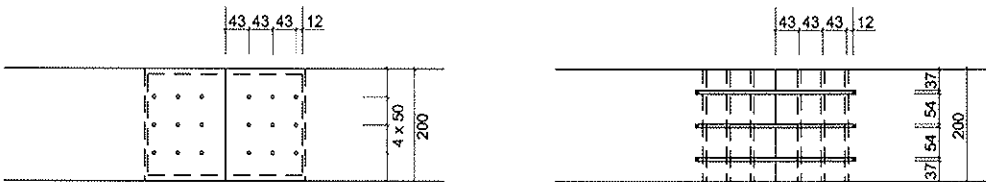


Figure 6 Connection D 03.1, 3x3 steel dowels



Figure 7 Connection D 04.1, 4x2 steel dowels with diameter of 12 mm

3.3 Connections with steel side plates and annular ringed shank nails

The geometry of the connections with steel side plates and annular ringed shank nails is shown in the following figure. The thickness of the steel side plates as well as the diameter of the annular ringed shank nails was 4.0 mm.

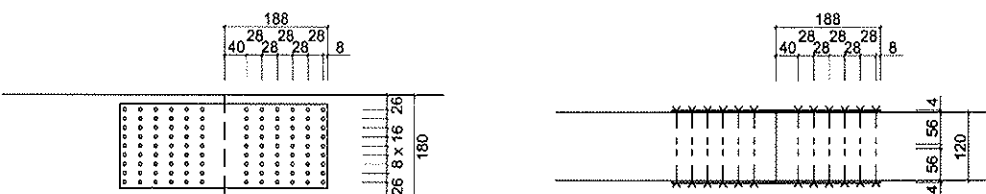


Figure 8 Connection N 01.1 and N 01.2 (the steel side plates of the connection N 01.2 were protected by a 2 mm fire-proof coat)

4 Tests at room temperature

4.1 Test specimens and test arrangement

Five specimens of each connection type were tested at room temperature according to standard EN 26891 [9]. The tests were carried out at the ETH in Zurich using the tension testing machine of the Structural Engineering Laboratory. Figure 9 shows the typical geometry of the test specimens. The connections were tested in tension parallel to the grain direction of the timber member.

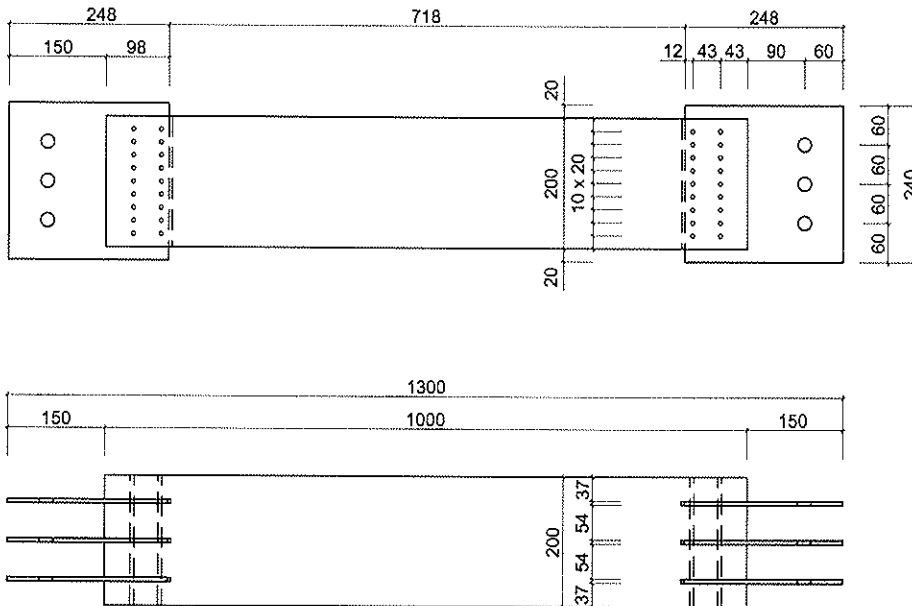


Figure 9 Geometry of the specimens for the tensile tests at room temperature (as example the connection D 01.1 is shown in the figure)

The loading curve according to EN 26891 as well as the load levels for the different connections are given in Table 3. The load-carrying capacity F_{cst} was estimated based on tests conducted in previous research projects. During the tests the load as well as the displacement was continuously measured.

Table 3 Loading curve and load levels for the different connections tested

connection type	$0.4 \cdot F_{\text{cst}}$ [kN]	$0.1 \cdot F_{\text{cst}}$ [kN]	$0.7 \cdot F_{\text{cst}}$ [kN]	$1.0 \cdot F_{\text{cst}}$ [kN]
D 01.1	200	50	350	500
D 01.2	236	59	413	590
D 02.1	252	63	441	630
D 03.1	100	25	175	250
D 04.1	184	46	322	460
N 01.1	112	28	196	280

4.2 Test results

Table 4 gives the failure loads for all tensile tests at room temperature. As statistical values also the mean values, the coefficient of variations as well as the 5% fractiles are given in

Table 4. A ductile failure due to plastic deformations of the steel dowels was observed for almost all tests.

Table 4 Failure loads for all tensile tests at room temperature

connection type	test number					mean value [kN]	coef. of variation [%]	5% fractile [kN]
	1	2	3	4	5			
D 01.1	487	506	522	422	473	482	8.0	419
D 01.2	551	584	568	610	577	578	3.8	542
D 02.1	651	571	595	668	649	627	6.6	558
D 03.1	227	220	240	235	230	230	3.3	218
D 04.1	404	426	423	404	415	414	2.5	397
N 01.1	287	307	283	326	290	299	6.0	269

The theoretical load-carrying capacity R_u of the connections was calculated using the plastic model given in SIA 265 [10] as well as in EN 1995-1-1 [11] and compared to the test results (see table 5). For the calculation the mean values of the measured densities r_w at 12% moisture content as well as the effective tensile strengths of the steel dowels were assumed. From table 5 it can be seen that the load-carrying capacities of the connections calculated according to SIA 265 are in good agreement with the test results, on the other hand the EN 1995-1-1 gives more conservative results.

Table 5 Comparison between test results and calculated load-carrying capacities

connection type	$r_{w=12\%}$ [kg/m ³]	$F_{u,test}$ [kN]	$R_{u,SIA\ 265}$ [kN]	$R_{u,EN\ 1995-1-1}$ [kN]
D 01.1	437	482	490	396
D 01.2	484	578	580	443
D 02.1	446	627	702	578
D 03.1	456	230	237	195
D 04.1	460	414	414	291
N 01.1	439	299	279	169

5 Tests under ISO-fire exposure

5.1 Test specimens and test arrangement

The fire behaviour of the connections subjected to tension parallel to the grain direction of the timber members was experimentally analysed with the test arrangement as shown in figure 10.

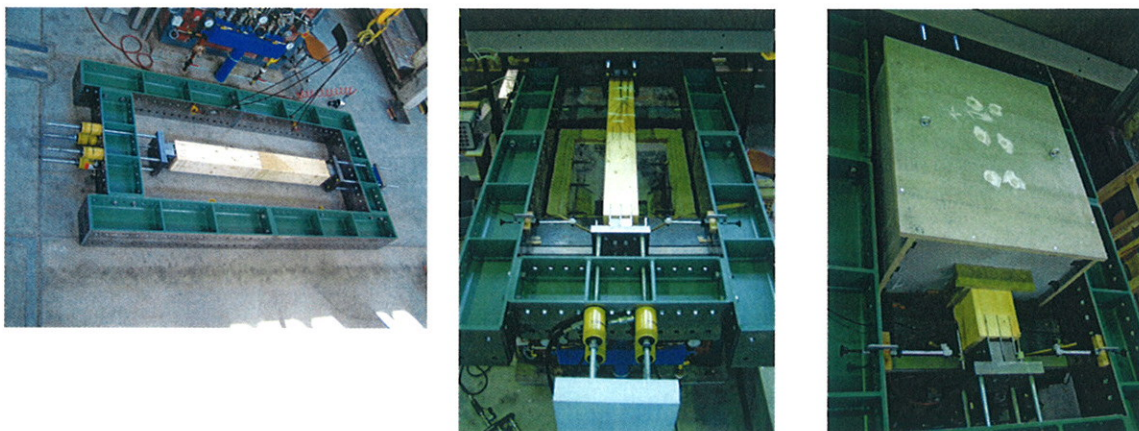


Figure 10 Test arrangement for the tensile tests under ISO-fire exposure

The fire tests were carried out on the small furnace (1.0x0.8 m) at the Swiss Federal Laboratories for Materials Testing and Research (EMPA) in Dübendorf and performed according to standard EN 1363-1 [12]. Figure 11 shows the typical geometry of the test specimens. The specimens were loaded with the defined load level ($0.3 \cdot F_u$, $0.15 \cdot F_u$ or $0.075 \cdot F_u$) about 15 minutes before the start of the fire test and then exposed to the ISO-fire until failure of the connection. For each connection type and load level two fire tests were performed (see table 1).

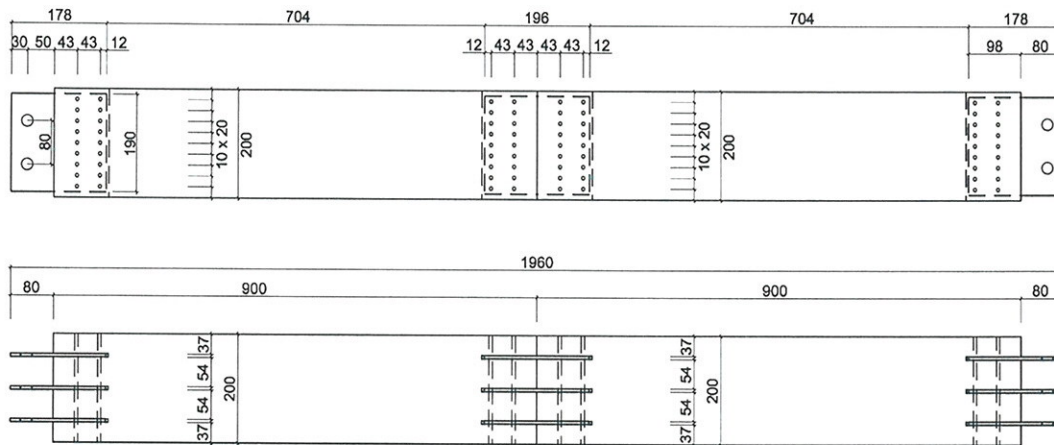


Figure 11 Geometry of the specimens for the tensile tests under ISO-fire exposure (as example the connection D 01.1 is shown in the figure)

During the tests, the temperature at selected locations was measured and recorded every minute with thermocouples of chromel-alumel, type K. At the end of the fire tests, the burners were immediately turned off, the specimen was removed and the fire was extinguished with water.

5.2 Results and discussion of the tests with dowels

After the fire tests, the outer timber members were completely charred. However during the fire tests the char-layer did not fall into the furnace, so that the slotted-in steel plates were not exposed directly to fire (see figure 12 left and center). An increased charring was observed on the upper and lower side by the internal timber members, thus the steel dowels located close to the edges of the timber members were completely embedded in charred wood (see figure 12 right). Table 6 gives failure times and failure modes for all fire tests with multiple shear steel-to-timber connections with dowels.

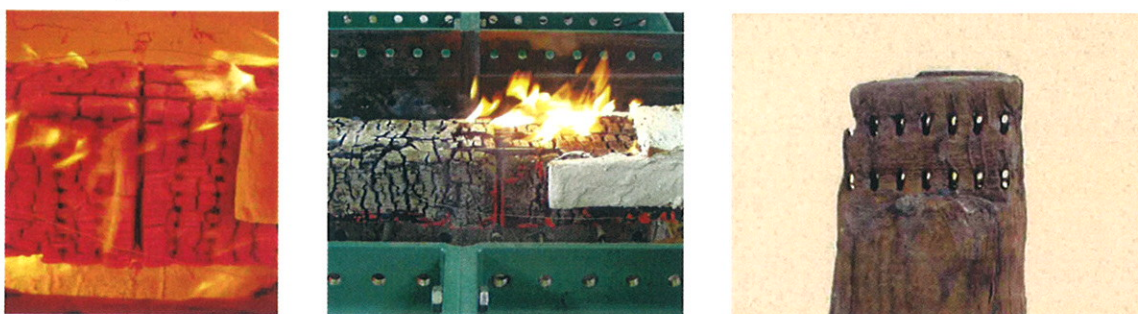


Figure 12 Test specimen D 01.1 during the fire test (left), at the end of the test (center) and after removing the char-layer (right)

The connection D 01.1 loaded with $0.3 \cdot F_u$ failed after 32 and 34 minutes, respectively. A reduction of the load level to $0.15 \cdot F_u$ and $0.075 \cdot F_u$ led only to an increased failure time of about 3 and 8 minutes, thus the load level seems not to be a relevant design parameter in order to increase the fire resistance of the connection. It is interesting also to observe that small plastic deformations of the steel dowels were observed for the connections loaded with $0.3 \cdot F_u$. However at load levels of $0.15 \cdot F_u$ and $0.075 \cdot F_u$ the steel dowels did not show

any plastic deformations more, on the other hand increased deformations due to embedment failure of the timber members were observed.

Table 6 Failure times and failure modes for all tensile tests with dowels under ISO-fire

connection type	load level [kN]	test number	failure time [minutes]	failure mode
D 01.1	$0.3 \cdot F_{u,D 01.1} = 145$	1	32	steel dowel deformations, timber embedment failure, net cross-section
		2	34	
	$0.15 \cdot F_{u,D 01.1} = 72$	1	38	timber embedment failure, timber splitting
		2	34.5	
	$0.075 \cdot F_{u,D 01.1} = 36$	1	41.5	timber embedment failure, timber splitting
		2	41	
D 01.2	$0.3 \cdot F_{u,D 01.2} = 173$	1	73	net cross-section, timber embedment failure
		2	73	
D 01.3	$0.3 \cdot F_{u,D 01.1} = 145$	1	72	net cross-section, block shear failure
		2	57	
D 01.4	$0.3 \cdot F_{u,D 01.1} = 145$	1	60.5	net cross-section, block shear failure
		2	61	
D 02.1	$0.3 \cdot F_{u,D 02.1} = 188$	1	30.5	net cross-section, block shear failure
		2	32	
D 03.1	$0.3 \cdot F_{u,D 03.1} = 69$	1	32	timber splitting
		2	33	
D 04.1	$0.3 \cdot F_{u,D 04.1} = 124$	1	34.5	steel dowel deformations, timber embedment failure
		2	35	

The failure times of the connections D 02.1, D 03.1 and D 04.1 loaded with $0.3 \cdot F_u$ varied between 30.5 and 35 minutes and were very similar to those of the connections D 01.1 loaded at the same level. Thus a reduction or increase of the number of the dowels (connections D 02.1 and D 03.1), as well as an increased of the diameter of the steel dowels (connections D 04.1) did not significantly improve the fire resistance of the connections. Although for these connections different failure modes were observed, it can be expected that the fire resistances of multiple shear steel-to-timber connections with dowels and slotted-in steel plates loaded with 30% of F_u is around 30 minutes.

For the connection D 01.2 the timber dimensions were increased from 200x200 mm to 280x280 mm, thus the timber covers of the slotted-in steel plates as well as the steel dowels facing the edges were increased of 40 mm. Also the end distances to the dowels were increased of 40 mm. For both fire tests the connection failed after 73 minutes, thus showing a much higher fire resistance in comparison with the other connections tested. The observed increased fire resistance by about 40 minutes in comparison to the connection D 01.1 corresponds to an improvement of about 1 minute for 1 mm of increased timber cover of the connection.

The connections D 01.3 and D 01.4 were protected by timber boards and gypsum plasterboards. The failure times of the connections protected by timber boards were 72 and 57 minutes. The observed high fire resistance for the first fire test may be due to a wrong position of the specimen in the furnace. The connections protected by gypsum plasterboards failed after 60 and 60.5 minutes, respectively. Thus by protecting the connection the fire resistance was increased by about 25 minutes, which for the 27 mm thick timber board correspond to an improvement of about 1 minute for 1 mm timber protection of the connection. It is further interesting to observe that the protected connections failed due to tensile failure of net cross-sections combined with block shear failure.

5.3 Results and discussion of the tests with nails

Table 7 gives failure times and failure modes for all fire tests on connections with steel side plates and annular ringed shank nails.

Table 7 Failure times and failure modes for all tensile tests with nails under ISO-fire

connection type	load level [kN]	test number	failure time [minutes]	failure mode
N 01.1	$0.3 \cdot F_{u,N 01.1} = 90$	1	11.5	nail deformations, timber embedment failure
		2	12	
	$0.15 \cdot F_{u,N 01.1} = 45$	1	14	nail deformations, timber embedment failure
		2	12.5	
N 01.2	$0.3 \cdot F_{u,N 01.1} = 90$	1	31	net cross-section, block shear failure
		2	28.5	
	$0.15 \cdot F_{u,N 01.1} = 45$	1	35.5	net cross-section, block shear failure
		2	38	

Due to the steel side plates exposed directly to fire, the connections with steel side plates and annular ringed shank nails showed increased deformations from beginning of the fire test in comparison with multiple shear steel-to-timber connections with dowels and as results of large deformations of the nails the unprotected connections N 01.1 loaded with $0.3 \cdot F_u$ already failed after 11.5 and 12 minutes, respectively.

The connection N 01.1 loaded with $0.15 \cdot F_u$ failed after 14 and 12.5 minutes, respectively. A reduction of the load level led only to an increased failure time of about 2 minutes, thus also for the connections with steel side plates and nails the load level seems not to be a relevant design parameter in order to increase the fire resistance of the connection.

The steel side plates of the connection N 01.2 were protected by a 2 mm thick fire-proof coat. The failure times of the connections loaded with $0.3 \cdot F_u$ were 31 and 28.5 minutes. Thus by protecting the connection the fire resistance was increased by about 18 minutes. A reduction of the load level led only to an increased failure time of about 7 minutes.

6 Conclusions

The structural behaviour of timber connections was experimental analysed by a series of tests at room temperature as well as under ISO-fire exposure. From the variety of timber connections, multiple shear steel-to-timber connections with dowels and slotted-in steel plates and connections with steel side plates and annular ringed shank nails are studied in the ongoing research project.

The tests at room temperature on multiple shear steel-to-timber connections with dowels and slotted-in steel plates showed high load carrying capacities as well as a ductile failure due plastic deformations of the steel dowels.

All unprotected multiple shear steel-to-timber connections with dowels tested under constant load of $0.3 \cdot F_u$ and subjected to ISO-fire exposure showed failure times between 30.5 und 35 minutes. A reduction of the load level to $0.15 \cdot F_u$ and $0.075 \cdot F_u$ led only to an increased failure time of about 3 and 8 minutes. A variation of the number or diameter of the steel dowels improved the fire resistance of max. 2 minutes. It can be generally concluded that the fire resistance of multiple shear steel-to-timber connections with dowels and slotted-in steel plates loaded with $0.3 \cdot F_u$ is around 30 minutes. The connections with dowels protected by timber boards or gypsum plasterboards showed failure times of around 60 minutes. By increasing the timber covers of the steel dowels and the slotted-in steel plates as well the end distance to the dowels by 40 mm, the fire resistance of the connections reached more than 70 minutes. Thus, from a fire design point of view these modifications were very favourable in order to increase significantly the fire resistance of the connections.

Unprotected connections with steel side plates and annular ringed shank nails failed already after about 12 minutes due to large deformations of the nails and the steel side plates directly exposed to fire. By protecting the steel side plates by a fire proof-coat the fire resistance of the connections was increased up to around 30 minutes.

The test results permit to check the design rules given in EN 1995-1-2 [13] (Eurocode 5) and to verify advanced calculation models recently developed by Povel [14]. Further, new simplified design models for timber connections with fire resistances of 60 minutes will be developed and compared to the test results. The temperature development will be also analysed using a FE-model. The design models should be published in a revised SIA Documentation 83.

7 References

- [1] Kolb, J., *Brandschutz in der Schweiz: das Projekt Brandsicherheit und Holzbau*, 10. DGfH-Brandschutz-Tagung 2004, Berlin, Proceedings published by German Society for Wood Research (DGfH), Munchen.
- [2] SIA 83 (Documentation): *Brandschutz im Holzbau*, Swiss Society of Engineers and Architects, Zurich, 1997.
- [3] Mischler, A., *Bedeutung der Duktilität für das Tragverhalten von Stahl-Holz-Bolzenverbindungen*, PhD Thesis No. 12561, ETH Zurich, 1998.
- [4] Gehri, E., Mischler, A., *Multiple shear steel-to timber joints*, in Madsen, B., *Behaviour of Timber Connections*, Timber Engineering Ltd., North Vancouver, Canada, 2000.
- [5] Norén, J., *Load-bearing Capacity of Nailed Joints exposed to Fire*, Fire and Materials, Vol. 20, December 1996.
- [6] Dhima, D., *Verification expérimentale de la résistance au feu des assemblages d'éléments en bois*, Département Incendie et Essais, CTICM, France, Ref. INC-99/399-DD/NB, 1999.
- [7] Kruppa, J., Lamadon, T., Racher, P., *Fire resistance tests on timber connections*, Département Incendie et Essais, CTICM, France, Ref. INC-00/187-JK/NB, 2000.
- [8] EN 1194: *Timber structures - Glued laminated timber - Strength classes and determination of characteristic values*, CEN, Brussel, 1999
- [9] EN 26891: *Timber structures. Joints made with mechanical fasteners. General principles for the determination of strength and deformation characteristics*. CEN, Brussel, 1991.
- [10] SIA 265 (Swiss Standard): *Holzbau (Timber)*, Swiss Society of Engineers and Architects, Zurich, 2003.
- [11] EN 1995-1-1 (Eurocode 5): *Design of timber structures, Part 1-1: General-Common rules and rules for buildings*, Final Draft, CEN, Brussel, December 2003, Final draft accepted and to be published in 2004.
- [12] EN 1363-1: *Fire resistance tests - Part 1: General requirements*, CEN, Brussel, 1999.
- [13] EN 1995-1-2 (Eurocode 5): *Design of timber structures, Part 1-2: General-Structural fire design*, Final Draft, CEN, Brussel, December 2003, Final draft accepted and to be published in 2004.
- [14] Povel, D., *Tragfähigkeit von Holzverbindungen mit stabförmigen Verbindungsmitteln im Brandfall*, PhD Thesis, Technical University Berlin, Fraunhofer IRB Publisher, Mai 2002.

INTERNATIONAL COUNCIL FOR RESEARCH AND INNOVATION
IN BUILDING AND CONSTRUCTION

WORKING COMMISSION W18 - TIMBER STRUCTURES

DETERMINATION OF FRACTURE MECHANICS PARAMETERS
FOR WOOD WITH THE HELP OF CLOSE RANGE PHOTOGRAMMETRY

S Franke
B Franke
K Rautenstrauch

Institute of Structural Engineering
Bauhaus-University Weimar

GERMANY

Presented by S Franke

A Asiz received clarification on the resistance curves.

B Yeh asked about the costs. S Franke responded that the costs of the equipment are less than 10000 Euro and the costs per test is 3 Euro.

Determination of fracture mechanics parameters for wood with the help of close range photogrammetry

Dipl.-Ing. Steffen Franke

Dipl.-Ing. Bettina Franke

Prof. Dr.-Ing. Karl Rautenstrauch

Institute of Structural Engineering

Chair of Timber and Masonry Engineering,

Bauhaus-University of Weimar, Germany

1 Introduction

An especially developed procedure, based on digital close range photogrammetry and image processing, enables the measuring of the progression of deformations, cracks and deteriorations during the loading and unloading of specimens. The significance of a test can be substantially increased by applying measuring marks or imaging the specimens surface. The contactless determination of the coordinates is done by a photo sequence over the total duration of the test followed by automated evaluation with the program OSPREY. As the evaluation is done in the post process, a frequency can be achieved in the test of up to 2 Hz. The gathered displacements of the coordinates of the measuring marks or other geometrical marks are easily transferable for a following processing in a numeric simulation by a Finite-Element-Program. The high degree of precision of this method of measurement in conjunction with the advantages of contact-free measurement give the opportunity to achieve a new quality in measuring deformations and the interpretation of mechanical conditions. With the achieved results, which have an accuracy in micrometer range, new insights could be obtained for timber construction.

2 Development of the Measuring System and its Application

2.1 System Components

The basis of the new measuring system is a high-resolution digital colour camera with a telecentric measuring objective. The camera has a resolution of 2580 x 1944 pixels with a picture rate of 5 images/second. The CCD- matrix camera sends a digital picture, which is transferred through the framegrabber to the PC. With the help of various software, the

image information can be taken out for processing and further analysis routines. Based on pure 2D-measurement, the specimens can move slightly depth wise without creating a distortion on the measuring results. Objectives with a smaller magnification provide a better clearness in the measuring field but they create fewer pixels in the figure of the marks and thus a higher uncertainty of measurement.

The contrast and the evenly distributed lighting of the entire image field are decisive for the results of measurement. Since the applied software requires a grey tone picture for the optical determination of the coordinates of the measuring points, the measuring field is lighted by a source of infrared light for the close infrared range. When simultaneously switching off the interpolation routines, the camera behaves like a grey tone camera with 5 million pixels. For marking the wood surface, the pretreatment of the surface with a white wax glaze combined with transfer marks applied afterwards turned out to be a good method. A sufficient black-white contrast is obtained by this combination, which provides the necessary grey tones by the infrared lighting. The transfer marks vary in diameter from 0.6 to 2.0 mm. This procedure of marking the specimens does not interfere or even destroy their structure as penetrating marks such as pins or drawing pins would do.

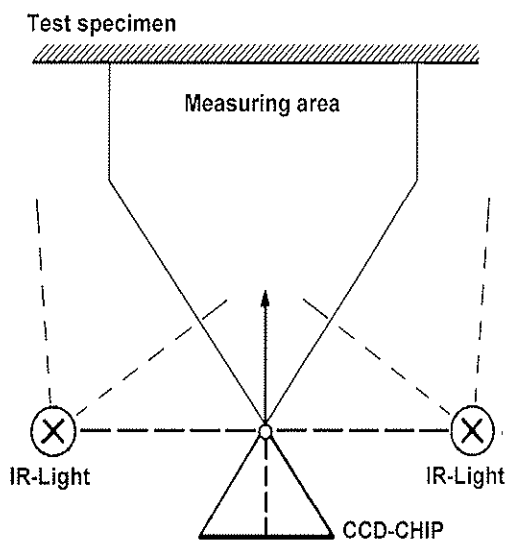


Figure 1: Measuring arrangement (sketch)



Figure 2: Measuring camera with IR-light

2.2 Application Routine

At first the specimens are marked with the measuring marks. During the test the coupling of the force signal and the picture sequence is necessary for the later evaluation of the results. Applying a suitable automation, it is presently possible to measure with a frequency of up to 2 Hz under real test conditions. The determination of the coordinates of the applied measuring points is carried out by the software program OSPREY. The program OSPREY serves the measurement of concrete geometry elements with the help of the coordinate measuring technique. In the current measuring tasks high-contrast object edges are touched. After the analysis of the picture brightness in the measuring field, the threshold value at the edge transition is automatically determined by a histogram. With this

procedure, a touching uncertainty of 1/5 pixel for the single point can be regarded as surely attainable. The attainable reproducibility of the photogrammetric touching of the measuring marks with the developed system, depends on the applied objective, shows a standard deviation of 0.5 μm respectively when the subpixel method is used.

3 Fields of Application of the Measuring System

3.1 Modification of the Measuring System with Strain Determination Tests

For the adaptation of the measuring system to the measuring tasks, test series with geometric and deformation measurements were carried out at first. Three-point and four-point bending tests with different wood species - beech, ash and spruce - were performed. The procedure of testing approximately corresponded to the German standard DIN 52 186. Cross sections of 44/44 mm², 70/20 mm² and 80/40 mm² with a uniform span of 600 mm were selected. By the arrangement of several measuring point rows over the full cross-sectional height it is possible to determine the development of strains over the height with plastic deformations also measured in the compression zone. Strains can be measured up to the failure range and can be recorded over the full measuring field by the contactless optical method. The failure strains can be determined at discrete measuring ranges. The bending tests show only small deviations between strain curves determined optical and manual by strain gauges, see Figure 3.

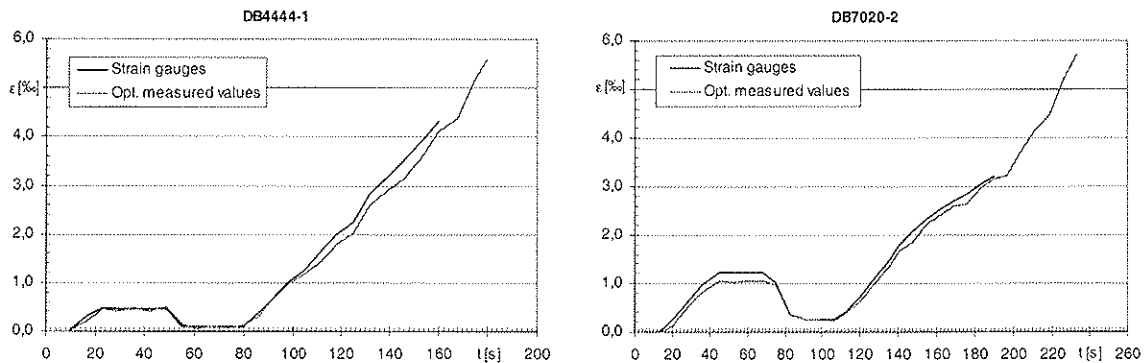


Figure 3: Strain-time-curves of the three point bending tests

For two exemplary cross sections the strain distributions over the cross sectional height under different loads is shown in Figure 4. Additionally the linear strain progression according to elastic theory are included in the figure as broken lines. The strains of the higher cross section clearly show plastic deformations in the area of the pressure zone. Compared to the linear strain distributions the plastic strains can be easily recognized. For application of elastic theory an E-modulus of approximately 12000 N/mm² has been determined.

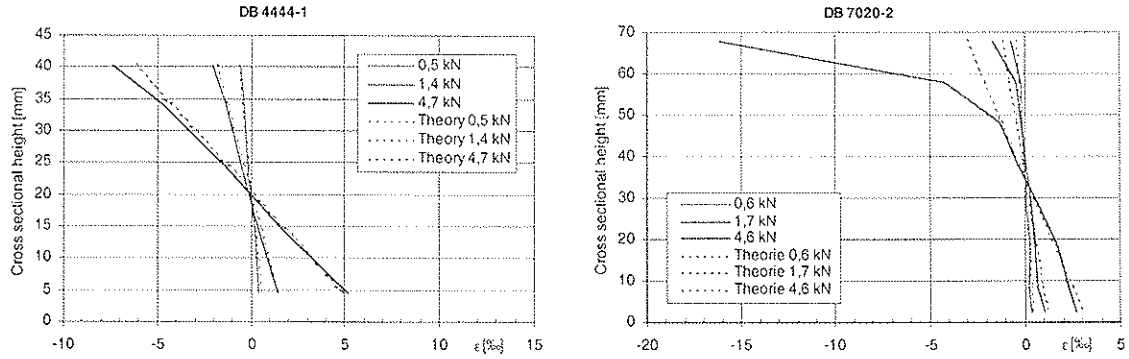


Figure 4: Strain distributions of different cross sections – bay centre

The presented results show, that strain distributions of different cross sections can be detected. In the lower load range an excellent agreement can be observed, which allow a reliable registration of low strain areas. This can be even be accomplished at a later time by recording the images. Based on the images the gained results may also be compared to the actual states of the loaded test specimen, which are fixed in the images.

3.2 Measurement of Crack Growth for the Determination of Fracture Mechanical Parameters

An important field of application of the introduced measuring system is the measurement of the crack opening and crack length for the determination of fracture mechanical parameters. Before the splitting of the wooden specimen a stable crack growth can often be observed. Numerous theoretical and experimental investigations to the application of fracture mechanics in timber engineering are documented and could be consulted for comparative reasons. It is obvious to examine the crack growth by photogrammetry because the measured values of tactile measuring procedures, which are obtained applying conventional methods, have not yet been sufficiently assigned up to now. The test series was carried out with CT-samples as illustrated in Figure 5.

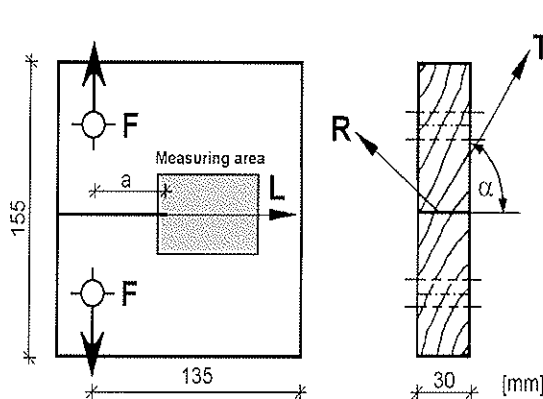


Figure 5: CT-samples for the test

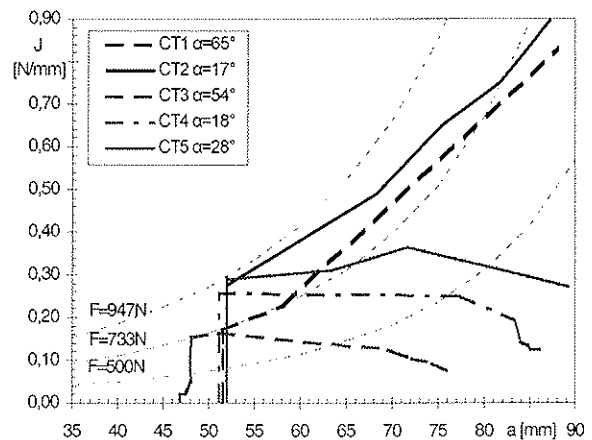


Figure 6: Crack resistance curves from the test results and the numeric simulations

In contrast to the usually common procedure to determine the fracture mechanics parameters on CT- samples in the post process, the optical measuring procedure can exactly measure the geometry of the cracks during the process. In the experimental investigations, the crack propagation could be determined exactly to within 100 μm . With the obtained values of crack length and their transmission to a Finite-Element simulation program, it was possible to determine the curves of resistance-to-cracking of timber. These first exemplary crack resistance curves show both a brittle material behaviour of wood and a ductile behaviour with increasing crack resistance (two curves). However, this knowledge must be protected and confirmed in secondary series of experiments.

3.3 Examination of the Transverse Tensile Area for Notched Structures

3.3.1 End notched beams of solid timber

Due to the redistribution of stress at an unstable change of the cross section the state of stress at the notch is characterized by a release of singular high stress concentrations. In particular high tensile stresses perpendicular to the grain arise at notches with stress of bending tension. The purpose of these test series was the determination of the strain distributions at the range of the notch during the continuous load increase. At the same time the crack formation and the crack growth were regarded in the test process.

In the research project altogether 25 tests with notches from solid wood with a cross section of $b \times h \times l = 40 \times 80 \times 650 \text{ mm}$ for all test specimens were examined. Figure 7 shows the applied measuring grid for the photogrammetric measurement, which is divided into two ranges. The internal two rows are to determine the strains perpendicular to the crack growth direction. In particular the strain conditions in the area in front of the crack for the determination of the transverse tension range was from special interest. The additional measuring points served for the following evaluation. Thereby the measured changes of coordinates are assigned to the associated knots in the FE- modelling.

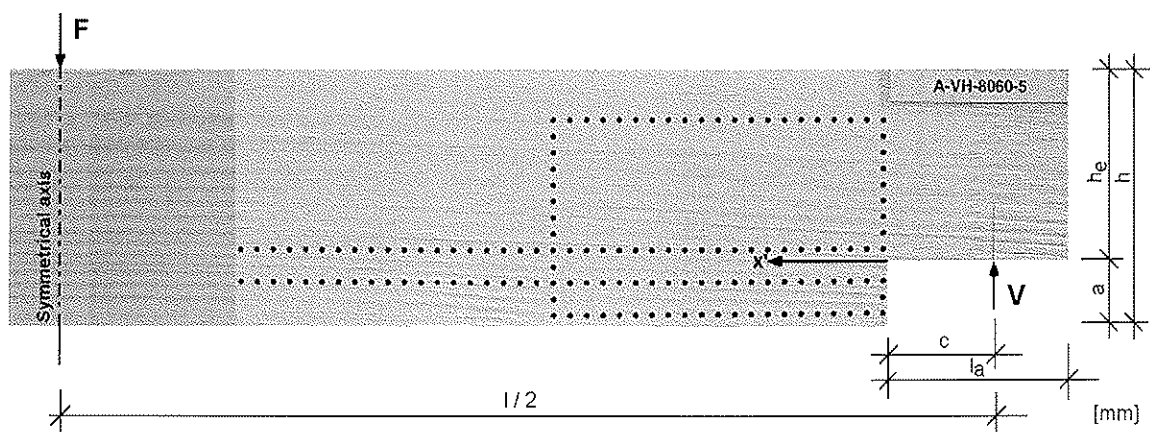


Figure 7: Definitions from test of notches

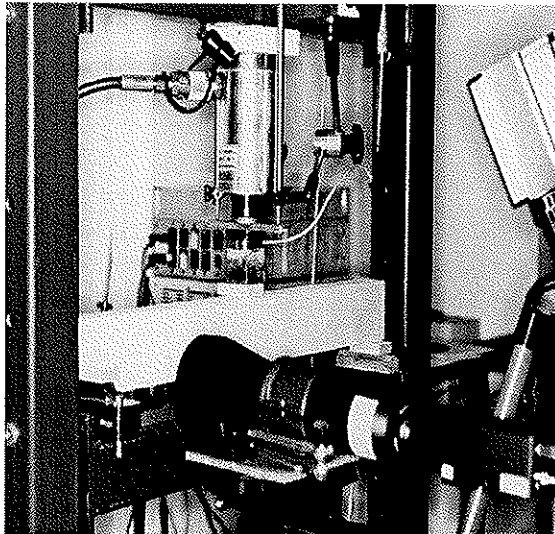


Figure 8: Experimental setup of endnotched beams of solid wood

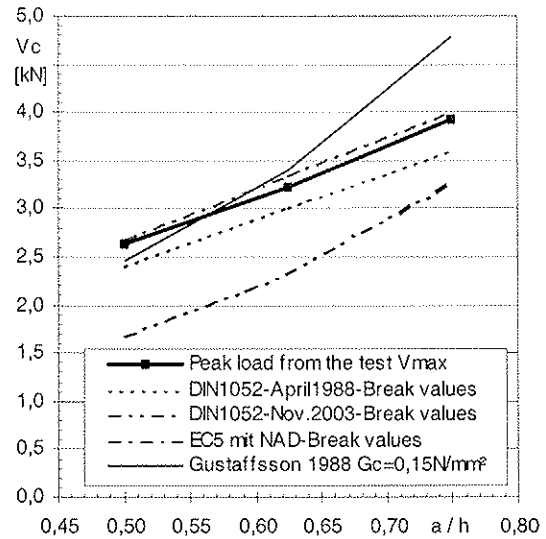


Figure 9: Ultimate loads of the tests in comparison with other calculating methods

For a calculation, e.g. of reinforcements, the estimation of the transverse tension range and the tension-resulting of the transverse tension range are needed. With the photogrammetric measuring technique the transverse strain progression in crack growth direction could be determined for the accomplished test series. The size of the transverse tension range could also be determined. Figure 10 and Figure 11 contain the determined transverse strain progression as individual measuring points and their linearization by means of an exponential curve for the comparison with the strains from the modelling with the program ANSYS®.

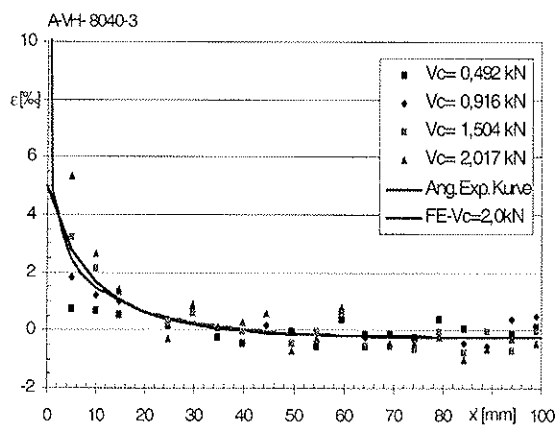


Figure 10: Transverse strain progression for a/h=0,5 – solid wood

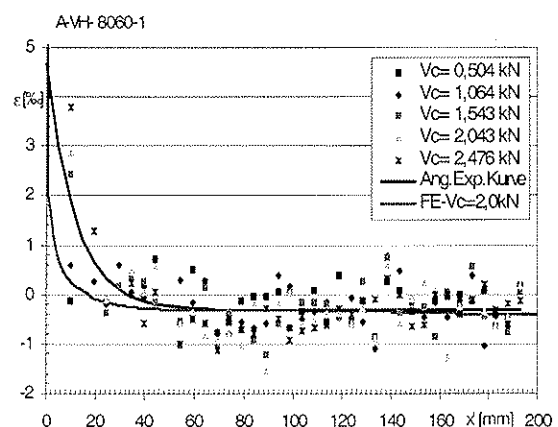


Figure 11: Transverse strain progression for a/h=0,75 – solid wood

Henrici investigated the load bearing performance of wood beams with notches and developed formulas for the determination of the transverse tension range and the arising transverse tensile force as a function of the substantial characteristic values of the beam. In Figure 12 the determined experimental values for the size of the transverse tension range with the FE- results from own simulation and the values from the estimation of Henrici are summarized. The evaluation of the measurements shows clearly that the estimation of the transverse tension range for notch ratios of $a/h = 0.5$ and 0.625 can be made relatively well with the procedure from Henrici and by a FE model. For the notch ratio of $a/h = 0.75$ a clearly larger transverse tension range, in relation to the calculated values, was determined.

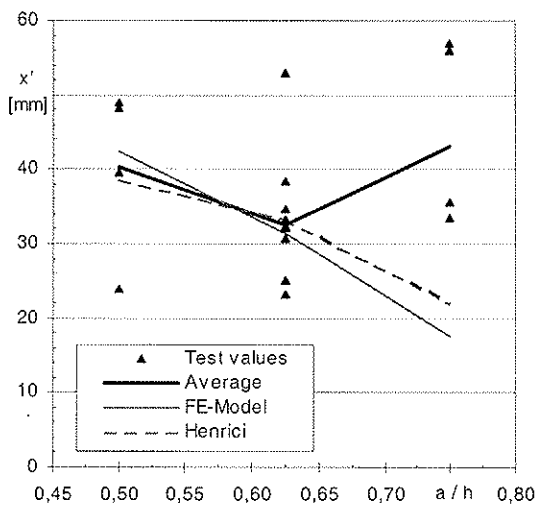


Figure 12: Transverse tension range

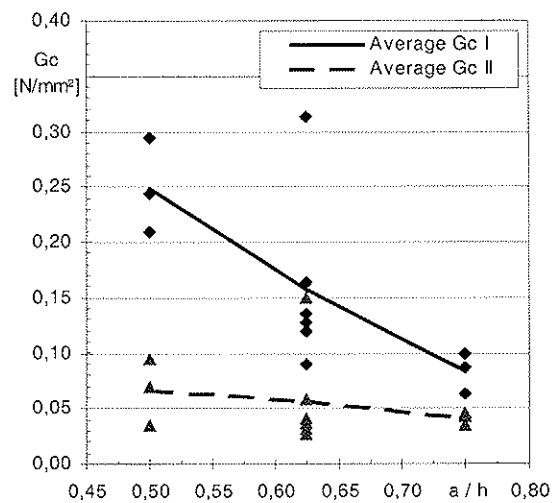


Figure 13: G_c depends on the notch ratio for mode I and II

The registration of the crack geometry during the test at the individual measuring photos with the dedicated loads makes possible to determine first the crack resistance curves with the help of FE- calculations and secondly the critical fracture energy G_c . In the following illustrations (Figure 14 and Figure 15) the determined crack resistance curves for two notch ratios are exemplary represented. The results show that here instead of brittle failure aspects of the non linear material behaviour become more important. The failure behaviour can be illustrated by means of the crack resistance curves. A constant crack resistance is equivalent to a brittle material failure and an increasing crack resistance is equivalent to a ductile material behaviour. If the crack length increases and the crack resistance decreases it indicates an edgeless initial crack or on an inhomogeneity in the material. By the results of the evaluation of the won crack resistance curves from the test series, a dependence on the critical fracture energy for the mode I and II to the notch ratio is presented in Figure 13. Until now, in publications for the estimation of the load capacity of notches, the critical fracture energy was regarded as constant for different notch ratios. This dependence should be also secured by further tests with additional notches.

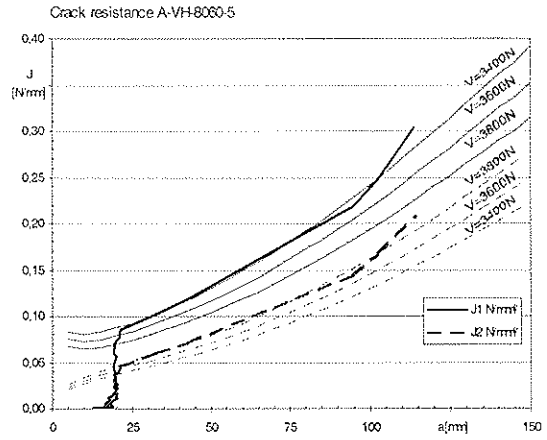
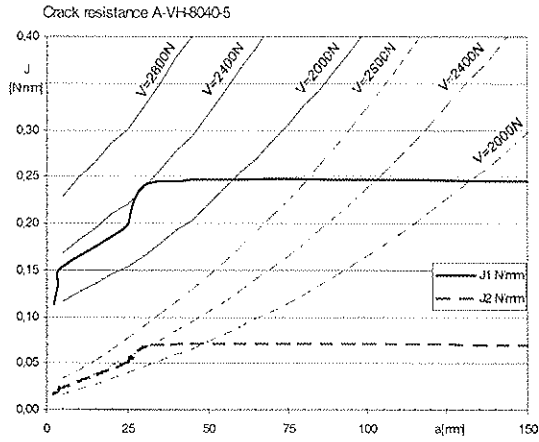


Figure 14: Crack resistance curves $\alpha = 0,50$

Figure 15: Crack resistance curves $\alpha = 0,750$

3.3.2 Endnotched beams of gluelam

First reached results from the recently finished test series with notches in glued laminated timber beams are exemplary for a beam specified here. In Figure 16 the applied measuring field within the area of a straight notch of a gluelam beam (cross section: 10/60 cm; $\alpha = 0,33$) is presented. In Figure 17 the strains perpendicular to the grain determined experimentally by optical measuring procedures and the strains calculated numerically with the substructure (represented by broken lines) are compared for different applied transversal forces. The curves show excellent agreement. The relocation and/or the reduction of the perpendicular-to-grain tensile stresses into less stressed areas is measurable by the new measuring procedure. Obviously, with the developed measuring procedure realistic strain distributions can be obtained.

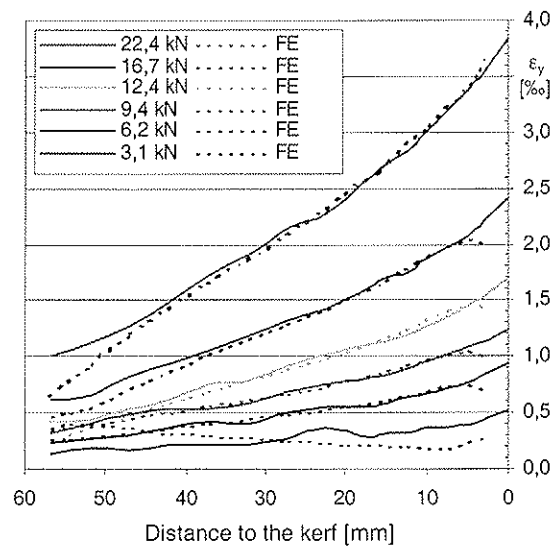
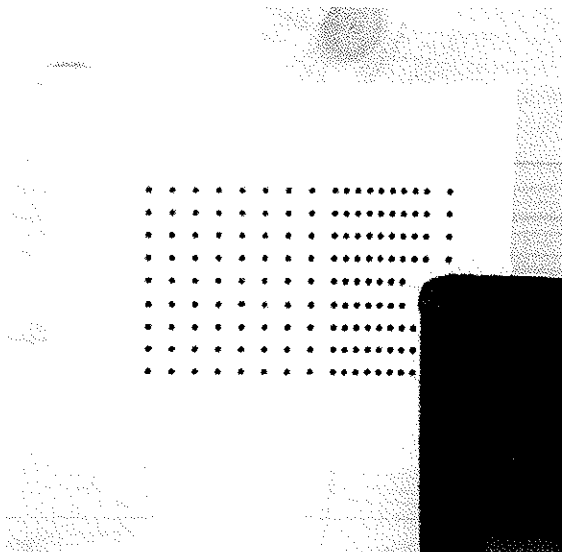


Figure 16: Measuring area of a gluelam beam in the notched area

Figure 17: Strain curves, measurement and FE-simulation

The modelling with the FE-method was done with a substructure, which includes the area of the measuring raster illustrated in Figure 16. The measured displacements, which were implemented into the FE-simulation enable the close-to-reality illustration of structural inhomogeneities (e.g. branches), which can be therefore simply considered for further calculations. For comparison the determined perpendicular-to-grain tensile stress distribution in the area of the notch is presented in Figure 18 and in Figure 19.

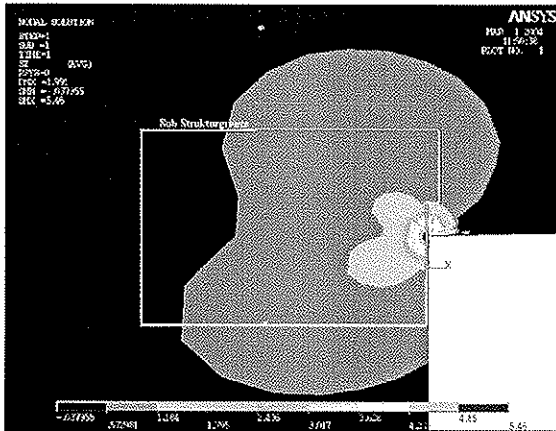


Figure 18 - Endnotched Beams: Stresses in the area of the notch (complete model)

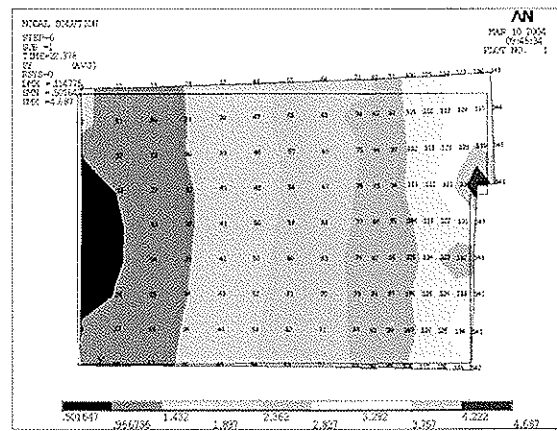


Figure 19 - Endnotched Beams: Stresses by applying measured displacements (substructure model)

4 Areas of future application

In many fields of structural engineering the photogrammetry measuring system, that has been developed within a research project, can lead to new insights. The test series that have already been completed provide many interesting results, which considerably contributed to new findings in timber engineering and new opportunities in the field of experimental stress-analysis and experimental technique. Especially the cracking of concrete seems to be a further field of work and interest.

The application will be extended to the continuation and the future development of the experimental investigations for the determination of the curves of cracking-resistance of timber and other important parameters for the fracture mechanical simulations. The measuring procedure will also be applied to improve the evaluation of the load bearing performance of connections with mechanical fasteners in timber constructions. The evaluation of the load bearing capacity of transverse connections including crack growth and the photogrammetric recording of relative displacements of the fasteners represents a main area of investigation.

References

- [1] Aicher, S. (1994): Bruchenergien, kritische Energiefreisetzungsraten und Bruchzähigkeit von Fichte bei Zugbeanspruchung senkrecht zur Faserrichtung. Holz als Roh- und Werkstoff, 52: 361-370.
- [2] Aicher, S., Reinhardt, W., Klöck, W. (1993): Nichtlineares Bruchmechanik-Maßstabgesetz für Fichte bei Zugbeanspruchung senkrecht zur Faserrichtung. Holz als Roh- und Werkstoff 51: 385-394.
- [3] Gustafsson, P.J. (1995): Ausgeklinte Träger und Durchbrüche in Brettschichtholz, Step B5. Informationsdienst Holz "Holzbauwerke Bemessung und Baustoffe nach Eurocode 5", Düsseldorf
- [4] Gustafsson, P.J. (1988): A study of strength of notched beams. CIB W18A- meeting 21, Canada
- [5] Henrici, D. (1984): Beitrag zur Spannungsermittlung in ausgeklinten Biegeträgern aus Holz. Dissertation, Universität München
- [6] Henrici, D. (1990): Beitrag zur Bemessung ausgeklinker Brettschichtholzträger. Bauen mit Holz 11/90: 806-881
- [7] Hujer, S., Franke, B., Rautenstrauch, K. (2003): Strain analysis of solid wood and glued laminated timber constructions by close range photogrammetry. International Symposium: Non Destructive Testing in Civil Engineering. Berlin
- [8] Hujer, S., Franke, B., Rautenstrauch, K. (2004): Strain analysis of solid wood and glued laminated timber constructions by close range photogrammetry. ESWM-II International conference of the European Society for Wood Mechanics, Villa Real, Portugal
- [9] Hujer, S., Franke, B., Rautenstrauch, K. (2004): Beanspruchungsanalyse von Bauteilen aus Voll- und Brettschichtholz durch Nahbereichsphotogrammetrie. Bauingenieur (Herbst 2004)
- [10] Logemann, M. (1991): Abschätzung der Tragfähigkeit von Holzbauteilen mit Ausklinkungen und Durchbrüchen. Dissertation, Universität Hannover
- [11] Luhmann, Th. (2000): Nahbereichsphotogrammetrie Grundlagen, Methoden und Anwendungen. Herbert Wichmann Verlag, 1. Auflage: Heidelberg
- [12] Linß, G.(Hrsg.), Brückner, P., Funk, W., Hamatscheck, U., Kühn, O., Nehse, U., Nopper, C.-B., Sichhardt, A., Volk, D. (1997): Quick Image/Development: Objektorientierte Softwarebibliothek für Bildverarbeitung, Qualitätssicherung, Messtechnik und Automation, Referenzhandbuch. STZ-Eigenverlag, 3. Auflage, Suhl.
- [13] Mistler, H.L. (1979): Die Tragfähigkeit des am Endauflager unten rechtwinklig ausgeklinten Brettschichträgers. Dissertation, Universität Karlsruhe
- [14] Schatz, T. (1994): Zur bruchmechanischen Modellierung des Kurzzeit-Bruchverhaltens von Holz im Rissöffnungsmodus I. Dissertation, Universität Stuttgart
- [15] Sinn, G., Reiterer, A., Stanzl-Tschegg, S.E., Tschegg, E.K. (2001): Determination of strains of thin wood samples using videoextensometry. Holz als Roh- und Werkstoff 29: 31-50
- [16] Schmid, M. (2002): Anwendung der Bruchmechanik auf Verbindungen mit Holz. Dissertation, Universität Karlsruhe

INTERNATIONAL COUNCIL FOR RESEARCH AND INNOVATION
IN BUILDING AND CONSTRUCTION

WORKING COMMISSION W18 - TIMBER STRUCTURES

A NEW DESIGN METHOD TO CONTROL VIBRATIONS
INDUCED BY FOOT STEPS IN TIMBER FLOORS

Lin J Hu

Forintek Canada Corp.

Ying Hei Chui

University of New Brunswick

CANADA

Presented by Y H Chui

F Rouger commented that the upper part of the regression curve has as many accepted as unacceptable floors.

Chui answered that this is a common issue with the acceptance criteria for serviceability studies.

P Glos commented that different countries have different acceptance criteria and this work only refers to acceptance based on Canadian surveys and experience.

T Williamson asked whether floor joist types were considered. Chui answered yes and the information is available in the paper.

B J Yeh asked how was the influence of dead weight and partition walls considered in the survey and the acceptance criteria. Chui answered that it is a sensitive issue and a large number of new construction were also considered in the survey. Furniture loads were not considered in the design proposal.

A New Design Method to Control Vibrations Induced by Foot Steps in Timber Floors

Lin J. Hu

Forintek Canada Corp., Canada

Ying Hei Chui

University of New Brunswick, Canada

ABSTRACT

Design methods contained in building codes and structural design standards to prevent excessive vibration in timber floors have not been found to provide satisfactory solutions for the broad range of floor systems encountered in contemporary timber construction. This paper describes the development of a new design method. The design method consists of a dual-parameter performance criterion and the associated calculation method for the performance criterion parameters. The derivation of the performance criterion was based on extensive field testing data and an occupant survey. The two parameters selected for design purpose are static deflection at floor centre under a point load and first natural frequency. The calculation method is based on the ribbed-plate theory and considers semi-rigid connections between joist and sheathing, torsional rigidity of joists, sheathing stiffness in the span and across-joist directions and the contribution of lateral performance enhancing elements such as between-joist bridging, strong-back and strapping. Comparison of predicted performance with recorded rating of a group of timber floors shows that the proposed design method works reasonably well. Only about 3 of the floors were slightly mis-classified as acceptable by the method. A few acceptable floors were 'conservatively' classified as unacceptable. This has provided some confidence for adopting the proposed method for design use.

1. Introduction

Although several design methods have been implemented in some building codes or proposed in the literature to control vibration in timber floors, complaints by users about unsatisfactory floor vibration performance are still received, especially in floors having long spans and large open space, or with cementitious toppings as reported in [1] and [2]. This implies that these design approaches are inadequate for the broad range of timber floor construction that is encountered today and that an alternative method is required.

A thorough review of design approaches already adopted in building codes and those proposed in the literature has revealed that these approaches generally provide satisfactory solutions only for certain classes of timber floors [3]. Further analysis of these design approaches has also revealed that the limited application of these design approaches arises

from the use of only a single design parameter, such as static deflection recommended in the National Building Code of Canada [4-6], fundamental natural frequency proposed by Dolan et al [7], initial peak velocity recommended in draft Eurocode 5 [8] and implicitly used by Foschi et al in their proposed design guidelines [9], and root-mean-square acceleration proposed by Smith and Chui [10] to control the vibrations. Another problem with some of these approaches is that the two-way system stiffness or mass of a floor is not accounted for. A design method, which is based on multiple parameters and a better representation of the effect of the two-way action and mass of a floor, can be a more effective general solution to the problem. This need motivated the project undertaken by Forintek Canada Corp. to develop a universally acceptable vibration controlled floor design method in collaboration with the University of New Brunswick.

2. Objective

The objective of this project was to develop a design method to control the vibrations induced by foot steps of normal walking for a broad range of timber floor systems. The new design method consisted of a mechanics-based calculation method to determine vibration performance parameters and a vibration-controlled floor design criterion associated with the calculation method.

3. Scope of Method

The proposed design method accounts for common construction details found in current construction practice, including various types of joist products and sub-floor materials, sub-floor gaps, semi-rigid connection between joist and sub-floor, lateral performance-enhancing elements such as between-joist bridging, strong-back and strapping, cementitious topping, and ceiling. Figure 1 shows a typical timber floor system considered by the proposed design method.

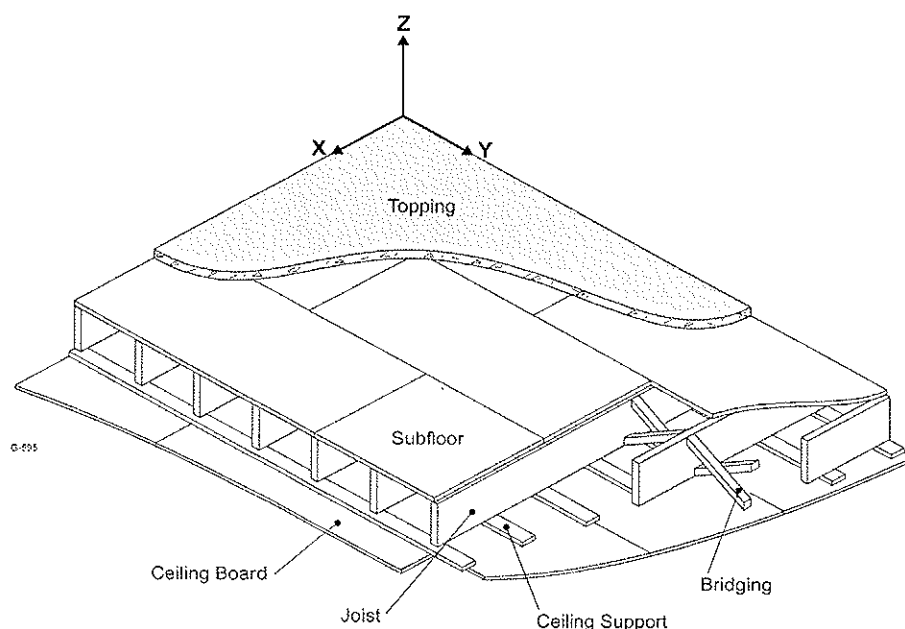


Figure 1 Timber floor system considered by the proposed design method.

4. Methodology

To develop the new design method, a three-phase approach was used.

4.1 Identification of Vibration Performance Parameters

In this phase, an occupant survey and an in-situ evaluation of about 130 field floors were conducted to identify vibration performance parameters that are closely correlated to the occupants' perception to vibrations in timber floors. In the survey, occupants were asked to rank vibration acceptance of the floors in their residences. At the same time static and dynamic tests were conducted on these floors to measure a number of response parameters that have been found to correlate with human response. These parameters include static point load deflection at floor centre, natural frequencies and acceleration time history response to a simulated foot step impulse. Logistic regression analysis was conducted to obtain the correlations between the measured vibration performance parameters and occupants' subjective evaluation of floor vibration performance. This led to the most suitable combination of response parameters for predicting vibrational performance of timber floors.

4.2 Development of Calculation Method for Design Parameters

A designer-useable calculation method based on ribbed plate theory [11] was developed to estimate the design parameters identified in Phase 1. Ribbed plate theory provides a simple and analytical approach to account for the two-way action in timber floors. This feature is very useful to overcome the difficulty in modelling the lateral performance-enhancement elements such as that shown in Figure 1. The numerical accuracy of the calculation method was checked by comparing its predictions with these from finite element method and tests.

4.3 Development of Design Criterion for Controlling Floor Vibration

The work mentioned in Phase 1 led to the identification of performance parameters and a possible form of a multi-parameter performance function based on measured responses. The performance function identified based on field measurements cannot be readily adopted for design use, since it is inevitable that field conditions deviate from the theoretical assumptions that are built into any calculation method. Therefore any design performance criterion needs to be calibrated to the calculation method. To this end a database consisting of 106 field floors was assembled. These floors were selected because a reasonably accurate description of floor construction details and properties of the floor components were available. All these floors were subjectively rated for their acceptance. The database covers a broad range of construction details found in current timber floor construction practice in North America, and a wide range of spans from 3 m to 13 m.

Chui's [11] calculation method was used to calculate the design parameters identified in Phase 1 for each floor. For floors built with sawn lumber joists, design properties for the joists were obtained from design documents [12-13]. For engineered wood joists such as wood I-joists and trusses, published design properties contained in the producers' specifications were used. Sub-floor properties were as those published in the Canadian timber design code [12]. Properties for fastening and concrete topping were adopted based on a review of literature [14]. Once the values of the identified performance parameters were calculated for the 106 floors, logistic regression analysis was conducted to develop a

design criterion that enables designers to discriminate unacceptable from acceptable floors. Once the design criterion was available it was further evaluated against current floor spans of solid sawn lumber and engineered wood joists and the industry's field experience.

5. Results and Discussion

5.1 Vibration Performance Parameters

5.1.1 Findings

Logistic regression analysis performed in Phase 1 showed that occupant perception to vibrations correlated with most of the measured performance parameters, including static deflection under a 1 kN load, fundamental natural frequency, initial peak velocity and acceleration, and root-mean-square (RMS) acceleration. The correlation was represented by five performance functions incorporating different combinations of performance parameters [1]. As an example, Figure 2 shows a plot of 1 kN static deflection and fundamental natural frequency for the 130 field floors. The performance curve as determined from the logistic regression analysis is superimposed onto the plot. Each symbol in the plot represents a floor. If the symbol is above the curve, it means that the floor vibration performance is not acceptable according to the correlation curve and vice versa. Comparison of the number of problem floors correctly identified by each function has revealed that the other four curves are very similar to this curve in terms of their ability to discriminate between acceptable and unacceptable floors as reported in [1].

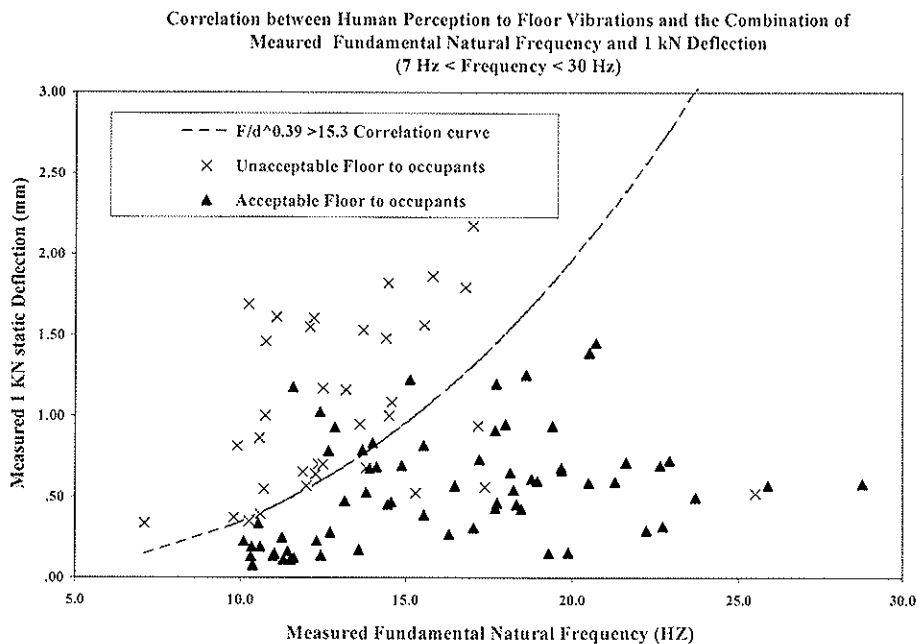


Figure 2 Correlation between human perception to floor vibrations, measured 1 kN static deflection and fundamental natural frequency of field floors.

It is interesting to note that these performance curves have a similar shape to the building vibration Z-axis (foot-to-head) base curve plotted in the frequency and RMS-acceleration plane presented in British Standard 6472 [15] and ISO 2631-2:1989(E) [16]. The BS or ISO base curve represents magnitudes of approximately equal human response to building vibrations.

5.1.2 Selection of Parameters for Vibration Controlled Floor Design

Based on the findings presented above, it was decided to use 1 kN static deflection and fundamental natural frequency as the design parameters to control vibrations in timber floors. The rationale behind their selection was that, unlike other dynamic-based variables such as peak velocity and rms or peak acceleration, they can be calculated using designer-useable equations and mechanical properties of floor components, or measured using relatively simple equipment with acceptable accuracy.

5.2 Calculation Method to Predict the Selected Design Parameters

Chui [11] developed a method to predict 1 kN static deflection and fundamental natural frequency. The method was based on the ribbed-plate theory and considered semi-rigid connections between joist and sheathing, torsional rigidity of joists, and sheathing stiffness in the span and across-joist directions. In addition, the contribution of lateral performance enhancing elements such as between-joist bridging, strong-back and strapping is accounted for in the formulas. Comparison with test results showed that the frequency formula tends to slightly over-estimate fundamental natural frequency, and the deflection formula predicts static deflection well. Overall, the predictive capability is considered acceptable for design use. A detailed description of the work can be found in Chui's paper [11]. The formulas are given below.

5.2.1 Formula to Predict 1 kN Static Deflection at Floor Centre

Static deflection at floor centre under a point load P (N) can be calculated from the following series-type equation:

$$d_p = \frac{4P}{ab\pi^4} \sum_{m=1,3,5..} \sum_{n=1,3,5..} \frac{1}{\left(\frac{m}{a}\right)^4 D_x + 4\left(\frac{mn}{ab}\right)^2 D_{xy} + \left(\frac{n}{b}\right)^4 D_y} \quad \text{in m} \quad (1)$$

where,

a = floor span in m;

b = floor width in m;

$$D_x = \frac{EI_{CJ}}{b_1} \quad \text{in Nm (System flexural rigidity in joist - direction);}$$

b_1 = joist spacing in m;

$$D_y = \frac{\sum_i^k (EI_b)^i}{a} + \frac{EI_p b_1}{b_1 - t + \alpha^3 t} \quad \text{in Nm (System flexural rigidity in cross-joist-direction);}$$

t = joist thickness in m;

$D_{xy} = \frac{G_p h^3}{12} + \frac{C}{2 b_1}$ in Nm (Shear rigidity of multi-layered floor deck + torsion rigidity of joist);

$$\alpha = \frac{h}{H};$$

h = thickness of floor deck in m;

H = height of floor system (joist depth + floor deck thickness) in m;

G_p = shear modulus of multi-layer floor deck in N/m^2 ;

EI_p = flexural rigidity of multi-layer floor deck in Nm;

EI_{CJ} = composite flexural rigidity of joist in Nm^2 ;

$(EI_b)^i$ = flexural rigidity of the i^{th} row of lateral performance enhancing element in Nm^2 ;

k = total number of rows of lateral bracing members (assumed equally spaced);

C = joist torsional constant.

To ensure convergence of solution, it is recommended that three terms be used for $m=1,3,5$, and 17 terms for $n=1,3,5, \dots, 35$.

5.2.2 Formula to Predict Fundamental Natural Frequency

Using the same ribbed plate theory, the fundamental natural frequency of a floor system can be calculated as follows:

$$f_1 = \frac{\pi}{2\sqrt{\rho}} \sqrt{D_x \left(\frac{1}{a}\right)^4 + 4D_{xy} \left(\frac{1}{ab}\right)^2 + D_y \left(\frac{1}{b}\right)^4} \text{ in Hz} \quad (2)$$

where,

$\rho = m_j / b_1 + \rho_s t_s + \rho_c t_c$ in kg/m^2 ;

m_j = mass per unit length of joists in kg/m ;

ρ_c = density of topping in kg/m^3 ;

ρ_s = density of sub-floor in kg/m^3 ;

t_c = thickness of topping in m;

t_s = thickness of sub-floor in m.

5.2.3 Modelling Lateral Performance Enhancing Elements

The ribbed plate theory considers lateral performance enhancing elements as ribs running perpendicular to the joists. To apply the ribbed plate method to floors with continuous lateral performance enhancing elements, such as strong-back and strapping, is relatively simple as these elements are essentially flexural elements themselves. For discontinued lateral performance enhancing elements, such as bridging and blocking, an equivalent beam approach, Figure 3, which leads to an estimation of the flexural rigidity of a row of elements is required. The formula for calculating flexural rigidity (EI_b) of an equivalent

beam was derived based on general beam theory [17]. The final form of the formula is: $EI_b = K_c \times (\text{Joist spacing})$, where K_c is defined as the rotational stiffness of a joist-to-bridging/blocking connection. It is expressed as the bending moment required for rotating a bridging/blocking panel by a unit angle from the joist to which the bridging/blocking panel is attached.

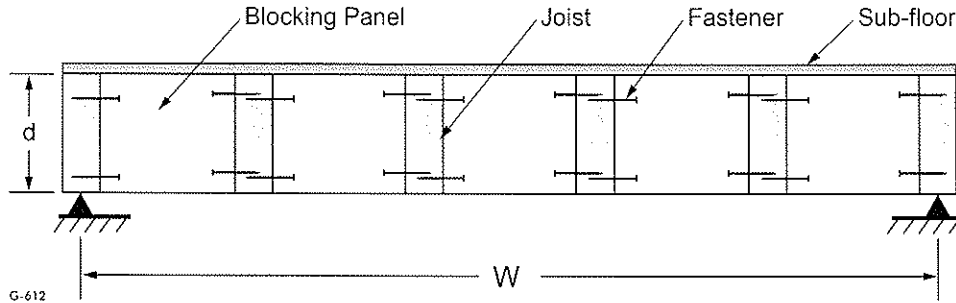


Figure 3 Cross-section of a timber floor with bridging/blocking panels

To determine the rotational stiffness, K_c , of an element type a test protocol was developed through Khokhar's thesis work [17] shown in Figure 4. According to this protocol, the specimen is composed of two bridging/blocking panels and three joist stubs. The two bridging/blocking panels are connected symmetrically on each side of the centre joist stub by fasteners following the fastener schedule used in practice. The beam like specimen is simply supported, and a vertical load is applied to the middle joist stub. The vertical deflection under the middle joist stub is measured by a linear variable displacement transformer (LVDT). K_c can be determined by Equation (3).

$$K_c = \frac{P}{VD} \frac{L^2}{2} \quad (3)$$

where P is the applied load, VD is the vertical displacement of the joist stub measured by the LVDT, and L is the joist spacing.

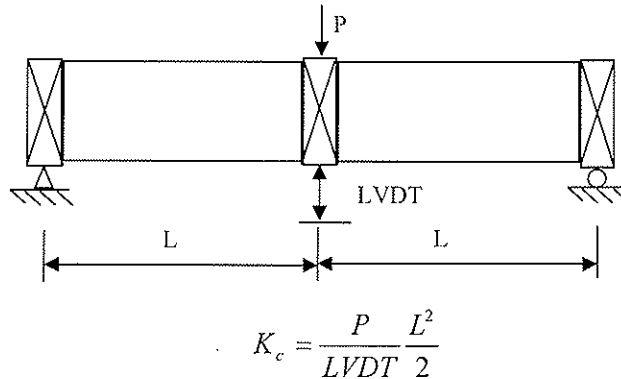


Figure 4 Test protocol to determine K_c of bridging/blocking-to-joist connection.

5.3 Vibration Controlled Floor Design Criterion

5.3.1 Design Criterion Based on 1 kN Static Deflection and Fundamental Natural Frequency

Through the logistic regression analysis on the 106 field floor database, the best correlation of the subjective rating with a combination of calculated 1 kN static deflection and fundamental natural frequency was determined to be of the form shown below:

$$\frac{f}{d^{0.44}} > 18.7 \text{ or } d < \left(\frac{f}{18.7}\right)^{2.27} \quad (4)$$

where d and f are the calculated 1 kN static deflection and fundamental natural frequency of a timber floor respectively using equations (1) and (2).

Equation (4) can be graphically expressed as the solid curve in Figure 4. For a floor, its calculated fundamental natural frequency and 1 kN static deflection can be plotted in the deflection-frequency plane as a symbol. If the symbol is above the curve, it means the floor vibration performance is not acceptable according to the criterion, and vice versa.

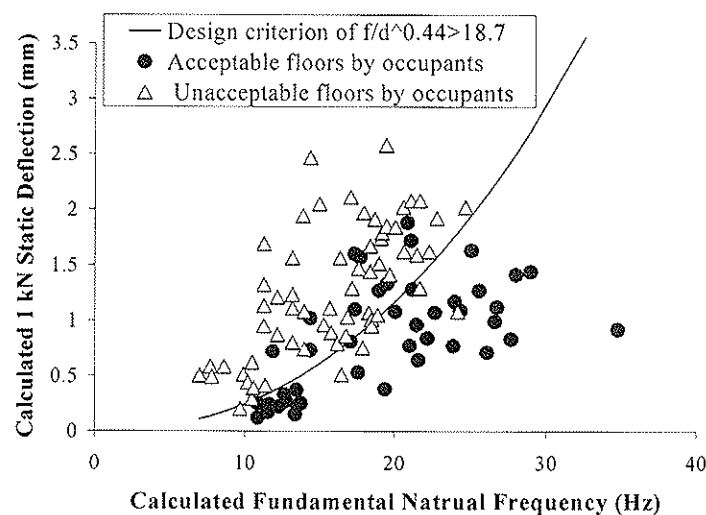


Figure 5 A comparison between the subjective rating of 106 field floors and their acceptance predicted by the new design criterion

Figure 5 presents a comparison between the subjective rating of these 106 floors and their acceptance according to the proposed design criterion. It can be observed that the proposed design criterion provides a fairly effective tool in discriminating between unacceptable and acceptable floors.

5.4 Impact of the New Design Method on Current Timber Floor Spans

The impact of the proposed new design method on the current timber floor spans was studied on floors built with wood I-joists and solid sawn lumber joists. The depth of joists ranged from 140mm to 450mm. The floor spans determined from this new design method were compared with the spans published in [5] for lumber joist floors, and the spans determined using the method proposed for engineered wood members in Canada [6].

Detailed results of the impact study can be found in a report by Hu [14]. In a nutshell, the study revealed that for floors having spans shorter than 4.8m the vibration-controlled spans allowed by the new design method were comparable with the spans allowed by the National Building Code of Canada [5] or the design method in [6]. For long-span floors, the new design method reduced the spans allowed by applying the span/480 deflection limit. Field survey results reported by Hu [1] and Johnson [2] revealed that the span/480 deflection limit did not provide an adequate control for vibrations of long span floors. It was found that the proposed design method led to a more rational increase in spans resulting from the addition of performance enhancing elements such as bridging/blocking, strong-back and strapping than that allowed by the method proposed in [6]. This finding was supported by results reported by Taylor et al [18]. For concrete topped timber floors, the new design method provided more rational solutions than the method in [6]. In fact, contrary to the method proposed in [6], the addition of concrete topping led to a deterioration in vibrational performance according to the proposed design method. This is in agreement with our field testing experience of concrete topped floors [1] and the results reported by Taylor and Hua [19]. For floors with concrete topping, the proposed design method reduced the spans by about 0.3m to 0.6m, depending on floor spans and other construction details. The proposed method showed great potential to properly address issues which are deemed to be problematic with the current design approaches. These include long span floors and the liberal treatment of the performance enhancing elements such as bridging, blocking, strapping and strong-backs, and heavy topping.

6. Conclusion and Recommendation

It can be concluded that the new design method shows great potential to provide rational vibration-controlled spans for a broad range of timber floor systems. The mechanics-based approach also lends itself to facilitate the acceptance of innovative building products. The new design method presented in this paper will provide a framework for the formulation of an acceptable design method for a broad range of timber floors. Additional calibration work may be required to apply the tentative design criterion to timber floor designs in other countries because it was calibrated to material properties published in the Canadian literature.

7. Acknowledgements

The authors would like to thank the Canadian Forest Service, Natural Resources Canada and the Natural Sciences and Engineering Research Council (NSERC) of Canada for their financial support.

8. References

- [1] Hu L. J., *Serviceability Design Criteria for Commercial and Multi-Family Floors*, Report No. 5 to Canadian Forest Service, Forintek Canada Corp., Sainte-Foy, 2002, 42 pp.
- [2] Johnson J.R., *Vibration Acceptability in Wood Floor Systems*, Master thesis, Virginia Polytechnic Institute and State University, Blacksburg, 1994, 127 pp.

- [3] Hu L. J., Chui Y. H. and Onysko D. M., "Vibration Serviceability of Timber Floors in Residential Construction", *Progress in Structural Engineering and Material*, Vol. 3, No. 3, 2001, pp. 228-237.
- [4] National Building Code of Canada, *Commentary A: Serviceability Criteria for Deflections and Vibrations*, National Research Council of Canada, Ottawa, 1985.
- [5] National Building Code of Canada, *Appendix A: Explanatory material for the NBCC*, National Research Council of Canada, Ottawa, 1990.
- [6] Canadian Wood Council et. al., *Development of Design Procedures for Vibration Controlled Spans Using Engineered Wood Members*, Concluding Report to Canadian Construction Materials Centre and Consortium of Manufactures of Engineered Wood Products Used in Repetitive Member Floor Systems, Canadian Construction Materials Centre, Ottawa, 1997, 39 pp.
- [7] Dolan J. D. et. al., "Preventing Annoying Wood Floor Vibrations", *Journal of Structural Engineering*, Vol. 125, No. 1, 1999, pp.19-24.
- [8] Larsen H. et. al., "Design of Timber Structures-Part 1: General Rules and Rules for Building", *Eurocode No. 5. EC5: Part 1, TC250/SC5 PT1*, European Committee for Standardisation, Brussels, 1992.
- [9] Foschi R. O. et. al., "Floor Vibration due to Occupants and Reliability-Based Design Guidelines", *Canadian Journal of Civil Engineering*, Vol. 22, No.3, 1995, pp.471-479.
- [10] Smith I. and Chui Y. H., "Design of Lightweight Wooden Floors to Avoid Human Discomfort", *Canadian Journal of Civil Engineering*, Vol.15, No.2, 1988, pp.254-262.
- [11] Chui Y. H., "Application of Ribbed-Plate Theory to Predict Vibrational Serviceability of Timber Floor Systems". *Proceedings of 7th World Conference in Timber Engineering*, Shah Alam, Malaysia, August 12-15, 2002, paper No. 9.3.1, Vol.4, pp.87-93.
- [12] Canadian Standards Association, *Engineering Design in Wood*, CSA Standard O86-01, CSA, Toronto, 2001, 196 pp.
- [13] Canadian Wood Council, *Wood Design Manual*, Canadian Wood Council, Ottawa, 2001, 702 pp.
- [14] Hu L. J., *Implementation of a New Serviceability Design Procedure for Wood Based Floors*, Report No. 9 to Canadian Forest Service, Forintek Canada Corp., Sainte-Foy, 2002, 67 pp.
- [15] British Standards Institution (BSI), *Evaluation of Human Exposure to Vibration in Buildings (1 Hz to 80 Hz)*, British Standard BS 6472. London, 1984.
- [16] International Organisation for Standard (ISO), *Evaluation of human exposure to whole-body vibration – Part 2: Continuous and shock-induced vibration in buildings (1-80 Hz)*, ISO Standard 2631-2: 1989 (E), Geneva, 1989.
- [17] Khokhar A. M., *Influence of Lateral Element Stiffness on Performance of Wooden Floors*, MScFE Thesis, Faculty of Forestry and Environmental Management, University of New Brunswick, Fredericton, 2004.
- [18] Taylor S., et al., "Dynamic Performance of Wood Framed Floor Systems with Bridging/Blocking Enhancements", *Presentation and Abstracts of Forest Products Society 54th Annual Meeting*, South Lake Tahoe, June 18-21, 2000, pp. 17-17.
- [19] Taylor S. and Hua G., "Dynamic Performance of Wood Framed Floor Systems with Poured Toppings", *Proceedings of Sixth World Conference on Timber Engineering*, July 31-August 3, 2000, Whistler, pp.4.6.3.1 – 4.6.3.6.

INTERNATIONAL COUNCIL FOR RESEARCH AND INNOVATION
IN BUILDING AND CONSTRUCTION

WORKING COMMISSION W18 - TIMBER STRUCTURES

SERVICEABILITY LIMIT STATES OF WOODEN FOOTBRIDGES

VIBRATIONS CAUSED BY PEDESTRIANS

P Hamm

Fachgebiet Holzbau, Technische Universität München

GERMANY

Presented by P Hamm

H Blass noted high damping factor was observed for simple beam. Hamm answered that concrete topped mechanical connections did not seem to have a large role in the damping. Hamm agreed that more tests should be done to check whether dowels or screws would make a difference.

C Clorius received clarification of framework bridge and truss beam bridge.

K Crews received confirmation that the dampers were installed under the bridge.

Y H Chui asked whether there would be an influence of the exciter used in the test to determine damping. He found in floor vibration test that the human exciter can make a big difference. Hamm answered that the mass of the exciter was too low compared to the bridge to make a difference.

F Lam asked whether ambient vibration techniques have been considered. Hamm answered that the exciter is the more direct method.

A Cecotti asked whether the 0.3% damping for the cable found by measurement as it seemed to low. Hamm answered that they were measured results and they were surprisingly low.

P Ross shared his experience with a bridge design by his firm that has a fn of 1.5 Hz and low damping. This bridge would be okay with few people. The assumption for a lot of people was that the randomness of the movement from the people could make the bridge response still acceptable. They found out that this assumption was wrong and dampers were added to remediate.

A discussion took place between point-wise applications of the exciter versus exciting the bridge over the whole span. Hamm found a moving excitation versus fixed excitation factor of 0.75 which is dependent on the damping and the bridge length.

K Crews commented that this issue of position of excitation would depend on the mode of excitation.

Serviceability limit states of wooden footbridges

Vibrations caused by pedestrians

PATRICIA HAMM

Fachgebiet Holzbau, Technische Universität München, Germany

1 General

This paper deals with Eurocode 5 – Design of timber structures, Part 2: Bridges, draft 2004 [1]. The verifications of vibrations of wooden footbridges caused by pedestrians in the serviceability limit state are explained and discussed.

Depending on the natural frequencies of the bridge the following verifications of the bridge acceleration are recommended in Annex B (informative) [1], see figure 1. a_{vert} and a_{hor} are the resulting accelerations of the bridge in the vertical and horizontal direction. If all vertical natural frequencies of the bridge are greater than 5 Hz and all horizontal natural frequencies are greater than 2,5 Hz no further verifications of the vibrations are needed.

Recognize that all these verifications are in the serviceability limit state. Although these criteria and formula are presented in a norm for timber structures EC5 [1], they are valid for all materials, with exception of the damping factor.

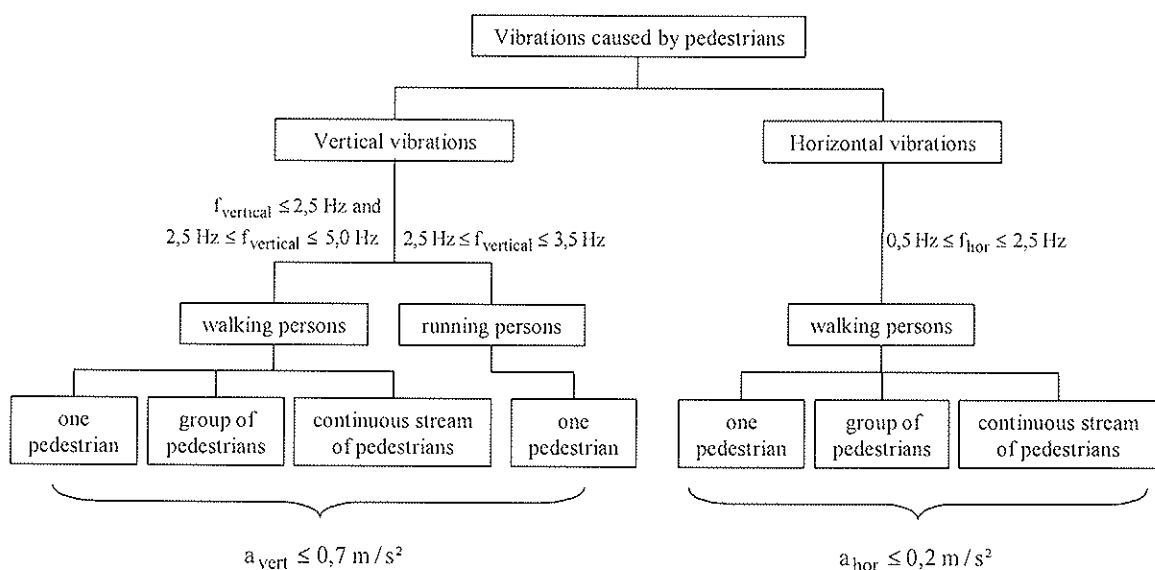


Figure 1: Verifications of bridge vibrations caused by pedestrians recommended in [1], [2]

2 Bridge acceleration due to passing pedestrians

2.1 Natural frequency

To get the natural frequencies of the bridge, one can use a finite element programme or transfer the bridge into a dynamic model with mass M^* and stiffness K^* , see figure 2.

$$f_{\text{vert}} = \frac{\omega}{2\pi} = \frac{1}{2\pi} \cdot \sqrt{\frac{K^*}{M^*}}, \text{ neglecting the damping of the bridge } R \quad (1)$$

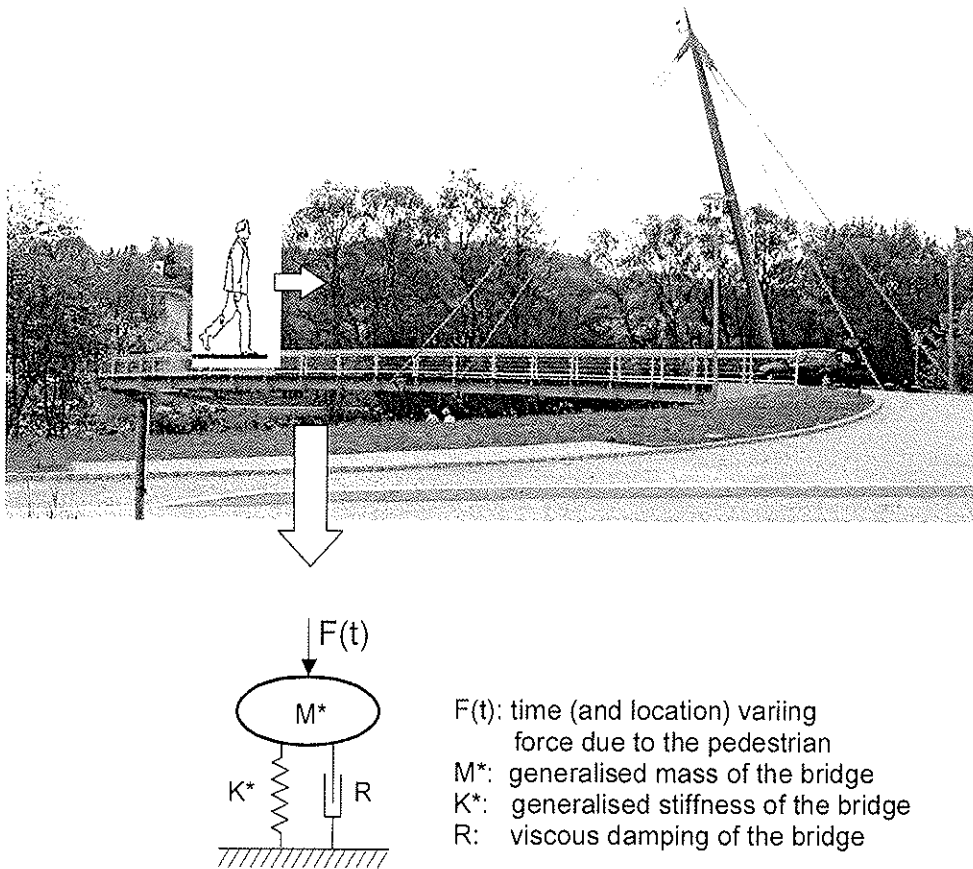


Figure 2: Footbridge in Zwiesel: Picture and dynamic model of the bridge incl. pedestrian

2.2 Dynamic load caused by pedestrians

The pedestrian crossing the bridge is transferred into a dynamic load $F(t)$. The graph of the function of $F(t)$ for walking and running is shown in figure 3 (thick line) as the sum of the first three Fourier coefficients (thin lines). In practice only one of the Fourier coefficients is relevant – the one closest to the natural frequency. For the Fourier decomposition see [3].

Table 1 shows the step frequencies and the first harmonic parts of the load depending on the kind of movement, with $F_0 \approx 700\text{N}$ = weight of the pedestrian.

Factor k in table 1 considers the fact, that the pedestrian is crossing the bridges and not acting on the same place all the time. It ranges between (0,4 ...) 0,6 ... 0,75 (... 0,8), depending on the static system and the damping of the bridge [4].

	step frequency f_s	vertical load on bridge	horizontal load on bridge
walking	1,5 ... 2,5 Hz	$k \cdot 0,4 \cdot F_0$	$k \cdot 0,1 \cdot F_0$
running	2,5 ... 3,5 Hz	$k \cdot 1,3 \cdot F_0$	$k \cdot 0,1 \cdot F_0$

Table 1: Step frequencies and 1st harmonic parts of the load for walking and running

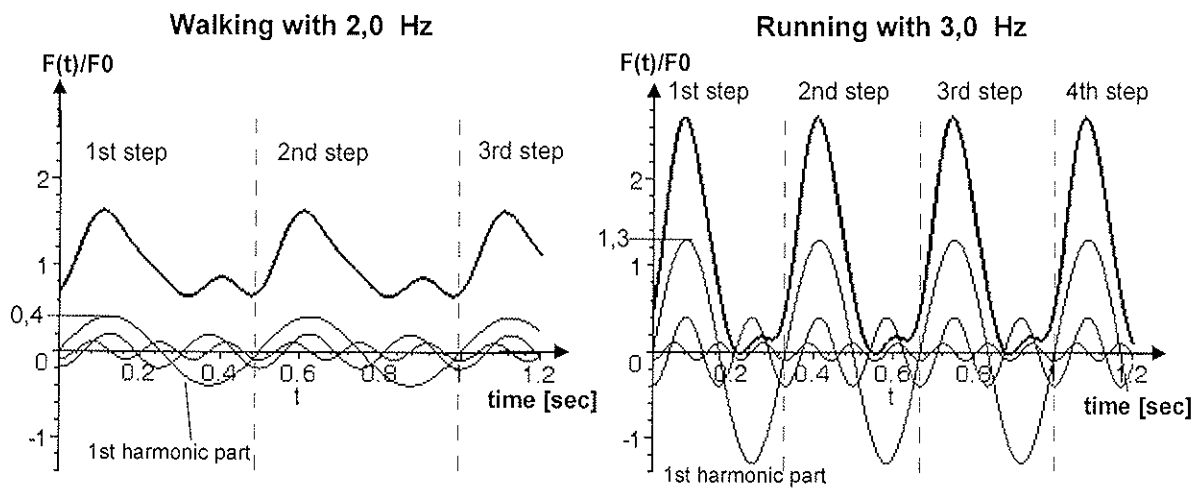


Figure 3: Graphs of the loads due to a walking and running pedestrian (total (thick line) and the first 3 harmonic parts (thin lines))

2.3 Acceleration caused by pedestrians

When the load on the bridge is known, the answer of the bridge can be calculated. Formula 3 gives the maximum value of the acceleration of the bridge, assuming resonance between bridge- and step frequency (because it is the worst case).

$$F_{\text{vert,walking}}(t) = k \cdot 0,4 \cdot F_0 \cdot \sin(2\pi \cdot f_s) \approx 200 \cdot \sin(2\pi \cdot f_s) \quad 2a$$

$$F_{\text{vert,running}}(t) = k \cdot 1,3 \cdot F_0 \cdot \sin(2\pi \cdot f_s) \approx 600 \cdot \sin(2\pi \cdot f_s) \quad 2b$$

$$a_{\text{vert,1,walking}} = \frac{200}{M \cdot 2\zeta} \quad 3a$$

$$a_{\text{vert,1,running}} = \frac{600}{M \cdot 2\zeta} \quad 3b$$

ζ is the damping factor (see chapter 3). The relation between the damping factor ζ and the viscous damping R is shown in formula 4 (for ω see formula 1):

$$R = 2 \cdot \zeta \cdot M \cdot \omega \quad 4$$

The formula 3a, b (taken from [1]) are a good approximation to calculate the bridge acceleration due to one pedestrian, see figure 6. The user of the formula needs some

experience in calculating the generalized mass of the bridge, or one can use a finite element programme therefore.

When using such a programme, one can perform a more detailed calculation with a time and location varying load. Depending on the natural frequencies of the bridge walking and/or running pedestrians should be considered (see table 1 and figure 3). The load velocity along the bridge is $0,9m \cdot f_s$, factor k is 1.

The load- acceleration- relation in the horizontal direction is a little bit different. This is because of the fact, that only each second step gives a load to the right, and the other ones to the left. The load frequency is half of the step frequency, see formula 5. For the maximum value of the horizontal acceleration see formula 6.

$$F_{hor,walking}(t) = k \cdot 0,1 \cdot F_0 \cdot \sin\left(2\pi \cdot \frac{1}{2} \cdot f_s\right) = 50 \cdot \sin\left(2\pi \cdot \frac{1}{2} \cdot f_s\right) \quad 5$$

$$a_{hor,1,walking} = \frac{50}{M \cdot 2\zeta} \quad 6$$

Formula 3a, b and 6 are given in Annex B (informative) in [1]. They give the acceleration due to one pedestrian in resonance.

What should one do to consider more than one pedestrian? Are they all acting in resonance? In [7] a study is described to get a synchronization factor depending on the natural frequency of the bridge. If the natural frequency is in the range of the usual step frequency for walking (see table 1), the synchronization factor is 0,23 for vertical vibrations and 0,18 for horizontal vibrations. This factor takes care of the fact that pedestrians are likely to fall into the frequency of the bridge vibration.

With help of this factor the acceleration due to a group or a continuous stream of pedestrians can be calculated.

$$a_{vert,group,walking} = 0,23 \cdot 13 \cdot k_{vert} \cdot a_{vert,1,walking}, \text{ for running corresponding} \quad 7a$$

$$a_{hor,group,walking} = 0,18 \cdot 13 \cdot k_{hor} \cdot a_{hor,1,walking} \quad 7b$$

13 is the number of pedestrians in the group.

$$a_{vert,stream,walking} = 0,23 \cdot (0,6 \cdot b \cdot \ell) \cdot k_{vert} \cdot a_{vert,1,walking}, \text{ for running corresponding} \quad 8a$$

$$a_{hor,stream,walking} = 0,18 \cdot (0,6 \cdot b \cdot \ell) \cdot k_{hor} \cdot a_{hor,1,walking} \quad 8b$$

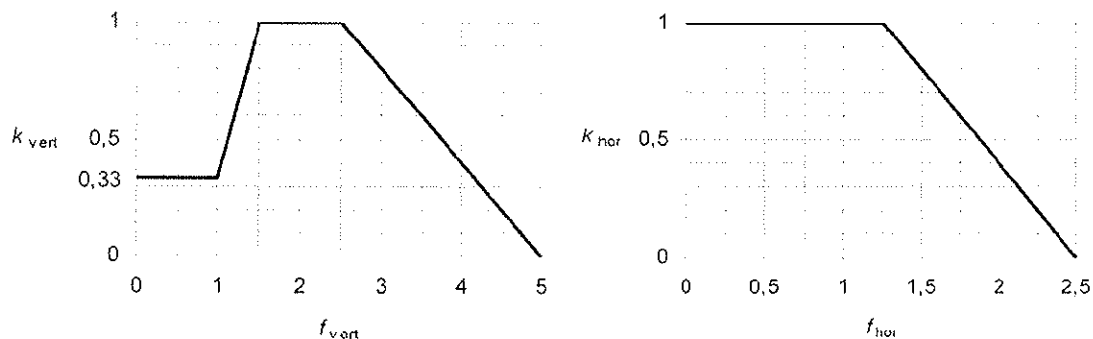
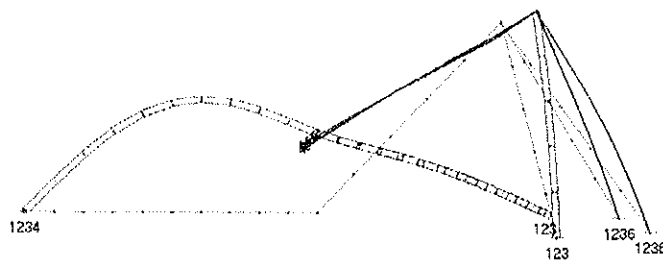


Figure 4a, b: Relationship between the vertical /horizontal natural frequency and the coefficient k_{vert}/k_{hor} , form [1]

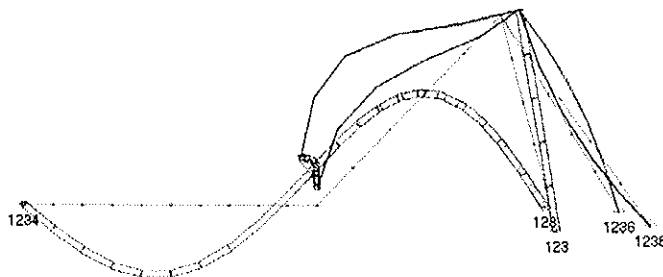
In formula 8a, b 0,6 pedestrians each square meter are assumed. b is the width of the bridge, ℓ the total length. The factor k_{vert} and k_{hor} [figure 4 a and b] consider, that the synchronization is possible only in the range of usual step frequencies.

2.4 Example: Bridge in Zwiesel across the creek Schwarzer Regen

The latest measurement the author has performed was on a Bridge in Zwiesel, see figure 2. Before the bridge was built, the natural frequencies and the expected accelerations had been calculated, see figure 5a, b. In table 2 the results are shown. The calculated accelerations had been such high, so that the installation of a vibration damper was planned. The measurement confirmed the calculation and the necessity of the damper. A running group of 7 pedestrians reached an acceleration of $5,4 \text{ m/s}^2$!



1st mode: $f_c = 1,81 \text{ Hz}$



2nd mode: $f_c = 2,58 \text{ Hz}$

Figure 5a, b: 1st and 2nd vertical bending modes and frequencies of the bridge in Zwiesel

	calculated	measured
first vertical natural frequency	1,78 Hz	1,81 Hz
second vertical natural frequency	2,41 Hz	2,58 Hz
acceleration due to a walking pedestrian	$\frac{200}{19750 \cdot 2 \cdot 0,01} = 0,50 \frac{\text{m}}{\text{s}^2}$	first f_c : $0,60 \text{ m/s}^2$ second f_c : $0,40 \text{ m/s}^2$
acceleration due to a running pedestrian	$\frac{600}{19750 \cdot 2 \cdot 0,01} = 1,5 \frac{\text{m}}{\text{s}^2}$	second f_c : $1,70 \text{ m/s}^2$

Table 2: Comparison of calculated and measured parameters of the bridge in Zwiesel

2.5 Further comparisons

Altogether more than 20 wooden footbridges have been examined. They have been excited by pedestrians walking and running in resonance. The measured accelerations have been compared with the calculated accelerations (see formula 3a, b, for the damping factor see table 3). The results are shown in figure 6.

The calculated and measured accelerations fit together in most of the cases. If the values do not fit, the calculation is on the “safe side”, this means, the calculated value is higher than the measured one.

There are some differences between the values, especially for the bridges with high natural frequencies. This is because of the fact, that running with step frequencies of 3,9 Hz and more is very difficult. In the other cases with “calculated accelerations are greater than measured accelerations”, the runner probably was not exactly in resonance with the bridge.

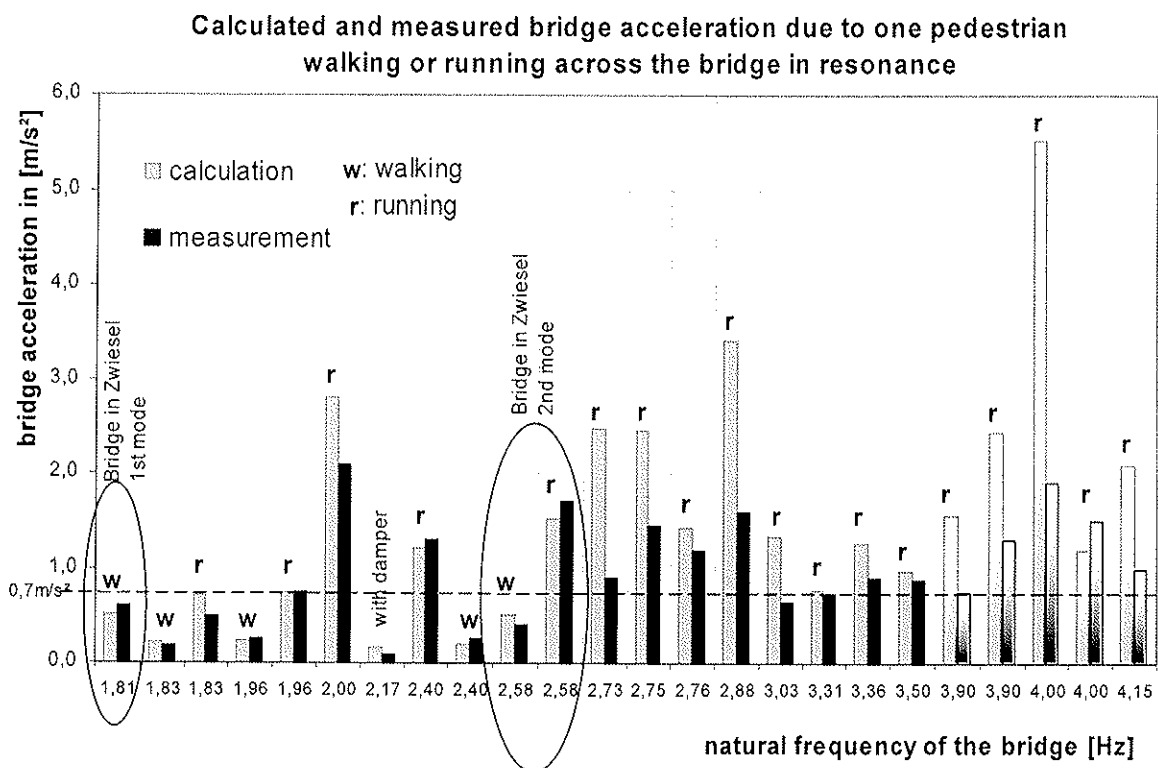


Figure 6: Comparison of calculated and measured bridge accelerations due to one pedestrian walking or running across the bridge in resonance

2.6 Discussion

As one can see in figure 6, most of the measured bridge accelerations due to a running pedestrian are greater than 0,7 m/s². With only few exceptions no bridge has a damper installed. So one can ask:

Is the requirement in Eurocode 5 [1] to strict?

What should one do with the running group or stream?

In the authors opinion the limit of the acceleration caused by running people can be greater than for walking groups. Vibrations caused by running people are more likely accepted than vibrations caused by walking people. The (new) limit of the bridge acceleration caused by running people should depend on the situation of the bridge, for example: the using frequency, the location of the bridge, the static system (see table 3).

Criteria:	The bridge is ...	
using frequency	used rather often.	used rather seldom.
number of pedestrians	often used by crowds of pedestrians.	used by single persons only.
location of the bridge	located centrally in the city.	located away in the country.
	located as a viewpoint (a place to stay).	
static system	covered with a roof (a place to stay).	a simple static system (e.g. simple supported beam).
	suspended by cables (fatigue and optic problem).	
Consequence:	The limit of the bridge acceleration due to running pedestrians should ...	
	be near the values given in figure 1.	be increased.

Table 3: Criteria to increase the acceleration limit for footbridges ... or not

3 Damping factor

In EC5 [1], chapter 6.5.1 (2) the following information is given:

“(2) Where no other values have been verified, the damping ratio should be taken as:

- $\zeta=0,010$ (=1,0%) for structures without mechanical joints,

- $\zeta=0,015$ (=1,5%) for structures with mechanical joints.

NOTE 1: For specific structures, alternative damping ratios may be given in the National annex.”

To specify the damping factor of wooden footbridges the following two methods were used.

3.1 Decreasing vibration

With a mechanical exciter a sinusoidal load is put on the bridge. Then the steady state vibration is reached, the excitation is stopped and the decreasing vibration can be measured (see figure 8b, c). The mechanical exciter in figure 7 was designed and constructed at the Technische Universität München, Fachgebiet Holzbau [4].

The damping factor can be calculated with formula 9, 10.

$$\Lambda = \frac{1}{n} \cdot \ln \frac{a_0}{a_n}; \quad \zeta = \frac{\Lambda}{2\pi} \quad 9; 10$$

Figure 7: Mechanical exciter

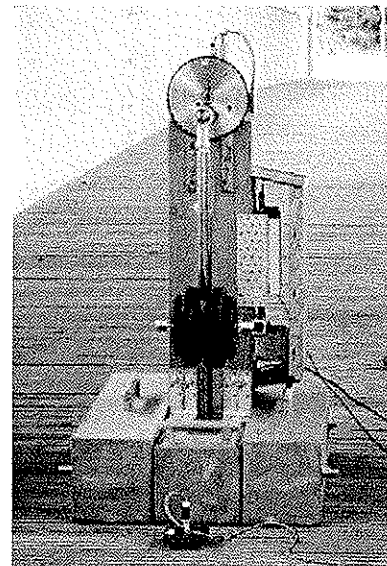


Figure 8 shows two “extreme” damping behaviours of wooden footbridges, a bending beam bridge made of glued laminated timber and bituminous mastic concrete in Uttenreuth and a cable stayed bridge with long cables in Oberesslingen.

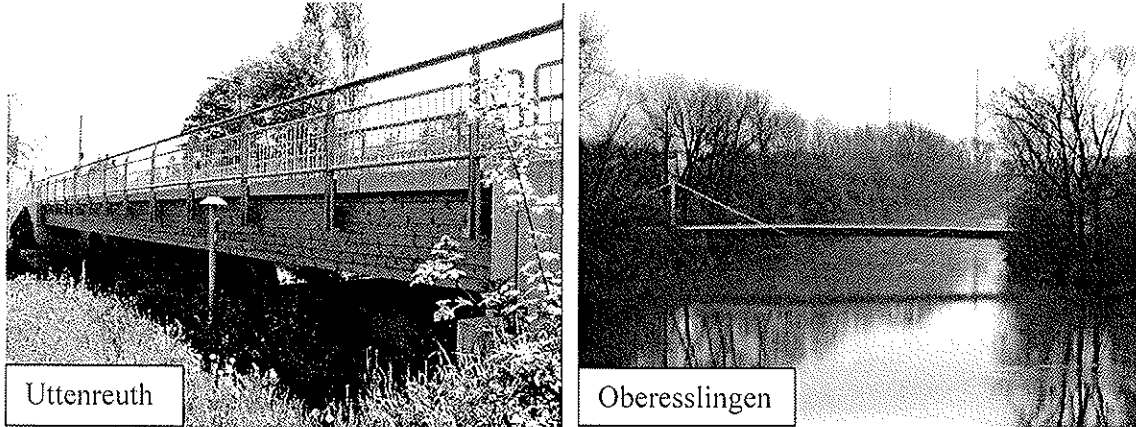
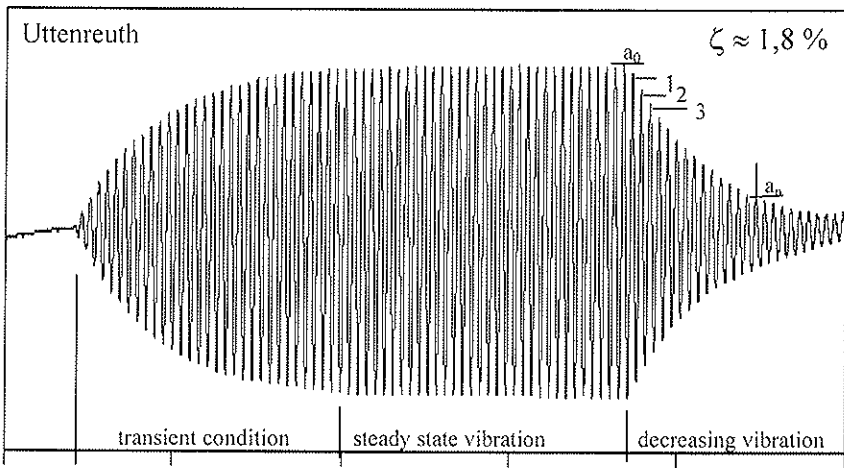


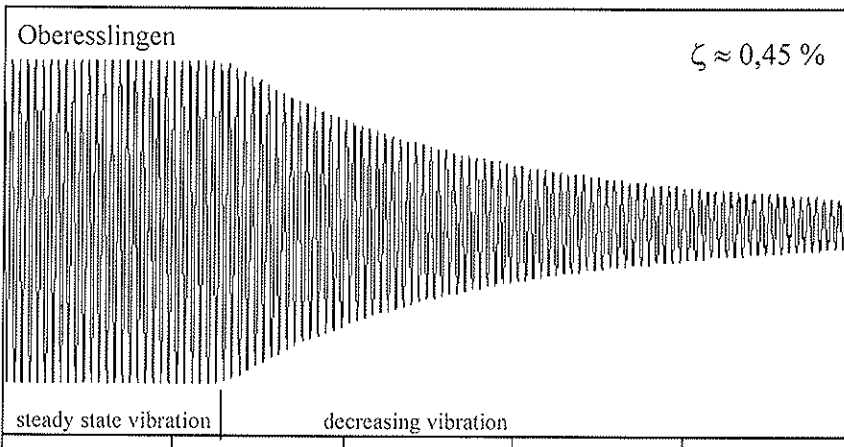
Figure 8a: Pictures of the footbridges in Uttenreuth and Oberesslingen

Zeitreihe Beschl. Datei:u2-240i Kanal: 0 Zeitabstand [sec]:0.5000E-02
 -0.2000E+00 ... 0.2000E+00 lin. Mi 22. 5.2002 12:27:57



0.000E+00 0.800E+01 0.160E+02 0.240E+02 0.320E+02 0.400E+02

Zeitreihe Beschl. Datei:es4-274i Kanal: 0 Zeitabstand [sec]:0.5000E-02
 -0.1000E+01 ... 0.1000E+01 lin. Mo 16.12.2002 10: 5:20



0.400E+02 0.480E+02 0.560E+02 0.640E+02 0.720E+02 0.800E+02

Figure 8b, c: Recordings of the measurements for Uttenreuth and Oberesslingen.

3.2 Resonance curve

The second method to measure and calculate the damping factor of a bridge deals with the resonance curve. Hereby the bridge is excited by the mechanical exciter with sinusoidal loads in different exciting frequencies. The amplitudes of the bridges in the steady state vibration due to the different loads are measured and the resonance curve can be drawn. The maximum amplitude a_{\max} is at resonance between the natural bridge and the exciting frequency. Take $a_{\max} / \sqrt{2}$ and calculate the corresponding exciting frequencies f_1 and f_2 . The difference between these frequencies divided through 2 times the natural frequency is the damping factor (see formula 11 and figures 9 a, b).

$$\zeta = \frac{f_2 - f_1}{2 \cdot f_e}$$

11

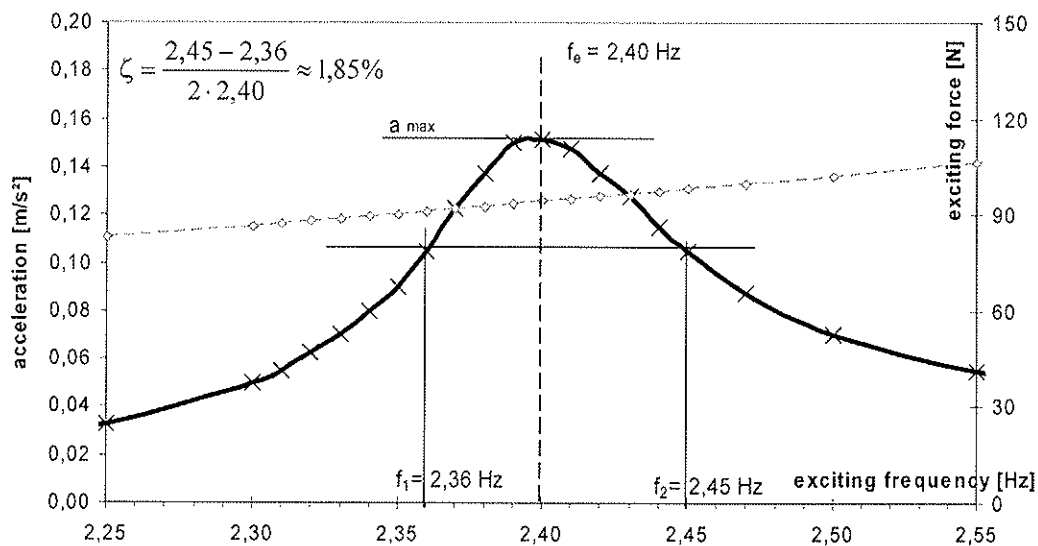


Figure 9a: Resonance curve (measured acceleration and exciting force) for a wooden footbridge in Uttenreuth.

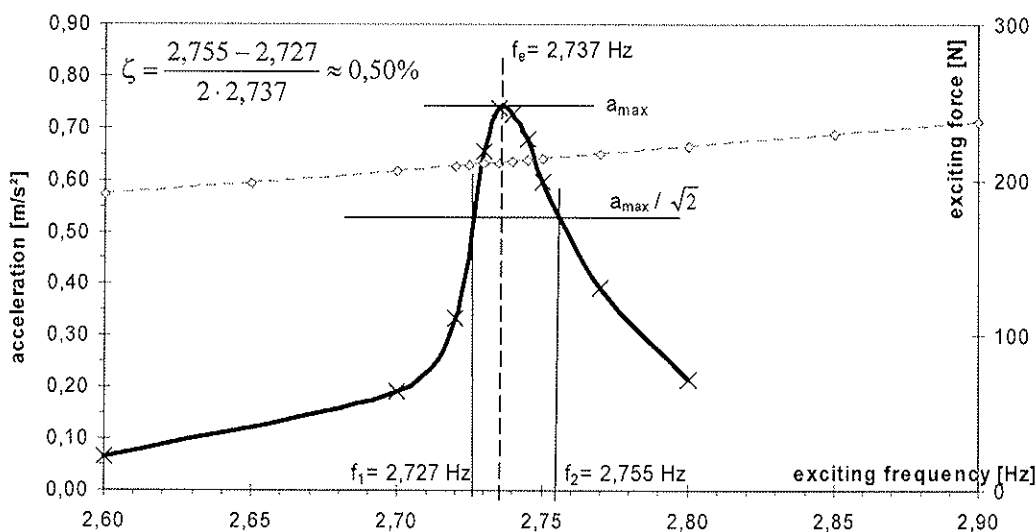


Figure 9b: Resonance curve (measured acceleration and exciting force) for a wooden footbridge in Oberesslingen.

3.3 Results for the damping factor

The damping factors of about 20 bridges have been measured by these two methods and sorted by their static systems. In table 4 suggestions for the damping factors are given.

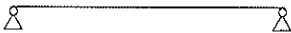
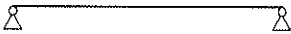
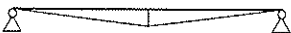

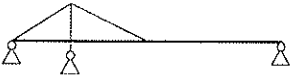
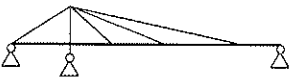
Static system of beam / bridge	Damping factor
Glued laminated beam 	0,50 %
Bending beam bridges made of glued laminated timber 	1,20 %
Suspended beam bridges 	0,90 %
Frame work bridges 	0,80 %
Cable stayed bridges with short cables 	1,00 %
Cable stayed bridges with long cables 	0,30 %
Bituminous mastic concrete	additional 0,30 %

Table 4: Suggestion for the damping factor of wooden beams and footbridges depending on their static system, which is exemplarily shown in the drawings

4. References

- [1] Eurocode 5 - Design of timber structures, Part 2: Bridges. prEN 1995-2: 2004, Stage 49.
- [2] Eurocode 5: Bemessung und Konstruktion von Holzbauten, Teil 2: Brücken. ENV 1995-2: 1997.
- [3] Bachmann, Hugo et al.: "Vibration Problems in Structures - Practical Guidelines". 2nd Edition, Birkhäuser Verlag Basel, Berlin, Boston, 1997.
- [4] Hamm, Patricia: "Ein Beitrag zum Schwingungs- und Dämpfungsverhalten von Fußgängerbrücken aus Holz". Dissertation. TU München, November 2003.
- [5] Hamm, Patricia: "Vibrations of wooden footbridges induced by pedestrians and a mechanical exciter". In: "footbridge 2002, Proceedings of the International Conference on the Design and dynamic behaviour of footbridges" Paris, 20. - 22. November 2002. Editor: AFGC and OTUA. pp 144-145.
- [6] Kreuzinger, Heinrich: "Dynamic design strategies for pedestrian and wind actions". In: "footbridge 2002, Proceedings of the International Conference on the Design and dynamic behaviour of footbridges" Paris, 20. - 22. November 2002. Editor: AFGC and OTUA. pp 129-141.
- [7] Grundmann, Harry; Kreuzinger, H.; Schneider, M. "Schwingungsuntersuchungen für Fußgängerbrücken". In: Bauingenieur 68 /1993. pp 215-225.

INTERNATIONAL COUNCIL FOR RESEARCH AND INNOVATION
IN BUILDING AND CONSTRUCTION

WORKING COMMISSION W18 - TIMBER STRUCTURES

ACTION COMBINATION PROCESSING TO THE EUROCODES

- BASIS OF SOFTWARE TO ASSIST THE ENGINEER

Y Robert

A V Page

R Thépaut

C J Mettem

TRADA Technology

UNITED KINGDOM

Presented by Y Robert

J Köhler asked whether the loads are taken random or from loading codes. Robert answered that they are taken from codes.

Zhang asked if only U.L.S is considered. Robert clarified that also S.L.S. is taken into account.

Action Combination Processing to the Eurocodes

- Basis of Software to Assist the Engineer

Yannig Robert, Arnold V Page, Rémi Thépaut, Christopher J Mettem.

TRADA Technology, UK

1 Introduction

The aim of this research is to provide for the designer a practical and transparent software solution for use with the structural Eurocode suite [1] [2] [3] [4] [5] [6]. This provides choice between speed of design and optimisation. It is also intended to leave the option to proceed to an accurate design with the result obtained from an anterior rapid design without reprocessing all the actions.

Eurocode 0 indicates that the actual effects of actions need to be combined together, rather than the values of the actions themselves as normal with permissible stress codes. This approach provides more accurate results but can be time consuming since the number of combinations to be performed increases quickly with the number of actions applied to the structure. Nevertheless, when a linear elastic analysis is carried out, as it is often the case in timber structural design, the scope of necessary checks can be reduced. Action combinations may be pre-processed to limit or even sometimes remove the need to combine effects of actions at a later stage. Also, the k_{mod} factor can be introduced early to reduce the number of cases to be investigated, by identifying the critical load duration cases.

Because of timber's moisture and time-dependent properties, conforming to the Eurocodes can become more complex and error prone especially for timber designers who lack a knowledge of limit states design, or for others whose knowledge of timber design is limited.

It should be noted that the basis of the logic is founded in EN 1990. Hence, the action combination processing method applies for steel or concrete structures as well as those in timber. With experience, mixed material structures (timber with steel, for example), or timber-concrete, timber steel composites are feasible.

The theoretical basis of the software will be discussed in this paper.

2 Design methodology

The software under development is intended to permit the designer to check a structure using the following sequence:

2.1 Preliminary tasks

- Quantify the actions on the structure: pattern; characteristic value(s); associated load duration.
- Group all of the actions with the same patterns together. Two actions are considered as having the same patterns as one another when they are applied at the same position, with the same distribution and in the same orientation. However, they can have different load durations, be of a different nature, and have favourable or unfavourable effects without being regarded as a separate group.
- Use the action pre-processor to pre-process each group into an equivalent action of the same pattern as the initial action with a design value for each duration, a reduced design value for each duration, a critical load duration case and, for each duration, an indication of the leading variable action of the group

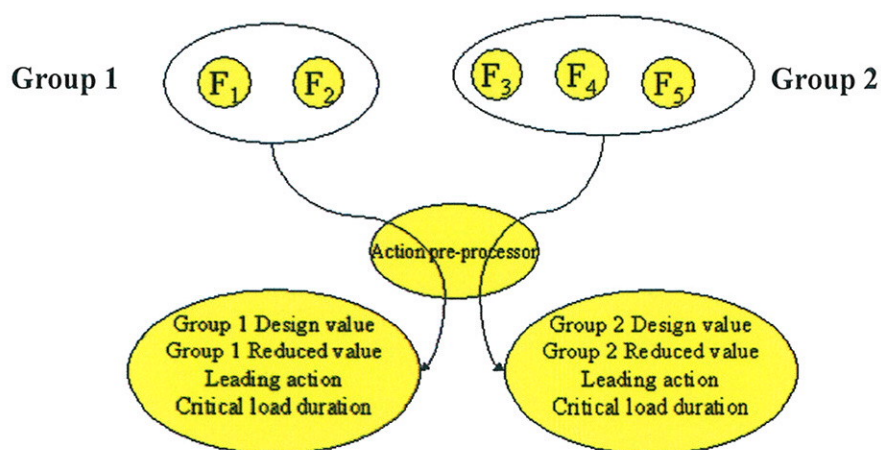


Figure 1 Example of a pre-processing logic with actions F1, F2 having one pattern and F3, F4, F5 another pattern

After this preliminary stage, the designer has the choice between a rapid but conservative method and a precise method.

2.2 Rapid method

The rapid method is illustrated in Figure 2. Below are the steps which the designer needs to take:

- For each load duration which proves to be critical for at least one group of actions, calculate the effects of the corresponding ULS design values of all the actions groups.

- For each SLS combination which has to be checked, calculate the effects using the SLS design values of all the actions groups.
- Check ULS and SLS to the relevant material code.

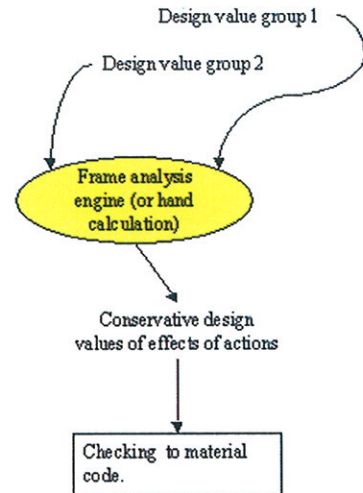


Figure 2 Rapid processing of above example

2.3 Precise method

The precise method is illustrated in Figure 3. The designer takes the following steps:

- For each load duration which proves to be critical for at least one group of actions, take each group in turn and combine the ULS design values of its equivalent action with the reduced design values of the other groups for that load duration.
- For each SLS combination which has to be checked, take each group in turn and combine the design values of its equivalent action with the reduced design values of the other groups.
- Check that ULS and SLS limits are not exceeded, by applying the relevant materials code.

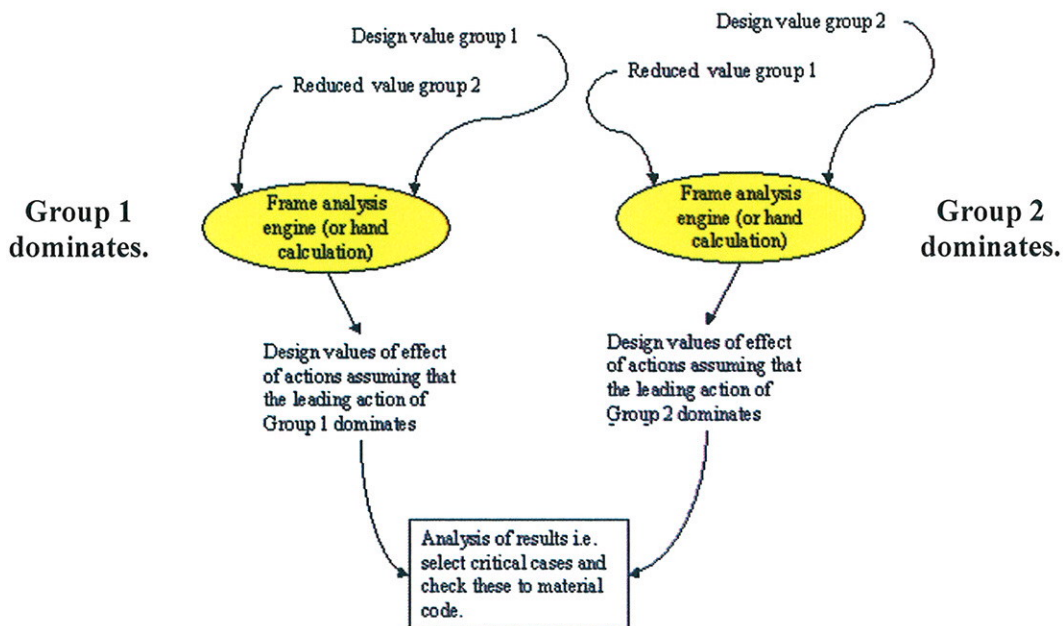


Figure 3 Accurate processing of Figure 1 example for one load duration or SLS combination

3 Basis of the action pre-processor

3.1 Restrictions and hypothesis

In order to make possible the design of the action pre-processor, the following assumptions were made:

- The structure is designed and checked using EN 1990, EN 1991, and the appropriate material codes.
- The structural model used to calculate the action effects assumes a linear deformational behaviour of the structure.

3.2 Design value and reduced values of a group of actions

The design value of a group for a particular combination is defined as the combination of the characteristic values of the actions part of this group in accordance with the relevant EN 1990:2002 equation.

Pre-processing actions into design values directly before performing a structural analysis leads to inaccurate results. As they are combined in separate groups, each design value has a leading variable action embedded in it. Thus if there is more than one group, some actions that are not actually “leading” are considered to be so. This normally results in a conservative design, since the representative value of a variable action (ψF) is always numerically larger when the action is assumed to be leading. Thus, the “rapid method” can be safely used when speed of design is of importance.

To overcome this conservatism, a new value, the “reduced value”, has been introduced into the logic. This is obtained using the combination of EN 1990:2002 appropriate to the limit state under consideration, but assuming that no particular variable action is leading. For instance, in the case of four actions $G_k, Q_{k,1}, Q_{k,2}, Q_{k,3}$ having the same geometrical pattern as one another, the design and reduced values of the actions group for the ultimate limit states fundamental combination are respectively:

$$F_{design} = \gamma_G G_{k,1} + \gamma_Q (Q_{k,1} + \psi_{0,2} Q_{k,2} + \psi_{0,3} Q_{k,3})$$

$$F_{reduced} = \gamma_G G_{k,1} + \gamma_Q (\psi_{0,1} Q_{k,1} + \psi_{0,2} Q_{k,2} + \psi_{0,3} Q_{k,3})$$

Thus when the “design value” of a group is combined with the “reduced value” of other groups, a result fully in accordance with EN 1990:2002 is obtained. Nevertheless, in non trivial cases, the group of actions containing the leading variable action cannot be determined immediately, particularly bearing in mind for timber the additional complication of the k_{mod} effect. Hence, it is necessary to assess in turn each of the groups as potentially leading.

Hence E_d , the design value of the effects of three actions groups for a specific design check can be obtained:

$$E_d = \text{Max} \begin{cases} E\{F_{design,1}; F_{reduced,2}; F_{reduced,3}\} \\ E\{F_{reduced,1}; F_{design,2}; F_{reduced,3}\} \\ E\{F_{reduced,1}; F_{reduced,2}; F_{design,3}\} \end{cases}$$

Where $E\{\text{Actions groups}\}$ = The effect due to the actions groups calculated with an appropriate structural model.

And $\text{Max}(\text{value1, value 2,...})$ defined as the value having the maximum absolute value.

3.3 Leading variable action

Within a group of actions and for each combination and load duration case, the action generating the greatest design value is the leading variable action. Thus, the software tests in turn each of the variable actions as leading.

3.4 Determination of the limiting load duration case

In the case of an ultimate limit states check, the time dependent properties of timber's strength implies that separate checks are necessary for each load duration case.

Indeed, in prEN 1995-1-1:2003 we have: $R_d = k_{\text{mod}} \cdot \frac{R_k}{\gamma_M}$

Where

	R_d the design value of a load carrying capacity
	k_{mod} modification factor for duration of load and moisture content
	γ_M partial factor for material properties
	R_k the characteristic load carrying capacity

Because, k_{mod} is load duration and moisture content dependent, R_d , the design resistance, alters for each load duration case. Consequently, checks need to be made for each case in turn. Nevertheless, governing cases can more rapidly be anticipated by integrating the k_{mod} factor early in the process.

According to EN 1990:2002 and prEN 1995-1-1, the following condition should be met:

$$E_d \leq k_{\text{mod}} \cdot \frac{R_k}{\gamma_M} \quad \text{Where } E_d \text{ is the design value of the relevant actions effect}$$

$$\text{Or } \frac{E_d}{k_{\text{mod}}} \leq \left(\frac{R_k}{\gamma_M} \right)$$

R_k and γ_M depend only upon the material, and in some cases the geometry of the structure, hence this particular ratio is not time dependent. Thus, for each load duration case in turn, the ratios of E_d and k_{mod} may be compared, with the highest result indicating the limiting case. Thus the action pre-processor logic uses this observation to predict the limiting load duration case for each group of actions.

4 Comparison of the three methods

The following compares three methods: Conventional post-processing, the rapid method using the software logic, and the precise method using the software logic.

4.1 Test case

To assess the various potential solutions to verify a structure, consider an imaginary structure, which is submitted to a variable number of actions. These actions can be grouped by patterns in n groups, each containing m variable actions and one permanent action. Below is an example for three groups of actions each containing three variable actions.

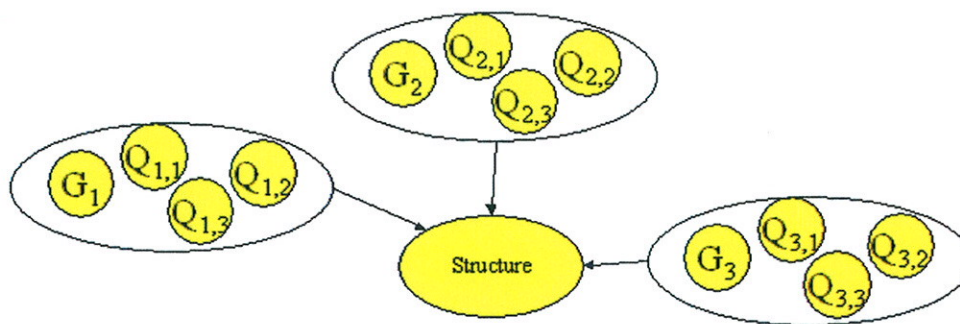


Figure 4 Test case comprising three groups of actions

The effect of an action $Q_{i,j}$ is written $q_{i,j}$. (Each action has various effects in different regions of the structure, but for simplicity, $q_{i,j}$ is the effect relevant to the context).

It is also assumed that k ultimate limit states checks are required. When comparing the methods below, the fundamental combination is considered in just one load duration case. Nevertheless in the case of a real life design, all appropriate load duration cases would need to be assessed. Also serviceability limit states checks would probably be required. It is emphasised that the logic explained, and the software outlined, is to assist rather than replace, the experience and judgement of the engineer.

4.2 Assessment of post-processing without the logic

The post-processing of actions entails calculating the effect of each action in turn and then processing characteristic values of effects into design values. This method leads to the optimum result. However the number of structural appraisals required is equal to the number of actions; furthermore in permutation. Each time the designer deems a check to be necessary, he or she needs to combine the characteristic effects of the actions together in all their permutation and then check the structure to the relevant code. For all but the most trivial structures and loading schemes this is a formidable task.

4.3 Assessment of the rapid method using the software logic

With the exception of the early pre-processing, the rapid method is similar to the design procedure which would be used while checking a structure with a permissible stress code. Thus, it can be expected to be quite practical. Nevertheless, the method generates somewhat conservative results.

Considering the test case, it can be shown that for an ultimate limit states check with the fundamental combination:

$$\frac{F_{rapid}}{F_d} \leq \frac{n}{n - \chi \times (1 - \psi_0) \times (n - 1)}$$

Where

- F_{rapid} = value obtained with this method
- F_d = value obtained by post - processing
- n = number of action groups as in 4.1
- $\chi = \frac{\sum q_{i,j}}{\sum q_{i,j} + \sum g_i}$
- ψ_0 as defined in EN1990 : 2002

These values are plotted in Figure 5 with a ψ_0 assumed to be 0.7. This shows that the simplified but rapid method is more conservative for very light structures, and for structures which are submitted to many different actions with varying patterns. In the case of timber structures, χ is typically between 0.5 and 0.8, so that values obtained with the simplified method are likely to be at the most 30% conservative.

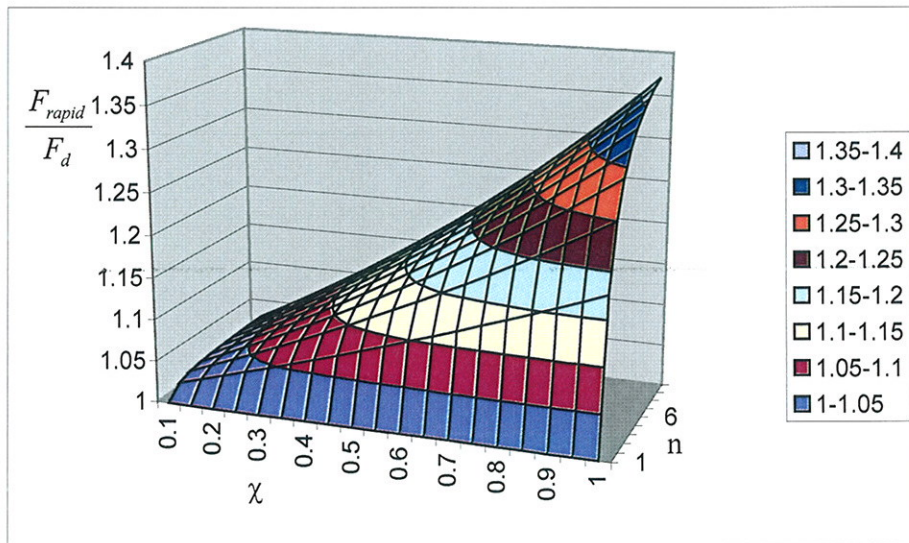


Figure 5 Rapid method compared with precise values

Since it is a time-efficient solution, designers are likely to regard it as of value, especially at the preliminary design stage. Particularly with bespoke or architect designed structures, many trade-offs and radical alterations occur before the final proposed solution is presented to the client and approving authorities. The entire structural form, element types and connection arrangements may be subject to alterations, and the engineer is expected swiftly to be able to indicate the likely implications. [7]

4.4 Assessment of the precise method using the software logic

As is to be expected, the precise method leads to the exact result, but involves evaluating more combinations. Each group of actions needs to be assessed as potentially leading in turn, so that as many structural analyses are required as there are groups of actions.

Second order linear-elastic analysis is defined as “an elastic structural analysis using linear stress/strain laws applied to the geometry of the deformed structure” [1]. In the case of timber construction such analysis may be necessary to analyse slender spatial structures such as gridshells. These types of structures bring into being the aesthetic exhilaration, architectural quality, and potentially the sustainability benefit of timber [8].

Generally frame or space analysis programs which perform second order linear analysis adopt a two step procedure. Firstly, the deformation of the structure is calculated, then stresses are re-computed integrating the estimated deformations. It is also verified at this stage that the structure is neither locally nor globally unstable. The action pre-processor logic is thus an efficient approach to performing more precise second order linear analyses, using commercially available, general-purpose structural software.

4.5 Comparison of methods

Table 1 below summarises and evaluates the number of tasks necessary to obtain design values to verify to ULS a case such as that described above, using each of different methods. It is clear that post-processing leads to the greatest number. Unless these are entirely performed by purpose-written and independently checked and assured software, such checking may be prohibitively elaborate.

Stage	Post-processing	Rapid method	Precise method
Pre-processing	No	Yes	Yes
Structural analysis	$n(m+1)$	1	n
Post-processing	Process design values from characteristics values k times.	No	Select the more severe result k times

Table 1 Summary and evaluation of tasks which each method entails.¹

The comparison outlined in table 1 considers a single load duration. With more than one load duration involved, pre-processing is likely to provide an even greater advantage.

¹ n = number of actions groups

m= number of variable actions per group

k= number of ULS checks which are required

5 Conclusion

This research indicates that the pre-processing of actions is an efficient way of designing with the structural Eurocodes. The logical approach provides the engineer with a choice between precision and speed of design. It enables the upgrade of a rapid design into a precise one, at “project stage 2”.

The logic and ensuing software under development requires testing with real life designs. Timber construction has many forms, ranging from the single family timber dwelling to long span structures such as sports halls and bridges. Thus different engineers designing various structures are likely to come up with several solutions to prove the safety and serviceability of these structures.

The authors would welcome comments on the paper and offer to test the prototype software. Please address any responses to Yannig Robert from whom copies of the software can be obtained.

6 Acknowledgement

The authors gratefully acknowledge the advice and assistance given by Buro Happold Engineers especially by Jamie Siggers and Jonathan Roynon, Glued Laminated Timber Association (UK), Gifford Consulting Engineers, Institution of Civil Engineers, Local Authority Building Control (LANTAC), NHBC Engineers, and the Steel Construction Institute.

7 References

- [1] CEN, *EN 1990:2002 Eurocode – Basis of structural design*, 2002, Brussels, CEN
- [2] CEN, *EN 1991-1.1:2002 Eurocode 1: Actions on structures. General actions – Densities, self-weight, imposed loads for buildings*, 2002, Brussels, CEN
- [3] CEN, *EN 1991-1.3:2003 Eurocode 1: Actions on structures. General actions – Snow loads*, 2003, Brussels, CEN
- [4] CEN, *DD ENV 1991-2.4:1997 Eurocode 1: Basis of design and actions on structures. Actions on structure – Wind actions*, 1997, Brussels, CEN
- [5] CEN, *DD ENV 1991-2.6:2000 Eurocode 1: Basis of design and actions on structures. Actions on structure – Actions during execution*, 2000, Brussels, CEN
- [6] CEN, *prEN 1995-1-1:2003 Eurocode 5 – Design of timber structures Part 1-1: General - common rules and rules for buildings*, 2003, Brussels, CEN
- [7] Natterer J and Sandoz J.L. “Conceptual design”, in Blass H J et al (eds) *Timber engineering STEP 2*, (The Netherlands, Centrum hout, 1995), pp E2/1-E2/8
- [8] Harris R et al, “The use of timber gridshells for long span structures”, *Proceedings of the 8th world conference on timber engineering WCTE 2004*, Vol 1 (June 2004), pp. 99-104

INTERNATIONAL COUNCIL FOR RESEARCH AND INNOVATION
IN BUILDING AND CONSTRUCTION

WORKING COMMISSION W18 - TIMBER STRUCTURES

PROBABILISTIC MODEL CODE FOR THE DESIGN OF TIMBER STRUCTURES

J Köhler

M H Faber

Swiss Federal Institute of Technology, Zürich

SWITZERLAND

Presented by J Köhler

R Steiger asked whether the Probabilistic Code is used as a design code or for calibration. Köhler answered that it supports the engineers in their decision as well as it is a basis for decision in code drafting.

P Glos stated that the probabilistic design code is important but that he cannot see any progress in the last 20 years. There are data available to check the model and find out which accuracy of information is really needed. The existing system for designing structures is good.

H Blass answered that off-shore structures are designed according to the probabilistic design methods.

J Köhler added that it is also important to compare the different building materials.

K Crews added that there is also an application for bridges.

Probabilistic Model Code for the Design of Timber Structures

Jochen Köhler¹, Michael H. Faber

Swiss Federal Institute of Technology, Zurich, Switzerland

1 Foreword

During the last 2-3 decades one of the main activities of the Joint Committee on Structural Safety (JCSS) has been to establish a Probabilistic Model Code (PMC) for Reliability Based Design of Structures. In early 2001 a first version of the JCSS PMC was published on the web: www.jcss.ethz.ch. Presently the JCSS PMC contains important information regarding the general probabilistic modeling of loads and load combinations together with probabilistic models for the resistance related material characteristics of concrete, steel and soil.

One of the remaining building stones required to complete the JCSS PMC is a set of relevant probabilistic models for reliability assessment of timber structures. This work in fact was initiated already some 6-8 years ago at which time the JCSS asked the timber engineering community for assistance in accomplishing this important task. This request resulted in the initiation of the European Community COST E24 Action Reliability of Timber Structures in the year 2001. The aim of this research project is to establish an operational basis for reliability analysis of timber structures.

The present document contains a summary of a draft proposal for the probabilistic modeling of timber material properties for design purposes. It reflects the current state of the art of the ongoing discussion among the participants of the COST action E24 and the members of the JCSS. The aim of presenting this document at the CIB-W18 meeting is to draw attention on the ongoing development of a probabilistic model code for timber structures and to raise discussions about this subject on a broader platform. Some models still have to be verified and many model parameters have to be quantified. Members of the CIB-W18 are kindly invited to join these discussions.

To obtain the complete version of the document and to find some background information about the COST action E24 the interested reader is invited to visit the homepage of the action at:

<http://www.km.fgg.uni-lj.si/coste24/coste24.htm>

2 Scope and limitations

The present proposal of the PMC for timber structures mainly concerns modeling the material properties of solid structural timber. Important sections about 'glued laminated timber' and 'other materials' have to be included. The proposed models are mainly based on test programs and investigations with North American and European softwoods. For some other softwood

¹ Institute of Structural Engineering IBK, Swiss Federal Institute of Technology ETH; CH-8093 Zürich, Switzerland. Direct Phone: +41 1 633 40 78, e-mail: jochen.koehler@ibk.baug.ethz.ch

and especially for hardwood the underlying assumptions are less or not appropriate. To become operational more specific information has to be included especially in section 8 where quantitative information of timber grades and species has to be specified. Furthermore several sections are still in progress and have to be further discussed within the international timber research community. Please note that quantitative information in this draft still has to be justified and agreed upon.

3 Modeling framework for timber material properties

Timber is by nature a very inhomogeneous material. The timber material properties depend on the specific wood species, the geographical location where the wood has been grown and furthermore on the local growing conditions of every single part of a tree. Timber is an orthotropic material, i.e. it consists of “high strength” fibers/grains which are predominantly orientated along the longitudinal axis of a timber log/ tree and packed together within a “low strength” matrix. Material properties such as e.g. the ultimate bending stress and the bending stiffness depend on the orientation of the moment axis to the fiber/grain direction. Considering the material properties of a timber structural element or a test specimen it has to be taken into account that the timber element is taken out from its natural configuration. Irregularities in regard to grain direction, knots, fissures, etc. become, in addition to the orthotropic characteristics mentioned above, highly decisive for the load bearing capacity of a timber structural element or a test specimen of structural dimension. Only in very small test specimens it is possible to depress these irregularities; with so called clear wood specimen it is possible to investigate the orthotropic material properties of timber. However, for timber in structural size the above mentioned irregularities are of highest interest and strength properties of structural timber are therefore usually determined by direct testing of timber elements of structural size; strength is defined on an element level rather than on a material level (Thelandersson and Larsen [2003]). Consequently, the strength data of timber material of structural size reflects the load bearing capacity of a test specimen in regard to the considered failure mode. Even if the test data are expressed in stress units it is important to note, that the stress is calculated assuming ideal elastic and homogeneous behavior of the material of the considered element. As the likelihood of occurrences of growth irregularities increases for increasing dimensions of the considered structural element the strength and stiffness related material properties strongly depend on the size and the cross sectional proportions of the structural element.

In addition to the above mentioned characteristics, the surrounding climate, i.e. temperature, humidity and the load history may have significant influence on the material properties. Therefore, in summary, timber material properties are always conditional on size, climate and loading characteristics.

In Figure 1 the general principle of the proposed modeling framework is illustrated. Reference timber material properties \mathbf{x} are defined; the bending strength, the modulus of elasticity and the density are the material properties with the highest experimental evidence. \mathbf{y} are denoted as other timber material properties. The material properties are seen in three different contexts. In the middle part of Figure 1 \mathbf{X}^0 and \mathbf{Y}^0 are defined as random variables of the material properties of finite reference volumes measured under reference test conditions². In the bottom part of Figure 1 \mathbf{X}^* and \mathbf{Y}^* are defined as random variables of the material properties under any conditions and any size of the component. Models for deviations in climate,

² Reference test condition is defined in regard to the climate in which the volumes are conditioned prior to the test and in regard to the type of loading.

loading and size compared to the reference volumes and conditions are proposed in this document. One special case of deviation from reference volume and conditions are test data x' and y' obtained under standardized test conditions. Various test standards for the evaluation of timber material properties exist on an international scale. However, nearly all available experimental evidence is related to these test standards. Therefore focus is directed to the problem of relating information from standardized tests to the models of reference volumes and conditions.

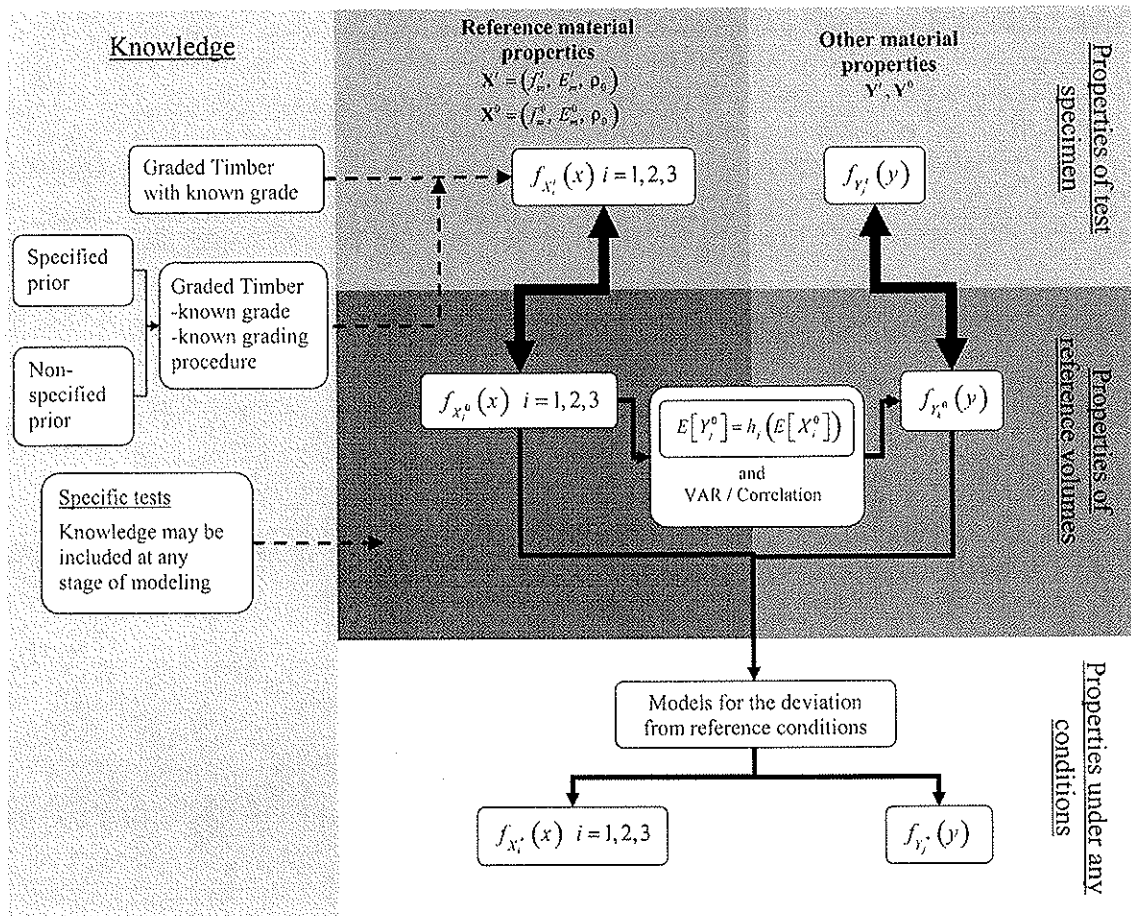


Figure 1 General principle of the modeling of timber material properties; integration of knowledge.

Beside the geometrical conditions, climate and loading, the timber material properties are strongly depending on the timber species, the origin and the quality control procedure which is applied. Information about these conditions may be present or not. Also test results about the material properties could be available. In the left part of Figure 1 different states of knowledge are illustrated and it is indicated how may be used in the modeling.

4 Reference Timber Material Properties

The reference timber material properties are the bending strength, the bending modulus of elasticity and the density.

Reference timber material properties are:

f_m bending strength

E_m bending modulus of elasticity

ρ_0 density

4.1 Spatial variation of timber material properties

4.1.1 Scales of modeling variations, hierarchical model

Three hierarchical levels of variation are distinguished: micro, local (meso) and global(macro).

The variability of the distribution parameters of timber specimen strength per sawmill represents a typical global parameter variation. This variation is primarily the result of different origins of the timber and the different procedures applied for identifying the considered grade. Parameter variations may also be due to statistical uncertainties.

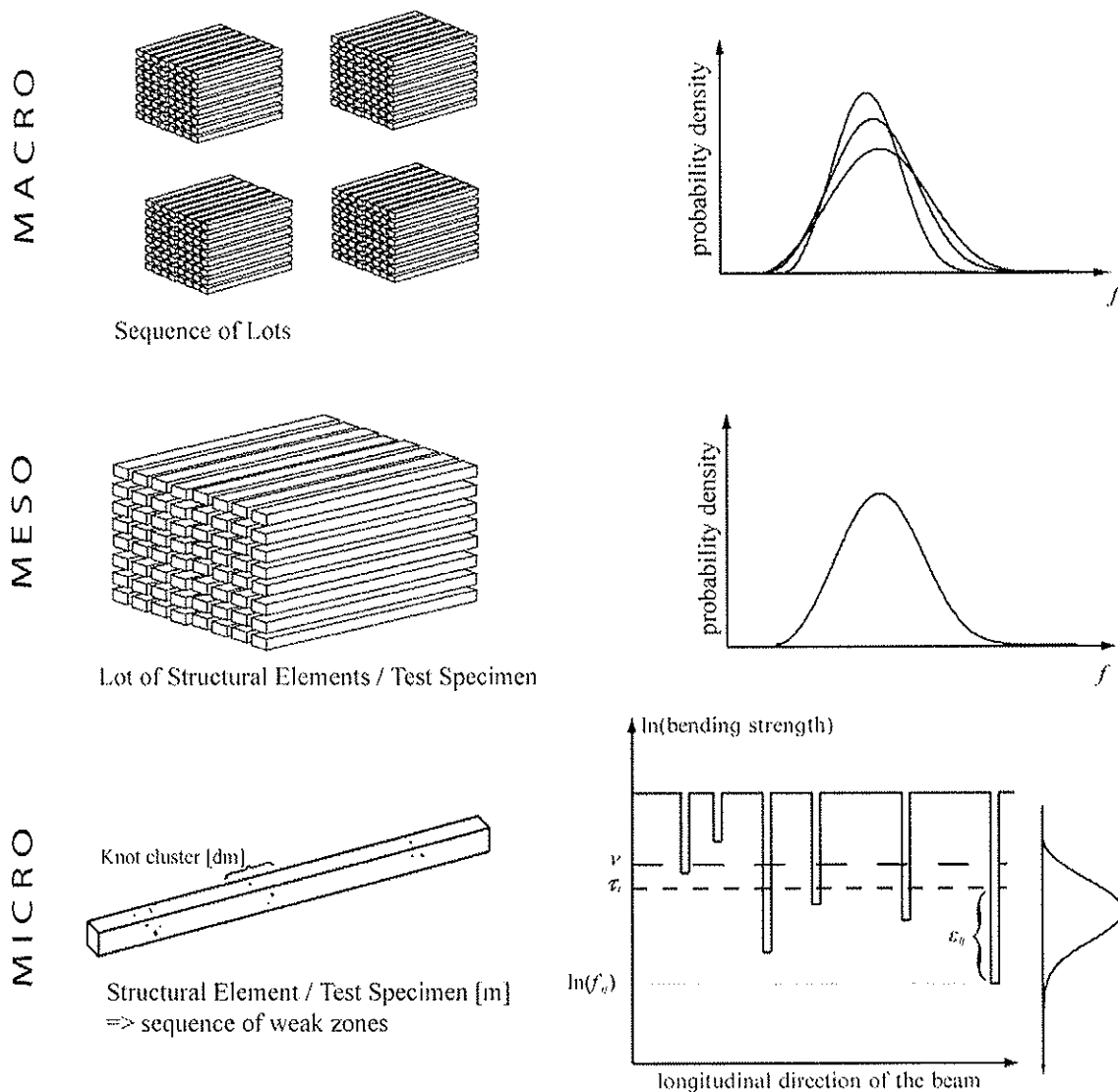


Figure 2 Different levels of modeling of timber material properties.

The variations between timber specimen or components of a specific sub-population are modeled at the meso level. Information about the specific sub-population may be obtainable

from tests with the purpose of reducing the parameter variation. The geometrical scale of the test specimens is in order of the size of a structural element and probably most conveniently measured in meters.

At the micro-level the irregularities in the timber material itself are represented. These are basically uncontrollable as they originate from natural variability such as the random distribution of knots fissures and grain deviations. The geometrical scale of these irregularities could be measured in μm at grain level or in cm if knots and weak sections are considered. The various material properties considered on element level, i.e. the load carrying capacity of such elements are qualified through the non homogeneous properties on this micro scale level. The models for timber material properties proposed are taking this into account.

In Figure 2 the three different scales of stochastic modeling are illustrated. At the micro level, the random variations in one single component are modeled. Different models can be used depending on the sensitivity of material properties to different irregularities in the material; and how these irregularities can be described. At the meso level the material properties of entire components or specimen from one population are modeled. Test samples can be used to estimate the parameters of proper probability distribution functions for describing the random nature of the properties on this level. Macro level variations are denoted as the variations between different populations (lots) of timber components. They can be taken from different suppliers which are taking the timber from different producers or different grading procedures are involved qualifying the populations to a specific grade. The distribution parameters of the modeled material properties of these different populations are varying. Since specific information about specific populations is rare this variations has to be taken into account at the macro level.

4.2 Bending Strength

In the present model a timber component is assumed to consist of a finite number of weak sections separated by strong sections. Failure of one single weak section is determining the strength of the entire component and consequently the component can be modeled as a series system of weak sections.

4.2.1 Variations of bending strength properties

The proposed model for the variation of bending strength properties is based on the findings in, among others, Riberholt and Madsen [1979], Czmocho et al [1991], Isaksson [1999] and Ditlevsen and Källsner [2004]. The main assumption is that failure can occur only at a finite number of locations in a structural component. These locations are called weak sections.

In Isaksson [1999] a hierarchical model is formulated, where the strength variability is treated at three different levels:

$$\ln(f_{ij}) = \nu + \tau_i + \varepsilon_{ij} \quad (2.1)$$

where,

f_{ij} is the strength of weak section j in component i .

ν is the logarithm of the mean strength of all weak sections of all components.

τ_i is the realization of the difference between the logarithm of the mean of the strength of the sections within a specific component i and ν . τ is modeled by a normal distributed random variable with zero mean and standard deviation equal to σ_τ .

ε_{ij} is the realization of the difference between the strength of weak section j in component i and $\nu + \tau_i$, i.e. the variability within one particular component in one particular population. ε is modeled by a normal distributed random variable with zero mean and standard deviation equal to σ_ε .

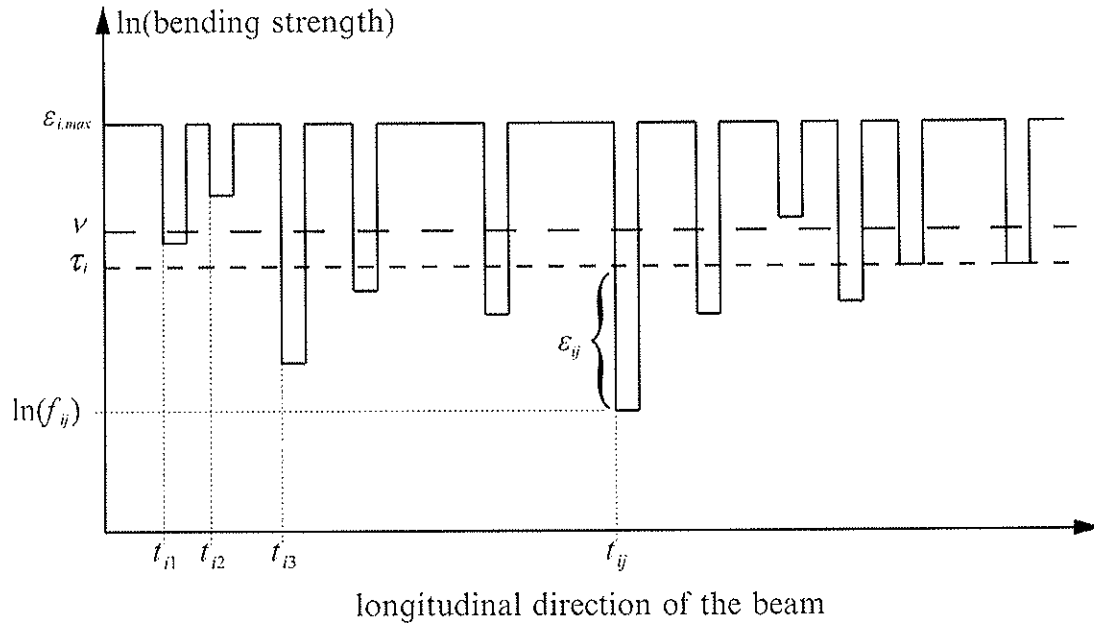


Figure 3 Modeling of the longitudinal variation of bending strength of a timber beam, Isaksson [1999].

For 'beam shape' components ($l \gg h, b$) it is assumed that weak sections (and correspondingly the number of weak sections) are distributed spatially according to events $(t_{i1}, t_{i2}, t_{i3}, \dots, t_{ij})$ of a Poisson process along the longitudinal axis of the component. As shown in Figure 3, two adjacent weak sections are separated by strong sections. The strength of the strong sections $\varepsilon_{i,max}$ in one component is assumed to be constant and has the same magnitude as the strongest of the modeled weak sections. Following the Poisson assumption the distances between the weak sections are exponentially distributed. The lengths of the weak sections are assumed to be constants equal to the depth of the cross section of the component. Sample parameter values for the Poisson process model are given in Isaksson [1999].

The reference volume for bending strength is defined through the random length of one strong section and one weak section and a depth of 150 mm. The width is assumed to be not relevant. According to Equation (2.1) the strength of a weak section is lognormal distributed and assumed to be correlated with the other reference material properties.

4.3 Modulus of Elasticity

The modulus of elasticity in general is considered as a property of an entire structural element. However, in some cases the lengthwise variations may be of concern.

4.3.1 Variations of Modulus of elasticity

The lengthwise variation of the bending modulus of elasticity is based on the lengthwise variation model for bending strength. The realizations of the modulus of elasticity are directly related to the realizations of the strength of a weak section following the model proposed for bending in the foregoing. As illustrated in Figure 4 the length l_{ij} of a section with modulus of elasticity E_{ij} is derived based on the bending model as follows

$$l_{ij} = \frac{(t_{ij} - t_{ij-1})}{2} + \frac{(t_{ij+1} - t_{ij})}{2} \quad (2.2)$$

where t_k are the events of the Poisson process.

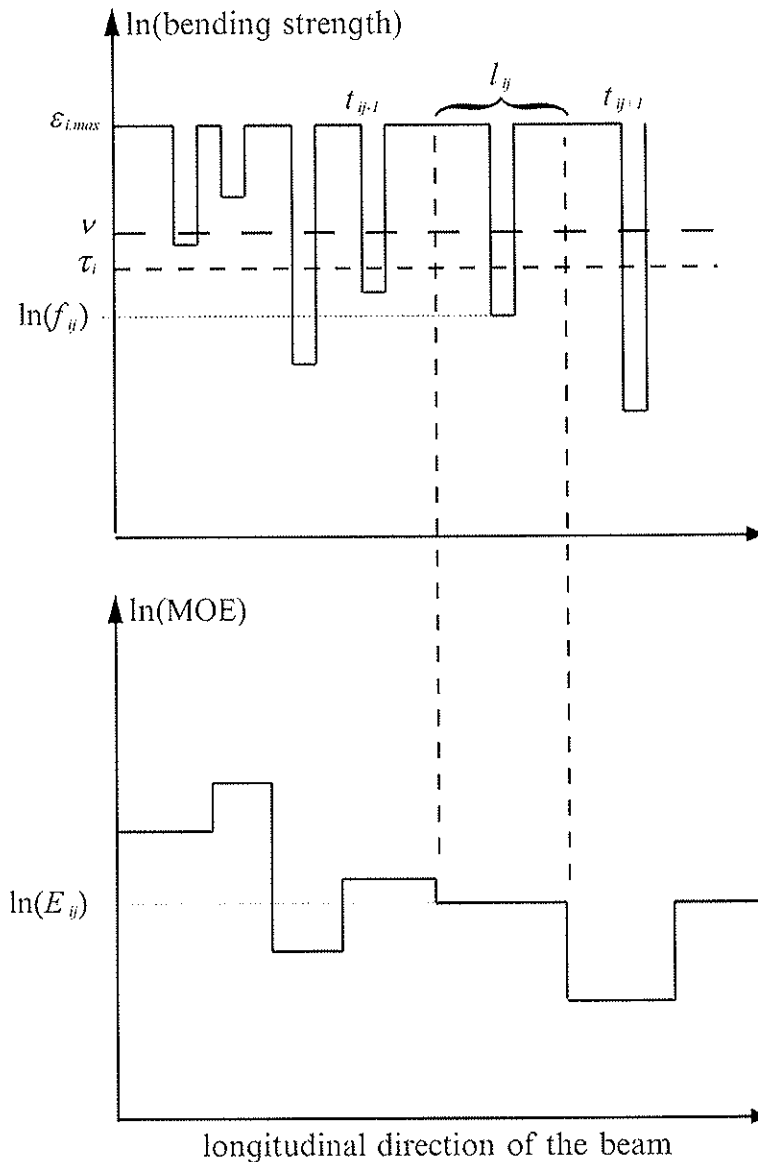


Figure 4 Modeling of the longitudinal variation of MOE of a timber beam.

E_{ij} is assumed to be a realization of a lognormal distributed random variable and assumed to be correlated with the other reference material properties.

4.4 Density

Density is assumed to be constant for the entire timber component. It is modeled as a normal distributed random variable and assumed to be correlated with the other reference material properties.

4.5 Parameters and correlation matrix

Quantitative information about the probabilistic models is given in sections 5 and 8.

5 Other Material Properties

In Table 1 other timber material properties are summarized. A probabilistic model and the relation of their parameters to the parameters of the reference material models is proposed. The size of the considered finite reference volume is referred as spatial reference.

Table 1: Probabilistic models of other timber material properties and their spatial reference. (quantities are tentative and basis for further discussion)

Property	Spatial reference Distribution	Expected Values $E[X]$	Coefficient of variation $COV[X]$
Tension strength parallel to the grain:	Weak section – as bending LOGNORMAL	$E[f_{t,0}^0] = 0.6 E[f_m^0]$	$COV[f_{t,0}^0] = 1.2 COV[f_m^0]$
Tension strength perp. to the grain:	Weibull concept WEIBULL	$E[f_{t,90}^0] = \min\{0.8; 0.0017 E[\rho_0]\}$	$COV[f_{t,90}^0] = COV[\rho_0]$
MOE - tension parallel to the grain:	Weak sections – as MOE-bending LOGNORMAL	$E[E_{t,0}^0] = E[E_m^0]$	$COV[E_{t,0}^0] = COV[E_m^0]$
MOE - tension perp. to the grain:	Constant – no reference LOGNORMAL	$E[E_{t,90}^0] = \frac{E[E_m^0]}{30}$	$COV[E_{t,90}^0] = COV[E_m^0]$
Compression strength parallel to the grain:	Weak sections – as MOE-bending LOGNORMAL	$E[f_c^0] = 6 E[f_m^0]^{0.45}$	$COV[f_c^0] = 0.8 COV[f_m^0]$
Compression strength per. to the grain:	Constant – no reference LOGNORMAL	$E[f_{c,90}^0] = 0.008 E[\rho_0]$	$COV[f_{c,90}^0] = COV[\rho_0]$
Shear modulus:	Constant – no reference LOGNORMAL	$E[G^0] = \frac{E[E_m^0]}{16}$	$COV[G^0] = COV[E_m^0]$
Shear strength:	Constant – no reference LOGNORMAL	$E[f_v^0] = \min\{3.8; 0.21 E[f_m^0]^{0.8}\}$	$COV[f_v^0] = COV[f_m^0]$

All properties are subject to the reference climate conditions outlined in the foregoing. The correlations are given as follows:

Table 2: Correlations

	E_m^0	ρ_0	$f_{t,0}^0$	$f_{t,90}^0$	$E_{t,0}^0$	$E_{t,90}^0$	f_c^0	$f_{c,90}^0$	G^0	f_v^0
f_m^0	0.8		0.8				0.8			
E_m^0										
ρ_0										
$f_{t,0}^0$										
$f_{t,90}^0$										
$E_{t,0}^0$										
$E_{t,90}^0$										
f_c^0										
$f_{c,90}^0$										
G^0										

6 Reference Conditions

The reference volumes are defined in section 4 and in Table 1. The reference conditions are defined as follows:

- Reference volumes are conditioned in the reference climate 20° C and 65% relative humidity
- Volumes are loaded to failure in short-term ramp loading with a time to failure of approximately 5 minutes.

7 Modeling deviations from reference conditions

7.1 Deviation in size

A structural member or a test specimen is regarded as constituted from a sequence of finite reference volumes. For strength related material properties which can be modeled according to the model in Figure 3 the probability distributions of ultimate load bearing capacity can be found by simulation. For the special case of constant applied stress an analytical solution can be obtained according to Ditlevsen and Källsner [2004]. However, the model proposed in Figure 3 is modeling lengthwise variations of material properties and is capable of describing length-effects.

Tension perpendicular to the grain is governed by the non-separable compositions of small defects in a given volume. The probability distribution function of this material property is thus conditional on the considered volumes. According to the Weibull theory (Weibull [1939])

the strength values of test specimen can be related to the strength values of the volume of interest, as follows:

$$\frac{f}{f^0} = \left(\frac{V^0}{V} \right)^{\frac{1}{k_v}} \quad (4.1)$$

The parameter k_v can be also referred to the shape parameter of the Weibull distribution.

The bending strength and the tension strength parallel to the grain of components of different heights can be related to each other according to the following expression:

$$\frac{f}{f^0} = \left(\frac{h^0}{h} \right)^{\frac{1}{k_h}} \quad (4.2)$$

It is proposed to model k_v and k_h as random variables.

7.2 Modification of strength due to the effect of the load history

Due to stresses, damage is accumulated during the lifetime of a timber structure. The damage accumulated is modeled by the factor α where $\alpha = 1$ corresponds to an undamaged material and $\alpha = \alpha_{ult}$ to the damage where the component fails. The limit state function is given as a function of damage factors by

$$g(\alpha_{ult}, \alpha) = \alpha_{ult} (S(t)) - \alpha(\mathbf{p}, S(t), f^0, z) \quad (7.2)$$

where \mathbf{p} is a vector of model parameters, $S(t)$ is the load (the applied stress) as a function of time, f^0 is the short term strength (evaluated under test conditions, i.e. 5min to failure in average) and z is the design variable.

The damage α is cumulated according to the following formulae (Nielsen [2000])

$$\alpha_0 = 1$$

$$\alpha_{i+1} = \alpha_i + \Delta\alpha_i$$

with

$$\frac{\Delta\alpha_i}{\Delta t} \stackrel{\Delta t \rightarrow dt}{=} \frac{d\alpha_i}{dt} = \Lambda \frac{\alpha_i (SL)^2}{\left((\alpha_i (SL)^2)^{-1} - 1 \right)^{\frac{1}{k}}} \quad (4.3)$$

where

$$\Lambda = \frac{(\pi FL)^2}{8q\tau}$$

q , τ , FL and b are model parameters. (Example values and a brief introduction to the model can be found in Köhler J., Faber M.H. [2003]) $SL = \frac{S(t)}{f^0}$ is the stress ratio; i.e. the ratio between the applied stress and the short term strength.

Ultimate damage is defined by $\alpha_{ult} = SL^{-2}$.

For quasi-harmonic pulse loads damage due to fatigue has to be considered. Therefore the model can be extended according to Nielsen [2000].

7.3 Modification of Strength due to change in climate

To be included

7.4 Combined effect of Climate and load history

The stress ratio in Equation (4.3) is modified by the moisture factor $\kappa(T(t), \omega(t))$, which is depending on temperature and load history. Therefore the stress ratio becomes $SL = \left(\kappa(t) \frac{S(t)}{f^0} \right)$. In the case of normal climate $\kappa(t) = 1$, the impact of climate variations is considered as additional load with, $\kappa(t) \geq 1$.

7.5 Modification of stiffness due to load and Climate history

(to be included, here or in the previous subsections)

8 Different states of knowledge

A challenging task is to establish probabilistic models reflecting the available knowledge. In the following a first proposal in this direction is given for the purpose of facilitating further discussions.

8.1 No prior knowledge

Due to the variability of timber material properties in regard to species, origin and quality control procedure, tests have to be involved to estimate the material properties. A low-informative prior distribution for the reference material properties can be defined as follows, and used for Bayesian updating involving information from tests.

	m'	n'	s'	v'
$\ln(\text{Bending strength } f_m^0 \text{ measured in } [MPa])$	3.8	3.0	1.2	10
$\ln(\text{Bending MOE } E_m^0 \text{ measured in } [MPa])$	9.2	3.0	3.2	10
Density ρ_0 measured in $[kg/m^3]$	400	3.0	100	10

where the parameters can be understand as:

m' is the hypothetical sample average of the mean

n' is the hypothetical number of observations for m'

s' is the hypothetical sample average of the standard deviation

v' is the hypothetical number of observations for s' .

8.2 Information on the code grade classification

It is assumed that at least some knowledge about the grade of the timber is available. However, a timber grade and its properties is the result of the applied grading rules; i.e. certain properties which have at least to be fulfilled to define a grade. In general these grading rules are standardized in codes.

Prior information about the parameters of the models for the reference material properties of reference volumes and under reference conditions can be given for different grades defined through different codes. As example parameters for grades according to EN 338 are presented:

MACHINE GRADED TIMBER EN 338 ³		m'	n'	s'	v'
C18	ln(Bending strength f_m^0 measured in [MPa])	3.38	5.0	0.246	10
	ln(Bending MOE E_m^0 measured in [MPa])	8.96	5.0	0.129	10
	Density ρ_0 measured in [kg/m ³]	399.2	5.0	39.92	10
C24	ln(Bending strength f_m^0 measured in [MPa])	3.66	6.0	0.246	10
	ln(Bending MOE E_m^0 measured in [MPa])	9.17	6.0	0.129	10
	Density ρ_0 measured in [kg/m ³]	435.2	6.0	43.52	10
C30	ln(Bending strength f_m^0 measured in [MPa])	3.88	6.0	0.246	10
	ln(Bending MOE E_m^0 measured in [MPa])	9.24	6.0	0.129	10
	Density ρ_0 measured in [kg/m ³]	472.5	6.0	47.25	10

8.3 Information about the grade and detailed information about the grading procedure

The probability distribution of the reference material properties of graded sub-populations can be modeled according to Faber et al [2004]. Basis is taken on the (prior) distributions of an

³ This is meant as an example for data representation. Quantities have to be verified! The parameters in the table are estimated under the assumption that the predictive 5% fractile values are matching the requirements in EN 338 assuming the following coefficients of variation:

	COV
Bending strength f_m^0	0.25
Bending MOE E_m^0	0.13
Density ρ_0	0.1

un-graded population and information about the grading procedure. (Relation between the reference material properties and an indicative property of the grading procedure, grading machine settings) If the parameters of the un-graded (prior) population can not be specified, the parameters from section 8.1 can be used. Otherwise the parameters from section 8.1 can be used as prior for Bayesian updating with specific information about the un-graded population.

8.4 Test Data

The information from test data of a specific material property under specific conditions can be intergraded at any stage of modeling. A prior distribution of the specific material property can be evaluated without integrating the test data. The test data can be used for updating the parameters of the prior distribution (according to sections 8.1-8.3).

(A brief guideline for Bayesian Updating can be found in the JCSS PMC Part III)

→ for major interest in the recent discussion is the weight of the information involved. (weight of prior, of new data, of virtual data generated with given grading information...)

9 Glulam

10 Other wood based building materials

11 Connections

This section is drafted by A.Jorissen and A. Leijten

In this section basic values are given for the distribution of strength determining characteristics for timber connections.

11.1 Dowel type fasteners

11.1.1 Dowel type fasteners loaded in shear

Generally, the strength of a multiple fastener connection loaded under an angle with the grain is the lowest of all values obtained by Equations (11.1), (11.2) (Jorissen [1998]).

$$F_{\alpha,multiple} = \frac{An^B \left(\frac{a_1}{d}\right)^C \left(\frac{b}{d}\right)^D F_0}{\cos(\alpha)} \quad [\text{N}] \quad (11.1)$$

$$F_{\alpha,multiple} = n \frac{b \sqrt{\frac{G_c E_0 d (2h-d)}{h}}}{\cos(\alpha)} \quad [\text{N}] \quad (11.2)$$

where:

F_0 is the strength of the connection loaded parallel to the grain. This value is the lowest of all values obtained by Equation (11.2), with $\alpha = 0$, and the so called “Johansen” Equations in which the embedment strength for loading parallel to the grain is substituted ($\alpha = 0$).

A, B, C, D regression coefficients as random variables

a_1 spacing or loaded end distance parallel to the grain

n	number of fasteners in a row in the grain direction
$F_{\alpha, multiple}$	strength of the multiple fastener connection [N]
G_c	the fracture energy for mixed mode according to Peterson [1995] loading parallel to the grain [Nmm/mm ²]
b	member thickness [mm]
h	member width [mm]
E_0	modulus of elasticity parallel to the grain [MPa]
d	diameter of the dowel type fastener [mm]
α	angle between load and grain directions

For connections with dowel type fasteners, the embedment strength should be obtained by Equation (11.3).

$$f_{h,\alpha} = \frac{f_{h,0}}{f_{h,0} \sin^2(\alpha) + f_{h,90} \cos^2(\alpha)} \quad [\text{MPa}] \quad (11.3)$$

with

$$f_{h,0} = S_0 \rho^{T_0} d^{U_0} \quad \text{and} \quad f_{h,90} = S_{90} \rho^{T_{90}} d^{U_{90}}$$

where:

$f_{h,\alpha}$	embedment strength under loading angle to the grain α
$f_{h,0}; f_{h,90}$	embedment strength parallel and perpendicular to grain
ρ	timber density [kg/m ³]
d	diameter of the fastener
S, T, U	fastener type and loading mode depending regression coefficients as random variables

The coefficients used in Equations (11.1) to (11.3) should be taken from tables 11.1 and 11.2.

Table 11.1: Regression parameters as normal distributed random variables

Parameter	A	B	C	D	Pre-drilled			Non pre-drilled		
					S_0/S_{90}	T_0/T_{90}	U_0/U_{90}	S_0/S_{90}	T_0/T_{90}	U_0/U_{90}
mean	0.42	0.91	0.28	0.19						
c.o.v.										

Table 11.2: Material depending statistical parameters.

Parameter	G_c	E_0	ρ	k_{90}				d
				nails	bolts	dowels	screws	
Model	Lognormal	Lognormal	Normal	Normal	Normal	Normal	Normal	Normal
mean								
c.o.v.								

References

- Blass H.J., Bienhaus A. and Krämer V. (2001) *Effective bending capacity of dowel-type fasteners*. Proc. PRO 22, Int. RILEM Symposium on Joints in Timber Structures, pp. 71-88.
- Czmoch I. Thelandersson S. and Larsen H.J. (1991) *Effect of within member variability on bending strength of structural timber*. CIB/W18 – Timber Structures. Paper 24-6-3, Oxford, UK.
- Ditlevsen O. and Källsner B. (2004) *Statistical series system size effects on bending strength of timber beams*. Reliability and Optimization of Structural Systems – Maes & Huysse (eds). Taylor and Francis Group, London.
- EN 338; Structural Timber – Strength Classes
- EN 408; Timber Structures – Test Methods – Determination of physical and mechanical properties.
- Faber, M.H., Köhler, J., Sorensen, J.D. (2004). *Probabilistic Modeling of Graded Timber Material Properties*. Journal of Structural Safety, Volume 26, Issue 3, Pages 295-309, July 2004.
- Gustafsson, P.J. (1992). *Some test methods for fracture mechanics properties of wood and wood adhesive joints*. RILEM TC133-TF workshop, Bordeaux, France, 1992.
- Isaksson T. (1999) *Modeling the variability of bending strength in structural timber – Length and load configuration effects*. Report TVBK-1015, Department of Structural engineering, Lund University, Sweden.
- Jorissen, A. (1998). *Double shear timber connections with dowel type fasteners*. PhD-Thesis, Delft University Press, Netherlands.
- Köhler J., Faber M.H. (2003) *A Probabilistic Creep and Fatigue Model for Timber Materials* Proc. ICASP03, San Francisco, California, 2003.
- Nielsen L.F., (2000). *Lifetime and Residual Strength of wood subjected to static and variable load – Part I +II*. Holz als Roh- und Werkstoff. Vol. 58: 81-90 and 141-152.
- Petersson, H. (1995). *Fracture design analysis of wooden beams with holes and notches*. Paper 28-19-3, Proc. CIB-W18 meeting, Copenhagen, Denmark, 1995.
- Riberholt H. and Madsen P.H. (1979) *Strength of timber structures, measured variation of the cross sectional strength of structural lumber*. Report R 114, Struct. Research Lab., Technical University of Denmark.
- Thelandersson S. and Larsen H.J. (2003) *Timber Engineering*. John Wiley & Sons Ltd. Chichester, UK.
- Joint Committee on Structural Safety. 2001. Probabilistic Model Code, Internet Publication: www.jcss.ethz.ch.